

Energy management strategies for battery electric bus fleet

Hussein Basma

▶ **To cite this version:**

Hussein Basma. Energy management strategies for battery electric bus fleet. Electric power. Université Paris sciences et lettres, 2020. English. ⟨NNT : 2020UPSLM036⟩. ⟨tel-03710820⟩

HAL Id: tel-03710820

https://pastel.hal.science/tel-03710820v1

Submitted on 1 Jul 2022

HAL is a multi-disciplinary open access archive for the deposit and dissemination of scientific research documents, whether they are published or not. The documents may come from teaching and research institutions in France or abroad, or from public or private research centers.

L'archive ouverte pluridisciplinaire **HAL**, est destinée au dépôt et à la diffusion de documents scientifiques de niveau recherche, publiés ou non, émanant des établissements d'enseignement et de recherche français ou étrangers, des laboratoires publics ou privés.



HAL Authorization

PSL UNIVERSITÉ PARIS

THÈSE DE DOCTORAT
DE L'UNIVERSITÉ PSL

Préparée à MINES ParisTech

Energy Management Strategies for Battery Electric Bus Fleet

Stratégies de Gestion de l'énergie pour des Flottes de Bus Electriques à Batterie

Soutenue par

Hussein BASMA

Le 03 Décembre 2020

Ecole doctorale n° 621

Ingénierie des Systèmes, Matériaux, Mécanique, Énergétique

Spécialité

Énergétique et Génie des Procédés

Composition du jury :

Rochdi, TRIGUI Directeur de Recherche Université Gustave EIFFEL	*Président*
Göran, LINDBERGH Professeur, KTH Sweden	*Rapporteur*
Lavinia, GROSU Maître de Conférences, Université Paris Nanterre	*Examinatrice*
Charbel, MANSOUR Associate Professor, Lebanese American University	*Examinateur*
Pascal, STABAT Professeur, PSL – Mines ParisTech	*Directeur de thèse*
Adnane, HOUBBADI Docteur, Transdev	*Invité*

MINES ParisTech | PSL

SUMMARY

The transport sector accounts for more than one-quarter of global greenhouse gas (GHG) emissions and several alternative vehicle technologies have been introduced and developed to replace oil-dependent mobility. Battery electric buses (BEB) present a promising solution thanks to their high energy efficiency and low GHG emissions. However, this technology still faces numerous challenges that prevent its deployment at a massive scale, especially its high total cost of ownership (TCO) and other operational factors such as the limited bus driving range (DR), the high energy refueling time, and the required charging technologies and strategies. The main objective of this thesis is to study different energy management strategies that would ease the deployment of BEB by overcoming these challenges.

In order to evaluate the BEB energy needs, a comprehensive multi-physical bus energy model is developed. The model considers the different energy systems encountered in electric buses, including the battery, propulsion system, heating ventilation and air conditioning unit, and other auxiliaries that are necessary for the operation of the bus, such as pneumatic, hydraulic and electric auxiliaries. All these energy systems are coupled together in order to assess the global energy consumption of the BEB. Each energy system model is validated against similar experimental studies in the literature at a variety of simulation conditions. The validation results show that the proposed model can precisely predict the energy consumption of the BEB.

The energy consumption of the bus is evaluated at a variety of operating conditions such as driving and weather conditions, and levels of passengers' occupancy. The energy performance of each energy system in the bus is analyzed as function of these operating conditions. Results show the drastic increase in BEB energy consumption at extreme cold weather conditions and at high levels of traffic congestion, which further reduces the BEB driving range. This urges bus manufacturers and operators to rethink their current approaches to tackle costs and driving range problem of BEB deployment.

Then, a techno-economic model of a bus fleet is developed in order to assess the impact of different battery sizing and charging methods on the costs and operation of BEBs. The model is developed in real-time and it includes BEBs, chargers, stop stations along the line, terminal stations at both ends of the line, and a depot. The energy interactions among these components are presented using 2 types of interactions: (1) passengers' flow and (2) electric power flow. In addition, a detailed total cost of ownership (TCO) model for BEB deployment is presented. The

model considers the BEB unit costs, battery purchase and replacement costs, energy and power costs, infrastructure, and maintenance costs. Besides, an approach to assess BEB operation is presented by evaluating a punctuality index (PI) that reflects on BEB departure delays to their schedule, resulting from their daily charging events. Finally, a case study representative of bus line number 21 in Paris city is introduced utilizing the proposed models. The presented results quantitatively show the trade-off between BEB operation (PI) and TCO at different battery sizes and charging strategies. The results conclude on the need to provide a systematic methodology to optimally size the batteries and charge the BEB in order to minimize the TCO of BEB deployment while respecting operation constraints.

A methodology to minimize the TCO of BEB deployment is presented providing the optimal battery sizing and charging strategy for BEB, in a way the TCO of BEB deployment is minimized while respecting the BEB operation constraints. The methodology is a 2-step optimization algorithm that utilizes both Dynamic Programming and Genetic Algorithm optimization routines. The proposed methodology is applied to Bus line number 21 in Paris city, and it outputs the optimal battery sizing, charging strategy, and the corresponding required charging infrastructure. The results show that the proposed methodology could reduce the BEB TCO between 15-25% compared to the currently adopted approaches to deploy BEB. Finally, this chapter concludes on the main parameters that drive the TCO of BEB deployment and their impact on the different cost components, optimal battery size, and charging strategy.

Keywords: Battery electric bus – propulsion – HVAC – auxiliaries – energy consumption – driving patterns – weather conditions – passengers' load – driving range – total cost of ownership – bus line – bus fleet – charging strategy – battery sizing – schedule – real-time analysis – optimization – dynamic programming – genetic algorithm – optimal design – optimal energy management.

" You have to be burning with an idea, or a problem, or a wrong that you want to right. If you are not passionate enough from the start, you'll never stick it out."

Steve Jobs

Acknowledgements

A PhD journey is a long one that hardly could it be completed without the continuous support of the people surrounding you. No words can express my deepest gratitude and appreciation to all those who accompanied me during this journey. This success belongs to you all as much as it belongs to me.

First, I would like to thank Dr. Charbel MANSOUR, my thesis co-supervisor, my mentor since 2014, my idol and role model, for his guidance and trust during this thesis. I thank you for teaching me how important it is to pursue my dreams, and why passion should be a main driver behind any decision I take. You lead by example, and this makes it easier for you students to excel.

I thank all my thesis supervisors, Dr. Maroun NEMER, Professor Pascal STABAT, and Dr. Marc HADDAD for your valuable contribution and guidance. I learned a lot from you during this journey.

I would like to thank CES – Palaiseau for this great opportunity, and for providing a perfect work environment where one can learn, achieve, and excel.

I thank LAU for being part of this thesis and for their generous contribution.

I thank all jury members for dedicating their time to improve my work.

Special thanks to Rabih AL-HADDAD, my colleague and friend, for his significant contribution to my work. Your assistance was of a great added value and your moral support was remarkable.

I want to express my gratitude to all my friends in France and Lebanon. You were always there by my side.

I dedicate this work to my family, my late father, my beloved mother, my siblings Hadi, Zaynab and Sukayna.

Last but definitely not least, I dedicate my PhD to my beloved Christina, my strongest support and encouraging partner. You made this journey bearable and achievable with your continuous understanding and help over the past 3 years.

Thank you all

Table of Contents

SUMMARY ---- **2**

NOMENCLATURE ---- **29**

1. Chapter 1 INTRODUCTION ---- **37**

1.1 Background ---- **38**

1.2 Alternative Bus Technologies ---- **39**

1.3 Implications of Battery Electric Buses ---- **42**

1.3.1 Benefits of Battery Electric Buses ---- 42

1.3.2 Challenges of Battery Electric Buses ---- 44

1.4 Key Players in the Deployment of BEB Fleet ---- **46**

1.4.1 Operator ---- 47

1.4.2 Energy Logistics (Supplier, Transmission and Distribution operators) ---- 47

1.4.3 Regulatory Authorities ---- 48

1.5 The Current State of Deployment of BEB ---- **48**

1.5.1 BEB Market ---- 49

1.5.2 Challenges of BEB Operators ---- 51

1.5.2.1 Range Anxiety ---- 51

1.5.2.2 The Know-How of Operation ---- 51

1.5.2.3 The Readiness of the Electric Power Grid ---- 52

1.6 Problem Statement ---- **52**

1.7 Research Approach ---- **53**

1.8 References ---- **60**

2. Chapter 2 BATTERY ELECTRIC BUS ENERGY MODEL ---- **65**

2.1 Introduction ---- **66**

2.2 Review of the Literature ---- **67**

2.3 Modeling Environment ---- **73**

2.4 Battery Electric Bus Model ---- **73**

2.4.1 Bus Configuration and Specification ---- 73
2.4.1.1 Bus Configuration ---- 73
2.4.1.2 Bus Specifications ---- 75
2.4.2 Battery ---- 76
2.4.2.1 Technology and Market ---- 76
2.4.2.2 Electrical Model ---- 78
2.4.2.3 Thermal Model ---- 81
2.4.2.4 Battery Thermal Management System ---- 87
2.4.3 Propulsion System ---- 89
2.4.3.1 Electric Machine ---- 89
2.4.3.2 Wheels, Transmission and Braking Systems ---- 90
2.4.3.3 Torque Control Strategy ---- 91
2.4.4 Cabin Thermal Load ---- 93
2.4.4.1 Thermal Comfort ---- 93
2.4.4.2 Model ---- 94
2.4.5 HVAC Unit ---- 99
2.4.5.1 Technology ---- 100
2.4.5.2 Model ---- 102
2.4.5.2.1 Reversible Heat Pump ---- 102
2.4.5.2.2 Battery Thermal Management System ---- 104
2.4.5.2.3 Control Scheme ---- 104
2.4.6 Auxiliaries ---- 108
2.4.6.1 Pneumatic Auxiliaries ---- 108
2.4.6.2 Electric Auxiliaries ---- 109
2.4.6.3 Hydraulic Auxiliaries ---- 110
2.5 Model Validation ---- 111
2.5.1 Propulsion System ---- 111

2.5.2 Cabin Thermal Load---------- 116

2.5.3 HVAC System (Heat Pump) ---------- 117

2.5.4 Auxiliaries ---------- 118

2.5.5 Battery ---------- 119

2.6 Conclusion ---------- 121

2.7 References ---------- 123

3. Chapter 3 ENERGY CONSUMPTION OF BATTERY ELECTRIC BUS-------- 136

3.1 Introduction ---------- 137

3.2 Impact of Driving Conditions on Energy Consumption ---------- 138

3.2.1 Propulsion System Energy Consumption ---------- 138

3.2.2 Auxiliaries' Energy Consumption ---------- 140

3.2.2.1 Steering Pump---------- 141

3.2.2.2 Air Compressor ---------- 142

3.2.2.3 Suspension System and Electric Auxiliaries ---------- 143

3.2.3 HVAC Unit Energy Consumption ---------- 143

3.3 Impact of Weather Conditions on Energy Consumption ---------- 145

3.3.1 Impact of External Temperature ---------- 145

3.3.2 Impact of Solar Flux---------- 151

3.3.3 Impact of HVAC Energy Recovery System ---------- 152

3.4 Impact of Passengers' Load on Energy Consumption ---------- 153

3.4.1 HVAC Unit Energy Consumption ---------- 154

3.4.2 BTMS Energy Consumption ---------- 156

3.4.3 Propulsion System Energy Consumption ---------- 158

3.5 Study of Bus Battery Sizing at Different Operating Conditions---------- 159

3.5.1 Preliminary Battery Sizing Methodology ---------- 159

3.5.2 Case Studies ---------- 166

3.5.2.1 Baseline Scenario ---------- 167

3.5.2.2 Improvement Scenario 1: BEB Cabin Pre-Conditioning ---------- 169

3.5.2.3 Improvement Scenario 2: Use of Alternative on-board Heat Source --------- 169

3.5.2.4 Improvement Scenario 3: Reduce BEB Ridership Capacity ---------- 170

3.5.2.5 Improvement Scenario 4: Increase Battery Operating SOC Window -------- 171

3.5.2.6 Improvement Scenario 5: Trip Number Reduction ---------- 171

3.5.2.7 Improvement Scenario 6: Increase Daily Charging Events ---------- 172

3.6 Conclusion ---------- 173

3.7 References ---------- 175

4. Chapter 4 TECHNO-ECONOMIC MODEL OF BATTERY ELECTRIC BUS LINE ---------- 177

4.1 Introduction ---------- 178

4.2 State of the Art of BEB Lines: Battery Sizing, Charging Strategy and Charging Technology ---------- 179

4.2.1 Overview of BEB Operating Lines Worldwide ---------- 180

4.2.2 Charging Scheme of Electric Vehicles ---------- 183

4.2.2.1 Charging Infrastructure ---------- 183

4.2.2.1.1 Stationary Charging ---------- 183

4.2.2.1.2 Dynamic Charging ---------- 184

4.2.2.2 Charging Power Level ---------- 185

4.2.2.2.1 AC Chargers ---------- 185

4.2.2.2.2 DC Chargers ---------- 186

4.2.2.3 Type of Charging System ---------- 187

4.2.2.3.1 Conductive Charging System ---------- 187

4.2.2.3.2 Inductive Charging System ---------- 187

4.2.2.3.3 Battery Swapping System ---------- 187

4.2.3 BEB Line Costs and Operation Tradeoff(s) ---------- 188

4.3 BEB Line Energy Model ---------- 191

4.3.1 System Overview ---------- 191

4.3.2 System Model ---------- 193

4.3.2.1 Charger ---------- 193
4.3.2.2 BEBs ---------- 194
4.3.2.3 Stop Stations ---------- 195
4.3.2.3.1 Passengers' Flow Interaction: Stop Stations - BEBs ---------- 196
4.3.2.3.2 Electric Power Flow Interaction: Stop Stations - BEBs ---------- 199
4.3.2.4 Terminal Stations ---------- 199
4.3.2.4.1 Passengers' Flow Interaction: Terminal Stations - BEBs ---------- 200
4.3.2.4.2 Electric Power Flow Interaction: Terminal Stations - BEBs ---------- 200
4.3.2.5 Depot ---------- 201
4.3.2.5.1 Electric Power Flow Interaction: Depot - BEBs ---------- 201
4.3.2.6 Operating Conditions ---------- 202
4.3.2.6.1 Driving Conditions ---------- 202
4.3.2.6.2 Weather Conditions ---------- 202
4.3.2.6.3 Passengers' Load ---------- 202
4.3.2.6.4 Schedule ---------- 202
4.3.2.7 Charging Strategy ---------- 202
4.4 Operation of BEB Line ---------- 204
4.4.1 BEB Line Punctuality Level ---------- 204
4.4.2 BEB Line Punctuality Penalty Fares ---------- 205
4.5 Costs of Deployment of BEB Lines ---------- 206
4.5.1 Unit Cost ---------- 206
4.5.2 Operating Costs ---------- 207
4.5.3 Maintenance Cost ---------- 209
4.5.4 Infrastructure Cost ---------- 209
4.5.5 Battery Replacement Cost ---------- 210
4.5.6 Total Cost of Ownership ---------- 211
4.5.6.1 TCO Model ---------- 211

4.5.6.2 Present Worth of TCO ---------- 212

4.6 Impact of Battery Sizing and Charging Strategy on Operation and Costs of BEB Lines --- 215

4.6.1 Case Study ---------- 215

4.6.1.1 Bus Line Specifications---------- 215

4.6.1.2 Driving Conditions ---------- 216

4.6.1.3 Weather Conditions ---------- 216

4.6.1.4 Passengers' Load ---------- 216

4.6.1.5 Schedule ---------- 217

4.6.1.6 Cost Model Parameterization ---------- 218

4.6.1.7 Baseline Scenarios---------- 219

4.6.2 Results and Discussion---------- 220

4.6.2.1 TCO Segmentation ---------- 220

4.6.2.1.1 Battery Replacement Costs ---------- 221

4.6.2.1.2 Infrastructure Costs ---------- 222

4.6.2.1.3 Operating Costs---------- 223

4.6.2.2 TCO – PI Trade-off ---------- 224

4.7 Conclusion ---------- 228

4.8 References ---------- 231

5. Chapter 5 OPTIMAL BATTERY SIZING AND CHARGING STRATEGY FOR BATTERY ELECTRIC BUSES ---------- 243

5.1 Introduction ---------- 244

5.2 Review of the Literature ---------- 245

5.3 Methods ---------- 251

5.3.1 Framework ---------- 252

5.3.2 Optimization Step 1: Dynamic Programming ---------- 257

5.3.2.1 Overview---------- 257

5.3.2.2 Formulation---------- 257

5.3.2.2.1 Optimization Objective ---------- 257
5.3.2.2.2 State, Control, and Input variables ---------- 257
5.3.2.2.3 Mathematical Model ---------- 259
5.3.2.2.4 State and Control Variables Constraints ---------- 260
5.3.2.2.5 Grid Selection ---------- 262
5.3.2.2.6 Cost Function Matrix ---------- 262
5.3.2.2.7 Cost-to-go Function Matrix ---------- 263
5.3.3 Optimization Step 2: Genetic Algorithm ---------- 263
5.3.3.1 Overview ---------- 263
5.3.3.2 Formulation ---------- 264
5.3.3.2.1 Terminology ---------- 264
5.3.3.2.2 Analogy ---------- 264
5.3.3.2.3 Objective Function ---------- 264
5.3.3.2.4 GA Steps ---------- 265
5.4 Application ---------- 267
5.4.1 Case Study ---------- 267
5.4.2 Results and Discussion ---------- 267
5.4.2.1 Optimal Charging Strategies at Different Battery Sizes ---------- 267
5.4.2.1.1 Energy Costs ---------- 271
5.4.2.1.2 Battery Replacement Costs ---------- 275
5.4.2.2 Optimal Battery Size and Charging Infrastructure ---------- 279
5.4.2.3 Impact of Schedule on Optimal Battery Size ---------- 283
5.4.2.4 BEB Charging Load at Different Battery Sizes and Charging Strategies ---- 284
5.4.2.5 Sensitivity Analysis of the Different TCO parameters ---------- 287
5.4.2.5.1 Impact of Lithium-ion battery cost ---------- 288
5.4.2.5.2 Impact of demand charge tariff ---------- 290
5.4.2.5.3 Impact of the charger's cost ---------- 294

5.5 Conclusion ---------- 296

5.6 References ---------- 298

6. Chapter 6 CONCLUSIONS AND PERSPECTIVES ---------- 302

6.1 Synthesis and Conclusions ---------- 303

6.2 Improvement and Future Work ---------- 308

7. APPENDICES ---------- 311

Appendix A : Vapor Compression Cycle (VCC) ---------- 312

Appendix B: HP Components Modeling and Specifications ---------- 314

Appendix C: Propulsion System Validation Data ---------- 318

Appendix D: Comparative Energy Analysis of Battery Electric Bus and Diesel Bus ---------- 322

Appendix E: Development of the BEB Energy Consumption Maps ---------- 332

Appendix F: Validation of the Map-Based BEB Energy Consumption Against Real-World Data ---------- 335

Appendix G: Supplement to Section 4.3.1 ---------- 337

Appendix H: Battery Aging Model ---------- 339

Appendix I: GA Global Optimum ---------- 343

8. LIST OF PUBLICATIONS ---------- 345

9. Résumé Français ---------- 347

9.1 Chapitre 1 INTRODUCTION ---------- 348

9.1.1 Contexte général ---------- 348

9.1.2 Technologies alternatives de bus ---------- 348

9.1.3 Bus Electrique à Batterie ---------- 349

9.1.4 Déploiement de flottes de BEB ---------- 352

9.1.5 Formulation du problème ---------- 354

9.1.6 Objectifs scientifiques ---------- 355

9.2 Chapitre 2 MODÈLE ÉNERGÉTIQUE du BUS ÉLECTRIQUE à BATTERIE ---------- 357

9.2.1 Introduction ---------- 357

9.2.2 Etat de L'art ---------- 358

9.2.3 Configuration et spécification du bus ---------- 359

9.2.4 Modélisation ---------- 360

9.2.4.1 Batterie ---------- 360

9.2.4.2 Système de Propulsion ---------- 361

9.2.4.3 Cabine ---------- 362

9.2.4.4 HVAC ---------- 363

9.2.4.5 Auxiliaires ---------- 364

9.2.5 Validation des Modèles ---------- 366

9.2.6 Conclusion ---------- 369

9.3 Chapitre 3 La CONSOMMATION d'ÉNERGIE du BUS ÉLECTRIQUE à BATTERIE -- 370

9.3.1 Introduction ---------- 370

9.3.2 L'impact des conditions de conduite ---------- 371

9.3.3 L'impact des conditions météorologiques ---------- 373

9.3.4 L'impact de la charge des passagers ---------- 374

9.3.5 Méthodologie préliminaire pour le dimensionnement des batteries ---------- 375

9.3.6 Conclusion ---------- 379

9.4 Chapitre 4 MODÈLE TECHNO-ÉCONOMIQUE de LIGNE de BUS ÉLECTRIQUES à BATTERIE ---------- 380

9.4.1 Introduction ---------- 380

9.4.2 État de l'art des lignes du BEB : dimensionnement des batteries, stratégie et technologie de recharge ---------- 381

9.4.3 Modèle énergétique de la ligne du BEB ---------- 384

9.4.4 Fonctionnement de la ligne du BEB ---------- 385

9.4.5 TCO du déploiement des BEB ---------- 386

9.4.6 Impact de la stratégie de recharge et de dimensionnement des batteries sur le fonctionnement et les coûts des lignes du BEB ---------- 389

9.4.7 Conclusion ---------- 393

9.5 Chapitre 5 Optimisation du dimensionnement de la batterie et stratégie de recharge des Bus Electriques à Batterie ---------- 394

9.5.1 Introduction ---------- 394

9.5.2 État de l'art ---------- 395

9.5.3 Méthode ---------- 396

9.5.4 Application et résultats ---------- 399

9.5.5 Conclusion ---------- 404

9.6 Chapitre 6 CONCLUSIONS et PERSPECTIVES ---------- 406

9.6.1 Synthèse et conclusions ---------- 406

9.6.2 Perspectives ---------- 409

Table of Figures

Figure 1.1: Annual global CO2 emissions until 2017 [7] 38
Figure 1.2: Global CO2 emissions by sector in 2018 [8] 39
Figure 1.3: Propulsion system configuration of CNG and Biofuel bus technologies 40
Figure 1.4: Propulsion system configurations of electrified bus technologies 41
Figure 1.5: WTW, WTT, and TTW GHG emissions of different bus technologies [1], [14]–[17] 42
Figure 1.6: WTW, WTT and TTW energy consumption of different bus technologies [1], [14], [15], [18] 43
Figure 1.7: Bus unit cost by technology [1] 44
Figure 1.8: Bus TCO by technology [19], [20], [29], [30], [21]–[28] 44
Figure 1.9: Bus driving range by technology [1] 46
Figure 1.10: Bus refueling time by technology [1] 46
Figure 1.11: Required infrastructure modification by bus technology [1] 46
Figure 1.12: Scheme of BEB deployment 47
Figure 1.13: Global electrified buses sales by type of propulsion systems [32] 49
Figure 1.14: Forecast on the European urban bus market share [33] 50
Figure 1.15: Research approach framework 59
Figure 2.1: BEB components configuration 74
Figure 2.2: Ragone plot of various electrochemical energy storage and conversion devices [30] 77
Figure 2.3: Reported Lithium-ion battery pack costs, average of reported values and observed average by Bloomberg New Energy Finance (BNEF) [40] 78
Figure 2.4: Internal resistance and open-circuit voltage variation for a single battery cell as function of the battery SOC 80
Figure 2.5: Scheme of battery cell cross-sectional view 83
Figure 2.6: Scheme of battery pack top view 83
Figure 2.7: Entropy change data for battery cell anode and cathode function of battery SOC [68] 84
Figure 2.8: Coolant flow across battery cells 85
Figure 2.9: Battery coupled electro-thermal model scheme 89
Figure 2.10: Electric machine efficiency map [86] 90
Figure 2.11: Torque control strategy flow chart 92

Figure 2.12: BEB cabin thermal scheme [*] 95
Figure 2.13: Mean heat losses due to doors opening 99
Figure 2.14: Reversible HP in Heating Mode [96] 100
Figure 2.15: Reversible HP in cooling mode [96] 101
Figure 2.16: HVAC unit scheme 102
Figure 2.17: BTMS control scheme 107
Figure 2.18: Schematic of the pneumatic system in BEB 108
Figure 2.19: Electro-Hydraulic steering pump power consumption function of BEB speed [27] 111
Figure 2.20: Propulsion system energy consumption validation 115
Figure 2.21 Propulsion system validation error distribution 115
Figure 2.22: Bus cabin thermal need validation 116
Figure 2.23: Bus HVAC unit validation 118
Figure 2.24: Non-Mechanical auxiliaries energy consumption validation 119
Figure 2.25: Battery SOC and core and surface temperature profiles over a charge depleting cycle simulation results 120
Figure 2.26: Battery SOC and core and surface temperature profiles over a charge depleting cycle as reported by [62] 120
Figure 3.1: Propulsion system energy consumption at different driving conditions 139
Figure 3.2: Variation of propulsion system energy consumption at different average speeds 140
Figure 3.3: Non-Mechanical auxiliaries' energy consumption at different driving conditions 141
Figure 3.4: Variation of steering pump energy consumption at different average speeds 141
Figure 3.5: Air compressor average power demand function of drive cycle's average deceleration 142
Figure 3.6: Variation of the suspension system and electric auxiliaries energy consumption function of the average number of stops per km 143
Figure 3.7: HVAC unit average electric power demand at different drive cycles 144
Figure 3.8: BEB cabin steady-state thermal load at different external temperatures 146
Figure 3.9: Thermal load segmentation at different external temperatures measured in W (Heating) 147
Figure 3.10: Thermal load segmentation at different external temperatures measured in W (Cooling) 148

Figure 3.11: HVAC unit average electric power consumption at different external temperatures 149
Figure 3.12: Cabin temperature evolution and HVAC unit instantaneous electric power demand - T = 0 °C - MB Drive Cycle 150
Figure 3.13: HVAC system heating COP (COP_HP) and cooling COP (COP_R) at different external temperatures 150
Figure 3.14: BTMS average electric power demand at different external temperatures 151
Figure 3.15: HVAC unit average power demand at different levels of solar flux 152
Figure 3.16: HVAC unit average power demand at different external temperatures with/without energy recovery system 153
Figure 3.17: HVAC unit average electric power demand at different passengers' load 154
Figure 3.18: Fresh air heat flux (ventilation load) at different passengers' load 155
Figure 3.19: Temperature of air upstream the condenser/evaporator at different passengers' load 156
Figure 3.20: BTMS average electric power demand at different passengers' load 157
Figure 3.21: Temperature of air upstream the electric resistance/evaporator at different passengers' load 158
Figure 3.22: Propulsion system specific energy consumption at different passengers' loads 159
Figure 3.23: Flowchart of preliminary battery sizing methodology 160
Figure 3.24: Propulsion system specific energy consumption map 161
Figure 3.25: HVAC unit average power demand map ($R_{door\text{-}open}$ = 0.3) – No Solar Flux 162
Figure 3.26: HVAC unit additional power demand due to solar flux 163
Figure 3.27: BTMS average power demand map 164
Figure 3.28: Pneumatic system average power demand 164
Figure 3.29: Steering pump specific energy consumption 165
Figure 3.30: Suspension system and electric auxiliary's specific energy consumption 166
Figure 3.31: Daily energy consumption segmentation in BEB: Baseline Scenario 168
Figure 4.1: New BEB and PHEB in China [13] 180
Figure 4.2: Number of BEB ordered in Europe between 2009 – 2018 [13] 180
Figure 4.3: Stationary charging station - Portal Charger 184
Figure 4.4: Stationary charging station - Overhead Charger 184
Figure 4.5: Scheme of dynamic charging 185
Figure 4.6: EV charging scheme 188
Figure 4.7: Schematic diagram of a BEB line 192

Figure 4.8: Schematic of power flow and passengers' flow interactions among the different bus line components 193
Figure 4.9: DC chargers' efficiency 194
Figure 4.10: Schematic of passengers flow interaction between the buses and stop stations 198
Figure 4.11: Example of BEB charging power profile during the day 203
Figure 4.12: Summary of TCO model components 214
Figure 4.13: Bus Line number 21 route in Paris city 215
Figure 4.14: Velocity profile of bus line 21 for a one-way trip 216
Figure 4.15: Daily outdoor temperature profile in Paris city 217
Figure 4.16: Passengers' flow daily profile into few stop stations of bus line 21 in Paris city 217
Figure 4.17: Passengers' flow daily profile out of the bus at few stop stations of bus line 21 in Paris city 218
Figure 4.18: TCO segmentation at the baseline scenarios 221
Figure 4.19: Batteries capacity fade function of time for the baseline scenarios 222
Figure 4.20: Operating Costs (OC) segmentation for the baseline scenarios 224
Figure 4.21: TCO - PI trade-off at different battery sizes and maximum charging power rates (DDC) 225
Figure 4.22: TCO - PI trade-off at different battery sizes and maximum charging power rates (ELC) 226
Figure 4.23: TCO - PI trade-off at different battery sizes and maximum charging power rates (OC) 226
Figure 4.24: Cumulative probability distribution function for bus trip delay: case of depot day charging (DDC) 227
Figure 4.25: Cumulative probability distribution function for bus trip delay: case of end-line charging (ELC) 227
Figure 4.26: Cumulative probability distribution function for bus trip delay: case of opportunity charging (OC) 228
Figure 5.1: Optimization Step 1 flowchart for any charging infrastructure 254
Figure 5.2: Methodology complete flowchart 256
Figure 5.3: Optimal charging strategy at different battery sizes (BEB number 1 - Month of January) 268
Figure 5.4: Optimal charging power profile for BEB number 1 during the month of January at a 500 *kWh* battery size with and without considering battery aging 270

Figure 5.5: Optimal energy and battery replacement costs at different battery sizes 271
Figure 5.6: BEB energy consumption at different battery sizes..... 272
Figure 5.7: Day and night charging energy distribution at different battery sizes..... 273
Figure 5.8: Summary of energy cost variation at different battery sizes 274
Figure 5.9: Degradation of battery capacity as function of time at different battery sizes 275
Figure 5.10: Charge/discharge rate function of time for different battery sizes (BEB number 1 - Month of January)..... 276
Figure 5.11: Average daily number of cycles per battery cell at different battery sizes..... 277
Figure 5.12: Summary of battery replacement cost variation at different battery sizes..... 278
Figure 5.13: Optimal battery size for each BEB 279
Figure 5.14: BEB line optimal required charging infrastructure..... 280
Figure 5.15: Variation of TCO function of battery size..... 281
Figure 5.16: TCO segmentation and components..... 282
Figure 5.17: Variation of the optimal battery size per BEB as function of the minimum BEB dwell time..... 284
Figure 5.18: BEB cumulative power demand from the electric grid (Month of January) 285
Figure 5.19: BEB power demand load factor at different battery sizes 286
Figure 5.20: Optimal BEB power demand profiles from the electric grid under three different months 287
Figure 5.21: Impact of Lithium-ion battery cost on TCO 288
Figure 5.22: Impact of demand charge tariff on TCO..... 291
Figure 5.23: Impact of Lithium-ion battery cost and demand charge tariff on BEB TCO at different battery sizes 293
Figure 5.24: Impact of chargers' cost on TCO at different battery sizes..... 295
Figure 7.1: Ideal VCC schematic 312
Figure 7.2: Ideal VCC P-V diagram..... 313
Figure 7.3: Ideal VCC T-S diagram 313
Figure 7.4: Fan pressure losses at different frequencies function of airflow rate 316
Figure 7.5: Velocity profiles of the test drive cycles used in model validation 321
Figure 7.6: DB configuration 323
Figure 7.7: DB and BEB resistive power curve 325
Figure 7.8: DB acceleration requirement curves..... 325
Figure 7.9: Engine fuel flow map..... 326
Figure 7.10: Gearbox Model of the DB in Dymola 327

Figure 7.11: DB and BEB propulsion system energy consumption at different traffic conditions 328
Figure 7.12: DB and BEB propulsion system energy segmentation 329
Figure 7.13: DB and BEB auxiliaries energy consumption at different traffic conditions 330
Figure 7.14: DB and BEB HVAC unit energy consumption at different weather conditions 331
Figure 7.15: Velocity profile of bus line 21 in Paris 335
Figure 7.16: Passengers occupancy profile for bus line 21 in Paris (recorded on a Monday, July 2019) 336
Figure 7.17: Scheme of battery aging model 342
Figure 7.18: GA optimal solution at different initial conditions 343
Figure 9.1: Émissions de GES et consommation d'énergie WTW, WTT et TTW des différentes technologies de bus 350
Figure 9.2: Coût unitaire du bus par technologie 351
Figure 9.3: TCO du bus par technologie 351
Figure 9.4: Schéma de déploiement du BEB 352
Figure 9.5: La configuration des composants du BEB 359
Figure 9.6: Schéma du modèle de batterie 361
Figure 9.7: Organigramme de TCS 362
Figure 9.8: Validation du modèle de BEB 367
Figure 9.9: Résultats des tests de validation de la batterie (Référence) 368
Figure 9.10: Résultats des tests de validation de la batterie (Simulation) 368
Figure 9.11: Consommation d'énergie du système de propulsion et des auxiliaires dans différentes conditions de conduite 372
Figure 9.12: Demande de puissance moyenne pour HVAC et BTMS à différentes températures extérieures 374
Figure 9.13: Consommation d'énergie / demande de puissance pour différentes charges de passagers 375
Figure 9.14: Organigramme de la méthodologie préliminaire de dimensionnement de batterie 376
Figure 9.15: Schéma d'une ligne de BEB 385
Figure 9.16: Segmentation du TCO dans les scénarios de référence 390
Figure 9.17: Compromis TCO - PI à différentes tailles de batterie et puissance de recharge maximum (DDC) 392
Figure 9.18: Schéma e de la méthodologie 398

Figure 9.19: Stratégie de recharge optimale pour différentes tailles de batterie (BEB numéro 1 - mois de janvier)..... 400
Figure 9.20: Taille de batterie optimale pour chaque BEB et infrastructure de recharge optimale requise 402
Figure 9.21: Segmentation du TCO 403

Table of Tables

Table 1.1: Thesis work plan 54
Table 2.1: Summary overview of the recent literature on assessing the energy consumption of BEB 68
Table 2.2: Auxiliaries technology in BEB 75
Table 2.3: Bus chassis parameters 76
Table 2.4: Bus curb mass and total mass 76
Table 2.5: Summary of Lithium-ion battery equivalent circuit models [47]–[52] 79
Table 2.6: Summary of battery pack parameters [53] 80
Table 2.7: Summary of lithium-ion batteries thermal and heat generation models [30], [59], [60] 82
Table 2.8: Battery lumped-thermal model parametrization [62] 85
Table 2.9: Battery cell and battery pack geometric parameters [53], [69] 86
Table 2.10: Summary of battery thermal management systems 88
Table 2.11: APTA Standards and performance specifications for public transit vehicles [87] 93
Table 2.12: Summary of components sizing 93
Table 2.13: Thermal comfort conditions in buses [87], [88] 94
Table 2.14: Thermal balance additional equations 97
Table 2.15: Bus geometry 97
Table 2.16: Walls thermal properties 97
Table 2.17: Summary of HP components 103
Table 2.18: Variables controlled by the HVAC system 3 control units 105
Table 2.19: Electric auxiliaries power demand whenever actuated 110
Table 2.20: Summary of the studies presented in the recent literature that report the energy consumption of BEB propulsion system 112
Table 2.21: Summary of studies used to validate the cabin thermal load 117
Table 2.22: Summary of studies used to validate the HVAC unit model 118
Table 2.23: Battery electro-thermal model validation summary 121
Table 3.1: Baseline scenario operating conditions 167
Table 3.2: Minimum required battery size: Baseline Scenario 168
Table 3.3: Minimum required battery size: Improvement Scenario 1 - Cabin Pre-Conditioning 169

Table 3.4: Minimum required battery size: Improvement Scenario 2 - Use of Alternative on-board Heat Source 170
Table 3.5: Minimum required battery size: Improvement Scenario 3 - Reduce BEB Ridership Capacity 170
Table 3.6: Minimum required battery size: Improvement Scenario 4 - Increase Battery Operating SOC Window 171
Table 3.7: Minimum required battery size: Improvement Scenario 5 – Trip Number Reduction 171
Table 3.8: Minimum required battery size: Improvement Scenario 6 - Increase Daily Charging Events 172
Table 3.9: Summary of improvement scenarios 172
Table 4.1: Review of recent operating BEB lines globally 181
Table 4.2: SAE J-1772 standard for AC charging power levels [44] 186
Table 4.3: SAE J-1772 standard for DC charging power levels [44],[46], [47]. 186
Table 4.4: Impact of battery size and charging strategy on BEB line operation and costs 190
Table 4.5: Bus trips punctuality index 205
Table 4.6: Punctuality index target values 205
Table 4.7: Penalty fare structure for bus punctuality index 206
Table 4.8: Summary of notations used in the costs of deployment of BEBs 213
Table 4.9: Schedule of bus line number 21 in Paris city 218
Table 4.10: Parametrization of the TCO model 219
Table 4.11: Case study baseline scenarios 220
Table 4.12: Chargers' number and power rating for the baseline scenarios 223
Table 5.1: Summary overview of the recent literature on reducing the cost of deployments of BEBs 247
Table 5.2: Summary of the considered control variables to minimize TCO 251
Table 5.3: Definition of the state, control and input variables 258
Table 5.4: Definition of DP input parameters 261
Table 5.5: State and Control Variables Grids 262
Table 7.1: Thermodynamic properties of refrigerants R1234yf and R134a [109] 313
Table 7.2: Compressor model equations 314
Table 7.3: Moving boundary energy and mass balances for heat exchangers 315
Table 7.4: Expansion valve model equations 316
Table 7.5: Fan model equations 317

Table 7.6: Summary of scenarios and case studies used to validate the energy consumption of the propulsion system 318
Table 7.7: Drive cycles specifications [116] 320
Table 7.8: Auxiliaries technology in DB and BEB 322
Table 7.9: Summary of bus performance requirement as set by APTA 323
Table 7.10: DB and BEB total mass segmentation 324
Table 7.11: Summary of DB and BEB component sizing 326
Table 7.12: Summary of the criteria used to develop BEB energy consumption maps 333
Table 7.13: Validation of BEB map-based energy consumption (kWh/km) 336
Table 7.14: Summary of Lithium-ion batteries aging modeling approaches 340
Tableau 9.1:Technologie des auxiliaires en BEB 360
Tableau 9.2: Résumé de la configuration du bus et des spécifications des composants 365
Tableau 9.3: Résumé de la validation du modèle électrothermique de la batterie 368
Tableau 9.4: Conditions de fonctionnement du scénario de référence 377
Tableau 9.5: Résumé des solutions techniques pour la réduction de la taille de la batterie 378
Tableau 9.6: Scénarios de référence de l'étude de cas 389

NOMENCLATURE

Symbols

M	Mass	*kg*
A	Area	*m²*
C_D	Aerodynamic Drag Coefficient	-
f_r	Friction Rolling Coefficient	-
r	Radius	*m*
J	Inertia	*kg.m²*
N	Number of (stages/buses/ …)	-
E	Energy	*J or Wh or kWh*
C	Charge Capacity | Heat Capacity	*Ah* | *J/K*
R	Resistance | Gas Constant	*Ohm or W/m.K* | *J/mol.K*
U	Voltage	*V*
N_S	Number of Battery Pack Series Sets	-
N_P	Number of Battery Pack Parallel Modules	-
I	Electric Current	*A*
P	Power	*W or kW*
U_T	Battery Terminal Voltage	*V*
T	Temperature | Torque | Period	*°C or K* | *N.m* | *mins*
$\dot{Q}$	Heat Flux	*W*
H	Enthalpy	*J*
h	Heat Transfer Coefficient | Specific Enthalpy	*W/m².K* | *J/kg*
D	Diameter	*m*
L	Length	*m*
N_u	Nusselt's number	-
K	Thermal Conductivity	*W/m.K*
R_e	Reynold's number	-
P_r	Prandtl's number	-
C_p	Heat Capacity at Constant Pressure	*J/K*

c_p	Specific Heat Capacity at Constant Pressure	$J/kg.K$
V	Speed | Volume	m/s | m^3
$\dot{m}$	Mass Flow Rate	kg/s
i	Gear Ratio	-
F	Force | Form Factor	N | -
u	Specific Internal Energy	J/kg
l_{lv}	Enthalpy of Vaporization of Water	J/kg
w	Absolute Humidity	kg/kg
W	Work Rate	W
$\dot{V}$	Volume Flow Rate	m^3/s
g	Gravity	m/s^2
t	Time	s
d	Distance	km
$\bar{E}$	Specific Energy Consumption	kWh/km
SF	Solar Flux Intensity	W/m^2
$\dot{n}$	Passenger Flow Rate	$Pass/s$
UC	Unit Costs	€
K_b	Battery Size	kWh
OC	Operating Costs	€
C_b	Cost of Building Charging Station	€
C_a	Charging Station Construction Cost per unit Area	$€/m^2$
IC	Infrastructure Cost	€
BRC	Battery Replacement Cost	€
MC	Maintenance Cost	€
SV	Salvage Value	€
Q	Normalized Charge Capacity	-
d_r	Discount Rate	%
i_r	Nominal Annual Interest Rate	%
B	Pre-exponential Factor (Battery Aging)	-
E_a	Activation Energy	J
A_h	Charge Throughput	Ah
C_{Rate}	Charge/Discharge Rate	$1/h$

Greek Letters

v	Kinematic Viscosity	$N/m^2.s$
μ	Dynamic Viscosity	$N/m^2.s$
ρ	Density	kg/m^3
ε	Emissivity	-
δ	Thickness	mm
α	Absorptivity	-
τ	Transmissivity	-
η	Efficiency	-
Ω	Bus Unit Cost without Battery	$€$
β	Cost of Lithium-ion Battery Pack	$€/kWh$
$\alpha(t)$	Cost of Electric Energy	$€/kWh$
λ	Demand Charge Rate	$€/kW$
σ	Charger Cost per Unit Power	$€/kW$

Subscripts and Superscripts

min	Minimum
max	Maximum
eq	Equivalent
ocv	Open Circuit Voltage
Batt	Battery Pack
Cell	Battery Cell
S	Surface
C	Core
∞	Coolant
mech	Mechanical
elec	Electrical
w	Wheel
RR	Rear Right
RL	Rear Left

RG	Reduction Gear
FD	Final Drive
FR	Front Rear
FL	Front Left
Br	Brakes
Reg	Regenerative
conv	Convection
cond	Conduction
rad	Radiation
sol	Solar
abs	Absorbed
ext	exterior
IR	Infra-red
env	Environmental
int	Internal
trans	Transmitted
cab	Cabin
pass	Passengers
sens	Sensible
lat	Latent
vap	Vapor
rec	Recirculation
exch	Exchanger
mix	Mixed
con	Condensed
comp	Compressor
Dr	Driver
Pneu	Pneumatic
EL	Electric
Susp	Suspension
Hyd	Hydraulic
avg	Average

Prop	Propulsion
CS	Charging Station
D	Electric Power Demand Period
eu	Energy Usage
dc	Demand Charge
EL	End Life
PW	Present Worth
b	Bus Number
i	Charging Station Number / Stage Number
w	Charger Number

Abbreviations

GHG	Green House Gas
GDP	Gross Domestic Product
CNG	Compressed Natural Gas
ICE	Internal Combustion Engine
DB	Diesel Bus
EM	Electric Machine
HEB	Hybrid Electric Bus
FCEB	Fuel Cell Electric Bus
BEB	Battery Electric Bus
FD	Final Drive
WTW	Well to Wheel
WTT	Well to Tank
TTW	Tank to Wheel
TCO	Total Cost of Ownership
Ser	Series
Par	Parallel
DR	Driving Range
PV	Passenger Vehicle
HVAC	Heating, Ventilating and Air Conditioning
HP	Heat Pump

ACS	Air Circulation System
BTMS	Battery Thermal Management System
PI	Punctuality Index
RG	Reduction Gear
MG	Motor-Generator
TCS	Torque Control Strategy
AC	Alternating Current / Air Conditioner
DC	Direct Current
EV	Electric Vehicle
SOFC	Solid Oxide Fuel Cell
BNEF	Bloomberg New Energy Finance
SOC	State of Charge
PCM	Phase Change Material
RWD	Rear Wheel Drive
BER	Brake Energy Recovery
PID	Proportional Integral Derivative
APTA	American Public Transportation Association
VCC	Vapor Compression Cycle
ERV	Energy Recovery Ventilator
GWP	Global Warming Potential
ODP	Ozone Depletion Potential
LMTD	Logarithmic Mean Temperature Difference
COP	Coefficient of Performance
SAE	Society of Automobile Engineers
XFC	Extremely Fast Chargers
BSS	Battery swapping system
ESS	Energy Storage System
BRC	Battery Replacement Cost
ONC	Overnight Charging
DDC	Depot Day Charging
ELC	End-Line Charging
OC	Opportunity Charging

DOD	Depth of Discharge
GA	Genetic Algorithm
DP	Dynamic Programming
SOE	State of Energy

Operators

$\frac{\partial}{\partial}$	Partial Derivative
Δ	Difference
$\frac{d}{d}$	Derivative

Scripts

$\mathcal{B}$	Set of Buses
$\mathcal{X}_B$	Vector of Buses Location
$\mathcal{V}$	Vector of Buses Speed
$\mathcal{N}^B$	Vector of Buses Passenger Occupancy
$\mathcal{P}_B$	Vector of Buses Charging Power Demand
$\mathcal{S}^r$	Set of Stop Stations in Direction r
$\mathcal{X}^{S^r}$	Vector of Stop Stations Location in Direction r
$\mathcal{N}^{S^r}$	Vector of Stop Stations Passenger Occupancy in Direction r
$\mathcal{P}^{S^r}$	Vector of Stop Stations Charging Power Demand in Direction r
$\mathcal{E}$	Vector of Chargers' Charging Efficiency
$\mathbb{T}$	Schedule: Vector of Bus Trip Departure Time
$\mathbb{C}$	Vector of Charging Stations
$\mathbb{D}$	Set of Electric Power Demand Period
Θ	Set of Chargers

This page is intentionally left blank

Chapter 1
INTRODUCTION

1.1 Background

Many initiatives are being implemented worldwide to decrease the Green House Gas (GHG) emissions and local pollutants. Even with the several efforts to introduce regulations and standards in order to decrease these emissions, it remains challenging to achieve the emissions' targets set by the different protocols and agreements such as the United Nations Framework Convention on Climate Change (1992), Kyoto Protocol (2005) and Paris Climate Accord (2016) [1]–[3]. The annual CO_2 global emissions are witnessing a continuous increase since 2008 (global economic recession) increasing by 1.3% in 2016 as shown in Figure 1.1 [4] where most of this increase is resulted from developing economies, such as China and Asian-Pacific regions.

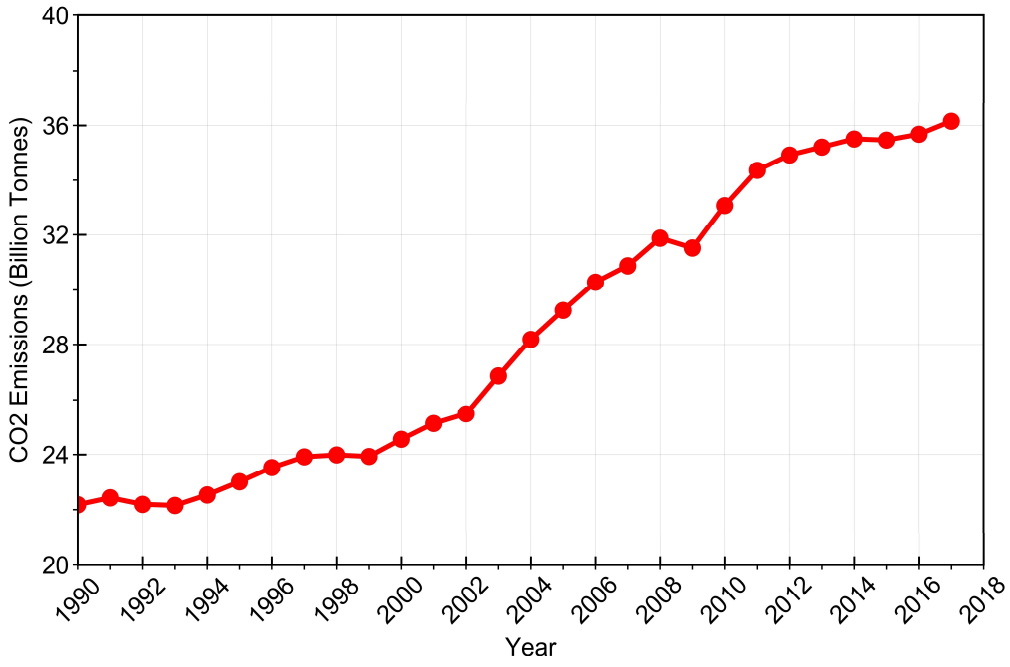


Figure 1.1: Annual global CO2 emissions until 2017 [7]

The transport sector contribution to global GHG emissions is around 23%, which is only second to the electricity and heat production sector as shown in Figure 1.2. Road transport, such as passenger vehicles and heavy-duty vehicles (trucks and buses), accounts for more than three-quarters of these emissions, whereas aviation and rail activities account for the rest. The transport sector CO_2 emissions are increasing at an annual rate of 1.6% in 2018 [5], the highest among all other sectors, mainly boosted by the increasing global gross domestic product (GDP), which increased road freight demand.

Emissions from buses and trucks are recording a continuous increase over the past 20 years at an annual rate of 2.2%, the highest segment within the transportation sector [5]. This trend is expected to be sustained despite all improvement in vehicle energy efficiency, mainly due to the increasing economic activity worldwide [6]. Although policies regarding heavy-duty vehicles still lag behind those concerned with passenger vehicles, such policies are gaining momentum, especially in the EU, China, and India. Cities such as Paris, Madrid, London, and Athens announced the ban of all diesel vehicles as of 2025 pushing towards alternative vehicle technologies.

Even though alternative technologies have been introduced and put in operation in the past years, oil-dependent mobility still holds the biggest share in the market due to the limited market penetration for new technologies [3]. The deployment of alternative technologies for road transport is highly dependent on several factors. Factors such as energy logistics, cost-benefits, infrastructure readiness, and public acceptance all affect the deployment of alternative technologies. However, public transport is less sensitive to these factors, especially in the context of transit buses. Public transport buses run on fixed routes, centralized starting and terminal locations, common infrastructure, and other factors that make the implementation of alternative technologies easier in public transport bus applications.

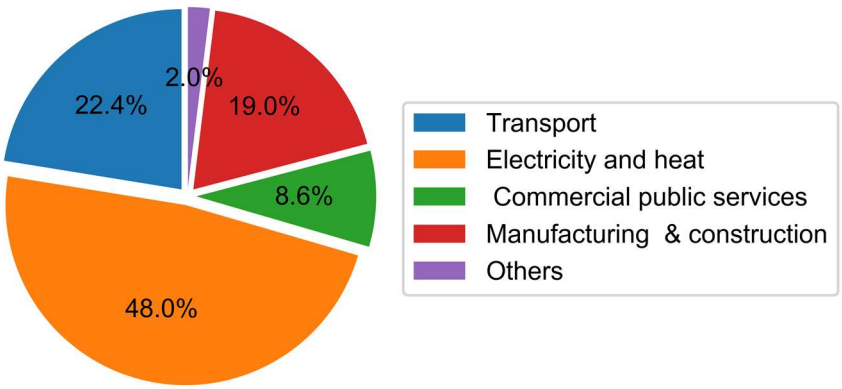


Figure 1.2: Global CO2 emissions by sector in 2018 [8]

1.2 Alternative Bus Technologies

Alternative bus technologies to the widely used Diesel Buses are mainly classified into 3 categories: (1) fossil fuel buses, (2) biofuel buses, and (3) electrified buses.

Alternative fossil fuel buses operate by burning compressed natural gas (CNG) using an internal combustion engine (ICE), similar to diesel buses (DB). CNG is mostly composed of Methane (CH_4) which is compressed at 250-350 bars in public transport bus applications. This technology is widely deployed worldwide mainly due to its environmental benefits and energy security of natural gas [9]. Another alternative fuel to fossil fuel buses consists of using biodiesel or ethanol in an ICE as well. The only major technological difference lies in the fuel storage system. The propulsion system configuration of CNG/biofuel buses is presented in Figure 1.3.

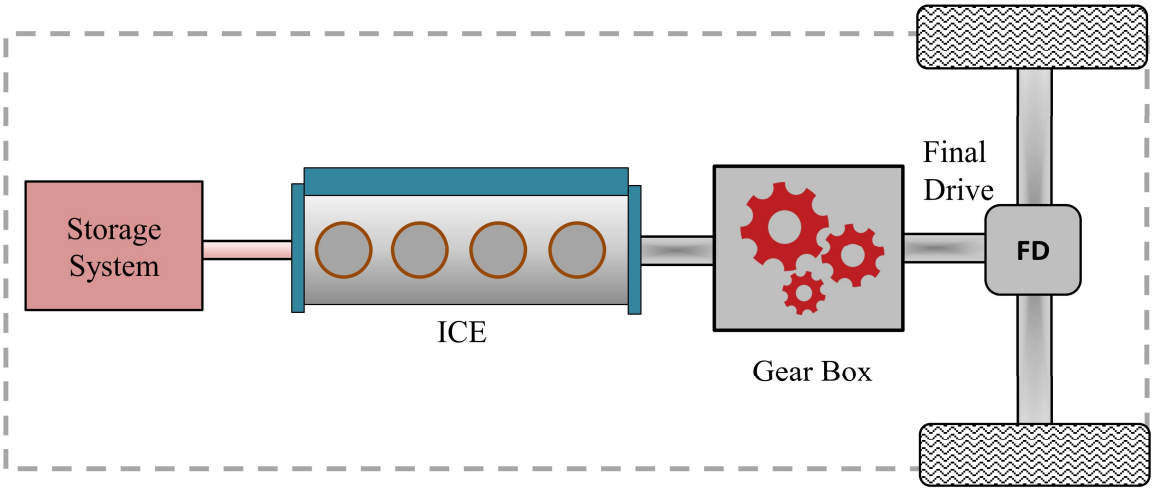


Figure 1.3: Propulsion system configuration of CNG and Biofuel bus technologies

Electrified buses are buses powered by electricity where an electric machine (EM) is used to propel the bus. There are several types of electrified buses depending on their propulsion system configuration. Electrified buses include Hybrid Electric Buses (HEB), Fuel Cell Electric Buses (FCEB), and Battery Electric Buses (BEB) [10]. HEB use both an ICE and one or more EMs in several architectures. The most common HEB architectures are series HEB and parallel HEB where the terms 'series' and 'parallel' describe the type of mechanical connection between the ICE and the EM [11]. FCEB use fossil fuels to generate electricity through an electrochemical process using fuel cells [12]. Hydrogen is the main fuel used in such technologies. Finally, BEB is a pure electric bus technology that is powered by the electric energy stored on-board in the battery pack [13]. Figure 1.4 shows the propulsion system configuration for the different electrified bus technologies.

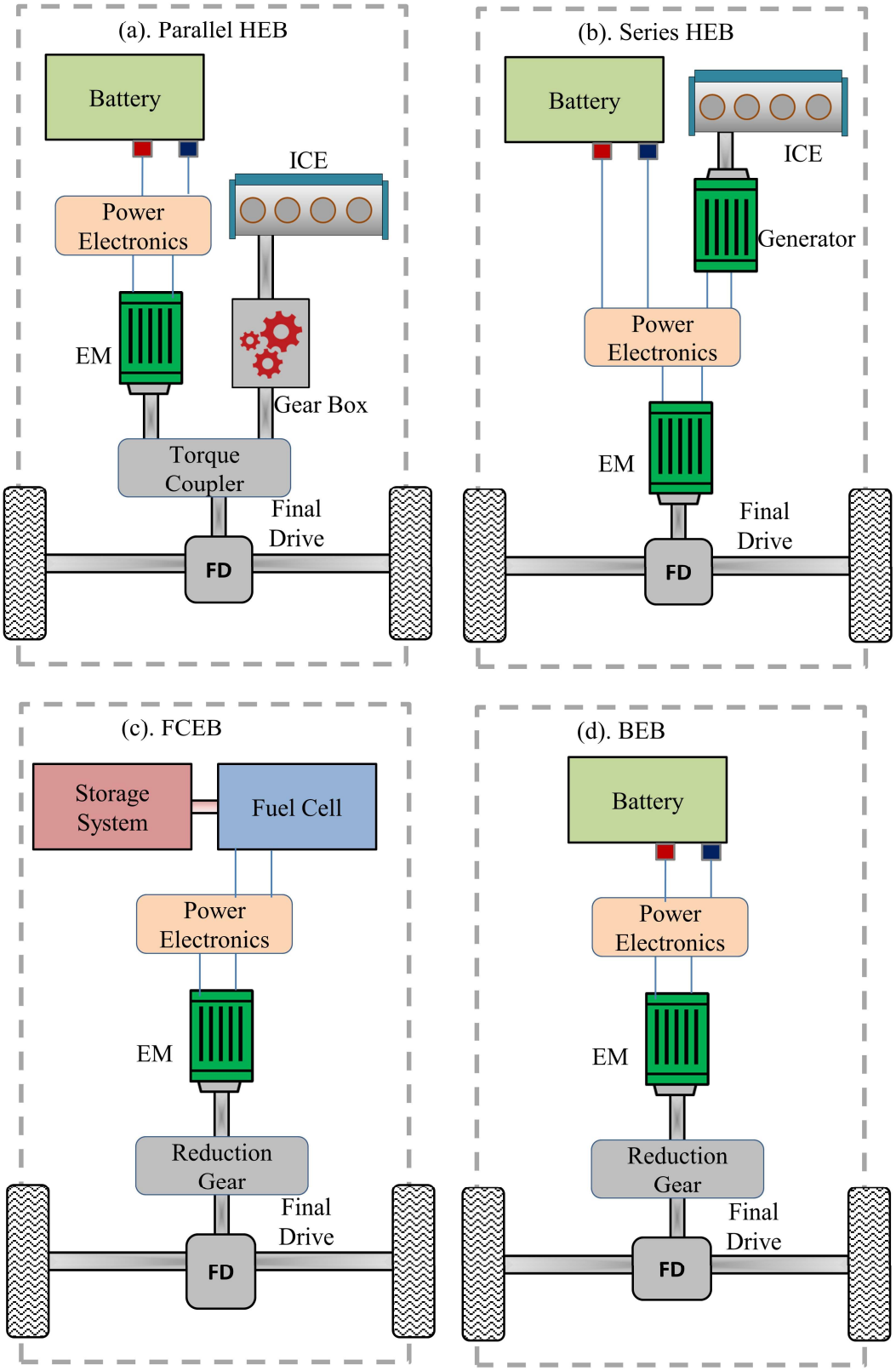


Figure 1.4: Propulsion system configurations of electrified bus technologies

1.3 Implications of Battery Electric Buses

BEB represent the most promising solution to replace current DB fleets due to their environmental advantages, however, this technology is still subject to many challenges. This section describes the benefits of BEB over DB and other alternative technologies, in addition to the challenges facing BEB and holding off their deployment at a massive scale.

1.3.1 Benefits of Battery Electric Buses

BEB have a great potential to reduce the total well-to-wheel (WTW) GHG emissions when compared to DB or other alternative technologies. Depending on the electricity generation energy mix, BEB can reduce the WTW - GHG emissions by 41 – 98 % compared to DB [1]. The WTW analysis considers the GHG emissions during the production and distribution phases of the energy source, referred to as Well-to-tank (WTT), and operation phases referred to as Tank-to-Wheel (TTW). These indices are measured in grams of equivalent CO_2 per driven km. BEB incur no tailpipe emissions and thus there are no TTW GHG emissions.

Figure 1.5 shows the WTT and TTW GHG emissions for different bus technologies, and the data labels represent the sum of the WTT and TTW GHG emissions, which corresponds to the WTW GHG emissions.

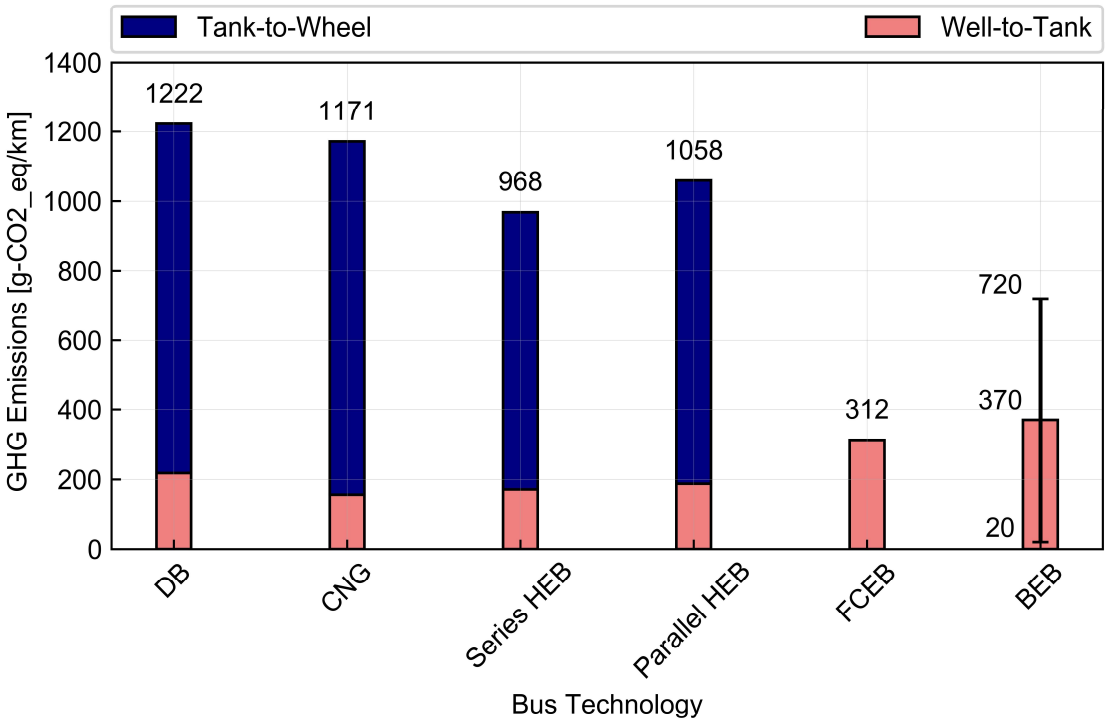


Figure 1.5: WTW, WTT, and TTW GHG emissions of different bus technologies [1], [14]–[17]

The minimum and maximum BEB GHG emissions are represented by an error bar considering the best- and worst-case scenarios of electricity generation energy mix as reported in [14]–[16]. The data collected are representative of BEB operating in Europe and the USA. BEB environmental performance is superior to all other alternative bus technologies regardless of the electricity generation energy mix except for FCEB. FCEB could achieve a 74% reduction in WTW GHG emissions when compared to DB. However, a clean electricity generation energy mix could achieve a 98% reduction in WTW GHG emissions for BEB.

BEB are also energy-efficient systems when compared to DB and other alternative bus technologies. The WTW energy consumption per driven km of BEB shows a significant reduction in energy consumption. Despite the relatively higher energy consumption during the electricity generation phase (WTT), BEB still attain a more efficient energy consumption due to their lower energy consumption during the operation phase (TTW), mainly thanks to their more efficient propulsion systems.

BEB reduction in WTW energy consumption ranges from 9.68 to 50% when compared to DB, depending on the electricity generation means as shown in Figure 1.6.

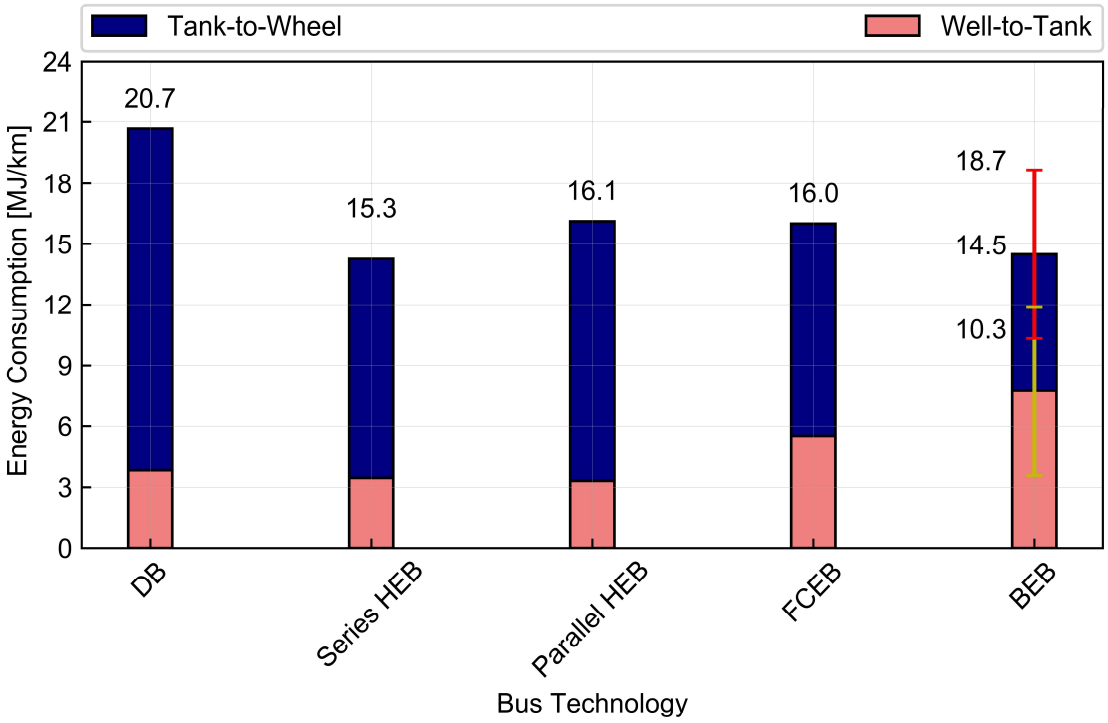


Figure 1.6: WTW, WTT and TTW energy consumption of different bus technologies [1], [14], [15], [18]

The data labels in Figure 1.6 represent the sum of the WTT and TTW energy consumption, which corresponds to the WTW energy consumption per driven km. The yellow error bar corresponds to the variation in the well-to-tank energy consumption as function of the electricity generation means and the red error bar represents the variation in the well-to-wheel energy consumption. BEB could achieve a higher energy efficiency when compared to alternative bus technologies, however, the energy efficiency could drastically deteriorate depending on the means of electricity generation. In addition, Appendix D presents a detailed analysis of the TTW energy consumption of BEB and DB.

1.3.2 Challenges of Battery Electric Buses

Despite their environmental and energy-efficiency benefits, BEB massive deployment is still subject to many challenges that hold off their market penetration.

BEB suffer poor economic performance when compared to DB. The economic performance of buses is presented by their total cost of ownership (TCO) which includes the unit cost, maintenance cost, running cost, and infrastructure cost. Figure 1.7 and Figure 1.8 introduce the unit cost and the TCO for the different bus technologies.

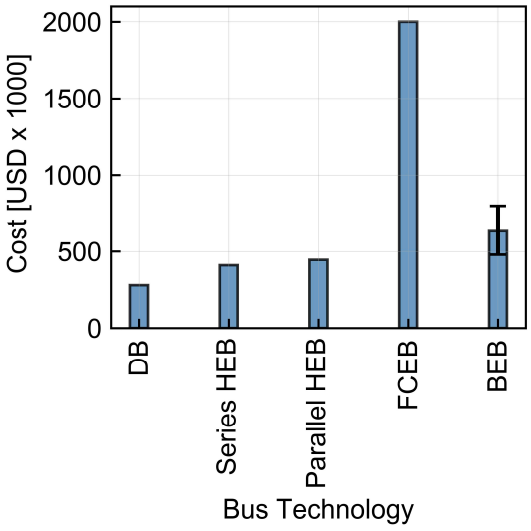


Figure 1.7: Bus unit cost by technology [1]

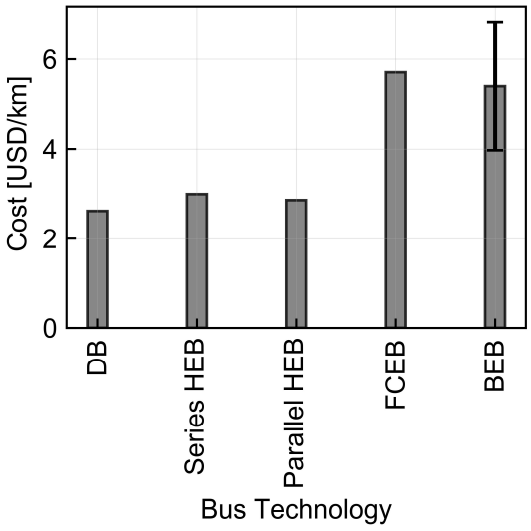


Figure 1.8: Bus TCO by technology[1] [19], [20], [29], [30], [21]–[28]

Except for FCEB, BEB unit price is higher than all other technologies, mainly due to the battery cost. The BEB unit cost is mainly driven by the size of its battery as BEB equipped with larger

[1] This figure is developed by studying the reported TCO by the different studies referenced in the figure caption. The average values of the TCO are shown in the figure per bus technology.

batteries incur a higher unit cost. BEB costs in Figure 1.7 are represented by error bars as they correspond to the minimum and maximum BEB unit costs in the market meanwhile depending on their battery sizes.

Moreover, even though BEB maintenance and running costs are way lower than all other bus technologies, they record the highest infrastructure costs, which increases their TCO significantly. BEB TCO ranges between 3.97 to 6.83 $/km depending on their battery sizes and infrastructure needs as shown in Figure 1.8. For instance, BEB with large battery capacities encounter higher unit cost but lower infrastructure costs, whereas BEB with smaller battery capacities encounter less unit cost but higher infrastructure costs due to the need for multiple fast-charging stations.

The operational features of BEB are another challenge facing this technology. Operational features include the bus driving range, refueling time, and infrastructure.

Driving range (DR) is the key barrier to BEB market penetration. DR is defined as the number of kilometers a bus can cover without the need for refueling. In BEB, DR is strongly related to the battery capacity, as battery packs with high energy capacity may help to reduce the range problem, however, this comes at the expense of additional bus costs. Figure 1.9 shows the DR for different bus technologies and highlights the BEB minimum and maximum DR depending on the battery size. BEB DR can reach up to 250 km for very large battery capacities, however, this comes at a very high unit price. Other bus technologies record a staggering 450 km DR, which is almost as twice as the BEB maximum DR in the meantime.

The energy refueling time is another challenge facing BEB. Refueling time is the time needed to refill the energy storage system in a bus. This feature is strongly coupled with DR of BEB as batteries with high energy capacity, effectively high DR, suffer a very long refueling time. On the contrary, batteries with a low energy capacity require a lower refueling time. Figure 1.10 shows the refueling time for different bus technologies. Most bus technologies require a refueling time between 5-10 mins, whereas a BEB may need up to 240 mins (BEB max) to fully refuel its energy storage system. BEB can be charged within 10 mins if equipped with a small battery size and with fast chargers.

The refueling infrastructure is a major operational aspect of BEB. Although other alternative bus technologies require some infrastructural modifications, BEB require major modifications in the current charging infrastructure as presented in Figure 1.11. First, there is a need to install charging stations to recharge the buses. Second, the impact of these charging stations on the

electric power grid might be major, and thus, grid modifications might be needed, especially in urban areas.

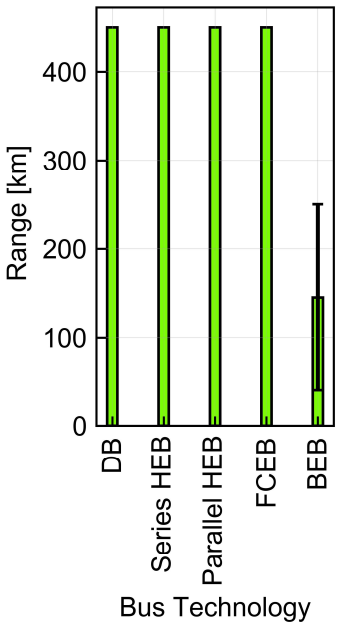


Figure 1.9: Bus driving range by technology [1]

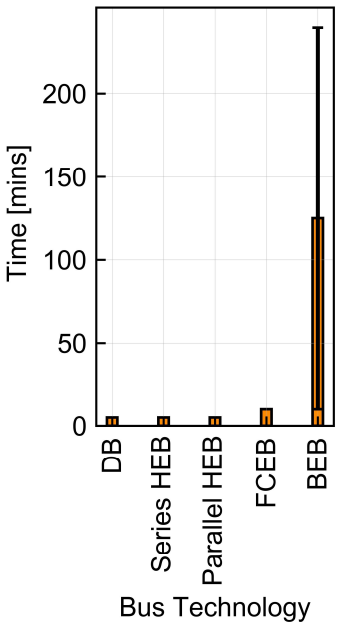


Figure 1.10: Bus refueling time by technology [1]

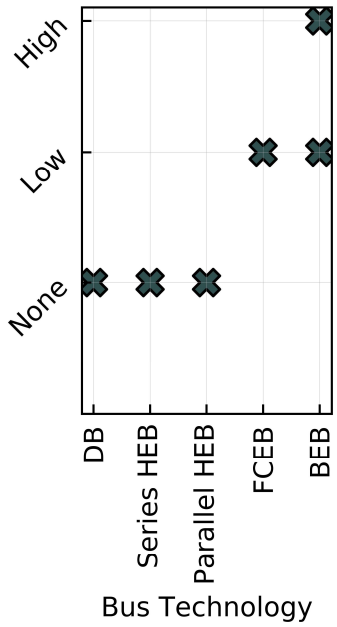


Figure 1.11: Required infrastructure modification by bus technology [1]

1.4 Key Players in the Deployment of BEB Fleet

The process of deployment of BEB is complicated and it concerns many key players. These players may have different objectives and constraints, and thus different approaches to deploying BEB at a massive scale.

These players can be narrowed into 3 categories:

1. BEB operators
2. Energy logistics (supplier, transmission, and distribution operators)
3. Regulatory authorities

Each player has its own role and concerns in the process of deployment of BEB.

Figure 1.12 presents a schematic of the BEB deployment showing the main sectors concerned in this process. Electricity generation, transmission and distribution processes are all included in the energy logistics category.

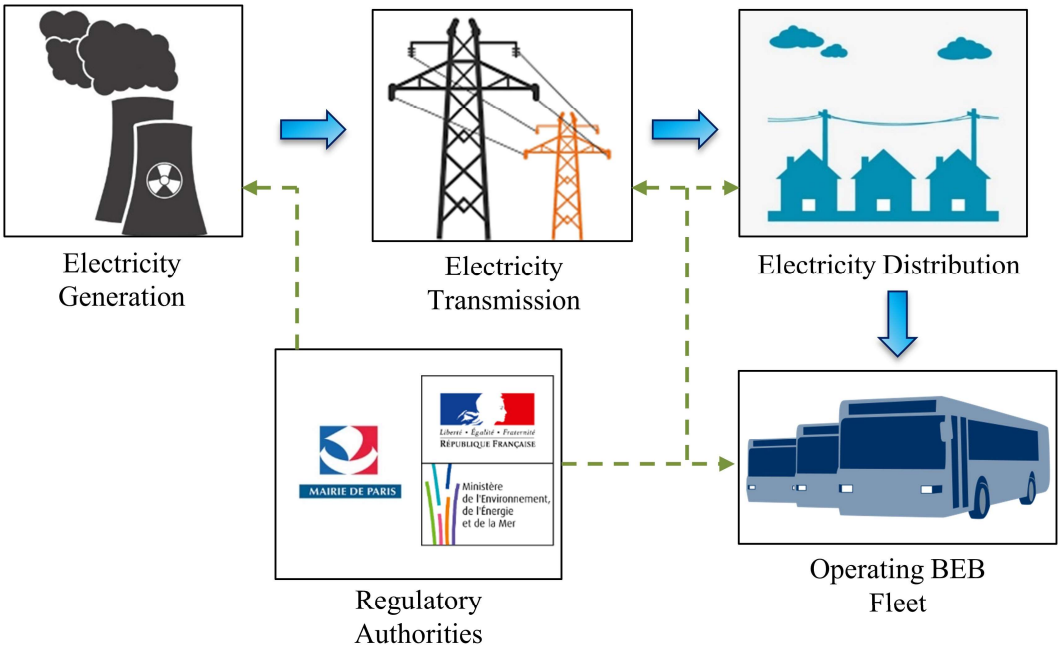


Figure 1.12: Scheme of BEB deployment

1.4.1 Operator

The operator of BEB is responsible for running the BEB fleet to meet passengers' transportation needs. With BEB deployment, the operator is supposed to replace the current oil-based bus fleet with BEB, while maintaining the same operation without any disruptions or disturbances in the BEB schedule. The deployment of BEB incurs additional costs for the operator, such as the BEB purchase costs and charging infrastructure costs, referred to as capital costs. In addition, the operator must deal with the fleet energy and maintenance costs, referred to as operating costs. Therefore, the operator's main concern is to minimize these costs while maintaining undisrupted bus fleet operation and complying with local and national authorities' requirements and regulations.

1.4.2 Energy Logistics (Supplier, Transmission and Distribution operators)

With BEB deployment, the electricity demand will increase which may impact the electricity market. The electricity sector could be summarized into 3 main processes: (1) electricity generation/supply, (2) electricity transmission, and (3) electricity distribution. The massive deployment of BEB could increase electricity power demand forcing a higher supply of electricity that may affect electricity suppliers, as new electricity generation power plants might be needed, mainly if the bus charging is carried out during peak hours. In addition, BEB

deployment will increase the power demand especially if charging takes place during peak hours and/or using super-fast chargers, which may incur infrastructural modifications in the power transmission and distribution grids at very high costs. Therefore, the energy supplier, transmitter and distributer concerns are to minimize the additional costs of electricity generation and power grid infrastructural modifications to cope with the additional electric power demand resulting from BEB charging.

1.4.3 Regulatory Authorities

Regulatory authorities include policymakers that enforce environmental regulations. Such authorities include governments or ministries and municipalities. The main role of these authorities is to reduce the total environmental impact of public transport buses through cost-effective solutions. Although BEB are zero-emission technology, their energy needs are met by generating electricity from different energy sources, and each energy source has a different impact on the environment. On the other hand, regulatory authorities are concerned about cost-effective solutions to deploy BEB, as they mainly finance such projects.

The mentioned key players in BEB deployment have different objectives and concerns regarding BEB deployment. BEB operator's main objective is to minimize the total operating and capital cost (charging infrastructure and bus unit cost) of BEB while maintaining smooth operation without schedule disruptions or service interruptions. On the other hand, electric energy suppliers, power transmitters and distributors are mainly concerned about the additional electricity generation cost and electric grid infrastructure modifications that may result from deploying BEB at a massive scale. Moreover, regulatory authorities' main objective is to maximize the environmental benefits of BEB through cost-effective solutions.

In this thesis, the main purpose is to study BEB deployment from the bus operator's point of view by minimizing the total cost of deployment of BEB encountered by the operator, while ensuring smooth fleet operation without schedule disruption or service interruption. This thesis also presents valuable insights for the other key players, especially those concerned with energy logistics, as it provides insights on the impact of BEB deployment on the electrical grid.

1.5 The Current State of Deployment of BEB

This section presents the current state of BEB market and then highlights the main challenges facing BEB operators.

1.5.1 BEB Market

BEB market has been witnessing a dynamic development in the past years. More than 460,000 vehicles were on the world's roads in 2018, which is almost 100,000 more compared to 2017 [31]. This increase is expected to be sustained as more countries are pushing towards bus fleet electrification amid the numerous environmental policies to cut GHG emissions and improve the air quality in urban areas. Figure 1.13 shows the global sales of electrified buses since 2016, classified according to their propulsion system configuration, and it introduces a projection on the electrified bus market until 2026. Since 2016, BEB and Plug-in HEB represent more than 90% of electrified bus sales, followed by HEB at 9%, and FCEB with less than 1% market share. This trend will be sustained until 2026 according to Guidehouse Insights study [32] with almost 120,000 new BEB will be introduced to the market annually, recording the fastest growth among all other electrified bus technologies. Unlike BEB, HEB and FCEB will continue to grow steadily and slowly until 2026 when their sales fall in favor of BEB.

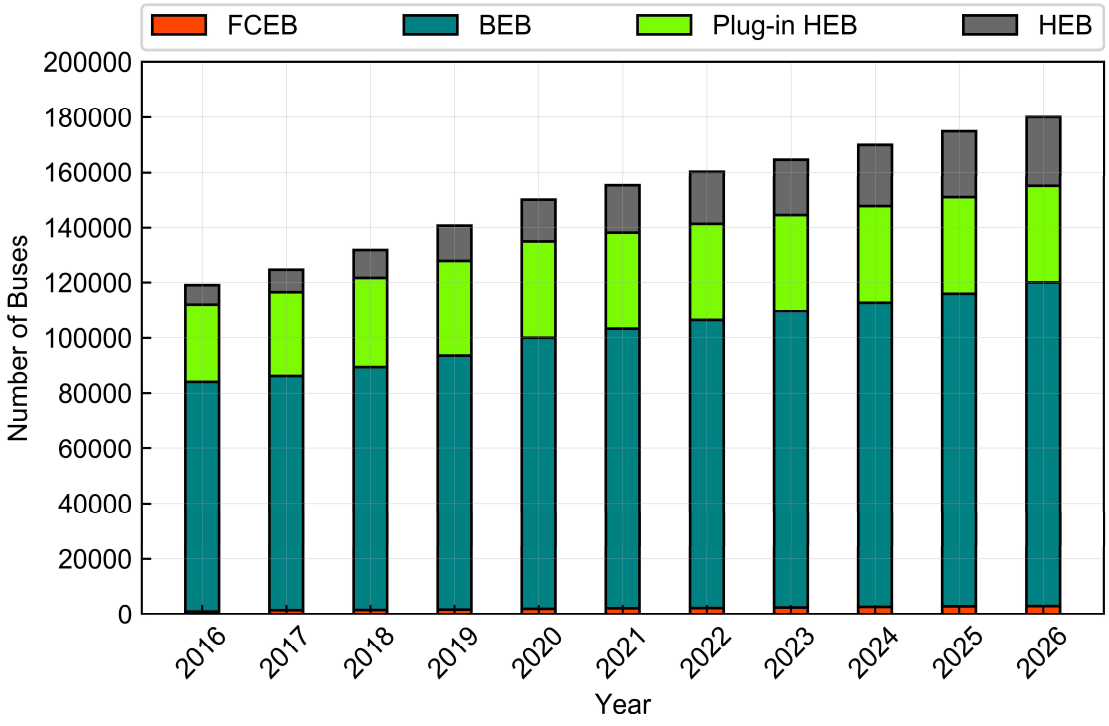


Figure 1.13: Global electrified buses sales by type of propulsion systems [32]

Zooming at the European market, studies reveal that more than 50% of the urban bus market share in Europe will be battery-electric by 2030, according to the ZeEUS project, which is concerned with BEB deployment in Europe [33], [34]. Several BEB deployment projects are studied within ZeEUS to review all operating BEB fleets in European countries in order to build

on such projects and assist in BEB deployment by providing technical and strategy-based solutions to help overcome BEB challenges. As shown in Figure 1.14, the transition to a cleaner urban bus fleet in Europe by 2030 will take place gradually as the market share of DB will drop from 53% in 2020 down to 31% in 2025 with BEB being the main alternative bus technology replacing DB. By 2030, only 10% of the urban bus market share in Europe will be oil-dependent. It is noteworthy to mention that FCEB market share will not exceed 10% by 2030 recording a slow growth whereas CNG and bio-diesel buses will record a slight decline in their market share in favor of BEB and HEB as well.

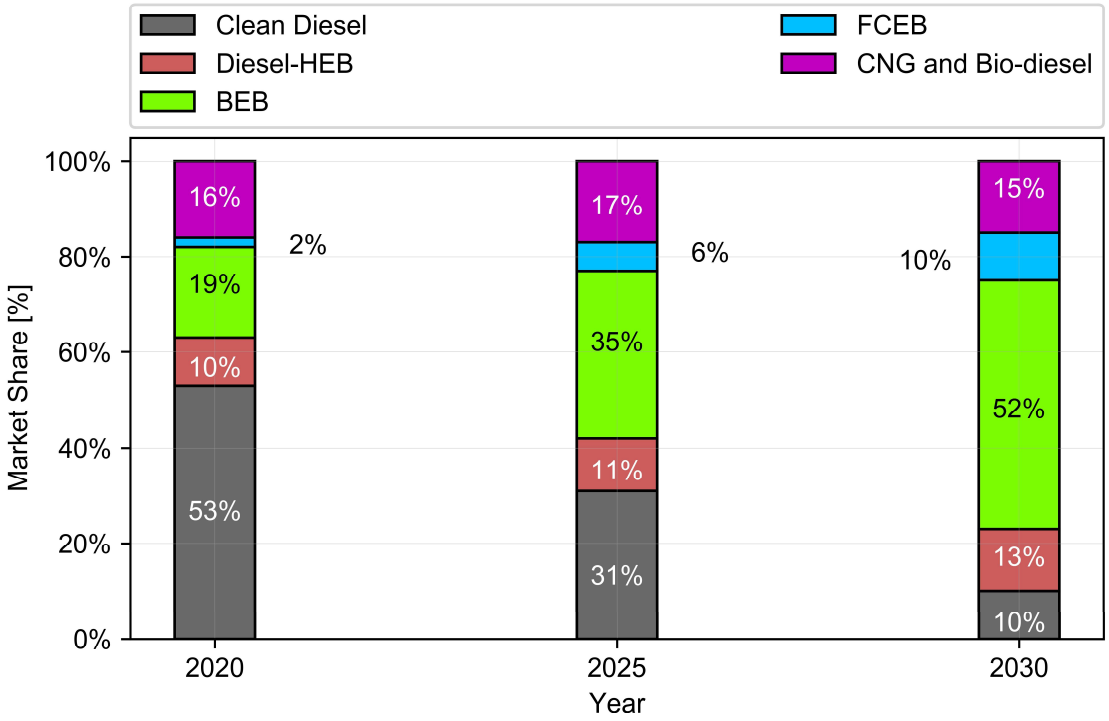


Figure 1.14: Forecast on the European urban bus market share [33]

France, Poland, the Netherlands, Sweden, and the United Kingdom are the main players in the European BEB market. In the past few years, many BEB trials were undertaken to study the feasibility of deploying BEB. For example, in the city of Paris, RATP (La Régie Autonome des Transports Parisiens) launched the first BEB line in Paris back in 2016. It was bus line 341 between Porte de Clignancourt and Charles de Gaulle Etoile. Afterward, RATP announced that by 2025, 80% of the Parisian bus fleet will be electric, which is almost 4000 new BEB. To achieve this goal, RATP ordered 800 electric buses in 2019 from three bus manufacturers: Bolloré, Alstom, and Heuliez. Until 2025, the French urban bus market will grow by 1000 BEB annually [35] to reach the energy transition goals set by national authorities.

1.5.2 Challenges of BEB Operators

BEB operators face many challenges when it comes to BEB deployment. The operator's main concern is to ensure that the bus fleet is operating without any schedule disruptions to meet passengers' transport needs and at minimal costs. From the operator's point of view, BEB challenges can be synthesized in three main points: (1) range anxiety, (2) the know-how of operation, and (3) readiness of the electric power grid.

1.5.2.1 Range Anxiety

Range anxiety is a term used to reflect on the concerns regarding the driving range (DR) of BEB. BEB DR is the major challenge facing the operator due to the limited energy capacity of the on-board energy source, and the relatively long energy refueling time. Several approaches have been considered to overcome the range anxiety problem of BEB. For example, BEB are being equipped with oversized batteries at a very high energy capacity to prolong the BEB DR. This increases the battery costs, adding more cost to the already-expensive technology, not to mention the reduction in the bus ridership capacity with such batteries. Charging mainly takes place during the night when the BEB is out of service and at low power.

Another approach to overcome the BEB DR problem is to reduce the battery energy capacity and charge the BEB frequently during the day. This reduces the battery cost but incurs high infrastructure costs due to the need for multiple charging stations. For both approaches, there is a clear trade-off between BEB deployment costs and DR depending on the choice of the battery energy capacity.

1.5.2.2 The Know-How of Operation

Operating a fleet of BEB is way more complicated when compared to the DB fleet, mainly due to the energy refueling process, or in other words, the charging of BEB. BEB charging strategy is critical to ensure a smooth operation of the BEB fleet. There are 2 main concerns regarding the operation of a BEB fleet: (1) schedule disruptions and (2) service interruption. Schedule disruption is the BEB failure to stay punctual to its daily schedule mainly due to delays related to its charging, whereas service interruption is the BEB failure to complete its trip due to lack of energy on-board.

The choice of the charging strategy directly drives the needed charging technology, corresponding costs, and operation of the BEB fleet. For example, adopting an overnight charging strategy will require the buses to be charged only at night using slow chargers. Such charging technology mainly incurs low infrastructure and operating costs; however, the risk of

service interruption is high as it is not possible to charge the BEB during the day. On the contrary, adopting a strategy based on frequent day-charging will require the BEB to be charged at high power rates utilizing super-fast chargers. Such chargers are expensive incurring high infrastructure and operating costs. Although a frequent day-charging strategy reduces the risk of service interruption, schedule disruption is highly probable with such a charging strategy due to the possible delays that may result from the frequent charging events.

Each charging strategy encounters different capital and operating costs and affects the operation of the BEB fleet differently. Therefore, the choice of the charging strategy directly drives the costs of deployment of BEB and the corresponding needed charging technology.

1.5.2.3 The Readiness of the Electric Power Grid

Deployment of BEB at a massive scale raises questions about the readiness of the electric power grid to host such high additional power demand. Even though BEB will represent a minor portion of the total electric vehicle fleet, which includes passenger vehicles (PV), BEB larger batteries compared to PV batteries make BEB charging power demand considerable. In addition, buses, in general, cover more kilometers per day when compared to PV, which effectively means a higher daily energy consumption yielding to a more frequent charging. That being said, the impact of BEB on the electric power grid cannot be ignored. Although the operator does not have any control over the electric power grid and it is the electricity distributor problem in the first place, yet it remains a concern for the BEB operator as it may impose additional constraints. Such constraints may affect the operator's choice of the charging strategies and technologies impacting the TCO of BEB deployment.

1.6 Problem Statement

Initiatives to decrease emissions from the transport sector are increasing worldwide by seeking alternative technologies to replace oil-based mobility. BEB present a promising solution to replace the current oil-based bus fleets and eliminate their environmental burden thanks to their higher energy efficiency and lower GHG emissions. However, this technology still faces many challenges, especially its high TCO and other operational factors such as the limited bus DR, energy refueling time, and costly infrastructure. Different key players interfere in BEB deployment including bus operators, energy suppliers, and public authorities. Each player has its own objectives and constraints for BEB deployment, and these objectives have to be considered.

BEB range anxiety and the know-how of operation are the main challenges facing bus operators to ensure a smooth BEB fleet operation without schedule disruptions or service interruption in order to meet passengers' transportation needs and at minimal costs. Currently, there are 2 main approaches considered in BEB deployment. First, designing BEB with very high energy capacity batteries accompanied with slow overnight charging and second, designing BEB with smaller batteries accompanied with frequent charging during the day at very high-power rates. The first approach results in very high batteries costs and incurs a high probability of service interruption while the second approach leads to very high infrastructural and operating costs and is more likely to result in schedule disruptions.

Therefore, there is a need to introduce a methodology capable of providing optimal battery sizing and charging strategy for BEB to minimize the total cost of ownership of BEB deployment, while ensuring no schedule disruption or service interruption during operation.

1.7 Research Approach

The choice of the battery size and the adopted charging strategies drive the total cost of ownership of BEB deployment and affect their operation. Oversizing the batteries and adopting an overnight charging strategy increase the battery acquisition cost, which increases the TCO, but incurs low risk of schedule disruption. However, the BEB are at a higher risk of service interruption as it is not possible to charge during the day. On the other hand, reducing the battery size and adopting a frequent charging strategy during the day requires a large number of chargers to be installed and at high power, which increases the infrastructure costs. In this case, the BEB are at a lower risk of service interruption as it is always possible to charge during the day, however, the BEB are prone to schedule disruption due to delays during charging.

This thesis presents a methodology for optimal battery sizing and charging strategies for BEB to minimize their TCO while respecting the BEB schedule and operation constraints.

Thus, this thesis answers the following main research question: How to minimize the total cost of deployment of battery electric buses in order to ease their market penetration and take maximum advantage of their environmental benefits?

In order to systematically answer this question, a set of sub-questions are identified and addressed in this thesis:

1. What are the different energy systems used in a BEB and how to evaluate their energy consumption and the total BEB energy consumption?
2. How does the energy consumption of a BEB change at different operating conditions and what are the main factors showing a significant impact on its energy consumption?
3. What is a proper battery sizing for a BEB considering the energy needs as function of the various operating conditions?
4. How to evaluate the TCO and operation of BEB fleets and how are they impacted by battery sizing and charging strategy?
5. What is the optimal battery sizing and charging strategy of BEB fleet minimizing the TCO of BEB deployment while respecting schedule and punctuality constraints?

Each chapter of this thesis answers one or more research questions as shown below.

For this sake, the following work plan is developed in order to answer the mentioned research questions as shown in Table 1.1.

Table 1.1: Thesis work plan

1. Identify BEB components technology and energy systems onboard	Chapter 2
2. Develop a comprehensive BEB energy model	
3. Validate the proposed bus model	
4. Analyze and quantify the energy consumption for each energy system of the BEB at varying operating conditions	Chapter 3
5. Deduce the required minimum bus battery size as function of the varying operating conditions	
6. Develop a techno-economic model for BEB lines	Chapter 4
7. Analyze the impact of battery size and charging strategy on BEB TCO and operation	
8. Develop a methodology to minimize BEB TCO	Chapter 5
9. Apply the proposed methodology through a real-life case-study in Paris city	
10. Introduce the related future work that would improve or complete this research	Chapter 6

- In order to evaluate the global energy consumption of BEB, a comprehensive battery-electric bus energy model is developed in Chapter 2. The bus configuration is thoroughly presented first highlighting the different energy systems encountered in a BEB and explaining the state-of-the-art technologies used in BEB. The proposed model considers these energy systems as they significantly impact the bus energy performance. Four main energy systems are identified in a BEB: (1) battery (2) propulsion system, (3) Heating, Ventilating and Air Conditioning System (HVAC), and (4) auxiliaries.

1. The battery model is a coupled electro-thermal model that captures both the electric and thermal behaviors of the cells within the battery pack.
2. The propulsion system is modeled considering its main components (electric machine, transmission, and braking system) and their corresponding control units.
3. The HVAC unit is composed of 3 main sub-systems: (1) reversible heat pump (HP), (2) air circulation system (ACS), and (3) battery thermal management system (BTMS).
4. The auxiliaries are essential features for the BEB operation, and they consume a considerable amount of energy. These auxiliaries are classified into 3 main categories: (1) pneumatic auxiliaries (braking system), (2) hydraulic auxiliaries (steering pump and suspension system), and (3) electric auxiliaries (doors, lighting, parking brakes, and wipers).

All these energy systems are coupled together in order to assess the global energy consumption of the BEB. Each energy system model is validated against similar experimental studies in the literature at a variety of simulation conditions. The validation results show that the proposed model can precisely predict the energy consumption of the BEB within a +/- 5% error margin.

The originality of this chapter is reflected in the proposed comprehensive methodology to model the bus energy performance considering all its energy systems as they significantly impact its energy consumption. In addition, the proposed model presents a tool that can help in assessing the required bus battery size by precisely assessing the BEB energy needs.

Finally, the BEB energy model developed in Chapter 2 allows the assessment of the bus energy consumption at any operating condition. This helps to understand how the energy consumption of a BEB, and each energy system within, varies as function of the different encountered operating conditions as will be shown in Chapter 3.

- After modeling and validating the different energy systems encountered in a BEB, the BEB energy consumption is evaluated. BEB energy consumption is subject to high variations

due to the different operating conditions it encounters during its operation. These operating conditions are driving conditions, weather conditions, and passengers' occupancy inside the BEB. The precise assessment of BEB energy consumption is critical as it directly drives the needed battery size and the corresponding charging strategy.

In Chapter 3, the proposed BEB energy model is simulated at a variety of operating conditions to analyze the energy performance of each system in the BEB, and the total BEB energy consumption as well. The analysis reveals how the BEB energy consumption drastically increases under extreme hot and cold weather conditions and extreme driving conditions with high levels of traffic congestion and low average speed.

This energy analysis opens a door on the required battery sizing for any BEB by simply identifying its operating conditions and assessing its energy consumption. A preliminary battery sizing framework is then introduced in this chapter where the bus required battery size can be estimated as function of its energy consumption and operating conditions. The required bus battery size shows a very sensitive behavior to the variations in weather conditions, especially in extremely cold climates, as the bus heating needs increase drastically.

At the end of this chapter, a variety of recommendations and technical solutions that may reduce the battery size are presented.

The originality of this chapter is that it provides a detailed energy assessment on the impact of driving and weather conditions, and passengers occupancy on the BEB energy consumption and therefore, the minimum required battery size.

The chapter concludes that an adequate charging strategy could significantly reduce the BEB battery size, and thus reducing the total BEB costs without affecting the BEB schedule or operation. However, the BEB charging strategy is highly affected by the bus schedule, the number of buses operating along the same route, and the bus energy consumption as function of its operating conditions. Therefore, a complete bus line model is needed to better analyze the interactions between the bus battery size and charging strategies and their impact on BEB total costs and operation. This will be presented in Chapter 4.

- BEB battery sizing and charging strategy are directly driven by the BEB operating conditions. In addition to the driving conditions, weather conditions, and passengers' load, the BEB schedule has a significant influence on the required charging strategies as it imposes constraints regarding the BEB operation. In order to assess the interactions among the battery sizing, charging strategy, and BEB operating conditions, a techno-economic model for the BEB line is developed in Chapter 4.

Chapter 4 starts with an introduction about the state-of-the-art BEB lines worldwide regarding their battery sizing and charging strategies. The complete scheme of BEB charging is then presented explaining the different charging infrastructure, technologies, and systems, while qualitatively highlighting the trade-offs between BEB costs and operation as function of the battery size and charging strategy. Then, a BEB line techno-economic model is presented and it is composed of three parts:

1. A BEB line energy model developed in real-time considering the following components: BEBs, chargers, stop stations along the line, terminal stations at both ends of the line, and a depot. The energy interactions among the different BEB line components are presented using 2 types of interactions: (1) passengers' flow and (2) electric power flow.
2. A detailed total cost of ownership (TCO) model for BEB deployment is presented in this chapter. The model considers the BEB unit costs, battery purchase and replacement costs, energy and power costs, infrastructure, and maintenance costs.
3. An approach to assess BEB operation is presented by evaluating a punctuality index (PI) that reflects on BEB departure delays to their schedule, resulting from daily charging events.

Then, a case study representative of bus line number 21 in Paris city is introduced utilizing the proposed models. The presented results quantitatively show the trade-off between BEB operation (PI) and TCO at different battery sizes and charging strategies. Notably, the impact of battery sizing, charging power, and charging infrastructure on the BEB schedule disruption and TCO are thoroughly evaluated.

The proposed techno-economic model of BEB lines in this chapter allows the assessment of the total cost of ownership (TCO) of BEB deployment and the operation of the BEB at any combination of battery sizes and charging strategies, and this is the novelty of this chapter as up to the author's knowledge, no study up to this date, presents a detailed techno-economic model of BEB lines capable of evaluating the BEB techno-economic performance.

The results of the case study show that different combinations of battery sizes and charging strategies result in different tradeoffs between the TCO and operation of BEB lines. Thus, there is a need to provide a systematic methodology to optimally size the batteries and charge the BEB in order to minimize the TCO of BEB deployment while respecting operation constraints. This is introduced in chapter 5.

- The proposed methodology is a 2-step optimization algorithm that utilizes both Dynamic programming and Genetic Algorithm optimization routines as will be shown in

Chapter 5. The optimization problem controls most of the variables that affect the TCO of BEB deployment including the size of the battery pack and the charging strategy. The charging strategy includes the BEBs charging energy and power profiles during the day, and the chargers' location and maximum power rate.

The methodology is applied to a case study representing bus line number 21 in Paris city. The reduction in BEB TCO is significant as it ranges between 15-20% when compared to the currently considered approaches regarding battery sizing and charging strategy of BEB.

The proposed methodology in this chapter is original and novel in many ways:

1. It is the only optimization-based methodology that minimizes the TCO of BEB deployment considering a comprehensive cost function while respecting the schedule constraints, in comparison to other heuristic approaches in the literature that can't achieve the maximum potential of minimizing the TCO of BEB deployment.
2. It is a generalizable methodology that can be applied to any charging infrastructure and any BEB line.
3. The methodology optimizes most of the variables that impact the cost and operation of BEB deployment from the bus operator point of view.

Further analysis is conducted in this chapter where the impact of the different battery sizing and charging strategies on the electric power demand is evaluated. Also, a sensitivity analysis is introduced to study the behavior of the TCO and optimal battery size and charging strategy relative to variations in the different TCO parameters.

Finally, Figure 1.15 illustrates a framework summarizing the proposed research approach considered in this thesis.

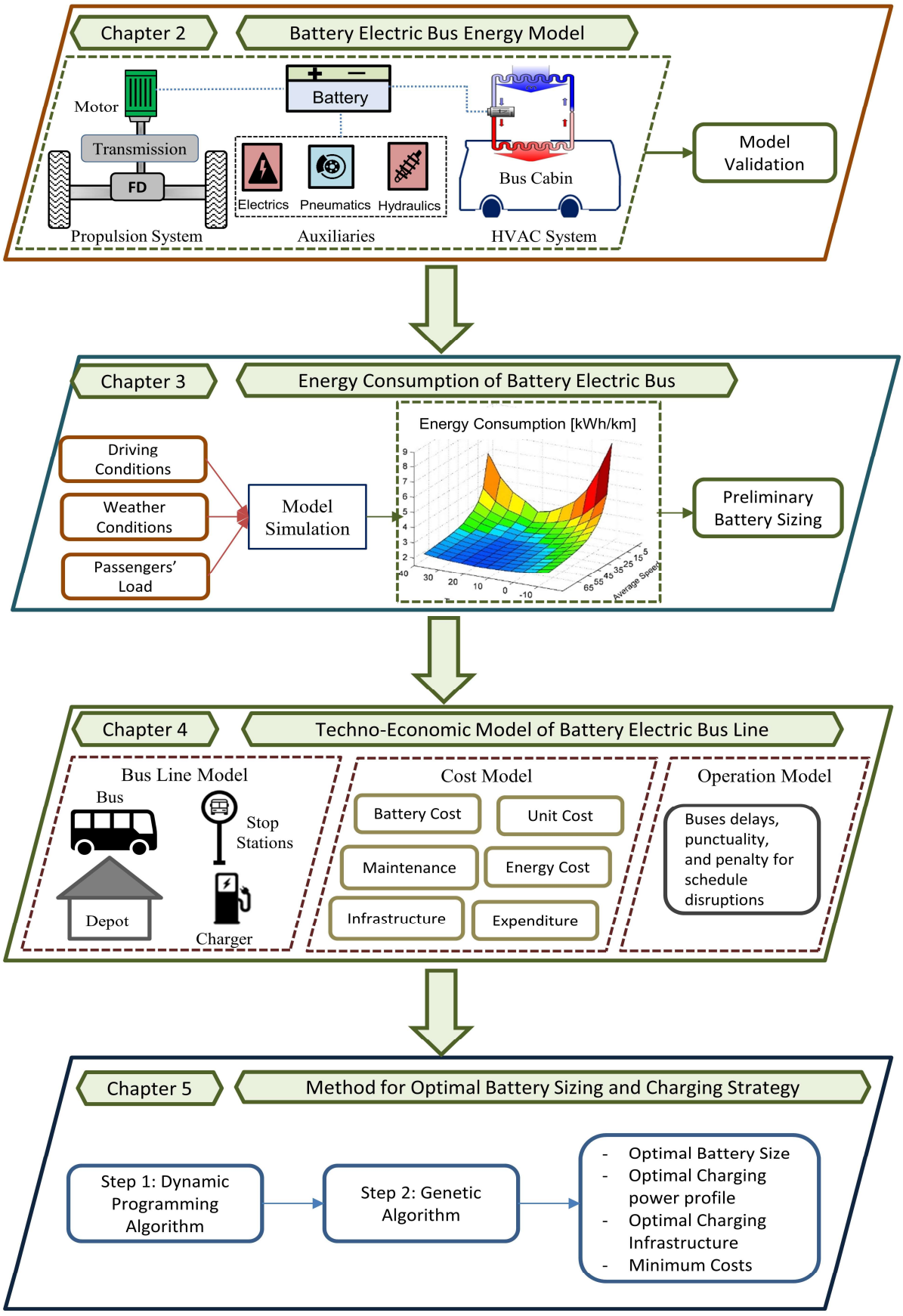


Figure 1.15: Research approach framework

1.8 References

[1] M. Mahmoud, R. Garnett, M. Ferguson, and P. Kanaroglou, "Electric buses: A review of alternative powertrains," *Renew. Sustain. Energy Rev.*, vol. 62, pp. 673–684, 2016, doi: 10.1016/j.rser.2016.05.019.

[2] J. Miles and S. Potter, "Research in Transportation Economics Developing a viable electric bus service : The Milton Keynes demonstration project," *Res. Transp. Econ.*, vol. 48, pp. 357–363, 2014, doi: 10.1016/j.retrec.2014.09.063.

[3] D. Beeton and G. Meyer, *Electric Vehicle Business Models*. 2015.

[4] C. Le Quéré *et al.*, "Global Carbon Budget 2018," *Earth Syst. Sci. Data Discuss.*, vol. pre print, no. November, pp. 1–54, 2018, doi: 10.5194/essd-2017-123.

[5] IEA, "Tracking Transport," Paris, 2019. [Online]. Available: https://www.iea.org/reports/tracking-transport-2019.

[6] "Transport emissions | Climate Action." https://ec.europa.eu/clima/policies/transport_en (accessed May 11, 2020).

[7] "CO_2 and Greenhouse Gas Emissions - Our World in Data." https://ourworldindata.org/co2-and-other-greenhouse-gas-emissions (accessed May 11, 2020).

[8] Global Alliance for Buildings and Construction, "2018 Global Status Report," 2018. doi: https://doi.org/10.1038/s41370-017-0014-9.

[9] T. L. F. Brito, E. Moutinho dos Santos, R. Galbieri, and H. K. de M. Costa, "Qualitative Comparative Analysis of cities that introduced compressed natural gas to their urban bus fleet," *Renew. Sustain. Energy Rev.*, vol. 71, no. December, pp. 502–508, 2017, doi: 10.1016/j.rser.2016.12.077.

[10] J. Ying, V. K. Ramachandaramurthy, K. Miao, and N. Mithulananthan, "A review on the state-of-the-art technologies of electric vehicle , its impacts and prospects," *Renew. Sustain. Energy Rev.*, vol. 49, pp. 365–385, 2015, doi: 10.1016/j.rser.2015.04.130.

[11] M. A. Gözüküçük and A. Teke, "A comprehensive overview of hybrid electric vehicle : Powertrain configurations , powertrain control techniques and electronic control units," vol. 52, pp. 1305–1313, 2011, doi: 10.1016/j.enconman.2010.09.028.

[12] G. J. Offer, D. Howey, M. Contestabile, R. Clague, and N. P. Brandon, "Comparative analysis of battery electric , hydrogen fuel cell and hybrid vehicles in a future sustainable road transport system," *Energy Policy*, vol. 38, no. 1, pp. 24–29, 2010, doi: 10.1016/j.enpol.2009.08.040.

[13] L. Kumar and S. Jain, "Electric propulsion system for electric vehicular technology : A review," *Renew. Sustain. Energy Rev.*, vol. 29, pp. 924–940, 2014, doi: 10.1016/j.rser.2013.09.014.

[14] J. Antonio, G. Sánchez, J. María, L. Martínez, and J. Lumbreras, "Impact of Spanish electricity mix , over the period 2008 – 2030 , on the Life Cycle energy consumption and GHG emissions of Electric , Hybrid Diesel-Electric , Fuel Cell Hybrid and Diesel Bus of the Madrid Transportation System," *Energy Convers. Manag.*, vol. 74, pp. 332–343, 2013, doi: 10.1016/j.enconman.2013.05.023.

[15] M. F. Torchio and M. G. Santarelli, "Energy , environmental and economic comparison of different powertrain / fuel options using well-to-wheels assessment , energy and external costs e European market analysis," *Energy*, vol. 35, no. 10, pp. 4156–4171, 2010, doi: 10.1016/j.energy.2010.06.037.

[16] N. Nylund and K. Koponen, "Fuel and Technology Alternatives for Buses Overall Energy Efficiency and Emission," 2012.

[17] J. Grutter, "Real World Performance of Hybrid and Electric Buses Environmental and Financial Performance of Hybrid and Battery Electric Transit Buses Based on Real World Performance of Large Operational Fleets," 2015.

[18] R. EDWARDS, J.-F. Larivé, D. Rickeard, and W. Weindorf, "WELL-TO-TANK Report Version 4 . a JEC WELL-TO-WHEELS ANALYSIS WELL-TO-WHEELS ANALYSIS OF FUTURE AUTOMOTIVE FUELS AND POWERTRAINS IN THE EUROPEAN CONTEXT," 2014. doi: 10.2790/95629.

[19] Z. Chen, Y. Yin, and Z. Song, "A cost-competitiveness analysis of charging infrastructure for electric bus operations," *Transp. Res. Part C Emerg. Technol.*, vol. 93, no. December 2017, pp. 351–366, 2018, doi: 10.1016/j.trc.2018.06.006.

[20] L. Eudy, M. Post, and C. Gikakis, "Fuel Cell Buses in U. S. Transit Fleets: Current Status 2014," 2014. [Online]. Available: http://gofuelcellbus.com/uploads/2012_Current_Status_Report_NREL.pdf.

[21] W. Feng and M. Figliozzi, “An economic and technological analysis of the key factors affecting the competitiveness of electric commercial vehicles : A case study from the USA market,” *Transp. Res. Part C Emerg. Technol.*, vol. 26, pp. 135–145, 2013, doi: 10.1016/j.trc.2012.06.007.

[22] A. Kunith, R. Mendelevitch, and D. Goehlich, “Electrification of a city bus network—An optimization model for cost-effective placing of charging infrastructure and battery sizing of fast-charging electric bus systems,” *Int. J. Sustain. Transp.*, vol. 11, no. 10, pp. 707–720, 2017, doi: 10.1080/15568318.2017.1310962.

[23] A. Lajunen, “Energy consumption and cost-benefit analysis of hybrid and electric city buses,” *Transp. Res. Part C Emerg. Technol.*, vol. 38, pp. 1–15, 2014, doi: 10.1016/j.trc.2013.10.008.

[24] Y. M. Nie and M. Ghamami, “A corridor-centric approach to planning electric vehicle charging infrastructure,” *Transp. Res. Part B*, vol. 57, pp. 172–190, 2013, doi: 10.1016/j.trb.2013.08.010.

[25] M. Rogge, E. Van Der Hurk, A. Larsen, and D. Uwe, “Electric bus fleet size and mix problem with optimization of charging infrastructure,” *Appl. Energy*, vol. 211, no. November 2017, pp. 282–295, 2018, doi: 10.1016/j.apenergy.2017.11.051.

[26] C. E. Thomas, “Fuel cell and battery electric vehicles compared,” *Int. J. Hydrogen Energy*, vol. 34, no. 15, pp. 6005–6020, 2009, doi: 10.1016/j.ijhydene.2009.06.003.

[27] J. Ribau, R. Viegas, A. Angelino, A. Moutinho, and C. Silva, “A new offline optimization approach for designing a fuel cell hybrid bus,” *Transp. Res. Part C Emerg. Technol.*, vol. 42, pp. 14–27, 2014, doi: 10.1016/j.trc.2014.02.012.

[28] J. P. Ribau, C. M. Silva, and J. M. C. Sousa, “Efficiency , cost and life cycle CO 2 optimization of fuel cell hybrid and plug-in hybrid urban buses,” *Appl. Energy*, vol. 129, pp. 320–335, 2014, doi: 10.1016/j.apenergy.2014.05.015.

[29] A. Elgowainy, A. Rousseau, M. Wang, M. Ruth, D. Andress, J. Ward, F. Joseck, T. Nguyen, and S. Das, “Cost of ownership and well-to-wheels carbon emissions / oil use of alternative fuels and advanced light-duty vehicle technologies,” *Energy Sustain. Dev.*, vol. 17, no. 6, pp. 626–641, 2013, doi: 10.1016/j.esd.2013.09.001.

[30] F. C. and H. J. Undertaking, “Urban buses : alternative powertrains for Europe,” 2012.

[31] IEA, “Global EV Outlook 2019 to electric mobility,” 2019.

[32] “Medium and Heavy Duty Buses with Hybrid, Plug-In Hybrid, Battery Electric, and Fuel Cell Powertrains: Global Market Analysis and Forecasts,” 2017.

[33] L. Eudy and M. Jeffers, “Zero-Emission Bus Evaluation Results: County Metro Battery Electric Buses,” *Nrel*, no. FTA Report No. 0118, 2018.

[34] “ZeEUS eBus Report 2: An updated overview of electric buses in Europe,” 2017.

[35] E. Jan, P. Stabat, and F. Neirac, “Compétitivité et déploiement du bus électrique en Europe à horizon 2025,” 2016.

**** End of Chapter 1 ****

Chapter 2

BATTERY ELECTRIC BUS ENERGY MODEL

2.1 Introduction

The massive deployment of BEB faces many challenges, such as the bus limited driving range, the high capital cost of the bus unit, and the readiness of the charging infrastructure [1]–[6]. BEB limited driving range raises concerns over the ability of the bus to operate without schedule disruptions during the day. In addition, BEB high capital costs, mainly due to the cost of the battery pack, make BEB an expensive and unattractive solution for investors, especially when compared to diesel buses or other alternative bus technologies [5]. Moreover, deployment of BEB requires major infrastructural modifications, such as the installation of charging stations and electricity grid adjustments. This results in high infrastructural costs.

Proper sizing of the battery energy capacity is essential to overcome the previously mentioned challenges. The bus driving range is limited by the energy capacity of the battery. Batteries with high energy capacity increase the bus driving range, however, they suffer high capital costs and additional energy consumption due to the battery weight. On the other hand, small batteries with low energy capacity incur lower capital costs but they suffer a reduced driving range. In addition, the choice of the battery size drives the infrastructural costs, such as the cost of chargers. Batteries with low energy capacity mainly require more frequent charging at high power rates [7], [8] to avoid any disruption in operation, which yields to a higher chargers cost.

Being the sole energy and power source on the bus, the battery should be capable of supplying the energy and power needs of the different energy systems encountered in BEB. In addition to the propulsion system, the HVAC system and the bus auxiliaries result in significant energy consumption in BEB. The HVAC unit energy consumption represents the energy needs to heat, ventilate, and air condition the bus cabin to sustain thermal comfort conditions inside the bus. On the other hand, bus auxiliaries are features that require a significant amount of energy to operate. These auxiliaries are electric, hydraulic, pneumatic, and battery-thermal auxiliaries that are essential to the bus operation. These energy systems demand power from the battery.

To that end, a detailed and comprehensive energy assessment of BEB is needed considering its different energy systems. The objective of this chapter is to present, in detail, the bus architecture, and the technology and modeling approach of each component in the bus, in addition to the criteria used to validate the proposed models. Finally, this chapter answers the following research question:

- ***What are the different energy systems used in a BEB and how to evaluate their energy consumption and the total BEB energy consumption?***

2.2 Review of the Literature

Several studies have been published over the past decade in the academic literature on assessing the energy consumption of BEB. Most of these studies focus on quantifying the energy consumption of the propulsion system in buses or evaluating the HVAC system energy consumption to maintain thermal comfort conditions inside the bus cabin. The studies propose different modeling approaches for the different energy systems encountered in BEB.

These studies are summarized in Table 2.1. The focus of each study is presented alongside the relevant findings and insights. The summary table also identifies the considered energy systems (propulsion, HVAC, auxiliaries) in each study. In addition, the application of each study is recognized such as the adopted driving and weather conditions.

It is important to mention that in addition to the different energy systems, these studies model the energy/power source as well to meet the BEB energy and power demands. Different battery models are introduced in these studies and they will be presented in the upcoming section where the battery modeling approach will be discussed.

The majority of the studies assess the energy consumption of the propulsion system by introducing and utilizing models for the propulsion system and its components. These studies model the components of the propulsion system and evaluate their energy performance at certain driving conditions such as fixed driving cycles, road topographies, and passengers' load [9]–[14]. The battery model is considered as a component in the propulsion system.

Few studies tackle the HVAC system energy consumption in electric vehicles by providing static thermal models [15] for the cabin and providing simplified HVAC system models with no clear control strategy. Out of these studies, the majority have tackled the HVAC system energy consumption for passenger electric vehicles rather than electric buses [16], [17]. Most of the proposed cabin models lack the comprehensiveness of the heat transfer processes that take place between the bus cabin and its environment, and this sacrifices the model's accuracy and misestimates the thermal needs. In addition, most of the presented HVAC models in the literature are simplified which may provide imprecise HVAC system energy consumption, not to mention their unclear control strategy that needs to be well-defined as it may alter the energy behavior of the HVAC unit.

Table 2.1: Summary overview of the recent literature on assessing the energy consumption of BEB

Reference	Focus	Considered Energy Systems	Application	Results/Insights
Halmeaho et al. (2017) [11]	Introducing a Multi-physical powertrain model with a focus on the electric machine losses.	- Propulsion	2 bus line drive cycles.	Modeling Electric machines as simple efficiency is at a satisfying level of accuracy and can be used instead of complicated models.
Gao et al. (2019) [10]	Presenting battery electric vehicle (including bus) powertrain model and conducting energy performance evaluation.	- Propulsion - Constant electric auxiliaries	Real road drive cycles and eco-drive cycles.	Eco-driving shows great potential to reduce battery electric vehicles' energy consumption.
Xu et al. (2015) [14]	Assessing energy consumption and emissions of transit buses using a Fuel and Emissions Calculator modal modeling approach.	- Propulsion - Constant auxiliaries	Different drive cycles, road topographies, and passengers' load.	The choice of optimal bus technology to minimize GHG is highly dependent on the route location and characteristics.
Delgado et al. (2011) [9]	Predicting heavy-duty vehicles energy consumption and emissions over drive cycles using a statistical data-based modeling approach.	- Propulsion	17 heavy-duty drive cycles for buses and trucks.	Metrics such as average velocity, average positive acceleration, and the number of stops affect the energy consumption of the bus and can be used to characterize drive cycles.
Perrotta et al. (2014) [13], [18]	Assessing electric bus propulsion system energy performance during brake energy recovery using a	- Propulsion	3 bus lines with different distances and number of stops.	Electric bus energy performance deteriorates when operating at short-distance bus lines representing urban routes.

	mathematical backward modeling methodology.			
Kim et al. (2015) [19]	Investigating battery exchange system for electric bus using energy models built in Autonomy.	- Propulsion - HVAC - Constant auxiliaries.	1 bus route and 2 external temperatures (30 °*C* and 18 °*C*).	The battery exchange system ensures quick recharging, yet it requires a robotized mechanism to put into practice.
Mallon et al. (2017) [20]	Investigating the impact of installing photovoltaic cells in electric buses on their battery life cycle using mathematical models.	- Propulsion - Constant HVAC consumption	1 drive cycle and a sample of yearly weather conditions.	Photovoltaic cells reduce the battery energy consumption depending on weather conditions and may prolong battery life by 19%.
Varga et al. (2015) [21]	Assessing energy consumption and emissions of electric bus using AVL Cruise energy simulation tool.	- Propulsion - Constant electric auxiliaries	1 drive cycle	Proper battery sizing is essential for BEB cost and design considerations.
Göhlich et al. (2014) [22]	Assessing bus energy consumption, design, and total cost of ownership in the city of Berlin using a multi-physical modeling approach.	- Propulsion - HVAC - Constant auxiliaries	1 drive cycle and 2 external temperatures (-17 °*C* and 18 °*C*).	Bus heating requires a significant amount of energy at extreme weather conditions.
Lourido et al. (2016) [12]	Evaluating the energy needs of rapid transit electric bus in the city of Bogota using a low-order longitudinal model.	- Propulsion	1 bus route is used to create synthesized drive cycles from real-world data.	A hybrid electric storage system composed of battery packs and ultra-capacitors reduces energy consumption due to lower ohmic losses.

Suh et al. (2015) [15]	Design of an efficient HVAC system for BEB.	- Propulsion - Constant HVAC consumption	1 local bus route, 1 drive cycle, and 2 HVAC loads (26 kW for heating and 28 kW for cooling).	A proper HVAC control scheme may reduce the HVAC unit electric energy consumption by 20%, and thus enhancing the driving range.
Göhlich et al. (2015) [23]	Economic assessment of different air-conditioning and heating systems for electric city buses based on comprehensive energetic simulations.	- HVAC	Long-term average yearly temperature	Heat Pump HVAC system is a promising technology that reduces the HVAC unit's electric energy consumption and enhances the driving range. However, its high cost remains the main limitation.
Lee et al. (2013) [24]	Characterizing the performance of mobile heat pump for a large passenger electric vehicle using the Dymola modeling environment.	- HVAC	Varying external temperature from 8 $°C$ to 40 $°C$.	Heat pump system can help to improve the driving range in electric buses.
Lajunen (2017) [16]	Evaluating and enhancing the energy efficiency and performance of cabin thermal management in electric vehicles using Amesim advanced modeling environment.	- Propulsion - HVAC	2 drive cycles, 1 measured real-world driving cycle, and varying external temperatures from -30$°C$ to 40 $°C$ for electric vehicle (not electric bus).	Driving range can be enhanced by 22 % when using a heat pump instead of a positive temperature coefficient heating system.
Fayazbakhsh et al. (2013) [17]	Comprehensive modeling of vehicle air conditioning loads using heat balance method.	- Propulsion - HVAC	2 specified driving and weather conditions for electric vehicles (not electric bus).	The proposed modeling approach presents a time-efficient computational tool without sacrificing accuracy.

Lajunen et al. (2015) [25]	Investigation of thermal energy losses in the propulsion system of an electric city bus using Amesim simulation environment.	- Propulsion - Constant HVAC consumption	4 drive cycles and a variety of external temperatures from -25°*C* to 10°*C*.	Drive cycle characteristics and weather conditions highly affect the thermal energy losses in powertrain components.
Yan et al. (2016) [26]	Improving the performance of air conditioning system in electric bus at variable passengers' load using a mathematical model.	- HVAC	1 drive cycle, 1 external temperature (35°*C*), and variable passengers' load.	Adjusting the bus cooling needs function of passengers' load can save up to 8% of the total AC energy consumption.
Andersson (2004) [27]	Identification and modeling of auxiliaries in commercial vehicles using an empirical data-based modeling approach.	- Constant HVAC consumption - Auxiliaries	1 drive cycle and a variety of external temperatures for a hybrid electric bus.	HVAC unit auxiliaries have a significant impact on the total energy consumption in commercial vehicles.
Petersson et al. (2007) [28]	Modeling and control of auxiliary energy systems in diesel heavy vehicles	- Propulsion - Auxiliaries	1 drive cycle	Driving the auxiliaries electrically could achieve energy consumption reduction but at higher investment costs.

Moreover, there is no study, up to the author's knowledge and this point in time, that evaluates the auxiliaries' energy consumption in electric buses. The presented studies rather discuss these auxiliaries in hybrid electric buses and diesel buses, and they are dated at this moment [27], [28]. In addition, this energy consumption is often simplified in the various energy models presented in the literature, by assuming a fixed auxiliary load [10], [14], [19], [21], [22]. However, in heavy-duty applications, the electric, pneumatic and hydraulic auxiliaries are not negligible [10], [27], [29], and a dynamic modeling approach is essential to estimate their energy consumption. In addition, battery thermal auxiliaries are exclusive features in electrified vehicles and their energy consumption is significant in high energy and power density applications which is the case in BEB [30].

Across the presented studies, none presents a comprehensive energy modeling methodology that considers all the energy systems encountered in BEB using a dynamic approach to provide a detailed energy consumption analysis of BEB. The very few studies that consider all the energy systems either assume a fixed HVAC unit energy consumption or a fixed auxiliaries' power demand.

Based on what has been presented, the following gaps and limitations in the recent literature of BEB energy consumption assessment are identified:

- There is no comprehensive energy modeling methodology that considers all the energy systems encountered in BEB to precisely assess its global energy consumption.
- HVAC system energy consumption in BEB has either been considered a fixed load or a simplified static load with no consideration of the dynamic heat transfer processes that take place between the bus cabin and its environment.
- HVAC unit models in BEB are simplified and do not introduce a clear control strategy which impacts their energy consumption significantly.
- No study considers a dynamic and detailed auxiliaries' model in BEB.

Based on the presented summary of the literature and the highlighted gaps within, this chapter presents a modeling methodology to assess the energy consumption of BEB at a variety of driving and weather conditions. The methodology considers all the energy systems encountered in BEB such as the propulsion system, HVAC system, and auxiliaries in order to precisely evaluate the global energy consumption of BEB.

In summary, this chapter presents a comprehensive modeling methodology to assess the energy performance of the different energy systems encountered in BEB.

The rest of the chapter is organized as follows: section 2.3 introduces the modeling environment, then section 2.4 thoroughly explains the BEB energy model considering all its energy systems. Section 2.5 presents the model validation and section 2.6 concludes on what has been presented in this chapter.

2.3 Modeling Environment

Dymola software is used to model the energy behavior of the BEB. It utilizes the Modelica modeling language to describe physical systems and components. Modelica is an object-oriented and equation-based language that allows convenient and component-oriented modeling of complex physical systems [31]. The defined libraries in Dymola contain electrical, mechanical, thermal, hydraulic, pneumatic, and control components, in addition to a variety of other libraries. The fact that Modelica is an open-source language allows the user to define, modify, and build new systems and components. The different systems and components in Dymola are defined by discrete, differential, and algebraic equations. "Modelica supports both high-level modeling by composition and detailed library component modeling by equations. This attracted a variety of industrial applications, especially automotive companies such as Audi, BMW, Daimler, Ford, Toyota, and VW" [32].

2.4 Battery Electric Bus Model

This section presents the energy modeling methodology in detail. First, the technology of BEB is explained. Then, the battery model is introduced followed by the propulsion system model. The bus cabin thermal model is then presented proceeded by the HVAC system model. Finally, the relevant bus auxiliaries are modeled and explained.

2.4.1 Bus Configuration and Specification

The BEB configuration is presented in Figure 2.1 as it shows the multiple energy systems within the BEB and their components. The battery, propulsion system, bus cabin, HVAC unit, and the set of auxiliaries are shown in Figure 2.1.

2.4.1.1 Bus Configuration

The bus propulsion system, also referred to as the powertrain, is responsible for propelling the bus by meeting the driver acceleration and braking demands. The propulsion system

architecture consists of the following main components: a propulsion unit, a transmission unit, and a braking system.

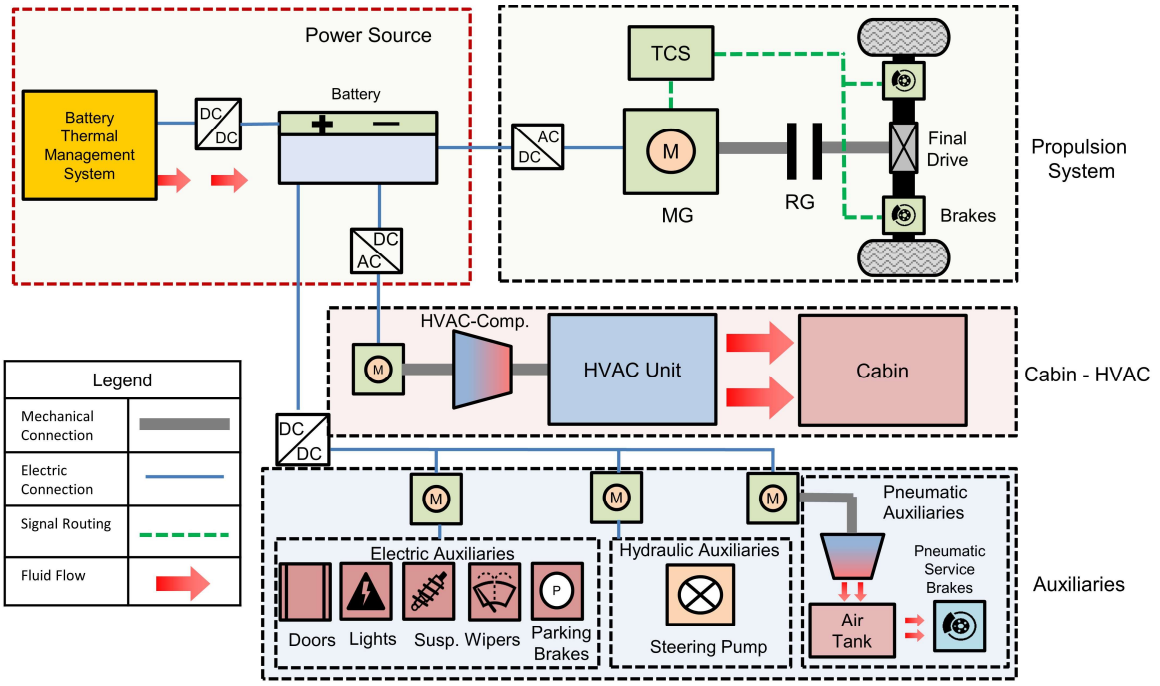


Figure 2.1: BEB components configuration

The propulsion unit is an electric machine (EM), powered by the battery and controlled by a torque control strategy (TCS) to ensure propulsion as well as to recover part of the braking energy. The EM operates as an electric motor during propulsion as it provides mechanical torque to move the bus whereas during braking, it operates as an electric generator where it recovers part of the vehicle's kinetic energy and converts it into electric energy to recharge the battery. In Figure 2.1, the EM is referred to as MG, which is an abbreviation for Motor-Generator, describing its two operating modes. The transmission unit contains only a single reduction gear (RG) and a differential, often referred to as the final drive, given the high torque capability of the electric machine. The braking system consists of pneumatic brakes used to dissipate the unrecovered braking energy by the electric machine and it is controlled by the TCS as well in order to ensure safe vehicle braking.

The HVAC unit is responsible for meeting the bus cabin thermal needs during all weather conditions by heating, cooling, ventilating, and dehumidifying the cabin whenever needed. A heat pump (HP) is used to meet the thermal comfort needs of the bus cabin. The use of a HP instead of other HVAC technologies will be thoroughly discussed in section 2.4.4. Unlike DB, the HP compressor in BEB is driven by a dedicated electric motor whereas the HP compressor in DB is directly driven by the diesel engine. This gives more flexibility in controlling the

compressor speed. Waste heat can be recovered from the powertrain components such as the battery and EM in order to assist the heating unit.

The bus auxiliaries are essential features for the bus operation and consume a significant amount of energy. The technology of these auxiliaries differs depending on bus technology. In BEB, most of these features are electrically-operated, however, DB auxiliaries rely more on hydraulic and pneumatic systems to operate. Table 2.2 lists these auxiliaries and their corresponding technologies in BEB. In general, electrically-operated auxiliaries are more energy-efficient compared to hydraulic or pneumatic auxiliaries as they are decoupled from the engine and can be controlled separately, however they require more frequent maintenance [28]. One important auxiliary that is exclusively found in BEB is battery thermal management (BTM). BTM is essential at extreme weather conditions to ensure efficient and safe operation of the battery pack [33].

Table 2.2: Auxiliaries technology in BEB

Auxiliary	Technology
Service Brakes	Pneumatic
Parking Brakes	Electric
Suspension System	Hydro-Electric
Steering Pump	Hydro-Electric
Lights	Electric
Wipers	Electric
Doors	Electric
BTM	Thermal

Finally, the mentioned energy systems demand energy from the Lithium-ion battery, being the sole energy and power source onboard. The choice of Lithium-ion battery technology will be discussed in the battery modeling section 2.4.2.

2.4.1.2 Bus Specifications

There is a variety of BEB operating in the market globally. The specifications of these buses differ in terms of the bus length, passengers' capacity, and use such as urban buses that operate inside the cities or inter-city buses that travel from one city to another. In this thesis, a reference 12-*m* bus chassis with 3 doors is considered, being the most common bus in the market meanwhile for urban use [34]–[37]. The bus characteristics [20], [33] are summarized in Table 2.3. The maximum allowable number of passengers on-board, including both seated and standing passengers, depends on the battery weight and the bus floor area [33]. For the current

bus configuration, the maximum allowable number of passengers is 55 with an average mass of 68 kg per passenger.

Table 2.3: Bus chassis parameters

	Parameter	Variable	Value	Unit
Chassis	Glider Mass	M_{Glider}	11600	kg
	Frontal Area	A_f	8.2	m^2
	Drag Coefficient	C_D	0.55	-
	Rolling Resistance Coefficient	f_r	0.008	-
Wheels	Wheel Radius	r_W	0.48	m
	Wheel Inertia	J_W	20.52	$Kg.m^2$
	Number of Wheels	N_W	4	-

The glider mass is defined as the mass of the bus without the propulsion system components. Accordingly, the total mass of the bus is computed by adding the mass of the corresponding propulsion system components, presented in Table 2.4. The mass of the battery is directly dependent on its energy capacity. The most common battery size of operating BEB at the moment is 300 kWh [37].

Table 2.4: Bus curb mass and total mass

Component	Weight [kg]
Glider mass	11600
Battery pack	4200
Transmission	80
Electric Machine	100
4 Auxiliary Electric Motors	100
Curb mass	**16080**
Passenger mass	3400
Total mass	**19480**

2.4.2 Battery

This section introduces the current Lithium-ion battery market and technology used for BEB. The battery electrical and thermal models are introduced in addition to the battery thermal management highlighting the interactions among these different sub-systems.

2.4.2.1 Technology and Market

Lithium-ion battery cells show superior energy and power performance when compared to other cell chemistries used in electric vehicles (EV) [30]. Figure 2.2 shows a Ragone plot of various

electrochemical energy storage and conversion devices, including the recently reported solid oxide fuel cells [38] (SOFC). Lithium-ion batteries are the most suitable battery chemistry for EV meanwhile due to their high energy density and specific energy (400 *Wh/L* and 150 *Wh/kg*) especially when compared to the widely used Nickel-metal Hydride (NiMH) batteries in hybrid electric vehicles (240 *Wh/L*, 75 *Wh/kg*) [39]. As illustrated in Figure 2.2, a higher battery specific energy implies a higher vehicle range which is one of the main operational challenges facing BEB. On the other hand, a higher battery specific power implies a better vehicle acceleration which is a key performance constraint in the design of BEB.

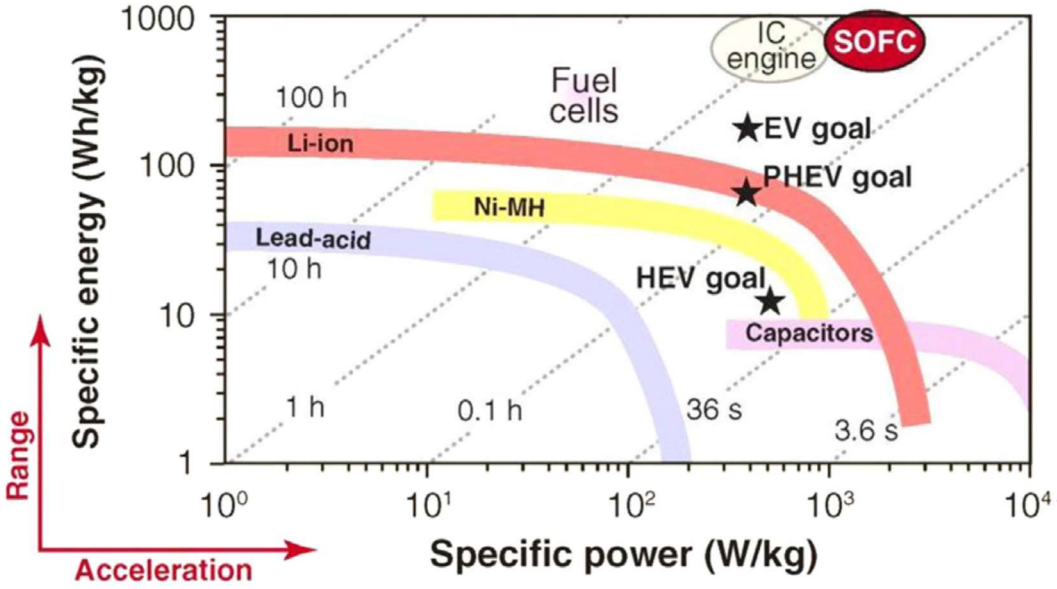


Figure 2.2: Ragone plot of various electrochemical energy storage and conversion devices [30]

In addition, the cost of Lithium-ion battery packs has been reduced significantly during the past decade due to the huge investment in this technology by tech giants, especially in China [40]. Figure 2.3 shows the reported Lithium-ion battery pack costs, an average of reported values, and observed average by Bloomberg New Energy Finance (BNEF). This cost has dropped from almost 800 *€/kWh* in 2010 down to less than 200 *€/kWh* in 2017. This trend is expected to be sustained in the next decade [40].

The superior energy and power performance of Lithium-ion batteries, alongside their continuous cost reduction, have expanded their current EV market share which explains their wide deployment in EV applications.

For these considerations, a Lithium-ion battery pack model is presented in the upcoming sections.

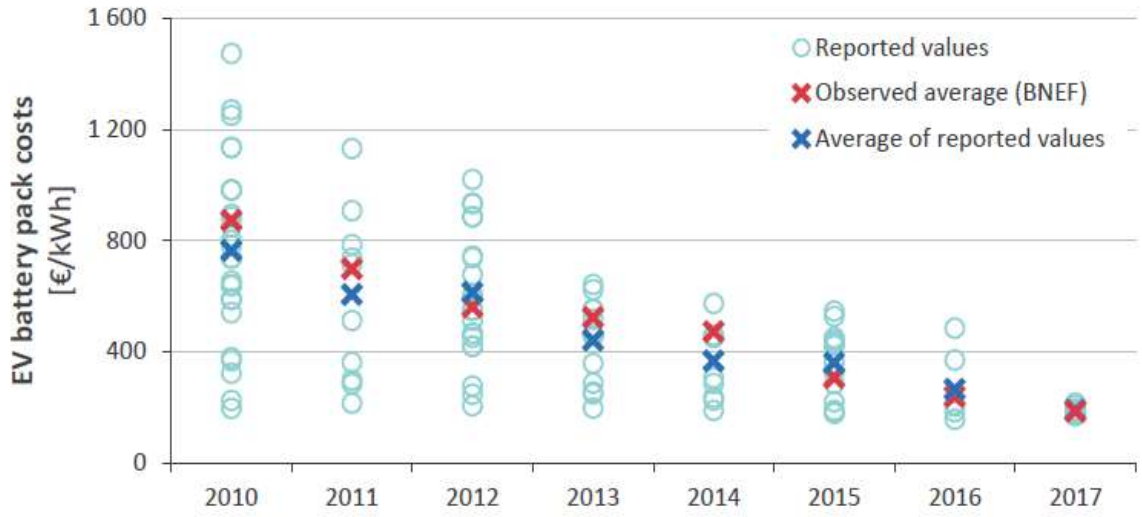


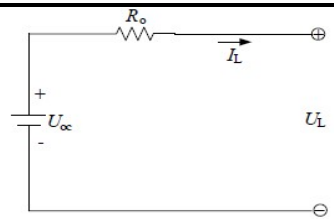
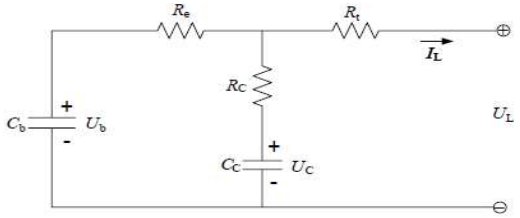
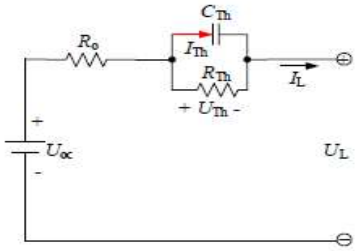
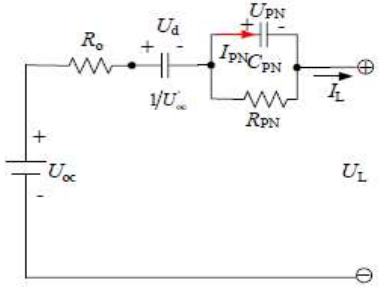
Figure 2.3: Reported Lithium-ion battery pack costs, average of reported values and observed average by Bloomberg New Energy Finance (BNEF) [40]

2.4.2.2 Electrical Model

There are two main approaches to model the electrochemical behavior of Lithium-ion batteries: (1) first-principle models and (2) equivalent circuit models [30]. First-principle models are physics-based electrochemical models that describe the kinetics and energy dissipation within battery cells, in addition to the different mass transport phenomena [41]–[43]. Such models have shown high accuracy in predicting Lithium-ion batteries behavior for any application, yet they result in high computation time [44]. On the other hand, equivalent circuit models are rather simplified input-output models that quantify the battery main variables such as state of charge (SOC), voltage, internal resistance, electric current, and power which make them practical for modeling the battery energy behavior at the system level. Table 2.5 summarizes the different Lithium-ion Battery equivalent circuit models highlighting their performance in terms of battery SOC and voltage estimation. The performance of each model is assessed based on its estimation accuracy regarding the battery cell SOC and voltage. A higher number of plus (+) signs indicates a better estimation accuracy.

In this thesis, a Rint equivalent circuit model is used to describe the behavior of the Lithium-ion battery, as it presents a satisfying trade-off among model complexity, accuracy, and data availability which made it widely used in EV modeling applications [11], [20], [45], [46]. The model considers the battery empirical data such as the open-circuit voltage and internal resistance of each cell as function of the battery SOC, as illustrated in Figure 2.4.

Table 2.5: Summary of Lithium-ion battery equivalent circuit models [47]–[52]

Model Name	Scheme	Description	Model Performance
Rint		Voltage source alongside internal resistance in series, both function of battery SOC.	SOC estimation: ++ Voltage Estimation: +
RC		2 capacitors representing battery surface effect and ample capability, in addition to 3 resistors.	SOC estimation: ++ Voltage Estimation: +
Thevenin		Connection of a parallel RC network in series to the Rint model to describe the battery dynamic characteristics.	SOC estimation: +++ Voltage Estimation: +
PNGV		Addition of a capacitor in series to the Thevenin model to predict the time-accumulation open-circuit voltage change.	SOC estimation: + Voltage Estimation: +++

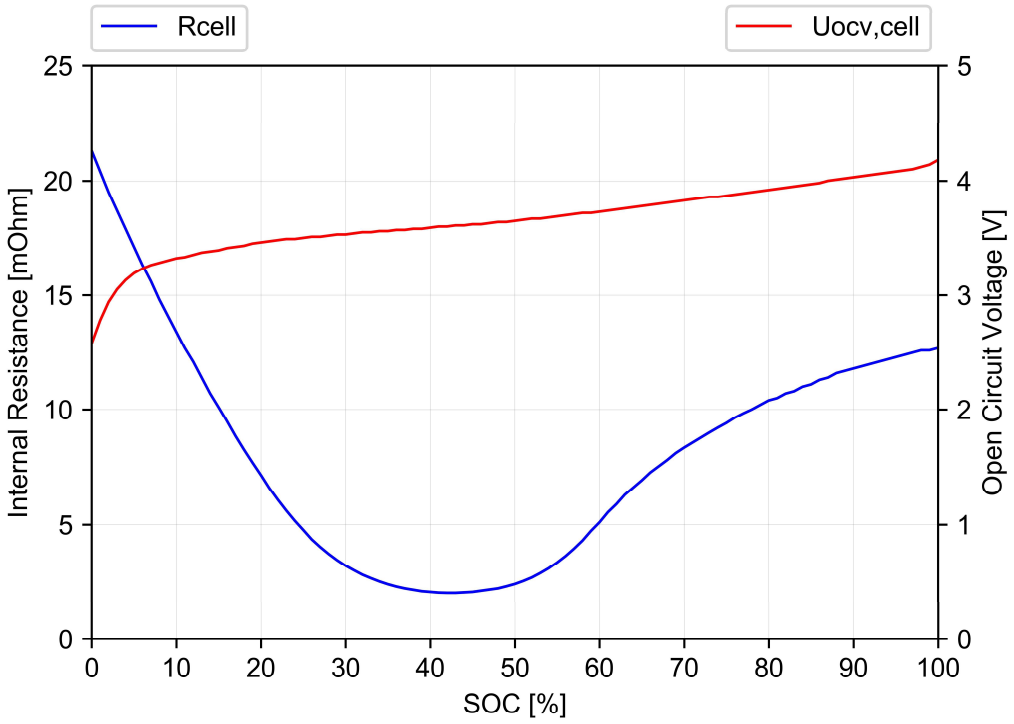


Figure 2.4: Internal resistance and open-circuit voltage variation for a single battery cell as function of the battery SOC

The battery cell parameters are summarized in Table 2.6. The battery pack consists of a set of modules that are connected in parallel. Each module is formed of a set of battery cells that are connected in series. The number of cells connected in series and the number of parallel modules both determine the battery specifications such as its maximum energy capacity (E_{max}), total charge capacity (C_{max}), equivalent internal resistance (R_{eq}), and its open-circuit voltage range (U_{ocv}) as shown in equations (2.1) to (2.5).

Table 2.6: Summary of battery pack parameters [53]

Parameter	Variable	Value	Unit
Energy Capacity per Cell	E_{Cell}	14.6	Wh
Charge Capacity per Cell	C_{Cell}	4.3	Ah
Mass of a Battery Cell	M_{Cell}	205	g
Number of Parallel Modules	N_P	108	-
Number of Series Sets	N_S	190	-

The resulting battery maximum energy capacity is around 300 kWh with a 465 Ah total charge capacity and an open-circuit voltage range between 600-800 V, which is the current state of the art for electric buses [54]. The battery can operate between 30 and 80% SOC window to avoid deep discharges that degrade the battery health, and reduce voltage drop at low SOC [55].

$$U_{OCV} = N_S \,.\, U_{OCV,Cell} \tag{2.1}$$

$$R_{eq} = R_{Cell} \,.\, \frac{N_S}{N_P} \tag{2.2}$$

$$C_{Max} = N_P \,.\, C_{Cell} \tag{2.3}$$

$$E_{Max} = N_P \,.\, N_S . C_{Cell} \tag{2.4}$$

$$M_{Batt} = N_P \,.\, N_S . M_{Cell} \tag{2.5}$$

This Rint battery model determines the battery terminal voltage (U_T), electric current (I_{Batt}), SOC, and the battery total discharge power (P_{Batt}) as shown in equations (2.6) to (2.9).

$$I_{Batt} = \frac{P_{Batt}}{U_T} \tag{2.6}$$

$$SOC\ (t) = \frac{C_0 - \int_0^t I_{Batt}(t) \,.\, dt}{C_{Max}} \tag{2.7}$$

$$U_T = \frac{1}{2}\left(U_{OCV} + \sqrt{U_{ocv}^2 - 4 . P_{Batt} . R_{eq}}\right) \tag{2.8}$$

$$P_{Batt} = \sum P_i \ \forall \ energy\ system\ i \tag{2.9}$$

As stated in equation (2.9), the battery power is the sum of the total power demand from the different energy systems. Note that the impact of battery cell temperature on the cell internal resistance behavior is considered. The internal resistance sharply increases at low temperatures (0 °*C* and below) whereas it is almost indifferent within a temperature range between 25°*C* to 40 °*C* [56].

2.4.2.3 Thermal Model

The application of Lithium-ion batteries in BEB is considered a high-voltage battery application. Such applications are subject to safety measures at the cell level, module level, and pack level [57]. A critical safety measure is to ensure that the temperature of the battery cells is within a safe operating range set by the international standard ISO 6469 for electrically-propelled vehicles [58]. For this sake, it is essential to model the thermal behavior of the battery cells.

Lithium-ion batteries thermal models are composed of 2 parts: (1) thermal model to estimate the temperature of the battery cell and (2) heat generation model to estimate the internal heat generation within the battery cell. Table 2.7 summarizes Lithium-ion battery thermal and heat generation models.

Table 2.7: Summary of lithium-ion batteries thermal and heat generation models [30], [59], [60]

	Model Name	Description	Model Performance
Thermal Model	Battery Thermal Model	Accounts for battery cell heat accumulation, convection, conduction, and heat generation.	Computation Complexity: -- Temperature Estimation: ++ Data Requirement: --
	Lumped Thermal Model	Balance of heat accumulation, heat dissipation due to convection to the surroundings, and heat generation.	Computation Complexity: - Temperature Estimation: + Data Requirement: -
Heat Generation Model	Local Heat Generation	Accounts for irreversible heat generation, reversible heat generation due to the entropic effect, ohmic heat generation from both solid and electrolyte phases.	Complexity: -- Generation Estimation: ++ Data Requirement: --
	Simplified Heat Generation	Accounts for joule's heating and reversible heat generation due to entropy effect.	Computation Complexity: - Generation Estimation: + Data Requirement: -
	Empirical Heat Generation	Empirical heat generation models include Joule's, reaction, and polarization heat generation.	Computation Complexity: - Generation Estimation: ++ Data Requirement: ---

Legend	+	++	+++	-	--	---
	Fair	Good	Very Good	Acceptable	Bad	Very Bad

In this thesis, a lumped thermal model alongside a simplified heat generation model are considered as they are widely used in vehicular applications [30], [61]–[67].

The proposed thermal model is a two-state model that captures the lumped thermal dynamics of a cylindrical battery. Figure 2.5 and Figure 2.6 introduce a scheme of the battery pack thermal model. The cross-section view shows the two thermal nodes considered in the lumped thermal modeling approach: (1) cell core at temperature (T_C) and (2) cell surface at temperature (T_S). Internal heat generation ($\dot{Q}$) heats the battery cell core. This heat is conducted to the cell surface which is in contact with the coolant at temperature (T_∞). As the coolant flows over the consecutive and adjacent battery cells, its temperature varies from one cell to another as it gets heated due to convection with the cell surface. Thus, this approach considers the difference in coolant temperatures among the different battery cells, and consequently, the temperature gradients inside the battery pack are considered. Equations (2.10) and (2.11) describe the governing equations of battery cell core and surface temperatures, where C_C and C_S are the heat capacities of the core and the surface respectively. R_1 is the conductive thermal resistance between the cell core and the cell surface, and R_2 is the convective thermal resistance between the cell surface and the coolant.

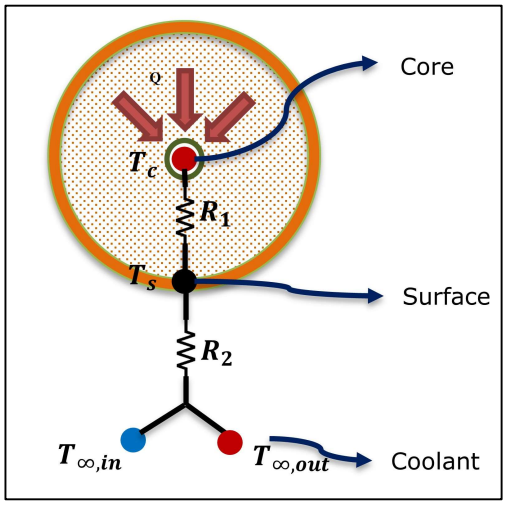


Figure 2.5: Scheme of battery cell cross-sectional view

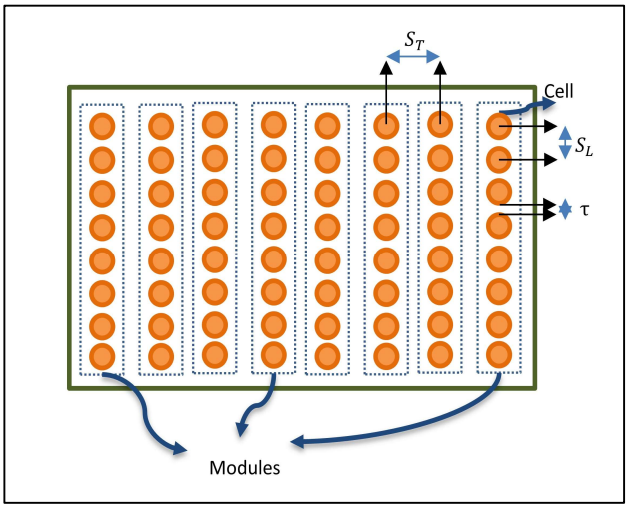


Figure 2.6: Scheme of battery pack top view

$$C_c \frac{dT_C}{dt} = \dot{Q} + \frac{T_S - T_C}{R_1} \tag{2.10}$$

$$C_S \frac{dT_S}{dt} = \frac{T_\infty - T_S}{R_2} - \frac{T_S - T_C}{R_1} \tag{2.11}$$

The internal heat generation $\dot{Q}$ is a byproduct of the chemical reactions taking place in the electrode assembly during battery operation [62]. The internal heat generation is governed by equation (2.12) according to [63]:

$$\dot{Q} = I_{Batt}(U_T - U_{OCV}) + I_{Batt}.T_C.\frac{\partial U}{\partial T} - \sum_i \Delta H_i r_i - \int \sum_j (H_j - H_j^{avg}).\frac{\partial c_j}{\partial t}\partial v \qquad (2.12)$$

The first and the second terms in this equation represent the resistive dissipation heat and reversible entropic heat within the battery cell, respectively. The last two terms represent the chemical reaction heat and mixing within the cell due to temperature gradient, however, they can be neglected [63], [65]. The previously presented electrical model and the lumped thermal model compute all the needed parameters for the calculation of the internal heat generation except for the entropy change parameter, denoted by $(\frac{\partial U}{\partial T})$ in equation (2.12). This term is experimentally obtained according to [68], and it is presented in Figure 2.7.

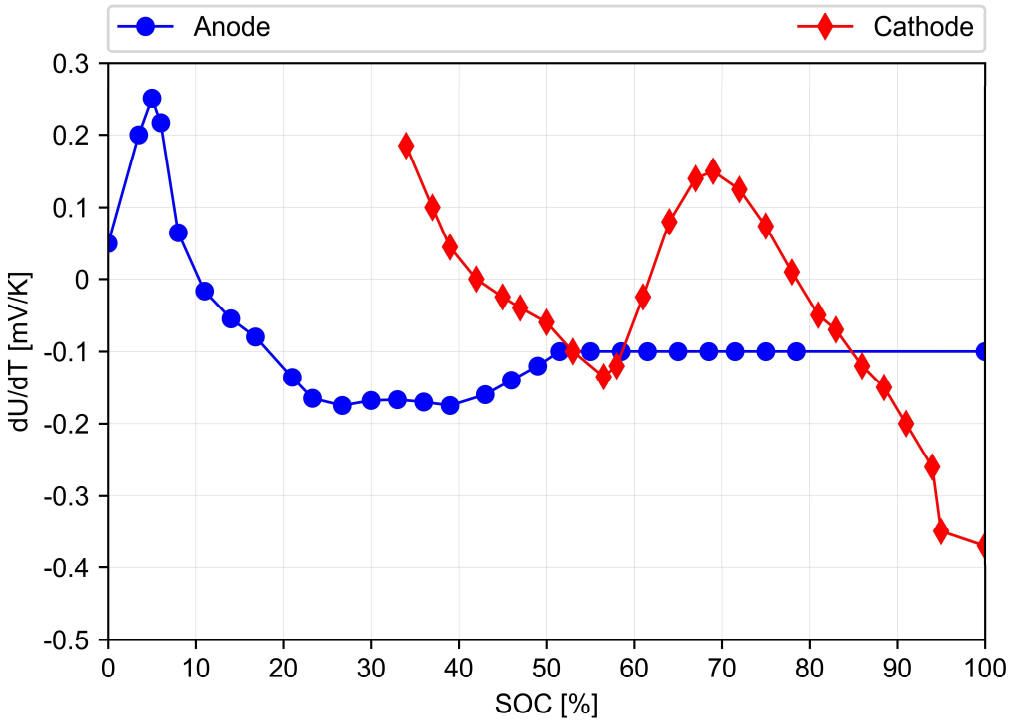


Figure 2.7: Entropy change data for battery cell anode and cathode function of battery SOC [68]

It is essential to parametrize the thermal resistances in lumped-thermal models. Concerning the value of the conductive thermal resistance (R_1), the different materials of the anode, cathode, casing, wiring, and electrolyte complicate the calculation of R_1 theoretically [64], therefore, the

conductive thermal resistance parametrization is done experimentally [61], [62]. Table 2.8 presents the model parameters.

Table 2.8: Battery lumped-thermal model parametrization [62]

Parameter	Variable	Value	Unit
Conductive Thermal Resistance	R_1	3.2 - 3.3	*K/W*
Battery Cell Core Heat Capacity	C_C	4.5	*J/K*
Battery Cell Surface Heat Capacity	C_S	62.7	*J/K*

As for the convective thermal resistance R_2, its value depends on the coolant flow characteristics, the geometry of the battery cells, and the layout of the battery pack. The coolant used in this study is air and this choice will be discussed thoroughly in section 2.4.2.4. The coolant is flowing across the cells composed in an in-line layout [69] as shown in Figure 2.8.

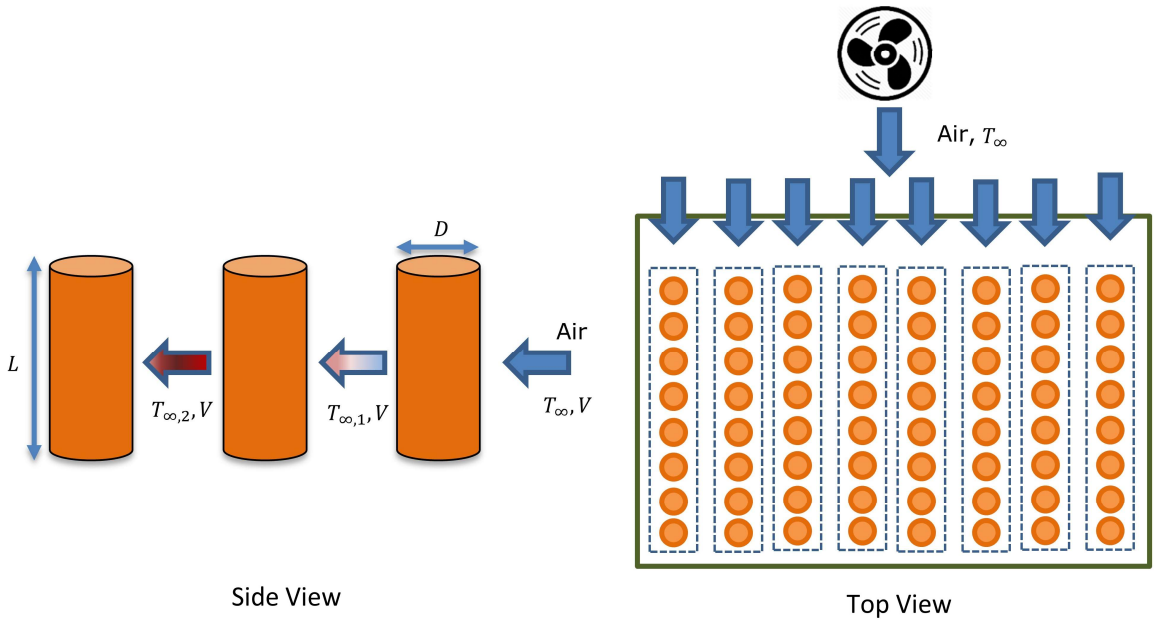


Figure 2.8: Coolant flow across battery cells

The convective thermal resistance (R_2) is inversely proportional to the air heat transfer coefficient (h_{air}) as shown in equation (2.13) where D and L are the diameter and the height of the battery cell respectively. Air heat transfer coefficient (h_{air}) is dependent on Nusselt's number (N_u) as shown in equation (2.14), where K_{air} is air thermal conductivity. Finally, Nusselt's number (N_u) is dependent on the coolant flow characteristics reflected in Reynold's number (R_e) and Prandtl's number (P_r). For airflow over an in-line layout, Nusselt's number (N_u) is

calculated based on equation (2.15) according to [69]. The variables v_{air}, $\mu_{air,}$ and $C_{P,air}$ are air kinematic viscosity, dynamic viscosity, and specific heat capacity at constant pressure, respectively. These parameters are dependent on the air temperature and pressure [70]. Note that in equation (2.15), Pr_s is Prandtl's number evaluated at the surface of the cell with m and c being dimensionless geometric parameters. Table 2.9 summarizes the battery cell and battery pack geometric parameters.

$$R_2 = \frac{1}{\pi . D . L . h_{air}} \tag{2.13}$$

$$h_{air} = \frac{N_u . K_{air}}{D} \tag{2.14}$$

$$N_u = 0.97 . c . R_e^m . {P_r}^{0.36} . \left(\frac{P_r^{\frac{1}{4}}}{P_{r,s}} \right) \tag{2.15}$$

$$R_e = \frac{V_{max} . D}{\nu_{air}} \tag{2.16}$$

$$P_r = \frac{C_{P,air} . \mu_{air}}{K_{air}} \tag{2.17}$$

Table 2.9: Battery cell and battery pack geometric parameters [53], [69]

	Parameter	Variable	Value
Battery Cell	Length	L	113 *mm*
	Diameter	D	32 *mm*
Battery Pack	Clearance between cells	τ	3 *mm*
	Distance between the center of 2 adjacent cells within the same module	S_L	35 *mm*
	Distance between the center of 2 adjacent cells in 2 different modules	S_T	35 *mm*
	N_u dimensionless geometric coefficient	c	0.27
	N_u dimensionless geometric exponent	m	0.63

In equation (2.16), Reynold's number is function of the variable V_{max} which is the maximum airspeed around the battery cell. V_{max} is calculated according to equation (2.18) where $\dot{m_{air}}$ is the air mass flow rate, ρ_{air} is the air density, A_{Cell} is the cell cross-sectional area. The air mass flow rate and temperature are determined by the cooling unit which will be discussed in section 2.4.2.4.

$$V_{max} = \frac{\dot{m_{air}}}{\rho_{air}.A_{Cell}}.\frac{S_T}{S_T - D} \quad (2.18)$$

2.4.2.4 Battery Thermal Management System

The Battery Thermal Management System (BTMS) is responsible for keeping the battery cells temperature within a desired operating range for performance and safety considerations. The BTMS is composed of 2 main components: (1) the cooling unit and (2) the cooling unit controller.

There are many battery cooling technologies under assessment meanwhile. These technologies are categorized under 4 main categories: (1) Air cooling technologies, (2) liquid cooling technologies, (3) phase change materials (PCM), and (4) heat pipes. Each category is further segmented into a set of sub-categories based on additional technological considerations. Table 2.10 introduces a summary of battery thermal management systems.

Based on the synthesis presented in Table 2.10, active air cooling/heating is considered in this study as it is capable of achieving a good compromise between adequate cooling and system complexity [71].

The cooling unit consists of a fan supplying air to cool the battery cells and an evaporator. The fan used is FB020-2E, its datasheet is available with flow rate, static pressure, and power consumption data [72]. The fan can supply air to cool the battery cells from three different air sources: (1) ambient air, (2) bus cabin air, (3) cooled air by the evaporator that is connected to the main HVAC unit.

In addition, at extreme cold weather conditions, there might be a need to heat the air before using it to cool the battery cells. For battery aging consideration, it is advised to cool battery cells with a minimum blown air temperature equals to 10 $°C$. For this sake, an electric resistance heater is coupled to the cooling unit.

The cooling unit modeling and controller will be discussed alongside the HVAC unit in section 2.4.4 as they are directly connected.

Finally, the coupled electro-thermal model scheme is presented in Figure 2.9.

Table 2.10: Summary of battery thermal management systems

BTM Technology		Advantages	Disadvantages
Air Cooling	Passive Air Cooling [73]–[75]	- Cheap - Variety of applications. - Simple	- High-temperature gradients. - Low heat extraction. - High space requirement - Additional weight - No battery heating during winter
	Passive Air Cooling/Heating [73]–[75]	Similar to passive air-cooling but it allows **battery heating during winter**	
	Active Air Cooling/Heating [74], [75]	Similar to passive air-cooling/heating but it incurs **acceptable temperature gradients** and **acceptable heat extraction** for high power applications	
Liquid Cooling	Refrigerant Liquid Cooling [76]	- High heat extraction - Low space requirement - Low-temperature gradients	- No battery heating during winter - Possibility of liquid leakage
	Coolant Liquid Cooling [75]	- High heat extraction - Low-temperature gradients - Battery heating during winter	- High space requirement - Additional weight - High complexity - Possibility of liquid leakage - Expensive
PCM		- Improved thermal conductivity [77], [78] - No need for a storage system [79], [80]	- Complex process to ensure critical thermo-mechanical properties for battery safety consideration [81].
Heat Pipes		- High and efficient heat extraction [82], [83]	- Immature technology [30]

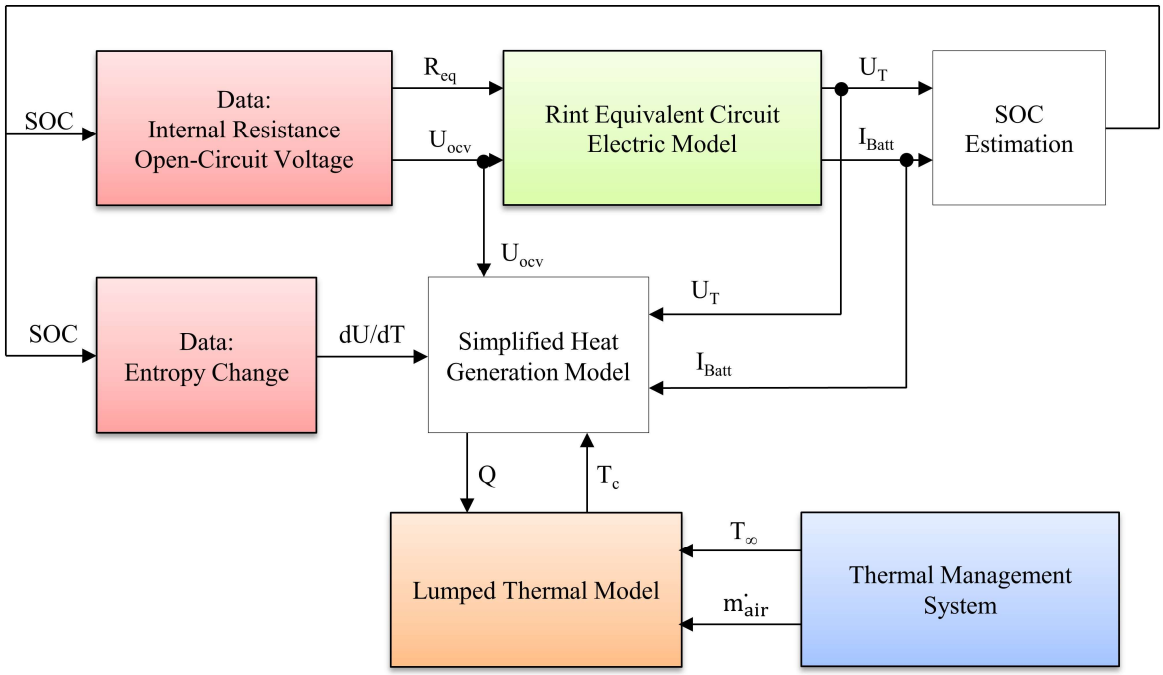


Figure 2.9: Battery coupled electro-thermal model scheme

2.4.3 Propulsion System

In this section, the main propulsion system components models will be discussed, such as the electric machine model, transmission and braking systems, wheels, and the Torque Control Strategy.

2.4.3.1 Electric Machine

There is a variety of modeling approaches to assess the energy behavior of electric machines (EM). By far, static efficiency map-based models are the most used in EV [11], [20], [84], [85] as they are at a good accuracy level and thus can be used instead of complicated models [11]. The proposed static efficiency maps include the efficiency of the electric machine and the efficiency of the inverter, as function of the EM torque and speed as illustrated in Figure 2.10. The EM peak and rated torque are considered. In addition, inertial components are added to capture the machine's dynamic performance imposing resistance to its velocity change.

During bus propulsion mode, the EM operates in motor mode and converts the battery electrical power into mechanical torque and speed; and during deceleration and braking modes, the machine operates in generator mode and converts part of the bus kinetic energy into electric energy, which is then restored to the battery. Note that this brake power recovery is limited by the maximum power of the machine and the battery maximum charging power.

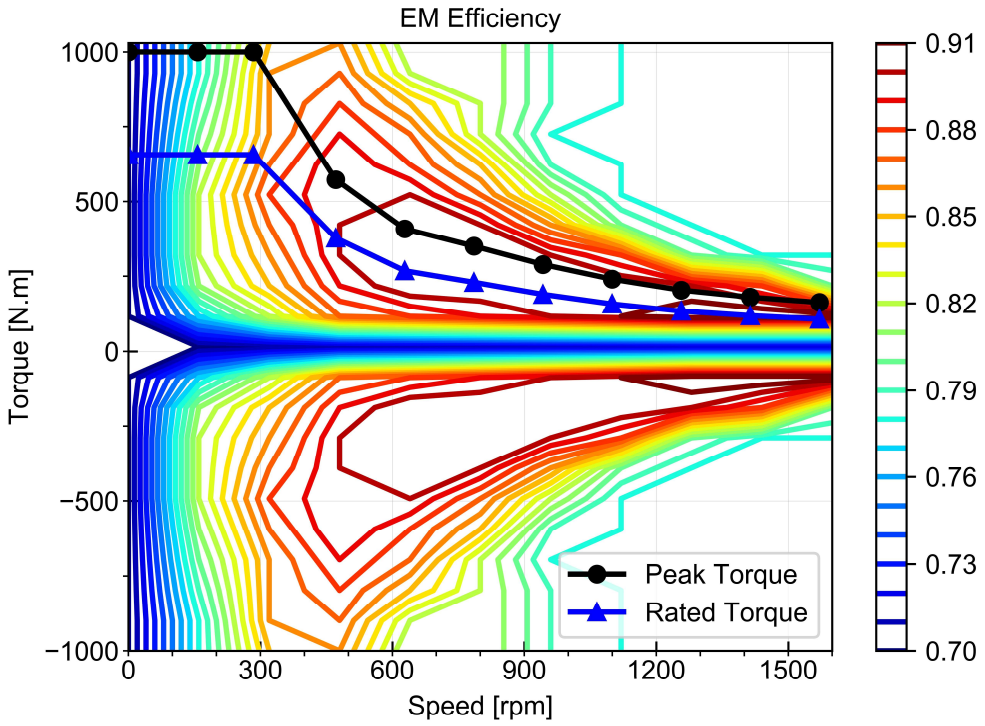


Figure 2.10: Electric machine efficiency map [86]

The EM torque (T_{EM}) is controlled for both modes by the Torque Control Strategy presented in section 2.4.3.3. Equations (2.19) to (2.22) determine the EM performance parameters, namely the electric current (I_{EM}) and the mechanical and electrical power of the machine ($P_{EM,mech}$, $P_{EM,elec}$).

$$P_{EM,mech} = \omega_{EM}.T_{EM} \tag{2.19}$$

$$P_{EM,elec} = P_{EM,mech}.\eta_{EM}^{k} \tag{2.20}$$

$$I_{EM} = \frac{P_{EM,elec}}{U_T} \tag{2.21}$$

$$k = \begin{cases} 1 \ (Traction) \\ -1 \quad (BER) \end{cases} \tag{2.22}$$

2.4.3.2 Wheels, Transmission and Braking Systems

The bus is considered to have two front wheels and two rear wheels. During traction, the transmission system, which consists of a reduction gear and a differential, transmits the traction torque from the EM to the rear wheels. There is no traction torque transmitted from the EM to the front wheels which makes this bus a Rear Wheel Drive (RWD) bus. The differential splits the torque between the rear wheels based on the slip ratio (s) defined as the torque ratio between the right rear wheel torque ($T_{W,RR}$) and the left rear wheel torque ($T_{W,RL}$).

During braking, there are 2 different modes to decelerate the bus, the first being friction braking and the second being regenerative braking through brake energy recovery (BER). Regenerative braking could only be applied to the rear wheels as they are coupled to the EM. On the contrary, friction braking could be applied to all rear and front wheels. The choice of the braking mode and braking torque values for each wheel is controlled by the TCS discussed thoroughly in section 2.4.3.3.

During Traction mode, equations (2.23) to (2.26) apply, where i_{RG} is the reduction gear ratio and i_{FD} is the final drive ratio.

$$T_{W,FR} = 0 \tag{2.23}$$

$$T_{W,FL} = 0 \tag{2.24}$$

$$T_{W,RR} = \frac{s}{1+s}.T_{EM}.i_{RG}.i_{FD} \tag{2.25}$$

$$T_{W,RL} = \frac{1}{1+s}.T_{EM}.i_{RG}.i_{FD} \tag{2.26}$$

During braking, equations (2.27) to (2.30) apply where the front wheels braking torque ($T_{Front,Br}$), rear wheels braking torque ($T_{Rear,Br}$), and regenerative brake torque (T_{Reg}) are all determined by the TCS.

$$T_{W,FR} = T_{Front,Br} \tag{2.27}$$

$$T_{W,FL} = T_{Front,Br} \tag{2.28}$$

$$T_{W,RR} = \frac{s}{1+s}.T_{Reg}.i_{RG}.i_{FD} + T_{Rear,Br} \tag{2.29}$$

$$T_{W,RL} = \frac{1}{1+s}.T_{Reg}.i_{RG}.i_{FD} + T_{Rear,Br} \tag{2.30}$$

Consequently, the total force propelling or braking the bus is expressed in equation (2.31).

$$F_{Total} = \frac{\sum T_W}{r_W} \tag{2.31}$$

2.4.3.3 Torque Control Strategy

The TCS in electric powertrains must ensure that the driver torque demand, communicated through the acceleration and brakes pedals, is always met. The driver is modeled as a proportional integral derivative controller (PID) that has a reference velocity profile defined by the drive cycle. The PID compares the bus actual speed and reference speed and outputs the required torque in order to follow the reference speed. The TCS receives and analyses the driver torque to control the EM propulsion and braking torques accordingly. During traction, the TSC

mainly controls the EM torque to be equal to the driver torque demand respecting its maximum torque limitation. However, during braking, the TCS controls the frictional braking torque depending on the regenerative braking torque imposed by the EM and the driver torque demand as well. In addition to the EM maximum power and the battery maximum charging power, the regenerative braking torque also depends on the battery SOC. The TCS will ensure that the battery is not overcharged and will stop the BER if the battery SOC is at its maximum set value. Figure 2.11 explains the logic behind the TCS.

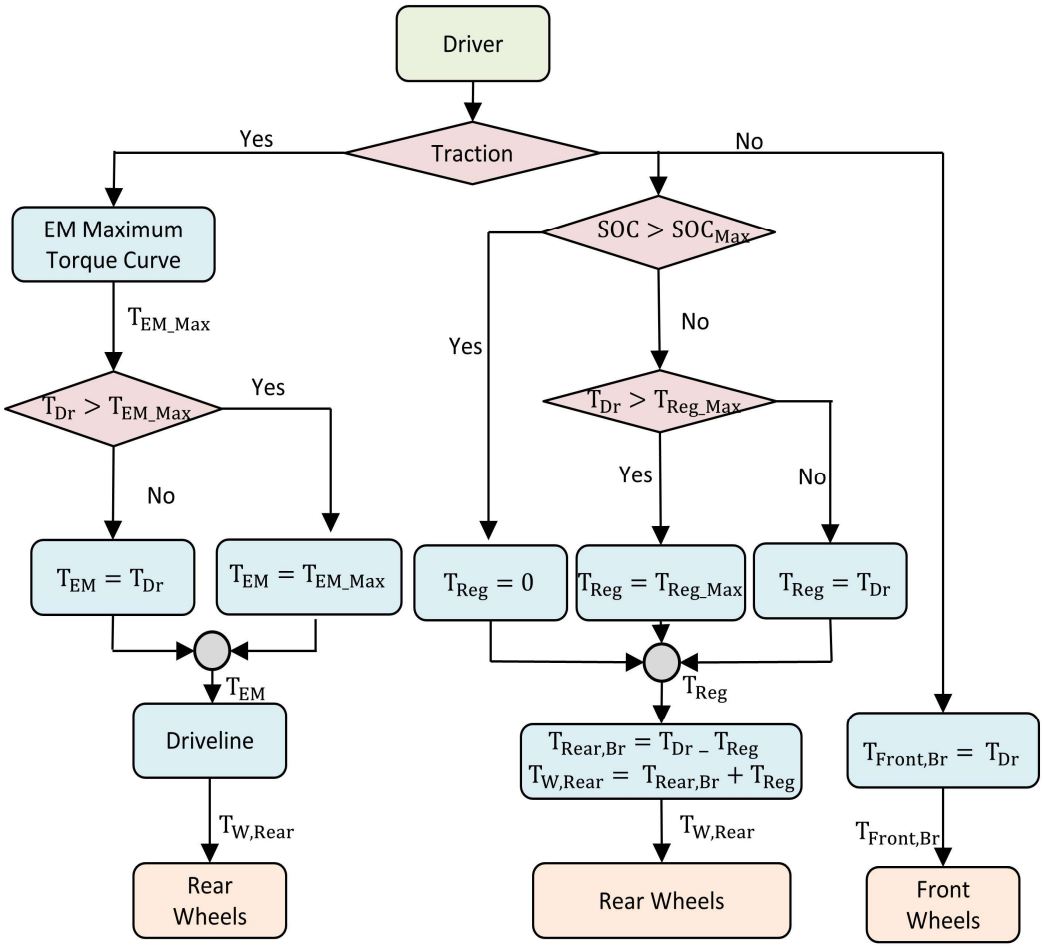


Figure 2.11: Torque control strategy flow chart

Finally, the propulsion system components are sized to meet public transit performance specifications set by the American Public Transportation Association (APTA) as shown in Table 2.11. A summary of components sizing is presented in Table 2.12. Appendix D provides details regarding the propulsion system components sizing.

Table 2.11: APTA Standards and performance specifications for public transit vehicles [87]

Top Speed	Maintain a speed of 105 *km/h* on a straight level road	
Gradeability	Maintain a speed of 65 *km/h* on a 2.5% ascending grade Maintain a speed of 25 *km/h* on a 10% ascending grade	
Acceleration	Speed (*km/h*)	Maximum time (s)
	16	5
	32	10
	48	18
	64	30
	80	60
	105	-

Table 2.12: Summary of components sizing

Component	Sizing Parameters	
Electric Machine	Rated Power	135 *kW*
	Maximum Continuous Torque (Rated Torque)	650 *N.m*
	Maximum Transient Torque (Peak Torque)	1000 *N.m*
Transmission	Reduction Gear Ratio	5.5
	Final Drive Ratio	5

2.4.4 Cabin Thermal Load

The thermal load in a BEB should be assessed to better understand its impact on the BEB driving range, given the significant incurred energy consumption. This section introduces the thermal comfort conditions standards and regulations inside a bus cabin followed by the cabin thermal load model.

2.4.4.1 Thermal Comfort

Thermal comfort is defined by ASHRAE as "the condition of mind that expresses satisfaction with the thermal environment and is assessed by subjective evaluation" [88]. Several parameters define thermal comfort conditions inside bus cabins. These conditions are classified under two main categories: (1) cabin related parameters and (2) HVAC unit related parameters. Table 2.13 summarizes thermal comfort conditions inside BEB cabins. It is important to mention that these conditions are defined during heating whereas during cooling, thermal comfort conditions need further investigation, however, the cabin temperature is to be maintained between 23 °*C* and 26 °*C*.

Table 2.13: Thermal comfort conditions in buses [87], [88]

	Parameters	Conditions
Cabin	Temperature	19℃ - 23 *°C*
	Convergence Time: time needed to reach the set cabin temperature	$T_{ext} > 0$ *°C* → 10 *mins* $T_{ext} < 0$ *°C* → 20 *mins*
	Relative Humidity	30% - 50%
	Maximum CO_2 Concentration	1000 *ppm*
HVAC unit	Maximum blown air temperature	49 *°C*
	Minimum fresh airflow per passenger	15 *cfm*
	Maximum blown air velocity	0.508 *m/s*

2.4.4.2 Model

A cabin thermal model is developed in [89], [90] for an electric vehicle (EV) using Dymola-Modelica software. The model is further developed in this thesis to fit an electric bus application. The proposed model is a combination of multiple sub-models that interact with each other by means of heat transfer. The cabin model consists of four main sub-models: (1) cabin interior, (2) cabin walls, (3) passengers, and (4) cabin internal materials. This model estimates the temperature of the bus cabin by considering the different modes of heat exchange that take place. The importance of this model lies in the fact that the amount of energy needed to heat up or cool down the bus cabin directly depends on the heat transfer between the bus cabin and its surroundings.

The cabin interior is modeled as a single thermal node using a mono-zonal approach that considers both the transient and steady-state phases. The air volume inside the cabin is represented as a single node with uniform temperature which is a convenient energy assessment methodology for the thermal load in EV [91]. Even though a mono-zonal single node model is not very appropriate for indoor thermal comfort study of a bus, the model remains a good initial representation to study the impact of the cooling and heating loads on total energy consumption. The cabin interior experiences three different heat exchanges: (1) heat exchange with the environment through the cabin walls, (2) heat exchange with passengers occupying the cabin, and (3) heat exchange with internal cabin materials such as the seats and dashboards. Figure 2.12 introduces the cabin thermal scheme.

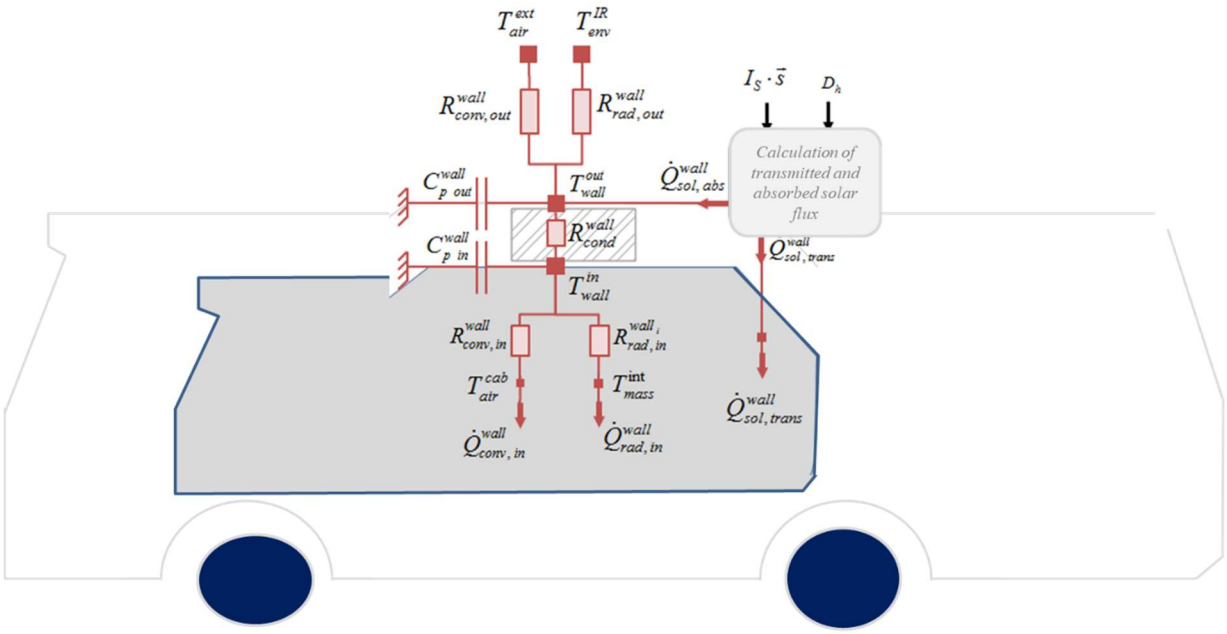


Figure 2.12: BEB cabin thermal scheme [*]

[*] This figure is taken from [90]. The scheme is slightly modified; however, the content is preserved.

The wall sub-model is an array of walls representing the bus body (Top, bottom, two sides, front, and back). The walls are of two types, either opaque (bus body metal) or glazing (bus glass). The total areas of these two types of walls are determined by the bus geometry as shown in Table 2.15. Each wall has two sides, an outer side facing the environment and an inner side facing the cabin interior. Through the walls, six modes of heat exchange are considered in this model: (1) convection between the wall outer side and the environment, (2) conduction from the wall outer side to the wall inner side, (3) convection between the wall inner side and the cabin interior, (4) incident radiation, (5) transmitted radiation heat flow through glazing and (6) absorbed radiation heat flow in glazing. The heat exchange by convection between the wall outer side and the environment considers the bus variable speed during its trip.

- **Thermal balance at the wall outer surface node T_{wall}^{out}**

Equation (2.32) shows the thermal balance at the wall outer surface:

$$C_{p\ out}^{wall} \frac{d(T_{wall}^{out})}{dt} = \dot{Q}_{conv,out}^{wall} + \dot{Q}_{rad,out}^{wall} - \dot{Q}_{cond}^{wall} + \dot{Q}_{sol,abs}^{wall} \quad (2.32)$$

The convection term $\dot{Q}_{conv,out}^{wall}$ between the wall outer surface and the exterior environment is expressed in equation (2.33):

$$\dot{Q}_{conv,out}^{wall} = h_{conv}^{out}.A_{wall}.(T_{air}^{ext} - T_{wall}^{out}) \quad (2.33)$$

Due to the cabin complex geometry, it is difficult to estimate the convection coefficients h_{conv}^{out}. In addition, a mix of natural and forced convection occur which complicates the calculation of the convection coefficients even more. Equation (2.34) is used and Brèque and Nemer [89] thoroughly explain this choice. The constants *a*, *b* and *c* are dependent on the wall geometry and *v* is air velocity.

$$h_{conv}^{out} = a + b.v^{c} \quad (2.34)$$

The radiation term $\dot{Q}_{rad,out}^{wall}$ and the conduction term $\dot{Q}_{cond}^{wall}$ from the wall outer surface to the wall inner surface are expressed in equations (2.35) and (2.36) respectively:

$$\dot{Q}_{rad,out}^{wall} = \varepsilon_{wall}^{out}.A_{wall}.({T_{env}^{IR}}^{4} - {T_{wall}^{out}}^{4}) \quad (2.35)$$

$$\dot{Q}_{cond}^{wall} = \frac{1}{R_{cond}^{wall}}.\left(T_{wall}^{out} - T_{wall}^{in}\right) \quad (2.36)$$

- **Thermal balance at the wall inner surface node T_{wall}^{in}**

Equation (2.37) shows the thermal balance at the wall inner surface:

$$C_{p\ in}^{wall}\frac{d(T_{wall}^{in})}{dt} = \dot{Q}_{cond}^{wall} - \dot{Q}_{conv,in}^{wall} - \dot{Q}_{rad,in}^{wall} \quad (2.37)$$

The convection term $\dot{Q}_{conv,in}^{wall}$ between the wall inner surface and cabin air is expressed in equation (2.38) and the corresponding convective heat coefficient h_{conv}^{in} is shown in equation (2.39) according to [92]:

$$\dot{Q}_{conv,in}^{wall} = h_{conv}^{in}.A_{wall}.(T_{wall}^{in} - T_{air}^{cab}) \quad (2.38)$$

$$h_{conv}^{in} = 3.\left|T_{wall}^{in} - T_{air}^{cab}\right|^{\frac{1}{3}} \quad (2.39)$$

The radiation term between the wall inner surface and the cabin internal materials is shown in equation (2.40):

$$\dot{Q}_{rad,in}^{wall} = \varepsilon_{wall}^{in}.F_{wall-int}.A_{wall}.\sigma.({T_{wall}^{in}}^{4} - {T_{mass}^{int}}^{4}) \quad (2.40)$$

Finally, Table 2.14 describes the rest of the variables presented in the thermal balance equations. Table 2.15 and Table 2.16 summarizes the bus cabin geometry.

Table 2.14: Thermal balance additional equations

Variable	Equation
$C_{p\,out}^{wall}$: heat capacity of the wall outer surface	$C_{p\,out}^{wall} = \delta_{skin}^{out}.A_{wall}.\rho_{skin}^{out}.c_{p\,skin}^{out} + \frac{\delta_{lining}}{2}.A_{wall}.\rho_{lining}.c_{p\,lining}$ skin refers to either metal or glass
$C_{p\,in}^{wall}$: heat capacity of the wall inner surface	$C_{p\,in}^{wall} = \delta_{skin}^{in}.A_{wall}.\rho_{skin}^{in}.c_{p\,skin}^{in} + \frac{\delta_{lining}}{2}.A_{wall}.\rho_{lining}.c_{p\,lining}$
T_{env}^{IR}: Infrared Environmental Temperature	$T_{env}^{IR} = 0.0552.T_{air}^{ext\,1.5}$ for surfaces facing the sky [93] $T_{env}^{IR} = T_{air}^{ext}$ for other surfaces
R_{cond}^{wall}: Wall conductive thermal resistance	$R_{cond}^{wall} = \frac{\delta_{skin}^{out}}{A_{wall}.k_{skin}^{out}} + \frac{\delta_{lining}}{A_{wall}.k_{lining}} + \frac{\delta_{skin}^{in}}{A_{wall}.k_{skin}^{in}}$
$F_{wall-int}$: form factor (geometric)	$F_{wall-int} = 0.75$ (assumption similar to [90])

Table 2.15: Bus geometry

Wall	Dimensions	Glazing		Metal		Lining
		Area (A_{Wall})	Thickness (δ)	Area (A_{Wall})	Thickness (δ)	Thickness (δ)
Top/Bottom	12 *m* x 2.55 *m*	0	4 *mm*	61.2 m^2	3 *mm*	13 *mm* / 15 *mm*
Sides	12 *m* x 3.2 *m*	40 m^2		24 m^2		75 *mm*
Back	3.2 *m* x 2.55 *m*	3.5 m^2		4.6 m^2		-
Front	3.2 *m* x 2.55 *m*	6.1 m^2		2 m^2		-

Table 2.16: Walls thermal properties

	Density (ρ)	Specific heat capacity c_p	Thermal conductivity (k)	Emissivity (ε)	Transmissivity (τ)	Absorptivity (α)
Glazing	2530 $kg.m^3$	795 $J.kg^{-1}.K^{-1}$	1.4 $W.m^{-1}.K^{-1}$	0.85	0.85	0.08
Metal	7800 $kg.m^3$	500 $J.kg^{-1}.K^{-1}$	25 $W.m^{-1}.K^{-1}$	0.85	-	0.8
Lining	250 $kg.m^3$	700 $J.kg^{-1}.K^{-1}$	.08 $W.m^{-1}.K^{-1}$	-	-	-

- **Thermal balance at the internal mass node T_{mass}^{int}**

The cabin internal material sub-model is a thermal node with a certain heat capacity and geometry that interacts with the cabin interior through convection and radiation as shown in equation (2.41).

$$C_{p\,in}^{int}\frac{d(T_{mass}^{int})}{dt} = \dot{Q}_{conv}^{int} + \sum_{i=1}^{nWall}(\dot{Q}_{sol,tra}^{wall} + \dot{Q}_{rad,in}^{wall}) \quad (2.41)$$

The absorbed and transmitted solar flux ($\dot{Q}_{sol,abs}^{wall}$ and $\dot{Q}_{sol,trans}^{wall}$) through the walls are explained in [90].

- **Energy balance at the cabin control volume**

The energy balance equation applied at the cabin air control volume is shown in (2.42)

$$V_{air}^{cab}.\left(u_{air}^{cab}.\frac{\partial\rho_{air}^{cab}}{\partial t} + \rho_{air}^{cab}.\frac{\partial u_{air}^{cab}}{\partial t}\right) = \sum_{i=1}^{nWall}\dot{Q}_{conv,in}^{wall} - \dot{Q}_{conv}^{int} + \dot{Q}_{pass} + \dot{Q}_{HVAC} + \dot{Q}_{doors} \quad (2.42)$$

The passengers' heat rejection $\dot{Q}_{pass}$ represents both sensible and latent heat rejection and it is dependent on the number of passengers in the bus as shown in equation (2.43) where $\dot{Q}_{pass}^{sens}$ is constant equals to 70 W and $\dot{Q}_{pass}^{lat}$ equals to 35 W [94]:

$$\dot{Q}_{pass} = n_{pass}.(\dot{Q}_{pass}^{sens} + \dot{Q}_{pass}^{lat}) \quad (2.43)$$

In addition, during the bus daily operation, doors opening has a considerable influence on the cabin temperature due to their frequent openings. This results in an increased energy demand that cannot be neglected. This is considered by adding a variable heat flow rate $\dot{Q}_{doors}$ in/out of the cabin which depends on the ambient temperature, bus cabin temperature, and the duration of open-doors [95]. Figure 2.13 shows the heat losses due to the doors opening.

Finally, $\dot{Q}_{HVAC}$ is the sum of the different heat flux interactions that take place between the HVAC unit and the bus cabin, and it includes: (1) sensible heat rejection/extraction ($\dot{Q}_{HVAC}^{sens}$), (2) latent heat rejection due to humidity condensation at the evaporator ($\dot{Q}_{HVAC}^{lat}$), and (3) ventilation load due to fresh air circulation ($\dot{Q}_{air}^{fresh}$). These terms are explained in section 2.4.5.2 through equations (2.45) to (2.48).

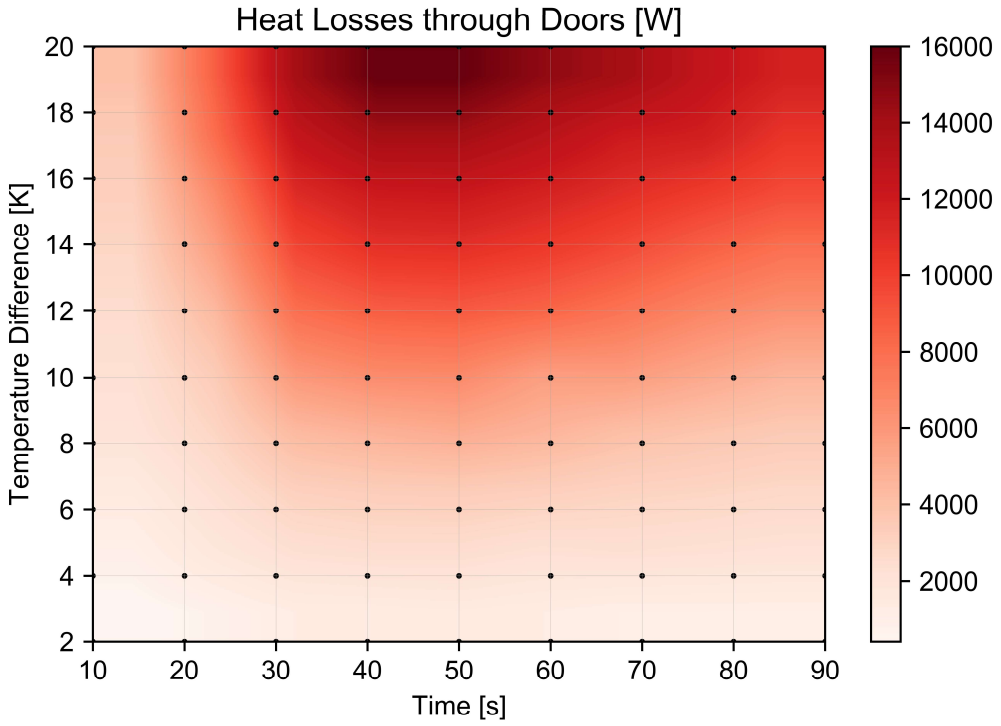


Figure 2.13: Mean heat losses due to doors opening

- **Mass balance at the cabin control volume**

The mass balance equation applied at the control volume is shown in equation (2.44)

$$V_{air}^{cab} . \left(\frac{\partial \rho_{air}^{cab}}{\partial t} \right) = \dot{m}_{air}^{blown} - \dot{m}_{air}^{fresh} - \dot{m}_{air}^{rec} \qquad (2.44)$$

The mass balance does not consider infiltration through windows or due to doors opening.

2.4.5 HVAC Unit

The HVAC unit should meet the bus cabin thermal needs by supplying or extracting heat and ventilating the cabin to sustain thermal comfort conditions. Several HVAC technologies are being used in bus applications. Electric resistance, positive temperature coefficient (PTC), diesel heaters, and heat pumps are commonly used heating technologies, whereas air conditioner (AC) is the main cooling technology [23].

Air source HP is the current state of the art heating technology for EV due to their superior energy performance [96]. A HP operation can be reversed to consider cooling as well. This is achieved by using a set of valves to change the working fluid flow. In this section, the reversible HP technology is presented first. The proposed model is then introduced followed by the HP control scheme.

2.4.5.1 Technology

A reversible HP is used to heat or cool the bus cabin. During heating, the reversible HP operation is exactly similar to any HP. However, during cooling, it operates as an AC using a 4-way valve which reverses the refrigerant flow. Figure 2.14 and Figure 2.15 show the reversible HP configuration in heating and cooling modes, respectively.

During heating, the fresh air flows into the ERV (Energy Recovery Ventilator) where it exchanges heat with the return air from the cabin. Fresh air is then mixed with the recirculated air (a fraction of the return air) and flows to the internal heat exchanger, which acts as a condenser in this case, where it gets heated further through heat exchange with the refrigerant. The heated air can be reheated again using an auxiliary heater before blowing it to the cabin. This heater could be simply bypassed. Meanwhile, the refrigerant follows the conventional vapor compression cycle (VCC) where the external heat exchanger acts as an evaporator.

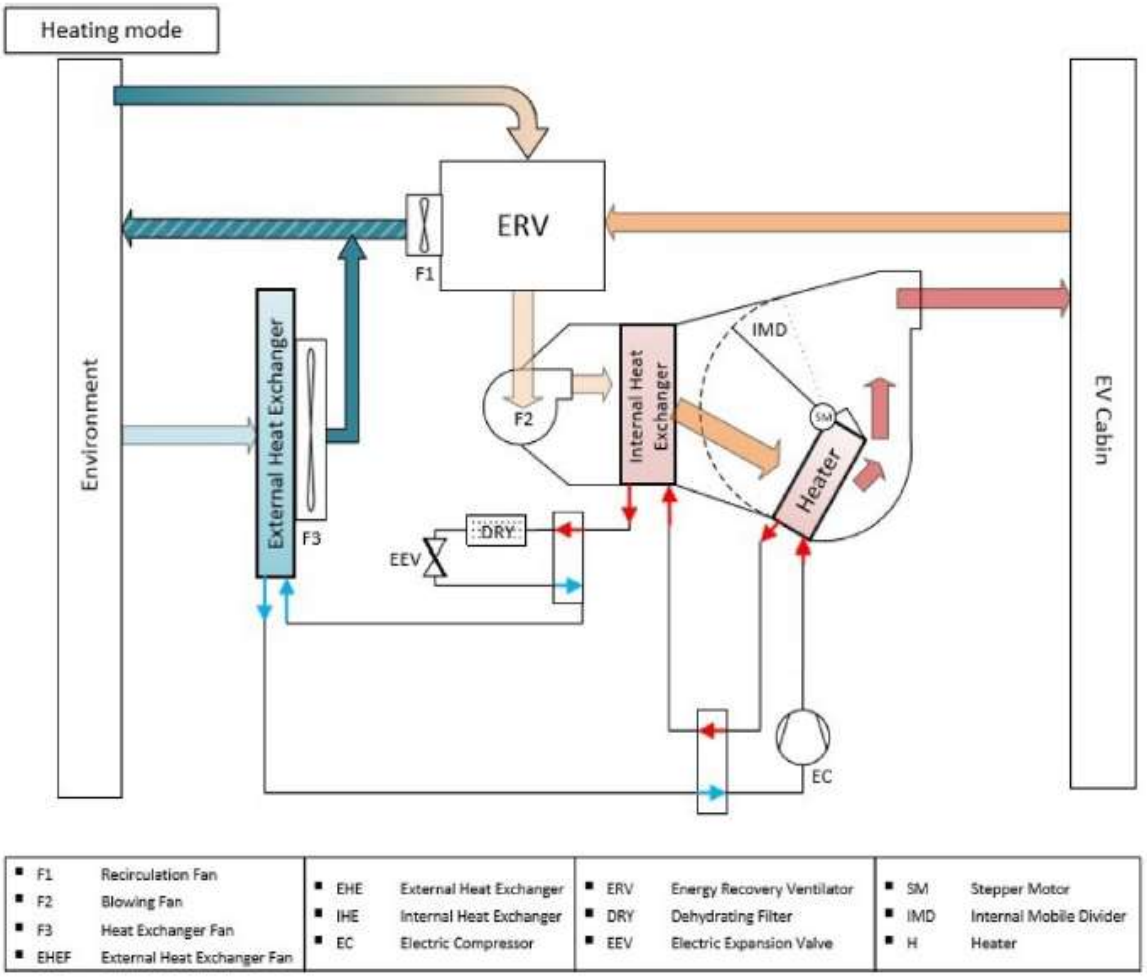


Figure 2.14: Reversible HP in Heating Mode [96]

During cooling, the 4-way valve changes the direction of the compressed refrigerant, so it passes through the external heat exchanger, and thus the external heat exchanger acts as a condenser in this case. The discharged refrigerant undergoes expansion and cools down the air passing through the internal heat exchanger which acts as an evaporator. It is possible to heat up the cold air using the auxiliary heater. This could be beneficial if the compressor supplies excessive power at its minimum speed which might be encountered during moderate-hot weather conditions.

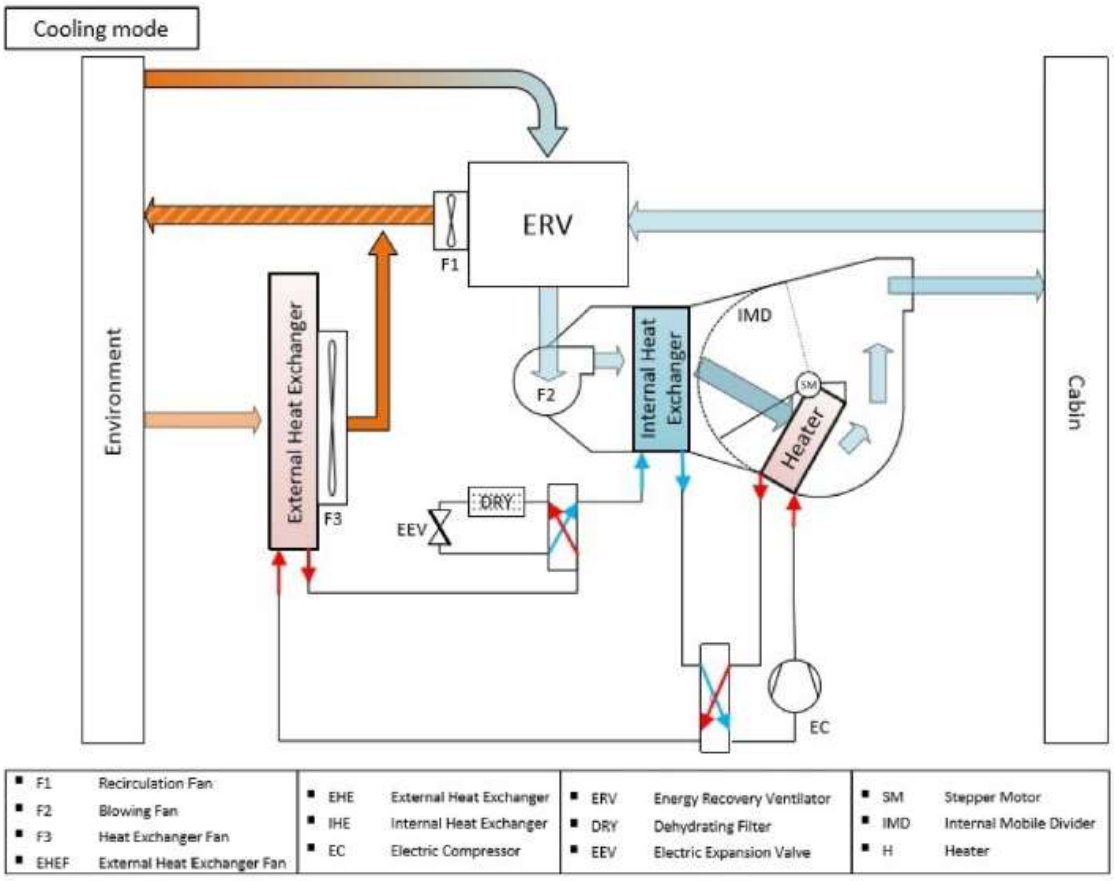


Figure 2.15: Reversible HP in cooling mode [96]

R1234yf is the chosen working refrigerant for the HP. R1234yf has zero ODP (Ozone Depletion Potential) and a low GWP (Global Warming Potential). In addition, it is a good replacement for refrigerant R134a as they carry similar physical properties [97]. The interest in replacing refrigerant R134a is due to the European regulations that ban the use of R134a and propose R1234yf as its replacement in mobile air conditioning applications [97]. Appendix A explains in detail the VCC.

2.4.5.2 Model

The complete HVAC unit consists of the 2 reversible heat pumps, the air circulation system, and the battery thermal management system (BTMS). Figure 2.16 introduces the HVAC unit scheme. This section explains the modeling of the HP, air recirculation system, and the BTMS.

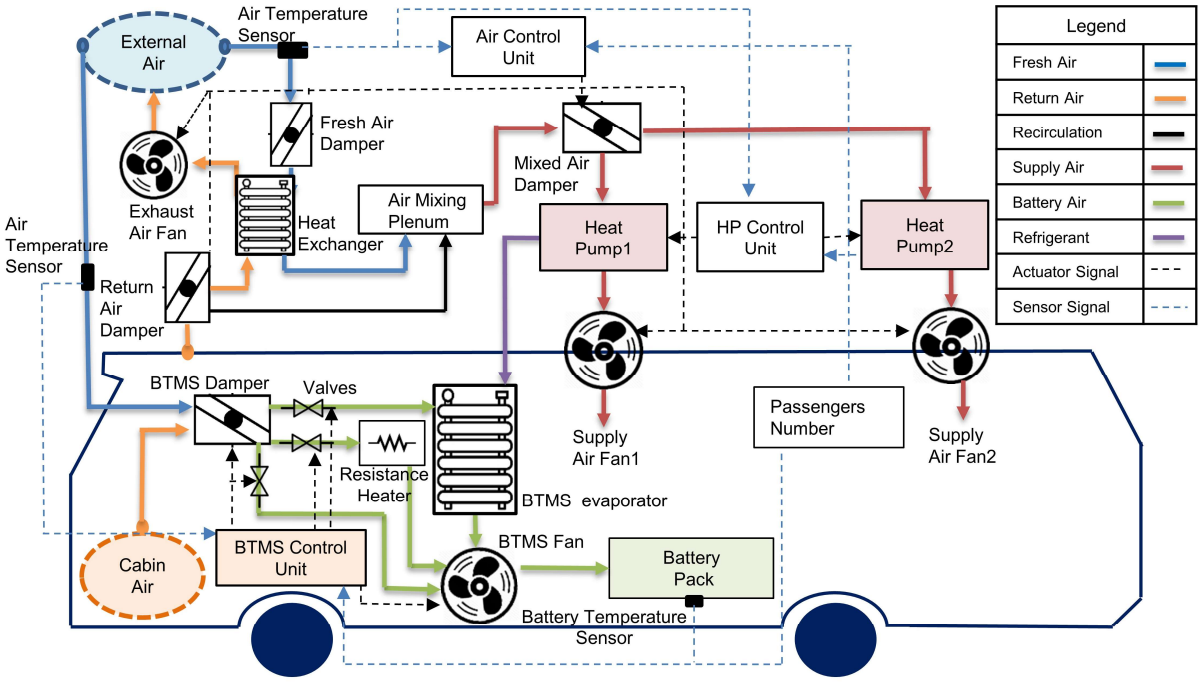


Figure 2.16: HVAC unit scheme

2.4.5.2.1 Reversible Heat Pump

Thermal load calculations for a bus of similar specifications show that the maximum required heating capacity is around 35 kW [15]. In BEB, the use of multiple HP is common as there are many buses equipped with more than 1 HP. 2 reversible HPs are considered, each rated at 20 kW, placed in the middle and the back of the bus. It is assumed that the 2 HPs share the thermal load equally. 5 kW is added to the HP capacity to supply the BTMS with the required thermal load whenever needed.

Each HP is composed of a compressor, expansion valve, 2 heat exchangers, in addition to the blower and the evaporator fans. A summary of these components specifications is shown in Table 2.17. These components are chosen to meet the maximum thermal load.

The model is developed in Dymola using the built-in TSMedia AC library. All the HP components are chosen from this library without any modification. The total HVAC unit heat flux ($\dot{Q}_{HVAC}$) is expressed in equation (2.45).

Table 2.17: Summary of HP components

Compressor	Scroll (Hermetic) variable speed electric compressor Displacement: 121 cm^3/rev
Heat Exchangers	Multi-port extruded tube crossflow heat exchanger Heat exchange area: 0.2067 m^2
Expansion Valve	Thermostatic expansion valve
Blower/ Fan	Centrifugal fans Operating frequency: 60 – 80 Hz Maximum air volume: 4000 m^3/h

The heat exchanger (evaporator/condenser) is modeled using the Logarithmic Mean Temperature Difference (LMTD) approach as shown in (2.46), where h_{exch} is the heat transfer coefficient of the heat exchanger and A_{exch} is the contact area between the air and the refrigerant through the tube walls. Typical values of h_{exch} are considered as inputs to the model (100 $W/K.m^2$ for automobile applications) [90]. $\dot{Q}_{HVAC}^{lat}$ is expressed in equation (2.47) with l_{lv} being the latent heat of vaporization of water and $\dot{m}_{Water}^{Con}$ is the mass of condensed water. $\dot{Q}_{air}^{fresh}$ is the ventilation load expressed in equation (2.48).

$$\dot{Q}_{HVAC} = \dot{Q}_{HVAC}^{sens} + \dot{Q}_{HVAC}^{lat} + \dot{Q}_{air}^{fresh} \quad (2.45)$$

$$\dot{Q}_{HVAC}^{sens} = h_{exch}.A_{exch}.LMTD(T_{air}^{mix}, T_{exch}^{out}) \quad (2.46)$$

$$\dot{Q}_{HVAC}^{lat} = l_{lv}.\dot{m}_{Water}^{Con} \quad (2.47)$$

$$\dot{Q}_{air}^{fresh} = \dot{m}_{air}^{fres}\ .Cp.(T_{Cabin} - T_{External}) \quad (2.48)$$

Detailed equations within these models are presented in Appendix B.

The air circulation system (ACS) is responsible for supplying/discharging conditioned air to/from the bus cabin. The ACS is mainly composed of a set of fans, dampers, and mixers. As shown in Figure 2.16, two air supply fans provide heated/cooled air to the cabin, 1 exhaust air fan that discharges air from the cabin and 2 fans (masked inside the HP block) draw fresh air from the exterior. The fan model is presented in Appendix B. In addition, a set of dampers is used to regulate airflow. A fresh air damper is used to stop and regulate the fresh air flow rate. Another damper (mixed air splitter damper) is used to split the mixed air flowing from the mixing plenum into two flows supplying both HPs. A return air damper is installed to discharge air from the cabin and split it into two flows. A fraction of the airflow is recirculated to the bus

cabin where it gets mixed with the fresh airflow in the air mixing plenum. The remaining exhaust air flows through an air-air heat exchanger where the fresh air flow recuperates part of the remaining exhaust air energy. Mixed air properties are calculated according to equations (2.49) and (2.50) derived from the energy and mass balance of mixing 2 airstreams where '*rec*' is cabin air recirculation rate which is a control variable.

$$T_{air}^{mix} = (1 - rec).T_{air}^{fres} + rec.T_{air}^{cabin} \quad (2.49)$$

$$w_{air}^{mix} = (1 - rec).w_{air}^{fr} + rec.w_{air}^{cabin} \quad (2.50)$$

The temperature of the fresh air (T_{air}^{fres}) is not necessarily equal to the exterior temperature as it recuperates the heat of the exhaust airflow.

The air mass flow rate blown into the cabin is another control variable in the HVAC unit. It is the sum of the fresh air and recirculated airflow rates as shown in equation (2.51).

$$\dot{m}_{air}^{blown} = \dot{m}_{air}^{fres} + \dot{m}_{air}^{rec} \quad (2.51)$$

Consequently, the fresh air and recirculated air mass flow rates are calculated according to equations (2.52) and (2.53).

$$\dot{m}_{air}^{fres} = (1 - rec).\dot{m}_{air}^{blown} \quad (2.52)$$

$$\dot{m}_{air}^{rec} = rec\ .\ \dot{m}_{air}^{blown} \quad (2.53)$$

2.4.5.2.2 Battery Thermal Management System

The final component of the HVAC system is the battery thermal management system (BTMS). As discussed in section 2.4.2.4 and shown in Figure 2.16, the BTMS is composed of a fan and an evaporator, and the generic models of these components are presented in Appendix B. The BTMS air damper determines the air source (cabin, exterior, or conditioned exterior/cabin air) to be blown over the battery cells. An electric resistance heater is used to heat up extremely cold air during winter.

Finally, the total power consumption of the HVAC unit is the sum of powers needed to operate the two HP, ACS, and BTMS as shown in equation (2.54).

$$P_{HVAC} = \frac{\dot{W}_{comp.} + \sum P_{fans}}{\eta_{EM}} + P_{resistance} \quad (2.54)$$

2.4.5.2.3 Control Scheme

As shown in Figure 2.16, there are three control units in the HVAC system: (1) Air control-unit, (2) HP control-unit, and (3) BTMS control-unit. Each unit is responsible for controlling a

set of variables in the HVAC system. Table 2.18 summarizes the variables controlled by the different control units.

Table 2.18: Variables controlled by the HVAC system 3 control units

Control Unit	Variables	Description/Impact
Air control unit	- Supply air fans speeds:	Air mass flow rate into the cabin
	- External fans speeds	Air mass flow rate over external heat exchangers
	- Exhaust air fan speed:	Discharge air flow rate
	- Return air damper:	Cabin air recirculation rate
	- Fresh air damper:	Fresh air flow rate
HP control unit	- Compressor Speed	Heat rejection/extraction rate to/out of the cabin
	- Expansion valve	Super heat-level
BTMS control unit	- BTMS fan speed	Airflow rate over the battery cells
	- BTMS damper	Air source to cool the battery cells
	- Electric resistance	Temperature of airflow rate over the battery cells

The air control unit and the HP control unit are directly related as they both control the heat rejection/extraction rate from/to the bus cabin. The default controllers in buses are ON-OFF controllers. This approach aims at maintaining the cabin temperature at the desired value within certain low and high limits by controlling the compressor speed. During heating, the controller turns the compressor ON until the cabin temperature reaches its high limit (23°*C*) and then the compressor is turned off. When cabin temperature drops below its low limit (19 °*C*), the compressor is turned ON again. The speed of the compressor is dependent on the exterior temperature. On the other hand, during cooling, the compressor will be turned OFF when cabin temperature reaches the lower limit (defined to be 23 °*C*) and will be turned ON back again when cabin temperature exceeds its higher limit (27 °*C*).

The remaining control parameters are controlled as follows:

a. All fans operate at their maximum speeds providing maximum airflow rate.
b. Fresh air damper is controlled to provide the minimum amount of required fresh air depending on the number of passengers inside the bus as shown in equation (2.55).

$$\dot{m}_{air}^{fresh} = n_{pass}.\dot{m}_{air,min\ per\ passenger}^{fres} \quad (2.55)$$

However, the number of passengers occupying the bus varies throughout the day and during the bus trips. For this sake, 4 levels of passengers' occupancy are defined: (1) Low level of occupancy (less than 10 passengers), (2) medium-low level of occupancy (from 10 to 25 passengers), (3) medium-high level of occupancy (from 25 to 40 passengers) and (4) high level of occupancy (greater than 40 passengers). At each level of occupancy, the minimum amount of fresh air is taken as the upper limit of the range. There are many technologies nowadays that allow an accurate estimation of the number of passengers occupying the bus, such as counting the passage of passengers through entrance and exit doors, or by estimating the weight of the passenger compartment in the bus.

c. Return air damper circulates the remaining airflow rate to be supplied to the cabin.
d. Expansion valve opening is controlled to ensure sufficient levels of super-heat for the refrigerant.
e. At moderate hot/cold conditions, the minimum compressor speed may still supply excessive power, in such cases, the mass flow rates are reduced to lower values (not maximum fans speed).
f. The returning air damper should ensure that the exhaust airflow rate is equal to the fresh air flow rate as shown in equation (2.56).

$$\dot{m}_{air}^{exhaust} = \dot{m}_{air}^{fresh} \tag{2.56}$$

When the compressor is in the OFF state, the air circulation system remains ON to ensure cabin ventilation.

Concerning the BTMS control unit, the required air mass flow rate over the battery cells is calculated function of the number of cells in the battery (different mass flow rates for different battery sizes) in an approach similar to [69]. The BTMS fan speed is adapted to provide this mass flow rate.

$$\dot{m}_{air}^{BTMS} = N_s . N_P . \dot{m}_{air\ per\ cell}^{BTMS} \tag{2.57}$$

The choice of the air source is complicated as it directly depends on the exterior temperature and the amount of fresh air entering the bus cabin (number of passengers). In addition, the decision to cool the air through the evaporator or to heat it using the electric resistance heater is also dependent on the BTMS air temperature. Figure 2.17 presents the BTMS control scheme.

First, the parameter λ is defined as the ratio of the BTMS required airflow rate to the ratio of the fresh air flow rate into the bus cabin as shown in equation (2.58).

$$\lambda = \frac{\dot{m}_{air}^{BTMS}}{\dot{m}_{air}^{fresh}} \tag{2.58}$$

The BTMS control scheme is dependent on the exterior temperature and the fresh air flow rate to the cabin. At high exterior temperatures above 35 °*C*, the BTMS air flow rate is cooled to 10 °*C*. The choice of the air source depends on the ratio λ. For λ values lower than 1, 100% of the BTMS airflow is drawn from the cabin. On the other hand, for λ values higher than 1, this implies that the needed BTMS air flow rate is higher than the fresh air flow rate. In this case, only a fraction of the BTMS air flow rate is drawn from the cabin ($\frac{1}{\lambda}$) which is equal to the entire fresh air flow rate. The deficit is compensated by drawing air from the exterior.

For exterior temperatures between 20 °*C* and 30 °*C*, the control strategy is similar to the previous case, however, air cooling reaches 20 °*C* due to the lower exterior temperature.

When the exterior temperature is between 10 °*C* and 20 °*C*, no cooling or heating is required and 100% of the BTMS air flow rate is drawn from the exterior.

Finally, for temperatures below 10 °*C*, heating is required when λ is higher than 1 as the BTMS air temperature might drop below 10°*C* at extreme cold conditions due to mixing cabin air and ambient air.

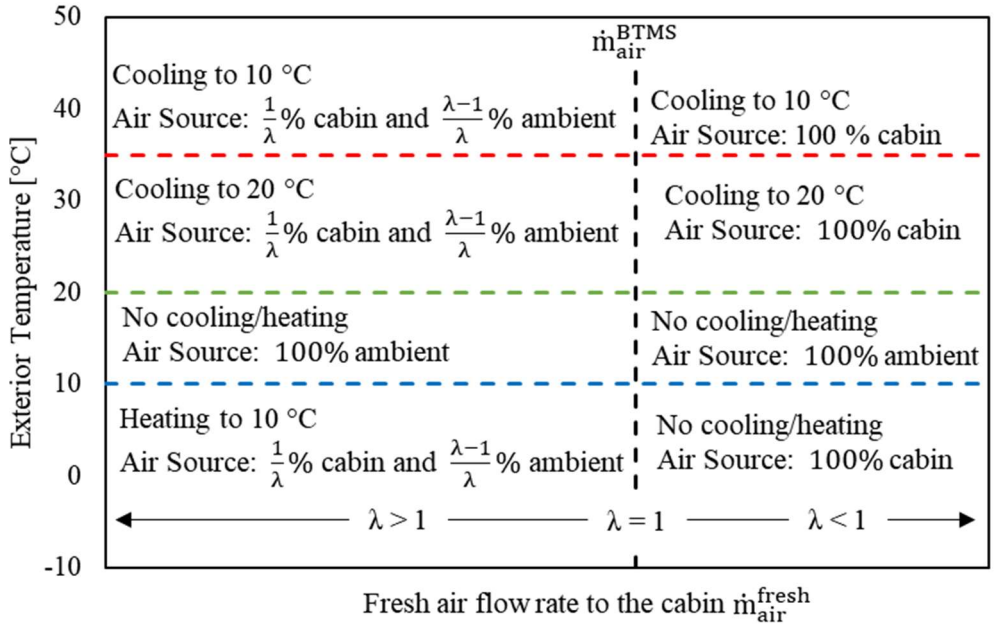


Figure 2.17: BTMS control scheme

2.4.6 Auxiliaries

The auxiliaries have always been neglected or simplified in the energy consumption calculation of EV. However, for BEB, their energy consumption is significant, and thus, a dynamic modeling approach is considered. This section introduces the models of the pneumatic, electric, and hydraulic auxiliaries.

2.4.6.1 Pneumatic Auxiliaries

Pneumatic auxiliaries in BEB are less likely to be found compared to DB. However, one very important feature that still operates using a pneumatic system is the service brakes. Pneumatic brakes (Air Brakes) are friction brakes that use the energy stored in compressed air at around 10 bars to press the pistons, so they apply the needed pressure on the brakes' pads to decelerate the bus. The pneumatic auxiliary's energy consumption is then dependent on the driver's behavior. An aggressive driving behavior with frequent decelerations will result in higher pneumatic auxiliary consumption.

The pneumatic system in BEB is formed of a compressor, an air tank to store compressed air, an electric machine to drive the compressor, and a foot valve that regulates the airflow as shown in Figure 2.18. In some applications, two or more air tanks are used to ensure safe operation in case of air leakage.

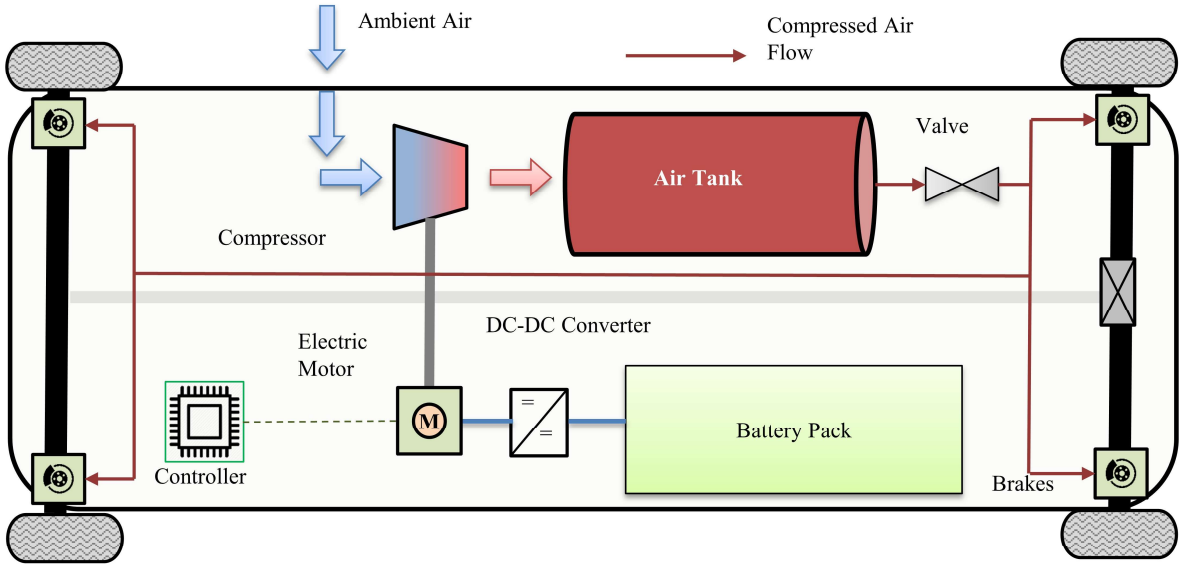


Figure 2.18: Schematic of the pneumatic system in BEB

The driver actuates the brakes pedal which results in opening the foot valve at a certain angle. This causes compressed air to flow from the air tank to press the brakes' pistons. The air

volumetric flow rate is dependent on the valve opening. Equation (2.59) describes this flow rate ($\dot{V}_{air}^{Br.}$) as function of the driver's braking torque ($T_{Dr,Br.}$), the maximum braking torque ($T_{Br.Max}$) and the maximum air flow rate through the valve ($\dot{V}_{air,max}^{Br.}$). The valve can supply up to 4 *L/s* of compressed air at 10 bars.

$$\dot{V}_{air}^{Br.} = \frac{T_{Dr,Br.}}{T_{Br.Max}} . \dot{V}_{air,max}^{Br.} \quad (2.59)$$

Being the most essential safety feature, the pneumatic system should always be capable of supplying enough compressed airflow to operate the service brakes as required. For this sake, it is essential to monitor the level of compressed air inside the air tank as shown in equation (2.60) where ($\dot{V}_{air}^{comp.}$) is the compressor volumetric flow rate to the air tank.

$$V_{air}^{Tank}(t) = V_{air}^{Tank}(0) + \int_0^t \left(\dot{V}_{air}^{comp.} - \dot{V}_{air}^{Br.}\right) . dt \quad (2.60)$$

An ON-OFF buffer controller controls the compressor to ensure that the air tank volume is always maintaining a minimum level of compressed air at 10 bars. This minimum threshold is set to be 50% of the maximum air tank volume. The compressor is a 2-cylinder piston compressor, directly belt-driven by a dedicated electric motor. When the air tank volume drops below 50% of its maximum volume, the compressor is turned ON at maximum speed until the air tank is full. The compressor can provide 240 *L/min* of compressed air consuming 2.7 *kW*. The electric motor driving the compressor operates at a fixed speed and constant efficiency of 80%. The pneumatic auxiliaries' power consumption is expressed in equation (2.61).

$$P_{Pneu} = \frac{P_{Comp.}}{\eta_{EM}} \quad (2.61)$$

2.4.6.2 Electric Auxiliaries

The electric auxiliaries in BEB are the doors, parking brakes, wipers, and lightings. These components are modeled as a power demand directly from the battery whenever actuated. The model receives the driver's commands to actuate these auxiliaries. For example, whenever there is a bus stop, the parking brakes are enabled, and the doors are opened. In addition, weather conditions determine if the wipers are actuated or not, and the lighting system on the bus is actuated at night. Table 2.19 quantifies these power demands according to [27]. These energy and power demands are met by means of an auxiliary electric motor consuming energy from the battery. The total electric auxiliaries' power consumption is shown in equation (2.62).

$$P_{Ele} = \frac{P_{Doors} + P_{PB} + P_L + P_W}{\eta_{EM}} \quad (2.62)$$

Table 2.19: Electric auxiliaries power demand whenever actuated

	Variable	Consumption	Process Duration [sec]
A pair of doors opening and closure	P_{Doors}	90 *W*	3
Parking brakes activation	P_{PB}	560 *W*	1
Lighting system	P_L	500 *W*	-
Wipers	P_W	500 *W*	-

2.4.6.3 Hydraulic Auxiliaries

The main hydraulic auxiliaries on a bus are the steering pump and the suspension system. The steering pump must always provide the required hydraulic pressure in the bus steering system. The power consumption of the steering pump can be characterized as function of the bus speed [27]. Figure 2.19 shows the used steering pump characteristics.

The suspension system is responsible for kneeling and lifting the bus front at the stops. This feature aims at easing passengers' entrance and exit to/from the bus. A hydrostatic system is used to lift the bus using pressurized liquid. The height of the bus floor changes by ($\Delta h = 65$ *mm*) for the considered bus. Equation (2.63) describes the suspension system power consumption. M_{Front} is the bus front weight which corresponds to the mass of the front axle and the mass of the chassis supported by the front axle. In addition, it is assumed that the weight of 1/3 of the passengers is supported by the front axle based on the bus geometry. The suspension system efficiency $\eta_{Susp.}$ is considered constant and equals to 70% and Δt represents the duration of the lifting process taken to be 3 seconds [27].

$$P_{Susp.} = \frac{M_{Front}.g.\Delta h}{\eta_{Susp.}.\Delta t} \quad (2.63)$$

The total hydraulic auxiliaries' power demand is expressed in equation (2.64).

$$P_{Hyd} = P_{pump} + P_{Susp.} \quad (2.64)$$

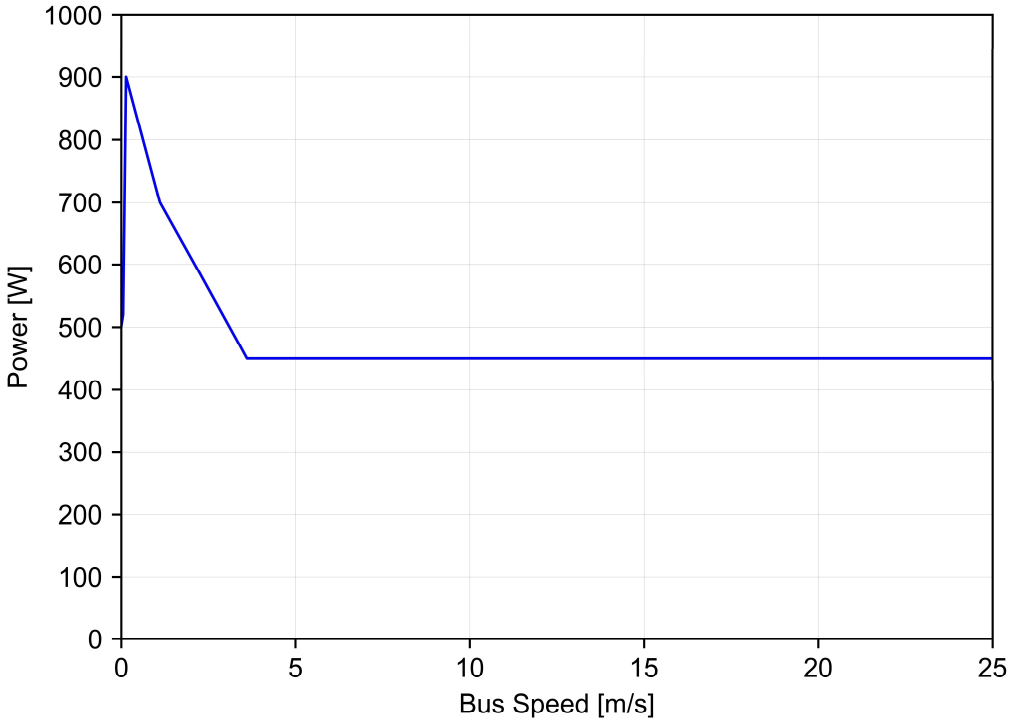


Figure 2.19: Electro-Hydraulic steering pump power consumption function of BEB speed [27]

2.5 Model Validation

The BEB model validation is essential to assess the accuracy of the proposed models and assumptions. The model validation is split into 5 parts: (1) validation of the propulsion system energy consumption, (2) validation of the bus cabin thermal needs, (3) validation of the HVAC system energy consumption, (4) validation of the auxiliaries energy consumption, and (5) validation of the battery electro-thermal model.

2.5.1 Propulsion System

The propulsion system model validation is conducted by comparing its energy consumption to the reported energy consumption values in the literature. The energy consumption comparison is performed over a variety of bus specifications, driving conditions, and passengers' loads. Table 2.20 summarizes the studies presented in the recent literature that report the energy consumption of the BEB propulsion system. Across the presented studies, all other energy systems apart from the propulsion system are not considered.

Table 2.20: Summary of the studies presented in the recent literature that report the energy consumption of BEB propulsion system

Scenario #	Reference	Energy Consumption Estimation Method	Available Buses Specifications	Experiment/Simulation Conditions
1	Zhou et al. (2016) [1]	Experimental	Two 12-*m* buses: - Curb weight: 13800 *kg* - Battery 1: 170 *kWh* – 1800 *kg* - Battery 2: 324 *kWh* – 3564 *kg* - EM1: 2 x 100 *kW* - EM2: 1 x 80 *kW* One 8-*m* bus: - Curb weight: 8800 *kg*. - Battery: 104 *kWh* – 1340 *kg* - EM: 2 x 75 *kW*	- Variety of drive cycles at different average speeds. - Variety of passengers' loads.
2	Torzynski et al. (2016) [98]	Experimental and Simulation.	11.6-m standard bus (SB): - Curb weight: 12500 *kg*. - Battery: 90 *kWh*. - A_f: 8.28 m^2 - C_D: 0.66 - EM: 250 *kW*	- One drive cycle - Variety of passengers' loads.
3	Rios et al. (2014) [99]	Experimental and Simulation.	12-*m* bus: - Curb weight: 12759 *kg*. - Battery: 50 *Ah*. - A_f: 7.1 m^2	- One drive cycle.

4	Gao et al. (2017) [100]	Simulation	Two 12-*m* buses: - Curb weight: 9600 *kg*. - Battery: 150 - 324 *kWh* – 2500 - 6300 *kg*. - A_f: 8.5 m² - C_D: 0.79	- Three drive cycles. - Variety of Battery sizes.
5	Raab et al. (2019) [101]	Simulation	12-*m* standard bus (SB): - Curb weight: 12500 *kg*. - Battery: 175 *kWh*. - A_f: 8.28 m² - C_D: 0.66 18-*m* articulated bus (AB): - Curb weight: 17500 *kg*. - Battery: 225 *kWh*. - A_f: 8.28 *m²* - C_D: 0.66 Double-decker bus (DD): - Curb weight: 18500 *kg*. - Battery: 250 *kWh*. - A_f: 10.35 *m²* - C_D: 0.66	- One drive cycle - Two passengers' loads.
6	Lajunen (2014) [5] – Lajunen et Lipman (2016) [4]	Simulation	12- *m* bus: - Curb weight: 10000 *kg*. - Battery: 149 *kWh* – 1515 *kg*. - EM: 150 kW - A_f: 6.2 *m²* - C_D: 1.2	- Variety of drive cycles at different average speeds. - One passengers' load.

The studies presented in Table 2.20 are referred to as scenarios. Each scenario includes a set of case studies. For each case study, there are different bus specifications, driving conditions, and passengers' loads. Table 7.6 in Appendix C summarizes the different scenarios and case studies used to validate the energy consumption of the propulsion system. The following parameters define each case study:

- Bus length varies from 8 to 12 *m*.
- Bus curb weight varies from 8.8 to 18.5 tons including standard buses, articulated buses, and double-decker buses.
- Bus drag coefficient varies from 0.55 to 1.2.
- Bus frontal area varies from 6.5 to 10.35 m^2.
- EM rated power varies from 75 to 275 *kW*. EM efficiency maps are sized based on the base-efficiency map presented in Figure 2.10. Sizing is done linearly by scaling the torque values of the EM and preserving the speed values to achieve the rated EM power.
- Battery voltage varies from 400 to 750 *V*.
- Battery weight, which reflects battery energy capacity, varies from 280 to 5400 *kg*.
- A variety of drive cycles are used, and they are presented in Table 7.7 in Appendix C. Concerning the studies that conducted experiments to estimate the energy consumption of the propulsion system (scenarios 1, 2, and 3), representative drive cycles are used to imitate the real-world velocity profiles of the buses. The cycles are chosen based on parameters such as the average speed, distance, duration, number of stops, idling time, average and maximum acceleration, and deceleration. Table 7.7 in Appendix C lists these drive cycles alongside their specifications and Figure 7.5 in Appendix C shows the velocity profiles of the mentioned drive cycles.
- Passengers' number occupying the bus ranges from 1 (empty bus) to full bus (maximum number of passengers depends on bus length and battery size).

The scenarios and case studies presented in Table 2.20 and Table 7.6 are simulated, and the resulting propulsion system energy consumption is compared to the reported values in the literature. The specific energy consumption measured in *kWh/km* is considered in the validation process. Figure 2.20 presents the mean, minimum and maximum errors for the propulsion system energy consumption validation at the different case studies across the 6 presented scenarios. The mean error is always less than 5% in all scenarios. In addition, the maximum error does not exceed 6% across all studies. The values between the parentheses on the

horizontal axis represent the number of simulations per scenario, which is effectively the number of case studies per scenario.

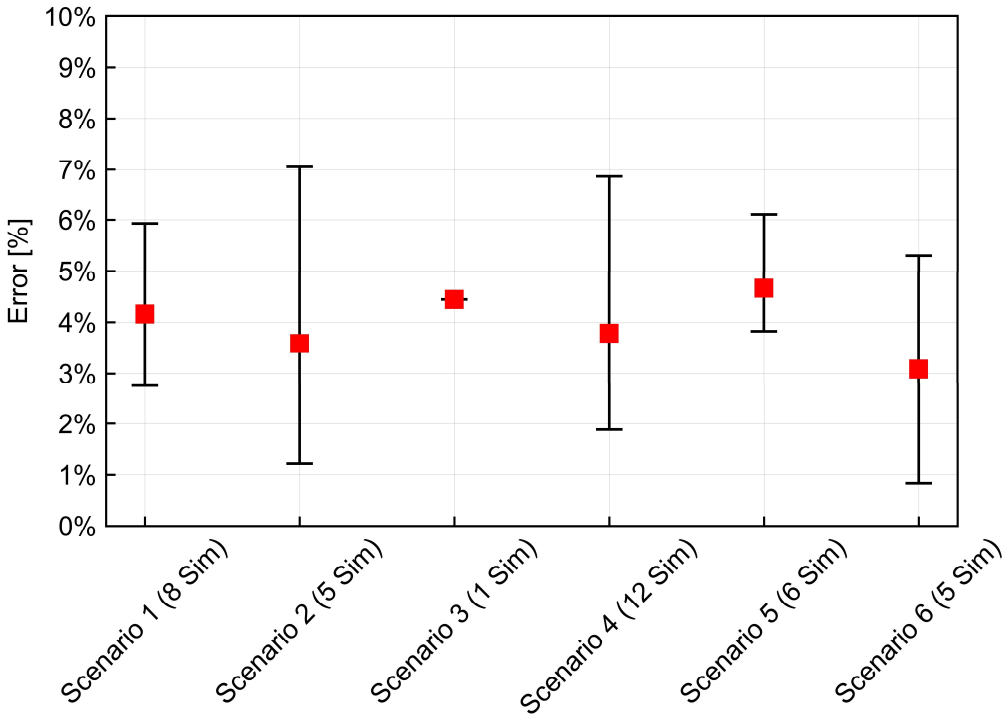


Figure 2.20: Propulsion system energy consumption validation

Moreover, the error distribution is presented in Figure 2.21.

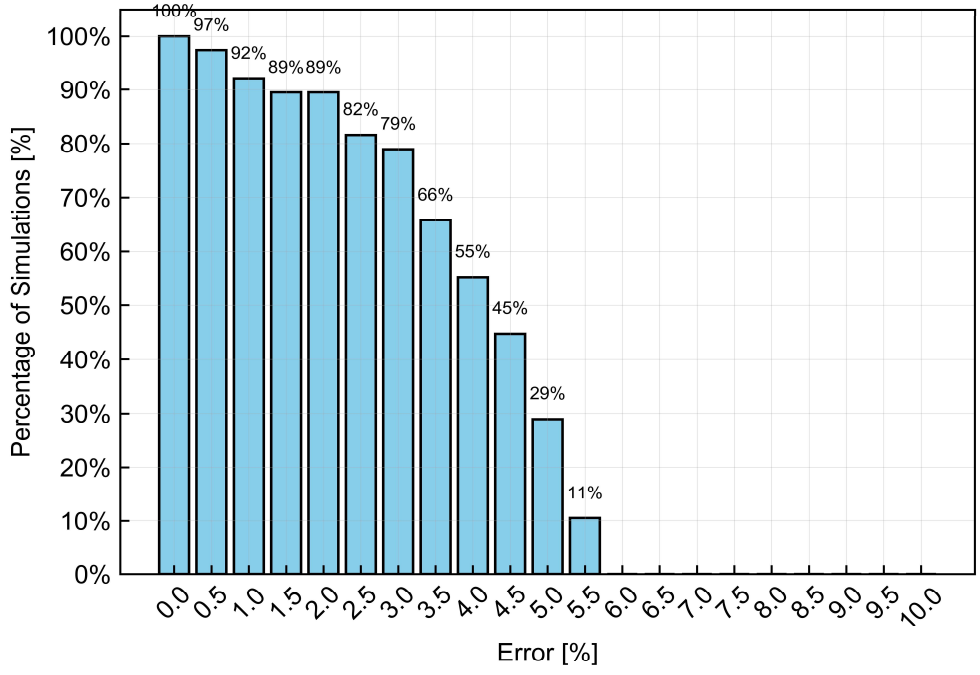


Figure 2.21 Propulsion system validation error distribution

29% of the simulations witness an error that exceeds 5% and only 11% of the simulation result in an error above 5.5%. The error does not exceed 6% in any of the proposed simulations.

One of the main reasons behind the % errors between the proposed propulsion system model and the reference values is the EM efficiency map, especially in scenarios 2 and 5. In addition, synthesized drive cycles are used to imitate real-world velocity profiles (scenarios 1, 2, and 3) which yields additional errors as well. However, the achieved % errors for the estimation of the propulsion system energy consumption are acceptable and serve the purpose of this thesis.

2.5.2 Cabin Thermal Load

Cabin thermal load is the heat flux to be supplied/extracted to meet the cabin thermal conditions at certain weather conditions. The cabin validation is done by comparing the thermal loads estimated by the model to those reported in the literature at different weather conditions. Many parameters affect the thermal load such as external temperature, solar flux, bus geometry, and number of passengers. The main studies in the literature report the thermal load of BEB at extreme weather conditions such as extreme hot weather (> 35 °*C*) and extreme cold weather (< -10 °*C*). Table 2.21 introduces the different studies used to validate the cabin thermal load.

Figure 2.22 shows the bus thermal load validation across the different presented scenarios.

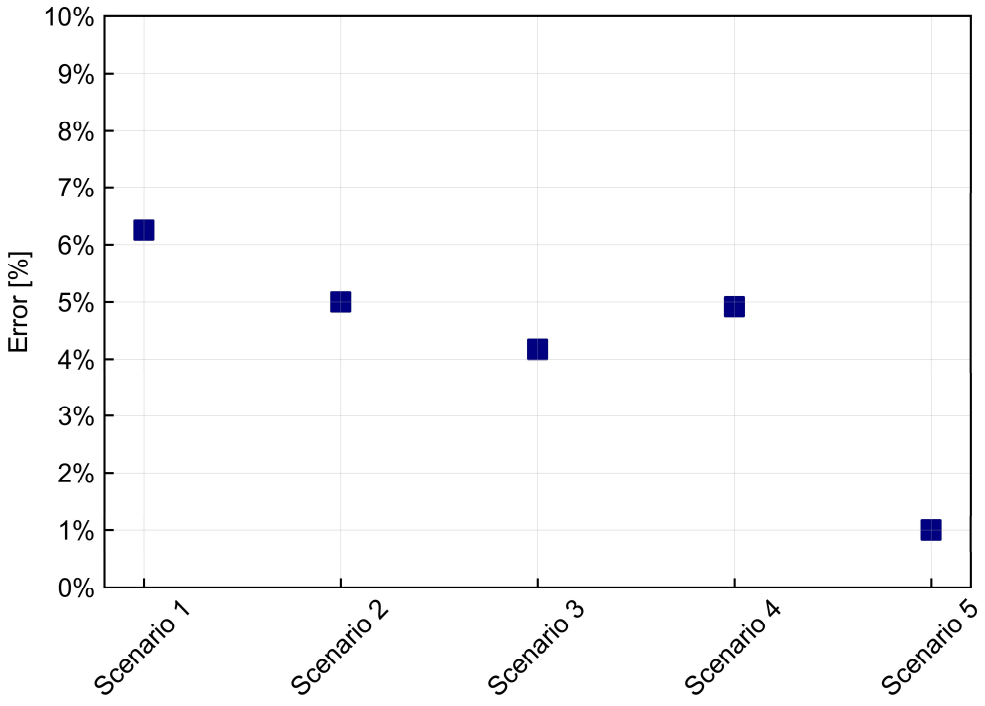


Figure 2.22: Bus cabin thermal need validation

All cooling scenarios (scenario 2-5) achieve an error of less than 5% whereas the only heating scenario (scenario 1) witnesses a 6.2% error. The lack of sufficient data concerning fresh air supply might be one reason for this error. In addition, not all studies present in detail the composition of the cabin walls insulation which impacts the heat transfer between the bus interior and the environment.

Table 2.21: Summary of studies used to validate the cabin thermal load

	Scenario #	1	2	3	4	5
	Study	Göhlich et al (2018) [33]	Suh et al (2013) [15], [102]	Pathak et al (2017) [103]	Unai (2017) [104], [105]	Liebold et al (2016) [106]
	Approach	Simulation	Experimental	Experimental	Experimental	Simulation
Bus Geometry	Length [m]	12	12	12	12.8	12
	Width [m]	2.55	2.55	2.6	2.6	2.48
	height [m]	3.5	3.5	2.8	2.8	3.22
	Glazing Area [m^2]	50	45	40.5	50	35
	Body Area [m^2]	90	95	107.5	90	125
Passengers #		-	20	90	60	20
Weather Conditions	Temperature [$°C$]	-10	36	32	35	32
	Sun Flux [W/m^2]	200	200	200	200	1000
Setup	T-Set [$°C$]	17	24	24	22	20
	Fresh Air Requirements	-	f(n_Pass)	rec = 0.8 (fixed)	f(n_Pass)	f(n_Pass)

2.5.3 HVAC System (Heat Pump)

The performance of the HP is validated by comparing the compressor electric power demand or the HP COP to the reported values in the literature, mainly to studies conducted experimental validation and measurements for HP in BEB or electric vehicles in general. The majority of the studies tackle BEB cooling using HP whereas very few studies consider BEB heating with a HP, mainly because positive temperature coefficient (PTC) is the main heating technology for BEB at the moment. Table 2.22 shows the studies used to validate the HVAC unit model.

Figure 2.23 shows the bus HVAC unit validation across the different presented scenarios. All cooling scenarios (scenario 1-3) record a mean error of less than 4%, whereas the heating scenarios (scenario 4-5) witness a mean error between 2-3 %. The highest error is recorded in scenario 5 at 6.8% (heating scenario with the external temperature at – 7°C). It is not possible

to further investigate the reasons behind this error as the data provided for this scenario are performance data published in the HP datasheet by the manufacturer. Other than that, the HVAC unit energy performance is acceptable with the current mean error.

Table 2.22: Summary of studies used to validate the HVAC unit model

Scenario #	Study	Approach	Application	Setup
1	Suh et al (2015) [15]	Experimental	Cooling	- Ambient Temperature: 35 *°C* - Compressor Speed: 55 – 65 *Hz*
2	Göhlich et al (2018) [33]	Experimental	Cooling	Ambient Temperature: 35 *°C*
3	Lee et al (2013) [107]	Experimental	Cooling	Ambient Temperature: 27 *°C* to 35 *°C*
4	Lajunen (2017) [16]	Simulation	Heating	Ambient Temperature: -30 *°C* to 0 *°C*
5	Thermo King (OEM) [108]	Data by OEM	Heating	Ambient Temperature: -7 *°C* to 15 *°C*

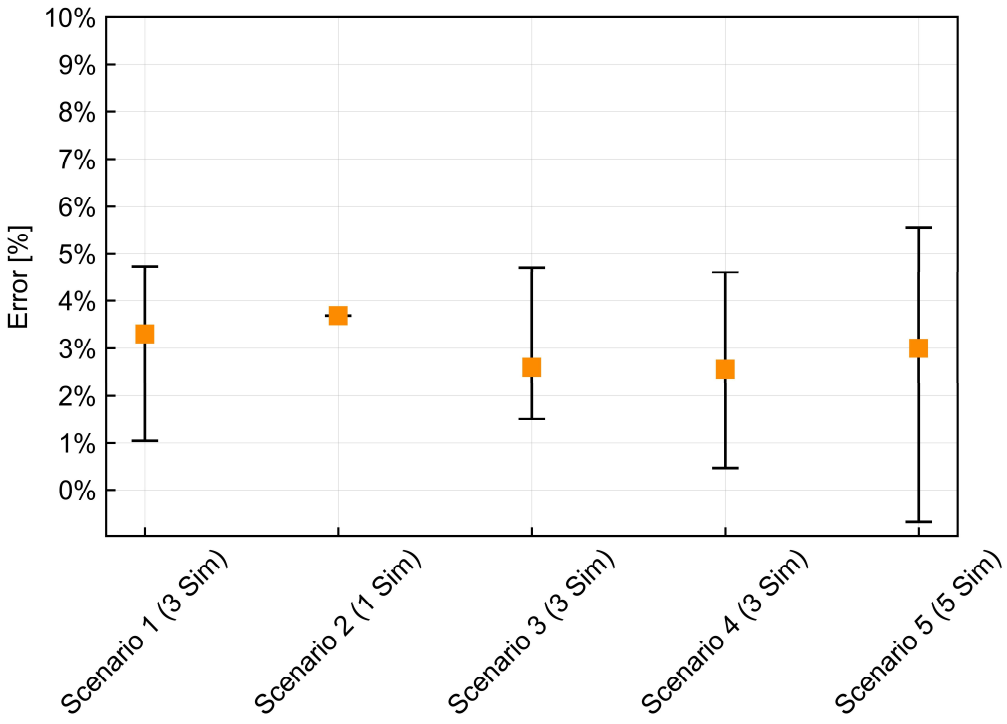


Figure 2.23: Bus HVAC unit validation

2.5.4 Auxiliaries

No study in the recent literature provides a thorough evaluation of the auxiliaries' energy consumption for electric buses. The only reference is dated back to 2004 (Andersson [27]). In the mentioned study, an experimental approach is used to assess the auxiliaries' energy

consumption using a roller test bench, where the bus was driven in a way to imitate the Braunschweig drive cycle. The model validation is achieved by comparing the average power of the different auxiliaries over the Braunschweig drive cycle. The average power is calculated as the auxiliary unit energy consumption divided by the drive cycle's duration. The validated auxiliary units' models are the air compressor operating the pneumatic system, steering pump, doors, suspension system, and parking brakes. Figure 2.24 presents the errors for the different auxiliary units' average power demand over the Braunschweig drive cycle. All auxiliary units achieve an error of less than 6%, which is acceptable for this thesis.

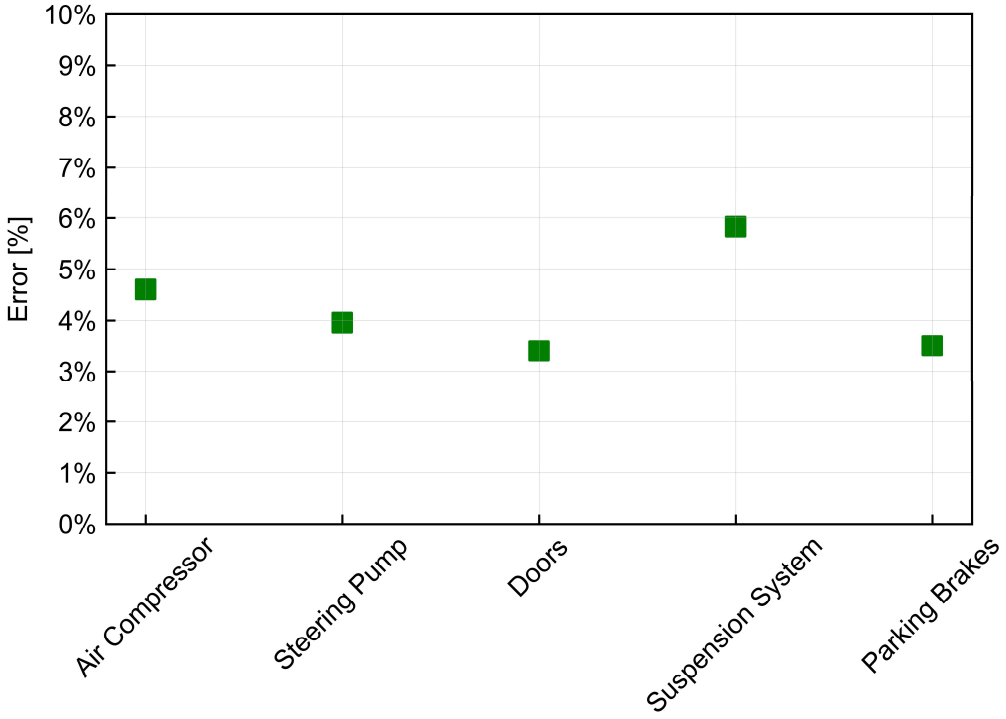


Figure 2.24: Non-Mechanical auxiliaries energy consumption validation

2.5.5 Battery

Very few studies present detailed data regarding the battery electro-thermal model validation. One study in specific is used to validate the battery electro-thermal model [62]. The validation is done by operating the battery at a charge depleting cycle, and then the battery *SOC* and temperature are compared between the proposed model and the values reported in [62]. It is not possible to mimic the exact charge depleting cycle used in [62] due to the lack of the required data, however, a cycle of constant discharge rate equals to 4C is used, where 4C is the average discharge rate of the charge depleting cycle used in [62]. Figure 2.25 and Figure 2.26 show the battery *SOC* and temperature profiles, with *Tc* being the cell core temperature and *Ts* the cell

surface temperature, and Table 2.23 compares the values of the battery *SOC* and temperature profiles between the model and the reference study at specific time instants. The *SOC* profiles are very similar and the slight fluctuations observed in the reference study are due to the non-constant charge depleting cycle. However, at the end of the cycle, the final *SOC* value is within 5% from the reference study. The temperature profiles witness high error % at the beginning of the cycle (23%). This value decreases to less than 1% at the end of the cycle, mainly as the moving time-average of the cycle becomes closer to the total average (4C).

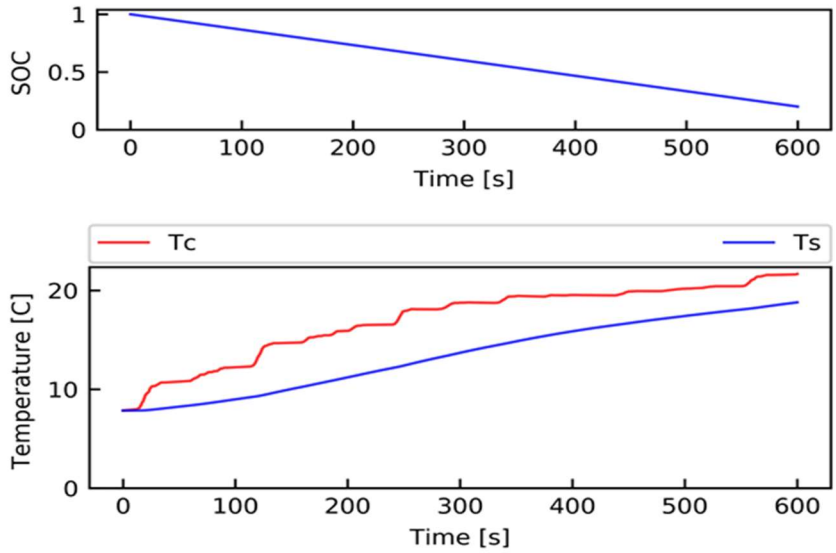


Figure 2.25: Battery SOC and core and surface temperature profiles over a charge depleting cycle simulation results

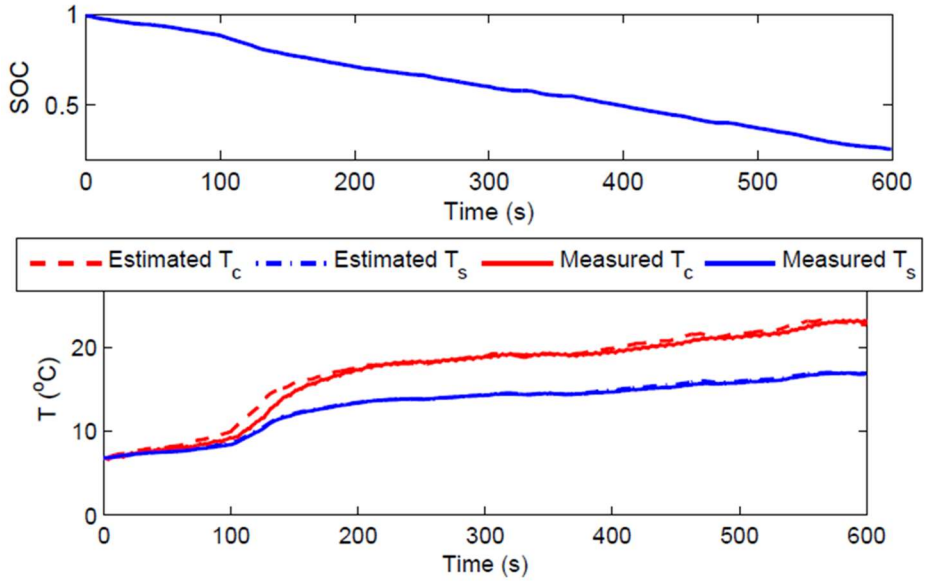


Figure 2.26: Battery SOC and core and surface temperature profiles over a charge depleting cycle as reported by [62]

Table 2.23: Battery electro-thermal model validation summary

Time		*SOC*	*Tc [°C]*	*Ts [°C]*
100 sec	Model	0.867	12.3	8.93
	Ref	0.9	10	8.75
	Error	3.60%	23%	2%
200 sec	Model	0.73	15.9	11.2
	Ref	0.7	17.5	13
	Error	4.20%	9.20%	13%
300 sec	Model	0.6	18.72	13.73
	Ref	0.6	19.5	14.8
	Error	0%	4%	7.30%
400 sec	Model	0.47	19.51	14.82
	Ref[62]	0.49	20	15
	Error	4.20%	2.40%	1.20%
500 sec	Model	0.33	20.12	15.41
	Ref	0.35	21	16
	Error	5.70%	4.20%	3.60%
600 sec	Model	0.19	21.96	18.74
	Ref	0.18	22	18.9
	Error	5.50%	0.20%	0.80%

2.6 Conclusion

This chapter provides a detailed energy modeling methodology to assess the energy consumption of BEB. The proposed model considers the different energy systems encountered in BEB such as the battery, propulsion system, HVAC system, and auxiliaries. The model integrates all these energy systems into a single platform to better assess the total bus energy consumption. A coupled battery electro-thermal model is introduced capable of capturing the battery cells' electric and thermal behavior. A detailed propulsion model is introduced to assess the energy consumption due to propulsion. An electric vehicle cabin model is adapted to fit a bus application and an HVAC unit model is developed to assess the heating and cooling needs of the bus and the resulting energy consumption. Moreover, dynamic auxiliaries' models are developed such as the pneumatic, hydraulic, electric, and battery thermal auxiliaries.

The proposed model is validated in terms of energy consumption and power demand of the different energy systems. The propulsion system model validation is conducted by comparing its specific energy consumption, measured in *kWh/km*, to values reported in the literature.

Several case studies for simulation are considered. The obtained mean error is around 3% and the maximum recorded error is 7%.

The bus cabin validation is conducted by comparing the cabin thermal load at different external temperatures to similar studies in the literature. In addition, the HVAC unit model is validated by comparing the HP COP to performance sheets supplied by manufacturers. The HVAC unit model shows an error between 2-3% for cooling scenarios; however, a 6% error is recorded for heating scenarios.

The auxiliaries' model is validated by comparing their energy consumption over a single regulatory cycle due to a lack of data. All auxiliaries show a mean error below 5%, except for the hydro-static suspension system which records a 7% error in energy consumption.

Finally, the battery electric and thermal behaviors are examined over one discharge cycle for a single battery cell. The battery SOC error is between 0 to 5.5% while the battery core and surface temperatures show a cumulative error of less than 1% at the end of the discharge cycle.

That being said, the model can be used to estimate the energy consumption of BEB at different operating conditions to reflect on their real world-energy consumption as will be presented in the next chapter.

2.7 References

[1] B. Zhou, Y. Wu, B. Zhou, R. Wang, W. Ke, and S. Zhang, "Real-world performance of battery electric buses and their life-cycle benefits with respect to energy consumption and carbon dioxide emissions," *Energy*, vol. 96, pp. 603–613, 2016, doi: 10.1016/j.energy.2015.12.041.

[2] J. Neubauer and E. Wood, "The impact of range anxiety and home, workplace, and public charging infrastructure on simulated battery electric vehicle lifetime utility," *J. Power Sources*, vol. 257, pp. 12–20, 2014, doi: 10.1016/j.jpowsour.2014.01.075.

[3] M. Mohamed, M. Ferguson, and P. Kanaroglou, "What hinders adoption of the electric bus in Canadian transit ? Perspectives of transit providers," *Transp. Res. Part D Transp. Environ.*, vol. 64, no. September 2017, pp. 134–149, 2018, doi: 10.1016/j.trd.2017.09.019.

[4] A. Lajunen and T. Lipman, "Lifecycle cost assessment and carbon dioxide emissions of diesel, natural gas, hybrid electric, fuel cell hybrid and electric transit buses," *Energy*, vol. 106, pp. 329–342, 2016, doi: 10.1016/j.energy.2016.03.075.

[5] A. Lajunen, "Energy consumption and cost-benefit analysis of hybrid and electric city buses," *Transp. Res. Part C Emerg. Technol.*, vol. 38, pp. 1–15, 2014, doi: 10.1016/j.trc.2013.10.008.

[6] S. Bakker and R. Konings, "The transition to zero-emission buses in public transport – The need for institutional innovation," *Transp. Res. Part D Transp. Environ.*, vol. 64, no. March 2017, pp. 204–215, 2018, doi: 10.1016/j.trd.2017.08.023.

[7] C. Botsford and A. Szczepanek, "Fast Charging vs . Slow Charging : Pros and cons for the New Age of Electric Vehicles," *Evs24*, no. May, pp. 1–9, 2009, [Online]. Available: http://www.cars21.com/assets/link/EVS-24-3960315 Botsford.pdf.

[8] G. Jung, B. Song, S. Shin, S. Lee, J. Shin, Y. Kim, and S. Jeon, "High efficient inductive power supply and pickup system for on-line electric bus," *2012 IEEE Int. Electr. Veh. Conf. IEVC 2012*, 2012, doi: 10.1109/IEVC.2012.6183263.

[9] O. F. Delgado, N. N. Clark, and G. J. Thompson, "Modeling Transit Bus Fuel Consumption on the Basis of Cycle Properties," *J. Air Waste Manag. Assoc.*, vol. 61, no.

4, pp. 443–452, 2011, doi: 10.3155/1047-3289.61.4.443.

[10] Z. Gao, T. Laclair, S. Ou, S. Huff, G. Wu, P. Hao, K. Boriboonsomsin, and M. Barth, "Evaluation of electric vehicle component performance over eco-driving cycles," *Energy*, vol. 172, pp. 823–839, 2019, doi: 10.1016/j.energy.2019.02.017.

[11] T. Halmeaho, P. Rahkola, K. Tammi, J. Pippuri, A.-P. Pellikka, A. Manninen, and S. Ruotsalainen, "Experimental validation of electric bus powertrain model under city driving cycles," *IET Electr. Syst. Transp.*, vol. 7, no. 1, pp. 74–83, 2017, doi: 10.1049/iet-est.2016.0028.

[12] W. N. Lourido, G. Member, and L. Mu, "Design of Electric Buses of Rapid Transit using Hybrid Energy Storage and Local Traffic Parameters," *IEEE Trans. Veh. Technol.*, vol. 66, no. 7, 2016, doi: 10.1109/TVT.2016.2616401.

[13] D. Perrotta, A. Teixeira, H. Silva, and B. Ribeiro, "Electrical Bus Performance Modeling for Urban Environments," *SAE Int. J. Altern. Powertrains*, pp. 34–45, 2012, doi: 10.4271/2012-01-0200.

[14] Y. Xu, F. E. Gbologah, D. Y. Lee, H. Liu, M. O. Rodgers, and R. L. Guensler, "Assessment of alternative fuel and powertrain transit bus options using real-world operations data: Life-cycle fuel and emissions modeling," *Appl. Energy*, vol. 154, pp. 143–159, 2015, doi: 10.1016/j.apenergy.2015.04.112.

[15] I. S. Suh, M. Lee, J. Kim, S. T. Oh, and J. P. Won, "Design and experimental analysis of an efficient HVAC (heating, ventilation, air-conditioning) system on an electric bus with dynamic on-road wireless charging," *Energy*, vol. 81, pp. 262–273, 2015, doi: 10.1016/j.energy.2014.12.038.

[16] A. Lajunen, "Energy Efficiency and Performance of Cabin Thermal Management in Electric Vehicles," *SAE Tech. Pap.*, 2017, doi: 10.4271/2017-01-0192.

[17] M. A. Fayazbakhsh and M. Bahrami, "Comprehensive Modeling of Vehicle Air Conditioning Loads Using Heat Balance Method," *SAE Tech. Pap.*, no. x, 2013, doi: 10.4271/2013-01-1507.

[18] D. Perrotta, J. Luís, R. J. F. Rossetti, J. F. De, Z. Kokkinogenis, B. Ribeiro, and J. L. Afonso, "Route planning for electric buses : a case study in Oporto," *Procedia - Soc. Behav. Sci.*, vol. 111, pp. 1004–1014, 2014, doi: 10.1016/j.sbspro.2014.01.135.

[19] J. Kim, I. Song, and W. Choi, "An Electric Bus with a Battery Exchange System," *Energies*, pp. 6806–6819, 2015, doi: 10.3390/en8076806.

[20] K. R. Mallon, F. Assadian, and B. Fu, "Analysis of on-board photovoltaics for a battery electric bus and their impact on battery lifespan," *Energies*, vol. 10, no. 7, 2017, doi: 10.3390/en10070943.

[21] B. O. Varga and C. Iclodean, "ELECTRIC BUSES FOR URBAN TRANSPORTATION: ASSESSMENTS ON COST, INFRASTRUCTURE AND EXPLOITATION Bogdan," *Ann. Univ. ORADEA. Fascicle Manag. Technol. Eng.*, vol. 10, no. May, 2015.

[22] D. Göhlich, A. Kunith, and T. Ly, "Technology assessment of an electric urban bus system for berlin," in *WIT Transactions on the Built Environment*, 2014, vol. 138, pp. 137–149, doi: 10.2495/UT140121.

[23] D. Göhlich, T. Ly, A. Kunith, and D. Jefferies, "Economic assessment of different air-conditioning and heating systems for electric city buses based on comprehensive energetic simulations," in *EVS28 International Electric Vehicle Symposium and Exhibition*, 2015, pp. 1–9.

[24] D. Y. Lee, C. W. Cho, J. P. Won, Y. C. Park, and M. Y. Lee, "Performance characteristics of mobile heat pump for a large passenger electric vehicle," *Appl. Therm. Eng.*, vol. 50, no. 1, pp. 660–669, 2013, doi: 10.1016/j.applthermaleng.2012.07.001.

[25] A. Lajuneni and A. Kalttonen, "Investigation of Thermal Energy Losses in the Powertrain of an Electric City Bus," 2015, doi: 10.1109/ITEC.2015.7165776.

[26] M. Yan, H. He, C. Sun, H. Jia, and M. Li, "Stochastic Dynamic Programming of Air Conditioning System under Time-varying Passenger Condition for Electric Bus," *Energy Procedia*, vol. 104, pp. 360–365, 2016, doi: 10.1016/j.egypro.2016.12.061.

[27] C. Andersson, "On auxiliary systems in commercial vehicles," Lund University, 2004.

[28] N. Pettersson and K. H. Johansson, "Modelling and control of auxiliary loads in heavy vehicles," *Int. J. Control*, vol. 79, no. 5, pp. 479–495, 2007, doi: 10.1080/00207170600587333.

[29] R. Basso, B. Kulcsár, B. Egardt, P. Lindroth, and I. Sanchez-diaz, "Energy consumption estimation integrated into the Electric Vehicle Routing Problem," *Transp. Res. Part D*

Transp. Environ., vol. 69, pp. 141–167, 2019, doi: 10.1016/j.trd.2019.01.006.

[30] Q. Wang, B. Jiang, B. Li, and Y. Yan, "A critical review of thermal management models and solutions of lithium-ion batteries for the development of pure electric vehicles," *Renew. Sustain. Energy Rev.*, vol. 64, pp. 106–128, 2016, doi: 10.1016/j.rser.2016.05.033.

[31] "Dymola Modelling Environment," 2019. https://www.claytex.com/products/dymola/.

[32] "Modelica Modelling Language," 2019. https://www.claytex.com/products/dymola/modelica-modelling-language/.

[33] D. Göhlich, T. A. Fay, D. Jefferies, E. Lauth, A. Kunith, and X. Zhang, "Design of urban electric bus systems," *Des. Sci.*, vol. 4, no. August, pp. 1–28, 2018, doi: 10.1017/dsj.2018.10.

[34] "Electric Bus Market Report: Trends, Forecast and Competitive Analysis," 2019. doi: 4832758.

[35] "Global Electric Bus Market Report 2019: $71.9 Bn Market Trends, Forecast and Competitive Analysis to 2024," 2019. Accessed: Nov. 15, 2019. [Online]. Available: https://www.prnewswire.com/news-releases/global-electric-bus-market-report-2019-71-9-bn-market-trends-forecast-and-competitive-analysis-to-2024--300926256.html.

[36] "Global Electric Bus Market Size, Share | Price Forecast Report 2025," 2019. Accessed: Nov. 15, 2019. [Online]. Available: https://www.adroitmarketresearch.com/industry-reports/electric-bus-market.

[37] "Electric Bus Market Size, Share, Trends | Industry Report 2025," 2018. Accessed: Nov. 15, 2019. [Online]. Available: https://www.psmarketresearch.com/market-analysis/electric-bus-market/segmentation.

[38] E. D. Wachsman and K. T. Lee, "Lowering the temperature of solid oxide fuel cells," *Science (80-.).*, vol. 334, no. 6058, pp. 935–939, 2011, doi: 10.1126/science.1204090.

[39] D. Linden and T. Reddy, *Handbook of Batteries*, 3rd ed. NewYork: Mcgrow-Hill, 2002.

[40] I. Tsiropoulos, D. Tarvydas, and N. Lebedeva, "Li-ion batteries for mobility and stationary storage applications, JRC Science for Policy Report, EU Commission.," 2018. doi: 10.2760/87175.

[41] M. Doyle, T. F. Fuller, and J. Newman, "1-Modeling of Galvanostatic Charge and Discharge," *J. Electrochem. Soc.*, vol. 140, no. 6, pp. 1526–1533, 1993.

[42] T. F. Fuller, M. Doyle, and J. Newman, "Simulation and Optimization of the Dual Lithium Ion Insertion Cell," *J. Electrochem. Soc.*, vol. 141, no. 1, pp. 1–10, 1994, doi: 10.1149/1.2054684.

[43] J. Newman and K. Thomas-Alyea, *Electrochemical Systems*, 3rd ed. Wiley, 2004.

[44] M. Doyle, J. Newman, A. S. Gozdz, C. N. Schmutz, and J. M. Tarascon, "Comparison of modeling predictions with experimental data from plastic lithium ion cells," *J. Electrochem. Soc.*, vol. 143, no. 6, pp. 1890–1903, 1996, doi: 10.1149/1.1836921.

[45] C. J. Mansour, "Trip-based optimization methodology for a rule-based energy management strategy using a global optimization routine: The case of the Prius plug-in hybrid electric vehicle," *Proc. Inst. Mech. Eng. Part D J. Automob. Eng.*, vol. 230, no. 11, pp. 1529–1545, Sep. 2016, doi: 10.1177/0954407015616272.

[46] W. S. Bou Nader, C. J. Mansour, M. G. Nemer, and O. M. Guezet, "Exergo-technological explicit methodology for gas-turbine system optimization of series hybrid electric vehicles," *Proc. Inst. Mech. Eng. Part D J. Automob. Eng.*, vol. 232, no. 10, pp. 1323–1338, Sep. 2018, doi: 10.1177/0954407017728849.

[47] H. He, R. Xiong, and J. Fan, "Evaluation of lithium-ion battery equivalent circuit models for state of charge estimation by an experimental approach," *Energies*, vol. 4, no. 4, pp. 582–598, 2011, doi: 10.3390/en4040582.

[48] V. H. Johnson, "Battery performance models in ADVISOR," *J. Power Sources*, vol. 110, no. 2, pp. 321–329, 2002, doi: 10.1016/S0378-7753(02)00194-5.

[49] J. Wehbe and N. Karami, "Battery equivalent circuits and brief summary of components value determination of lithium ion: A review," in *2015 3rd International Conference on Technological Advances in Electrical, Electronics and Computer Engineering, TAEECE 2015*, 2015, pp. 45–49, doi: 10.1109/TAEECE.2015.7113598.

[50] X. Zhang, W. Zhang, and G. Lei, "A review of li-ion battery equivalent circuit models," *Trans. Electr. Electron. Mater.*, vol. 17, no. 6, pp. 311–316, 2016, doi: 10.4313/TEEM.2016.17.6.311.

[51] H. W. You, J. I. Bae, S. J. Cho, J. M. Lee, and S. H. Kim, "Analysis of equivalent circuit

models in lithium-ion batteries," *AIP Adv.*, vol. 8, no. 12, 2018, doi: 10.1063/1.5054384.

[52] S. S. Madani, E. Schaltz, and S. K. Kær, "A review of different electric equivalent circuit models and parameter identification methods of lithium-ion batteries," *ECS Trans.*, vol. 87, no. 1, pp. 23–37, 2018, doi: 10.1149/08701.0023ecst.

[53] "Nanophosphate High Power Lihtium Ion Cell AHR32113m1Ultra-B." www.a123systems.com (accessed Nov. 17, 2019).

[54] S. Rothgang, M. Rogge, J. Becker, and D. U. Sauer, "Battery Design for Successful Electrification in Public Transport," *Energies*, pp. 6715–6737, 2015, doi: 10.3390/en8076715.

[55] A. Kunith, R. Mendelevitch, and D. Goehlich, "Electrification of a city bus network—An optimization model for cost-effective placing of charging infrastructure and battery sizing of fast-charging electric bus systems," *Int. J. Sustain. Transp.*, vol. 11, no. 10, pp. 707–720, 2017, doi: 10.1080/15568318.2017.1310962.

[56] V. H. Johnson, A. a Pesaran, and B. Court, "Temperature-Dependent Battery Models for High-Power Lithium-Ion Batteries," in *17th Annual Electric Vehicle Symposium*, 2000, no. January, pp. 1–15, [Online]. Available: http://www.nrel.gov/vehiclesandfuels/energystorage/pdfs/evs17paper2.pdf.

[57] D. Doughty and E. P. Roth, "A general discussion of Li Ion battery safety," *Electrochem. Soc. Interface*, vol. 21, no. 2, pp. 37–44, 2012, doi: 10.1149/2.F03122if.

[58] ISO, "ISO 6469-1: Electrically propelled road vehicles — Safety specifications — Part 1: Rechargeable energy storage system," 2019. Accessed: Nov. 16, 2019. [Online]. Available: https://www.iso.org/standard/45477.html.

[59] D. Bernardi, E. Pawlikowski, and J. Newman, "A General Energy Balance for Battery Systems_Bernadi D, Powlikowski E and Newman," *J. Electrochem. Soc.*, vol. 132, no. 1, pp. 5–12, 1985.

[60] N. Sato, "Thermal behavior analysis of lithium-ion batteries for electric and hybrid vehicles," *J. Power Sources*, vol. 99, no. 1–2, pp. 70–77, 2001, doi: 10.1016/S0378-7753(01)00478-5.

[61] C. Forgez, D. Vinh, G. Friedrich, M. Morcrette, and C. Delacourt, "Thermal modeling of a cylindrical LiFePO 4 / graphite lithium-ion battery," *J. Power Sources*, vol. 195, pp.

2961–2968, 2010, doi: 10.1016/j.jpowsour.2009.10.105.

[62] X. Lin, H. E. Perez, S. Mohan, J. B. Siegel, A. G. Stefanopoulou, Y. Ding, and M. P. Castanier, "A lumped-parameter electro-thermal model for cylindrical batteries," *J. Power Sources*, vol. 257, pp. 1–11, 2014, doi: 10.1016/j.jpowsour.2014.01.097.

[63] K. E. Thomas and J. Newman, "Thermal Modeling of Porous Insertion Electrodes," *J. ofThe Electrochem. Soc.*, no. 3401, pp. 176–192, 2003, doi: 10.1149/1.1531194.

[64] D. J. Becker, T. Wetzel, and D. Werner, "Thermal conductivity of Li-ion batteries and their electrode con fi gurations e A novel combination of modelling and experimental approach," *J. Power Sources J.*, vol. 364, pp. 72–83, 2017, doi: 10.1016/j.jpowsour.2017.07.105.

[65] K. E. Thomas, C. Bogatu, and J. Newman, "Measurement of the Entropy of Reaction as a Function of State of Charge in Doped and Undoped Lithium Manganese Oxide," *J. ofThe Electrochem. Soc.*, pp. 570–575, 2001, doi: 10.1149/1.1369365.

[66] X. Lin, H. E. Perez, J. B. Siegel, A. G. Stefanopoulou, Y. Li, R. D. Anderson, Y. Ding, and M. P. Castanier, "Online Parameterization of Lumped Thermal Dynamics in Cylindrical Lithium Ion Batteries for Core Temperature Estimation and Health Monitoring," *IEEE Trans. Control Syst. Technol.*, vol. 21, no. 5, pp. 1745–1755, 2013, doi: 10.1109/TCST.2012.2217143.

[67] C. Park and A. K. Jaura, "Dynamic Thermal Model of Li-Ion Battery for Predictive Behavior in Hybrid and Fuel Cell Vehicles," in *Future Transportation Technology Conference*, 2003, no. 724.

[68] Y. Ye, Y. Shi, N. Cai, J. Lee, and X. He, "Electro-thermal modeling and experimental validation for lithium ion battery," *J. Power Sources*, vol. 199, pp. 227–238, 2012, doi: 10.1016/j.jpowsour.2011.10.027.

[69] X. W. Tao, "Design , Modeling and Control of a Thermal Management System for Hybrid Electric Vehicles," Clemson University, 2016.

[70] J. C. Dixon, "Appendix B Properties of Air," in *The Shock Absorber Handbook*, 2nd ed., John Wiley & Sons, 2007, pp. 375–378.

[71] G.-H. Kim and A. Pesaran, "Battery Thermal Management and Design," *World Electr. Veh. Assoc. J.*, vol. 1, pp. 1–61, 2007.

[72] "Axial Fans Main Catalogue," 2012. https://termocom.com.ua/images/catalogs/Axial_fan_FB.pdf.

[73] K. W. Choi and N. P. Yao, "Heat Transfer in Lead-Acid Batteries.," *Am. Soc. Mech. Eng.*, vol. 126, no. 78-HT-52, pp. 1321–1328, 1978.

[74] Y. Chen and J. W. Evans, "Heat Transfer Phenomena in Lithium/Polymer–Electrolyte Bafteries for Electric Vehicle Application," *J. Electrochem. Soc.*, vol. 140, no. 7, pp. 1833–1838, 1993, doi: 10.1149/1.2220724.

[75] T. M. Bandhauer, S. Garimella, and T. F. Fuller, "A critical review of thermal issues in lithium-ion batteries," *J. Electrochem. Soc.*, vol. 158, no. 3, 2011, doi: 10.1149/1.3515880.

[76] A. Pesaran, "Battery Thermal Management in EVs and HEVs : Issues and Solutions," in *Advanced Automotive Battery Conference*, 2001, p. 10.

[77] S. A. Khateeb, S. Amiruddin, M. Farid, J. R. Selman, and S. Al-Hallaj, "Thermal management of Li-ion battery with phase change material for electric scooters: Experimental validation," *J. Power Sources*, vol. 142, no. 1–2, pp. 345–353, 2005, doi: 10.1016/j.jpowsour.2004.09.033.

[78] S. A. Khateeb, M. M. Farid, J. R. Selman, and S. Al-Hallaj, "Design and simulation of a lithium-ion battery with a phase change material thermal management system for an electric scooter," *J. Power Sources*, vol. 128, no. 2, pp. 292–307, 2004, doi: 10.1016/j.jpowsour.2003.09.070.

[79] V. Shatikian, G. Ziskind, and R. Letan, "Numerical investigation of a PCM-based heat sink with internal fin," *Int. J. Heat Mass Transf.*, vol. 48, pp. 3689–3706, 2005, doi: 10.1016/j.ijheatmasstransfer.2004.10.042.

[80] M. Akgün, O. Aydin, and K. Kaygusuz, "Thermal energy storage performance of paraffin in a novel tube-in-shell system," *Appl. Therm. Eng.*, vol. 28, no. 5–6, pp. 405–413, 2008, doi: 10.1016/j.applthermaleng.2007.05.013.

[81] A. Alrashdan, A. T. Mayyas, and S. Al-Hallaj, "Thermo-mechanical behaviors of the expanded graphite-phase change material matrix used for thermal management of Li-ion battery packs," *J. Mater. Process. Technol.*, vol. 210, no. 1, pp. 174–179, 2010, doi: 10.1016/j.jmatprotec.2009.07.011.

[82] Q. Wang, B. Jiang, Q. F. Xue, H. L. Sun, B. Li, H. M. Zou, and Y. Y. Yan, "Experimental investigation on EV battery cooling and heating by heat pipes," *Appl. Therm. Eng.*, vol. 88, pp. 54–60, 2014, doi: 10.1016/j.applthermaleng.2014.09.083.

[83] X. Yang, Y. Y. Yan, and D. Mullen, "Recent developments of lightweight, high performance heat pipes," *Appl. Therm. Eng.*, vol. 33–34, no. 1, pp. 1–14, 2012, doi: 10.1016/j.applthermaleng.2011.09.006.

[84] W. S. Bou, C. J. Mansour, and M. G. Nemer, "Optimization of a Brayton external combustion gas-turbine system for extended range electric vehicles," *Energy*, vol. 150, pp. 745–758, 2018, doi: 10.1016/j.energy.2018.03.008.

[85] C. Mansour, M. Haddad, and E. Zgheib, "Assessing consumption , emissions and costs of electri fi ed vehicles under real driving conditions in a developing country with an inadequate road transport system," *Transp. Res. Part D Transp. Environ.*, vol. 63, no. June, pp. 498–513, 2018, doi: 10.1016/j.trd.2018.06.012.

[86] Matlab, "AVDVISOR." 2003.

[87] "Apta-bus-Procurement-Guidelines," 2013.

[88] ASHRAE, "Standard 55 – Thermal Environmental Conditions for Human Occupancy," 2013. Accessed: Nov. 21, 2019. [Online]. Available: https://www.ashrae.org/technical-resources/bookstore/standard-55-thermal-environmental-conditions-for-human-occupancy.

[89] F. Brèque and M. Nemer, "Cabin Thermal Needs: Modeling and Assumption Analysis," in *Proceedings of the 12th International Modelica Conference*, 2017, pp. 771–781, doi: http://dx.doi.org/10.3384/ecp17132771.

[90] F. Brèque, "Etude et amélioration d'une pompe à chaleur pour véhicule électrique en conditions de givrage," PSL Research University - Mines Paristech, 2017.

[91] C. Mansour, W. Bou Nader, F. Breque, and M. Haddad, "Assessing additional fuel consumption from cabin thermal comfort and auxiliary needs on the worldwide harmonized light vehicles test cycle," *Transp. Res. Part D Transp. Environ.*, vol. 62, no. February, pp. 139–151, 2018, doi: 10.1016/j.trd.2018.02.012.

[92] A. Fujita, J. ichi Kanemaru, H. Nakagawa, and Y. Ozeki, "Numerical simulation method to predict the thermal environment inside a car cabin," *JSAE Rev.*, vol. 22, no. 1, pp. 39–

47, 2001, doi: 10.1016/S0389-4304(00)00101-6.

[93] W. Swinbank, “Long-wave radiation from clear skies,” *J. R. Meteorol. Soc.*, no. 1927, 1963.

[94] *ASHRAE Handbook - Fundamentals*. 2009.

[95] M. Liebers, D. Tretsiak, S. Klement, B. Bäker, and P. Wiemann, “Using Air Walls for the Reduction of Open-Door Heat Losses in Buses,” *SAE Int. J. ACommercial Veh.*, 2018, doi: 10.4271/2017-01-9179.

[96] Z. Qi, “Advances on air conditioning and heat pump system in electric vehicles - A review,” *Renew. Sustain. Energy Rev.*, vol. 38, pp. 754–764, 2014, doi: 10.1016/j.rser.2014.07.038.

[97] “Climate Friendly Alternatives for HFCs,” *European Commission*, 2012. https://ec.europa.eu/clima/policies/f-gas/alternatives_en.

[98] S. Torzynski, D. Göhlich, D. Hahn, and B. Bryl-Radziemska, Maria Verkehrsbetriebe, “Demonstration of An Electric Bus Fleet Operated on Line 204 with Inductive Charging System in Berlin,” 2016.

[99] J. Rios, P. Sauras-Perez, A. Gil, A. Lorico, J. Taiber, and P. Pisu, “Battery electric bus simulator - A tool for energy consumption analysis,” *SAE Tech. Pap.*, vol. 2014-Janua, 2014, doi: 10.4271/2014-01-2435.

[100] Z. Gao, Z. Lin, T. J. LaClair, C. Liu, J. M. Li, A. K. Birky, and J. Ward, “Battery capacity and recharging needs for electric buses in city transit service,” *Energy*, vol. 122, pp. 588–600, 2017, doi: 10.1016/j.energy.2017.01.101.

[101] A. F. Raab, E. Lauth, K. Strunz, and D. Göhlich, “Implementation schemes for electric bus fleets at depots with optimized energy procurements in virtual power plant operations,” *World Electr. Veh. J.*, vol. 10, no. 1, pp. 1–14, 2019, doi: 10.3390/wevj10010005.

[102] I. S. Suh, K. Lee, and M. Lee, “Dynamic model and control algorithm of HVAC system for dynamic wireless charging EV application,” *Proc. 2013 IEEE Int. Electr. Mach. Drives Conf. IEMDC 2013*, pp. 241–246, 2013, doi: 10.1109/IEMDC.2013.6556259.

[103] A. Pathak, R. Khoo, A. Ongel, and M. Lienkamp, “Feasibility of Using Air Curtains in

Urban Buses Reducing cooling requirements by minimising heat infiltration during boarding / alighting."

[104] Ş. Ünal, "Determination of the ejector dimensions of a bus air-conditioning system using analytical and numerical methods," *Appl. Therm. Eng.*, vol. 90, pp. 110–119, 2015, doi: 10.1016/j.applthermaleng.2015.06.090.

[105] S. Üna, "An experimental study on a bus air conditioner to determine its conformity to design and comfort conditions," *J. Therm. Eng.*, vol. 3, no. 1, pp. 1089–1101, 2017, doi: 10.18186/thermal.277288.

[106] A. Liebold, P. Lin, B. Vetsch, C. Arpagaus, and S. S. Bertsch, "Simulation of a VRF system applied in electric buses in Taiwan," *Int. Compress. Eng. Refrig. Air Cond. High Perform. Build. Conf.*, pp. 1–10, 2016.

[107] D. Y. Lee, C. W. Cho, J. P. Won, Y. C. Park, and M. Y. Lee, "Performance characteristics of mobile heat pump for a large passenger electric vehicle," *Appl. Therm. Eng.*, vol. 50, no. 1, pp. 660–669, 2013, doi: 10.1016/j.applthermaleng.2012.07.001.

[108] ThermoKing, "Fall 2017 A Thermo King publication for the mobile climate control industry," 2017.

[109] P. Reasor and R. Radermacher, "Refrigerant R1234yf Performance Comparison Investigation," 2010.

[110] Y. Lee and D. Jung, "A brief performance comparison of R1234yf and R134a in a bench tester for automobile applications," *Appl. Therm. Eng.*, vol. 35, pp. 240–242, 2012, doi: 10.1016/j.applthermaleng.2011.09.004.

[111] A. Gomaa, "Performance Characteristics of Automotive Air Conditioning System with Refrigerant R134a and Its Alternatives," *Int. J. Energy Power Eng.*, vol. 4, no. 3, p. 168, 2015, doi: 10.11648/j.ijepe.20150403.15.

[112] A. Gużda and N. Szmolke, "Compressors in Heat Pumps," *Mach. Dyn. Res.*, vol. 39, no. 2, pp. 71–82, 2015.

[113] EmersonClimateTechnologies, "Copeland Compressor Datasheet." p. 2019, 2019.

[114] F. Fardoun, O. Ibrahim, A. Zoughaib, F. Fardoun, O. Ibrahim, and A. Zoughaib, "Dynamic modeling of an air source heat pump water heater," 2011.

[115] A. G. Rasmussen, Bryan P.; Alleyne, "Dynamic Modeling and Advanced Control of Air Conditioning and Refrigeration Systems," 2009. [Online]. Available: http://hdl.handle.net/2142/12355.

[116] "NREL DriveCAT - Chassis Dynamometer Drive Cycles by National Renewable Energy Laboratory," 2019. www.nrel.gov/transportation/drive-cycle-tool.

**** End of Chapter 2 ****

Chapter 3
ENERGY CONSUMPTION OF BATTERY ELECTRIC BUS

3.1 Introduction

The precise assessment of BEB energy consumption is critical, mainly due to its driving range limitation. Unlike DB, BEB suffers a limited driving range resulting from the limited battery capacity on-board [1]–[3]. Moreover, the use of the HVAC unit and other pneumatic, hydraulic, and electric auxiliaries further reduces the BEB driving range as they consume energy from the battery [4]–[6]. In addition to the propulsion unit energy consumption, the HVAC unit and auxiliaries' energy consumption directly drive the sizing of the battery energy capacity in BEB.

BEB energy consumption is subject to high variations at different operating conditions. These operating conditions are driving conditions, weather conditions, and passengers' load. Driving conditions are the bus velocity profile, driving behavior, trip distance and duration, road topography, and the number of stops along the route. These driving conditions affect the energy behavior of the BEB. On the other hand, weather conditions, such as temperature and solar flux, impact the bus thermal needs, and thus affect the HVAC unit energy consumption. Moreover, the passengers' load influences the energy consumption of the bus due to the additional weight on-board and the varying thermal loads depending on the number of passengers occupying the bus.

Based on the review of the literature conducted in Table 2.1, none of the studies assesses the energy consumption of BEB at a variety of operating conditions to reflect on their real-world energy consumption.

Such assessment helps in properly sizing the battery energy capacity of BEBs under certain operating conditions. A proper battery sizing helps in overcoming the driving range and the cost challenges that face the massive deployment of BEB. That being said, it is essential to assess the energy consumption of BEB under a variety of operating conditions representing the different patterns of driving conditions and passengers' load, as well as the varying weather conditions to consider the various thermal needs of the bus.

In summary, this chapter presents a detailed analysis of the energy behavior of the BEB in general, and the different energy systems encountered within, at varying operating conditions. The following research questions will be answered in this chapter:

- ***How does the energy consumption of a BEB change at different operating conditions and what are the main factors showing a significant impact on its energy consumption?***

- ***What is a proper battery sizing for a BEB considering its energy needs as function of the various operating conditions?***

This chapter is organized as follows: section 3.2 describes the impact of driving conditions on the BEB energy consumption. Sections 3.3 and 3.4 analyze the impact of weather conditions and passengers' load on the BEB energy consumption respectively. In section 3.5, a preliminary methodology for battery sizing is introduced with different case studies for battery sizing and simple technical solutions to reduce the battery size.

3.2 Impact of Driving Conditions on Energy Consumption

This section presents the impact of driving conditions on the different energy systems within the bus. The BEB model is simulated at all drive cycles presented in Table 7.7 each representing specific driving conditions in terms of traffic levels, driver's behavior, and route type (urban or intercity route depending on the number of stops per km). Weather conditions and passengers' load are held constant across the different simulations where external temperature is set to 20 $°C$, solar flux is considered as 100 W/m^2 and the passengers' load is 30 passengers (60% occupancy rate).

3.2.1 Propulsion System Energy Consumption

Figure 3.1 introduces the propulsion system energy consumption at different driving conditions. The figure shows the energy consumed during the bus acceleration mode, the energy recovered during the brake energy recovery (BER) mode, and the total propulsion energy consumption, which is the sum of the 2 mentioned energy entities. The data labels shown in the figure correspond to the total propulsion energy consumption.

The propulsion system energy consumption shows high variations at the different simulated driving conditions. The highest energy consumption is recorded during the NYB drive cycle at 2.62 *kWh/km,* whereas the lowest value is recorded during the CSHV drive cycle at 1.7 *kWh/km,* which represents a 35% reduction in the propulsion system energy consumption for the presented bus configuration.

The main reason behind this variation is related to the drive cycle average speed. Figure 3.2 plots the propulsion system energy consumption function of the drive cycle average speed. At higher average speeds, the energy consumption decreases. This indicates that with heavier traffic, resulting in lower average speeds, the propulsion system energy consumption increases.

When more frequent starts and stops are encountered, the EM does not operate a lot at steady-state conditions, resulting in additional consumption due to frequent accelerations reducing its efficiency. Furthermore, the EM maximum efficiency is at medium to high speeds which explains the additional energy consumption at very low average speeds. On the other hand, despite the higher BER at lower average speeds due to more frequent decelerations, the high energy consumption due to acceleration dominates the propulsion system energy consumption behavior.

At very high speeds, a slight increase in energy consumption is observed due to lower EM efficiency when compared to medium-high speeds, in addition to the lower BER.

The presented analysis shows the impact of traffic conditions and route specification on the propulsion system energy consumption. Buses consume more energy along routes that encounter high levels of traffic such as urban buses or city center buses, whereas buses operating along routes with fewer traffic levels benefit from reduced energy consumption which is the case for inter-city buses for example.

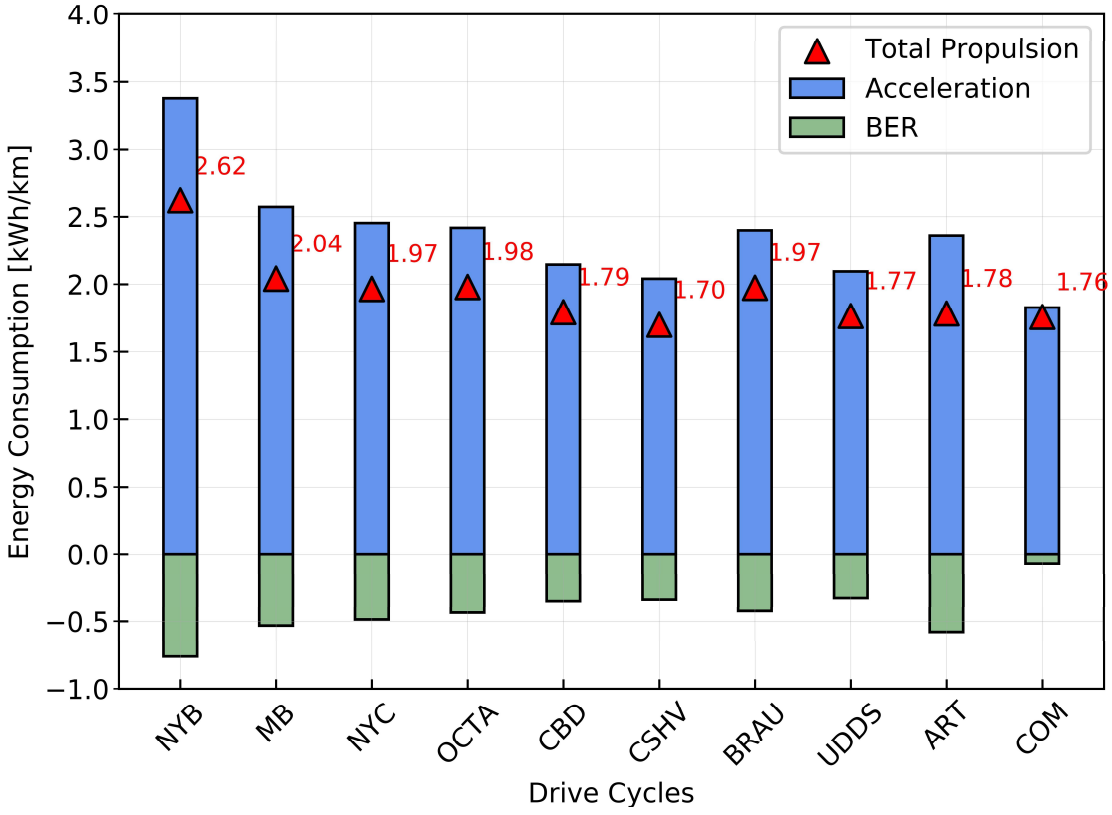


Figure 3.1: Propulsion system energy consumption at different driving conditions

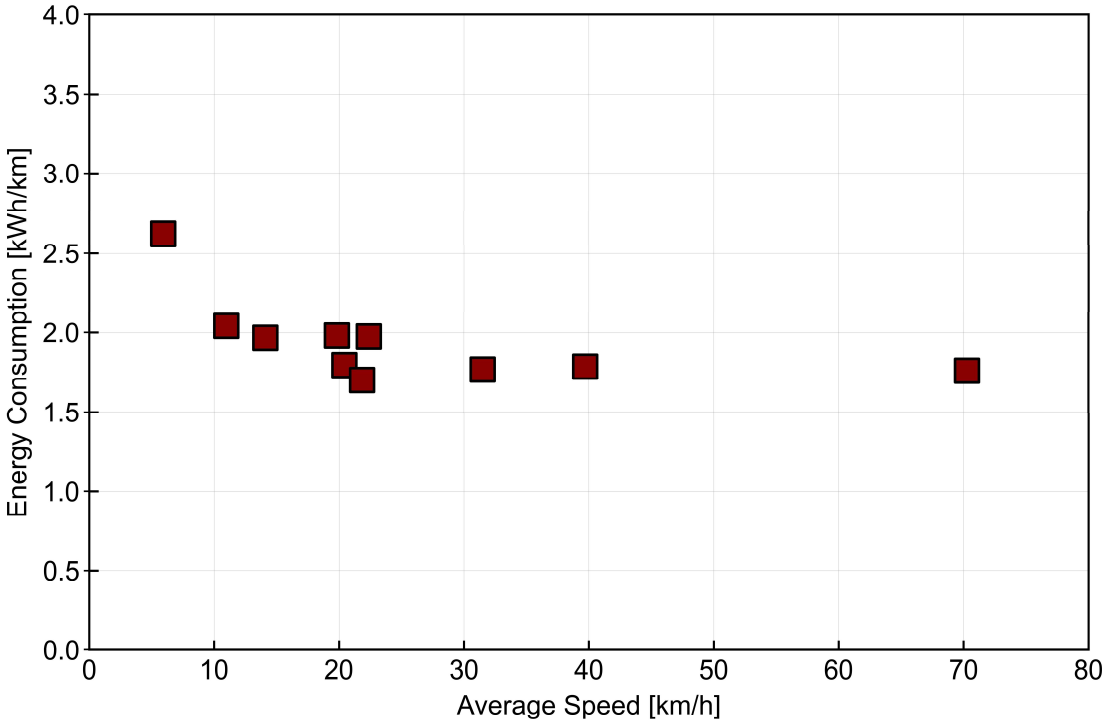


Figure 3.2: Variation of propulsion system energy consumption at different average speeds

3.2.2 Auxiliaries' Energy Consumption

Similar to the propulsion system, the auxiliaries' energy consumption is varying across the different drive cycles. The auxiliaries are the air compressor operating the pneumatic system, steering pump, suspension system, electric system, and the BTMS.

Figure 3.3 shows the energy consumption partition among the different auxiliaries at different drive cycles. The air compressor and the steering pump are the main energy consumers, followed by the suspension system, and finally the doors and the parking brakes representing the electric system. There is no electric auxiliary consumption due to lighting or wipers' actuation as they are not considered in these simulations. BTMS energy consumption is negligible as this simulation is conducted at 20 $°C$ and it doesn't show any variation with respect to the varying driving conditions, thus it is not presented in Figure 3.3.

The auxiliaries' energy consumption is highly affected by the different driving conditions, especially the air compressor and the steering pump. The total auxiliaries' energy consumption can represent up to 6% (NYB and MB) of the total BEB energy consumption as their energy consumption reaches 0.15 *kWh/km*. Other drive cycles record very low auxiliaries' energy consumption below 0.01 *kWh/km*, and the reasons behind these variations are explained in the following sections.

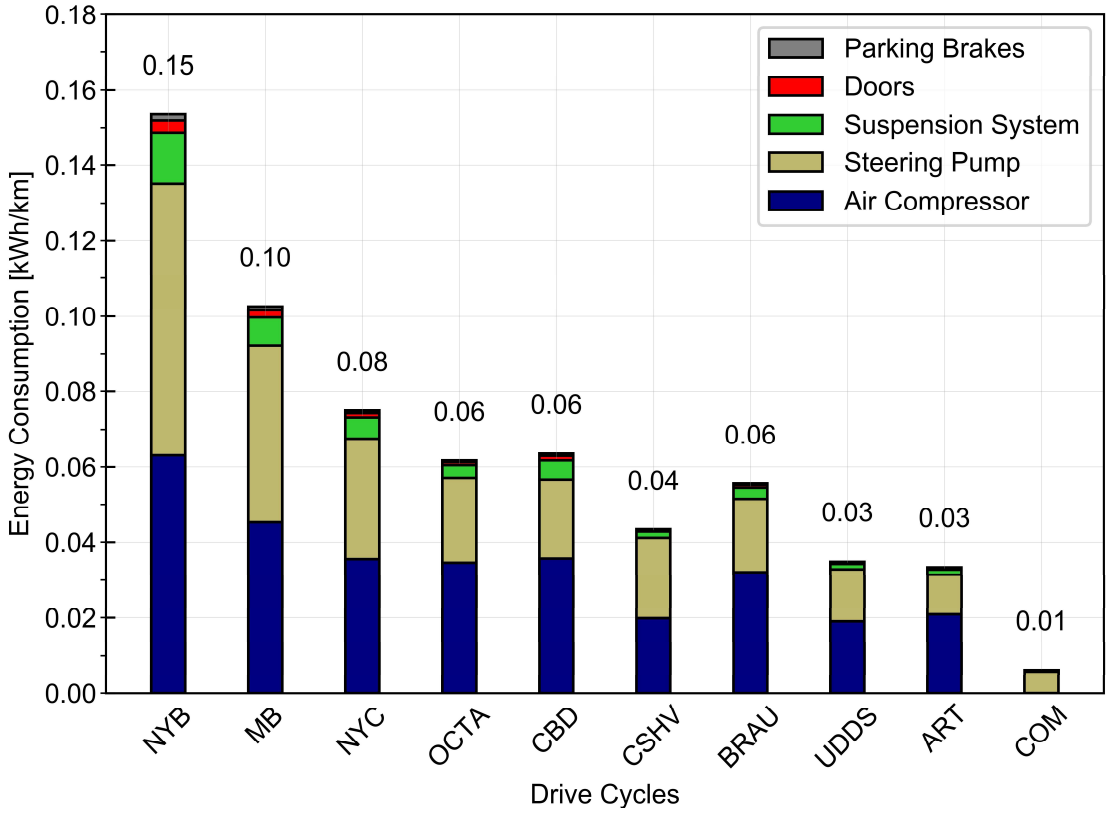


Figure 3.3: Non-Mechanical auxiliaries' energy consumption at different driving conditions

3.2.2.1 Steering Pump

Figure 3.4 plots the steering pump energy consumption as function of the cycle average speed.

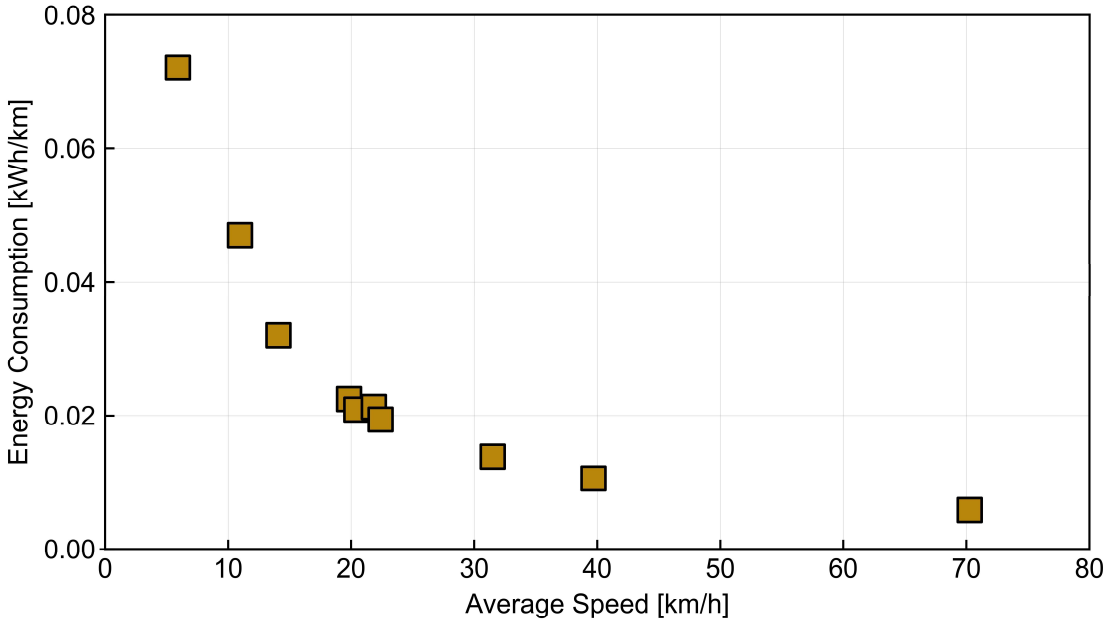


Figure 3.4: Variation of steering pump energy consumption at different average speeds

The steering pump power consumption is directly related to the bus speed. The higher the drive cycle average speed is, the lower is the steering pump energy consumption. The energy consumption exceeds 0.07 *kWh/km* at low speeds due to the pump efficiency deterioration at low speeds. At high speeds, the pump energy consumption is negligible. Once again, heavy traffic conditions increase another auxiliary feature energy consumption up to 3 times compared to lighter traffic conditions.

3.2.2.2 Air Compressor

The main pneumatic feature in a BEB is the service brakes and it is operated by the air compressor. Figure 3.5 plots the air compressor average power demand as function of the average drive cycle deceleration, which is representative of the level of braking encountered during the trip.

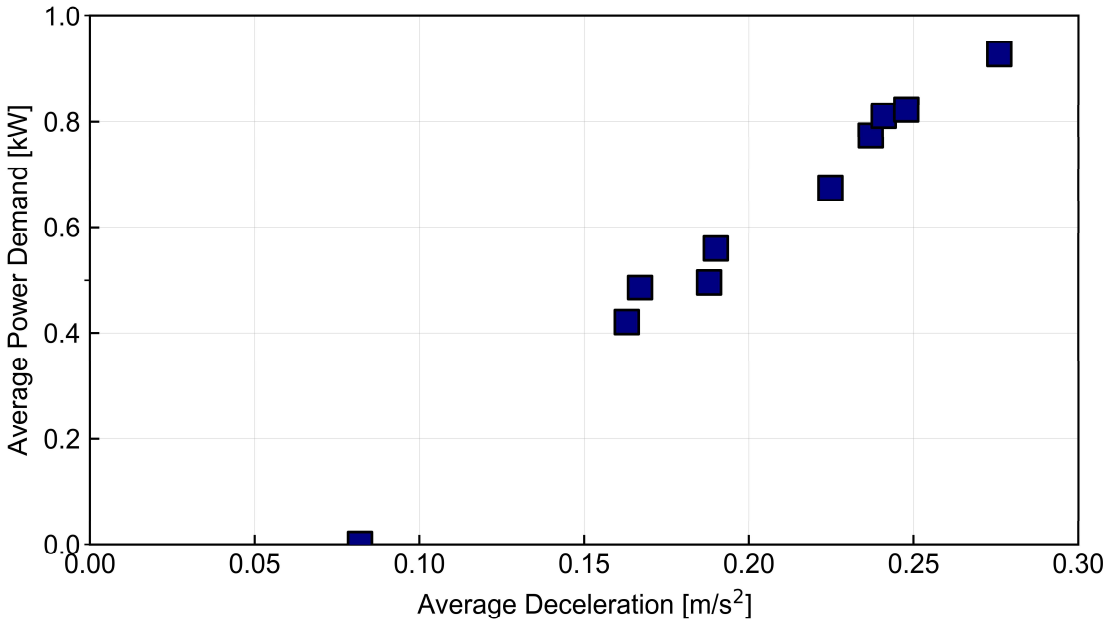


Figure 3.5: Air compressor average power demand function of drive cycle's average deceleration

The higher the drive cycle average deceleration is, the higher is the air compressor power demand. In other words, heavy traffic conditions associated with high decelerations can increase the pneumatic system energy consumption in a BEB. With more deceleration, more compressed air is needed to actuate the service brakes, and thus, the air compressor is turned on more frequently resulting in increased energy consumption or average power demand. At high trip deceleration (> 0.3 *m/s²*), the air compressor average power demand reaches 1 *kW*, whereas this value decreases during trips with normal decelerations reaching 0.5 *kW*. Driving

conditions with high levels of traffic and deceleration are mainly encountered in urban areas and inside city centers resulting in this additional energy consumption.

3.2.2.3 Suspension System and Electric Auxiliaries

The main electric features in BEB are the doors and the parking brakes. In addition to the suspension system, these features are only actuated when there is a bus stop, and the number of stops differs from one drive cycle to another. Figure 3.6 shows the energy consumption of these features function of the number of bus stops per kilometer. The higher the number of bus stops per kilometer is, the higher is the energy consumption. The cycle with the highest number of stops per km (NYB) records the highest energy consumption. The number of bus stops per km is related to the route specifications as the number of stops will increase in urban areas and inside city centers resulting in additional energy consumption.

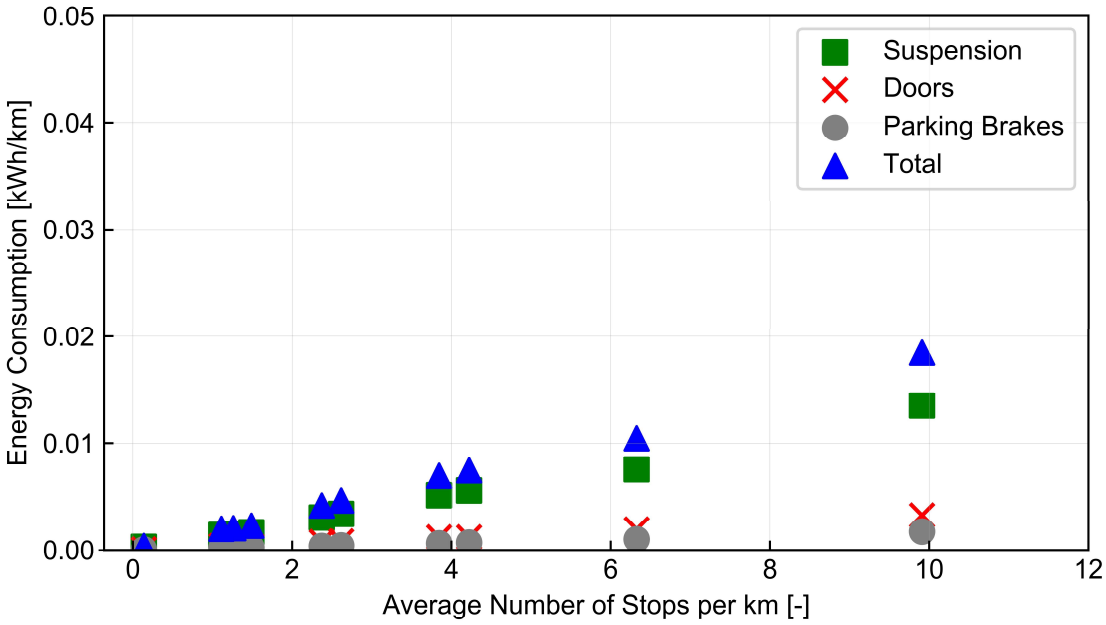


Figure 3.6: Variation of the suspension system and electric auxiliaries energy consumption function of the average number of stops per km

3.2.3 HVAC Unit Energy Consumption

The HVAC unit energy consumption is affected by the doors opening on the bus. The different drive cycles incur a different number of stops and different stoppage time at each stop where the doors are opened for passengers to get in and out of the bus. The doors' opening results in heat losses which affect the bus cabin temperature and diverges it from the set thermal comfort temperature range. As a result, the HVAC unit compressor switches ON more frequently to compensate for these heat losses. Figure 3.7 shows the HVAC unit average electric power

demand at different drive cycles. The average HVAC unit electric power ($P_{HVAC.avg}^{elec}$) is calculated by dividing the total HVAC unit energy consumption at the end of the trip (E_{HVAC}^{Total}) by the trip duration (Δt) as shown in equation (3.1).

$$P_{HVAC.avg}^{elec} = \frac{E_{HVAC}^{Total}}{\Delta t} \tag{3.1}$$

The different drive cycles are represented on the horizontal axis of Figure 3.7 by the ratio of bus stoppage time at stops to trip duration, and this ratio is referred to as $R_{door\text{-}open}$. Due to the lack of data on bus doors opening duration at each bus stops, it is assumed that the bus doors are always open when the bus is waiting at a certain stop. Consequently, the presented ratio reflects on how long the bus doors remain open during the trip.

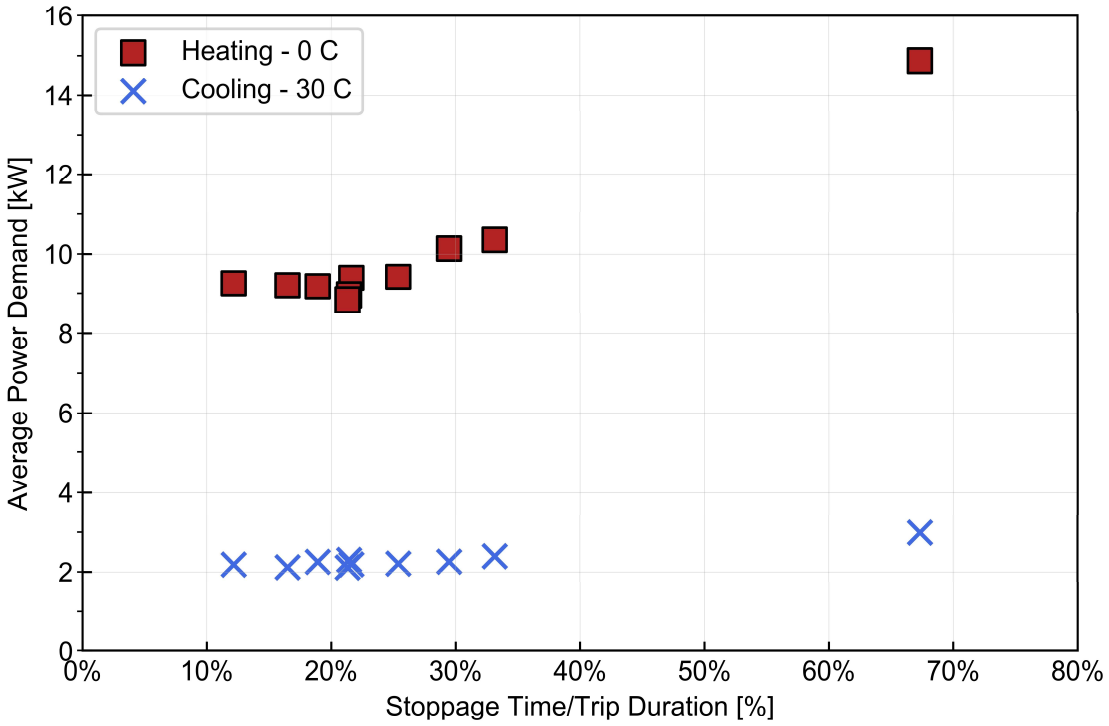


Figure 3.7: HVAC unit average electric power demand at different drive cycles

There are two scenarios considered, 1 heating scenario where the external temperature is 0 °*C*, and another cooling scenario where the external temperature is 30 °*C* as shown in Figure 3.7. For low to medium values of $R_{door\text{-}open}$ between 10 to 35 %, the average power demand increases from 9 to 10.5 *kW* during heating, and from 2 to 2.5 *kW* during cooling. At high $R_{door\text{-}open}$ values around 70%, which correspond to the NYB drive cycle, the average power demand reaches 15 *kW* during heating and 3 *kW* during cooling, which is almost a 50 % increase in the power demand when compared to the drive cycle that incurs the minimum $R_{door\text{-}open}$ value. Note that

the average power demand behavior is not linear because, with higher door opening duration, the HVAC system operates more during transient states with fluctuations in total COP.

This analysis implies that buses that operate along routes with a high number of stops and stoppage time at the stop stations require more energy to ensure thermal comfort conditions. This is mainly associated with buses operating in urban areas where the number of stops is high, and the doors are opened more frequently and for longer durations. On the contrary, buses operating outside urban areas such as inter-city buses require less energy.

3.3 Impact of Weather Conditions on Energy Consumption

This section presents the impact of weather conditions on the different energy systems, mainly the HVAC unit and the BTMS. The BEB model is simulated at a variety of weather conditions. The considered parameters are the external temperature and the solar flux. The external temperature ranges between -10 $°C$ and 40 $°C$ as they represent the extreme temperatures encountered in the city of Paris throughout the year. In addition, 3 levels of solar flux are considered: no flux, low flux (100 W/m^2), and high flux (400 W/m^2). Note that the solar flux values refer to the solar flux intensity over a horizontal surface area, and thus each wall of the bus is subject to different total solar flux depending on its orientation. Driving conditions and passengers' load are held constant across the different simulations where the MB drive cycle is used, and the passengers' load is fixed at 30 passengers (60% occupancy rate). This section is organized as follows: first, the impact of external temperature on the HVAC unit and BTMS is considered without solar flux, second, the impact of solar flux is evaluated and finally, the performance of the proposed heat recovery system is assessed.

3.3.1 Impact of External Temperature

Figure 3.8 shows the BEB cabin steady-state thermal load at different external temperatures. To recall the definition of thermal load, it is the heat supply to the BEB cabin or the heat extraction from the BEB cabin by the HVAC unit in order to attain thermal comfort conditions. During heating, for temperatures below 15 $°C$, the HP condensers should supply from 9.5 kW up to 30 kW at extreme cold conditions. This thermal load increases as external temperature decreases. On the other hand, during cooling, for temperatures above 25 $°C$, the HP evaporators should extract between 3 kW to 18 kW at extreme hot conditions.

For temperatures between 15$°C$ and 20 $°C$, neither heating nor cooling is required, and the HVAC unit only works in ventilation mode.

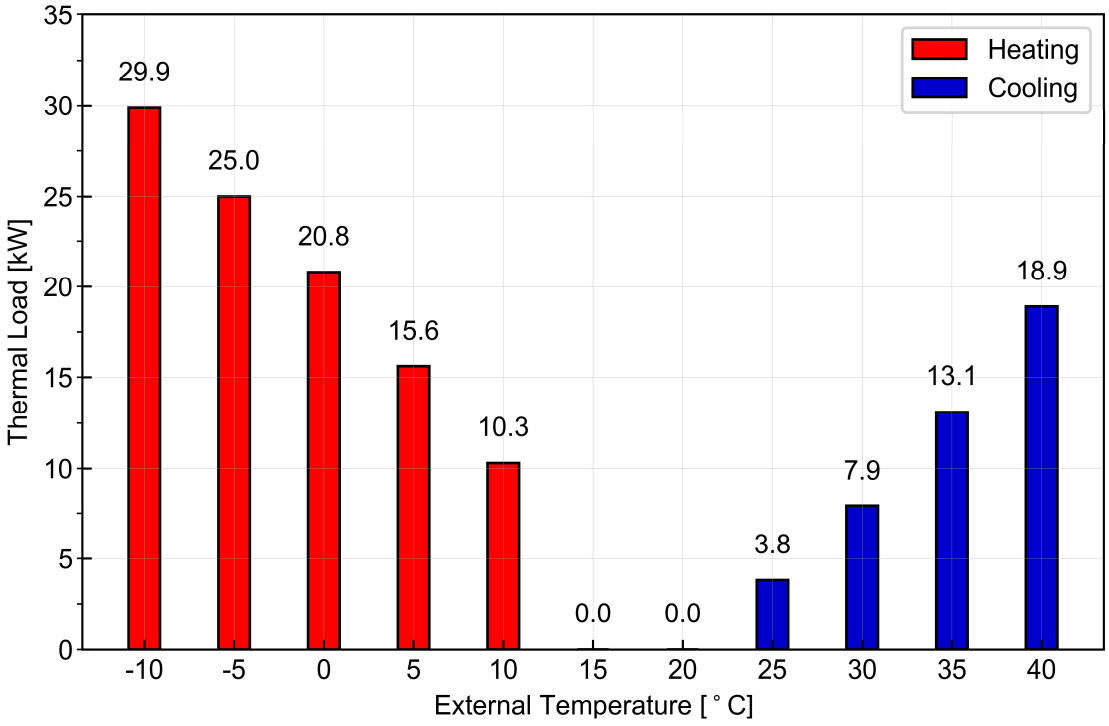


Figure 3.8: BEB cabin steady-state thermal load at different external temperatures

The thermal load during cold conditions exceeds that at hot conditions due to the higher temperature difference between the exterior and the cabin thermal comfort temperature (19-23 *°C* for cold conditions and 23-26 *°C* for hot conditions) despite the high latent heat load during cooling resulting from humidity condensation at the evaporator. Figure 3.9 and Figure 3.10 presents the thermal load segmentation at different external temperatures for heating and cooling, respectively.

During heating, the thermal load is mainly composed of heat losses through the cabin body and glazing walls, ventilation, door opening losses, and passengers' heat rejection. Heat losses through the cabin body are the biggest contributor to the thermal load representing almost 50% of this load. This is mainly due to the large body surface area when compared to the glazing surface area. In addition, heat losses due to ventilation (fresh air) are another main contributor to the thermal load representing more than 20%. Note that the ventilation heat losses are directly dependent on the number of passengers inside the bus. For the current simulations, only 30 passengers are occupying the bus, and thus, with a higher passenger occupancy rate, more ventilation heat losses are expected.

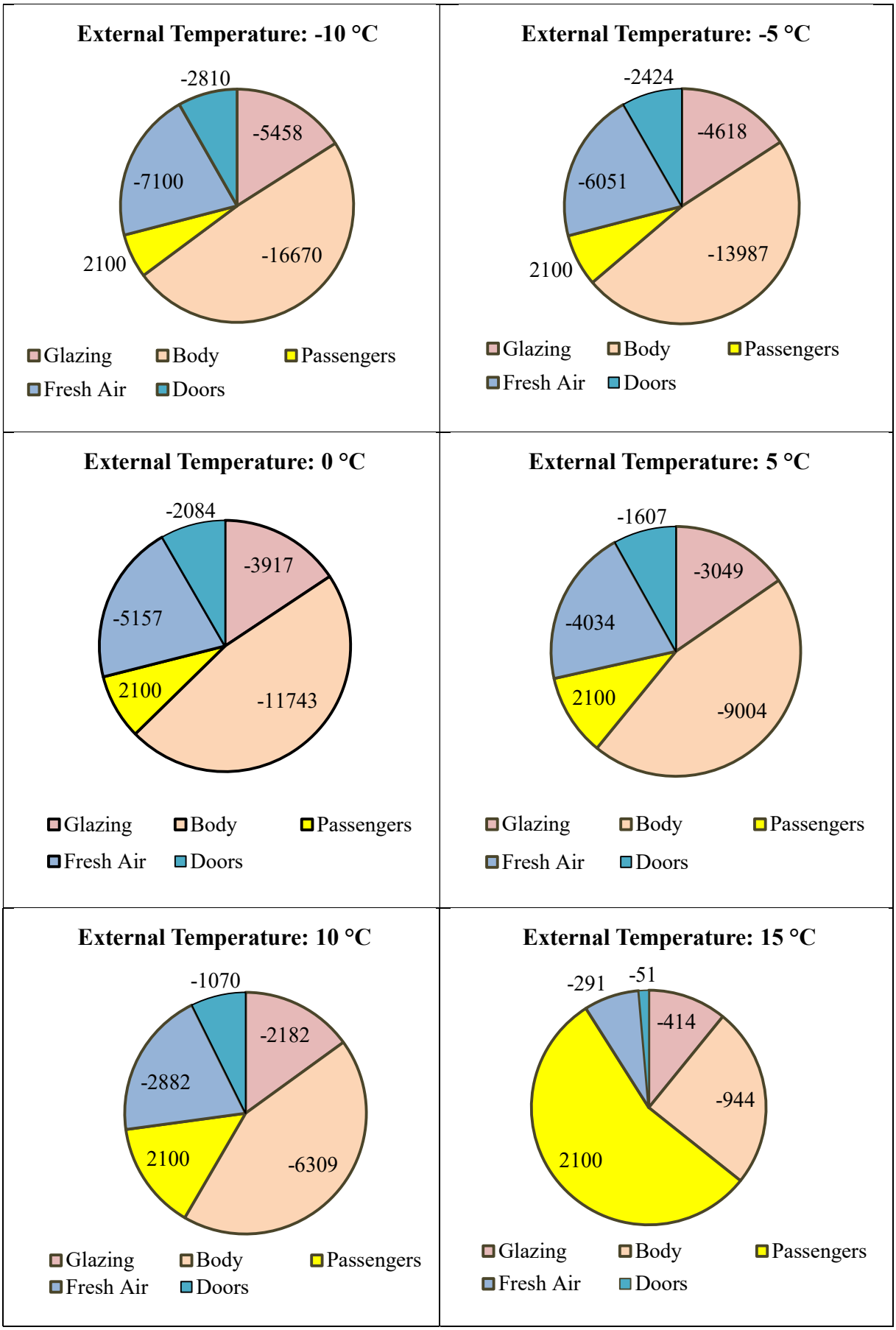


Figure 3.9: Thermal load segmentation at different external temperatures measured in W (Heating)

In addition, heat losses due to doors opening can represent up to 8% of the thermal load depending on the external temperature. Furthermore, passengers' sensible heat rejection is a positive contributor to the thermal load during winter.

On the other hand, during cooling, latent heat rejection is an additional contributor to the thermal load. Similar to cold weather conditions, heat losses through cabin body walls remain the biggest contributor to the thermal load, followed by ventilation heat losses, latent heat rejection, and door losses. Unlike cold weather conditions, the passengers' sensible heat rejection increases the thermal load during summer.

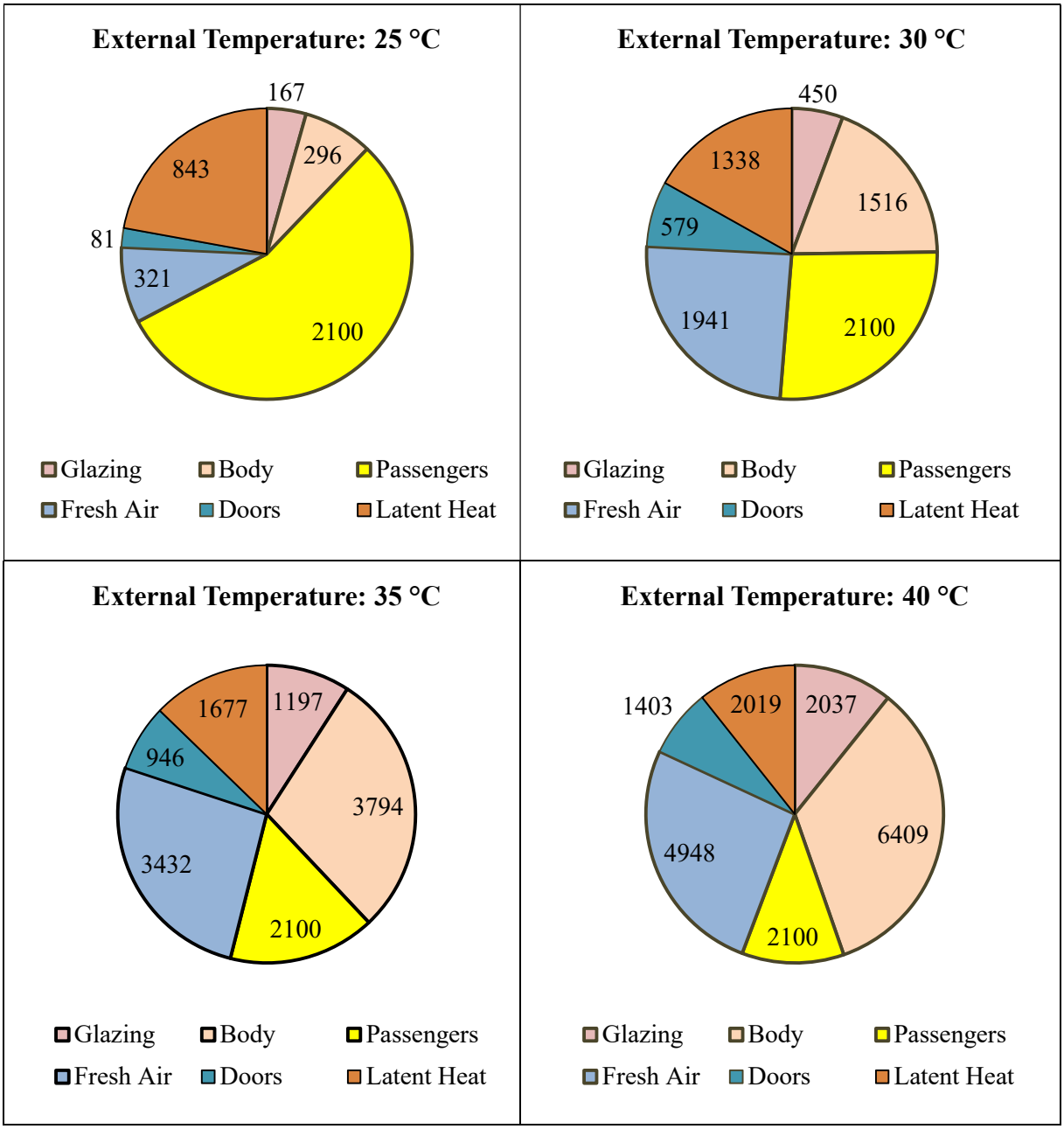


Figure 3.10: Thermal load segmentation at different external temperatures measured in W (Cooling)

After assessing the cabin thermal load, the corresponding HVAC unit energy consumption can be evaluated. Figure 3.11 shows the HVAC unit average electric power consumption at different external temperatures. The HVAC unit average power demand is the highest at extreme weather conditions due to the high thermal load at these conditions. The maximum electric power is always higher than the average power presented in Figure 3.11. The minimum electric power is around 1 kW when the external temperature is between 15-20 $°C$ as neither heating nor cooling is required, and the sole energy demand in this case is associated with the HVAC unit fans in order to ensure air ventilation. Figure 3.12 shows the cabin temperature evolution and the HVAC unit instantaneous electric power demand at 0 $°C$ external temperature simulated over 1 MB drive cycle (1089 seconds). The maximum electric power demand reaches 12.2 kW at 0$°C$ whereas the average reported power demand is around 10.4 kW as shown in Figure 3.11. In addition, the HVAC system COP is lowest at extreme weather conditions as shown in Figure 3.13, which further deteriorates the HVAC unit performance at these conditions. The COP increases as the external temperature approaches room temperature. The slight decrease in the COP at 15 $°C$ and 25 $°C$ is due to the very low condenser and evaporator power compared to the fans' power, which reduces the COP as the fans' power demand becomes dominant at these conditions.

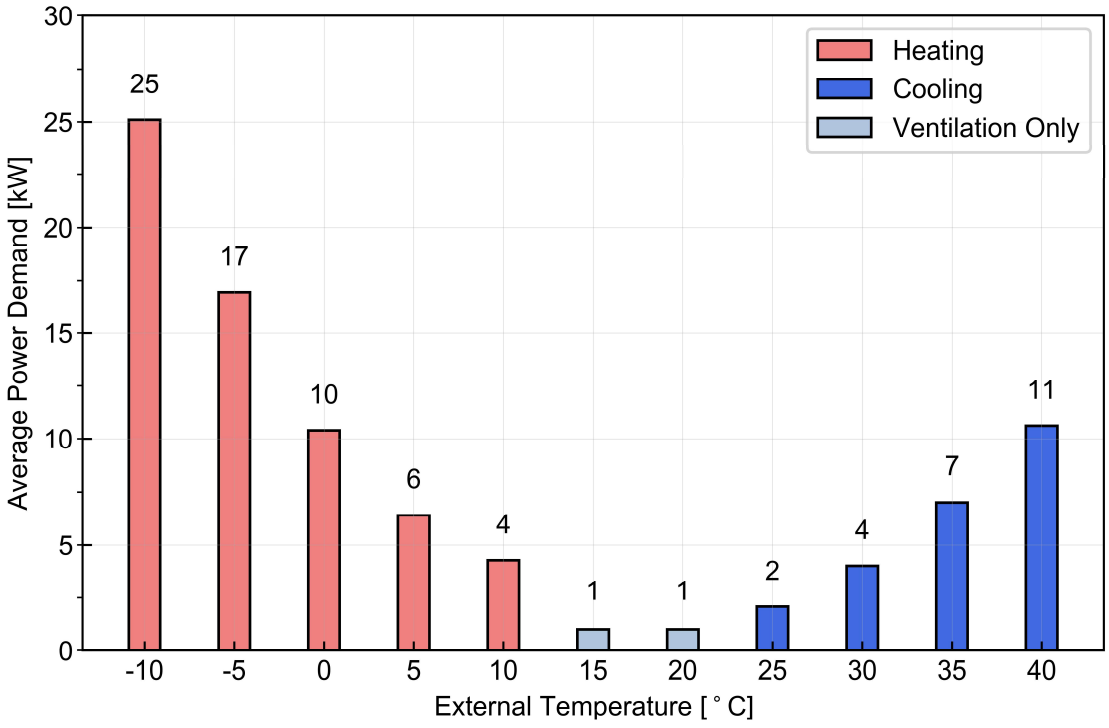


Figure 3.11: HVAC unit average electric power consumption at different external temperatures

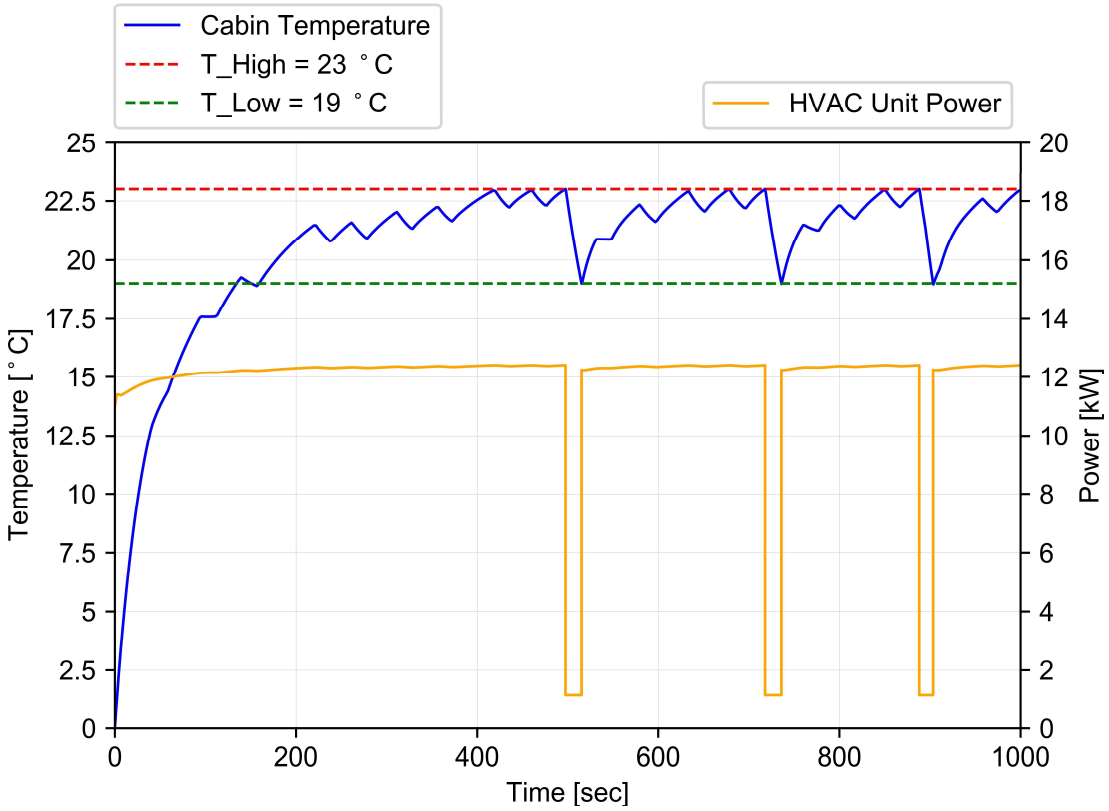


Figure 3.12: Cabin temperature evolution and HVAC unit instantaneous electric power demand - T = 0 °C - MB Drive Cycle

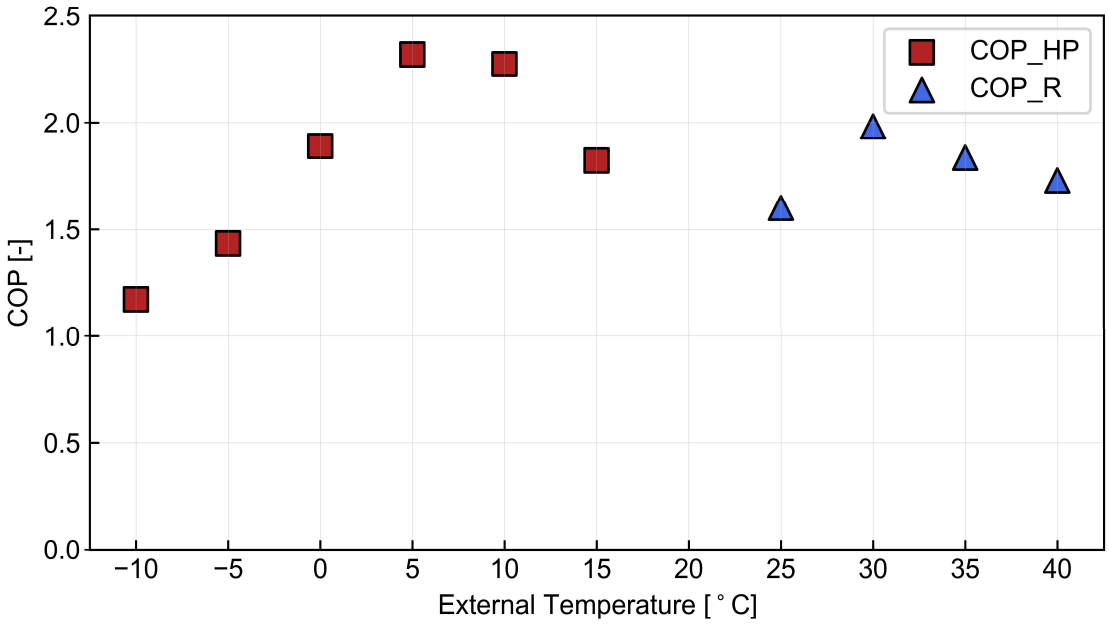


Figure 3.13: HVAC system heating COP (COP_HP) and cooling COP (COP_R) at different external temperatures

In addition to the HVAC unit power demand, the variation in external temperatures affects the BTMS power demand. Figure 3.14 shows the BTMS average electric power demand at different external temperatures. Similar to the HVAC unit average power demand, the BTMS average power demand is calculated by dividing the total BTMS energy consumption at the end of the trip (E_{BTMS}^{Total}) by the trip duration (Δt) as shown in equation (3.2).

$$P_{BTMS.avg}^{elec} = \frac{E_{BTMS}^{Total}}{\Delta t} \tag{3.2}$$

The BTMS average power demand is highest at extreme weather conditions as the air used to cool the battery cells requires cooling during extremely hot conditions and heating during extremely cold conditions. The BTMS average power demand can reach 6 *kW* at extreme hot conditions, which is one-third of the total HVAC unit power demand. It is important to note that the number of passengers occupying the bus has an indirect impact on the BTMS average power demand as explained in the previous chapter. With varying passengers' number, the BTMS average power demand varies, and this will be discussed in the next section.

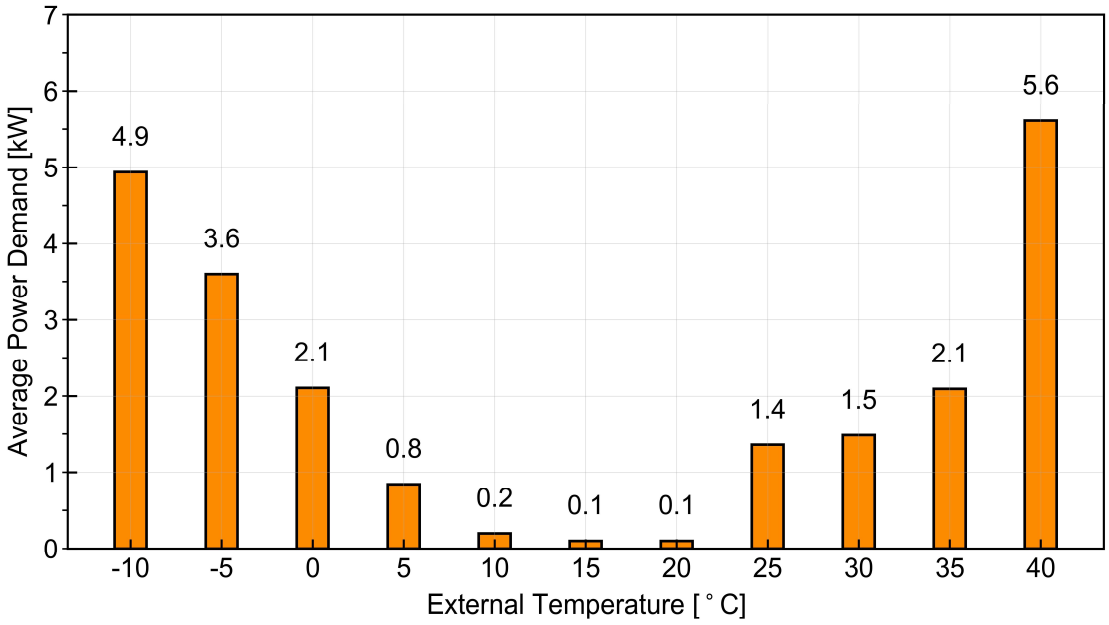


Figure 3.14: BTMS average electric power demand at different external temperatures

3.3.2 Impact of Solar Flux

The previous analysis is conducted considering no solar flux. However, the solar flux varies depending on the weather conditions. For instance, cloudy weather conditions will result in lower solar flux, and thus less solar flux will be absorbed and transmitted through the walls.

For this sake, the impact of solar flux on the HVAC unit average electric power demand is studied as shown in Figure 3.15.

During heating, higher solar flux reduces the thermal load as there is more solar flux transferred to the bus cabin, reducing the energy needed to heat the bus cabin. With higher solar flux, the bus cabin gets heated up faster, and thus the compressor will turn off more often reducing the total average power demand. This reduction can reach 15% at extreme cold conditions.

On the contrary, during cooling, the solar flux increases the thermal load, and thus more heat extraction from the bus cabin is needed resulting in additional average power demand by the HVAC unit. At extreme hot conditions, the high solar flux may result in a 30% increase in the HVAC unit power demand.

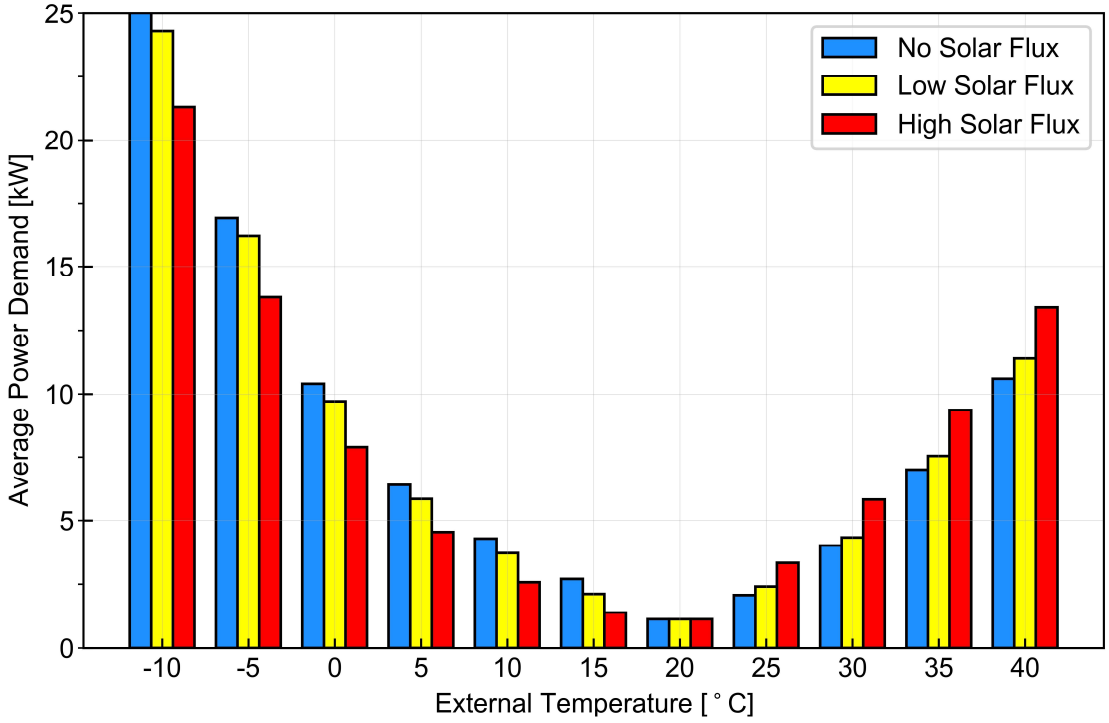


Figure 3.15: HVAC unit average power demand at different levels of solar flux

3.3.3 Impact of HVAC Energy Recovery System

The proposed HVAC unit installed on the bus includes an air-air heat exchanger to recover part of the exhaust air energy. This energy recovery system helps in reducing the energy consumption of the HVAC unit. Figure 3.16 shows the HVAC unit average power demand at different external temperatures with and without the energy recovery system. The recovery system can reduce the average power demand of the HVAC unit by 20 to 25%. The effectiveness of the heat exchanger to recover the exhaust air energy ranges from 50 to 60%

depending on the external temperature. The effectiveness can be significantly improved if the geometry of the heat exchanger is optimized, and thus more energy can be recovered.

In addition to the heat exchanger effectiveness, the number of passengers occupying the bus affects the amount of energy that can be recovered due to varying fresh air requirements, which will be discussed in the next section.

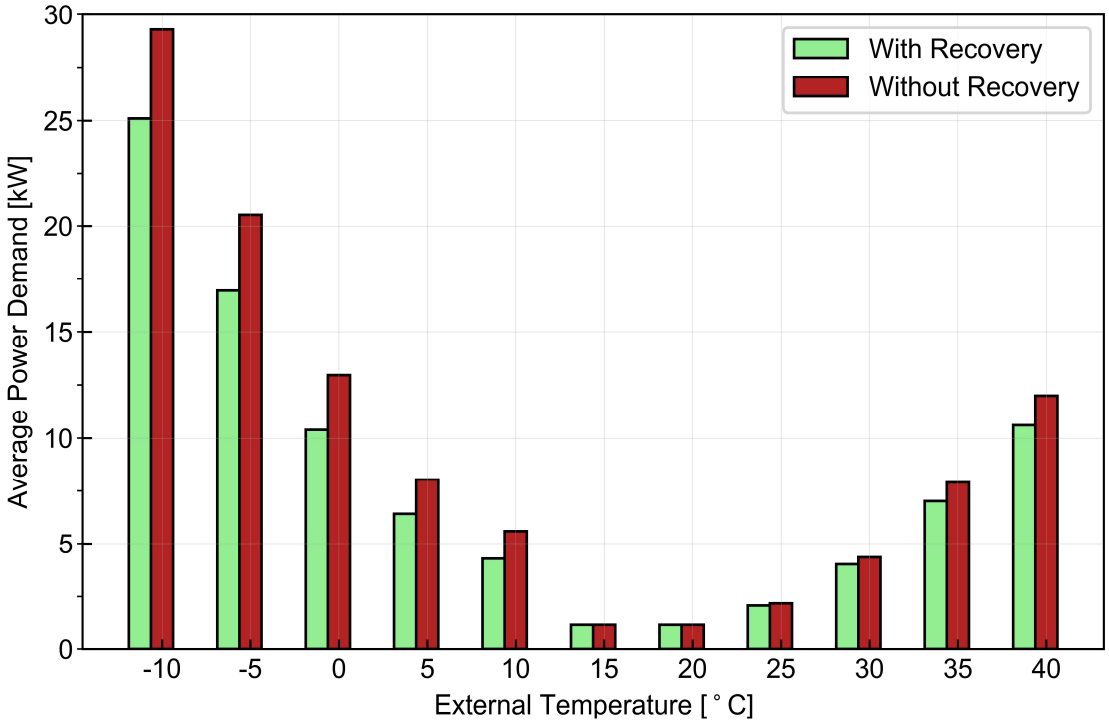


Figure 3.16: HVAC unit average power demand at different external temperatures with/without energy recovery system

3.4 Impact of Passengers' Load on Energy Consumption

This section presents the impact of passengers' load on the different energy systems within the bus. The BEB model is simulated at a variety of passengers' loads representing the different occupancy rates encountered on the bus during the day. The passengers' load varies from 5 to 80 passengers where the latter represents a case where the bus maximum passengers' capacity is exceeded by 50%. Driving conditions are held constant across the different simulations where the MB drive cycle is used. Concerning weather conditions, 2 external temperatures are considered (0 °*C* for a heating scenario and 30 °*C* for a cooling scenario) and the solar flux is set to low intensity. This section is organized as follows: first, the impact of passengers' load on the HVAC unit is assessed. Second, the impact of passengers' load on BTMS energy consumption is evaluated and finally, the effect on the propulsion system is assessed as well.

3.4.1 HVAC Unit Energy Consumption

Figure 3.17 shows the HVAC unit average electric power demand at different passengers' loads. For the heating scenario at 0 °*C* external temperature, the average power demand slightly increases from 10.5 *kW* to 11.1 *kW* between the minimum and the maximum passengers' loads, which represents a 5 % increase in the power demand and energy consumption as well. On the other hand, when considering the cooling scenario at 30 °*C* external temperature, the average power demand drastically increases from 2.9 *kW* to 6 *kW* between the minimum and the maximum passengers' loads, which represents a 100 % increase in the power demand, or almost doubling the power demand and energy consumption as well.

It is noteworthy to mention that the illustrated average power demand of the HVAC system increases by steps as a function of the passengers' occupancy. This is due to the adopted control strategy of the HVAC system, which adjusts the control variables of the system according to the four defined levels of passengers' occupancy.

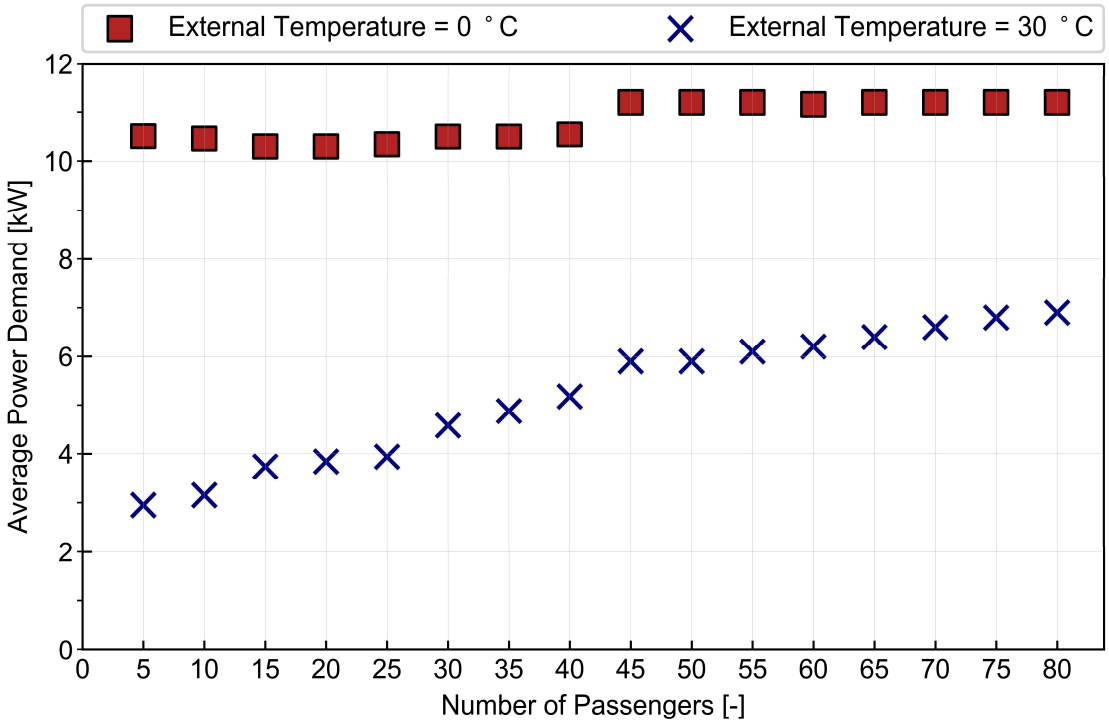


Figure 3.17: HVAC unit average electric power demand at different passengers' load

In order to explain the behavior of the HVAC unit average power demand at varying passengers' loads, it is important to recall that a higher number of passengers implies a larger amount of fresh air to be injected into the bus cabin to attain thermal comfort conditions. The amount of fresh air injected into the bus cabin affects two main parameters: (1) the fresh air

heat flux due to ventilation (ventilation load) and the mixed air upstream the condenser/evaporator (or downstream the mixing plenum).

Figure 3.18 shows the fresh air heat flux (ventilation load) at different passengers' loads. For the heating scenario at 0 °*C* external temperature, the heat flux increases from almost -2 *kW* to – 10.5 *kW* resulting in a higher ventilation load. This increase is only dependent on the passengers' load. Similarly, for the cooling scenario, the heat flux increases from almost 0.5 *kW* to 4 *kW* resulting in a higher ventilation load. Based on the HVAC unit control strategy, in particular ACU, for all number of passengers above 45, the bus is considered to be at its maximum occupancy (bus maximum seated occupancy is 55, and an additional 25 can stand inside the bus), which explains the constant heat flux after 45 passengers. The negative sign during the heating scenario indicated that the cabin is losing heat to the exterior. At higher passengers' loads, more fresh air is required, and thus more exhaust air is extracted from the bus cabin, and consequently more heat. This high heat extraction is compensated by increasing the HVAC unit heat supply resulting in additional power demand and energy consumption as presented in Figure 3.17. Moreover, Figure 3.17 shows a less sensitive behavior during the heating scenario compared to the cooling scenario, this is due to the fact with a higher passengers' load, more heat is rejected into the bus cabin from the passengers, and thus it helps in heating the bus cabin and reducing the heating needs, unlike the cooling scenario where this factor contributes negatively and increases the cooling needs.

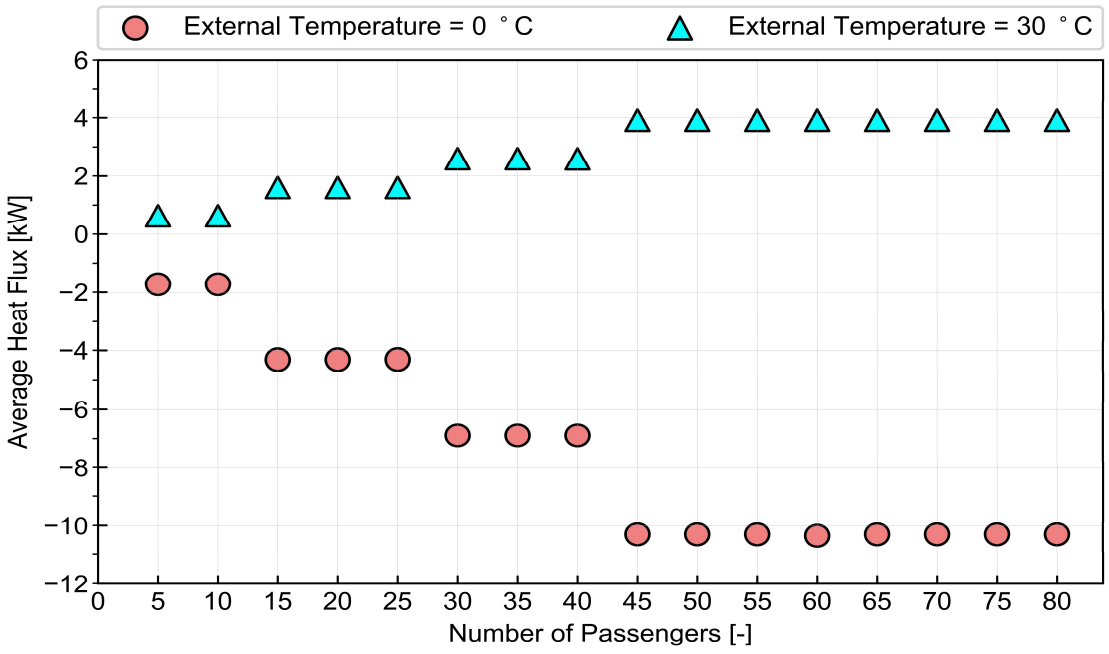


Figure 3.18: Fresh air heat flux (ventilation load) at different passengers' load

On the other hand, Figure 3.19 shows the air temperature upstream the condenser/evaporator at different passengers' loads. Note that the reported temperature values in Figure 3.19 are average values taken over the entire steady-state period. At higher passengers' loads, more fresh air is required, and thus less air is being recirculated from the bus cabin and mixed with the fresh air. This decreases the air temperature upstream the condenser in the heating scenario and increases the air temperature upstream the evaporator in the cooling scenario. In both cases, the inlet temperature diverges from the desired blown air temperature (outlet temperature), and in order to compensate for this variance, the compressor speed is increased resulting in higher power demand as presented in Figure 3.17, and consequently higher energy consumption.

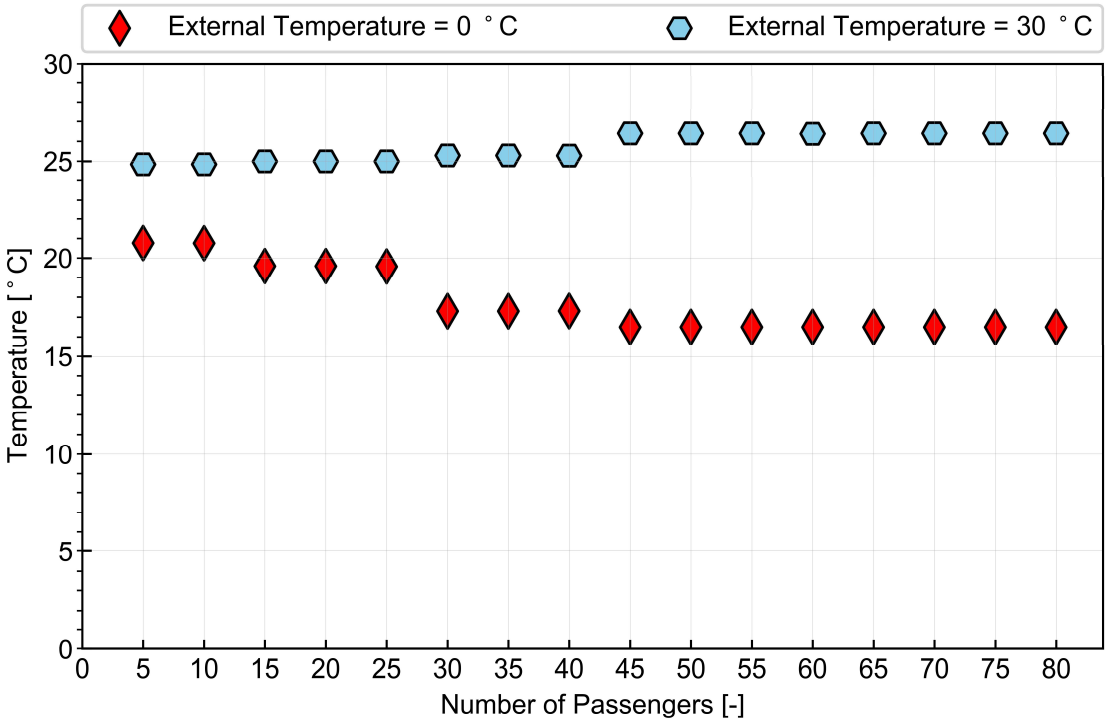


Figure 3.19: Temperature of air upstream the condenser/evaporator at different passengers' load

3.4.2 BTMS Energy Consumption

Figure 3.20 shows the BTMS average electric power demand at different passengers' load. For the heating scenario at 0 $°C$ external temperature, the average power demand is highest at low passengers' loads reaching 5.5 kW. This value decreases down to 0.3 kW at passengers' load equal to 45 where it remains almost constant afterward. Similar trends are observed when considering the cooling scenario at 30 $°C$ external temperature as the average power demand

decreases from 2.3 *kW* to 1 *kW* at passengers' load equal to 45 where it remains almost constant afterward for higher passengers' loads.

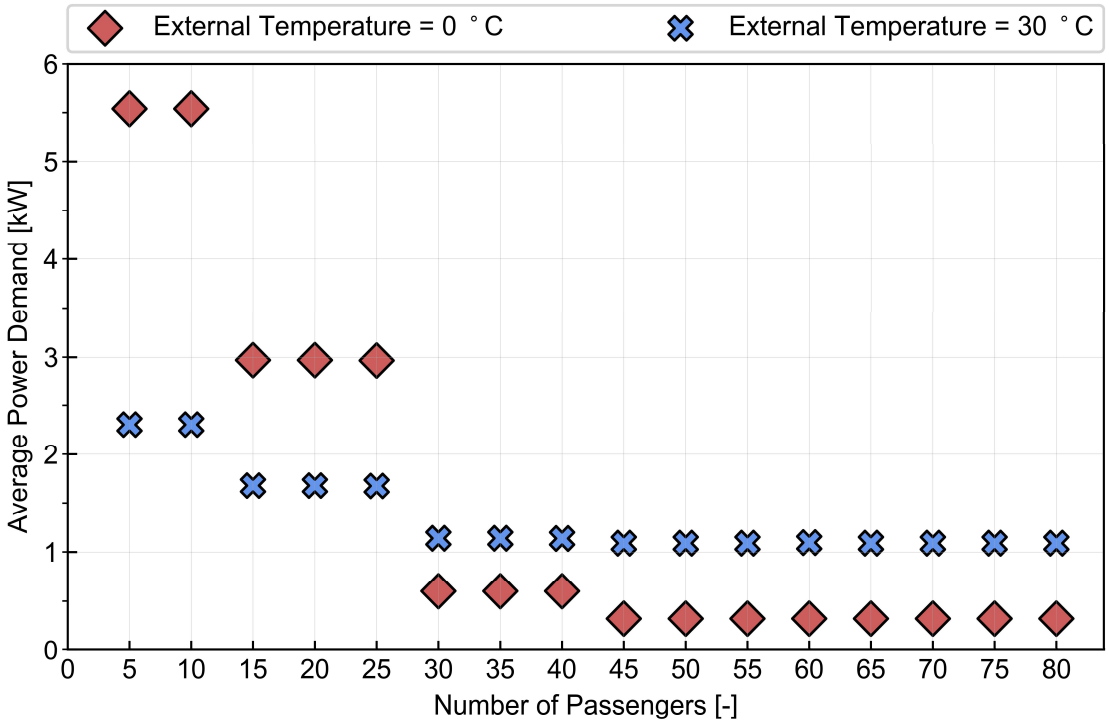


Figure 3.20: BTMS average electric power demand at different passengers' load

This behavior can be explained by recalling the BTMS control strategy presented in the previous chapter. During the heating scenario at 0 °*C* external temperature, the temperature of the blown air over the battery pack should be around 10 °*C,* and the air source is determined based on the ratio λ defined as the ratio of the BTMS required airflow rate to the ratio of the fresh air flow rate into the bus cabin ($\dot{m}_{air}^{BTMS}/\dot{m}_{air}^{fresh}$). For passengers' loads less than 45, the ratio λ is greater than 1 as the flow of fresh air ($\dot{m}_{air}^{fres}$) entering the bus cabin is less than the airflow needed to cool the battery pack ($\dot{m}_{air}^{BTMS}$), and thus the remaining required airflow is extracted from the exterior. Higher values of λ are obtained at lower passengers' loads and as a result, the temperature of the mixed air upstream the electric resistance decreases as shown in Figure 3.21. This implies that more power is needed to reach the desired blown air temperature at 10 °*C*. For passengers' load higher than 45, the ratio λ is less than 1, and the air blown over the battery pack is entirely drawn from the bus cabin at a temperature between 21 – 22 °*C* regardless of the λ values. No air heating is required in this case and the slight power demand observed is due to the fans' electric power consumption.

Concerning the cooling scenario at 30 °*C* external temperature, the temperature of the blown air over the battery pack should be around 20 °C and the air source is determined based on the ratio λ as well, as presented earlier in Figure 2.17. For passengers' loads less than 45, the ratio λ is greater than 1, and the temperature of the mixed air upstream the evaporator increases at lower passengers' loads as shown in Figure 3.21. This implies that more power is needed to reach the desired blown air temperature at 20 °*C*. For passengers' load higher than 45, the ratio λ is less than 1, and the air blown over the battery pack is entirely drawn from the bus cabin at a temperature between 23 – 24 °*C* regardless of the λ values. Slight air cooling is required in this case as the desired air temperature is around 20 °*C*.

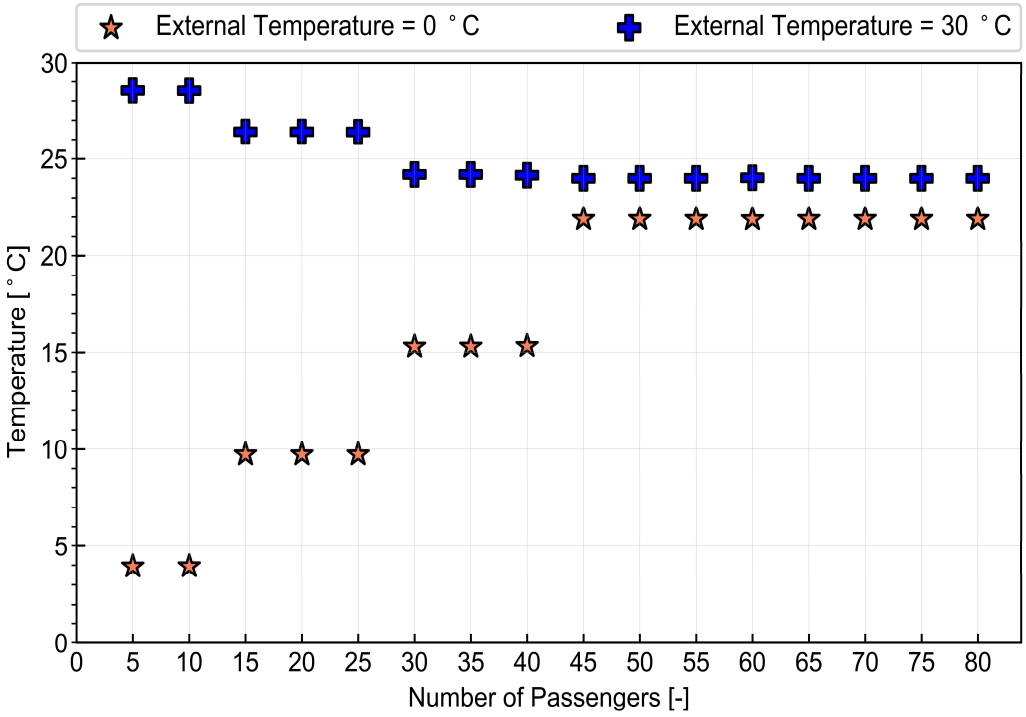


Figure 3.21: Temperature of air upstream the electric resistance/evaporator at different passengers' load

3.4.3 Propulsion System Energy Consumption

The passengers' load has a significant impact on the propulsion system energy consumption. Trivially, a higher number of passengers increases the propulsion system energy consumption due to the higher bus weight as presented in Figure 3.22. The energy consumption might increase by more than 15% for an overridden bus (80 passengers).

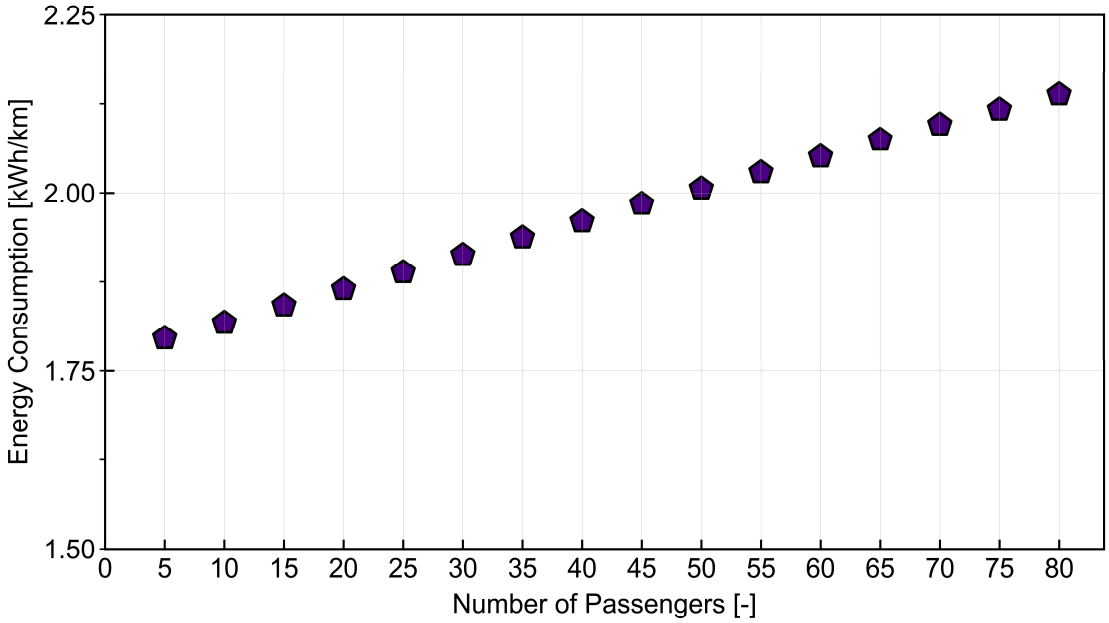


Figure 3.22: Propulsion system specific energy consumption at different passengers' loads

3.5 Study of Bus Battery Sizing at Different Operating Conditions

This section presents a study on the impact of the varying operating conditions the bus encounters during its operation on the required battery size. This study helps in understanding the proper battery sizing as function of the operating conditions and gives insights on the main parameters that drive the battery size. A preliminary battery sizing methodology is presented first, followed by several case studies.

3.5.1 Preliminary Battery Sizing Methodology

In this section, a preliminary battery sizing approach is presented based on the previous detailed analysis of BEB energy consumption at varying operating conditions. This approach is based on four basic steps as presented in Figure 3.23:

1. Determination of the bus operating conditions for a given bus trip.
2. Determination of the specific energy/average power demand of each energy system in the bus using the presented figures and cartographies.
3. Calculation of the total energy consumption of the bus per trip.
4. Estimation of the battery size by considering the battery available *SOC* window, and the number of trips that should be completed prior to a full battery recharge.

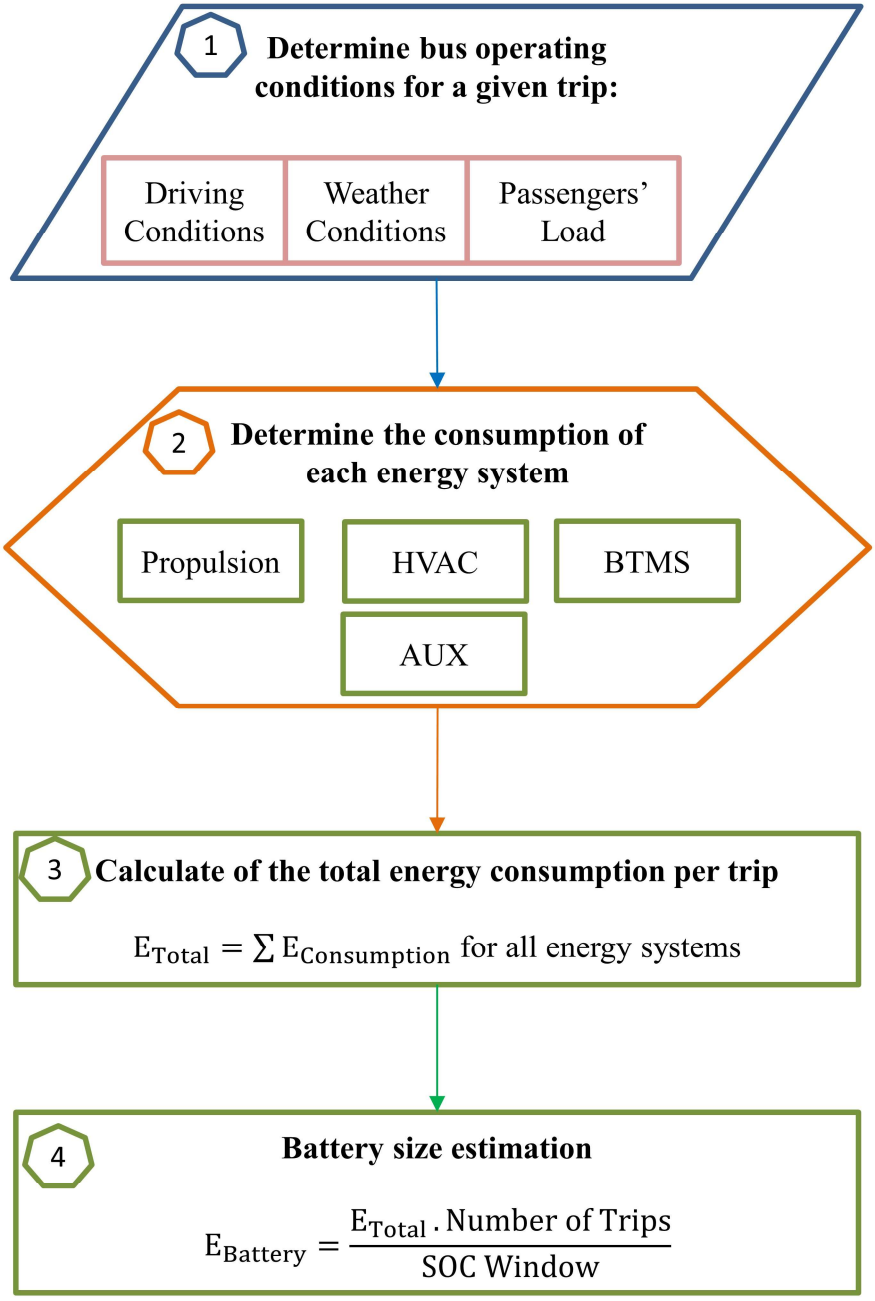


Figure 3.23: Flowchart of preliminary battery sizing methodology

The use of simplified energy consumption cartographies and maps rather than the presented dynamic models in Chapter 2 allows the users to be able to calculate the bus energy consumption with very simple inputs. However, the dynamic models require detailed inputs that may not be available to all users such as detailed drive cycles and passenger occupancy profiles. Despite its practicality, this simplification sacrifices part of the energy assessment accuracy, however, the difference can be neglected. Appendix F shows the criteria used to validate the energy consumption cartographies in comparison to the dynamic models.

- **Step 1: Determination of the Bus Operating Conditions**

The required operating conditions are basic information on any bus trip that can be easily obtained. These conditions are split into 3 parts as discussed earlier:

1. Driving Conditions: trip average speed, deceleration, duration, distance, number of stops.
2. Weather Conditions: external temperature and solar flux intensity.
3. Passengers' load: average number of passengers occupying the bus during the trip.

- **Step 2: Extracting Energy/Power Consumption Data**

The energy consumption and power demand of the different energy systems encountered in a BEB are presented in the following figures and cartographies. These cartographies are built by simulating the BEB dynamic energy model presented in Chapter 2 at a variety of drive cycles, weather conditions, and passengers' occupancy. More details regarding the development of these cartographies are presented in Appendix E.

1. Propulsion System

The propulsion system specific energy consumption is presented in Figure 3.24 and it is measured in *kWh/km*.

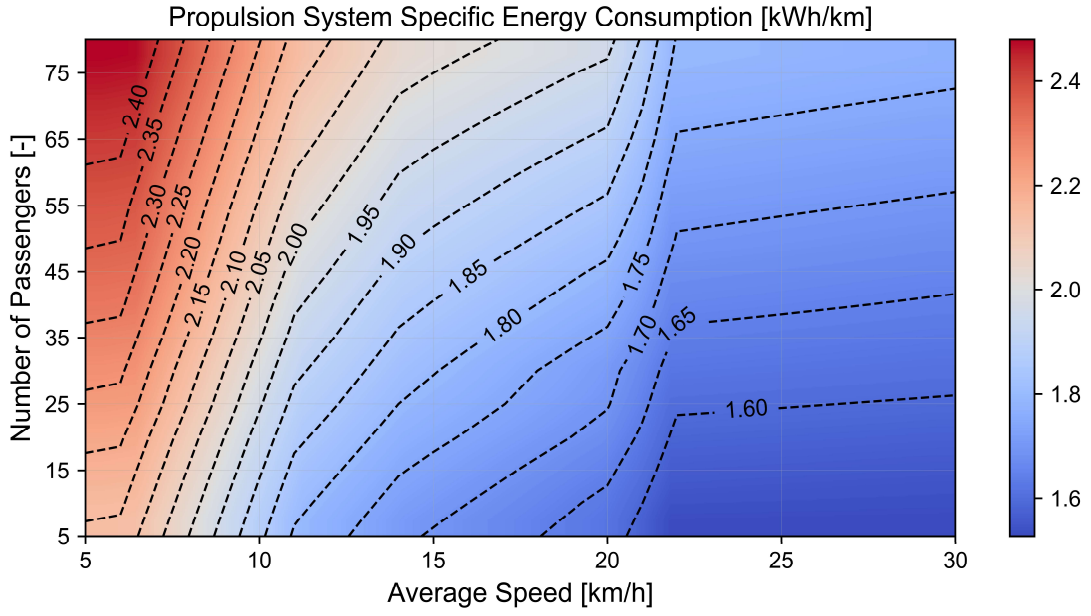


Figure 3.24: Propulsion system specific energy consumption map

The specific energy consumption map is function of the trip average speed (V_{avg}) measured in *km/h,* and the average number of passengers occupying the bus during the trip (n_{Pass}). Therefore, the energy consumption of the propulsion system (E_{Prop}) for a given trip, measured in *kWh*, is

the product of the specific energy consumption ($\bar{E}_{Prop}$) extracted from Figure 3.24, multiplied by the trip distance (d) measured in *km*, as shown in equation (3.3):

$$E_{Prop} = \bar{E}_{Prop}(V_{avg}, n_{Pass}).\, d \tag{3.3}$$

2. *HVAC Unit*

As presented earlier in this chapter, many operating conditions affect the HVAC unit energy consumption. First, Figure 3.25 shows the HVAC unit average power demand map for the MB drive cycle without considering solar flux.

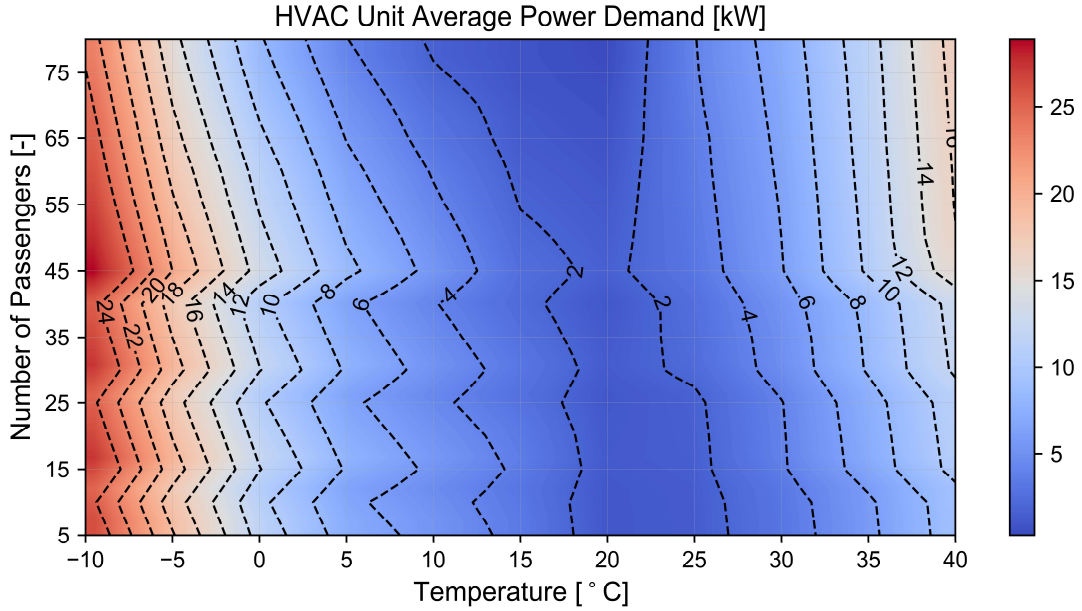


Figure 3.25: HVAC unit average power demand map ($R_{door\text{-}open}$ = 0.3) – No Solar Flux

The HVAC average power demand map is function of the external temperature (T), and the average number of passengers occupying the bus during the trip (n_{Pass}). However, for drive cycles other than the MB drive cycle, a correction factor multiplies the average power demand values extracted from Figure 3.25 in order to account for the different door opening durations, which is dependent on the trip driving conditions. Finally, to consider the impact of solar flux, Figure 3.26 shows the additional HVAC unit power demand due to solar flux at different external temperatures and intensities of solar flux. Therefore, the energy consumption of the HVAC unit for a given trip (E_{HVAC}), measured in *kWh*, is presented in equation (3.4):

$$E_{HVAC} = (C_F.\, P_{HVAC}(T, n_{Pass}) + P_{HVAC-SF}(T, SF)).\, \Delta t \tag{3.4}$$

P_{HVAC} , measured in *kW*, is the HVAC unit average power demand during the MB drive cycle without considering solar flux, and it is extracted from Figure 3.25 as function of external

temperature (T) and the average number of passengers occupying the bus (n_{Pass}). $P_{HVAC\text{-}SF}$ is the additional HVAC unit power demand due to solar flux, and it is extracted from Figure 3.26 as function of external temperature (T) and solar flux intensity (SF).

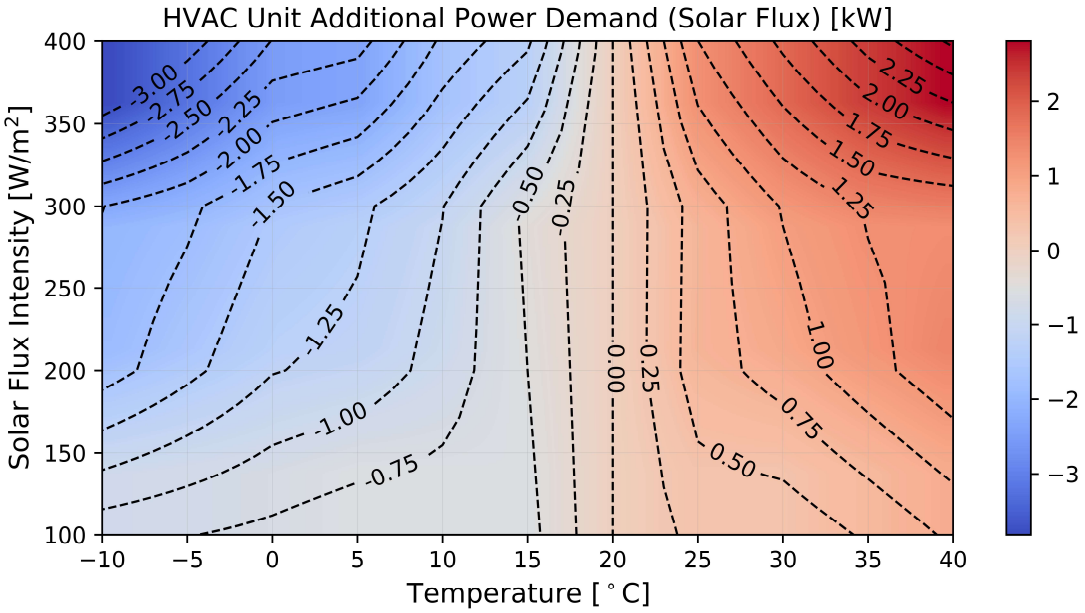


Figure 3.26: HVAC unit additional power demand due to solar flux

Δt is the trip duration measured in hours and C_F is the correction factor to consider different drive cycles each incurring different $R_{door\text{-}open}$ ratios. Recall that $R_{door\text{-}open}$ is the ratio of bus stoppage time to the total trip duration, assuming that bus doors are always open at the stops. C_F empirical formula is derived from data similar to those presented in Figure 3.7 and it is shown in equation (3.5):

$$C_F = \alpha . R^2 + \beta . R + \gamma \qquad (3.5)$$

α, β and γ are constants equal to ($\alpha = 0.0544$), ($\beta = 1.2305$) and ($\gamma = 0.6156$) respectively and R is the ratio of bus stoppage time to trip duration, referred to previously as $R_{door\text{-}open}$, ranging between 0 and 1. C_F is a positive real number.

3. BTMS

Figure 3.27 shows the BTMS average power demand function of the external temperature (T) and the average number of passengers occupying the bus during the trip (n_{Pass}). The energy consumption of the BTMS for a given trip (E_{BTMS}), measured in *kWh*, is presented in equation (3.6):

$$E_{BTMS} = P_{BTMS}(T, n_{Pass}) . \Delta t \qquad (3.6)$$

P_{BTMS} is extracted from Figure 3.27 as function of external temperature (T) and the number of passengers (n_{Pass}), measured in kW.

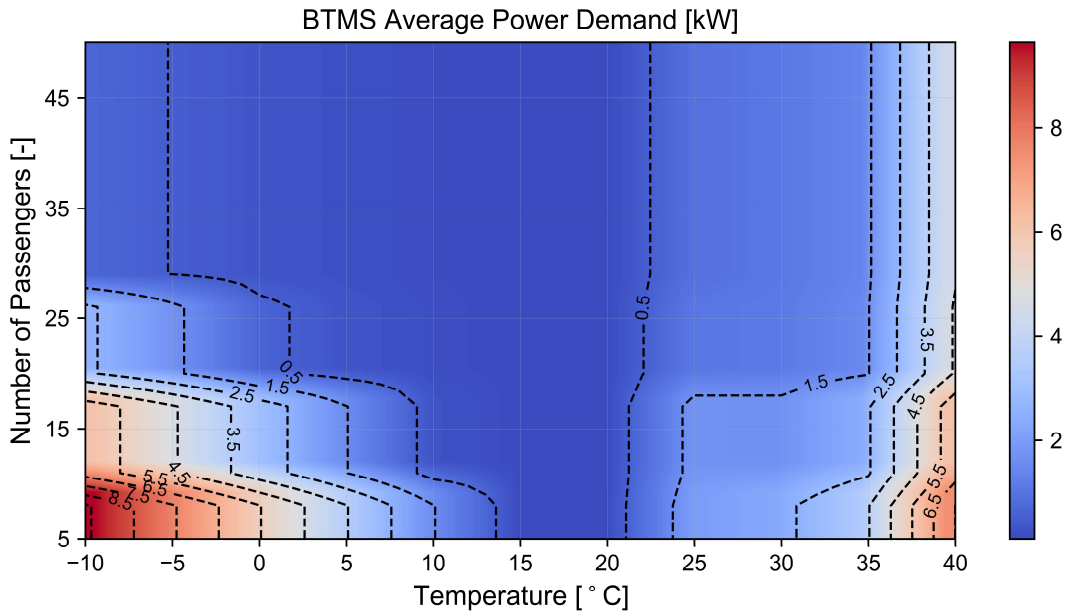


Figure 3.27: BTMS average power demand map

4. Pneumatic System

Figure 3.28 shows the pneumatic system average power demand as function of the drive cycle average deceleration. The energy consumption of the pneumatic system (E_{Pneu}) for a given trip, measured in kWh, is presented in equation (3.7):

$$E_{Pneu} = P_{Pneu}.\Delta t \tag{3.7}$$

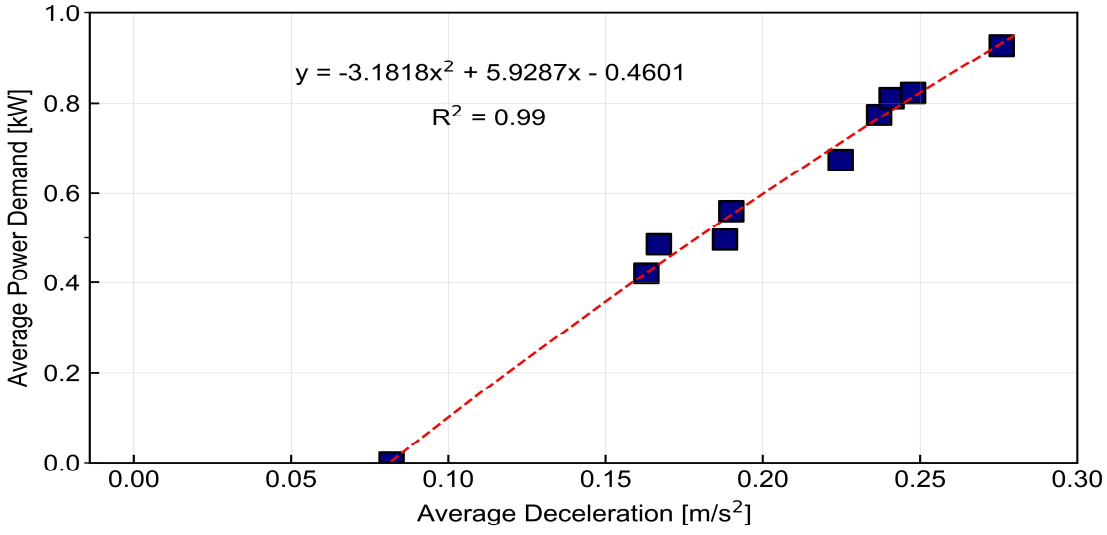


Figure 3.28: Pneumatic system average power demand

P_{Pneu} is extracted from Figure 3.28 measured in kW, and Δt is the trip duration measured in hours.

5. *Steering Pump*

Figure 3.29 shows the steering pump specific energy consumption as function of the drive cycle average speed.

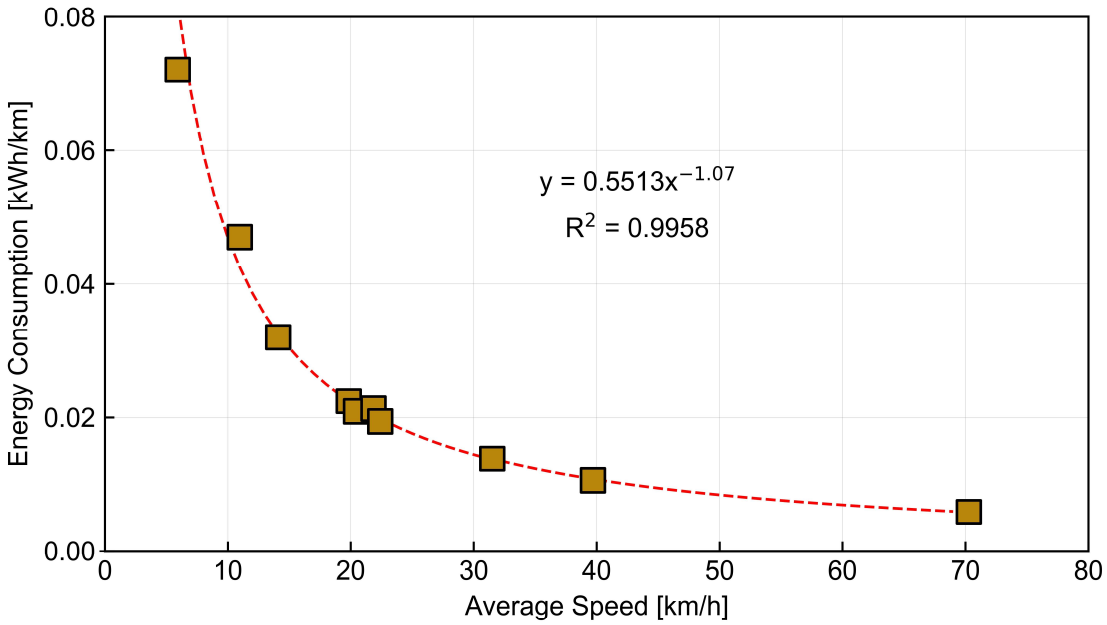


Figure 3.29: Steering pump specific energy consumption

The energy consumption of the steering pump for a given trip (E_{Pump}), measured in kWh, is presented in equation (3.8):

$$E_{Pump} = \bar{E}_{Pump}.d \qquad (3.8)$$

$\bar{E}_{Pump}$ is extracted from Figure 3.29 measured in kWh/km and d is the trip distance measured in km.

6. *Electric and Suspension System*

Figure 3.30 shows the suspension system and electric auxiliaries' specific energy consumption as function of the drive cycle average number of stops per km. Their energy consumption for a given trip ($E_{Susp\text{-}Ele}$), measured in kWh, is presented in equation (3.9) with $\bar{E}_{Sus-Ele}$ is extracted from Figure 3.30 measured in kWh/km, and d is the trip distance measured in km.

$$E_{Susp-Ele} = \bar{E}_{Sus-E} \ .d \qquad (3.9)$$

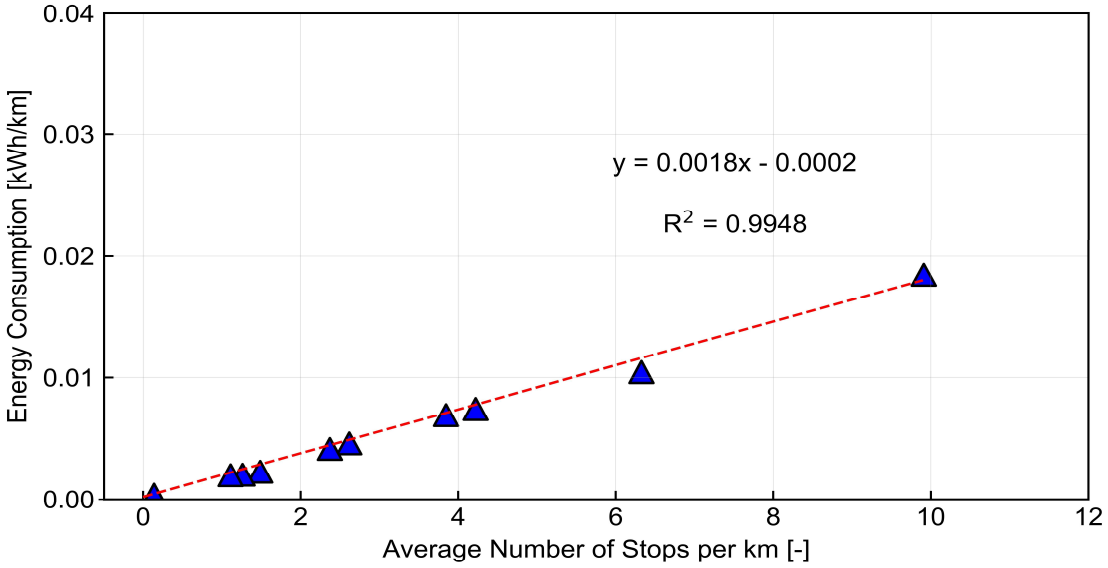


Figure 3.30: Suspension system and electric auxiliary's specific energy consumption

- **Step 3: Calculation of Bus Energy Consumption per Trip**

The bus energy consumption per trip (E_{Trip}) measured in kWh, is the sum of the energy consumption of the different energy systems determined in step 2, as shown in equation (3.10):

$$E_{Trip} = E_{Prop} + E_{HVAC} + E_{BTMS} + E_{Pneu} + E_{Pump} + E_{Susp-Ele} \quad (3.10)$$

- **Step 4: Estimating the Required Battery Size**

After calculating E_{Trip}, the battery size E_{Batt} measured in kWh can be estimated as shown in equation (3.11), where N_{Trips} is the number of trips a bus completes prior to a full battery recharge, and ΔSOC is the battery allowable SOC window. ΔSOC window is mainly recommended by the battery manufacturer in order not to deteriorate battery health, especially at very low SOC resulting in severe voltage drop. In addition, this ΔSOC window is considered as a safety margin as well to accommodate possible aggressive variations in operating conditions (mainly traffic conditions) that may increase the BEB energy consumption and delay its scheduled charging.

$$E_{Batt} = \frac{E_{Trip}.N_{Trips}}{\Delta SOC} \quad (3.11)$$

3.5.2 Case Studies

The previously discussed battery sizing preliminary methodology is utilized in this section where a BEB operating in the city of Paris is considered.

3.5.2.1 Baseline Scenario

The bus is only charged at night when it is out of service. The round-trip operating conditions for this bus are presented in Table 3.1.

Table 3.1: Baseline scenario operating conditions

	Parameter	Normal Conditions	Extreme Conditions 1	Extreme Conditions 2
Driving Conditions	Average Speed	11 *km/h*	8 *km/h*	8 *km/h*
	Distance	20 *km*	20 *km*	20 *km*
	Duration	1.81 *h*	2.5 *h*	2.5 *h*
	Average Deceleration	0.2 m/s^2	0.3 m/s^2	0.3 m/s^2
	Number of Stops	120	120	120
	Stoppage Time	0.51 *h*	0.51 *h*	0.51 *h*
Weather Conditions	Temperature	10 °*C*	-5 °*C*	35 °*C*
	Solar Flux	100 W/m^2	30 W/m^2	400 W/m^2
Passengers' Load		30	50	50
Additional Considerations	Battery SOC Window	0.7	0.7	0.7
	Number of Daily Trips	5	5	5
	Charging Events per day	1	1	1

Three types of operating conditions are considered: (1) normal conditions where all operating conditions are calculated based on annual average data and (2 and 3) extreme conditions where the extreme rarely occurring conditions are considered. These values are based on data collected for this bus line

The bus is supposed to complete 5 trips prior to its full battery recharge at night. This implies that there is only one charging event per day. The battery *SOC* operating window is 0.7 (minimum SOC is 0.2 and maximum SOC is 0.9).

Based on the previously discussed battery sizing preliminary methodology, the minimum battery capacity under normal conditions is **348 *kWh***, under extreme conditions 1 is **647 *kWh***, and under extreme conditions 2 is **571 kWh** as presented in Table 3.2. The main reason behind this vast increase is due to the HVAC unit energy consumption at -5 °*C* and 30 °*C*, followed by the heavier traffic conditions and higher passengers' load as shown in Figure 3.31.

Table 3.2: Minimum required battery size: Baseline Scenario

Operating Conditions	Normal	Extreme 1 - Cold	Extreme 2 - Hot
Minimum Required Battery Size	348 *kWh*	647 *kWh*	571 *kWh*

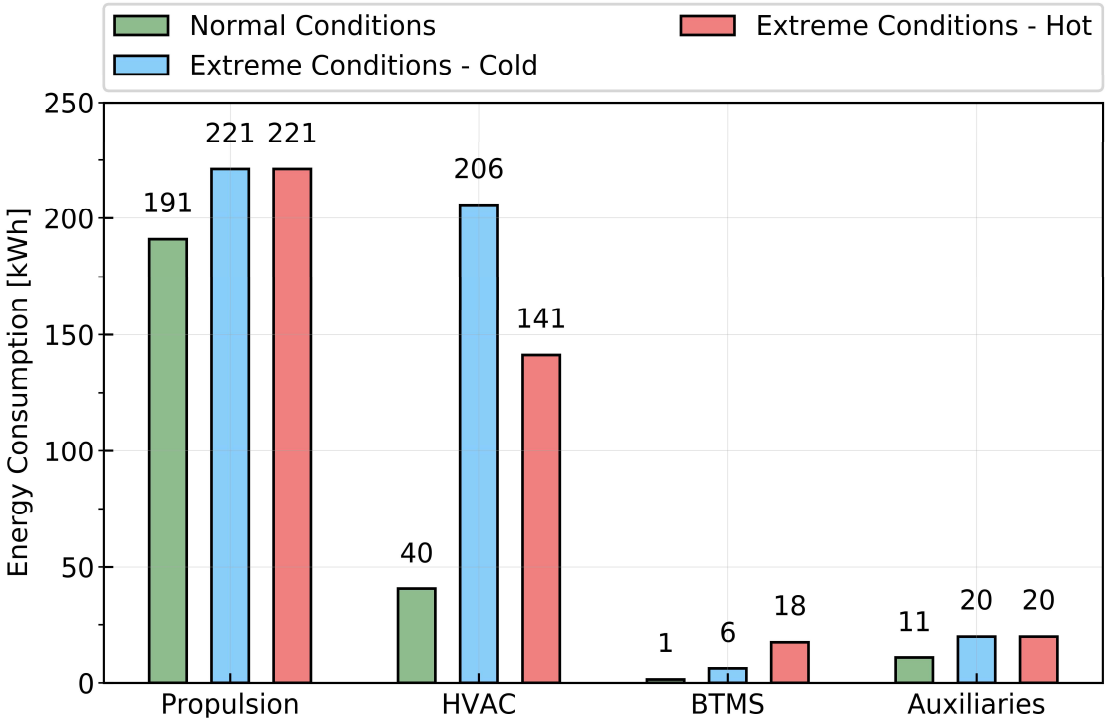


Figure 3.31: Daily energy consumption segmentation in BEB: Baseline Scenario

Bus operators will be forced to size the BEB battery at extreme operating conditions (extreme cold conditions in this case), rather than normal conditions in order to ensure proper operation of the BEB without schedule disruptions during these extreme conditions. However, rarely do these extreme conditions occur during the year, and thus, the battery size is largely oversized for normal operating conditions that are encountered frequently. A largely oversized battery means a more expensive and heavier BEB leading to additional capital and operating costs to the already expensive technology.

In order to tackle this problem, 6 improvement scenarios are considered in this section that may help to reduce the battery minimum required size at extreme conditions. These improvement scenarios aim at reducing the energy consumption of the different energy systems in the BEB. These scenarios are compared to the baseline scenario.

3.5.2.2 Improvement Scenario 1: BEB Cabin Pre-Conditioning

Cabin pre-conditioning is achieved by heating /cooling the BEB cabin to the desired temperature when it is parked at the depot using an external heating/cooling unit other than the onboard HVAC unit. Cabin pre-conditioning reduces the HVAC unit energy consumption at the end of the bus trip as the HVAC unit directly starts operating at a steady-state, eliminating the transient state operation and the consequent energy consumption.

As shown in Table 3.3, the minimum required battery size is reduced by 2 to 3 % at extreme conditions. This improvement is not significant at these operating conditions due to the relatively long trip duration when compared to the transient state duration which is around 10 minutes. However, a higher percentile reduction in battery size can be achieved if shorter trips are considered.

Table 3.3: Minimum required battery size: Improvement Scenario 1 - Cabin Pre-Conditioning

Operating Conditions		Extreme 1 - Cold	Extreme 2 - Hot
Minimum Required Battery Size	Baseline Scenario	647 *kWh*	571 *kWh*
	Improvement Scenario	627 *kWh*	557 *kWh*

3.5.2.3 Improvement Scenario 2: Use of Alternative on-board Heat Source

Using an alternative heat source on-board reduces the HVAC unit energy consumption, and thus reduces the battery size. Alternative heating sources might be diesel fuel heaters, gas heaters (ethanol), water heaters (Hot water storage on-board where the water is heated off-board the bus) if applicable, or any other heating technology that does not consume electric energy from the battery. Two cases are considered in this scenario: (Case 1) an alternative heat source that assists the HVAC unit during heating allowing to shut down one of the 2 operating heat pumps and (Case 2) an alternative heat source that replaces the entire HVAC system during heating allowing to shut down both heat pumps. The latter case eliminates most of the HVAC unit electric energy consumption and the remaining energy consumption is just due to the fans operating the air circulation system.

As shown in Table 3.4, the minimum required battery size can be reduced from 647 *kWh* to 500 *kWh* in case 1 (21% reduction), and to 353 *kWh* (43% reduction) in case 2. As for the extreme hot conditions, there are no external cooling technologies that can be used on-board other than the HVAC unit.

To that end, despite the significant reduction in battery size for extreme cold conditions, the extreme hot conditions drive the battery sizing limiting the benefits of an external heat source on-board. Effectively, the new reduced battery size is 571 *kWh* rather than 647 *kWh* which only represents a 12% reduction. Such a solution is only effective at extreme cold conditions.

Table 3.4: Minimum required battery size: Improvement Scenario 2 - Use of Alternative on-board Heat Source

Operating Conditions		Extreme 1 - Cold	Extreme 2 - Hot
Minimum Required Battery Size	Baseline Scenario	647 *kWh*	571 *kWh*
	Improvement Scenario: Case 1	500 *kWh*	571 *kWh*
	Improvement Scenario: Case 2	353 *kWh*	571 *kWh*

3.5.2.4 Improvement Scenario 3: Reduce BEB Ridership Capacity

One way to reduce the BEB energy consumption at extreme conditions is to reduce its ridership capacity whenever these extreme conditions occur. Reducing the allowable number of passengers on-board directly reduces the propulsion system and HVAC unit energy consumption as shown previously in this chapter. Two cases are considered in this scenario: (Case 1) reducing the BEB ridership capacity by 30 % and (Case 2) by 50 %. As shown in Table 3.5, at extreme cold conditions, there is no reduction in the minimum required battery size. On the contrary, a slight increase is observed. Although a reduced BEB ridership capacity reduces the energy consumption of the propulsion system and HVAC unit, the BTMS energy consumption increases. This is due to the lack of sufficient air supply to the BEB cabin at low passengers' load, which forces the battery cooling unit to draw air from the exterior and heat it using electric resistance heaters at relatively lower efficiency when compared to the HVAC unit. On the other hand, during extreme cold conditions, the battery size can be reduced by 10% when reducing the BEB ridership capacity by 50%. Therefore, such a solution is only effective during extreme hot conditions, not to mention the resulting lack of customers' satisfaction.

Table 3.5: Minimum required battery size: Improvement Scenario 3 - Reduce BEB Ridership Capacity

Operating Conditions		Extreme 1 - Cold	Extreme 2 - Hot
Minimum Required Battery Size	Baseline Scenario	647 *kWh*	571 *kWh*
	Improvement Scenario: Case 1	640 *kWh*	528 *kWh*
	Improvement Scenario: Case 2	655 *kWh*	514 *kWh*

3.5.2.5 Improvement Scenario 4: Increase Battery Operating SOC Window

Increasing the battery operating *SOC* window implies that a higher percentage of the battery available energy can be utilized. The recommended *SOC* window by battery manufacturers is 0.7 (minimum *SOC* = 0.2 and maximum *SOC* = 0.9) which is considered in the baseline scenario. Two cases are considered in this scenario: (Case 1) a battery *SOC* window of 0.8 (minimum *SOC* = 0.2 and maximum *SOC* = 1) and (Case 2) a battery *SOC* window of 0.9 (minimum *SOC* = 0.1 and maximum *SOC* = 1).

As shown in Table 3.6, trivially, the minimum required battery size can be significantly reduced by more than 20% at both extreme conditions. However, it is important to note that utilizing a battery SOC window higher than that recommended by the battery manufacturer accelerates battery aging, and thus reduces the battery lifetime.

Table 3.6: Minimum required battery size: Improvement Scenario 4 - Increase Battery Operating SOC Window

Operating Conditions		Extreme 1 - Cold	Extreme 2 - Hot
Minimum Required Battery Size	Baseline Scenario	647 *kWh*	571 *kWh*
	Improvement Scenario: Case 1	566 *kWh*	500 *kWh*
	Improvement Scenario: Case 2	503 *kWh*	445 *kWh*

3.5.2.6 Improvement Scenario 5: Trip Number Reduction

Another way to reduce the daily energy consumption of the BEB, and thus reducing the minimum required battery size, is to reduce the number of trips during the day at extreme conditions. At these conditions, alternative buses compensate for this reduction such as diesel buses or any available bus technology. Two cases are considered in this scenario: (Case 1) a 20 % reduction in the number of bus daily trips and (Case 2) a 40 % reduction in the number of bus daily trips.

As presented in Table 3.7, the minimum required battery size can be reduced by 40% at extreme conditions.

Table 3.7: Minimum required battery size: Improvement Scenario 5 – Trip Number Reduction

Operating Conditions		Extreme 1 - Cold	Extreme 2 - Hot
Minimum Required Battery Size	Baseline Scenario	647 *kWh*	571 *kWh*
	Improvement Scenario: Case 1	518 *kWh*	457 *kWh*
	Improvement Scenario: Case 2	388 *kWh*	342 *kWh*

3.5.2.7 Improvement Scenario 6: Increase Daily Charging Events

The baseline scenario and all the previously presented improvement scenarios are based on one charging event during the day, which takes place at night when the bus is out of service. This input highly affects the battery size at normal and extreme conditions. An alternative solution to that is to increase the number of daily charging events. For example, fully charging the BEB battery once at night and once during the day would theoretically reduce the battery size to half.

As shown in Table 3.8, increasing the number of charging events per day can reduce the minimum required battery size down by 80% at extreme conditions. Such a solution helps to reduce the battery size; however, it should be carefully implemented as it may result in some schedule disruptions if the BEB charging time is long, not to mention the additional investment costs in the required charging infrastructure. In addition, frequent charging during the day mainly takes place at high power to avoid schedule disruption, this results in a high-power demand from the electric grid, and thus major infrastructure modifications might be required in this case.

Table 3.8: Minimum required battery size: Improvement Scenario 6 - Increase Daily Charging Events

Operating Conditions		Extreme 1 - Cold	Extreme 2 - Hot
Minimum Required Battery Size	Baseline Scenario	647 *kWh*	571 *kWh*
	3 Charging Events per day	258 *kWh*	228 *kWh*
	5 Charging Events per day	130 *kWh*	115 *kWh*

Finally, the different proposed improvement scenarios and their resulting drawbacks are summarized in Table 3.9.

Table 3.9: Summary of improvement scenarios

Improvement Scenario	Battery Size Reduction	Drawbacks
BEB Cabin Pre-Conditioning	2 ~ 3 %	- Negligible Improvement
Use of Alternative on-board Heat Source	20 – 40 % during extreme cold conditions	- Not applicable for extreme hot conditions
Reduce BEB Ridership Capacity	10 % during extreme hot conditions	- No improvement during extreme cold conditions - Reduction in customers' satisfaction

Increase Battery Operating SOC Window	10 – 20 %	- Accelerating battery aging and reduction in battery lifetime
Trip Number Reduction	20 – 40 % (depending on the reduction in number of daily trips)	- Use of alternative buses that might be banned for environmental concerns.
Increase Daily Charging Events	20 – 80 %	- Additional investment costs due to multiple charging events (more chargers). - Risk of schedule disruption

3.6 Conclusion

The energy consumption of BEB has a direct impact on its minimum required battery size. Mainly batteries are oversized in order to meet the BEB energy needs at extreme weather conditions. Although the occurrence of these extreme conditions is rare, they drive the size of the battery in order to ensure smooth uninterrupted BEB operation at such conditions.

The energy consumption of BEB shows a very sensitive behavior relative to its operating conditions. The driving conditions could impact the propulsion system energy consumption by 35%, where it increases during high levels of traffic congestion (speed less than 10 km/h). The Steering Pump Auxiliary energy consumption is also affected by driving conditions as its efficiency drastically deteriorates at low speeds, doubling its energy consumption in comparison to normal traffic conditions (10-15 km/h). The Air Compressor Auxiliary power demand is directly related to the levels of braking and deceleration during the trip, and thus its power demand increases with high levels of congestion. In general, The BEB total energy consumption drastically deteriorates for highly congested trips as it can increase by 50% implying that city buses suffer from high energy consumption when compared to other types of bus service, for example, inter-city buses.

On the other hand, the weather conditions impact the HVAC unit energy consumption and the total BEB energy consumption as well. The HVAC Unit average power demand increases as external temperatures deviate from thermal comfort temperature (19-26 °C). Extreme weather conditions could increase the total BEB energy consumption by 50%, in comparison to normal weather conditions. Such weather conditions are encountered during winter (temperatures below -5 °C) and during summer (Temperature above 35 °C and high solar flux intensity). In addition, the BTMS power demand also has a considerable impact and it could represent more than one-third of the total HVAC unit energy consumption.

Furthermore, the passenger's occupancy inside the BEB impacts its energy consumption. The HVAC Unit power demand could increase by 100% during cooling and by 15% during heating due to the high cabin ventilation needs and high heat rejection at passengers' occupancy. In addition, the propulsion System energy consumption increases due to the additional weight. This increase could reach 15% when comparing an empty bus to a full one.

Sizing the battery in BEB is affected by many factors as shown in Table 3.9. However, the adopted charging patterns, such as the number of daily charging events, induce the highest impact. Charging the battery during the day raises questions regarding the bus schedule disruptions that may result due to the increased number of charging events. Moreover, additional investment costs might be incurred resulting from the needed infrastructure to charge the buses throughout the day. Further than that, the choice of charging technology directly drives the charging duration and investment costs. However, proper sizing of the battery alongside an adequate charging strategy may ensure a smooth bus operation without disruptions, and at relatively lower total investment costs.

This needs further investigation as the BEB charging strategy is highly affected by the schedule of the bus, the number of buses operating along the same route, and the energy consumption of the bus depending on the variable operating conditions. Therefore, a complete bus line model is needed to better assess these improvement scenarios.

3.7 References

[1] M. Mahmoud, R. Garnett, M. Ferguson, and P. Kanaroglou, "Electric buses: A review of alternative powertrains," *Renew. Sustain. Energy Rev.*, vol. 62, pp. 673–684, 2016, doi: 10.1016/j.rser.2016.05.019.

[2] J. Neubauer and E. Wood, "The impact of range anxiety and home, workplace, and public charging infrastructure on simulated battery electric vehicle lifetime utility," *J. Power Sources*, vol. 257, pp. 12–20, 2014, doi: 10.1016/j.jpowsour.2014.01.075.

[3] B. Zhou, Y. Wu, B. Zhou, R. Wang, W. Ke, and S. Zhang, "Real-world performance of battery electric buses and their life-cycle benefits with respect to energy consumption and carbon dioxide emissions," *Energy*, vol. 96, pp. 603–613, 2016, doi: 10.1016/j.energy.2015.12.041.

[4] A. Lajunen, "Energy Efficiency and Performance of Cabin Thermal Management in Electric Vehicles," *SAE Tech. Pap.*, 2017, doi: 10.4271/2017-01-0192.

[5] D. Y. Lee, C. W. Cho, J. P. Won, Y. C. Park, and M. Y. Lee, "Performance characteristics of mobile heat pump for a large passenger electric vehicle," *Appl. Therm. Eng.*, vol. 50, no. 1, pp. 660–669, 2013, doi: 10.1016/j.applthermaleng.2012.07.001.

[6] D. Göhlich, A. Kunith, and T. Ly, "Technology assessment of an electric urban bus system for berlin," in *WIT Transactions on the Built Environment*, 2014, vol. 138, pp. 137–149, doi: 10.2495/UT140121.

**** End of Chapter 3 ***

Chapter 4

TECHNO-ECONOMIC MODEL OF BATTERY ELECTRIC BUS LINE

4.1 Introduction

BEB battery sizing is significantly impacted by the bus energy consumption, which depends on the bus operating conditions such as the driving conditions, weather conditions, and passengers' load [1]. Therefore, the required battery size is driven by these conditions, as high energy-demanding operating conditions will result in a larger battery size [2], [3]. More often, batteries are sized to ensure uninterrupted bus operation under extreme operating conditions such as cold ambient temperatures, heavy traffic conditions, and high passengers' load. This results in increased battery costs due to these rarely-occurring conditions, not to mention the additional battery weight which increases the total bus weight and reduces its ridership capacity [4], [5].

The adopted charging strategies of BEB affect the battery size [2], [6]. Charging the BEB during the night outside the bus service hours will result in a large battery size as it should be capable of supplying the BEB energy needs throughout the day. For such a charging scenario, slow chargers are used as there is plenty of time to charge the buses. However, implementing multiple charging events during the day creates room for reducing the battery size. Such charging scenarios are associated with fast chargers due to the limited available time to charge the buses [7], [8].

The battery sizing and charging strategy of BEB are driven by the operating conditions of the BEB line. In addition to the driving conditions, weather conditions, and passenger load, many studies have concluded that the BEBs schedule directly influences the charging strategies [9]–[11]. BEBs that operate along lines that encounter high passenger flow are mainly running on tight schedules and are expected to complete a high number of trips per day, thus the available charging time for these buses during the day is limited. On the contrary, inter-city BEBs operate for longer trips between the cities but less frequently, which possibly allows more charging opportunities during the day.

Proper battery sizing and charging strategy are critical to ensure uninterrupted operation of the BEB. Two main indicators reflect on the operation of BEB: (1) schedule disruption and (2) service interruption. Schedule disruption is the failure to stay punctual to the bus schedule due to delays related to its charging, while service interruption is the failure to complete a trip due to lack of energy on-board. Charging the BEB only overnight eliminates any risk of schedule disruption during operation, however, the risk of service interruption is high as it is not possible to charge the BEB during the day. On the contrary, frequent day-charging lowers the risk of

service interruption, whereas schedule disruption is highly probable with such a charging strategy due to the possible delays that may result from the frequent charging events.

The total cost of deployment of BEB is directly driven by the choice of battery size, charging strategy, and the BEB operating conditions. For instance, BEB equipped with large batteries are mainly accompanied by slow charging during the night, whereas BEB equipped with small batteries require frequent charging during the day at very high-power rates. The former approach yields in high batteries acquisition costs and incurs a high probability of service interruption whereas the latter approach results in high infrastructural and operating costs and is more likely to result in schedule disruptions.

In order to assess the interactions among the battery sizing, charging strategy, and BEB operating conditions, and their impact on the BEB operation and costs, it is essential to develop a BEB line techno-economic model where the mentioned components are considered alongside their interactions.

This chapter is organized as follows: section 4.2 introduces the current state-of-the-art operating BEB lines and presents the complete scheme of BEB charging. A detailed BEB line energy model is developed in section 4.3, followed by a BEB line operation model in section 4.4 and a comprehensive TCO model in section 4.5. Section 4.6 presents a case study utilizing the proposed models, highlighting the impact of different battery sizing and charging strategies on BEB TCO and operation. Finally, section 4.7 concludes on the main findings in this chapter.

4.2 State of the Art of BEB Lines: Battery Sizing, Charging Strategy and Charging Technology

Many cities globally have already implemented several projects to electrify their bus fleets. China leads the bus fleet electrification race where almost 99% of all global electric buses are operating in China as shown in Figure 4.1. This is due to the promotions and incentives set by the Chinese authorities to deploy BEB rapidly [12]. On the other side, Europe is a big market for BEB as shown in Figure 4.2 where many bus lines are 100% operating using BEB. Netherlands, Sweden, and the UK are the leading countries in bus fleet electrification followed by France and Germany [13], [14].

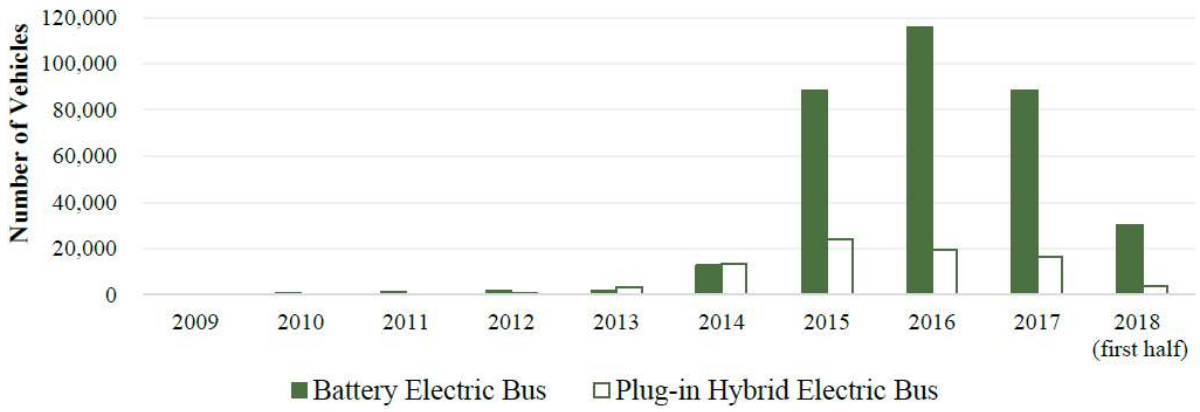


Figure 4.1: New BEB and PHEB in China [13]

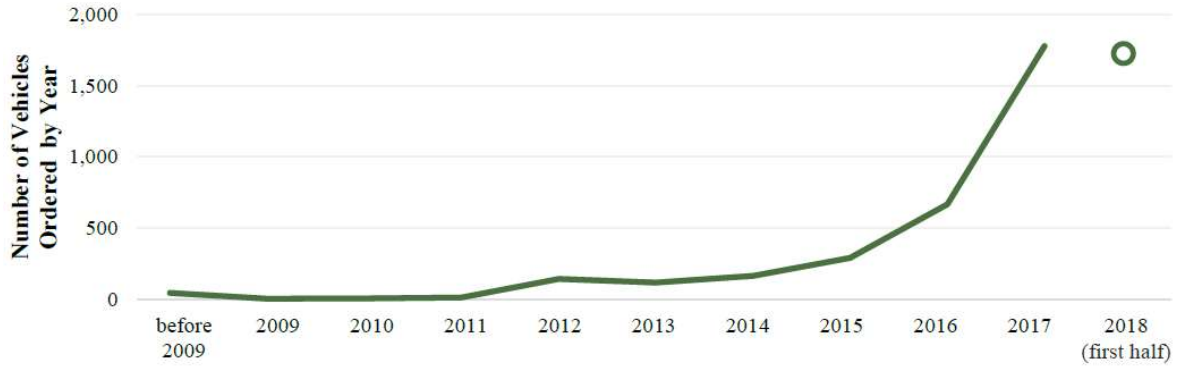


Figure 4.2: Number of BEB ordered in Europe between 2009 – 2018 [2][13]

4.2.1 Overview of BEB Operating Lines Worldwide

Table 4.1 introduces a review of the recent operating BEB lines in Europe, China, and the USA. The table compares the different adopted battery sizes and charging strategies in each country/city.

A variety of battery sizes and charging strategies for BEB lines are implemented worldwide. The battery size ranges from 65 *kWh* (China-Guangzhou) to 660 *kWh* (California-USA). This high discrepancy in the choice of the battery size reflects on the different energy needs for each bus line. In addition, a variety of charging strategies are adopted worldwide where charging takes place at the bus depot or stop stations, and at different power levels as the charging ranges from 40 *kW* (London-UK) to 600 *kW* (Amiens-France).

To that end, it is essential at this point to thoroughly define the charging strategy of a BEB line.

[2] The number of vehicles ordered per year for the year 2018 is estimated based on the first half of the year. The value for the first half of the year is multiplied by 2 to estimate the yearly value.

Table 4.1: Review of recent operating BEB lines globally

Country/City	Bus Manufacturer/Operator	Reported Battery Size and Driving Range	Reported Charging Strategy
China: Shenzhen – Beijing – Guangzhou [15]–[17]	BYD	- 250 *kWh* – 300 *km* - NA – 65 *km*	- Night Charging at Depot - Day Charging at high power within 10 minutes
Netherlands: Amsterdam [18]	VDL Bus and Coach.	- 216 to 288 *kWh*	- A mixed strategy of slow night charging at the depot and fast charging during the day at a dedicated station
UK: London [19]–[21]	BYD – ADL Partnership	- 382 *kWh* – 256 *km* double-decker - NA – 256 *km* Standard 12 *m*	2x40 *kW* dual plug to charge the buses at the depot.
Sweden: Gothenburg [22], [23]	Volvo	- 396 *kWh*	- Fast charging along the route up to 150 *kW*
Sweden: Ostersund [24]–[26]	Scania	250 *kWh*	- Possibility of night charging at depot up to 150 *kW* and opportunity charging during the day using pantographs at 300 *kW*.
Germany: Hamburg [27]–[29]	MAN	480 *kWh* – 200 to 270 *km*	- Not Specified, but most probably the buses will be charged at night using slow chargers due to the large battery size.

USA: California [30], [31]	- BYD	- 240 *km*	- Depot Charging within 3 hours
	- Proterra	- 220 *kWh* to 660 *kWh* – 150 to 400 *km*	- Not Specified
France: Amiens [32], [33]	Irizar – Keolis	- 350 *kWh* – 240 *km*	- Bus Rapid Transit (BRT) with day charging using pantographs at 600 *kW*
France: Paris [34]	Blue Bus	- 240 *kWh* – 180 to 240 *km*	- Night Charging at Depot

In general, a charging strategy integrates the following three questions:

- Where to charge?
- When to charge?
- What is the charging duration?

First, the charging location of the buses might be at the bus depot, at the terminal stations of the line, or at any stop station along the line. Second, the charging time of the buses may take place at night during out-of-service hours or at any time during the day, and at different frequencies. In addition, it is critical to decide on the charging duration as it may disturb the bus operation resulting in schedule delays. In this thesis, the charging duration is considered by looking into the amount of energy to charge the buses and the charging power rate. These headlines of the charging strategy, alongside the battery size, affect each other as they highly interact. For example, deciding to locate the chargers at the bus depot enforces a large battery size that can only be charged at night.

4.2.2 Charging Scheme of Electric Vehicles

In recent years, extensive research and development have been put through concerning EV charging. An EV charger is the "vehicle refueling point" to transfer electric energy from an electricity source [35]. Charging of EVs is defined by identifying the following three modules: (1) Charging Infrastructure, (2) Charging Power Level, and (3) Type of Charging System.

4.2.2.1 Charging Infrastructure

The charging infrastructure identifies the charging facility and location. There are two main types of charging facilities: (1): stationary charging and (2) Dynamic charging [36].

4.2.2.1.1 Stationary Charging

Stationary charging facilities require the vehicles to be parked at a certain charging station [36]. This is the most common charging infrastructure deployed worldwide. As shown in Figure 4.3 and Figure 4.4, stationary charging can be through portal chargers or overhead chargers (mounted pantographs).

Stationary charging is further categorized based on the charging method or location. There are 3 stationary charging methods: (1) overnight charging, (2) end-line charging, and (3) opportunity charging [37].

Overnight charging takes place during the night when the buses are out of service. No charging is conducted during the day. It is a single charging event methodology that should supply the entire bus daily energy needs during the night. Overnight charging is mainly conducted at low power rates and for long durations. The order of magnitude of charging duration during overnight charging is in hours.

End-line charging takes place at both terminal stations of the bus line where the bus can be charged prior to its return trip, depending on its schedule. This methodology incurs a high number of charging events during the day or a maximum of 2 charging events per round trip. Compared to overnight charging, BEBs operating on an end-line charging methodology can utilize smaller battery sizes due to the higher number of available charging events during the day. The charging duration at the end-lines is in the order of tens of minutes.

Opportunity charging is conducted at stop stations along the bus line. The charging duration is the shortest when compared to the other charging methodologies as it should take place in a very short time mainly equivalent to the bus layover duration at the stop stations. This charging duration ranges from 30 seconds to a couple of minutes. This charging methodology is mainly associated with high power chargers due to the short available charging time at the station.



Figure 4.3: Stationary charging station - Portal Charger



Figure 4.4: Stationary charging station - Overhead Charger

4.2.2.1.2 Dynamic Charging

Dynamic charging facilities, referred to as “on the move charging”, can charge the vehicles while they are in motion [36], [38]. Dynamic charging facilities are still under development and require further testing. Very few BEB lines operate on dynamic charging facilities such as the OLEV system in South Korea [39]. Many studies report that dynamic charging could have numerous benefits especially its potential to reduce the battery size as it allows charging during

the BEB operation [40], [41]. In addition, dynamic charging eliminates BEBs waiting time at the charging stations due to charger's unavailability.



Figure 4.5: Scheme of dynamic charging

Furthermore, dynamic charging can be classified into either quasi-dynamic or dynamic charging. The power transfer during quasi-dynamic charging is conducted at low bus speed or fast stop-and-go mode. On the contrary, dynamic charging takes place when the bus is in motion regardless of its speed [38].

4.2.2.2 Charging Power Level

Many standards define the charging power levels for electric vehicles. The Society of Automobile Engineers (SAE) standards are the most commonly used standards when it comes to charging power levels [35], [40], [42], [43]. The main standard in use currently is the SAE-J1772 standard that categorizes chargers based on their power level.

First, the chargers are either classified into AC (alternating current) or DC (direct current) chargers.

4.2.2.2.1 AC Chargers

AC chargers are mainly mounted on-board inside the vehicle and they draw electric power directly from the grid. An AC-DC converter inside the vehicle converts the AC power source to charge the DC energy storage system (Battery) [44]. The maximum power in AC chargers is limited by the rectifier size and its cooling needs, as there is limited space inside the vehicle to place large rectifiers that can convert high AC power rates. Three levels of AC chargers are identified by SAE J-1772 standard as shown in Table 4.2.

AC level 1 chargers are standard chargers that can utilize household outlets. The maximum electric power output of AC level 1 chargers is around 1.4 kW. Such chargers are used for

passengers EV [43]. AC Level 1 chargers utilize the standard 120V AC household outlets and the maximum usable current is around 16 A [45].

AC level 2 chargers are the preferred chargers meanwhile and most commonly used for private and public facilities. At this level, power rates can reach up to 14.4 kW. AC level 2 chargers utilize 240-V outlets, and the resulting maximum current exceeds 60 A.

AC level 3 chargers achieve a power rate greater than 14.4 kW. AC level 3 chargers are also referred to as AC fast chargers. It is important to mention that fast chargers are defined as "any charger that can charge an average electric vehicle battery pack in less than 30 minutes" [44]. Thus, the charging power depends on the battery size.

Table 4.2: SAE J-1772 standard for AC charging power levels [44]

SAE Standards	Level of Charging	Maximum Power Rate [kW]	Nominal Voltage Supply [V]	Maximum Current [A]
AC Charging	Level 1	1.44	120	16
	Level 2	14.4	208 - 240	60
	Level 3	> 14.4	-	-

4.2.2.2.2 DC Chargers

DC chargers are off-board chargers mounted outside the vehicle and they supply regulated DC power to the battery. Unlike AC chargers, DC chargers can reach higher power rates as they are not constrained by the limited space inside the vehicle. Similar to AC chargers, three levels of DC chargers are identified by SAE J-1772 standard as shown in Table 4.3.

Table 4.3: SAE J-1772 standard for DC charging power levels [44],[46], [47]**.**

SAE Standards	Level of Charging	Maximum Power Rate [kW]	Nominal Voltage Supply [V]	Maximum Current [A]
DC Charging	Level 1	36	200 - 450	80
	Level 2	90	200 - 450	200
	Level 3	240	200 - 600	400

Further than that, extreme fast chargers (XFC) are under continuous development and these chargers can exceed 400 kW maximum power rating [42]. In addition, the recently published SAE J-3105 standard introduces practices for high voltage automatic charging for heavy-duty vehicles and buses. This standard introduces 2 levels of automatic charging for buses using

mounted pantograph where the voltage ranges from 250 V to 1000 V: (1) level 1 automatic charging rated at 350 kW (600 A) and (2) level 2 automatic charging rated at 1200 kW (1200 A) [48]–[50].

4.2.2.3 Type of Charging System

The type of the charging system is defined by the mode of energy transfer from the energy source to the rechargeable battery. Three modes of energy transfer are identified according to [43]: (1) conductive charging system, (2) inductive charging system, and (3) battery swapping.

4.2.2.3.1 Conductive Charging System

In conductive charging systems, the power transfer from the energy source to the battery takes place through direct contact by means of a conductor. This is the simplest and most common charging system and it incurs a high energy transfer efficiency [43].

4.2.2.3.2 Inductive Charging System

Inductive charging systems, or wireless charging systems, transfer power to the battery using an electromagnetic field without any contact between the energy source and the battery. This technology is still under further development. Inductive charging systems provide benefits such as electric safety at any weather conditions. However, this technology suffers from high costs and relatively lower efficiency, and higher power losses when compared to conductive charging systems [51].

4.2.2.3.3 Battery Swapping System

Battery swapping system (BSS) allows the user to swap their batteries at a certain BSS station where the batteries charging takes place. BSS provides more flexibility concerning the charging techniques which helps in prolonging battery life and reducing the peak power demand from the electricity grid [43]. However, there are many concerns regarding the costs and safety of BSS.

Finally, Figure 4.6 summarizes the scheme of EV charging where the three mentioned charging modules alongside their sub-modules are presented. The charging of EV is completely defined by identifying these 3 modules, and any other charging method is a combination of these modules.

Note that XFC in Figure 4.6 refers to extreme fast chargers.

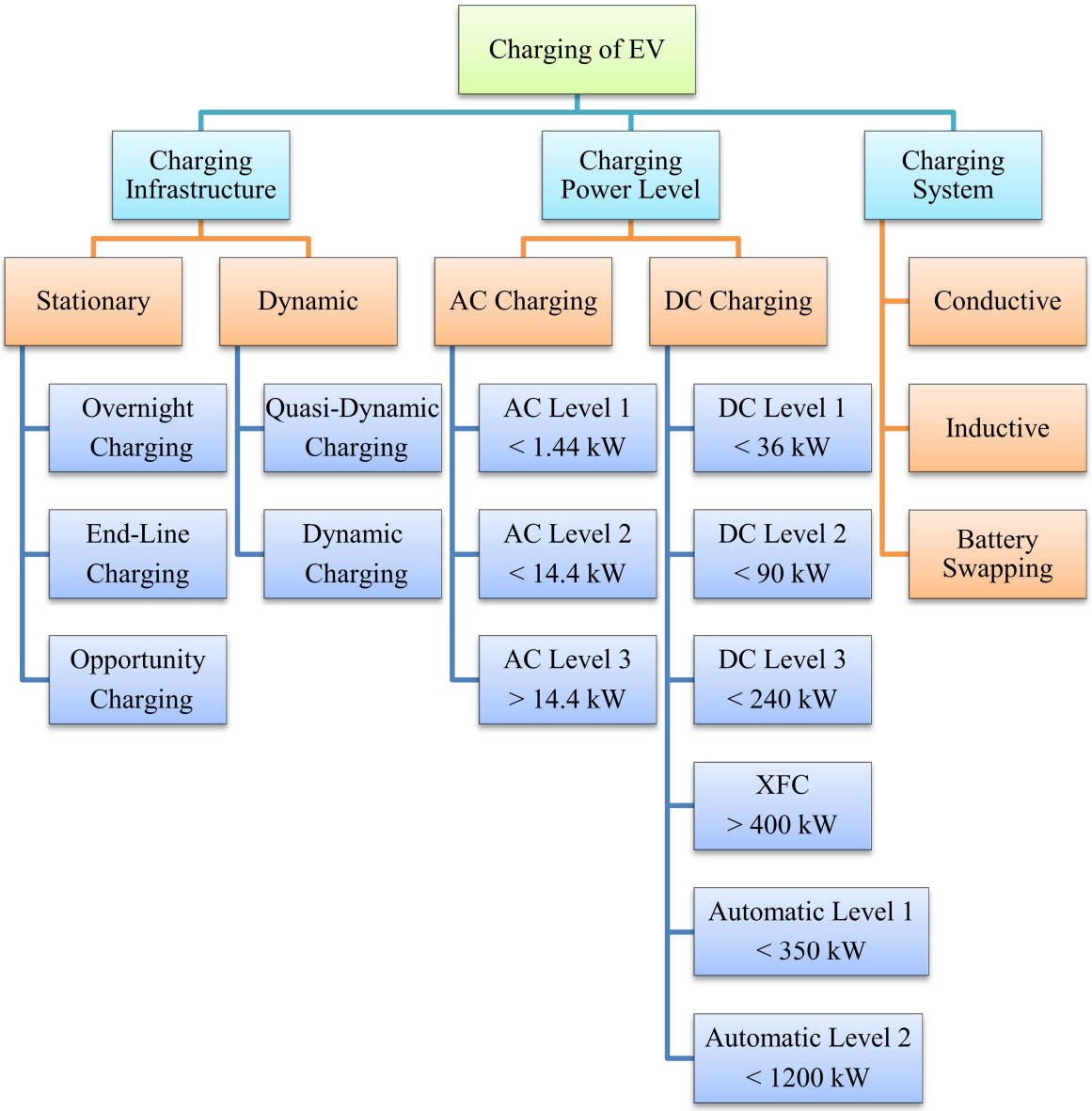


Figure 4.6: EV charging scheme

4.2.3 BEB Line Costs and Operation Tradeoff(s)

The battery size and the adopted charging strategy for a BEB line drive its operation and costs. Features such as the available energy on-board and charging duration affect the operation of BEB. Long charging durations may result in disruptions in the BEB operation, especially if the bus operates along a high-demand line that runs on a tight schedule. In addition, the available energy on-board determines the available BEB driving range which should always be sufficient to complete the BEB trips to avoid any service interruption. On the other hand, costs of BEB

deployment are directly driven by the choice of battery size and charging strategy. In addition to the cost of the battery, the chargers' cost is affected by the choice of charging technology and location. High-power fast chargers are more expensive when compared to slow chargers, and the costs of installation of a charging station at the depot are different from those at a certain stop station. Each combination of battery size and charging strategy yields different costs and affects the BEB line operation differently, where the goal is to reduce the costs and ensure smooth operation.

BEB line operation is defined by two main features: (1) risk of schedule disruption and (2) risk of service interruption. Schedule disruption occurs when the bus is not capable of following its pre-defined schedule resulting in delays, whereas service interruption is when the bus is not capable of completing a certain trip due to energy shortage in its battery on-board.

Table 4.4 shows qualitatively the trade-offs in terms of BEB line operation and costs depending on the battery size and the charging strategy. Starting with the battery size, larger batteries result in lower risks in schedule disruption and service interruption when compared to smaller batteries, but this comes at higher battery cost.

Concerning the charging location, depot charging incurs lower schedule disruption risk when compared to stop station charging since the latter may cause delays during charging. However, the risk of service interruption is higher in depot charging as there is no opportunity to charge the buses along the route. On the contrary, stop station charging provides the opportunity to charge the bus along the route, reducing the risk of service interruption. Terminal stations charging present a moderate solution in terms of schedule disruption and service interruption as it results in moderate daily charging frequencies. The incurred costs are dependent on the geographic location of the chargers, local authorities' regulations, construction in the geographic area (mainly these highly vary among city centers, suburbs, and countryside)

Another important headline in the charging strategy is charging time and frequency. Charging the buses at night only (once) eliminates any risk of schedule disruption as no charging takes place during the day, unlike multiple charging events during the day where there is a higher risk of schedule disruption. On the other hand, night charging faces a higher risk of service interruption as the battery should be sufficiently charged to operate throughout the entire day. As for the costs, multiple charging during the day is generally more expensive due to the higher number of needed chargers.

Table 4.4: Impact of battery size and charging strategy on BEB line operation and costs

			Operation		Costs
			Schedule Disruption	Service Interruption	
Battery Size		large (High energy capacity)	Lower Risk	Lower Risk	Higher cost
		Small (Low energy capacity)	Higher Risk	Higher Risk	Lower cost
Charging Strategy	Location	Depot	Lower risk	Higher risk	Dependent on geographic location.
		Terminal Stations	Medium risk	Medium risk	
		Stop Station	Higher risk	Lower risk	
	Time / Frequency	Night (Once)	No Risk	Higher Risk	Lower cost
		Day (Multiple charging events during the day)	Higher Risk	Lower Risk	Higher cost
	Energy	large amount	Higher Risk	Lower Risk	Higher cost
		Small amount	Lower Risk	Higher Risk	Lower cost
	Power	High- power fast chargers	Lower risk	Lower risk	Higher cost
		Low- power slow chargers	Higher risk	Higher risk	Lower cost

The amount of charging energy also affects the BEB line operation and costs. Aiming to charge a large amount of energy results in higher schedule disruption risk due to the higher resulting charging duration. However, a lower risk of service interruption is expected due to the sufficient amount of energy on-board.

Finally, the charging power rate has the strongest impact on BEB line operation and costs. The use of high-power fast chargers reduces schedule disruption and service interruption risks due to the lower charging duration and higher amount of charged energy. However, the costs of chargers increase drastically with the increase in their power rating.

To that end, BEB lines operation and costs are directly driven by the BEB battery size and the adopted charging strategies. Therefore, this chapter answers the following research question:

- ***How to evaluate the TCO and operation of BEB lines and how are they impacted by battery sizing and charging strategy?***

4.3 BEB Line Energy Model

This section presents the BEB line energy model in detail. First, a global overview of the system is presented describing each component as an energy entity that contributes to the global system energy scheme. Then, BEB line components are modeled including the stop stations, terminal stations, and depot.

4.3.1 System Overview

Figure 4.7 shows a schematic of a BEB line. The line consists of many BEBs, chargers, stop stations along the line, terminal stations at both ends of the line, and a depot. Stop stations, terminal stations, and the depot may be equipped with chargers to charge the BEBs. The line operating conditions are shown as well including the weather conditions, driving conditions, and passengers' load. In addition, the line schedule is introduced in the figure and the charging strategy as well.

The stop stations along the BEB line incorporate 2 tasks that affect the system global energy scheme. First, stop stations host passengers waiting for the bus arrival, and the number of passengers at the stop station directly determines the passengers' load inside the BEB, which impacts the energy consumption of all the BEBs operating along the line. Second, any stop station is a potential location to install a charger to transfer energy to the BEBs as long as the BEB is stopped at the station.

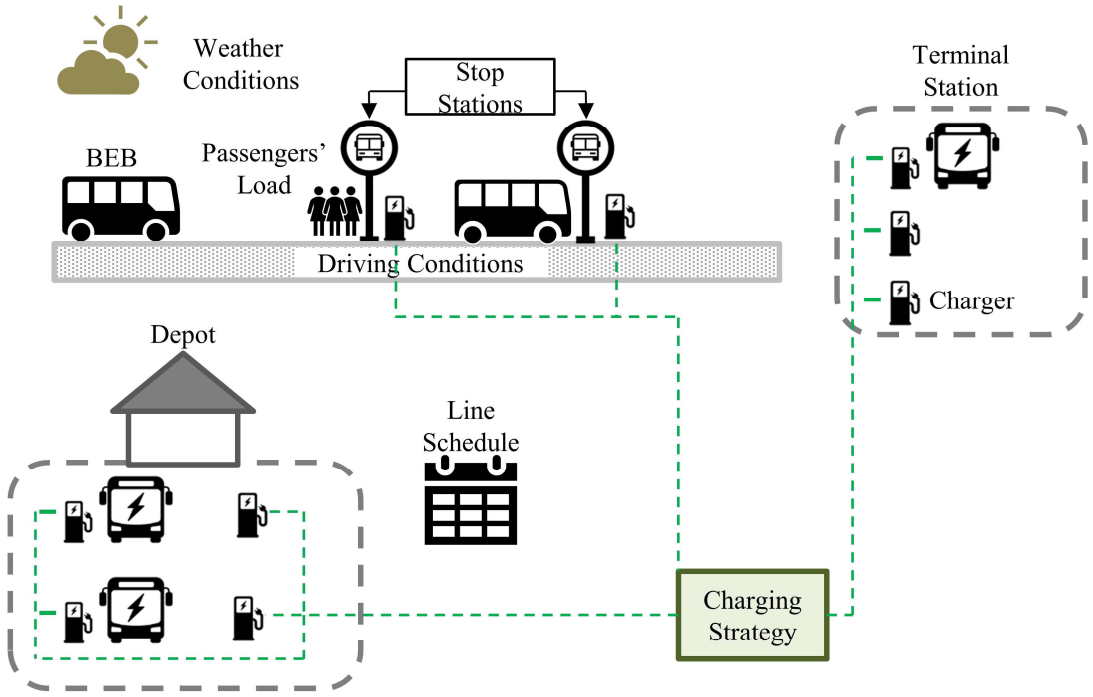


Figure 4.7: Schematic diagram of a BEB line

The terminal stations are actually stop stations located at both ends of the BEB line. Similar to the stop stations, terminal stations can be equipped with chargers to transfer energy to the BEBs. However, the main difference is that the BEBs normally stop for longer durations at the terminal stations, mainly waiting for their return trips.

The Depot is the place where the buses are parked when they are not operating during the day or when they are out of service at night. The bus depot may be located a few kilometers away from one of the bus terminals stations, or in some cases, it may serve as a terminal station itself. At the depot, BEBs can be charged as it is a potential location to install chargers as well. Charging at the depot mainly takes place at night when BEBs are out of service, or during the day if some BEBs are not operating for long durations. There is no passengers' flow to the depot or from the depot to the BEB unless the depot serves as a terminal station.

In addition, the line schedule impacts the energy scheme of the BEB line. It is considered as an additional operating condition. The schedule determines the starting time of the trips for each bus and the daily number of trips per bus. Thus, the schedule directly impacts the energy consumption of the BEBs and the charging strategy.

Finally, the charging strategy controls the power flow from the chargers to the BEBs.

4.3.2 System Model

This section introduces the mathematical modeling of the different BEB line components. The energy interactions among the different BEB line components are presented using 2 types of interactions: (1) passengers' flow and (2) electric power flow. Figure 4.8 shows the power flow and passengers' flow interactions among the different bus line components.

Similar to the BEB energy model presented in Chapter 2, Dymola is used to model the BEB line which is based on the Modelica language. This allows a real-time assessment of the system as the Modelica language is object-oriented programming language and equation-based, where each variable should be presented by a unique equation at each instant in time.

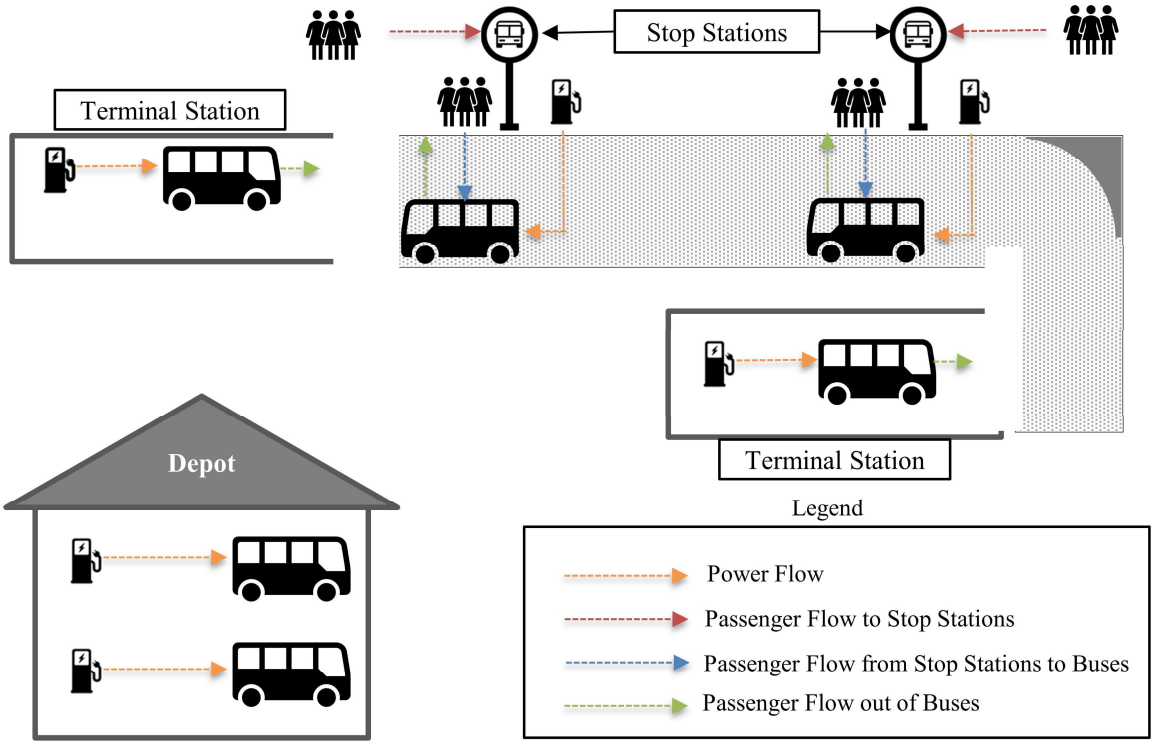


Figure 4.8: Schematic of power flow and passengers' flow interactions among the different bus line components

4.3.2.1 Charger

As discussed in section 4.2.2, BEBs can be charged by a variety of charging technologies. For public transport applications and namely BEBs, DC conductive chargers are utilized to transfer electric power from the energy source to the batteries. A charger is modeled as an efficiency map as a function of the charger output power and the soaking temperature of the charger. Data are collected from [52], [53]. It is important to mention that if a charger is placed at a certain stop station, then its soaking temperature is equal to the exterior temperature if no housing is

provided for the charger. On the other hand, chargers that are located at the depot or the termini are usually housed in pre-conditioned rooms or booths.

Figure 4.9 shows the efficiency of a DC charger at varying power outputs and varying temperatures. The charger's efficiency increases with increasing power output. On the other hand, the charger's efficiency deteriorates as its soaking temperature diverges from the optimal operating temperature considered to be 25 °C [52], [53].

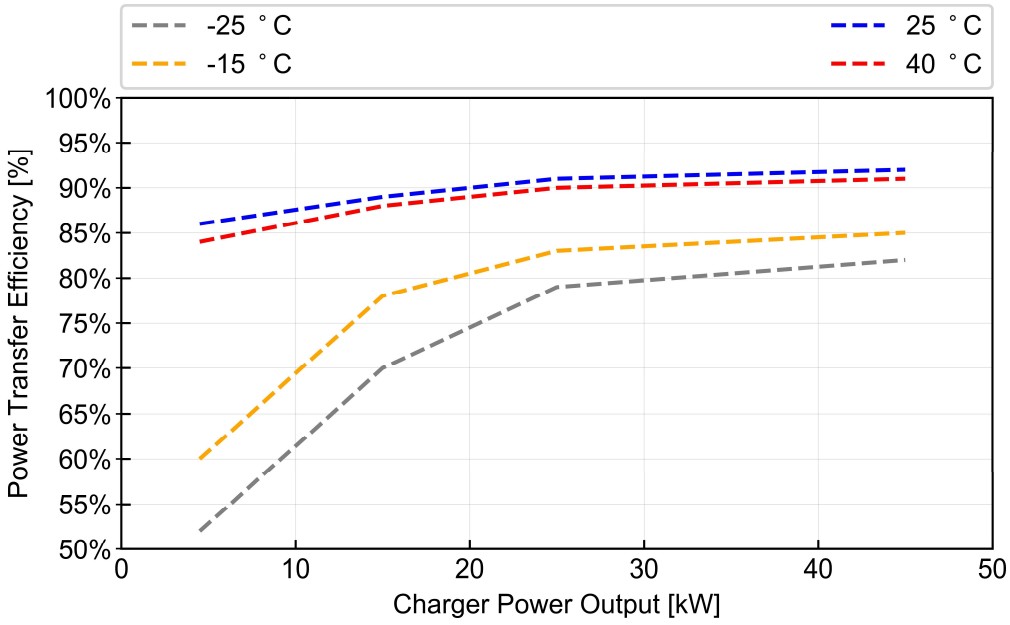


Figure 4.9: DC chargers' efficiency

4.3.2.2 BEBs

The main component in a BEB line is the bus itself. Chapter 2 thoroughly describes the energy model of a BEB. A set $\mathcal{B}$ of BEBs contains a number n_B of buses that operate along a certain BEB line. Subscript b represents a BEB number (identity).

$$\mathcal{B} = \{B_1, B_2, \dots, B_b, \dots B_{n_B}\} \ \forall\, b \in \{1,2, \dots, n_B\} \tag{4.1}$$

Each bus in set $\mathcal{B}$ is defined by two variables: its spatial location and speed at any time instant t. Therefore, two additional variables are needed to completely define the set $\mathcal{B}$: (1) a 1-D dynamic matrix $\mathcal{X}_B$ that represents the spatial location of each BEB at any time instant t, and (2) another 1-D dynamic matrix $\mathcal{V}_B$ that represents the speed of each BEB at any time instant t. The spatial location of any bus is defined as its coordinates in any discretized space, relative to a reference point to be defined.

$$\mathcal{X}_B(t) = \left[X_{B_1}, X_{B_2}, \dots, X_{B_b}, \dots\ X_{B_{n_B}}\right] \tag{4.2}$$

$$\mathcal{V}_B(t) = \left[V_{B_1}, V_{B_2}, \dots, V_{B_b}, \dots\ V_{B_{n_B}}\right] \tag{4.3}$$

In order to present the energy interaction between the BEB and the other BEB line components, the following 2 variables are defined: (1) a 1-D dynamic matrix $\mathcal{N}_P^B$ representing the number of passengers occupying each BEB at any instant *t,* and (2) another 1-D dynamic matrix $\mathcal{P}_B$ which represents the electric power flow to each BEB at any instant *t*.

$$\mathcal{N}_P^B(t) = \left[N_P^{B_1}, N_P^{B_2}, \dots, N_P^{B_b}, \dots\ N_P^{B_{n_B}}\right] \tag{4.4}$$

$$\mathcal{P}_B(t) = \left[P_{B_1}, P_{B_2}, \dots, P_{B_b}, \dots\ P_{B_{n_B}}\right] \tag{4.5}$$

4.3.2.3 Stop Stations

The number and location of the stop stations along the line may differ depending on the trip direction. Normally, each line has 2 directions representing both the onward trip and the return trip of the bus. Let $\mathcal{S}^r$ be a set of stop stations in direction *r* containing a certain number n_S^r of stop stations. Subscript *s* represents a stop station number and *r* is a natural number equals to 1 in direction 1 (onward trip) or equals to 2 in direction 2 (return trip).

$$\mathcal{S}^r = \left\{S_1^r, S_2^r, \dots, S_s^r, \dots\ S_{n_S^r}^r\right\}\ \ \forall\, s\ \in \{1,2,\dots,n_S^r\} \tag{4.6}$$

Each stop station in all sets $\mathcal{S}^r$ is defined by a static variable representing its spatial location in reference to the line depot. Thus, additional variables are needed to completely define sets $\mathcal{S}^r$. 1-D static matrices $\mathcal{X}_{S^r}$ represent the spatial location of each stop station in direction *r*.

$$\mathcal{X}_{S^r} = \left[X_{S_1^r}, X_{S_2^r}, \dots, X_{S_s^r}, \dots\ X_{S_{n_S^r}^r}\right] \tag{4.7}$$

In addition, 2 sets of variables are defined to present the energy interaction between the stop stations and the other BEB line components, mainly the BEB itself: (1) a 1-D dynamic matrix $\mathcal{N}_P^{S^r}$ representing the number of passengers waiting at each stop station in direction *r* at any instant *t* and (2) another 1-D dynamic matrix $\mathcal{P}_{S^r}$ which represents the electric power demand from each stop station in direction *r* at any instant *t*. The electric power demand from each stop station is the sum of all the BEBs charging power demand at this station.

$$\mathcal{N}_P^{S^r}(t) = \left[N_P^{S_1^r}, N_P^{S_{12}^r}, \dots, N_P^{S_S^r}, \dots\ N_P^{S_{n_S^r}^r}\right] \tag{4.8}$$

$$\mathcal{P}_{S^r}(t) = \left[P_{S_1^r}, P_{S_2^r}, \dots, P_{S_s^r}, \dots\ P_{S_{n_S^r}^r}\right] \tag{4.9}$$

4.3.2.3.1 Passengers' Flow Interaction: Stop Stations - BEBs

In order to model the passengers' flow interaction between the stop stations and the BEBs, it is essential first to detect if a certain BEB B_b is waiting at any stop station S_s^r at any instant *t*. Let $\mathcal{J}^r$ be a dynamic binary matrix of size n_S^r x n_B.

$$\mathcal{J}^r(t) = \begin{bmatrix} I_{1,1} & \dots & I_{1,b} & \dots & I_{1,n_B} \\ \vdots & & \vdots & & \vdots \\ I_{s,1} & \dots & I_{s,b} & \dots & I_{s,n_B} \\ \vdots & & \vdots & & \vdots \\ I_{n_S^r,1} & \dots & I_{n_S^r,b} & \dots & I_{n_S^r,n_B} \end{bmatrix} \quad \forall\ B_b \in \mathcal{B}\ \wedge \forall\ S_s^r \in \mathcal{S}^r \tag{4.10}$$

For any element $I_{s,b}$ in matrix $\mathcal{J}^r$, if bus B_b is parked at stop station S_s^r, then $I_{s,b}$ is assigned a value of 1. Otherwise, $I_{s,b}$ is assigned a value of 0 as shown in equation (4.11).

$$I_{s,b}(t) = \begin{cases} 1, & \forall\ X_{B_b}(t) = X_{S_s^r}\ \wedge\ V_{B_b}(t) = 0 \\ 0, & otherwise \end{cases} \quad \forall\ I_{s,b} \in \mathcal{J}^r \tag{4.11}$$

At the stop stations, there is an inward flow of passengers to the stop stations and an outward flow of passengers from the stop stations to the BEBs. At any instant *t*, the number of passengers at stop station *s* in direction *r* is described in equation (4.12). Similarly, at any instant *t*, the number of passengers in BEB *b* is described in equation (4.13).

$$N_P^{S_s^r}(t) = \int_0^t (\dot{n}_{In}^{S_s^r} - \dot{n}_{out}^{S_s^r}).\, dt \tag{4.12}$$

$$N_P^{B_b}(t) = \int_0^t (\dot{n}_{In}^{B_b} - \dot{n}_{out}^{B_b}).\, dt \tag{4.13}$$

$\dot{n}_{In}^{S_s^r}$ is the inward passengers' flow rate to stop station S_s^r, and $\dot{n}_{out}^{S_s^r}$ is the outward passengers' flow rate from the stop station to any BEB waiting at S_s^r. Similarly, $\dot{n}_{In}^{B_b}$ is the inward passengers' flow rate to BEB B_b and $\dot{n}_{out}^{B_b}$ is the outward passengers' flow rate from the same BEB.

The inward passengers' flow $\dot{n}_{In}^{S_s^r}$ at a certain stop station is dependent on its location, direction, and time of the day as there are some busier stop stations depending on the aforementioned

parameters. Therefore, $\dot{n}_{In}^{S_s^r}$ is evaluated as function of the stop station number (location), direction, and time of the day as shown in equation (4.14). $\dot{n}_{In}^{S_s^r}$ is an input to the BEB line model and the data are collected for each bus line.

$$\dot{n}_{In}^{S_s^r} = f(s, r, t) \tag{4.14}$$

The outward passengers' flow $\dot{n}_{out}^{S_s^r}$ from a certain stop station to all BEB waiting at this stop station is described in equation (4.15).

$$\dot{n}_{out}^{S_s^r}(t) = \begin{cases} \sum_{b=1}^{n_B} I_{s,b}(t).\alpha\,, & \forall\, I_{s,b} \in \mathcal{J}_s^r \subseteq \mathcal{J}^r \,|\, N_P^{S_s^r}(t) > 0 \wedge N_P^{B_b}(t) < N_{P,Max}^B \forall\, B_b \in \mathcal{B} \\ 0, & \text{otherwise} \end{cases} \quad \forall\, S_s^r \in \mathcal{S}^r \wedge \forall\, r \tag{4.15}$$

α is a positive non-zero constant measured in (passengers/s) which reflects on the rate at which passengers move from the stop to the BEB. $N_{P,Max}^B$ is the maximum allowable number of passengers on any bus. $\mathcal{J}_s^r$ is a horizontal sub-vector at row index *s* of matrix $\mathcal{J}^r$. In equation (4.15), there might be more than one non-zero element $I_{s,b}$ in the binary vector $\mathcal{J}_s^r$ at any instant *t*. This implies that there might be more than one bus at the same stop station and at the same time instant *t*. This is common in case of schedule disruptions.

The inward passengers' flow rate $\dot{n}_{In}^{B_b}$ to BEB B_b is dependent on the number of passengers waiting at the stop station where the bus is stopped as described in equation (4.16).

$$\dot{n}_{In}^{B_b}(t) = \begin{cases} \sum_{r=1}^{2} \sum_{s=1}^{n_S^r} I_{s,b}(t).\beta\,, & \forall\, I_{s,b} \in \mathcal{J}_b^r \subseteq \mathcal{J}^r \,|\, N_P^{B_b}(t) < N_{P,Max}^B \wedge N_P^{S_s^r}(t) > 0 \,\forall\, S_s^r \in \mathcal{S}^r \\ 0, & \text{otherwise} \end{cases} \quad \forall\, B_b \in \mathcal{B} \tag{4.16}$$

β is a positive non-zero constant measured in (passengers/s), where β is equal to α. $\mathcal{J}_b^r$ is a vertical sub-vector at column index *b* of matrix $\mathcal{J}^r$. In equation (4.16), there is only one non-zero element $I_{s,b}$ in the set of binary vectors $\mathcal{J}_b^r$ ($\mathcal{J}_b^1$ and $\mathcal{J}_b^2$ as there are 2 directions) at any instant *t*. This implies that the bus can be at only one stop station in one direction *r* at any time instant *t*.

The outward passengers' flow $\dot{n}_{out}^{B_b}$ from BEB B_b is an input to the BEB line model. The data collected is in the form of a certain number of passengers $N_{out}^{B_b}$ leaving the bus at a certain stop station S_s^r at time t. Therefore, $N_{out}^{B_b}$ is dependent on the stop station location, direction, and time of the day as well, as shown in equation (4.17). Consequently, $\dot{n}_{out}^{B_b}$ is defined as shown in equation (4.18).

$$N_{out}^{B_b} = f(s,r,t) \tag{4.17}$$

$$\dot{n}_{out}^{B_b}(t) = \begin{cases} \sum_{r=1}^{2} \sum_{s=1}^{n_S^r} I_{s,b}(t).\kappa, & \forall\ I_{s,b} \in \mathcal{J}_b^r \subseteq \mathcal{J}^r \mid N_{out}^{B_b}(s,r,t) > 0\ \forall\ S_s^r \in \mathcal{S}^r \\ 0, & \text{otherwise} \end{cases} \quad \forall\ B_b \in \mathcal{B} \tag{4.18}$$

κ is a positive non-zero constant measured in (passengers/s).

Finally, Figure 4.10 presents a schematic of the passengers' flow interaction between the buses and stop stations.

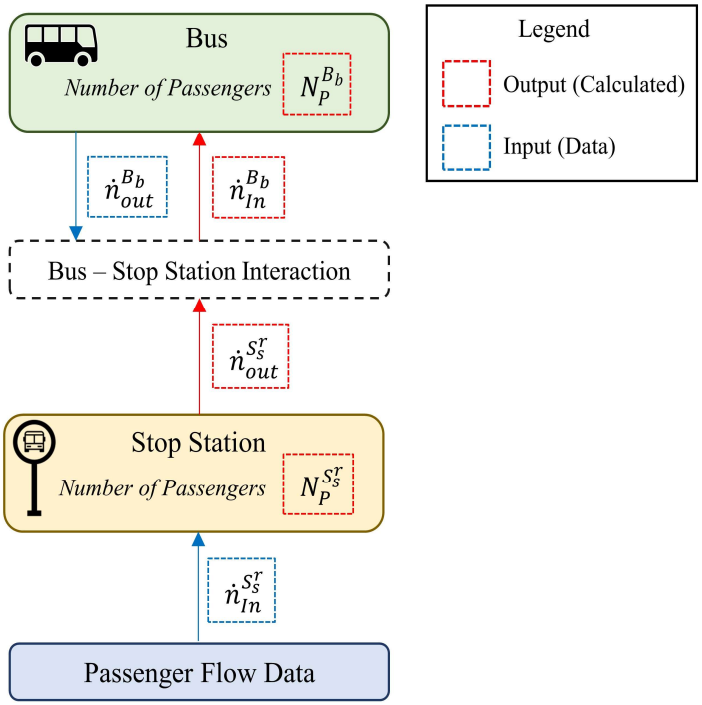


Figure 4.10: Schematic of passengers flow interaction between the buses and stop stations

4.3.2.3.2 Electric Power Flow Interaction: Stop Stations - BEBs

Electric power flow from the stop stations to the BEBs denotes the charging of BEBs at the stop stations. The electric power flow from the stop stations to the BEBs is conducted by means of chargers. Charging at the stop stations is referred to as opportunity charging. It is assumed that there is only one charger at each stop station. Each charger has a specific charging efficiency depending on its required power output and soaking temperature as presented in section 4.3.2.1. Therefore, a 1-D matrix $\mathcal{E}_{S^r}$ represents the charging efficiency of the charger at each stop station in direction *r*.

$$\mathcal{E}_{S^r} = \left[\eta_{S_1^r}, \eta_{S_2^r}, \dots, \eta_{S_s^r}, \dots \eta_{S_{n_S^r}^r}\right] \tag{4.19}$$

The electric power transfer from the stop stations to the BEBs is expressed in equation (4.20). The first term in the equation enclosed by parentheses is the Hadamard product of 2 matrices of the same dimension where the size of both $\mathcal{P}_{S^r}$ and $\mathcal{E}_{S^r}$ is 1xn_S^r. The Hadamard product is also referred to as the element-by-element product of 2 matrices, and the resulting matrix is of size 1xn_S^r as well. Then, the matrix product of the Hadamard product $(\mathcal{P}_{S^r}(t) \circ \mathcal{E}_{S^r})$ and the binary matrix $\mathcal{J}^r$ results in a matrix of size 1xn_B, which is the electric power flow to the BEBs from the stop stations located along direction *r*. Finally, the total electric power delivered to the BEBs is the matrix sum of the electric power flow from all the stop stations located in both directions.

$$\mathcal{P}_B(t) = \sum_{r=1}^{2} (\mathcal{P}_{S^r}(t) \circ \mathcal{E}_{S^r}).\mathcal{J}^r(t) \tag{4.20}$$

The electric power demand at the stop stations $\mathcal{P}_{S^r}(t)$ is directly controlled by the charging strategy.

4.3.2.4 Terminal Stations

Normally for each bus line, there is one terminal station in each direction. Thus, for each bus line, there exist 2 terminal stations along this line. Let $\mathcal{T}$ be the set of terminal stations.

$$\mathcal{T} = \{T^1, T^2\} \tag{4.21}$$

Similar to the stop stations, terminal stations are defined by their spatial location in reference to the line depot. Let $\mathcal{X}_T$ be a static matrix containing the spatial locations of both terminal stations.

$$\mathcal{X}_T(t) = [X_{T^1}, X_{T^2}] \quad (4.22)$$

In addition, let $\mathcal{N}_P^T$ be a 1-D dynamic matrix representing the number of passengers waiting at each terminal station at any instant *t*.

$$\mathcal{N}_P^T(t) = \left[N_P^{T^1}, N_P^{T^2}\right] \quad (4.23)$$

Unlike the stop stations, there might be more than one charger at each terminal station. Let $\mathcal{P}_{T^r}$ be a 1-D dynamic matrix of size 1 x n_C^r where n_C^r is the number of chargers installed at a terminal station T^r. $\mathcal{P}_{T^r}(t)$ represents the power demand from each charger installed at the terminal station T_r. The number of chargers at each terminal station might be different.

$$\mathcal{P}_{T^r}(t) = \left[P_1^{T^r}, P_2^{T^r}, \dots, P_c^{T^r}, \dots P_{n_C^r}^{T^r}\right] \quad (4.24)$$

4.3.2.4.1 Passengers' Flow Interaction: Terminal Stations - BEBs

Passengers' flow at the terminal station takes place in 3 stages: first, the bus arrives at the terminal station and discharges all passengers on-board, and in this stage, there is no passengers flow from the terminal station to the bus. Then the bus waits at the terminal station for its return trip and during this time no passengers are allowed to get into the bus. Finally, prior to the bus departure from the terminal station to start its return trip, passengers flow into the bus.

The passengers' flow interaction between the terminal stations and the BEBs is modeled in a similar approach to that used in passengers' flow interaction between the stop stations and the BEBs, but with very few differences. The complete model is presented in Appendix G.

4.3.2.4.2 Electric Power Flow Interaction: Terminal Stations - BEBs

Charging the BEBs at the terminal stations incurs more complications when compared to charging at the stop stations, mainly due to the chargers' availability problem. At the terminal stations, it is possible to charge multiple BEBs at the same time if there are enough available chargers. At this stage, it is important to define the chargers' allocations to the BEBs. Thus, a dynamic binary matrix $\mathcal{O}_{T_r}$ is defined to determine which charger should be allocated to any BEB that requires charging at a terminal station T^r. The size of the matrix $\mathcal{O}_{T^r}$ is n_C^r x n_B where the number of rows equals the number of chargers at the terminal station T_r and the number of columns is the number of BEBs. $\mathcal{O}_{T^r}$ is controlled by the charging strategy.

Let $\mathcal{E}_{T^r}$ be a 1-D matrix representing the charging efficiency of the chargers installed at a terminal station T^r.

$$\mathcal{E}_{T^r} = \left[\eta_1^{T^r}, \eta_2^{T^r}, \dots, \eta_c^{T^r}, \dots \eta_{n_C^r}^{T^r}\right] \quad (4.25)$$

The power transfer to the BEBs is expressed in equation (4.26).

$$\mathcal{P}_B(t) = \sum_{r=1}^{2} (\mathcal{P}_{T^r}(t) \circ \mathcal{E}_{T^r}).\mathcal{O}_{T_r}(t) \quad (4.26)$$

The electric power demand at the terminal stations $\mathcal{P}_{T^r}(t)$ and the chargers' allocation matrix $\mathcal{O}_{T^r}$ are directly controlled by the charging strategy.

4.3.2.5 Depot

Normally for each bus line, there is one depot where the buses are parked when they are out of service. The depot is the reference point in the bus line and its spatial location $X_D = 0$.

Similar to the terminal stations, there might be multiple chargers installed at the depot. Let $\mathcal{P}_D$ be a 1-D dynamic matrix of size 1 x n_C^D where n_C^D is the number of chargers installed at the depot. $\mathcal{P}_D(t)$ represents the power demand from each charger installed at the depot.

$$\mathcal{P}_D(t) = \left[P_1, P_2, \dots, P_d, \dots P_{n_C^D}\right] \quad (4.27)$$

As mentioned earlier, there is no passengers' interaction between the depot and the BEBs.

4.3.2.5.1 Electric Power Flow Interaction: Depot - BEBs

Similar to the terminal stations, it is possible to charge multiple BEBs at the same time if there are enough available chargers at the depot. A dynamic binary matrix $\mathcal{O}_D$ is defined to determine which charger should be allocated to any BEB that requires charging at the depot. The size of the matrix $\mathcal{O}_D$ is n_C^D x n_B where the number of rows equals the number of chargers at the depot and the number of columns is the number of BEBs.

Let $\mathcal{E}_D$ be a 1-D matrix representing the charging efficiency of the chargers installed at the depot.

$$\mathcal{E}_D = \left[\eta_1, \eta_2, \dots, \eta_d, \dots \eta_{n_C^D}\right] \quad (4.28)$$

The power transfer to the BEBs is expressed in equation (4.29).

$$\mathcal{P}_B(t) = (\mathcal{P}_D(t) \circ \mathcal{E}_D).\mathcal{O}_{\mathrm{D}}(t) \quad (4.29)$$

The electric power demand at the depot $\mathcal{P}_D(t)$ and the chargers' allocation matrix $\mathcal{O}_{\mathrm{D}}$ are directly controlled by the charging strategy.

4.3.2.6 Operating Conditions

The BEB line operating conditions highly affect its energy consumption. These operating conditions are driving conditions, weather conditions, passengers' load, and the schedule.

4.3.2.6.1 Driving Conditions

Driving conditions reflect on the bus route characteristics such as the road topography, distance, and traffic conditions. In addition, the number of stops and the location of each stop station, terminal station, and depot are all defined under the BEB line driving conditions. Typical driving conditions for BEB lines were presented in Appendix C. The driving conditions are summarized using velocity profiles as function of time for a specific bus trip. These profiles could be altered by traffic conditions during the day. Data such as average bus speed, acceleration, deceleration, number of stops, and stoppage time at the stations could all be inferred from these velocity profiles.

4.3.2.6.2 Weather Conditions

Weather conditions depend on the geographic location of the BEB line. The exterior temperature and the solar flux are the 2 considered parameters. Dynamic temperature and solar flux profiles throughout the day are considered on an hourly basis.

4.3.2.6.3 Passengers' Load

The passengers' load in the BEBs is already modeled in a dynamic approach between the BEBs and the stop and terminal stations in the previous sections. Data for passengers' flow into the stop stations and the number of passengers leaving the bus at each stop station are collected for each BEB line.

4.3.2.6.4 Schedule

The schedule of the BEBs determines the daily number of trips for each BEB and the starting time of each trip. A BEB b completes a daily number of trips n_t^b and the starting time for each trip is defined in the set $\mathbb{T}_b$. $t_b^{j,r}$ is the starting time of trip j in direction r for BEB b.

$$\mathbb{T}_b = \left\{ t_b^{1,1}, t_b^{1,2}, t_b^{2,1}, t_b^{2,2}, \dots, t_b^{j,r}, \dots, t_b^{n_t^b,1}, t_b^{n_t^b,2} \right\} \quad (4.30)$$

4.3.2.7 Charging Strategy

As defined earlier, the charging strategy determines the charging profile of the BEBs during the day by determining the charging location, time, energy, and power.

Deciding on the charging location is done in 2 parts: (1) deciding on where to install the chargers and (2) decide on where to charge during the day. First, the chargers could either be installed at the depot, terminal stations, or any stop station. In addition, it is essential to determine the number of chargers that should be installed at the terminal stations and the depot if any. Then, after deciding on the chargers' location, it is essential to decide where to charge during the day in case chargers are installed at multiple locations.

The charging location during the day, time, energy, and power can all be summarized in one variable which is the charging power profile of the BEB during the day. An example of a BEB charging power profile during the day is shown in Figure 4.11. The charging time, location, energy, and power can all be deduced from this charging power profile.

As shown in Figure 4.11, the first charging event starts at 03:00h and the second charging event starts at 15:00h. The charging power is 40 *kW* during the first charging event and 100 *kW* during the second charging event.

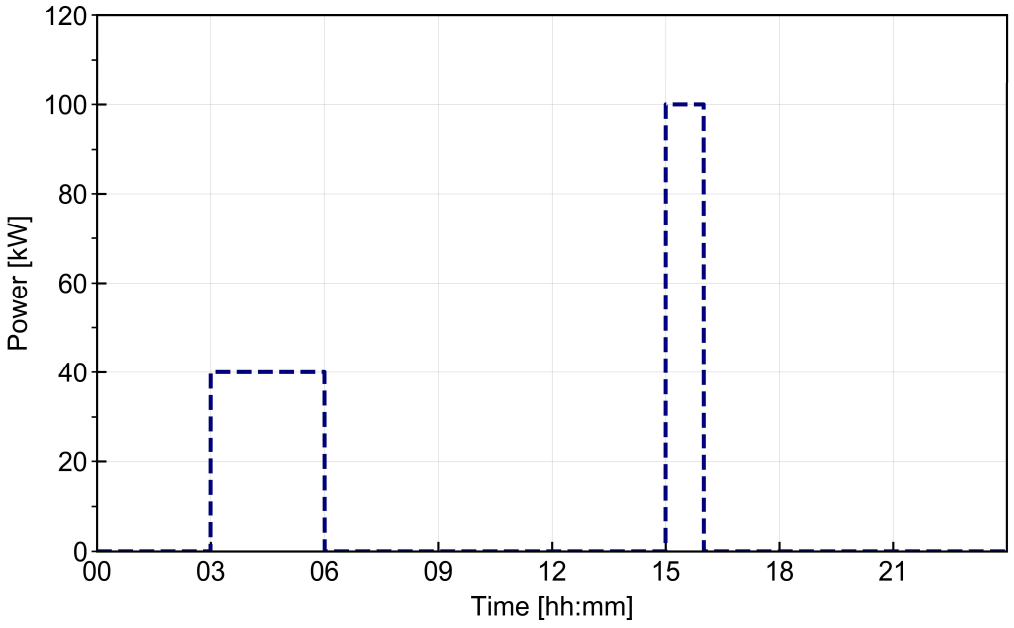


Figure 4.11: Example of BEB charging power profile during the day

In addition, the charging energy is controlled by determining the duration of each charging event. The first charging event duration is 3 hours, and it takes place at 40 *kW*, thus a total of 120 *kWh* of energy is transferred to the battery. Similarly, the second charging event takes place for 1 hour and at 100 *kW*, thus a total of 100 *kWh* of energy is transferred to the battery.

Furthermore, the charging location is reflected in the BEB charging power profile as the location of the bus is known at each instant during the day. In the presented example, both charging events take place at the depot as the bus is out of service from 3:00 – 6:00 and it is parked at the depot during this period. The second charging event takes place at the depot as well as the BEB is parked at the depot between 15:00 – 16:00 waiting for its next trip, as determined by its schedule.

4.4 Operation of BEB Line

The main task of any public transport bus line is to facilitate passengers' mobility along its line of operation. The operation of the bus line should ensure passengers' satisfaction at many levels. One level of passengers' satisfaction is related to bus punctuality. With the deployment of BEBs, there are many concerns regarding the BEBs' ability to follow their pre-defined schedule due to their charging needs, which may cause potential delays, and thus disrupting the BEBs schedule.

As defined earlier, BEB line operation is defined by two main indicators: (1) % schedule disruption and (2) % of service interruption. Bus operators are obliged to attain a certain level of punctuality when operating the bus fleet. Failure to attain this level of punctuality results in penalties that should be paid by the bus operator.

This section introduces the criteria used to assess the level of punctuality for a BEB line. Then, the structure of the penalty that should be paid by the operator is presented. The criteria to evaluate the punctuality level and penalty structure for any bus line are set by the relevant public establishments. In this thesis, the criteria used in Paris are presented.

4.4.1 BEB Line Punctuality Level

The punctuality level is presented by a punctuality index that reflects on the number of delayed and interrupted trips for a sample of buses. According to the contract between *le Syndicat des Transports d'Ile-De-France* et *la Régie Autonome des Transports Parisiens* [54], appendix II-C of the contract defines the punctuality index as follows [55]: " for a scheduled bus trip at a time t_d, the punctuality index is calculated as function of the amount of time delayed, in reference to the scheduled departure time t_d, from the bus terminal station". Table 4.5 presents the punctuality index (PI) calculation method where, t_d is the scheduled departure time and $t_{d,actual}$ is the actual departure time of a bus.

Table 4.5: Bus trips punctuality index

Case		Punctuality Index (PI)
Case 1: The actual departure time is delayed by less than 5 minutes.	$t_{d,actual} < t_d + 5'$	100 %
Case 2: The actual departure time is delayed from 5 to 10 minutes.	$t_d + 5' < t_{d,actual} < t_d + 10'$	50 %
Case 3: Actual departure time is delayed by more than 10 minutes	$t_{d,actual} > t_d + 10'$	0%

The total punctuality index (*PI*) over a period of time, mainly taken as 1 year, is the average of the recorded PIs over that same period.

The previous definition does not consider the bus service interruption, because, with the current diesel buses operating in Paris, there are no concerns regarding service interruption due to lack of energy on-board. In this thesis, if service is interrupted during any bus trip, the corresponding trip is assigned a PI equal to 0%.

The concerned authorities set a "goal" for *PI*, a "lower limit" and a "higher limit". For the case of Paris city, the goal is to achieve a 97% *PI* for all bus trips operated by a certain operator, the lower limit is 94% and the higher limit is 100%.

Table 4.6 summarizes the *PI* target values.

Table 4.6: Punctuality index target values

Parameter	Symbol	Value
Punctuality Index goal	$\widehat{PI}$	97 %
Punctuality Index lower limit	PI_{Low}	94 %
Punctuality Index higher limit	PI_{High}	100%

4.4.2 BEB Line Punctuality Penalty Fares

The structure of the penalty fare is also presented in appendix II-C of [55]. The penalty fare is calculated as function of PI. The annual amount to be paid in euros ($PF_{€}$) can either be a positive

or a negative amount. A positive $PF_{€}$ implies that the operator pays a penalty and a negative $PF_{€}$ implies that the operator gets a bonus. There is a maximum penalty fare M that is imposed on the penalty structure. The maximum penalty fare M is dependent on the size of the contract between the operator and the public establishment. Operators that run a higher number of bus lines are subjected to high M values. In the presented case for Paris city operator, the maximum penalty fare is 2.1 million €.

Table 4.7: Penalty fare structure for bus punctuality index

	Case	Penalty Fare Structure
Penalty Fare (**PF**$_{€}$ > 0)	$PI = \widehat{PI}$	No penalty fare is paid (PF$_{€}$ = 0)
	$PI_{Low} < PI < \widehat{PI}$	$PF_{€} = \frac{PI - \widehat{PI}}{PI_{Low} - \widehat{PI}}.M$
	$PI < PI_{Low}$	M
Bonus (**PF**$_{€}$ < 0)	$\widehat{PI} < PI < PI_{High}$	$PF_{€} = -\frac{PI - \widehat{PI}}{PI_{High} - \widehat{PI}}.M$

4.5 Costs of Deployment of BEB Lines

One of the main challenges facing BEBs is their deployment costs [9], [56]–[58]. The cost of deployment of BEBs can be segregated into 5 main components: (1) Bus unit cost, (2) operating costs, (3) maintenance costs (4) infrastructure costs, and (5) battery replacement costs [56].

4.5.1 Unit Cost

The unit cost is the purchase cost of a BEB. BEB unit cost is more expensive when compared to DB due to the additional cost of the electric components such as the battery pack and the electric machine [59]. The bus unit cost (UC) is composed of 2 parts: (1) a fixed cost including the bus chassis cost and electric components and (2) a variable cost depending on the size of the battery pack. The battery cost can be considered linearly proportional to its energy capacity in an approach similar to [9], [58], [60], [61]. The unit cost is expressed in equation (4.31) where Ω is the fixed cost of the BEB, β is the cost of the battery pack per unit energy measured in $€/kWh$ and K_b is the battery energy capacity of the BEB B_b.

$$UC = \Omega + \beta.K_b \tag{4.31}$$

For a set of BEBs operating along the line each with a battery capacity K_b, the total unit cost is expressed in equation (4.32).

$$UC_{Line} = n_B.\Omega + \sum_{b=1}^{n_B} \beta.K_b \quad \forall B_b \in \mathcal{B} \tag{4.32}$$

4.5.2 Operating Costs

In general, the operating costs include energy costs, maintenance costs, wages, and battery replacement costs as well. However, in order to differentiate among these components and thoroughly reflect on the impact of each cost component on the TCO, the operating costs are only considered to be the energy costs and wages, whereas maintenance and battery replacement costs are dealt with as separate cost components in this thesis.

The operating costs of BEBs are the electricity bills paid by the operator for the electric energy used to charge the BEBs batteries at the charging stations. A charging station is any BEB stop station, terminal station, or depot that is equipped with chargers. A charging station may contain one charger or a set of chargers, which might be the case at the terminal stations and the depot. Each charging station is an electricity node that is connected to the electric grid and incurs an electricity bill. Thus, the operating costs of a certain BEB line, defined over a specific billing period, are the sum of the electricity bills at all the charging stations during this billing period.

Let $\mathbb{C}$ be a set containing all the charging stations along a certain BEB line where the number of charging stations is denoted by n_{CS}. Denote by T_{Bill} the electricity billing period.

$$\mathbb{C} = \{CS_1, CS_2, \dots, CS_i, \dots\ CS_{n_{CS}}\} \quad \forall\, i\ \in \{1,2, \dots, n_{CS}\} \tag{4.33}$$

The operating cost is directly related to the energy consumption of the BEBs and the electricity bill structure set by local authorities. The structure of the electricity bill differs from one country to another, or even among cities within the same country. However, the most general electricity bill structure is composed of 2 components: (1) energy usage and (2) demand charge.

The energy usage is the amount of energy consumed at the charging station to charge the BEBs. The cost of electric energy consumption is proportional to the amount of electric energy consumed. However, the electric energy tariff may vary during the day depending on many factors, such as the electricity generation mix during the day, or the total power demand from the electricity grid.

At each charging station CS_i, the cost related to the energy usage is expressed in equation (4.34), where $OC_{CS_i}^{eu}$ is the energy usage component of the operating costs at the charging station CS_i, α is the electric energy tariff that varies as function of time, and P_{CS_i} is the power demand at charging station CS_i.

$$OC_{CS_i}^{eu} = \int_0^{T_{Bill}} \alpha(t).P_{CS_i}(t).dt \tag{4.34}$$

The other component of the electricity bill is the demand charge. The demand charge is also known as the power cost. The demand charge is an additional fee to be paid by the consumer and it is calculated based on the peak power demand during a defined time interval [61]. The demand charge is calculated as the peak demand multiplied by a demand charge rate. Unlike the cost of electric energy usage, demand charges are not cumulative, they are considered one-time occurrence costs proportional to the peak power demand during a defined billing period, which is the maximum recorded during a billing period [60]. The peak power demand is calculated as the average power demand over a defined time interval [62].

Utility companies that supply the BEB operators with electric energy define the demand charge time interval T_D. T_D mainly ranges from 15 minutes to 1 hour. Denote by $\mathbb{D}$ the set of demand periods within a certain billing period T_{Bill}.

$$\mathbb{D} = \{T_1, T_2, \dots, T_d, T_{d+1}, \dots\} \quad \forall\, d \in \left\{1,2, \dots, \frac{T_{Bill}}{T_D}\right\} \tag{4.35}$$

At each charging station CS_i, the cost related to the demand charge is expressed in equation (4.36) where $OC_{CS_i}^{dc}$ is the demand charge component of the operating costs at the charging station CS_i, λ is the demand charge rate, P_{CS_i} is the power demand at the charging station CS_i and τ_d and τ_{d+1} are the time stamps at the beginning and end of the demand period T_d.

$$OC_{CS_i}^{dc} = \lambda.\max\left(\frac{\int_{\tau_d}^{\tau_{d+1}} P_{CS_i}(t).dt}{T_D}\right) \quad \forall\ T_d \in \mathbb{D} \tag{4.36}$$

Then, the total operating costs at the charging station CS_i are the sum of the energy usage component and demand charge component of the electricity bill at the charging station CS_i.

$$OC_{CS_i} = OC_{CS_i}^{eu} + OC_{CS_i}^{dc} \tag{4.37}$$

In addition to the electricity bill, operating cost also includes the drivers' wages and all other personnel that are paid in exchange for services relevant to the BEB line operation. Let n_{per} be the number of personnel operating the BEB line and denote by W_P the average salary per person during a billing period T_{Bill}.

Finally, the total operating costs for a BEB line over a certain billing period T_{Bill} is the sum of the electricity bills at all the charging stations during this billing period, in addition to the paid salaries as shown in equation (4.38).

$$OC_{Line} = \sum_{i=1}^{n_{CS}} \left(\int_{0}^{T_{Bill}} \alpha(t).P_{CS_i}(t).dt + \lambda.\max\left(\frac{\int_{\tau_d}^{\tau_{d+1}} P_{CS_i}(t).dt}{T_D} \right) \right) + n_{per}.W_P$$
$$\forall\ T_d \in \mathbb{D} \ \wedge\ CS_i\ \in \mathbb{C} \qquad (4.38)$$

4.5.3 Maintenance Cost

Maintenance costs involve regular checks, repairing, or replacing components in the BEB (other than the battery in this thesis). The maintenance costs for BEBs are relatively lower when compared to DB due to the lower number of rotating mechanical parts [63]. Maintenance costs are mainly measured per driven km. Thus, the maintenance cost of a BEB line over a time period is the maintenance cost rate multiplied by the distance covered by all BEBs during this time period as shown in equation (4.39), where ω is the maintenance cost rate and X_b is the distance covered by BEB B_b.

$$MC_{Line} = \sum_{b=1}^{n_B} \omega.X_b \qquad \forall\ B_b \in \mathcal{B} \qquad (4.39)$$

4.5.4 Infrastructure Cost

The infrastructural modifications due to BEBs deployment can range from moderate to major modifications. Modifications such as building charging stations at the bus line are relatively moderate in terms of cost and construction complexity. However, a massive deployment of BEBs may require modifications at the electricity grid level or even modifications in the electricity generation powerplant to fulfill the high electricity demand. The scope of this thesis covers BEBs deployment from the operator's perspective and thus, the only considered infrastructure costs are those associated with the construction and installation of charging stations.

Let Θ_{CS_i} be the set containing all the installed chargers at a station CS_i, and denote by $n_C^{CS_i}$ the number of chargers installed at station CS_i, where each has a power rating P_{MAX}^w.

$$\Theta_{CS_i} = \left\{\theta_1, \theta_2, \dots, \theta_w, \dots, \theta_{n_C^{CS_i}}\right\} \tag{4.40}$$

The infrastructure cost of building a charging station can be approximated in equation (4.41) as presented by [64], [65] where $C_b^{CS_i}$ is the cost of building or remodelling a charging station, and σ is the cost per unit charger power measured in *€/kW*.

$$IC_{CS_i} = C_b^{CS_i} + \sum_{w=1}^{n_C^{CS_i}} \sigma . P_{MAX}^w \qquad \forall\, \theta_w \in \Theta_{CS_i} \tag{4.41}$$

$C_b^{CS_i}$ depends on the area needed to build or remodel the charging station. This is directly affected by the number of chargers installed at the charging station. $C_b^{CS_i}$ is expressed in equation (4.42) where A_0 is a construction area for the charging station, a_0 is the required construction area for 1 charger, and C_a is the construction cost per unit area measured in *€/m²*.

$$C_b^{CS_i} = (A_0 + a_0 . n_C^{CS_i}) . C_a \tag{4.42}$$

Finally, the total infrastructure cost for a BEB line is the sum of the infrastructure costs for all the charging stations as expressed in equation (4.43).

$$IC_{Line} = \sum_{i=1}^{n_{CS}} \left((A_0 + a_0 . n_C^{CS_i}) . C_a + \sum_{w=1}^{n_C^{CS_i}} \sigma . P_{MAX}^w \right) \qquad \forall\, \theta_w \in \Theta_{CS_i} \wedge CS_i \in \mathbb{C} \tag{4.43}$$

4.5.5 Battery Replacement Cost

Replacing the energy storage system (ESS) is a common practice for BEBs as the service life of the battery is shorter than the service life of the BEB itself. The battery replacement cost (*BRC*) in this thesis is defined for a given year. Equation (4.44) shows the BRC at year *y,* where $\beta(y)$ is the cost of the battery pack per unit energy measured in *€/kWh* purchased at year *y,* K_b is the energy capacity of the new battery measured in *kWh*, and $R_b(y)$ is a binary variable that decides if the battery of BEB B_b is replaced at year *y,* depending on the battery lifespan.

$$BRC(y) = R_b(y) . \beta(y) . K_b \tag{4.44}$$

The total BRC for a BEB line over a year is expressed in equation (4.45).

$$BRC(y)_{Lin} = \sum_{b=1}^{n_B} R_b(y).\beta(y).K_b \quad \forall B_b \in \mathcal{B} \tag{4.45}$$

In order to estimate the battery lifetime and the required battery replacement frequency, a basic battery aging model is developed as presented in Appendix H. Note that the battery life span depends on the discharge/charge cycle, battery voltage, temperature, and C-rate.

4.5.6 Total Cost of Ownership

The total cost of ownership (TCO) is a very common method to determine the direct and indirect costs of urban bus lines as presented in these studies [4], [66]–[68]. TCO is used to calculate the total costs encountered during the entire service life of the system [69]. The proposed TCO model quantifies these costs per driven kilometer which is a common practice when assessing the TCO of vehicles [56].

4.5.6.1 TCO Model

Let T_{EL} be the end life of the BEBs in years. The infrastructure cost and the unit cost (IC_{Line}+ UC_{Line}) are capital costs paid at year y = 1 (start of BEB line operation). On the contrary, the operating and maintenance costs ($OC_{Line} + MC_{Line}$) are paid monthly, and the battery replacement cost is paid at certain years y that corresponds to the year of the battery replacement. Finally, the salvage value of batteries is zero at their end life. In addition, the salvage value of the bus is zero after 12 years and that of the infrastructure is zero after 20 years [70]. TCO is expressed in equation (4.46) where $X_{b,m}$ is the distance covered by BEB B_b during month m. SV_B and SV_C are the battery salvage value and infrastructure salvage value at T_{EL} respectively, and they are presented in equation (4.47) and (4.48).

$$TCO = \frac{UC_{Line} + IC_{Line} + \sum_{y=1}^{T_{EL}} \sum_{m=1}^{12} (OC_{Line} + MC_{Line}) + \sum_{y=1}^{T_{EL}} BRC_{Line} - (SV_B + SV_{IC})}{\sum_{y=1}^{T_{EL}} \sum_{m=1}^{12} \sum_{b=1}^{n_B} X_{b,m}} \quad \forall B_b \in \mathcal{B} \tag{4.46}$$

$$SV_B = \frac{Q_{Batt}(T_{EL})}{Q_{Loss\ Max}}.\beta(y).K_b \quad \forall B_b \in \mathcal{B} \tag{4.47}$$

$$SV_{IC} = \frac{T_{IC}}{T_{EL}}.IC_{Line} \tag{4.48}$$

4.5.6.2 Present Worth of TCO

The present worth (PW) is a very common method used to compare different cash flows at different time periods [67]. PW is included to consider the time value of money due to the interest rate [71]. The PW is calculated based on the discount rate. The discount rate (d_r) is calculated as shown in equation (4.49), where i_r is the nominal annual interest rate, γ is the number of compounding periods per year, and δ is the number of periods per year.

$$d_r = \left(1 + \frac{i_r}{\gamma}\right)^{\frac{\gamma}{\delta}} - 1 \tag{4.49}$$

From equation (4.49), i_r and γ are mainly fixed depending on the country/city, however, the number of periods per year (δ) is dependent on the payment frequency per year (cash flow frequency). For example, the operating and maintenance costs are paid once every month, thus the value of δ is 12. On the other hand, battery replacement costs are paid yearly, if any, and thus the value of δ is 1 in this case. Infrastructure and unit costs are already paid at present; thus, their PW is not affected by the discount rate. For this sake, d_r varies depending on the cost component. d_r^y denotes annual discount rate and d_r^m denotes a monthly discount rate. Equation (4.50) presents the present worth of the TCO. For transportation projects, the interest rate ranges from 10-12% for developing countries according to the world bank [72], and it gets a bit lower for developed countries. In France, the interest rate for transportation projects is around 6.5% as reported by [73].

$$TCO_{PW} = \frac{\begin{array}{c} UC_{Line} + IC_{Line} + \sum_{y=1}^{T_{EL}} \sum_{m=1}^{12} (OC_{Line} + MC_{Line}).\left(1 + d_r^m\right)^{-(12.(y-1)+m)} + \\ \sum_{y=1}^{T_{EL}} BRC_{Line}.\left(1 + d_r^y\right)^{-y} - (SV_B + SV_{IC}).\left(1 + d_r^y\right)^{-T_{EL}} \end{array}}{\sum_{y=1}^{T_{EL}} \sum_{m=1}^{12} \sum_{b=1}^{n_B} X_{b,m}}$$
$$\forall\, B_b \in \mathcal{B} \tag{4.50}$$

Another cost component that could be considered is the penalty/bonus to be paid/received by the bus operators due to the bus's punctuality relative to their schedule as defined in section 4.4. For the presented PI penalty fare structure, the maximum penalty to be paid by the bus operator is negligible in comparison to the TCO. Preliminary calculations show that it represents 0.15% of the TCO. This mainly due to the fact that the current PI penalty fare structure is developed for diesel bus fleet, where TCO is way much lower in comparison to BEB, and there are no concerns regarding schedule delays due to charging. Table 4.8 summarizes the notations used in this section and, Figure 4.12 summarizes the different TCO model components.

Table 4.8: Summary of notations used in the costs of deployment of BEBs

	Notation	Description	Unit
Indices	b	BEB index	-
	i	Charging station index	-
	w	Charger index	-
	y	Year index	-
	m	Month index	-
Parameters	Ω	Cost of a BEB without a battery	*€*
	β	Cost of a battery pack	*€/kWh*
	α	Electric energy tariff	*€/kWh*
	λ	Demand charge rate	*€/kW*
	W_P	Average salary per person	*€*
	ω	Maintenance cost rate	*€/km*
	σ	Cost per unit charger power	*€/kW*
	C_a	Construction cost per unit area	*€/m²*
	T_D	Demand charge time interval	*minutes*
	T_{Bill}	Electricity billing period	*months*
	τ_d	Timestamp at the beginning of the demand period	*minutes*
	T_{EL}	BEB end lifetime	*years*
	n_B	Number of BEBs	-
	n_{per}	number of personnel operating the BEB line	-
	X_b	Distance covered by a BEB	*km*
	A_0	Minimum construction area for a charging station	*m²*
	a_0	required construction area per charger	*m²*
	d_r	Discount rate	*%*
Variables	K_b	Battery energy capacity	*kWh*
	n_{CS}	Number of charging stations	-
	$n_C^{CS_i}$	Number of chargers installed at station CS_i	-
	P_{MAX}^w	Charger's power rating	*kW*
	P_{CS_i}	Power demand at charging station CS_i	*kW*
	$R_b(y)$	Decision to replace the battery of BEB B_b at year y	-

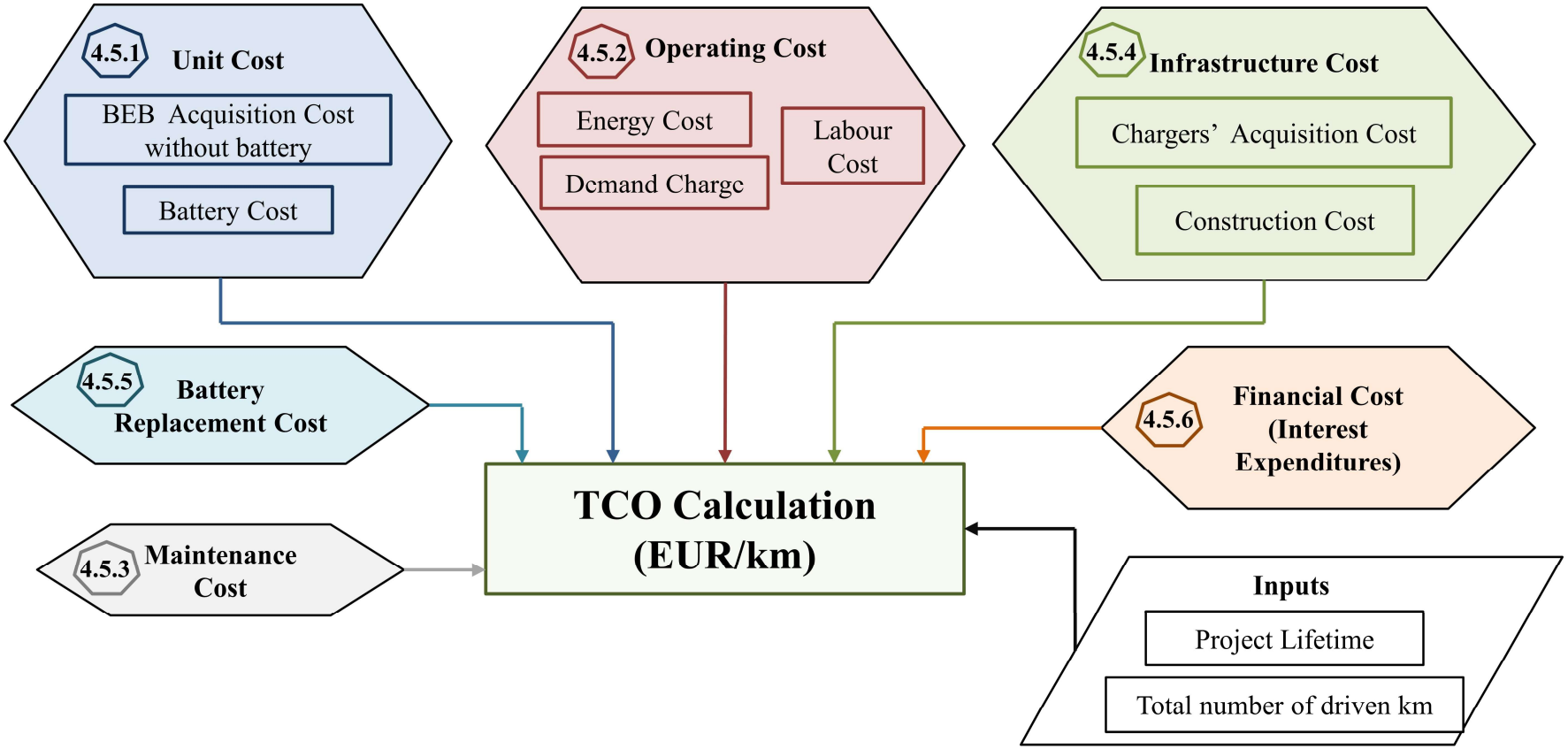


Figure 4.12: Summary of TCO model components

4.6 Impact of Battery Sizing and Charging Strategy on Operation and Costs of BEB Lines

In this section, a case study is presented in order to highlight the impact of BEB battery sizing and charging strategy on the TCO and operation of a BEB line, reflected in its punctuality index (PI), utilizing the proposed models. First, the case study is introduced highlighting the BEB line operating conditions and parameterizing the cost function. Then, different charging strategies and battery sizes are assessed in order to quantify their impact on the costs and operation of the BEB line. Finally, the tradeoffs between TCO and PI are also presented as function of the different battery sizes and charging strategies.

4.6.1 Case Study

4.6.1.1 Bus Line Specifications

The studied Bus line in this case is representative of Bus Line number 21 in Paris city. The bus route starts from *Stade Charlety* in the 13th arrondissement of Paris to *Gare Saint-Lazare* in Paris 8th arrondissement, as illustrated in Figure 4.13. The bus line depot is located 1 *km* away from *Stade Charlety – Porte de Gentilly* so it serves as a depot and a terminal station in this case. The other bus line terminal station is located at *Gare Saint-Lazare* where it is shared with other bus lines. The bus line contains 20 buses.

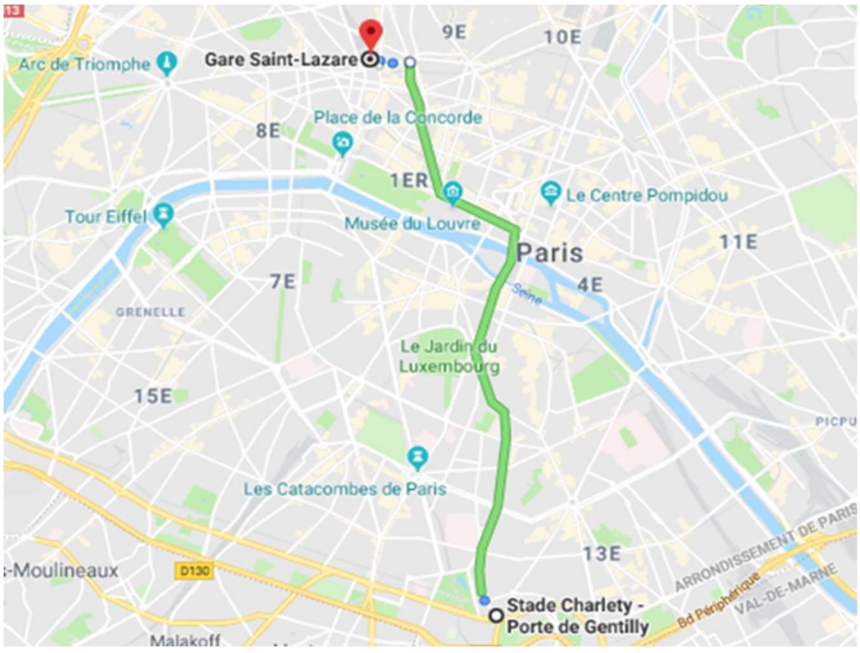


Figure 4.13: Bus Line number 21 route in Paris city

4.6.1.2 Driving Conditions

The distance of a one-way trip in any direction is around 9.7 *km,* and the trip duration is around 1 hour 15 minutes during normal traffic conditions. Along the bus line, there are 34 stop stations in each direction where the buses stop for 30 - 45 seconds. Figure 4.14 shows the speed profile for a one-way trip along the bus line, where the average speed along the bus line is 8.3 *km/h*. The road grade is assumed to be 0° along the entire route [74].

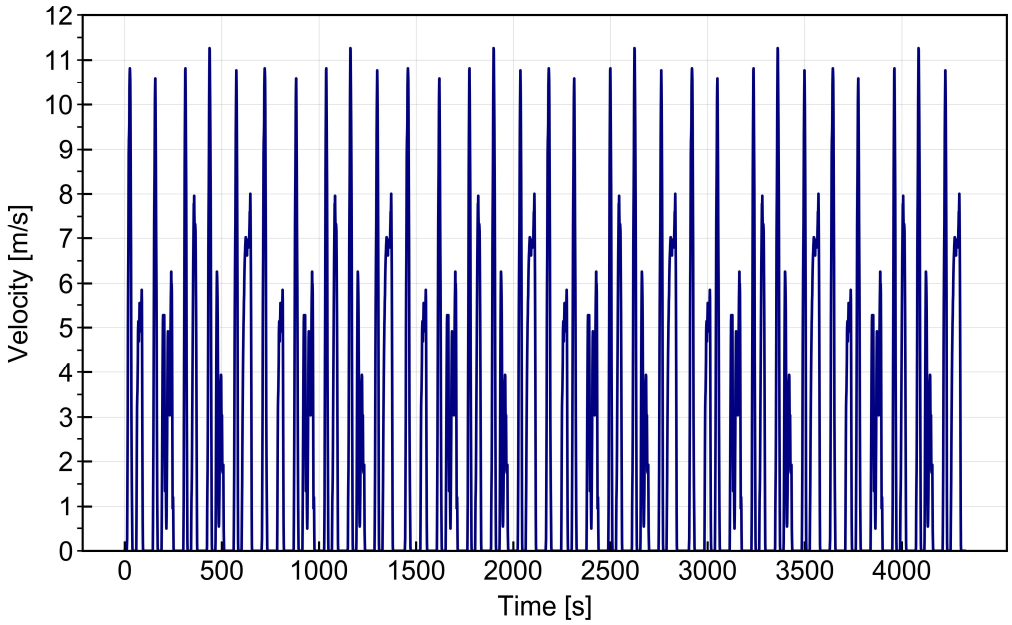


Figure 4.14: Velocity profile of bus line 21 for a one-way trip

4.6.1.3 Weather Conditions

The considered weather conditions are the daily average for each month during the year, recorded over the past 10 years in Paris city [75]. Figure 4.15 shows the daily outdoor temperature profile in Paris city just for 3 different months to simplify the figure. The temperature profile varies from one month to the other.

4.6.1.4 Passengers' Load

Passengers' flow data is collected for bus line 21 in Paris city for 3 weeks from the last week of June till the 2nd week of July 2019. The passengers' flow data is recorded at each stop station and multiple times during the day. The daily passengers' flow into the stop stations is shown in Figure 4.16 where only 5 stop stations are presented. As shown in the figure, the flow varies from one stop station to the other during the day.

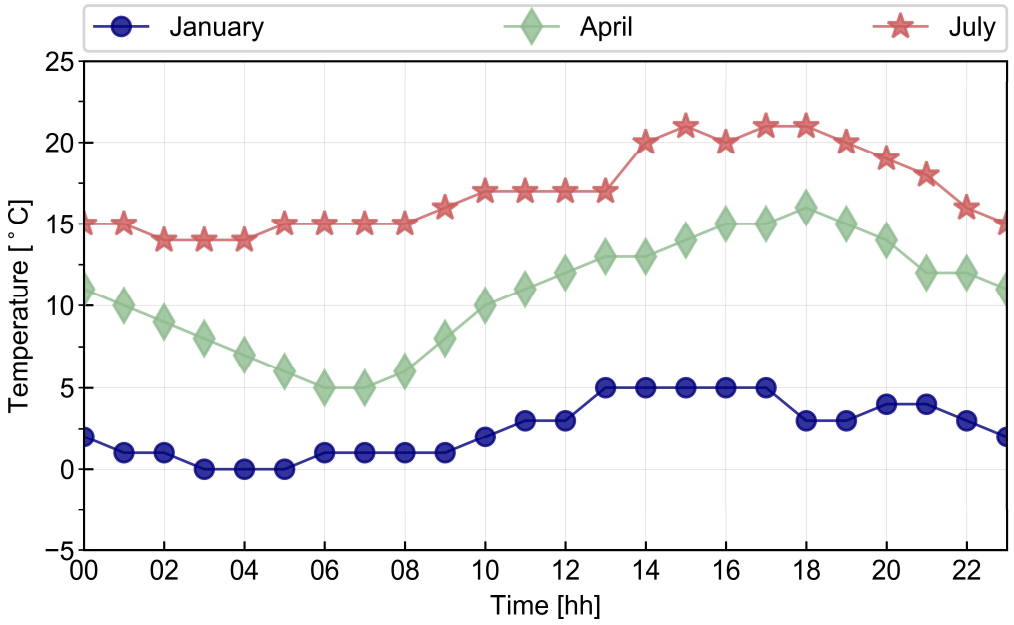


Figure 4.15: Daily outdoor temperature profile in Paris city

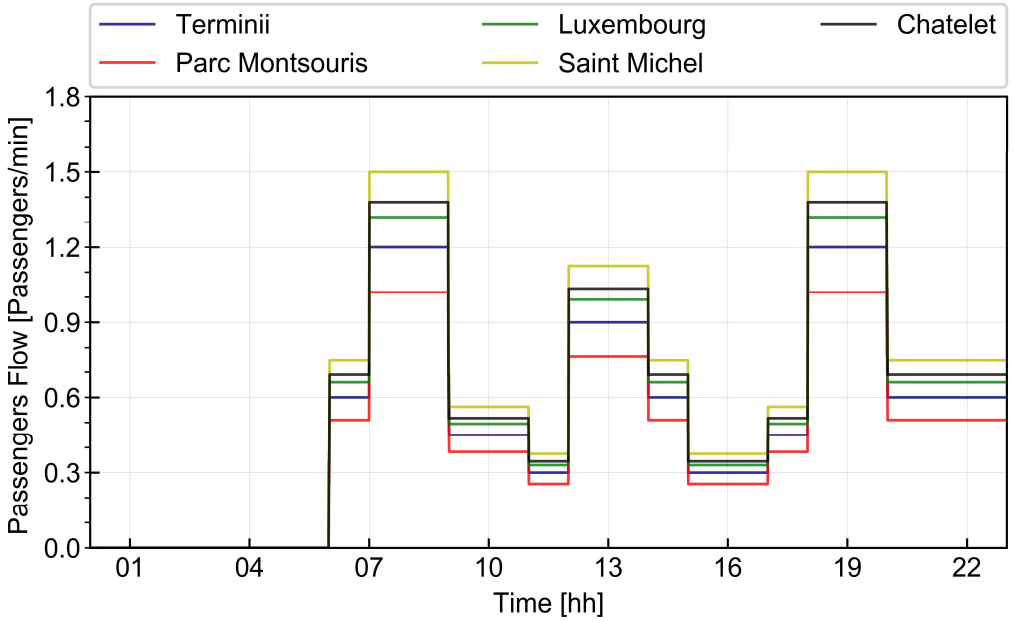


Figure 4.16: Passengers' flow daily profile into few stop stations of bus line 21 in Paris city

In addition, the number of passengers leaving the bus at each stop station is recorded during the day and presented in Figure 4.17.

4.6.1.5 Schedule

The bus line starts operating at 5:30 in the morning, and the last trip in both directions departs at 00:30 after midnight. The line schedule is presented in Table 4.9. Note that the bus frequency,

expressed in minutes, refers to the time passed between two buses at a given bus stop. For simplification, the bus is considered in the model to operate at the mentioned hours, Monday through Sunday, year-round.

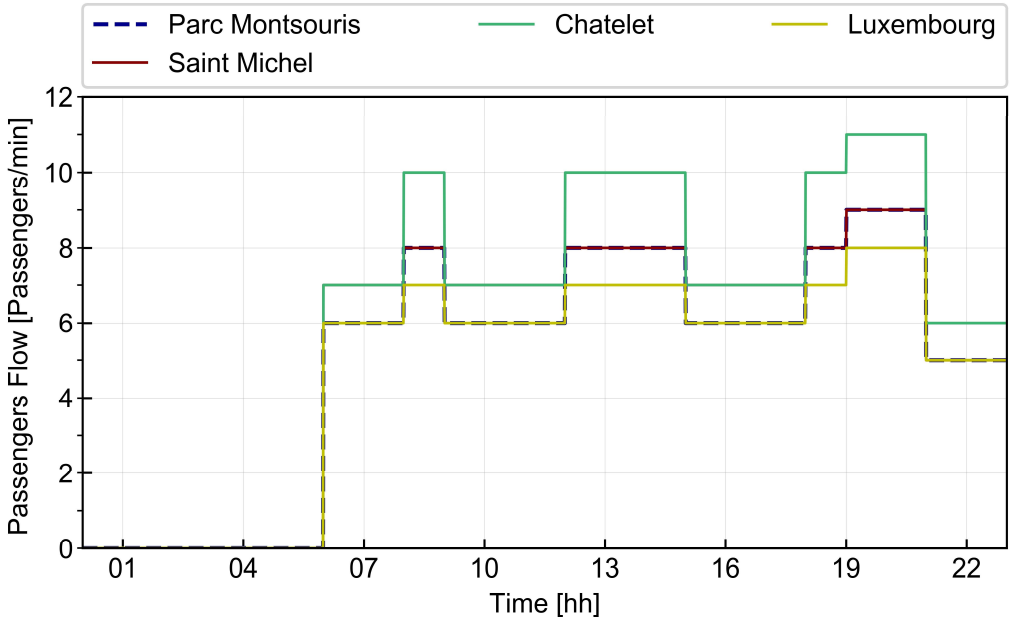


Figure 4.17: Passengers' flow daily profile out of the bus at few stop stations of bus line 21 in Paris city

Table 4.9: Schedule of bus line number 21 in Paris city

Time [hh: mm]	Bus Frequency [mins]
5:30 - 7:00	15
7:00 - 8:30	8
8:30 -13:15	10
13:15 - 17:45	12
17:45 - 20:00	8
20:00 - 00:30	15

4.6.1.6 Cost Model Parameterization

The TCO model is parameterized as shown in Table 4.10. There are slight variations in the different cost parameters across the literature, and for this sake, average values are considered for each cost parameter. Due to a lack of data availability, some assumptions are made, and this is stated directly next to the cost parameter. Finally, the monthly and yearly discount rates are calculated based on an annual interest rate of 6.5%, which is the case in France.

Table 4.10: Parametrization of the TCO model

Parameter	Value
Cost of a BEB without a battery	450,000 *€* [10], [76]
Cost of battery pack	580 *€/kWh* [66], [77], [78]
Electric energy tariff [79]	0.17 *€/kWh* between 6:00 – 23:00
	0.13 *€/kWh* between 23:00 – 6:00
Demand charge rate	11.5 *€/kW* [61], [80]
Average salary per person (Gross)	1600 *€/month* (assumption)
Maintenance cost rate	0.16 *€/km* [10], [66]
Cost per unit charger power	460 *€/kW* [10], [77], [78], [80]
Construction cost per unit area	1100 *€/m²* for new buildings
	220 *€/m²* for renovating old buildings
Demand charge time interval	15 minutes (assumption)
Electricity billing period	1 month
Time stamp at the beginning of demand period	[0, 0.25, 0.5, …. 23.5 – 24] hours
BEB end lifetime	12 years [66]
Minimum construction area for a charging station	Depot/Terminal: 185 *m²* [77], [78]
	Stop Station: -
Required construction area per charger	27.87 *m²* [77]
Annual interest rate	6.5 % [73]

4.6.1.7 Baseline Scenarios

Four different charging scenarios are considered in this case study. These scenarios represent all possible stationary charging methods, and any other method is a combination of these methods. Table 4.11 presents these scenarios. The exact battery size is estimated based on the methodology presented in section 3.5.1. The charging strategy column is split into 4 parts:

- Location: defines the charging location of the BEB mainly at the depot, terminal stations air stops stations.
- Time: decides on when to charge the buses during the day, night, and before which trips if applicable.
- Energy: the amount of energy to be charged.
- Power: the charging power rate.

Table 4.11: Case study baseline scenarios

		1	2	3	4
Scenario		**Overnight Charging (ONC)**	**Depot Day Charging (DDC)**	**End-Line Charging (ELC)**	**Opportunity Charging (OC)**
Battery Size		600 *kWh*	120 *kWh*	80 *kWh*	60 *kWh*
Charging Strategy	**Location**	Depot	Depot	Depot and Terminus	Depot, Terminus, and 8 selected stop stations
	Time	- Night (OFF service hours)	- Day (dwell times) - Night (OFF service hours)	- Day (dwell times) - Night (OFF service hours)	- Day (dwell times) - Night (OFF service hours) - During operation (along the route)
	Energy	Until SOC = SOC_{Max}			
	Power	Minimum power rate required to reach SOC_{Max} prior to BEB departure			

4.6.2 Results and Discussion

This section first presents the TCO segmentation among the different considered baseline scenarios, in order to study the impact of different charging strategies and battery sizing on TCO and its different components. Then, this section analyses the different tradeoffs between TCO and PI of a BEB line at different battery sizes and charging strategies.

4.6.2.1 TCO Segmentation

Figure 4.18 shows the TCO segmentation at the baseline scenarios. The TCO is composed of 6 components: 1. Maintenance Costs (MC), 2. Operating Costs (OC), 3. Infrastructure Costs (IC), 4. Battery Replacement Costs (BRC), 5. Unit Costs -Battery (UCB) and 6. Unit Costs – without Batteries (excluding the battery) (UCNB). Scenario 1 (ONC) shows the highest TCO as it reaches 2.83 *€/km,* whereas scenario 2 (DDC) reports the lowest TCO around 2.37 *€/km*. The relatively higher TCO in scenario 1 is mainly due to the high UCB as this scenario utilizes the largest battery size (600 *kWh*) despite its lower IC and OC. MC and UCNB are the same across the different scenarios. End-Line Charging scenario (ELC) and opportunity charging scenario (OC) yield a similar TCO around 2.39 *€/km*.

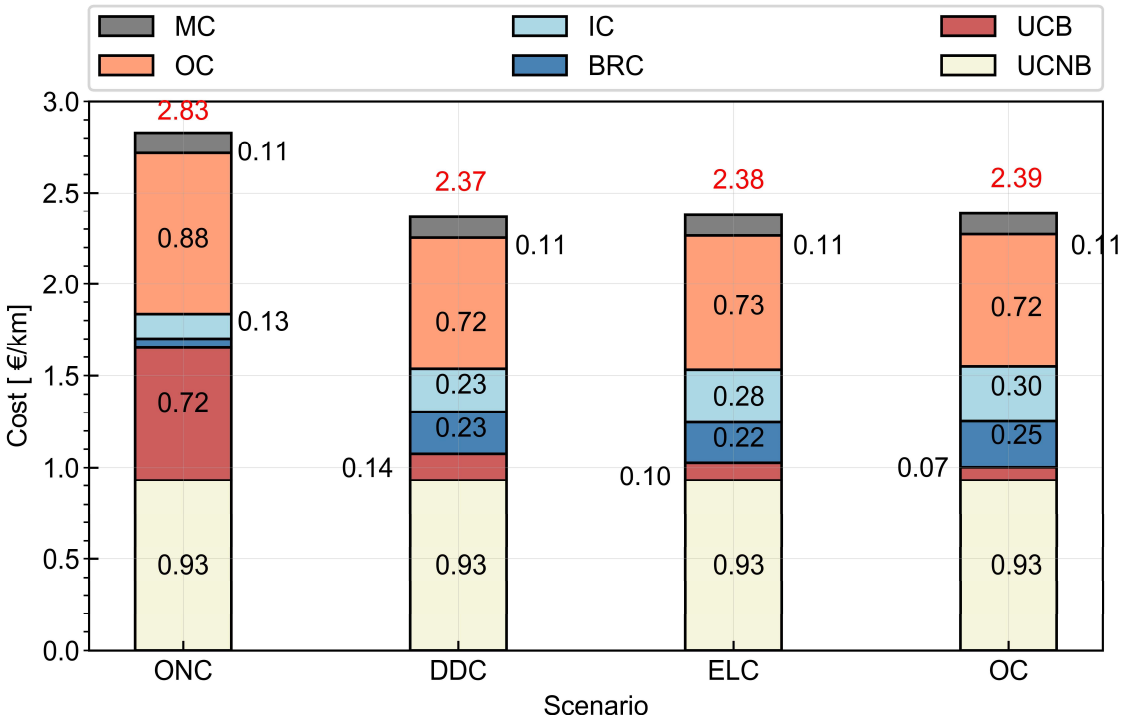


Figure 4.18: TCO segmentation at the baseline scenarios

Across the 4 scenarios, MC and UCNB are the same as they are not affected by the battery size nor the charging strategy. The other TCO components vary across the scenarios.

Concerning the UCB, trivially, the scenarios with the largest battery sizes report higher UCB.

4.6.2.1.1 Battery Replacement Costs

As for the BRC, the battery is replaced when it reaches its end life, considered as a 20% loss in its initial maximum charge capacity. As presented in the battery aging model; battery size and the charging strategy directly drive battery aging. Figure 4.19 shows the battery capacity fade as function of time for the baseline scenarios. In the ONC scenario, batteries lifetime is around 10.5 years, and thus one battery replacement is needed, which explains why the BRC in the ONC scenario is low. On the contrary, the DDC scenario reports a battery lifetime of 2.8 years, resulting in 5 battery replacement events. Similarly, the battery lifetime is 2.7 years in the ELC scenario (5 battery replacement events) and 2.1 years in the OC scenario (5 battery replacement events). Although scenarios 2,3 and 4 have a similar number of battery replacements, the BRC is different among these scenarios, mainly due to the battery salvage value (the salvage value of the final battery installed).

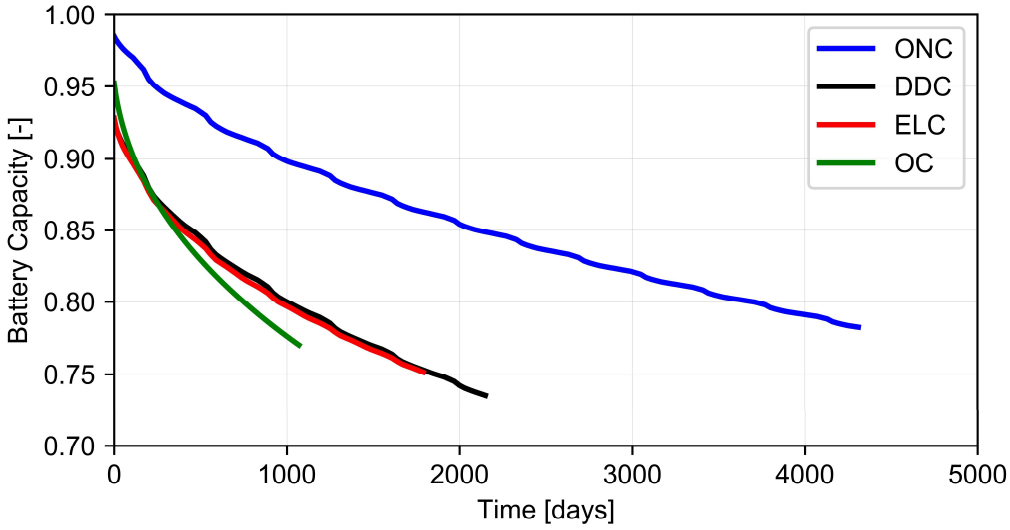


Figure 4.19: Batteries capacity fade function of time for the baseline scenarios

4.6.2.1.2 Infrastructure Costs

The IC is the acquisition and the installation costs of the chargers, and thus it is directly related to the number of chargers to be installed, and their corresponding power rating. Table 4.12 summarizes the required chargers' number (between parentheses) and their corresponding power rating for the baseline scenarios. The charging power of each charger is considered as the maximum power demand by the bus from this charger during its annual operation. The number of chargers to be installed at the depot is equal to the number of BEBs (20), however, their power rates vary across the different scenarios.

The ONC scenario witnesses the lowest chargers' power rates as the BEBs are charged at night during this scenario, and for long durations. All the charging events take place at the depot for this scenario, and thus there are no chargers installed at the terminus or the stop stations. Similarly, charging only takes place at the depot for the DDC scenario, however, day charging is possible during the BEBs dwell time, in addition to overnight charging. The charger's power rates are higher when compared to the ONC scenario due to the short available charging time during the day.

The ELC scenario utilizes chargers installed at both ends of the line (Depot and Terminus). Similar to the previous scenarios, 20 chargers are installed at the depot. In addition, 7 chargers are needed at the terminus in order to charge the BEBs during their dwell time prior to their return trips. The number of chargers to be placed at the terminus is determined by the maximum number of BEBs charging simultaneously at the terminal stations. Fast charging takes place at the terminus due to the very short available charging time.

Finally, the OC scenario is similar to the ELC scenario but with an additional 8 100-*kW* chargers installed at 8 equidistant stop stations (4 in each direction). This is an assumption considered in this case study as there exists a very high number of possibilities to install more chargers at other stations, and at higher power rates. Apart from scenario 1 (ONC), all other scenarios show a similar IC.

Table 4.12: Chargers' number and power rating for the baseline scenarios

Scenario	Chargers			
	Depot	Terminus	Stop Stations	Total
ONC	100 kW (7) - 140 kW (6) 180 kW (6) - 200 kW (1)	-	-	2820 kW
DDC	40 kW (2) - 150 kW (7) 260 kW (6) - 450 kW (5)	-	-	4940 kW
ELC	20 kW (2) – 80 kW (9) 140 kW (4) – 260 kW (5)	400 kW (7)	-	5520 kW
OC	20 kW (2) – 70 kW (12) 100 kW (2) – 220 kW (4)	350 kW (7)	100 kW (8)	5210 kW

4.6.2.1.3 Operating Costs

As for the OC, the ONC scenario shows the highest OC (0.88 *€/km*) among all scenarios where all other scenarios witness OC around 0.7 *€/km*. Figure 4.20 shows the OC segmentation for the baseline scenarios. The labor cost is the same across all scenarios as it is not affected by the battery size nor the charging strategy. However, the energy costs for the ONC scenario is slightly lower when compared to the other scenarios as it records 0.29 *€/km,* whereas other scenarios record energy costs around 0.33 *€/km*. 2 opposing effects take place here, first, larger batteries result in higher energy consumption due to their additional weight and higher cooling needs. On the other hand, charging takes place solely at night for the ONC scenario when electricity tariffs are low. On the contrary, the demand charge in the ONC scenario is the highest as it records 0.25 *€/km,* whereas other scenarios record 0.05-0.06 *€/km*. This high demand charge for the ONC scenario is due to the fact that all BEBs charge at the same time during this

scenario, and despite their relatively lower charging power, their cumulative power demand is very high as they are all charged at the same time during the night.

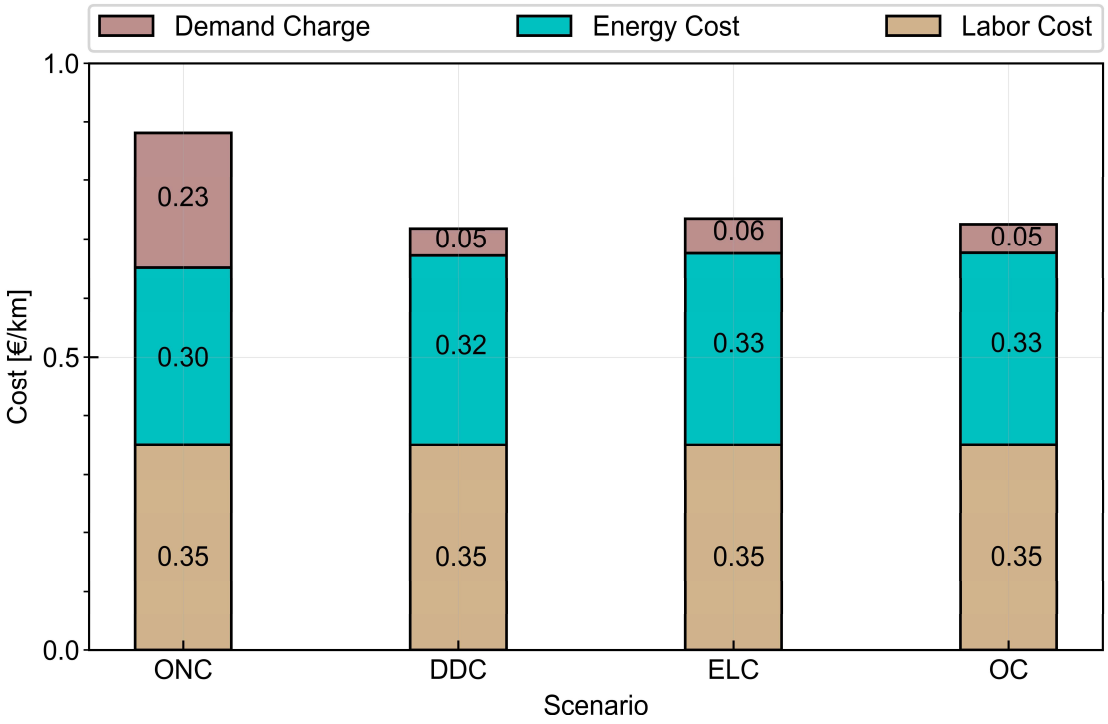


Figure 4.20: Operating Costs (OC) segmentation for the baseline scenarios

4.6.2.2 TCO – PI Trade-off

Although reducing the TCO of BEB deployment is a critical point for BEB operators, they are subjected to many constraints regarding the service quality of the BEB line, which limits their ability to reduce the TCO. This service quality is represented by the punctuality index (PI) as defined earlier in section 4.4 and section 4.2.3.

As shown in the TCO segmentation analysis, battery costs (acquisition and replacement), operating costs, and infrastructure costs can be reduced, contrary to the other cost components (unit cost and maintenance cost).

The battery, operating, and infrastructure costs are directly related to the choice of the battery size and the charging strategy of the BEBs. Figure 4.21 shows the TCO - PI trade-off at different battery sizes and maximum charging power rates for the DDC scenario.

All baseline scenarios (blue circles with different color tones) have a 100% PI and no limitation on the maximum charging power rate. Additional scenarios are considered, derived from the baseline scenarios, by limiting the maximum allowable charging power rate for each scenario

to 100, 120, and 150 *kW*. Limiting the maximum charging power may yield to prolonged charging events, resulting in some delays in the BEBs departure time from their stations, and thus reducing the PI. Each point presented in Figure 4.21 (markers), other than the baseline scenarios, is the intersection between a solid line and a dashed line. A solid line represents a constant battery size (K_b), and a dashed line represents a constant maximum power (P_{max}).

As the maximum allowable charging power decreases, the TCO decreases due to a reduction in the IC, BRC, and demand charge of the OC. However, this yields a reduction in the PI. For example, at a fixed battery size of 120 *kWh*, reducing the maximum allowable charging power to 100 *kW* reduces the TCO from 2.37 to 2.18 *€/km* (8%), however, the PI is reduced from 100% to 85%. On the other hand, increasing the battery size increases the TCO due to the additional battery costs and energy consumption, however, higher PI values are obtained. This is due to the fact that larger battery sizes require less charging during the day, and thus they are less sensitive to the maximum allowable charging power.

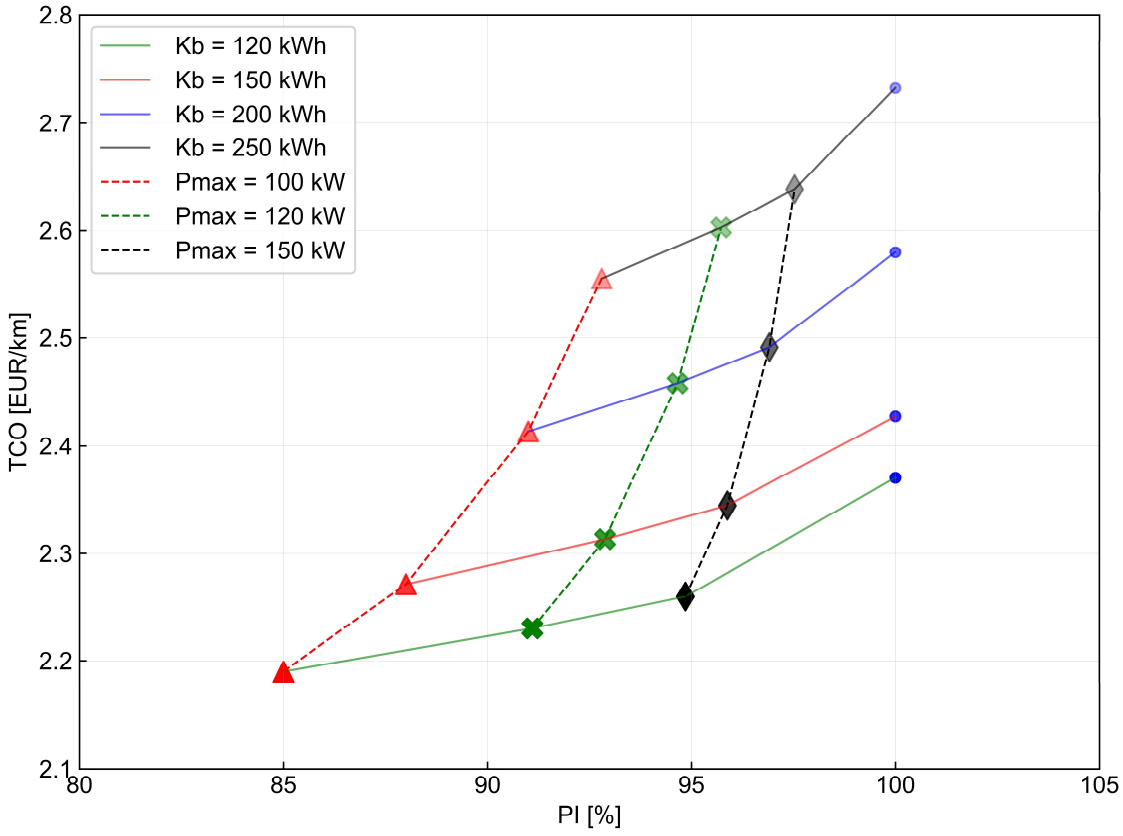


Figure 4.21: TCO - PI trade-off at different battery sizes and maximum charging power rates (DDC)

The other scenarios (ELC and OC) show similar behavior concerning the battery size and charging power as shown in Figure 4.22 and Figure 4.23. As the number of charging events

increases (OC>ELC>DDC), the TCO and PI become more sensitive to the maximum allowable charging power and less sensitive to the battery size.

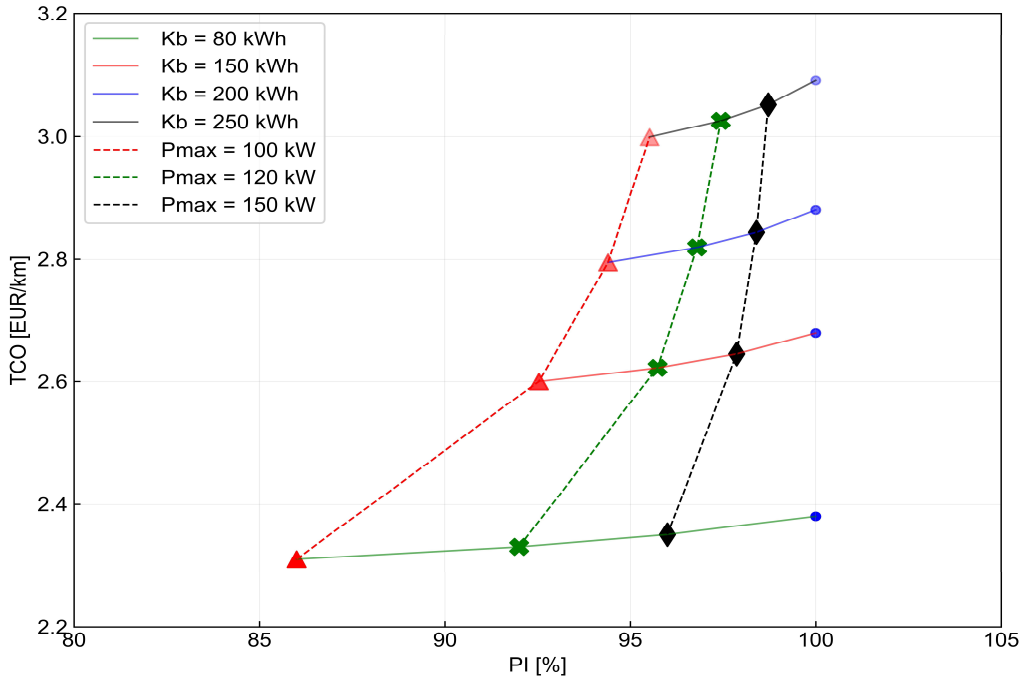


Figure 4.22: TCO - PI trade-off at different battery sizes and maximum charging power rates (ELC)

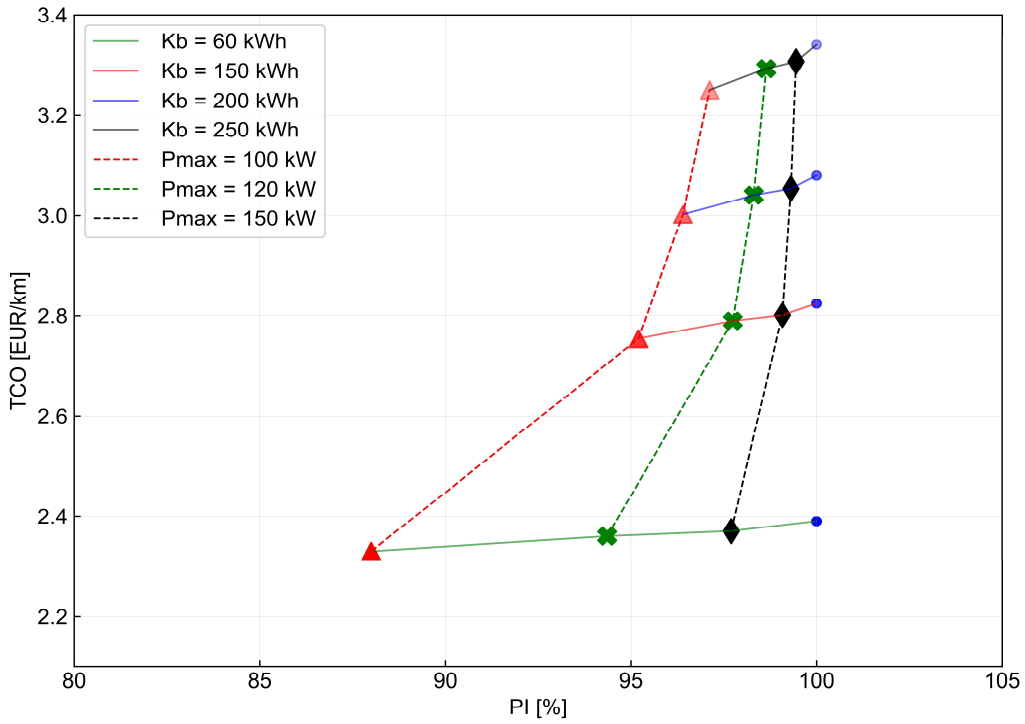


Figure 4.23: TCO - PI trade-off at different battery sizes and maximum charging power rates (OC)

Figure 4.24, Figure 4.25, and Figure 4.26 show the cumulative probability distribution function for bus trip delay in minutes, for the DDC, ELC, and OC scenarios respectively at different maximum allowable charging power. For the DDC scenario with P_{max} = 100 kW, 82% of the annual trips do not experience any delay in their departure from the line termini, and 90% of the trips experience a delay fewer than 10 minutes. At higher maximum charging power (120 kW and 150 kW), 87% and 93% of the trips do not experience any delay respectively, and 93% and 95% of the trips are delayed by less than 10 minutes. At higher charging power, the bus trip delay is reduced, which complies with the PI analysis presented in Figure 4.21.

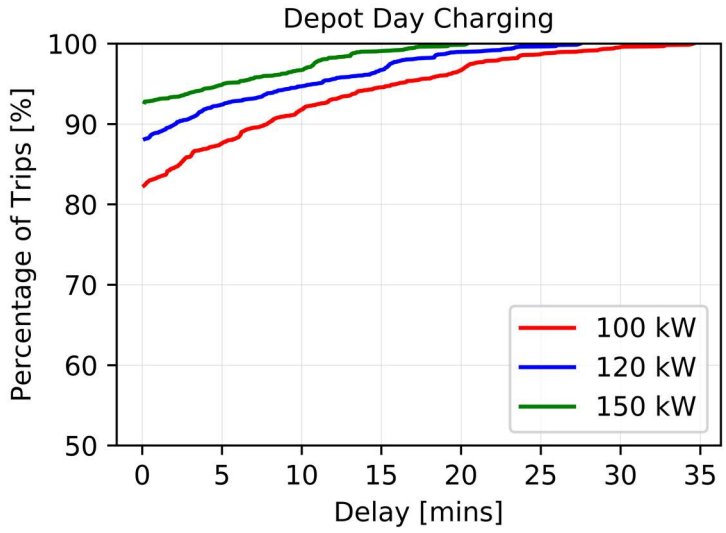


Figure 4.24: Cumulative probability distribution function for bus trip delay: case of depot day charging (DDC)

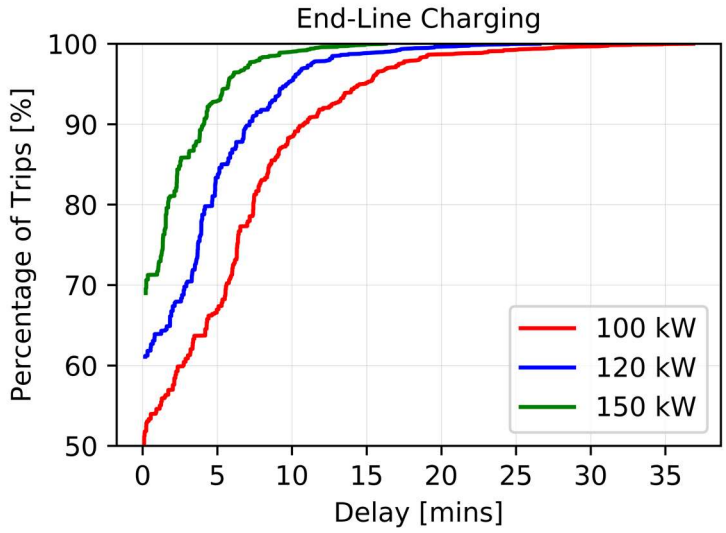


Figure 4.25: Cumulative probability distribution function for bus trip delay: case of end-line charging (ELC)

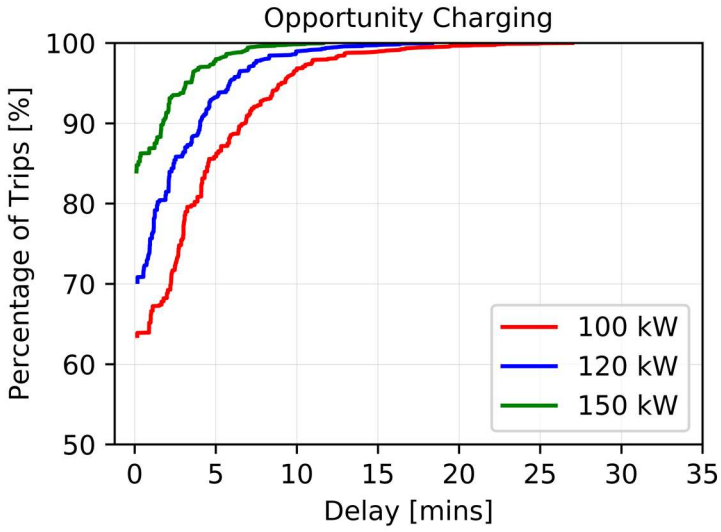


Figure 4.26: Cumulative probability distribution function for bus trip delay: case of opportunity charging (OC)

On the other hand, the ELC and OC scenarios show similar behavior concerning the maximum charging power when compared to the DDC scenario, however, the bus trip delay is much higher. For example, for the ELC and OC scenarios at P_{max} = 100 kW, only 50% and 64% of the annual trips do not experience any delay in departure respectively, which is very low when compared to the 82% witnessed in the DDC scenario. On the contrary, 98% of the trips experience a delay of less than 10 minutes during the ELC scenario, and 100% for the OC scenario, which is higher than the 93% observed during the DDC scenario. At higher P_{max} = 150 kW, 70% and 85% of the annual trips do not experience any delay in departure for the ELC and OC scenarios respectively, which is still lower than the 93% observed in the DDC scenario, whereas 100% of the trips are delayed by less than 10 minutes during the ELC and OC scenario, which is higher than the 95% observed during the DDC scenario.

That being said, fewer trips are delayed during the DDC scenario when compared to the ELC or OC scenario, whereas longer trip delays are observed in the DDC scenario. In addition, the ELC and OC scenarios are more sensitive to the maximum charging power when compared to the DDC scenario, mainly due to the higher number of charging events.

4.7 Conclusion

The operation of BEBs is sensitive to the battery sizing and the adopted charging strategy. A proper battery sizing alongside an adequate charging strategy are essential to ensure smooth

operation without schedule disruptions or service interruptions. In addition, the costs of BEBs deployment is driven by the choice of the battery sizing and charging strategy as well.

In this chapter, a bus line techno-economic model is developed which allows the assessment of the TCO and operation (reflected in PI) for any BEB line, at any combination of battery sizes and charging strategies. The model is developed in real-time and it considers the following components: buses, chargers, stop stations, terminal stations, and a depot. The energy interactions among the different BEB line components are presented using 2 types of interactions: (1) passengers' flow and (2) electric power flow. In addition, the TCO model considers the unit costs, battery purchase and replacement costs, electricity costs, infrastructure, and maintenance costs. The BEBs PI is also presented and modeled to reflect on the bus schedule disruptions or service interruption due to charging.

A case study is introduced to quantitatively show the impact of battery sizing and charging strategy on the TCO and PI of BEB. In addition, the case study highlights the resulting tradeoffs between BEB operation (PI) and TCO.

Adopting an overnight charging strategy associated with large battery sizes incurs low infrastructure and battery replacement costs, but high unit and operating costs due to the large battery size and high demand charge. For such an approach, the risk of service interruption is high as it is not possible to charge the BEB during the day, whereas the risk of schedule disruption is low as no charging takes during the day (during operating hours).

On the other hand, adopting a strategy based on frequent day-charging associated with small battery size will require the BEB to be charged at high power rates which incur high infrastructure costs, and high battery replacement costs due to accelerated battery aging. Unit costs and operating costs are mainly low due to the small battery size and low demand charge. Although this approach reduces the risk of service interruption, the risk of schedule disruption is high due to the delays that may result from frequent charging events.

Thus, the different battery sizing and charging strategies affect the TCO and PI of BEB line differently.

In addition, there are clear tradeoffs between the TCO and PI. For example, reducing the battery size helps in lowering the TCO, thanks to the reduced battery costs. However, this may impact the PI of the BEB line as it becomes more prone to service interruption during operation. On the other hand, adopting a charging strategy that utilizes high-power rating chargers reduces

the risks of schedule disruption due to the fast charging events, and also reduces the risk of service interruption as more energy is stored in the battery during charging, which enhances the PI of the BEB line. However, this increases the TCO, this time due to the high cost of chargers in the first place, and high battery replacement costs caused by the accelerated battery aging.

That being said, the different combinations of battery sizes and charging strategies result in different TCO-PI trade-offs. For this sake, there is a need for optimal battery sizing and charging strategy to minimize the TCO of BEBs deployment while maintaining acceptable PI values as set by local authorities.

4.8 References

[1] Z. Gao, Z. Lin, T. J. LaClair, C. Liu, J. M. Li, A. K. Birky, and J. Ward, "Battery capacity and recharging needs for electric buses in city transit service," *Energy*, vol. 122, pp. 588–600, 2017, doi: 10.1016/j.energy.2017.01.101.

[2] O. Lopez and D. B. Gorosabel, "Assessing the Construction of Charging Stations for Electric Buses : A Case Study for Stockholm Inner City," KTH Royal Institute of Technology, 2017.

[3] A. Ostadi and M. Kazerani, "A Comparative Analysis of Optimal Sizing of Battery-Only, Ultracapacitor-Only, and Battery-Ultracapacitor Hybrid Energy Storage Systems for a City Bus," *IEEE Trans. Veh. Technol.*, vol. 64, no. 10, pp. 4449–4460, 2015, doi: 10.1109/TVT.2014.2371912.

[4] D. Göhlich, T. A. Fay, D. Jefferies, E. Lauth, A. Kunith, and X. Zhang, "Design of urban electric bus systems," *Des. Sci.*, vol. 4, no. August, pp. 1–28, 2018, doi: 10.1017/dsj.2018.10.

[5] J. M. Clairand, P. Guerra-Terán, X. Serrano-Guerrero, M. González-Rodríguez, and G. Escrivá-Escrivá, "Electric vehicles for public transportation in power systems: A review of methodologies," *Energies*, vol. 12, no. 16, pp. 1–22, 2019, doi: 10.3390/en12163114.

[6] T. Ly, D. Goehlich, and L. Heide, "Assessment of the Interaction of Charging System and Battery Technology for the Use in Urban Battery Electric Bus Systems," 2016, doi: 10.1109/VPPC.2016.7791621.

[7] G. De Filippo, V. Marano, and R. Sioshansi, "Simulation of an electric transportation system at The Ohio State University," *Appl. Energy*, vol. 113, pp. 1686–1691, 2014, doi: 10.1016/j.apenergy.2013.09.011.

[8] M. Mohamed, H. Farag, N. El-Taweel, and M. Ferguson, "Simulation of electric buses on a full transit network: Operational feasibility and grid impact analysis," *Electr. Power Syst. Res.*, vol. 142, pp. 163–175, 2017, doi: 10.1016/j.epsr.2016.09.032.

[9] A. Lajunen, "Energy consumption and cost-benefit analysis of hybrid and electric city buses," *Transp. Res. Part C Emerg. Technol.*, vol. 38, pp. 1–15, 2014, doi: 10.1016/j.trc.2013.10.008.

[10] M. Xylia, S. Leduc, P. Patrizio, F. Kraxner, and S. Silveira, "Locating charging infrastructure for electric buses in Stockholm," *Transp. Res. Part C Emerg. Technol.*, vol. 78, pp. 183–200, 2017, doi: 10.1016/j.trc.2017.03.005.

[11] Y. Wang, Y. Huang, J. Xu, and N. Barclay, "Optimal recharging scheduling for urban electric buses: A case study in Davis," *Transp. Res. Part E Logist. Transp. Rev.*, vol. 100, pp. 115–132, 2017, doi: 10.1016/j.tre.2017.01.001.

[12] "China is adding a London-sized electric bus fleet every five weeks," *World Economic Forum*, 2018.

[13] H. F. and A. D. Jamie Lee-Brown, Meredith Baker, Oliver Joy, Chiara Amato, Roland Steinmetz, Roos Van der Ploeg, Evy Breen, Zita Koks, Bernard Aritua, Yi Yang, Huijing Deng, Edward Andrew Beukes, Li Qu, Alejandro Hoyos Guerrero, Philip Turner, "Electric Mobility & Development," 2019. [Online]. Available: https://www.electricmobilityeurope.eu/.

[14] A. P. and O. S. Till Bunsen, Pierpaolo Cazzola, Marine Gorner, Leonardo Paoli, Sacha Scheffer, Renske Schuitmaker, Jacopo Tattini and Jacob Teter. It benefited from the support provided by Simon Bennett, Emanuele Bianco, Paul Hugues, George Kamiya, Sarbojit Pal, Kate Pal, "Global EV Outlook 2018," 2018. doi: 10.1787/9789264302365-en.

[15] BYD, "60' Electric Transit Bus - BYD USA." https://en.byd.com/bus/60-electric-transit-bus/#specs (accessed Jan. 15, 2020).

[16] L. Poon, "Why China is Winning the Electric Bus Race - CityLab," *CITYLAB*, 2019. https://www.citylab.com/transportation/2019/06/electric-bus-china-grid-ev-charging-infrastructure-battery/591655/ (accessed Jan. 15, 2020).

[17] J. Margolis, "Electric buses: Cleaner and greener, but with limitations.," *PRI*, 2019. https://www.pri.org/stories/2019-10-08/china-dominates-electric-bus-market-us-getting-board (accessed Jan. 15, 2020).

[18] VDL, "31 electric VDL Citeas for urban transport in Amsterdam," 2019. https://www.vdlsteelweld.com/en/news/31-electric-vdl-citeas-for-urban-transport-in-amsterdam (accessed Jan. 15, 2020).

[19] BYD, "BYD ADL provide full installation service for RATP Dev London electric bus

fleet," 2018. http://www.byd.com/en/news/2018-11-16/BYD-ADL-provide-full-installation-service-for-RATP-Dev-London-electric-bus-fleet (accessed Jan. 15, 2020).

[20] J. Bernhardt, "London extends its' e-bus fleet - new ADL BYD buses enter service - Urban Transport Magazine," *Urban Transport Magazine*, 2019. https://www.urban-transport-magazine.com/en/londons-elektrobusflotte-waechst-weiter-neue-adl-byd-busse-im-einsatz/ (accessed Jan. 15, 2020).

[21] BYD, "Products - BYD ADL Electric Buses." https://www.evbus.co.uk/products/ (accessed Jan. 15, 2020).

[22] C. Hampel, "SE: Volvo to deliver 157 electric buses for Transdev - electrive.com," *electrive.com*, 2019. https://www.electrive.com/2019/11/06/volvo-to-deliver-157-buses-for-transdev-in-gottenburg/ (accessed Jan. 15, 2020).

[23] Volvo, "Volvo 7900 Electric Overview." https://www.volvobuses.com/en-wa/about-us/volvo-7900-electric1.html (accessed Jan. 15, 2020).

[24] Scania, "'Scania has created a very good battery bus' | Scania Group." https://www.scania.com/group/en/scania-has-created-a-very-good-battery-bus/ (accessed Jan. 15, 2020).

[25] Scania, "Scania citywide BEV | Scania Global." https://www.scania.com/global/en/home/products-and-services/buses-and-coaches/our-range/scania-citywide-bev.html (accessed Jan. 15, 2020).

[26] Scania, "Chapter 2: The energy expert: 'Change will be fast' | Scania Group," *Sustainability Stories*, 2019. https://www.scania.com/group/en/chapter-2-the-energy-expert-change-will-be-fast/ (accessed Jan. 15, 2020).

[27] C. Randall, "Hamburg operator orders 17 electric MAN buses - electrive.com," *electrive.com*, 2019. https://www.electrive.com/2019/12/10/hamburg-transport-operator-orders-17-electric-man-buses/ (accessed Jan. 15, 2020).

[28] MAN, "An electrifying achievement – MAN hands over first all-electric city buses to Hamburg," *MAN Newsroom*. https://press.mantruckandbus.com/an-electrifying-achievement--man-hands-over-first-all-electric-city-buses-to-hamburg/ (accessed Jan. 15, 2020).

[29] MAN, "First electric bus order for MAN: transport company Verkehrsbetriebe

Hamburg-Holstein is counting on the Lion's City E," *MAN Newsroom*. https://press.mantruckandbus.com/first-electric-bus-order-for-man-transport-company-verkehrsbetriebe-hamburg-holstein-is-counting-on-the-lions-city-e/ (accessed Jan. 15, 2020).

[30] Proterra, "Range | Proterra." https://www.proterra.com/vehicles/catalyst-electric-bus/range/ (accessed Jan. 15, 2020).

[31] C. Hampel, "Los Angeles orders 130 BYD electric buses - electrive.com," *electrive.com*, 2019. https://www.electrive.com/2019/11/14/los-angeles-orders-130-byd-electric-buses/ (accessed Jan. 15, 2020).

[32] Irizar, "Irizar ie bus - Irizar e-mobility." https://www.irizar-emobility.com/solutions-and-services/vehicles/ie-bus/?lang=en (accessed Jan. 15, 2020).

[33] "Electric buses roll out in Northern France - Smart Cities World," *Smart Cities World*, 2019. https://www.smartcitiesworld.net/news/news/electric-buses-roll-out-in-northern-france-4188 (accessed Jan. 15, 2020).

[34] CDE, "23 Bluebus pour « verdir » la ligne 341 à Paris," *CDE Newsletter*, 2016. https://www.connaissancedesenergies.org/23-bluebus-pour-verdir-la-ligne-341-paris-160603 (accessed Jan. 15, 2020).

[35] W. Khan, A. Ahmad, F. Ahmad, and M. Saad Alam, "A Comprehensive Review of Fast Charging Infrastructure for Electric Vehicles," *Smart Sci.*, vol. 6, no. 3, pp. 256–270, 2018, doi: 10.1080/23080477.2018.1437323.

[36] Z. Chen, W. Liu, and Y. Yin, "Deployment of stationary and dynamic charging infrastructure for electric vehicles along traffic corridors," *Transp. Res. Part C Emerg. Technol.*, vol. 77, pp. 185–206, 2017, doi: 10.1016/j.trc.2017.01.021.

[37] A. Lajunen, "Lifecycle costs and charging requirements of electric buses with different charging methods," *J. Clean. Prod.*, vol. 172, pp. 56–67, 2018, doi: 10.1016/j.jclepro.2017.10.066.

[38] Y. J. Jang, S. Jeong, and M. S. Lee, "Initial energy logistics cost analysis for stationary, quasi-dynamic, & dynamicwireless charging public transportation systems," *Energies*, vol. 9, no. 7, 2016, doi: 10.3390/en9070483.

[39] S. Jeong, Y. J. Jang, and D. Kum, "Economic Analysis of the Dynamic Charging Electric

Vehicle," *IEEE Trans. Power Electron.*, vol. 30, no. 11, pp. 6368–6377, 2015, doi: 10.1109/TPEL.2015.2424712.

[40] M. Yilmaz and P. T. Krein, "Review of battery charger topologies, charging power levels, and infrastructure for plug-in electric and hybrid vehicles," *IEEE Trans. Power Electron.*, vol. 28, no. 5, pp. 2151–2169, 2013, doi: 10.1109/TPEL.2012.2212917.

[41] J. Shin, S. Shin, Y. Kim, S. Ahn, S. Lee, G. Jung, S. J. Jeon, and D. H. Cho, "Design and implementation of shaped magnetic-resonance-based wireless power transfer system for roadway-powered moving electric vehicles," *IEEE Trans. Ind. Electron.*, vol. 61, no. 3, pp. 1179–1192, 2014, doi: 10.1109/TIE.2013.2258294.

[42] D. Ronanki, A. Kelkar, and S. S. Williamson, "Extreme fast charging technology—prospects to enhance sustainable electric transportation," *Energies*, vol. 12, no. 19, pp. 1–17, 2019, doi: 10.3390/en12193721.

[43] H. Shareef, M. M. Islam, and A. Mohamed, "A review of the stage-of-the-art charging technologies, placement methodologies, and impacts of electric vehicles," *Renew. Sustain. Energy Rev.*, vol. 64, pp. 403–420, 2016, doi: 10.1016/j.rser.2016.06.033.

[44] S. S. Williamson, S. Member, A. K. Rathore, and S. Member, "Industrial Electronics for Electric Transportation : Current State-of-the-Art and Future Challenges," *IEEE Trans. Ind. Electron.*, vol. 62, no. 5, pp. 3021–3032, 2015, doi: 10.1109/TIE.2015.2409052.

[45] K. Morrow, "Plug-in Hybrid Electric Vehicle Charging Infrastructure Review," 2008.

[46] A. Schroeder and T. Traber, "The economics of fast charging infrastructure for electric vehicles," *Energy Policy*, vol. 43, pp. 136–144, 2012, doi: 10.1016/j.enpol.2011.12.041.

[47] B. Lunz and D. U. Sauer, *Electric road vehicle battery charging systems and infrastructure*. Elsevier Ltd., 2015.

[48] M. Kosowski, E. S. A. E. J-, and C. Chairperson, "SAE J-3105 Heavy-Duty Conductive Automatic Charging Recommended Practice," 2018.

[49] J. Shuttleworth, "Conductive Automatic Charging Recommended Practice nears completion," *SAE Standard News*, 2019.

[50] M. Kosowski, "Update for SAE J-3105 SAE J3105 Automatic Charging Recommended Practice," 2019.

[51] T. Nguyen, S. Li, W. Li, C. C. Mi, and F. Ieee, "Feasibility Study on Bipolar Pads for Efficient Wireless Power Chargers," *2014 IEEE Appl. Power Electron. Conf. Expo. - APEC 2014*, pp. 1676–1682, 2014, doi: 10.1109/APEC.2014.6803531.

[52] G. Trentadue, A. Lucas, M. Otura, K. Pliakostathis, M. Zanni, and H. Scholz, "Evaluation of Fast Charging Efficiency under Extreme Temperatures," *Energies*, pp. 1–13, 2018, doi: 10.3390/en11071937.

[53] A. Genovese, F. Ortenzi, and C. Villante, "On the energy efficiency of quick DC vehicle battery charging," *Electr. Veh. Symp. 28*, vol. 7, pp. 570–576, 2015.

[54] T. Parisiens, "CONTRAT entre le Syndicat des Transports d ' Ile - et la Régie Autonome des Transports Parisiens," 2016.

[55] T. Parisiens, "ANNEXES au CONTRAT entre le Syndicat des Transports d ' Ile - et la Régie Autonome des Transports Parisiens," 2016.

[56] M. Mahmoud, R. Garnett, M. Ferguson, and P. Kanaroglou, "Electric buses: A review of alternative powertrains," *Renew. Sustain. Energy Rev.*, vol. 62, pp. 673–684, 2016, doi: 10.1016/j.rser.2016.05.019.

[57] D. Beeton and G. Meyer, "Energy Efficiency in Electric and Plug-in Hybrid Electric Vehicles and Its Impact on Total Cost of Ownership," in *Electric Vehicle Business Models*, 2015, p. 266.

[58] R. Kühne, "Electric buses - An energy efficient urban transportation means," *Energy*, vol. 35, no. 12, pp. 4510–4513, 2010, doi: 10.1016/j.energy.2010.09.055.

[59] W. Feng and M. Figliozzi, "An economic and technological analysis of the key factors affecting the competitiveness of electric commercial vehicles: A case study from the USA market," *Transp. Res. Part C Emerg. Technol.*, vol. 26, pp. 135–145, 2013, doi: 10.1016/j.trc.2012.06.007.

[60] Y. He, Z. Song, and Z. Liu, "Fast-charging station deployment for battery electric bus systems considering electricity demand charges," *Sustain. Cities Soc.*, vol. 48, no. October 2018, 2019, doi: 10.1016/j.scs.2019.101530.

[61] N. Qin, A. Gusrialdi, R. Paul Brooker, and A. T-Raissi, "Numerical analysis of electric bus fast charging strategies for demand charge reduction," *Transp. Res. Part A Policy Pract.*, vol. 94, pp. 386–396, 2016, doi: 10.1016/j.tra.2016.09.014.

[62] R. Hledik, “Rediscovering Residential Demand Charges,” *Electr. J.*, vol. 27, no. 7, pp. 82–96, 2014, doi: 10.1016/j.tej.2014.07.003.

[63] R. Nunno, “Battery Electric Buses : Benefits Outweigh Costs,” 2018. [Online]. Available: https://www.eesi.org/files/FactSheet_Electric_Bus_Benefits_Outweigh_Costs_1018.pdf.

[64] Y. M. Nie and M. Ghamami, “A corridor-centric approach to planning electric vehicle charging infrastructure,” *Transp. Res. Part B*, vol. 57, pp. 172–190, 2013, doi: 10.1016/j.trb.2013.08.010.

[65] Z. Chen, Y. Yin, and Z. Song, “A cost-competitiveness analysis of charging infrastructure for electric bus operations,” *Transp. Res. Part C*, vol. 93, no. April, pp. 351–366, 2018, doi: 10.1016/j.trc.2018.06.006.

[66] M. Rogge, E. van der Hurk, A. Larsen, and D. U. Sauer, “Electric bus fleet size and mix problem with optimization of charging infrastructure,” *Appl. Energy*, vol. 211, no. February 2017, pp. 282–295, 2018, doi: 10.1016/j.apenergy.2017.11.051.

[67] L. Nurhadi, S. Borén, and H. Ny, “A sensitivity analysis of total cost of ownership for electric public bus transport systems in Swedish medium sized cities,” *Transp. Res. Procedia*, vol. 3, no. July, pp. 818–827, 2014, doi: 10.1016/j.trpro.2014.10.058.

[68] A. Kunith, R. Mendelevitch, and D. Goehlich, “Electrification of a City Bus Network: An Optimization Model for Cost-Effective Placing of Charging Infrastructure and Battery Sizing of Fast Charging Electric Bus Systems,” *SSRN Electron. J.*, 2017, doi: 10.2139/ssrn.2782417.

[69] H. Malkki and K. Alanne, “An overview of life cycle assessment (LCA) and research-based teaching in renewable and sustainable energy education,” *Renew. Sustain. Energy Rev.*, vol. 69, no. November 2016, pp. 218–231, 2017, doi: 10.1016/j.rser.2016.11.176.

[70] D. Göhlich, A. Kunith, and T. Ly, “Technology assessment of an electric urban bus system for berlin,” in *WIT Transactions on the Built Environment*, 2014, vol. 138, pp. 137–149, doi: 10.2495/UT140121.

[71] L. Blank and A. Tarquin, *Engineering Economy*, 7th ed. 2012.

[72] THE WORLD BANK, “Transport Economics , Policy and Poverty Thematic Group,”

2005.

[73] F. Massimo, “Guide de l’analyse coûts-avantages des projets d’investissement,” 2003. [Online]. Available: http://ec.europa.eu/regional_policy/sources/docgener/guides/cost/guide02_fr.pdf.

[74] ADEME, “Panorama et évaluation des différentes filières d ’ autobus urbains,” 2015.

[75] “Historique-Meteo,” 2020. https://www.historique-meteo.net/france/ile-de-france/paris/.

[76] A. Kunith, R. Mendelevitch, and D. Goehlich, “Electrification of a city bus network—An optimization model for cost-effective placing of charging infrastructure and battery sizing of fast-charging electric bus systems,” *Int. J. Sustain. Transp.*, vol. 11, no. 10, pp. 707–720, 2017, doi: 10.1080/15568318.2017.1310962.

[77] Y. Nie and M. Ghamami, “A corridor-centric approach to planning electric vehicle charging infrastructure,” *Transp. Res. Part B Methodol.*, vol. 57, pp. 172–190, 2013, doi: 10.1016/j.trb.2013.08.010.

[78] Z. Chen, Y. Yin, and Z. Song, “A cost-competitiveness analysis of charging infrastructure for electric bus operations,” *Transp. Res. Part C Emerg. Technol.*, vol. 93, no. December 2017, pp. 351–366, 2018, doi: 10.1016/j.trc.2018.06.006.

[79] “Electricity Supply Services in France.” https://www.french-property.com/guides/france/utilities/electricity/tariff.

[80] Y. He, Z. Song, and Z. Liu, “Fast-charging station deployment for battery electric bus systems considering electricity demand charges,” *Sustain. Cities Soc.*, vol. 48, no. April, 2019, doi: 10.1016/j.scs.2019.101530.

[81] A. Barré, B. Deguilhem, S. Grolleau, M. Gérard, F. Suard, and D. Riu, “A review on lithium-ion battery ageing mechanisms and estimations for automotive applications,” *J. Power Sources*, vol. 241, pp. 680–689, 2013, doi: 10.1016/j.jpowsour.2013.05.040.

[82] E. Meissner and G. Richter, “The challenge to the automotive battery industry: The battery has to become an increasingly integrated component within the vehicle electric power system,” *J. Power Sources*, vol. 144, no. 2, pp. 438–460, 2005, doi: 10.1016/j.jpowsour.2004.10.031.

[83] G. Sarre, P. Blanchard, and M. Broussely, "Aging of lithium-ion batteries," *J. Power Sources*, vol. 127, no. 1–2, pp. 65–71, 2004, doi: 10.1016/j.jpowsour.2003.09.008.

[84] O. Erdinc, B. Vural, and M. Uzunoglu, "A dynamic lithium-ion battery model considering the effects of temperature and capacity fading," *2009 Int. Conf. Clean Electr. Power, ICCEP 2009*, pp. 383–386, 2009, doi: 10.1109/ICCEP.2009.5212025.

[85] A. G. Ritchie, "Recent developments and likely advances in lithium rechargeable batteries," *J. Power Sources*, vol. 136, no. 2 SPEC. ISS., pp. 285–289, 2004, doi: 10.1016/j.jpowsour.2004.03.013.

[86] W. Bögel, J. P. Büchel, and H. Katz, "Real-life EV battery cycling on the test bench," *J. Power Sources*, vol. 72, no. 1, pp. 37–42, 1998, doi: 10.1016/S0378-7753(97)02775-4.

[87] K. Ohue, T. Utsunomiya, O. Hatozaki, N. Yoshimoto, M. Egashira, and M. Morita, "Self-discharge behavior of polyacenic semiconductor and graphite negative electrodes for lithium-ion batteries," *J. Power Sources*, vol. 196, no. 7, pp. 3604–3610, 2011, doi: 10.1016/j.jpowsour.2010.12.073.

[88] R. B. Wright, C. G. Motloch, J. R. Belt, J. P. Christophersen, C. D. Ho, R. A. Richardson, I. Bloom, S. A. Jones, V. S. Battaglia, G. L. Henriksen, T. Unkelhaeuser, D. Ingersoll, H. L. Case, S. A. Rogers, and R. A. Sutula, "Calendar- and cycle-life studies of advanced technology development program generation 1 lithium-ion batteries," *J. Power Sources*, vol. 110, no. 2, pp. 445–470, 2002, doi: 10.1016/S0378-7753(02)00210-0.

[89] S. S. Zhang, K. Xu, and T. R. Jow, "Electrochemical impedance study on the low temperature of Li-ion batteries," *Electrochim. Acta*, vol. 49, no. 7, pp. 1057–1061, 2004, doi: 10.1016/j.electacta.2003.10.016.

[90] S. B. Peterson, J. Apt, and J. F. Whitacre, "Lithium-ion battery cell degradation resulting from realistic vehicle and vehicle-to-grid utilization," *J. Power Sources*, vol. 195, no. 8, pp. 2385–2392, 2010, doi: 10.1016/j.jpowsour.2009.10.010.

[91] R. Kötz, P. W. Ruch, and D. Cericola, "Aging and failure mode of electrochemical double layer capacitors during accelerated constant load tests," *J. Power Sources*, vol. 195, no. 3, pp. 923–928, 2010, doi: 10.1016/j.jpowsour.2009.08.045.

[92] H. Gong, Y. Yu, T. Li, T. Mei, Z. Xing, Y. Zhu, Y. Qian, and X. Shen, "Solvothermal synthesis of LiFePO4/C nanopolyhedrons and microellipsoids and their performance in

lithium-ion batteries," *Mater. Lett.*, vol. 66, no. 1, pp. 374–376, 2012, doi: 10.1016/j.matlet.2011.08.093.

[93] V. Ramadesigan, K. Chen, N. A. Burns, V. Boovaragavan, R. D. Braatz, and V. R. Subramanian, "Parameter Estimation and Capacity Fade Analysis of Lithium-Ion Batteries Using Reformulated Models," *J. Electrochem. Soc.*, vol. 158, no. 9, p. A1048, 2011, doi: 10.1149/1.3609926.

[94] V. Ramadesigan, V. Boovaragavan, and V. R. Subramanian, "Efficient Reformulation of Solid-Phase Diffusion in Physics-Based Lithium-ion Battery Models," vol. 16, no. 29, pp. 129–134, 2009, doi: 10.1149/1.3115314.

[95] T. F. Fuller, "Simulation and Optimization of the Dual Lithium Ion Insertion Cell," *J. Electrochem. Soc.*, vol. 141, no. 1, p. 1, 1994, doi: 10.1149/1.2054684.

[96] A. Eddahech, O. Briat, H. Henry, J. Y. Delétage, E. Woirgard, and J. M. Vinassa, "Ageing monitoring of lithium-ion cell during power cycling tests," *Microelectron. Reliab.*, vol. 51, no. 9–11, pp. 1968–1971, 2011, doi: 10.1016/j.microrel.2011.07.013.

[97] A. Eddahech, O. Briat, E. Woirgard, and J. M. Vinassa, "Remaining useful life prediction of lithium batteries in calendar ageing for automotive applications," *Microelectron. Reliab.*, vol. 52, no. 9–10, pp. 2438–2442, 2012, doi: 10.1016/j.microrel.2012.06.085.

[98] D. Andre, C. Appel, T. Soczka-Guth, and D. U. Sauer, "Advanced mathematical methods of SOC and SOH estimation for lithium-ion batteries," *J. Power Sources*, vol. 224, pp. 20–27, 2013, doi: 10.1016/j.jpowsour.2012.10.001.

[99] M. Einhorn, V. F. Conte, C. Kral, J. Fleig, and R. Permann, "Parameterization of an electrical battery model for dynamic system simulation in electric vehicles," *2010 IEEE Veh. Power Propuls. Conf. VPPC 2010*, 2010, doi: 10.1109/VPPC.2010.5729127.

[100] S. Sankarasubramanian and B. Krishnamurthy, "A capacity fade model for lithium-ion batteries including diffusion and kinetics," *Electrochim. Acta*, vol. 70, pp. 248–254, 2012, doi: 10.1016/j.electacta.2012.03.063.

[101] M. Safari, M. Morcrette, A. Teyssot, and C. Delacourt, "Life Prediction Methods for Lithium-Ion Batteries Derived from a Fatigue Approach," *J. Electrochem. Soc.*, vol. 157, no. 7, p. A892, 2010, doi: 10.1149/1.3432560.

[102] V. Marano, S. Onori, Y. Guezennec, G. Rizzoni, and N. Madella, "Lithium-ion batteries

life estimation for plug-in hybrid electric vehicles," *5th IEEE Veh. Power Propuls. Conf. VPPC '09*, pp. 536–543, 2009, doi: 10.1109/VPPC.2009.5289803.

[103] J. Schmalstieg, S. Käbitz, M. Ecker, and D. U. Sauer, "A holistic aging model for Li(NiMnCo)O2 based 18650 lithium-ion batteries," *J. Power Sources*, vol. 257, pp. 325–334, 2014, doi: 10.1016/j.jpowsour.2014.02.012.

[104] H. J. Ploehn, P. Ramadass, and R. E. White, "Solvent Diffusion Model for Aging of Lithium-Ion Battery Cells," *J. Electrochem. Soc.*, vol. 151, no. 3, p. A456, 2004, doi: 10.1149/1.1644601.

[105] M. Broussely, P. Biensan, F. Bonhomme, P. Blanchard, S. Herreyre, K. Nechev, and R. J. Staniewicz, "Main aging mechanisms in Li ion batteries," *J. Power Sources*, vol. 146, no. 1–2, pp. 90–96, 2005, doi: 10.1016/j.jpowsour.2005.03.172.

[106] M. Broussely, S. Herreyre, P. Biensan, P. Kasztejna, K. Nechev, and R. J. Staniewicz, "Aging mechanism in Li ion cells and calendar life predictions," *J. Power Sources*, vol. 97–98, pp. 13–21, 2001, doi: 10.1016/S0378-7753(01)00722-4.

**** End of Chapter 4*

Chapter 5

OPTIMAL BATTERY SIZING AND CHARGING STRATEGY FOR BATTERY ELECTRIC BUSES

5.1 Introduction

BEBs charging is a complex process that incurs a large number of variables interacting among each other and impacting the complete charging scheme. The charging strategy of BEB defines its charging energy and power profiles during the day and the charging infrastructure. The charging infrastructure identifies the charging facilities as it defines the charging location for the BEBs and the chargers' size (maximum power) [1], [2]. The different components of the charging strategy highly affect each other. For example, charging at the stop stations will require chargers with high power ratings due to the limited charging duration. In addition, such charging infrastructure results in frequent daily charging and at high power. On the other hand, deciding to charge at the depot overnight takes place at low power and for prolonged durations, and thus low power chargers are sufficient to supply the BEB charging needs.

Battery sizing and charging strategy of BEBs directly drive the TCO of BEBs deployment. BEBs TCO includes the acquisition costs of the BEBs, batteries, and infrastructure in addition to the operating, maintenance, and battery replacement costs due to aging. Oversizing the batteries results in a high battery acquisition cost increasing the TCO. However, large batteries are less prone to aging phenomena, and thus their replacement cost is low. On the other hand, the charging strategy has a huge impact on the TCO of BEBs as well. Frequent charging during the day requires a large number of chargers to be installed and thus increasing the infrastructure costs. Moreover, charging at high-power levels requires the installation of high-power supply chargers that incur high acquisition costs.

In addition, the choice of the battery size and the charging strategy have a straight impact on BEBs operation and punctuality to their schedule, reflected in their punctuality index (PI). BEBs equipped with large batteries are less prone to schedule disruptions but at a high risk of service interruption as most of their charging takes place during the night outside their service hours. On the other hand, BEBs equipped with small batteries associated with frequent charging during the day increases the risk of schedule disruption but are less prone to service interruption.

That being said, there is a need for an optimal battery sizing and charging strategy for BEB lines that minimize the TCO of BEB deployment while respecting BEBs schedule and punctuality constraints. This chapter introduced a methodology that minimizes the TCO of BEB deployment by optimizing the battery size and the charging strategy. A case study is considered utilizing the proposed methodology representative of bus line number 21 in Paris City. The

impact of the different battery sizes and charging strategies on the TCO is thoroughly explained. Finally, the chapter concludes with a sensitivity analysis of the main cost parameters and their impact on the TCO, battery size, and charging strategy.

5.2 Review of the Literature

Several studies have been published over the past decade on reducing the costs of deployment of BEBs by properly sizing the batteries and adopting adequate charging strategies. Table 5.1 introduces a summary overview of the recent literature on reducing the cost of deployments of BEBs. The focus of each study is presented alongside the methods used to reduce the deployment costs of BEBs. In addition, the cost function components of each study are highlighted next to the considered control variables.

The majority of the contributions in the literature present comparative cost analysis or feasibility studies among a variety of charging strategies, where variables such as battery size and maximum charging power are varied for predefined charging infrastructure as presented in [2], [3]. Other studies introduce methods to reduce the costs of deployment of BEBs as shown in [4], [5], however these heuristic methods that do not lead to optimal results.

On the other hand, several studies provide optimization methods to minimize certain cost components of the TCO of BEBs deployment. [6] and [7] present a linear programming optimization algorithm to minimize the chargers' acquisition costs by optimally locating the charging stations along the BEB line and identifying the maximum chargers' power. Other studies focus on minimizing battery replacement costs due to aging. [8] introduces a non-linear programming optimization algorithm that optimizes the BEBs charging power in order to minimize battery aging. Similarly, [9] utilizes a genetic algorithm multiple-objective optimization technique to minimize battery replacement costs and energy costs by controlling the BEBs charging power during overnight charging.

Very few studies consider the majority of the cost components of BEB deployment TCO. [10] uses a mixed-integer linear programming optimization technique to optimally locate the charging stations minimizing the battery, chargers, and energy costs. Similarly, [11] utilizes a mixed-integer linear programming technique to minimize battery, chargers, and energy costs for a single fast opportunity charging station by controlling the battery size. In addition, [12] and [13] introduce genetic algorithm-based optimization routines minimizing the battery,

chargers, and energy costs by controlling the charging time and battery *SOC* in [12] and the fleet size (number of buses) and chargers' number in [13].

Across the reviewed studies in the recent literature, none presents an optimization-based methodology that minimizes the TCO of BEB deployment including all the cost components such as battery and chargers' acquisition costs, battery replacement costs, infrastructure costs, energy costs, and demand charge, while respecting BEBs schedule constraints. In addition, none of the presented studies introduce a generalizable methodology to optimize, for any charging infrastructure, the BEBs battery size, daily charging power, energy, and time.

Based on what has been presented, the following gaps and limitations in the recent literature are identified:

- There is no optimization-based methodology that minimizes the TCO of BEB deployment considering a comprehensive cost function while respecting the schedule constraints.
- The presented optimization-based methodologies are only applicable for specific charging infrastructure and BEB lines and thus, they are not generalizable.
- Battery size is not optimized but rather considered as an input to the optimization models or a parameter that is subjected to sensitivity analysis, despite its significant contribution to the TCO of BEB deployment.
- None of the studies optimizes all the control variables of the charging strategy such as the daily charging power, energy, time, and location, whereas most of the studies optimize a single control variable.

Based on the presented summary of the literature and the highlighted gaps within, this chapter presents an optimization-based methodology to minimize the TCO of BEB deployment by optimally sizing the battery and controlling the charging strategy for any charging infrastructure, while respecting the BEBs schedule and punctuality constraints.

In summary, this chapter answers the following research question:

- ***What is the optimal battery sizing and charging strategy of BEB line minimizing the TCO of BEB deployment while respecting schedule and punctuality constraints?***

This chapter is organized as follows: section 5.3 introduces the proposed methodology to minimize TCO of BEB deployment, then section 5.4 presents an application of the proposed methodology. Finally, section 5.5 concludes on the main findings in this chapter.

Table 5.1: Summary overview of the recent literature on reducing the cost of deployments of BEBs

Reference	Focus	Cost Function Definition	Methods	Control Variables	Additional Considerations
Elin (2016) [3]	Investigating the investment cost of electrifying a complete bus system.	- Battery and chargers acquisition costs - Grid connection costs	Holistic approach (non-optimization).	- Battery Size - Chargers' Maximum Power	Study tackles the three stationary charging infrastructures (Depot, end-line, and opportunity charging).
Lajunen (2018) [2]	Assessing the lifecycle costs and the changing needs of different charging methods.	- BEB units, batteries and chargers acquisition costs and their salvage values. - Energy, maintenance, and CO2 emissions costs. - Battery replacement costs	Feasibility study (non-optimization).	- Battery Size - Chargers' Maximum Power	Study tackles the three stationary charging infrastructures.
Qin et al. (2016) [5]	Minimizing the energy costs and demand charge	Energy costs and demand charge.	Rule-Based (non-optimization)	- Scheduling daily BEBs charging.	Study tackles a single fast charger at a stop station (stationary opportunity charging).

Chen et al. (2018) [4]	Assessing the cost-competitiveness of different charging infrastructure for electric bus systems.	- BEB units, batteries, and chargers acquisition costs	- Enumeration of control variables (non-optimization) - $1^{st}/2^{nd}$ order non-linear problem.	- Number of BEBs - Battery Size	Study tackles the following three charging infrastructures: 1. Stationary opportunity charging 2. Dynamic charging lanes 3. Battery swapping stations
El-Taweel et al. (2017) [8]	Optimal design of a charging station	- Chargers' acquisition costs.	- Optimization using linear programming.	- Number of chargers - Chargers' power rating	Study tackles the three stationary charging infrastructures.
Kunith et al. (2015) [7]	Locating the charging stations of public transit bus systems	Chargers' acquisition costs.	Optimization using mixed integer optimization.	- Charger's location and number.	Study tackles fast chargers (stationary opportunity charging).

Xylia et al. (2017) [14]	Locating the charging stations of public transit bus systems.	- BEB units, batteries and chargers acquisition costs and their salvage values. - Energy, maintenance, and CO2 emissions costs.	Optimization using mixed integer linear programming.	- Location of the charging station.	Study tackles the stationary opportunity charging infrastructure.
Houbbadi et al. (2017) [9]	Multi-objective optimization considering charging costs and battery aging of BEBs.	- Energy costs - Battery replacement costs (aging)	- Optimization using genetic algorithm.	- BEBs charging power	Study tackles stationary charging infrastructure at the depot.
Houbbadi et al. (2019) [8]	Minimizing the battery replacement costs for overnight charging BEBs	- Battery replacement costs (aging)	- Optimization using non-linear programming.	- BEBs charging power	Study tackles stationary charging infrastructure at the depot.
Wang et al. (2017) [10]	Planning and operation of BEBs charging infrastructure.	- Chargers acquisition and charging station construction costs. - Energy and maintenance costs - Schedule delay costs	Optimization using mixed integer linear programming.	- Location of the charging station. - Schedule of the daily BEBs charging.	Charging takes place at a fixed duration/power during the day.

Rogge et al. (2018) [13]	Optimizing the fleet size and charging infrastructure of BEB line to reduce its TCO.	- BEB units, batteries, and chargers acquisition costs. - Energy and labor costs.	Optimization using grouping genetic algorithm.	- Fleet Size - Number of Chargers - Schedule of the daily BEBs charging.	Charging takes place at a fixed duration/power during the day.
Ke et al. (2016) [12]	Minimizing the construction cost of e-transportation system	- BEB units, batteries, and chargers acquisition costs - Energy Costs	- Optimization using genetic algorithm.	- Battery SOC - Charging Time	Battery size and charging infrastructure are fixed for a certain BEB line.
He et al. (2019) [11]	Deployment of fast-charging stations and energy storage systems to minimize demand charge tariffs.	- Battery and chargers acquisition costs - Demand charge tariff	Optimization using mixed integer linear programming	- Battery Size - Energy Storage System Size	Study considers fast-charging stations.

5.3 Methods

In order to minimize the TCO of BEB deployment, it is essential to find the optimal combinations of the different control variables that impact the TCO. As thoroughly mentioned in Chapter 4, the size of the battery pack and the charging strategy drive the TCO of BEB deployment. The battery size is defined as the maximum energy capacity of the battery. On the other hand, the charging strategy incurs a large number of variables:

- BEBs charging energy profile during the day.
- BEB charging power profiles during the day.
- Chargers' size (maximum power) and location, which are defined as the charging infrastructure.

These control variables are classified into two categories: (1) dynamic control variables and (2) static control variables. The BEBs charging energy and power profiles during the day are dynamic variables as they may vary at each time instant during the BEBs operation. On the contrary, battery size and charging infrastructure (chargers' maximum power and location) are static variables that are preferably fixed over the entire BEBs operation. Table 5.2 summarizes these variables.

Table 5.2: Summary of the considered control variables to minimize TCO

Control Variables	
Static Variables	Battery Size Charger Maximum Power Charger Location
Dynamic Variables	BEB daily charging energy profile BEB daily charging power profile

Each control variable impacts one or more cost components of the TCO. The dynamic control variables (daily charging energy and power profiles) mainly affect the operating costs and battery replacement costs. On the other hand, static variables affect capital costs such as infrastructure costs and battery acquisition costs. The BEBs unit and maintenance costs are not affected by any control variable.

This problem incurs a large number of control variables and they are of different types (static and dynamic). For this sake, this section presents an optimization-based methodology to minimize the TCO of BEB deployment considering all the mentioned control variables.

5.3.1 Framework

The methodology is mainly composed of two optimization steps where each step applies a different optimization algorithm. Each optimization step deals with a certain type of control variables. In the first step, the dynamic control variables are optimized to minimize the operating and battery replacement costs, whereas, in the second step, the static control variables are optimized to minimize the TCO taking into account the optimized dynamic control variables that resulted from step 1.

- **Optimization Step 1**

In this step, the dynamic control variables are optimized to minimize the energy costs and battery replacement costs for each BEB. A set $\mathcal{B}$ of BEBs contains a number n_B of buses that operate along a certain BEB line. Subscript b represents a BEB number.

$$\mathcal{B} = \{B_1, B_2, \dots, B_b, \dots B_{n_B}\} \quad \forall\, b \in \{1,2, \dots, n_B\} \tag{5.1}$$

Denote by $P_{B_b}(t)$ and $E_{B_b}(t)$ the daily charging power and energy profiles respectively for a BEB B_b.

$$\mathcal{P}_B(t) = \left[P_{B_1}, P_{B_2}, \dots, P_{B_b}, \dots P_{B_{n_B}}\right] \tag{5.2}$$

$$\mathcal{E}_B(t) = \left[E_{B_1}, E_{B_2}, \dots, E_{B_b}, \dots E_{B_{n_B}}\right] \tag{5.3}$$

In this optimization step, the cost components to be minimized are the energy costs and battery replacement costs. Let these two cost components be represented by the variable C_1, expressed in equation (5.4) where OC^{eu} is the energy cost and BRC is the battery replacement cost. The Dynamic Programming (DP) optimization technique is used to minimize C_1 by optimally controlling the dynamic variables $P_{B_b}(t)$ and $E_{B_b}(t)$. The choice of DP as an optimization technique and its mathematical formulation will be thoroughly discussed in section 5.3.2.

$$C_1 = OC^{eu} + BRC \tag{5.4}$$

This optimization step is further split into 3 sub-steps:

1.1- The dynamic control variables $P_{B_b}(t)$ and $E_{B_b}(t)$ of a bus are defined for a certain day. During each day, the BEBs operating conditions vary affecting the BEBs costs. Therefore, the optimal dynamic control variables $P_{B_b}(t)$ and $E_{B_b}(t)$ are different for each day due to the varying operating conditions. In general, the optimization problem aims at minimizing the TCO over a specified period measured in years. To simplify the problem, each month during the year is represented by one day which reflects the average operating conditions during this month.

Thus, the dynamic control variables $P_{B_b}(t)$ and $E_{B_b}(t)$ are optimized for each month during the year minimizing the daily C^d_{1,B_b} cost for each B_b. The obtained C^d_{1,B_b} cost results for each day are multiplied by the number of days of the corresponding month in order to estimate the C^m_{1,B_b} cost per month for each B_b. The sum of the optimal monthly C^m_{1,B_b} costs defines the yearly optimal C^y_{1,B_b} cost. Finally, the yearly optimal C^y_{1,B_b} cost is multiplied by the optimization period number of years to calculate the total optimal C_{1,B_b} cost over the entire optimization period.

1.2- Step 1.1 optimizes the dynamic control variables for a single battery size K_b. However, the battery size directly impacts the dynamic variables as small battery sizes require more frequent charging to supply the BEB energy needs when compared to large battery sizes. In addition, the BEB energy consumption increases for larger batteries, and this results in increases energy costs. Thus, step 1.1 is repeated for each possible battery size K_b.

1.3- The optimal dynamic control variables for each BEB are directly affected by the BEB operating conditions. These operating conditions highly vary among the BEBs. The bus schedule determines the trip operating conditions for each BEB as it determines the departure time for each bus trip. The departure time for each bus trip determines the trip driving conditions as traffic conditions vary during the day. In addition, trip departure time also determines the weather conditions such as the external temperature and solar flux as they vary during the day. Finally, passengers load inside the bus also varies during the day, and thus it is affected by the bus schedule. In addition, the bus schedule determines the number of daily trips to be completed by each bus and the departure time for each trip during the day. This defines the possible charging time slots, and it highly varies from one bus to another depending on their defined schedules. Therefore, step 1.2 is repeated for every bus operating along the line.

Concerning the static control variables in this step, the charging infrastructure is set as an input, and the optimization-based methodology is applied to each one of the three stationary charging

infrastructures (depot, end-line, and opportunity charging). The charging infrastructure defines the charger's location and number along the BEB line. As for the battery size, this static control variable directly affects the C_1 costs as previously shown in Chapter 4. Therefore, the battery is dealt with as an input at the beginning of the optimization period that will be held constant and for each battery size, the whole optimization step 1.1 process is applied as discussed in step 1.2 for every B_b resulting in different optimal dynamic control variables $P_{B_b}^{m,k_b}(t)$ and $E_{B_b}^{m,k_b}(t)$ and optimal costs C_{1,B_b}^{m,k_b}. Finally, Figure 5.1 shows the flowchart of optimization step 1.

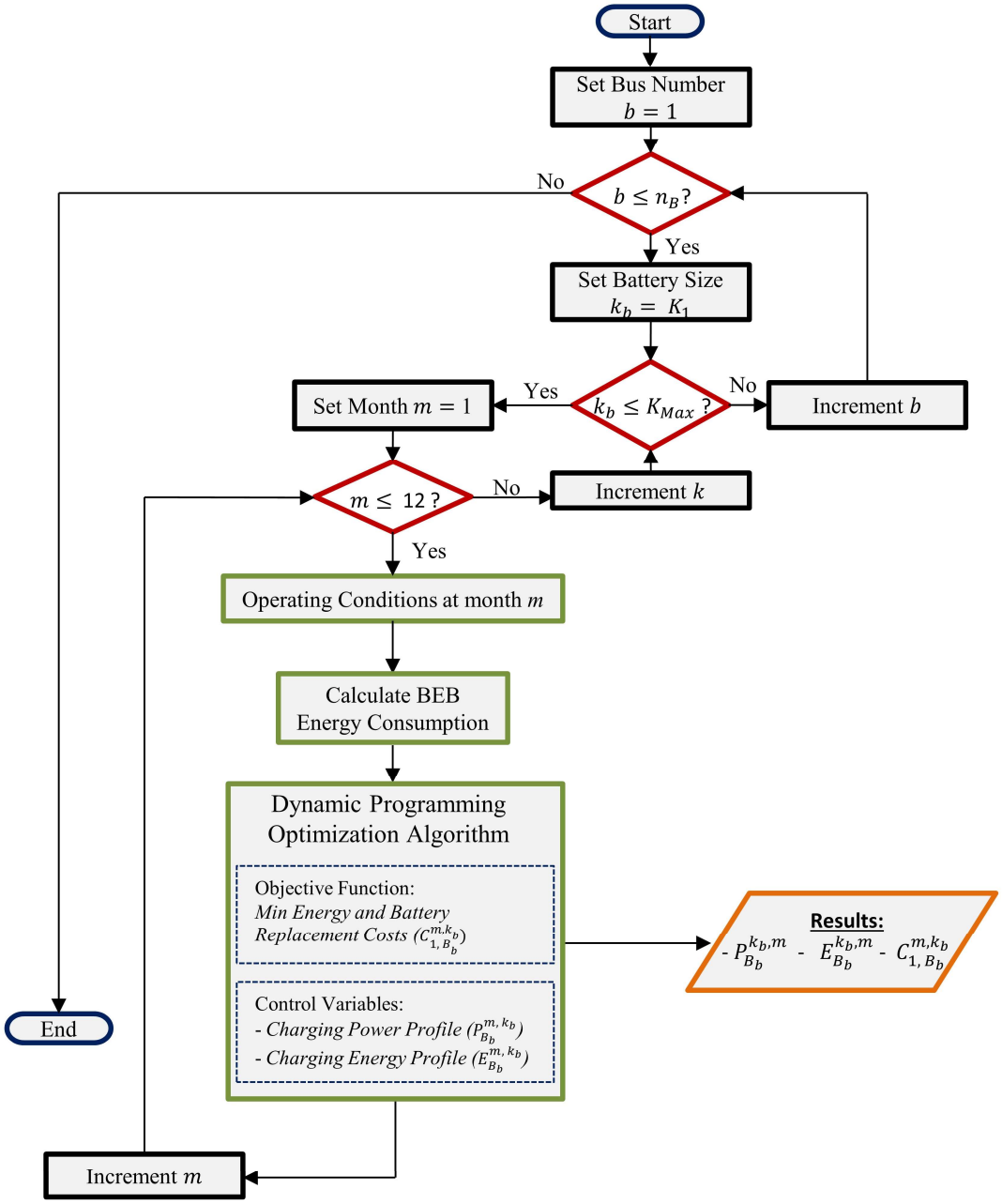


Figure 5.1: Optimization Step 1 flowchart for any charging infrastructure

- **Optimization Step 2**

In this step, the static control variables are optimized to minimize the TCO of BEB deployment. In step 1, the optimal dynamic control variables $P_{B_b}^{m,\,k_b}(t)$ and $E_{B_b}^{m,\,k_b}(t)$ are optimized for each month, at each battery size, and for each BEB as well, resulting in the minimal costs $C_{1,\,B_b}^{m,k_b}$. Therefore, for each BEB B_b, there exists a set of possible battery sizes $\mathcal{K}_{B_b}$ that contains K_{Max} different possible battery sizes each with its corresponding optimal $P_{B_b}^{m,\,k_b}(t)$ and $E_{B_b}^{m,\,k_b}(t)$, and at minimal $C_{1,\,B_b}^{m,k_b}$.

$$\mathcal{K}_{B_b} = \{K_1, K_2, \dots K_{Max}\} \quad \forall\ B_b\ \in \mathcal{B} \tag{5.5}$$

That being said, the TCO is minimized by optimally choosing the battery size K_b for each BEB. In step 1, the considered costs are the energy and battery replacement costs as they are directly affected by the dynamic control variables. In this step, the other cost components are considered. First, the battery acquisition costs are directly related to the choice of the battery size. In addition, the infrastructure cost is also considered as it is driven by the choice of the charging infrastructure and the chargers' maximum power rate. The chargers' maximum power rate is determined by the daily charging power profile $P_{B_b}^{m,\,k_b}$ maximum power demand for each BEB at each battery size.

A Genetic Algorithm – based (GA) optimization technique is used to optimize the battery size for each BEB minimizing the TCO. The choice of GA as an optimization technique and its mathematical formulation will be thoroughly discussed in section 5.3.3. The final output of optimization step 2 is the optimal battery size K_b for each BEB which determines the optimal daily charging power and energy profiles $P_{B_b}^{m,\,k_b}(t)$ and $E_{B_b}^{m,\,k_b}(t)$, and the chargers' maximum power rating $P_{C,Max}$.

Finally, Figure 5.2 shows the complete methodology flowchart.

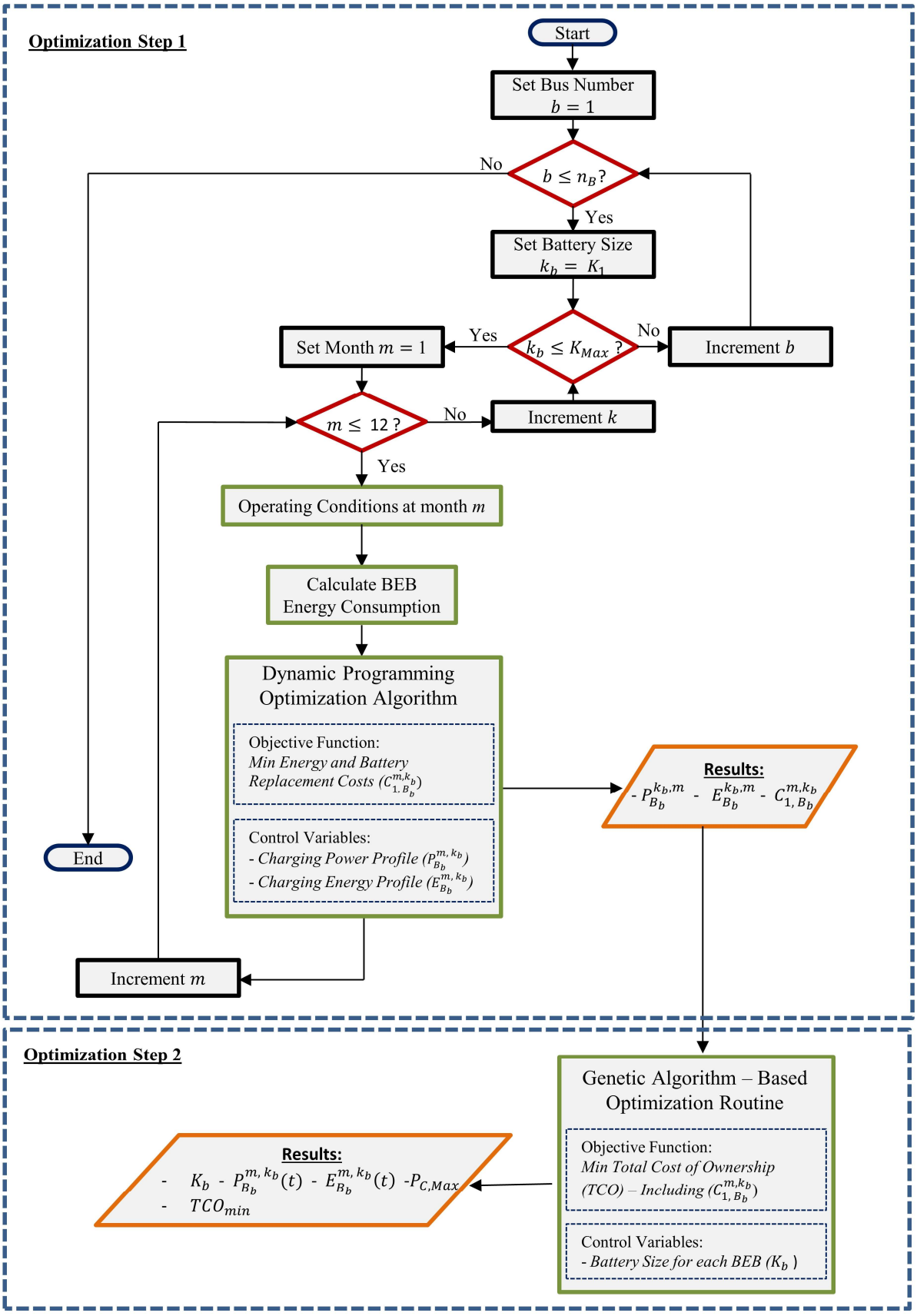


Figure 5.2: Methodology complete flowchart

5.3.2 Optimization Step 1: Dynamic Programming

This section describes the first optimization step and its corresponding mathematical formulation.

5.3.2.1 Overview

Dynamic programming (DP) is a mathematical technique developed by Richard Bellman in 1954 [15] to provide optimal solutions for multi-stage decision problems, based on the principle of the overall optimality of the problem. DP provides a globally optimal solution, and thus, it serves as a benchmark. However, it incurs some limitations, such as the heavy computation time, and the need for prior knowledge of all the inputs defined throughout the optimization period [16]. The choice of DP for this optimization step is due to the fact that it can handle a multi-stage dynamic-decision problem, which is the case in optimization step 1.

5.3.2.2 Formulation

In this section, the DP theory is discussed and applied to the problem addressed in this chapter.

5.3.2.2.1 Optimization Objective

The DP objective is to minimize the total energy and battery replacement costs of each BEB over a certain optimization period. Therefore, DP is used to minimize a cost function J, defined as the sum of the cumulative costs L, referred to as the cost-to-go, over the whole optimization period as shown in equation (5.6).

The cumulative cost L is defined at a stage i and it is function of the charging energy (u) and power (p) at every charging stage (i), and the bus battery size (k) over an optimization period which consists of N stages.

$$J = \min \sum_{i=0}^{N-1} L_i(u_i, p_i, k) \tag{5.6}$$

5.3.2.2.2 State, Control, and Input variables

The state, control, and input variables are all determined at each stage during the optimization period. The stage in this problem is defined as a charging event. The total number of stages is the total number of charging events, which varies depending on the charging infrastructure. The first state variable in this problem is the battery state of energy (SOE) when the bus arrives at a charging station i.e., before a possible charging event. This variable is denoted by x. The second

state variable is the time when a bus arrives at a certain charging station i.e., before a possible charging event, and it is denoted by t_a.

The control variables, as mentioned earlier, are the charging power (p) and charging energy fraction (u), defined as the ratio of the charging energy in *kWh* to the battery energy capacity in *kWh*, thus it is a dimensionless variable. The daily operating conditions are input parameters to the DP algorithm as they determine the energy consumption of the BEB. In addition, the BEBs schedule determines the available charging time slots during the day and the BEB departure time constraints as well.

These inputs can be represented by three variables: bus energy consumption per trip (c), bus departure time (t_{trip}) and trip duration (Δt). Table 5.3 summarizes the state, control, and input variables of this problem.

Table 5.3: Definition of the state, control and input variables

	Variable	Definition	Unit
State	x	Battery State of Energy	-
	t_a	Bus arrival time to a charging station	h
Control	u	The ratio of the "energy used to charge the battery, to the nominal battery energy''	-
	p	Charging Power	kW
Input	k	Battery Capacity	kWh
	c	Energy consumption per bus trip	kWh
	t_{trip}	Bus departure time for a certain trip	h
	Δt	Trip Duration	h
	N	Total Number of Stages	-
	n_B	Total Number of Buses	-
Index/node	b	Bus Number	-
	i	Stage Number	-

5.3.2.2.3 Mathematical Model

The state variables in this problem are determined using equations (5.7) and (5.8). The battery state of energy $x(t)$ at any time t is the ratio of the battery available energy $E(t)$ at time t to the nominal battery capacity k_b. The state variable t_a is simply the time when a bus arrives at a charging station, and it is deducted from the bus schedule only, as function of the bus number.

$$x(t)_{i,n} = \frac{E(t)_{i,b}}{k_b} \tag{5.7}$$

$$t_{a\,i,b} = f(b) \tag{5.8}$$

As for the control variables, they are mainly chosen from a set of available values.

$$u_{i,b} \in (u_1, u_2, u_3, \dots, u_{max}) \tag{5.9}$$

$$p_{i,b} \in (p_1, p_2, p_3, \dots, p_{max}) \tag{5.10}$$

Concerning the input variables, the bus departure time t_{trip} is directly determined by the schedule and the trip duration Δt is deducted from the driving conditions. A trip is defined between two charging events, which implies that the trip-related input variables are dependent on the considered charging infrastructure. For example, if the considered charging infrastructure is stationary charging at the depot, t_{trip} is the bus departure time from the depot and Δt is the duration of a round trip (Depot to Depot).

On the contrary, if the considered charging infrastructure is stationary end line charging, t_{trip} is the bus departure time from the termini (Depot and Terminus) and Δt is the duration of a one-way trip (Depot to Terminus or Terminus to Depot). Obviously, in the second case, there is a higher number of possible charging events, and thus a higher number of stages *N*.

Similarly, if the opportunity charging at the stops station is considered, t_{trip} is the bus departure time from a stop station where charging is possible and Δt is the duration of the trip between 2 consecutive stop stations where charging is possible. The energy consumption per bus trip input variable is dependent on the BEB operating conditions. For each trip, the operating conditions are determined, and the BEB energy consumption is calculated according to the methodology presented in Chapter 2 and Chapter 3.

After defining all the needed variables, the state equations can now be presented. The state equation, or system equation, is the equation that governs the transition of the system states

from one stage to another. There are 2 state equations that represent the two state variables in this problem as shown in equations (5.11) and (5.12).

$$x_{i+1,b} = x_{i,b} + u_{i,b} - c_{i,b} \ \forall \ i \ \in \{0 \dots N-1\} \ \wedge \ \forall \ B_b \ \in \ \mathcal{B} \tag{5.11}$$

$$t_{a\ i+1,\boldsymbol{b}} = t_{trip\ i,\boldsymbol{b}} + \Delta t_{i,\boldsymbol{b}} \ \forall \ i \ \in \{0 \dots N-1\} \ \wedge \ \forall \ B_b \ \in \ \mathcal{B} \tag{5.12}$$

Finally, the boundary conditions of the state variables are introduced in equation (5.13). They determine the battery's initial and final SOE in addition to the bus initial and final arrival time to the charging stations.

$$\begin{cases} x_{0,b} = \bar{x}_{0,b} \\ x_{N,b} = \bar{x}_{N,b} \\ t_{a\ 0,b} = \bar{t}_{a\ 0,b} \\ t_{a\ N,b} = \bar{t}_{a\ N,b} \end{cases} \tag{5.13}$$

5.3.2.2.4 State and Control Variables Constraints

The DP problem presented in this thesis is a constrained multi-stage problem. The state and control variables should respect some imposed constraints. As for the battery $SOE\ x$, it should remain between a minimum and a maximum threshold defined in order not to deteriorate the battery state of health (*SOH)*, as recommended by the battery manufacturer.

Let $\mathcal{X}_{i,b}$ be the set of allowable values of x at a stage i for BEB B_b.

$$\begin{cases} x_{i,b} \ \in \ \mathcal{X}_{i,b} \\ x_{min} < x_{i,b} < x_{max} \end{cases} \ \forall \ i \ \in \{0 \dots N-1\} \ \wedge \ \forall \ B_b \ \in \ \mathcal{B} \tag{5.14}$$

Concerning the control variables, both control variables are constrained as well between minimum and maximum values as shown in equations (5.15) and (5.16). Let $\mathcal{U}_{i,b}$ and $\mathcal{P}_{i,b}$ be the sets of allowable values of u and p respectively at a stage i for BEB B_b.

$$\begin{cases} u_{i,b} \ \in \ \mathcal{U}_{i,b} \\ u_{min} < u_{i,b} < u_{max} \end{cases} \ \forall \ i \ \in \{0 \dots N-1\} \ \wedge \ \forall \ B_b \ \in \ \mathcal{B} \tag{5.15}$$

$$\begin{cases} p_{i,b} \ \in \ \mathcal{P}_{i,b} \\ p_{min} < p_{i,b} < p_{max} \end{cases} \ \forall \ i \ \in \{0 \dots N-1\} \ \wedge \ \forall \ B_b \ \in \ \mathcal{B} \tag{5.16}$$

In addition, the main constraint in this problem is related to the schedule of the buses. The charging event should be completed prior to the bus departure time from the corresponding charging station. The duration of the charging event is function of the control variables as shown in equation (5.17). This constraint is presented in (5.18). In this thesis, it is assumed that the

BEB schedule is fixed throughout its operation during the year. However, the BEB schedule might be subject to some modifications, especially between winter and summer.

$$\Delta t_{Ch,i,b} = \frac{u_{i,b}.k_b}{p_{i,b}} \tag{5.17}$$

$$t_{a\,i,b} + \Delta t_{Ch,i,b} \leq t_{trip\,i,b} \tag{5.18}$$

As discussed earlier, the state is constrained in this problem, so a decision vector containing $u_{i,b}$ and $p_{i,b}$ at any stage i for BEB B_b must ensure that the future states vector containing $x_{i+1,b}$ and $t_{a\,i+1,b}$ is inside the feasible state area. The feasible state areas are defined in equations (5.19) and (5.20).

$$\mathcal{X}_{i,b}^{*} = \{x_{i,b} \in \mathcal{X}_{i,b}: u_{i,b} \in \mathcal{U}_{i,b} \wedge p_{i,b} \in \mathcal{P}_{i,b} : x_{i+1,b} \in \mathcal{X}_{i+1,b}\} \tag{5.19}$$

$$\mathcal{T}_{i,b}^{*} = \{t_{a\,i,b} \in \mathcal{T}_{i,b}: u_{i,b} \in \mathcal{U}_{i,b} \wedge p_{i,b} \in \mathcal{P}_{i,b} : t_{a\,i+1,b} \in \mathcal{T}_{i+1,b}\} \tag{5.20}$$

Consequently, the feasible control areas are expressed in equations (5.21) and (5.22).

$$\mathcal{U}_{i,b}^{*} = \{ u_{i,b} \in \mathcal{U}_{i,b} : x_{i+1,b} \in \mathcal{X}_{i+1,b} \wedge t_{a\,i+1,b} \in \mathcal{T}_{i+1,b}\} \tag{5.21}$$

$$\mathcal{P}_{i,b}^{*} = \{ p_{i,b} \in \mathcal{P}_{i,b} : x_{i+1,b} \in \mathcal{X}_{i+1,b} \wedge t_{a\,i+1,b} \in \mathcal{T}_{i+1,b}\} \tag{5.22}$$

Finally, Table 5.4 summarizes all the mentioned input parameters for DP.

Table 5.4: Definition of DP input parameters

	Parameter	Definition	Unit
State Variables	x_{min}	Battery Minimum State of Energy	-
	x_{max}	Battery Maximum State of Energy	-
	$\overline{x_0}$	Battery Initial State of Energy	-
	$\overline{x_N}$	Battery Final State of Energy	-
	$\overline{t_0}$	Bus First Arrival Time to a Charging Station	*h*
	$\overline{t_N}$	Bus Final Arrival Time to a Charging Station	*h*
Control Variables	u_{min}	Minimum Charging Energy Ratio	-
	u_{max}	Maximum Charging Energy Ratio	-
	p_{min}	Minimum Charging Power	*kW*
	p_{max}	Maximum Charging Power	*kW*

5.3.2.2.5 Grid Selection

DP algorithm is based on a discrete decision route [15]–[17], so it is critical to discretize the state and control variables' spaces. Each state and control variable has its own discretized space referred to as a grid. This problem includes four grids representing two state variables and two control variables. The choice of the element step of the grid determines the length of the state or control variable vector.

Table 5.5 introduces the four grids considered in this problem.

Table 5.5: State and Control Variables Grids

	Variable	Range	Element Step	Vector Length
State Variables	x	0 – 1	0.001	1001
	t_a	0 – 24 *h*	20 *s*	4320
Control Variables	u	0 – 1	0.001	1001
	p	0 – 500 *kW*	5 *kW*	101

5.3.2.2.6 Cost Function Matrix

The cost function matrix is dependent on three main variables: the two control variables u and p, in addition to the state variable t_a. The cost function is calculated at each stage i and stored in a matrix of five dimensions. These 5 dimensions represent the two control variables, the two state variables, and the stage index i.

The cost function includes operating costs and battery replacement costs. The operating costs include both energy costs and the demand charge. Unlike the energy costs, the demand charge is not cumulative, it is considered a one-time occurrence cost proportional to the peak power demand during a defined billing period [18]. However, the DP cost function can only handle cumulative costs evaluated at each instant, thus the demand charge term is not considered at this optimization step but rather in optimization step 2.

Equation (5.23) describes the cost function $\Omega_{i,b}$ defined at a stage i for BEB B_b.

$$\Omega_{i,b} = \alpha(t_{a\,i,b}).u_{i,b}.k_b + \frac{Q_{i,b}^{Loss}(u_{i,b}, p_{i,b}, k_b)}{Q_{Max}^{Loss}}.\beta.k_b \qquad (5.23)$$

The first term of this cost function is the energy cost. α is the electric energy tariff measured in *€/kWh*. It is function of the state variable t_a as there are different tariffs imposed during the day. The term $(u_{i,b}.k_b)$ is the amount of energy charged at charging event i. The second term corresponds to the battery replacement costs due to aging. $Q_{i,b}^{Loss}$ is the battery capacity loss during a charging event i and Q_{Max}^{Loss} is the maximum allowable capacity loss, which indicates the battery end life. β is the cost of the battery pack per unit energy measured in *€/kWh*. Such representation of the battery replacement cost allows its evaluation at each stage.

Many constraints are introduced in this section and if a certain vector of control variables at any stage *i* fails to meet any of these constraints, an infinite cost is imposed on this vector, and thus excluding it from the possible optimal solutions.

5.3.2.2.7 Cost-to-go Function Matrix

The cost-to-go at stage i is the cumulative cost from stage 0 to stage i. At the final stage N, the cost-to-go is the total cumulative cost for the entire optimization period. Equation (5.24) describes the cost-to-go function.

$$L_{i,b}(x_{i,b}) = \sum_{i=0}^{i} \Omega_{i,b}(u_{i,b}, p_{i,b}, t_{a\,i,b}) \tag{5.24}$$

The cost-to-go function matrix is of two dimensions, its lines being the stage number i and its columns being the state variable x. The cost-to-go at stage i depends on the state $x_{i,b}$ at this stage, which is a result of the different decisions $u_{i,b}$ and $p_{i,b}$ taken at the previous stages ($0 \rightarrow i-1$).

5.3.3 Optimization Step 2: Genetic Algorithm

This section describes the second optimization step and its corresponding mathematical formulation.

5.3.3.1 Overview

"Genetic algorithms (GAs) are search methods based on principles of natural selection and genetics. GAs encode the decision variables of a search problem into finite-length strings of alphabets of certain cardinality" [19]. In order to evolve a set of optimal solutions, certain measures are considered for distinguishing the best solutions. In mathematical models, such measures are referred to as objective functions [20]–[22]. In the first optimization step, the dynamic control variables of each BEB are optimized for every possible battery size,

minimizing the energy costs and battery replacement costs. In this step, the choice of the optimal battery size, and its corresponding optimal dynamic control variables, are optimized for each BEB in the line minimizing the TCO of BEB deployment.

5.3.3.2 Formulation

In this section, the GA theory is discussed and applied to the problem addressed in this chapter.

5.3.3.2.1 Terminology

The following terminology is used in GAs mimicking Darwin's Theory of Evolution.

- Population: a set of possible solutions to optimize the objective function. Each solution is referred to as an individual.
- Individual: a possible solution to optimize the objective function. Each solution is composed of a set of entities referred to as chromosomes.
- Chromosome: an entity carrying a set of control variables. These control variables are referred to as genes.
- Gene: Control variable.
- Allele: Value of a control variable.

5.3.3.2.2 Analogy

In this problem, a chromosome is a BEB, and thus the total number of chromosomes for each individual is the total number of BEBs in the line. Each BEB (chromosome) carries a certain battery ID which has 2 genes: the first being the battery size and the second being the optimal charging power profile during the day for each day of the optimization period. The values of the battery size and the power profiles are the alleles.

5.3.3.2.3 Objective Function

The GA objective is to minimize the TCO of BEB deployment over the entire defined optimization period. The TCO model is recalled from Chapter 4 - section 4.5.6 as shown in equation (5.25).

$$\mathcal{Z} = \frac{\begin{array}{c} UC_{Line} + IC_{Line} + \sum_{y=1}^{T_{EL}} \sum_{m=1}^{12} (OC_{Line} + MC_{Line}).(1 + d_r^m)^{-(12.(y-1)+m)} + \\ \sum_{y=1}^{T_{EL}} BRC_{Line}.\left(1 + d_r^y\right)^{-y} - SV(T_{EL}).\left(1 + d_r^y\right)^{-T_{EL}} \end{array}}{\sum_{y=1}^{T_{EL}} \sum_{m=1}^{12} \sum_{b=1}^{n_B} X_{b,m}} \quad \forall\, B_b \in \mathcal{B} \tag{5.25}$$

5.3.3.2.4 GA Steps

This section presents the steps of the GA optimization routine.

1. Initial Population

An initial population containing N individuals is generated randomly, where N is an even natural number. Let $\mathcal{S}$ be a population, and I be an individual. Initial population $\mathcal{S}_0$ can be expressed in equation (5.26).

$$\mathcal{S}_0 = \{I_1, I_2, I_3, \dots I_n, \dots I_N\} \ \forall \ n \in \{0,1,2 \dots N\} \quad (5.26)$$

The index 0 refers to the first generation of individuals and generally, at any generation g, a population $\mathcal{S}_g$ is expressed in equation (5.27).

$$\mathcal{S}_g = \{I_1, I_2, I_3, \dots I_n, \dots I_N\} \forall \ n \in \{0,1,2 \dots N\} \quad (5.27)$$

2. Fitness Evaluation

In this step, the fitness value of each individual in the population $\mathcal{S}_g$ is assessed. The fitness function is the objective function $\mathcal{Z}$ defined earlier. A lower value of $\mathcal{Z}(I_n)$ implies that individual I_n is a fitter individual, and thus a better solution. Therefore, each individual $I_n \in \mathcal{S}_g$ is assigned a fitness value $\mathcal{Z}(I_n)$, which reflects the TCO of this possible solution.

3. Natural Selection

In this phase, the fittest 50% of the total individuals in the population i.e., 50% of the individuals with minimal TCO, are chosen to form the parent population denoted by $\mathcal{S}_{p,g}$ of size $N/2$.

$$\mathcal{S}_{p,g} = \{I_1, I_2, I_3, \dots I_n, \dots I_{N/2}\} \forall \ n \in \left\{0,1,2 \dots \frac{N}{2}\right\} \quad (5.28)$$

4. Crossover

The individuals in the parent population $\mathcal{S}_{p,g}$ undergo crossover among each other where they exchange at least 1 allele. The total number of exchanged alleles is random and the individuals undergoing crossover are randomly chosen from the parent population. Let I_a and I_b be 2 individuals of the parent population $\mathcal{S}_{p,g}$, and let j be the set of chromosomes at which the crossover will take place, new individuals $\acute{I}_a$ and $\acute{I}_b$ are the resulting individuals at the end of the crossover process between I_a and I_b. Equation (5.29) shows the crossover process where N_B is the number of chromosomes in each individual.

$$\begin{cases} \acute{I}_a(i) = I_a(i) \ \forall\, i \in \{1,2,\dots N_B\} - \{j\} \\ \acute{I}_a(j) = I_b(j) \\ \acute{I}_b(i) = I_b(i) \ \forall\, i \in \{1,2,\dots N_B\} - \{j\} \\ \acute{I}_b(j) = I_a(j) \end{cases} \forall\, I_a \text{ and } I_b \in \mathcal{S}_{p,g} \qquad (5.29)$$

This results in a new population called the offspring population $\mathcal{S}_{o,g}$ of size $N/2$.

$$\mathcal{S}_{o,g} = \left\{\acute{I}_1, \acute{I}_2, \acute{I}_3, \dots \acute{I}_n, \dots I_{N/2}^{\acute{}}\right\} \forall\ n \in \left\{0,1,2 \dots \frac{N}{2}\right\} \qquad (5.30)$$

5. Mutation

Every chromosome of each individual in the offspring population $\mathcal{S}_{o,g}$ is subjected to mutation. A chromosome j undergoes mutation resulting in a mutated chromosome k as shown in equation (5.31).

$$I_n(k) = I_n(j + r) \ \forall\, I_n \in \mathcal{S}_{o,g} \wedge \forall\, j \in \{1,2,\dots N_B\} \qquad (5.31)$$

With *r* being a random integer mutation rate between a lower and a higher limit. The resulting mutated individual is referred to as I_n''. This results in a new mutated population referred to as $\mathcal{S}_{m,g}$ of size $N/2$ as shown in equation (5.32).

$$\mathcal{S}_{m,g} = \left\{I_1'', I_2'', I_3'', \dots I_n'' \dots, I_{N/2}''\right\} \forall\ n \in \left\{0,1,2 \dots \frac{N}{2}\right\} \qquad (5.32)$$

6. New Population

The parent population and the mutated population of generation *g* are combined together forming a new population of size *N*. This population serves as the initial population of the next generation $g + 1$.

$$\mathcal{S}_{g+1} = \mathcal{S}_{p,g} \cup \mathcal{S}_{m,g} \qquad (5.33)$$

7. Termination

Steps 2 – 6 are repeated until the termination criterion is met. The termination criterion is met when the fitness value of the fittest individual in each population over the last *G* generations varies by less than a certain percentage *T* %. The values of *G* and *T* are considered to be 100 and 1% respectively.

Finally, the result of this second optimization step is the optimal battery size K_b and its corresponding optimal charging power profile for each BEB that minimize the TCO of BEB deployment.

5.4 Application

5.4.1 Case Study

In this section, a case study is presented utilizing the proposed optimization methodology to minimize the TCO of BEB deployment by optimizing the BEBs battery size and charging strategies. This case study aims at showing the tradeoffs among the different TCO cost components, and how they are driven by the choice of battery size and charging strategy. In addition, this case study highlights the impact of the different battery sizes and charging strategies on the electric grid. The studied Bus line in this case is representative of Bus Line number 21 in Paris city similar to Chapter 4.

5.4.2 Results and Discussion

This section discusses the results of the proposed optimization methodology applied to the presented case study. The results are presented in four main sections:

- The results of optimization step 1 (DP) are presented analyzing the resulting optimal charging strategies at the different battery sizes for a single BEB.
- Then, the findings of optimization step 2 are introduced highlighting the optimal battery size and charging strategy that minimize the TCO of BEB deployment.
- The impact of the BEB schedule on the choice of the optimal battery size is presented.
- BEB charging load is assessed for different battery sizes and charging strategies.
- A sensitivity analysis is conducted by varying the main TCO parameters in order to study their effect on the optimal BEB battery size and charging strategy.

5.4.2.1 Optimal Charging Strategies at Different Battery Sizes

Figure 5.3 shows the optimal charging strategy at different battery sizes for BEB number 1 during the month of January. Panel (a) of Figure 5.3 introduces the optimal charging strategy at a 50-kWh battery. At this battery size, charging takes place at the depot, terminus, and at 8 stop stations along the route (4 in each direction). This is due to the undersized battery energy capacity that requires frequent charging during the day to supply the BEB energy needs.

The power profiles presented in panel (a) show that depot and terminus charging take place at 50-100 *kW* during the day, whereas charging along the route at the stop stations can take place at 200 *kW*. This is due to the shorter allowable charging duration at the stop stations (30 seconds – 1 minute) when compared to charging at the depot or terminus (tens of minutes).

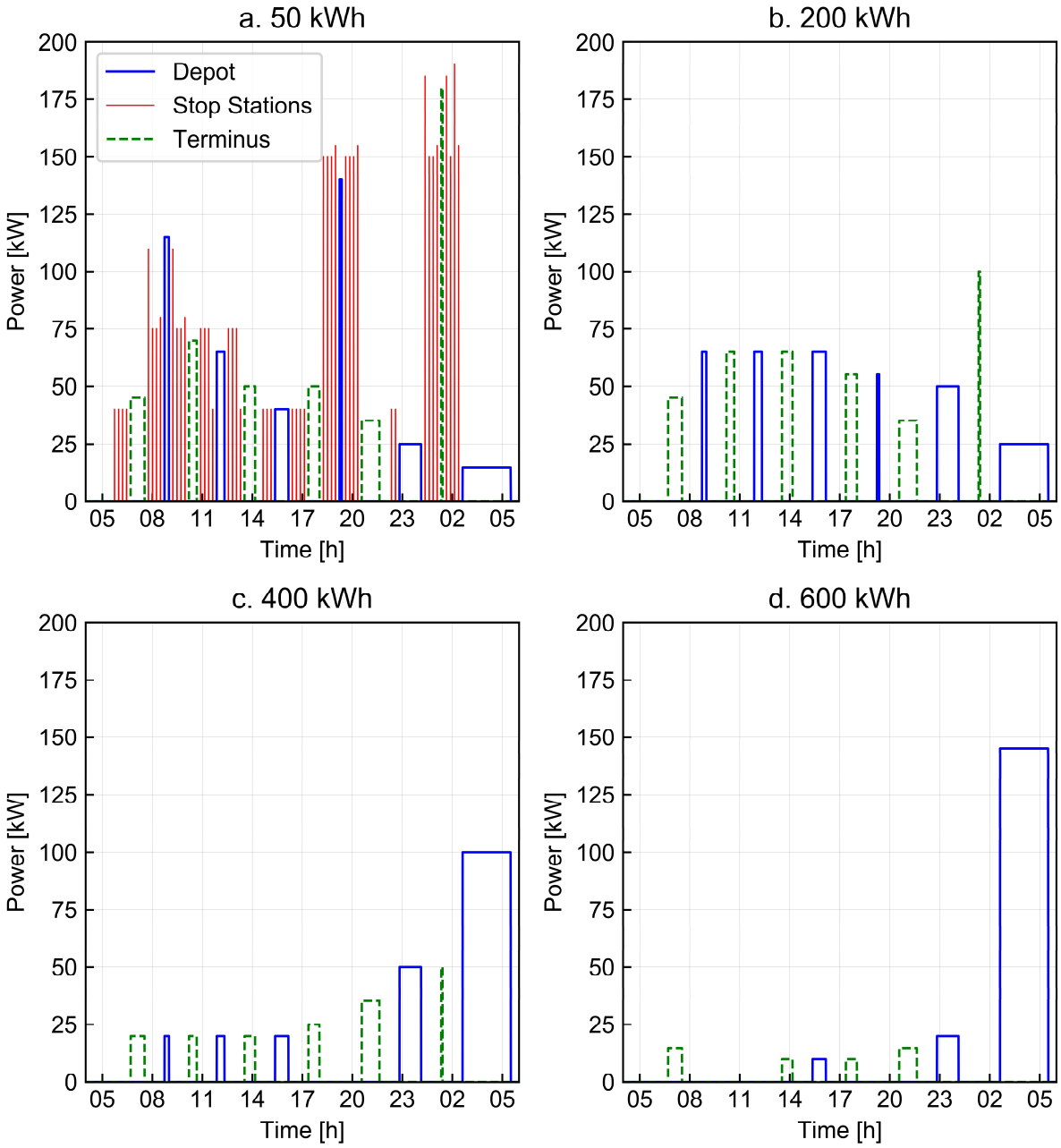


Figure 5.3: Optimal charging strategy at different battery sizes (BEB number 1 - Month of January)

In addition, the charging power highly fluctuates during the day as shown in panel (a) due to the varying daily operating conditions, and thus the varying daily BEB energy needs. The maximum charging power at the depot and the terminus is recorded around 09 hh and 19 hh as

shown in panel (a) of Figure 5.3. These times represent the peak hours during the day with the highest traffic congestion levels and the highest passengers' load, thus, the highest BEB energy demand. Furthermore, during such peak hours, the BEBs schedule is very tight, which reduces the BEB dwell time at the depot or the terminus, and thus reducing the BEB available charging time. These two factors result in a high-power charging during peak hours. Another high charging power event is observed at 01 hh (+1) mainly due to the extremely cold weather conditions at this time during the day.

For the presented BEB, the BEB is out of service after 02:30 hh mm and it is parked at the depot. At this stage, overnight charging takes place at low power as shown in panel (a) as the BEB is charged at 15 *kW* for almost 3 hours. The charging power during the night is much lower when compared to the daily charging power mainly due to the longer available charging time.

On the other hand, panels (b), (c), and (d) of Figure 5.3 show the optimal charging strategies at 200-*kWh*, 400-*kWh*, and 600-*kWh* battery sizes respectively for BEB number 1 during the month of January as well. At these battery sizes, optimal charging strategies take place only at the depot and the terminus ignoring charging along the route at the stop stations. This is due to the high-power charging at the stop stations that accelerates battery aging, and thus increases battery replacement costs. It is clear from Figure 5.3 that the charging frequency during the day decreases as the battery size increases. The charging frequency for the 200-*kWh* battery is 11 charging events during the day, 9 daily charging events for the 400-*kWh* battery, and 6 for the 600-*kWh* battery. The reason behind this decrease in the charging frequency during the day at larger battery sizes is due to the high initial battery energy level at the start of the day.

In addition, smaller battery sizes are charged at higher power during the day as the 200-*kWh* battery records a maximum charging power of 100 *kW* during the day. This value decreases to 50 *kW* for the 400-*kWh* battery and barely 20 *kW* for the 600-*kWh* battery. Despite their almost similar energy needs during the day, large batteries are charged at lower power when compared to smaller batteries due to their high initial energy level at the start of the day. With a higher initial battery energy level, the needed amount of energy to be charged decreases, which allows slower charging.

On the contrary, overnight charging (after 02:30 hh mm) takes place at higher power for larger batteries as presented in Figure 5.3. The 600-*kWh* battery is charged at 150 *kW* during the night. This value decreases to 100 *kW* for the 400-*kWh* battery and, 25 *kW* for the 200-*kWh* battery.

This is due to the lower energy charged during the day for BEBs with large batteries, and also considering that the energy needs are almost similar at the different battery sizes. BEBs with large batteries favor night charging due to the lower imposed electricity energy tariffs at night when compared to the electricity energy tariffs during the day as presented in this case study. BEBs with large batteries can supply the BEB energy needs during the day and with minimal charging due to their high initial energy level. This allows night charging at reduced electricity tariffs, and thus reducing the energy costs. However, charging solely at night may result in a very high charging power which accelerates battery aging, and thus increases the battery replacement costs. For this sake, a certain amount of energy is charged during the day in order to reduce the charging power at night. This results in increased energy costs. On the other hand, day charging is limited to a low amount of energy per charging event due to the short charging duration. Thus, the optimal charging strategy at each battery size finds the best trade-off between energy costs and battery replacement costs. Figure 5.4 shows the optimal charging power profile for BEB number 1 during the month of January at a 500-*kWh* battery size with and without considering battery aging. If the battery replacement is not considered in the DP cost function, the overnight charging event takes place at a higher charging power around 120 *kW*, in comparison to 110 *kW* when battery replacement cost is considered. This reduces the total energy cost as more energy is being charged at night and at low electricity tariff.

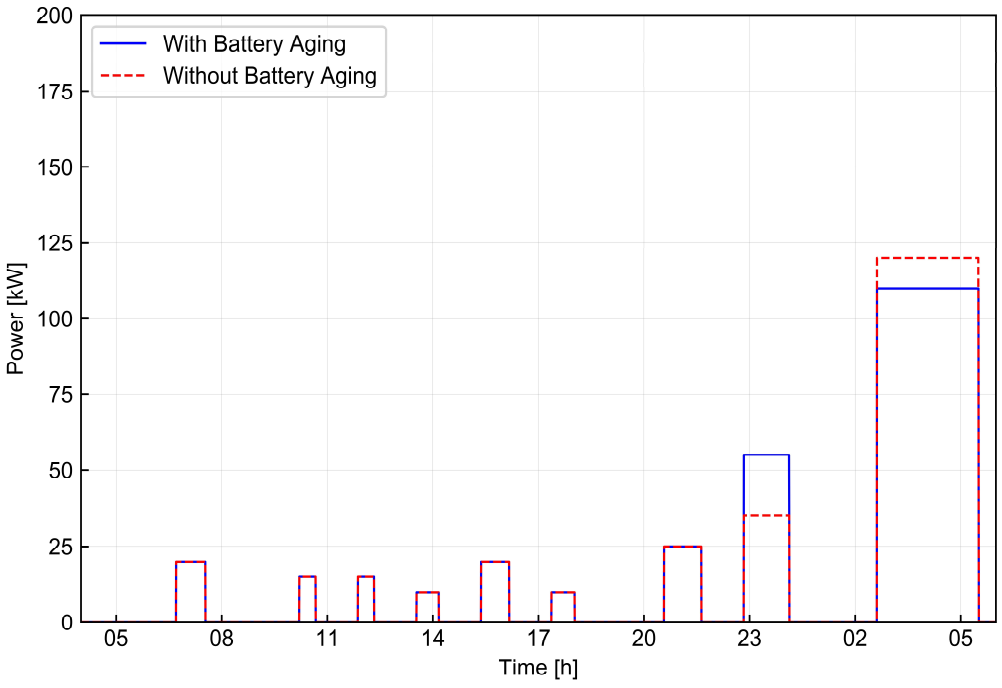


Figure 5.4: Optimal charging power profile for BEB number 1 during the month of January at a 500 *kWh* battery size with and without considering battery aging

Figure 5.5 shows the optimal energy and battery replacement costs at different battery sizes for BEB number 1. The energy costs follow a cubic polynomial behavior function of the battery size. For a very small battery size (50-100 *kWh*), the energy costs increase from 0.319 *€/km* to 0.321 *€/km* followed by a decrease until 0.3 *€/km* at 450 *kWh* battery size, which is approximately a 7% decrease in the energy costs. The energy costs increase again for battery sizes higher than 450 *kWh* reaching 0.31 *€/km* at 600 *kWh* (3.3 % increase). On the other hand, battery replacement costs follow a quadratic polynomial behavior function of the battery size. For small battery size (50-150 *kWh*), the battery replacement costs increase from 0.08 *€/km* to 0.12 *€/km,* which represents a 50% increase in the battery replacement costs. The battery replacement costs decrease for battery sizes larger than 150 *kWh* until it reaches 0.03 *€/km* at 600 *kWh*, which represents a 75% reduction in the battery replacement costs.

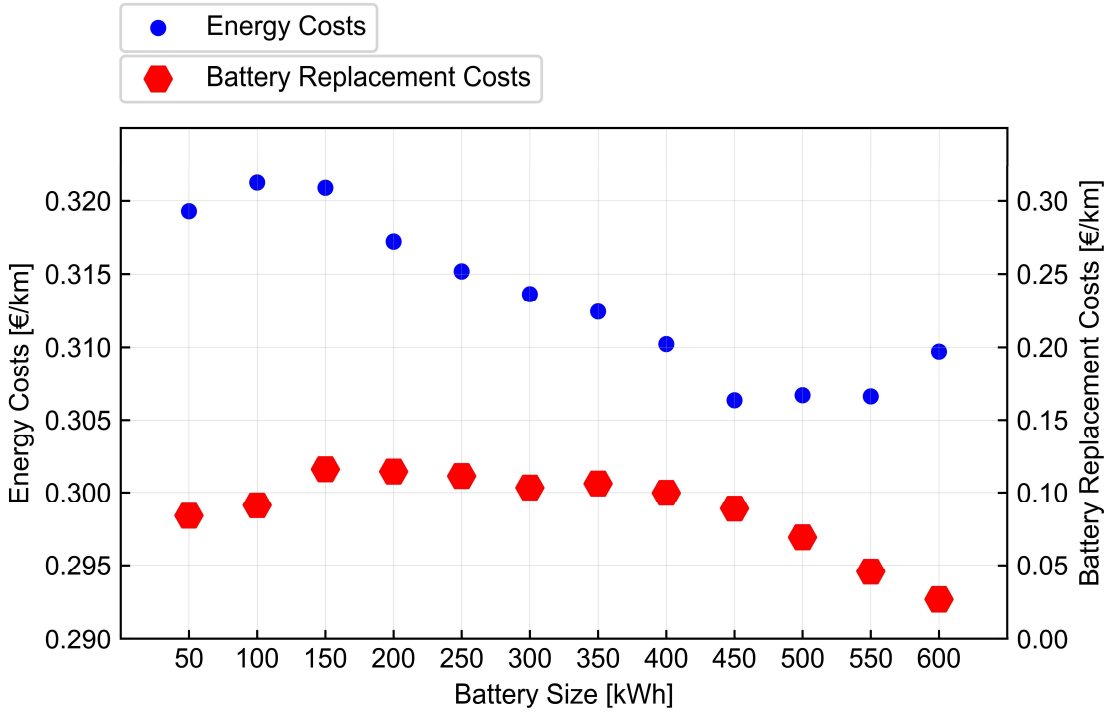


Figure 5.5: Optimal energy and battery replacement costs at different battery sizes

The trends observed in Figure 5.5 are explained in the following subsections.

5.4.2.1.1 Energy Costs

Two main opposing factors drive the energy costs:

- BEB energy consumption increases for large batteries due to the additional battery weight and additional cooling needs, which increases the energy costs.

- BEBs equipped with large batteries favor night-charging over day-charging which takes place at low electricity tariffs. This decreases energy costs.

Figure 5.6 shows the BEB energy consumption at different battery sizes where the error bars represent the variation in the BEB energy consumption due to the different daily operating conditions, and the red circular markers represent the average energy consumption across the different daily operating operations. It is clear that BEB energy consumption increases at large battery sizes due to the additional battery weight and cooling needs. For a BEB equipped with a 50-*kWh* battery, the BEB average energy consumption records 3.5 *kWh/km*. This value increases at 600-*kWh* battery size reaching 4 *kWh/km* recording a 15% increase in energy consumption.

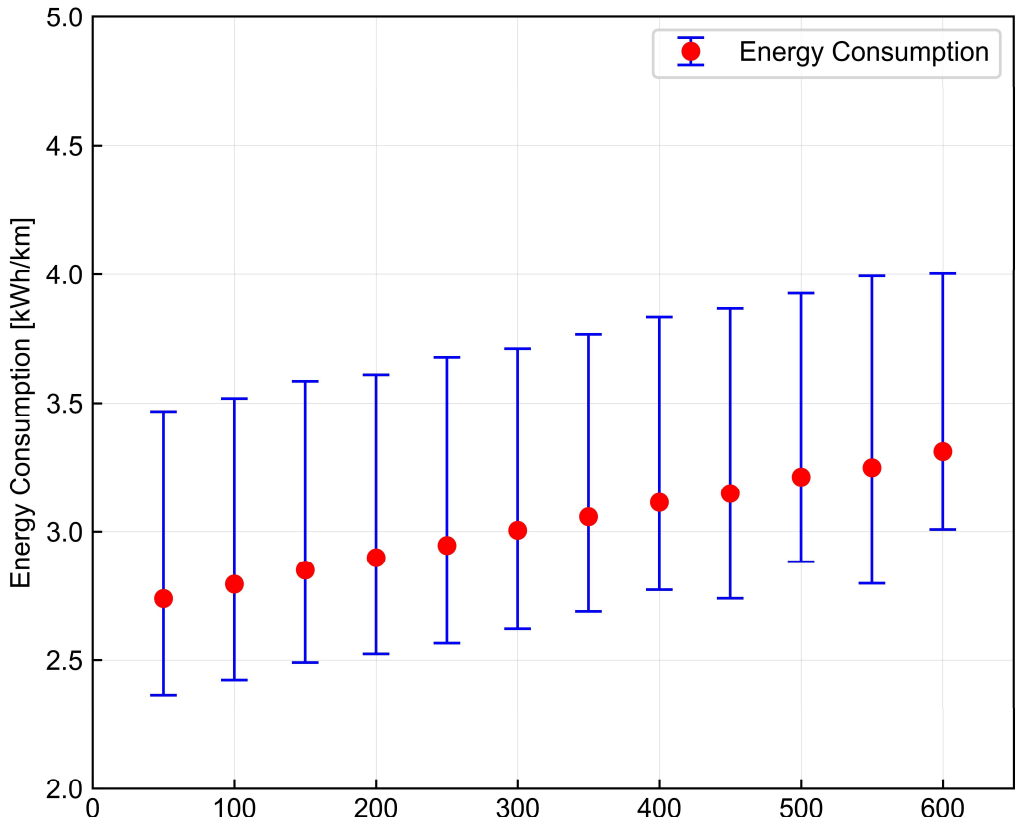


Figure 5.6: BEB energy consumption at different battery sizes

On the other hand, Figure 5.7 shows the day and night charging energy distribution at different battery sizes for 1 day of operation. The blue and red bars represent the average daily charging energy during the day and night and the error bars represent the variation in the BEB energy consumption due to the different daily operating conditions. It is important to mention that night charging is considered as any charging event that takes place during the off-peak hours (after

23 hh in this case) including the overnight charging event. As the battery size increases, the amount of day charging energy decreases whereas the amount of night charging energy increases. A BEB equipped with a 50-*kWh* battery charges 85% of its daily energy needs during the day, whereas a 600-*kWh* battery charges only 5% of its daily energy needs during the day taking advantage of the reduced electricity tariffs at night.

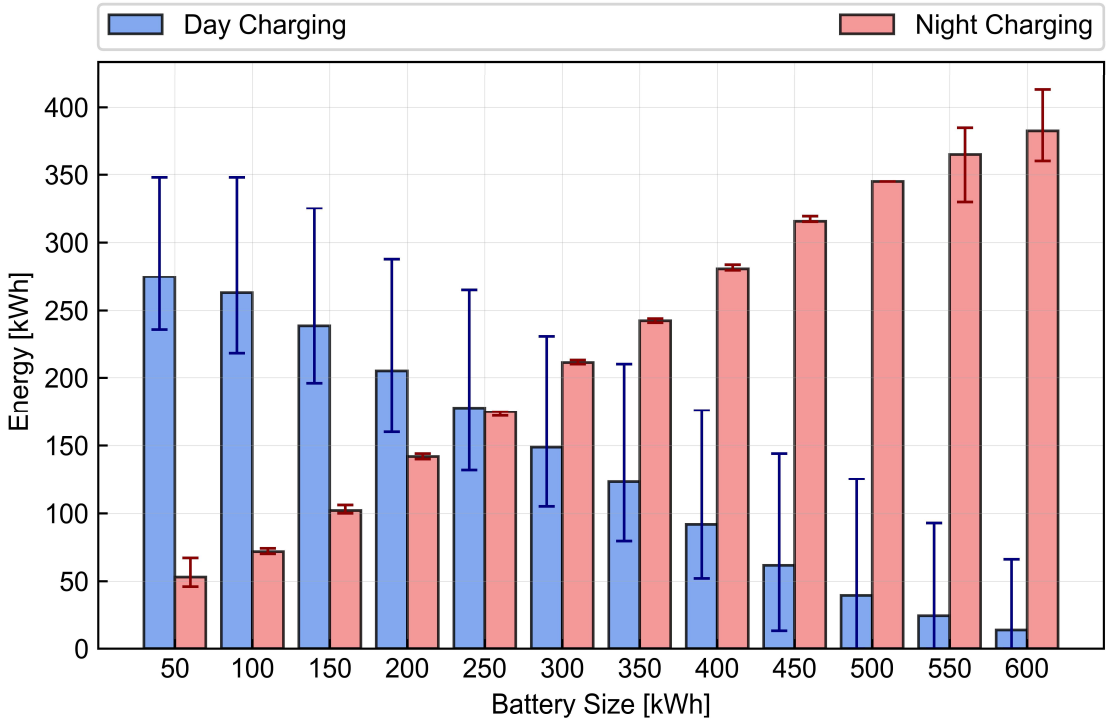


Figure 5.7: Day and night charging energy distribution at different battery sizes

Two opposing factors drive the optimal energy costs at each battery size as observed in Figure 5.5: (1) the energy consumption which varies as function of the battery size, and (2) the charging energy distribution during (day/night) at different electricity tariffs.

- For small battery sizes less than 100 *kWh*, the BEB energy consumption is the lowest, however, the majority of charging takes place during the day at a high electricity tariff. As the battery size slightly increases from 50 to 100 *kWh*, the energy costs increase as the increase in the energy consumption for larger battery sizes dominates the energy cost reduction due to charging more energy at night at reduced tariffs. This is due to the very low amount of energy to be charged at night (15-20% of the total BEB energy needs during the day).
- For battery size between than 100 - 450 *kWh,* the energy costs are reduced further as the impact of charging at night outweighs the increase in energy consumption with larger

batteries. 25-80% of the BEB energy needs are charged at night, outweighing the increased energy consumption.

- Finally, at very large battery sizes (above 450 *kWh*) the increase in the energy consumption overweighs the benefits of increased night charging at reduced electricity tariffs resulting in increased energy costs. Even though 85-95% of the BEB energy needs are charged at night at reduced electricity tariffs, the very large battery size is resulting in increased energy costs mainly due to the large battery weight and high cooling needs.

Figure 5.8 summarizes the energy costs variation at different battery sizes.

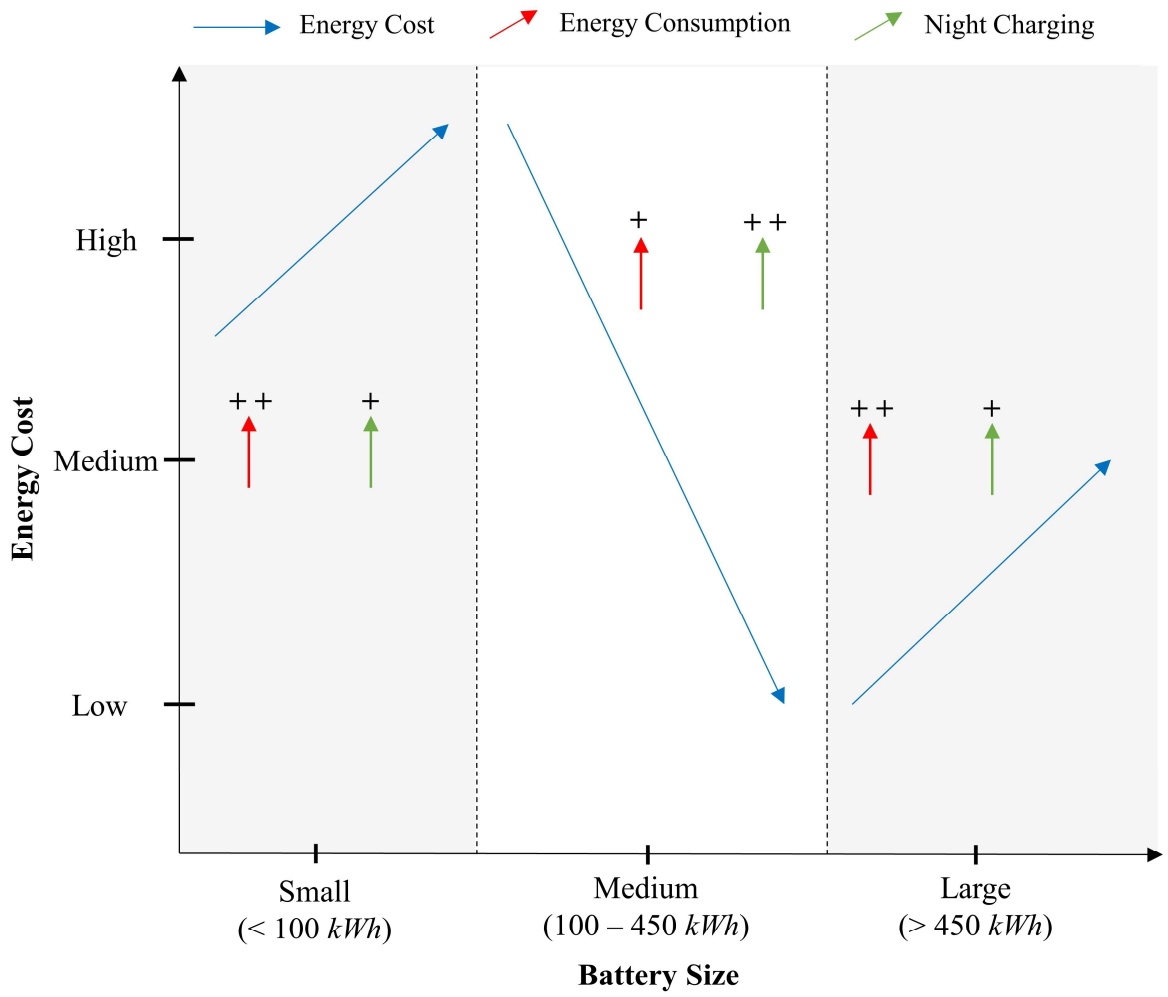


Figure 5.8: Summary of energy cost variation at different battery sizes

It is clear in the figure that there are 3 main regions each corresponds to a certain range of battery sizes. For each region, the energy cost trend as function of the battery size is different, driven by the 2 main factors impacting the energy cost: (1) energy consumption and (2) night-charging energy at reduced tariffs. For each region, one factor dominates the other and drives

the energy cost trend. A factor associated with two plus (+ +) signs in each region in the figure is the dominant factor.

5.4.2.1.2 Battery Replacement Costs

The battery replacement costs are affected by 2 opposing factors: (1) the frequency of battery replacement and (2) the cost of the battery pack.

The battery replacement costs are directly related to the frequency of battery replacement over the considered optimization period. Figure 5.9 shows the battery normalized capacity at different battery sizes. The battery is considered to reach its end of life when the battery capacity reaches 80% of its initial capacity. The 80% limit is highlighted with the red dashed line shown in the figure below. As the battery size increases, the battery life increases which reduces the battery replacement costs. A 50-*kWh* battery reaches its end of life after 1080 days (~ 3 years), whereas a 200-*kWh* battery reaches its end of life after 5.8 years. This number increases to 9.12 years at a 400-*kWh* and 11 years at 600 *kWh*. Thus, larger batteries require less frequent replacement which reduces their battery replacement costs.

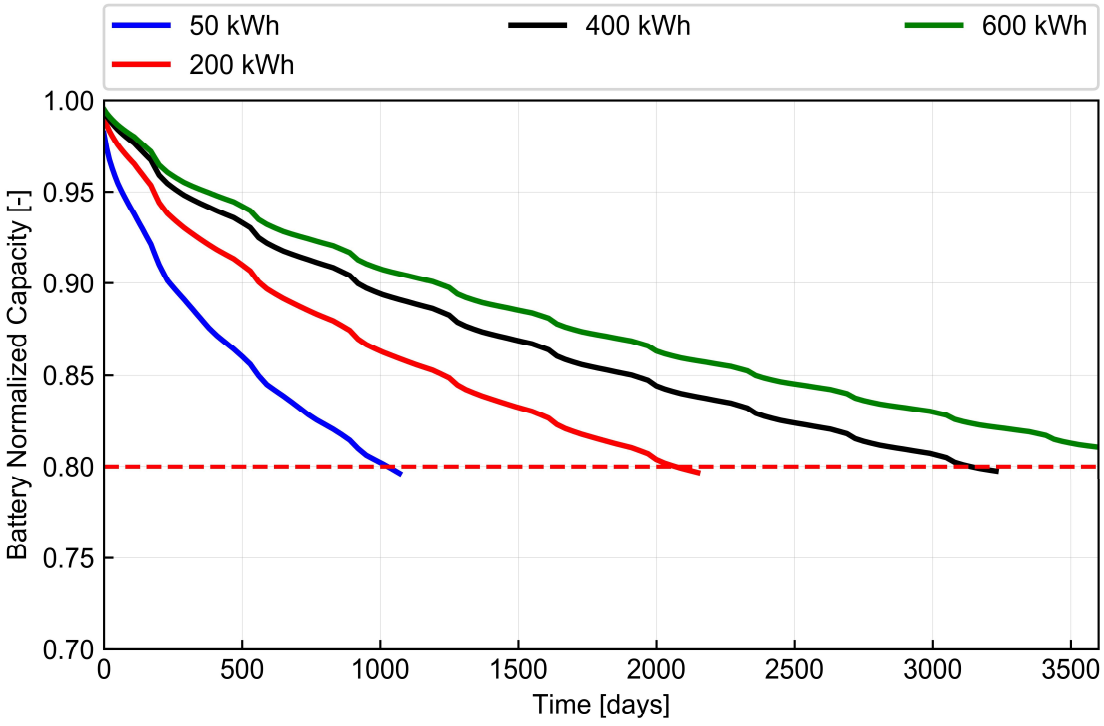


Figure 5.9: Degradation of battery capacity as function of time at different battery sizes

There are 2 main reasons behind the accelerated battery aging phenomenon for smaller batteries: (1) charging power per battery cell and (2) charge throughput per battery cell.

The charging power per battery cell could be normalized to better compare batteries with a different number of cells (i.e. different sizes). This is represented by the battery C-Rate. The C-Rate is the charge/discharge rate and it is presented in Figure 5.10 at different battery sizes.

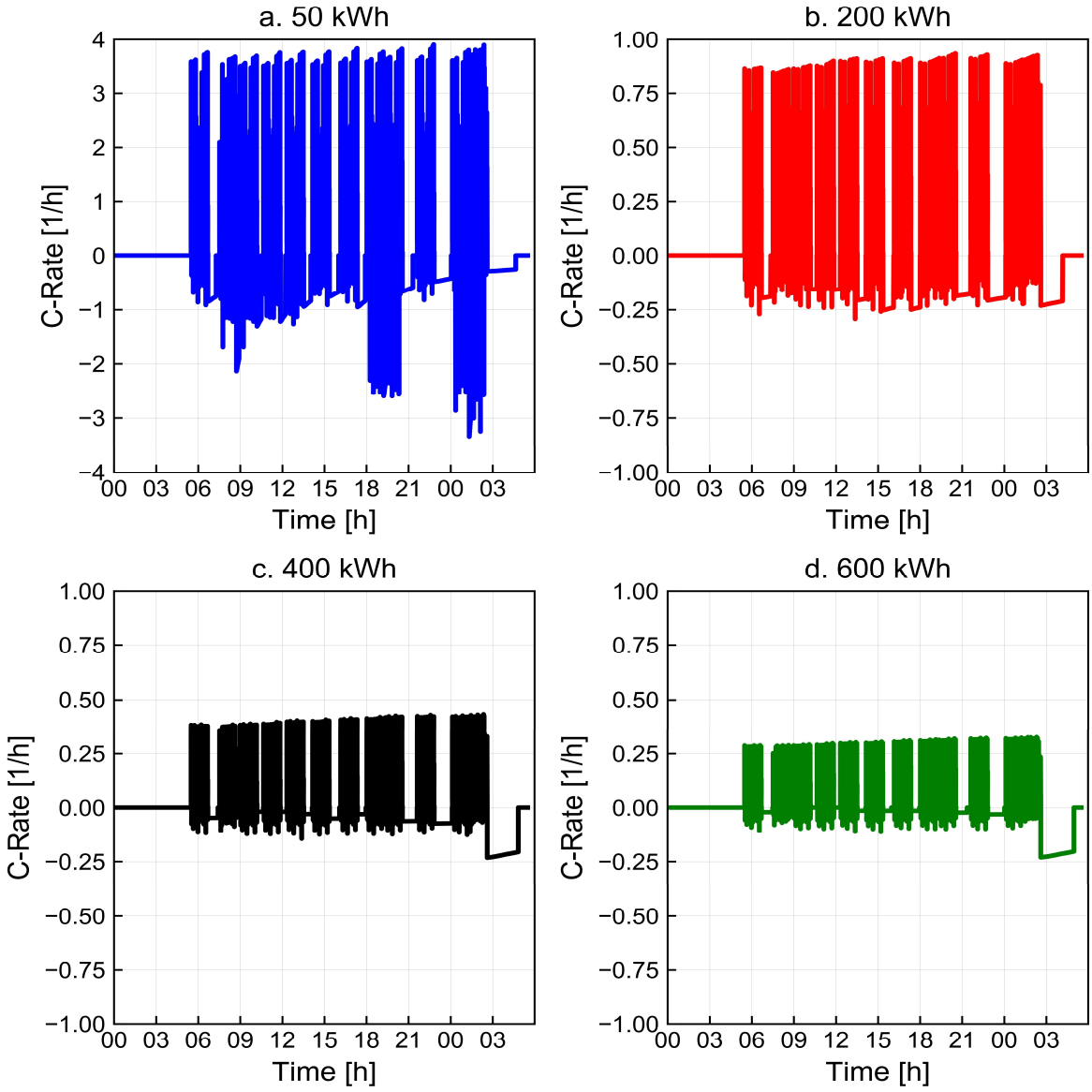


Figure 5.10: Charge/discharge rate function of time for different battery sizes (BEB number 1 - Month of January)

A positive C-rate implies battery discharging and a negative C-rate implies battery charging. Starting with battery discharging (C-rate >0), mainly all battery sizes share the same discharge power profiles (with slight variations due to the additional battery weight and cooling needs) as they all operate under the same operating conditions. However, smaller battery sizes contain a lower number of battery cells, thus the power load per cell is higher, resulting in high positive

C-rates at smaller battery sizes as shown in Figure 5.10. A 50-*kWh* battery records a maximum C-rate of 4, whereas this value decreases to 0.4 for a 600-kWh battery. Higher values of the C-rate accelerate battery aging mainly due to the increased battery cell temperature at high C-rate. As for battery charging, a similar analysis applies as the negative C-rate is going to be higher (in absolute terms) for smaller batteries. In addition, smaller batteries are being charged at higher power during the day, increasing the charging C-rate further, and thus worsening the battery aging phenomenon for small batteries.

The other factor that affects battery aging is the charge throughput per battery cell. The charge throughput can be represented by the average number of daily cycles per battery cell. Cycles include both charging and discharging of the cells. Figure 5.11 shows the average daily number of cycles per battery cell at different battery sizes. The average daily number of cycles decreases as the battery size increases due to the higher number of cells for large batteries, which reduces the charge throughput per battery cell. A higher number of cycles accelerates battery aging and in particular battery cycle aging.

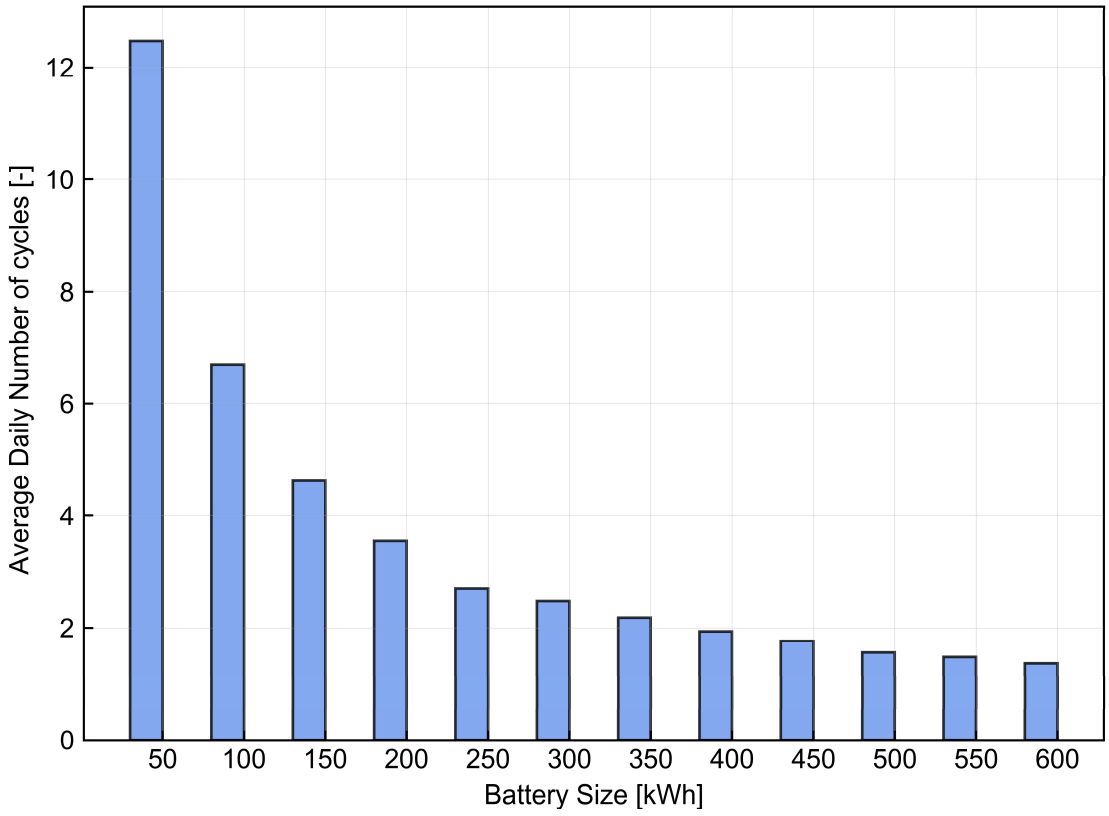


Figure 5.11: Average daily number of cycles per battery cell at different battery sizes

As for the battery pack costs, trivially larger batteries incur high battery costs.

That being said, the two main factors driving the battery replacement cost are the (1) frequency of battery replacement and (2) battery cost.

- for large batteries above 200 *kWh*, the battery replacement frequency decreases due to the slow aging phenomenon that takes place. This overweighs the high battery pack costs for large batteries. Thus, battery replacement cost decreases as the battery size increases.
- For small battery sizes between 50 – 200 *kWh*, battery replacement cost increases. Despite the low battery pack costs at such battery sizes, the high battery replacement frequency is dominant, and it increases the battery replacement costs.

Figure 5.12 summarizes the battery replacement cost variation at different battery sizes.

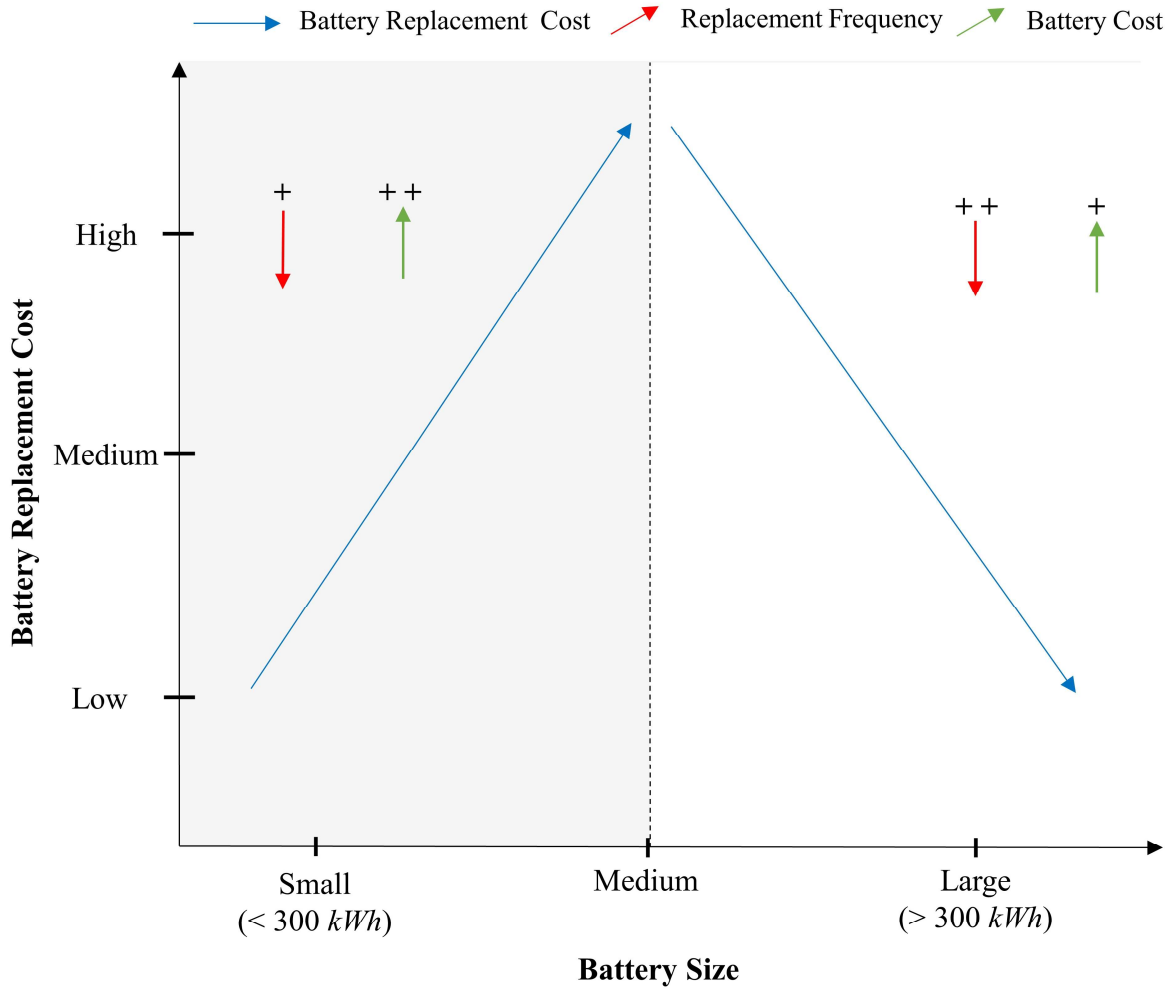


Figure 5.12: Summary of battery replacement cost variation at different battery sizes

Two main regions are highlighted in this figure each corresponds to a certain range of battery sizes. The battery replacement cost behavior as function of the battery size is different across the two regions, and this is mainly due to the two opposing factors impacting the battery

replacement cost: (1) battery cost and (2) frequency of battery replacement. For each region, one factor is dominant over the other and drives the battery replacement cost trend. A factor associated with two plus (+ +) signs in each region in the figure is the dominant factor.

That being said, optimization step 1 (DP) minimizes the total energy and battery replacement costs at different battery sizes by optimally controlling the daily charging strategy per BEB throughout its entire operation during the year.

In what follows, the results of optimization step 2 (GA) are presented showing the optimal battery size for each BEB operating along the line and the corresponding needed charging infrastructure.

5.4.2.2 Optimal Battery Size and Charging Infrastructure

Figure 5.13 shows the optimal battery size for each BEB operating along the line proposed in this case study. Out of the 20 BEBs operating along the line, 13 BEBs should be equipped with 90-100 *kWh* batteries, 6 BEBs to be equipped with 70-80 *kWh* batteries, and a single BEB with a 60-*kWh* battery. The optimal battery size for each BEB is highly dependent on its schedule and its energy consumption during the day, which varies from one BEB to another despite their operation along the same line.

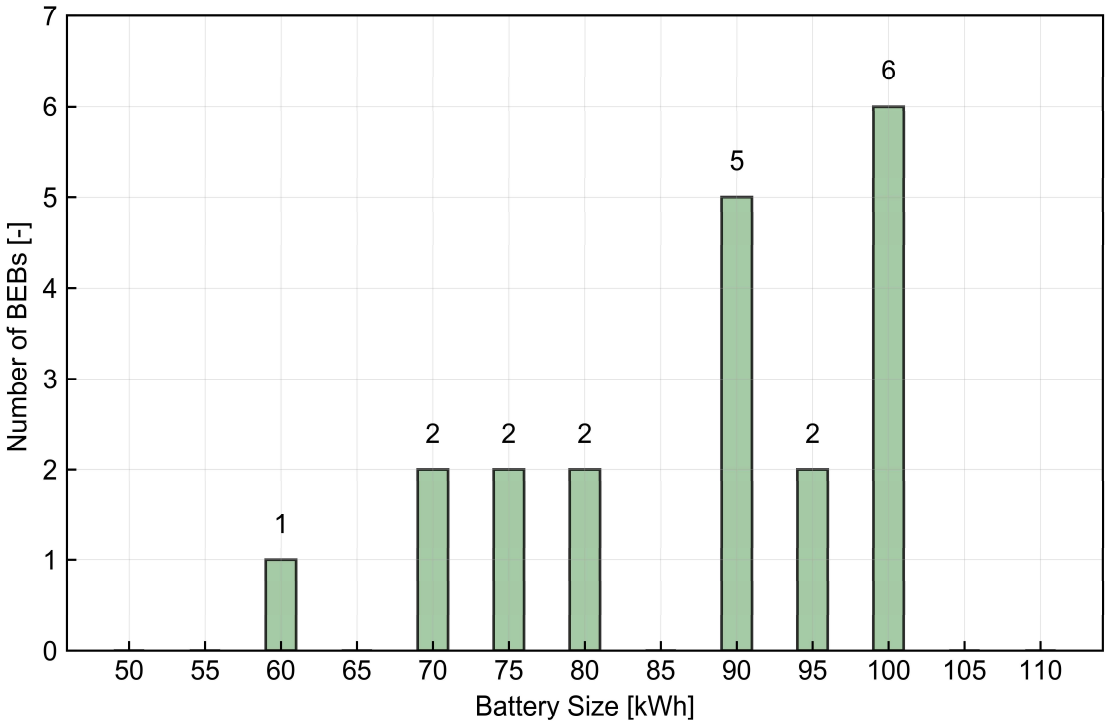


Figure 5.13: Optimal battery size for each BEB

In addition, Figure 5.14 shows the optimal required charging infrastructure for the BEB line proposed in this case study. 20 chargers should be installed at the depot with their power rating ranges between 65-95 *kW* where the majority of these chargers are rated at 70 *kW*. 7 additional chargers to be placed at the terminus as well and their power rate ranges from 100-115 *kW*. No chargers to be installed at the stop stations. Note that Appendix I verifies the optimality of the chosen solution by the GA algorithm as it shows the resulting optimal solution at different initial conditions.

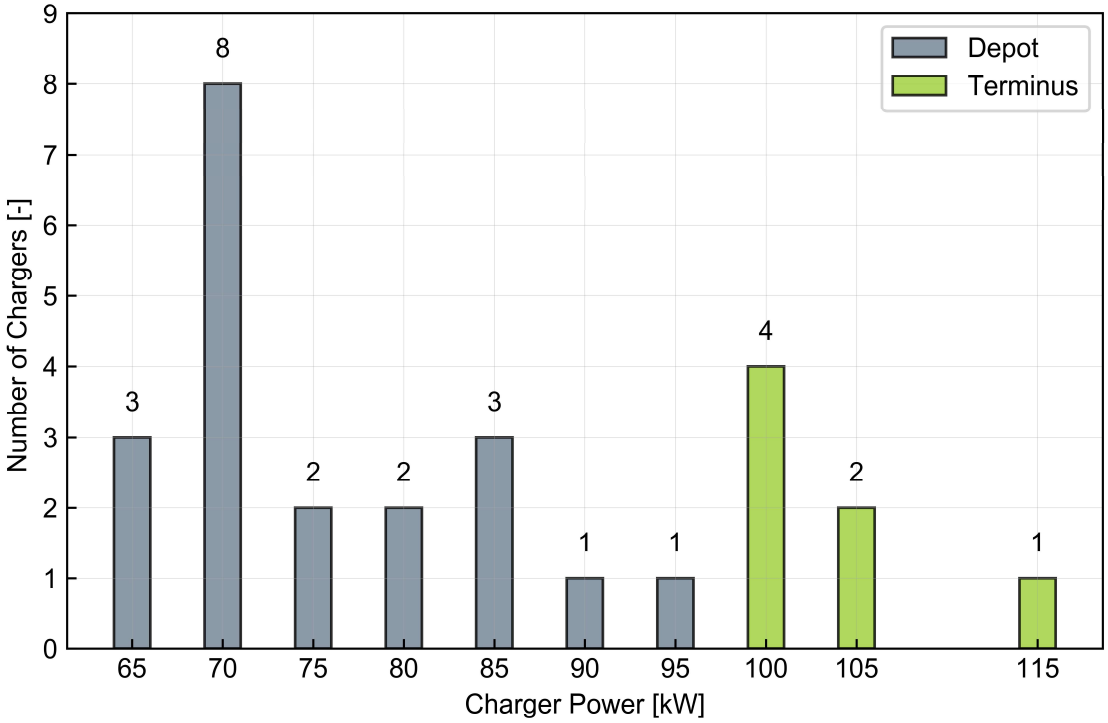


Figure 5.14: BEB line optimal required charging infrastructure

In order to analyze the choice of the optimal battery sizes and the corresponding required charging infrastructure, it is essential to study the TCO at different battery sizes. Figure 5.15 presents the TCO variation as function of battery size. To simplify the analysis, it is assumed that all BEBs are equipped with the same battery size, i.e., a battery size on the horizontal axis of Figure 5.15 represents the battery size of all the BEBs operating along the line.

As shown in Figure 5.15, the TCO decreases from 2.27 to 2.157 *€/km* (~ 6% reduction) as the battery size increases from 50 kWh to approximately 100 *kWh*. At 100 *kWh* battery size, the TCO reaches its minimum and starts increasing afterward continuously until it reaches 2.87 *€/km* (~ 34% increase) at 600 *kWh* battery size. The resulted optimal solution of battery sizes presented earlier in Figure 5.13 records a TCO equals to 2.14 *€/km* as shown in the bar plot

situated at the bottom right of Figure 5.15. This value is lower than the minimum recorded value of 2.157 *€/km* at the 100-*kWh* battery size mainly since each BEB is equipped with different battery size.

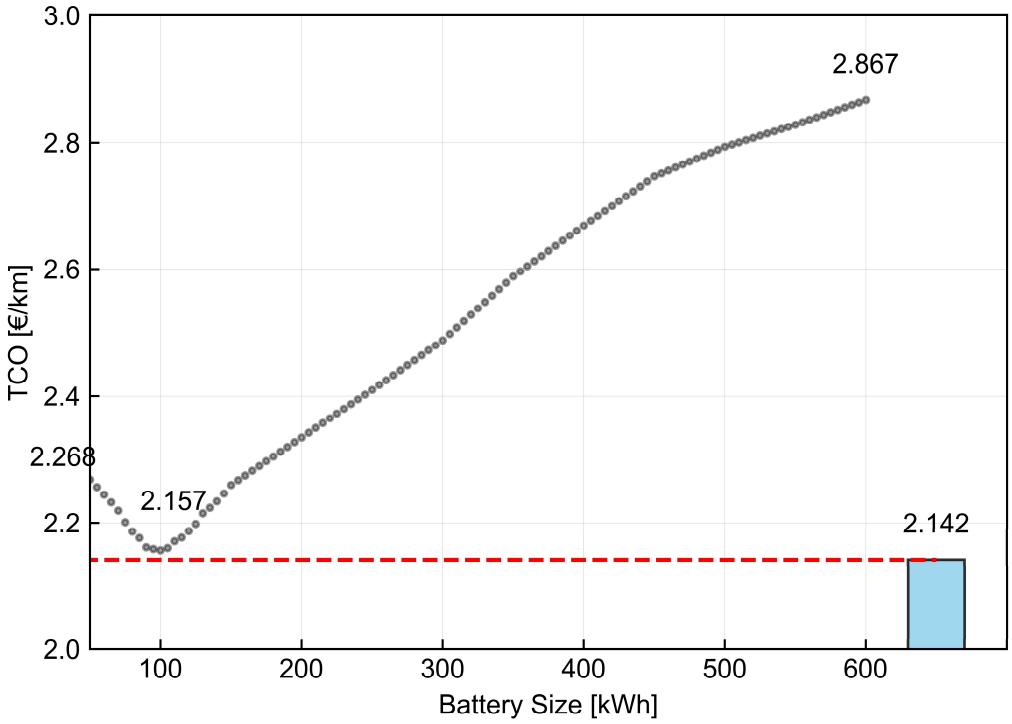


Figure 5.15: Variation of TCO function of battery size

Figure 5.16 shows the TCO segmentation and the different cost components to better understand the behavior of the TCO at different battery sizes. Panel (b) of Figure 5.16 shows the bus unit cost (including the battery cost) function of the battery size. The unit cost linearly increases with the increase in battery size. It ranges from 1 *€/km* at 50 *kWh* battery size to 1.6 *€/km* at 600-*kWh* battery size. The unit cost could represent 45-55 % of the TCO, which is the biggest portion of all the other cost components. The optimal solution presented in the bar plot records a unit cost equals to 1.029 *€/km* as most of the optimal battery sizes are below 100 *kWh*.

On the other hand, panel (c) of Figure 5.16 shows the infrastructure cost variation as function of battery size. For very small battery sizes, the infrastructure cost reaches 0.3 *€/km* at 50-*kWh* battery size mainly due to the fast chargers needed at the stop stations for such small battery sizes. The infrastructure costs decrease as the battery size increases and it reaches 0.1 *€/km* (67% reduction) at 250 *kWh* battery size. At such average battery sizes (100-300 *kWh*), end-line charging is favored at the depot and the terminus, thus charging takes place at relatively lower power when compared to smaller battery sizes. This results in reduced chargers' power

rates and thus reduced infrastructure costs. For battery sizes above 300 *kWh*, infrastructure costs increase reaching 0.15 *€/km* at 600 *kWh* battery size (50 % increase). This increase in infrastructure costs is justified by the fact that large batteries favor night charging at the depot rather than frequent day-charging, and thus the entire energy needs are charged at night and at relatively high power. This results in increased infrastructure costs (refer back to Figure 5.3). The infrastructure costs represent 5-15% of the TCO.

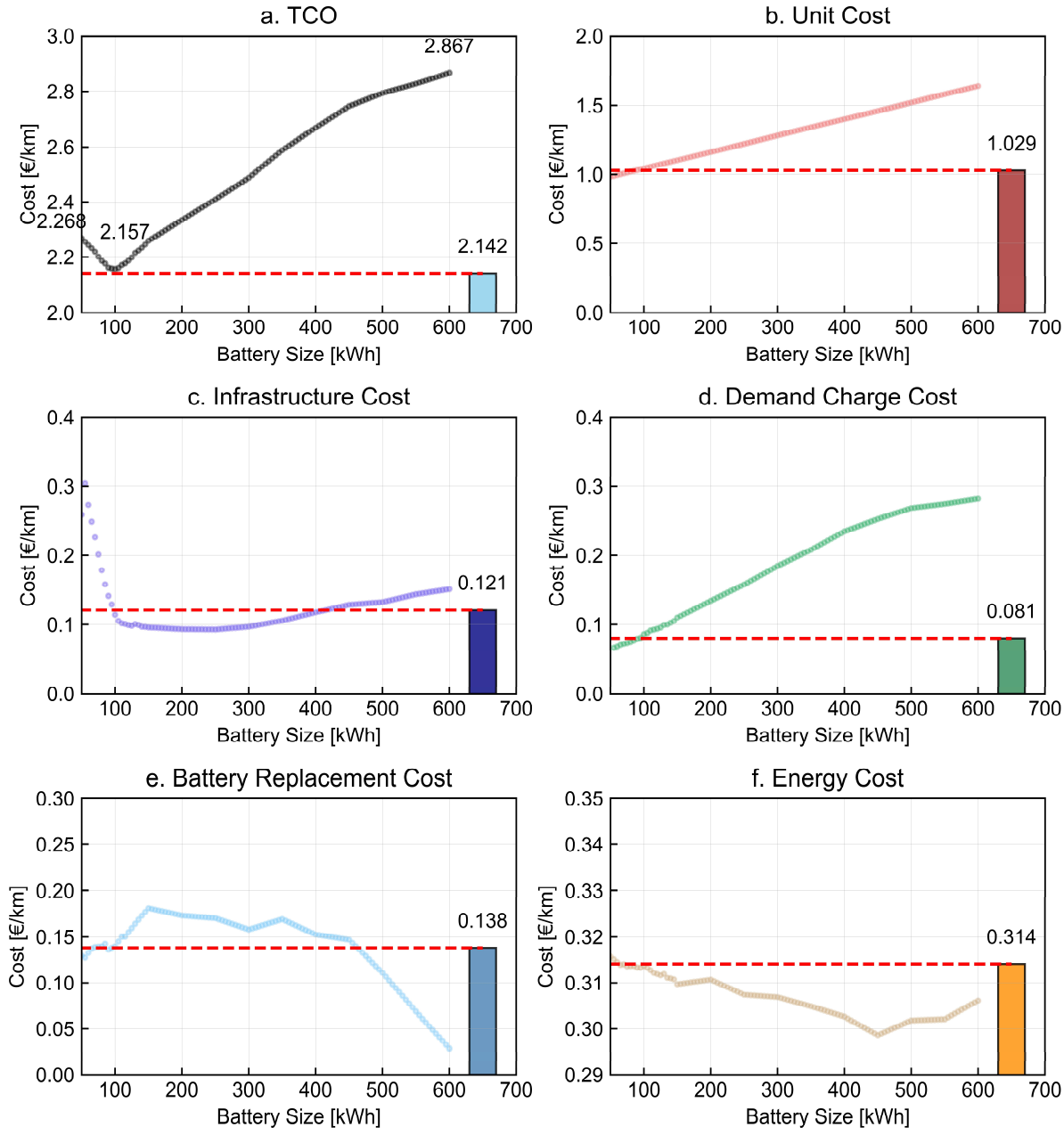


Figure 5.16: TCO segmentation and components

The demand charge cost component is not negligible, and it could exceed the infrastructure, costs especially at large battery sizes. The demand charge costs are strictly increasing as the

battery size increases. Even though smaller batteries are charged at higher power, these batteries record the lowest demand charge cost. The demand charge cost is the cumulative power demanded by the BEB line from the electricity network. As battery sizes increase, the BEBs will be charged at the terminus and the depot, and mainly multiple BEBs are charged simultaneously resulting in increased demand charge costs. On the other hand, charging smaller batteries at the stop stations (opportunity charging) takes place one BEB at a time, and thus the demand charge is lower despite the higher charging power per BEB. For very large battery sizes, the demand charge costs record 0.3 *€/km* representing 10% of the TCO.

5.4.2.3 Impact of Schedule on Optimal Battery Size

The optimal battery size for each BEB along the line is different due to several factors, mainly the BEBs schedule and their energy consumption. During the day, each BEB completes a certain number of trips and at varying operating conditions resulting in different energy consumption for each BEB during the day. However, the BEBs schedule has a higher impact on the battery size as it determines the available charging time during the day as well.

The optimal battery sizes for the BEBs presented in Figure 5.13 are plotted as function of the minimum dwell time at the depot/terminus as shown in Figure 5.17. The minimum dwell time is determined by each BEB's schedule and it is the minimum available charging duration before a certain trip. As the minimum BEB dwell time increases, the optimal battery size decreases. For BEBs with a minimum dwell time around 5 minutes, the recorded optimal battery sizes are the highest at 90-100 *kWh*. The optimal battery size decreases to reach 60 *kWh* for BEBs with a minimum dwell time above 20 minutes.

At a very low minimum dwell time for BEBs, charging should take place at very high power increasing the infrastructure costs, demand charge costs, and battery replacement costs. Increasing the battery size prevents this high increase in these cost components as BEBs start their daily trips with higher initial energy levels (oversized batteries) reducing the charging needs during these very fast dwell times. On the contrary, longer BEB dwell time allows reducing the battery size and thus, decreasing the BEB unit cost.

For BEBs operating along the same bus line, and similar operating conditions, the optimal battery size could change by more than 40% due to schedule modifications. Normally, the bus schedule is subject to some modifications mainly between winter and summer as bus frequency and number of trips decrease during the summer. In addition, the bus daily schedule might be subject to some modifications set by the bus operator. Thus, it is essential to consider the

variabilities in the bus schedule and its impact on the choice of the optimal battery size and charging strategy. This needs further investigation.

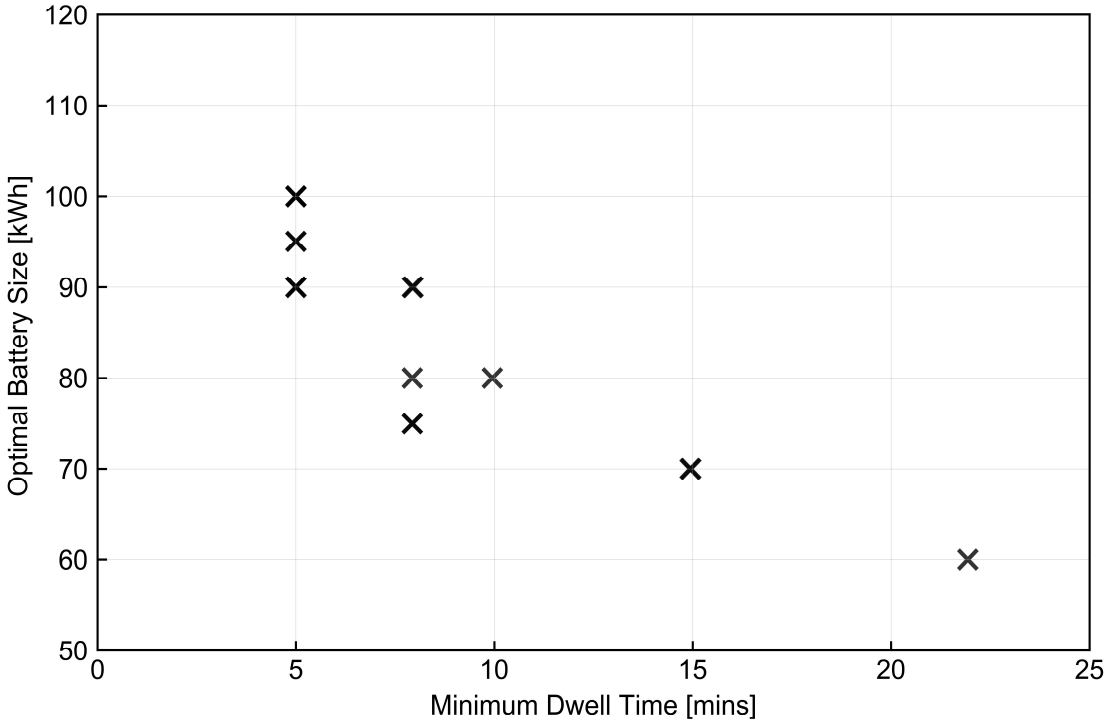


Figure 5.17: Variation of the optimal battery size per BEB as function of the minimum BEB dwell time

5.4.2.4 BEB Charging Load at Different Battery Sizes and Charging Strategies

One of the main challenges facing the massive deployment of BEB is the electric grid ability to host the additional power demand needed to charge these buses. The BEB cumulative power demand profile from the electric grid is shown in Figure 5.18 at different battery sizes (panels (a) to (e)) and the BEB cumulative power demand profile under the optimal solution resulted from the proposed optimization methodology is presented in panel (f). If all the BEBs are equipped with a 50-*kWh* battery, the maximum power demand from the grid exceeds 1000 *kW* (around 09:00 hh: mm). During the overnight charging events (after 02:00 hh: mm), the peak power demand reaches 250 *kW*. As the battery size increases from 50-600 *kWh*, the peak power demand during the day decreases from 1000 *kW* to 250 *kW*, whereas the peak power demand during the overnight charging events increases from 250 *kW* to 2600 *kW* (2.6 *MW*). This behavior complies with the analysis presented in Figure 5.3 as buses equipped with large batteries favor night charging to take advantage of reduced electricity tariffs.

Panel (f) of Figure 5.18 shows the BEB power demand under the proposed optimal solution. The proposed optimal solution is composed of different battery sizes (majority around 100 *kWh*), and the power demand from the grid is leveled with low fluctuations in the peak power during the day when compared to the other battery sizes. The proposed optimization methodology is resulting in reduced peak power demand from the grid during the day and the night, mainly due to the demand charge cost component considered in the optimization objective function.

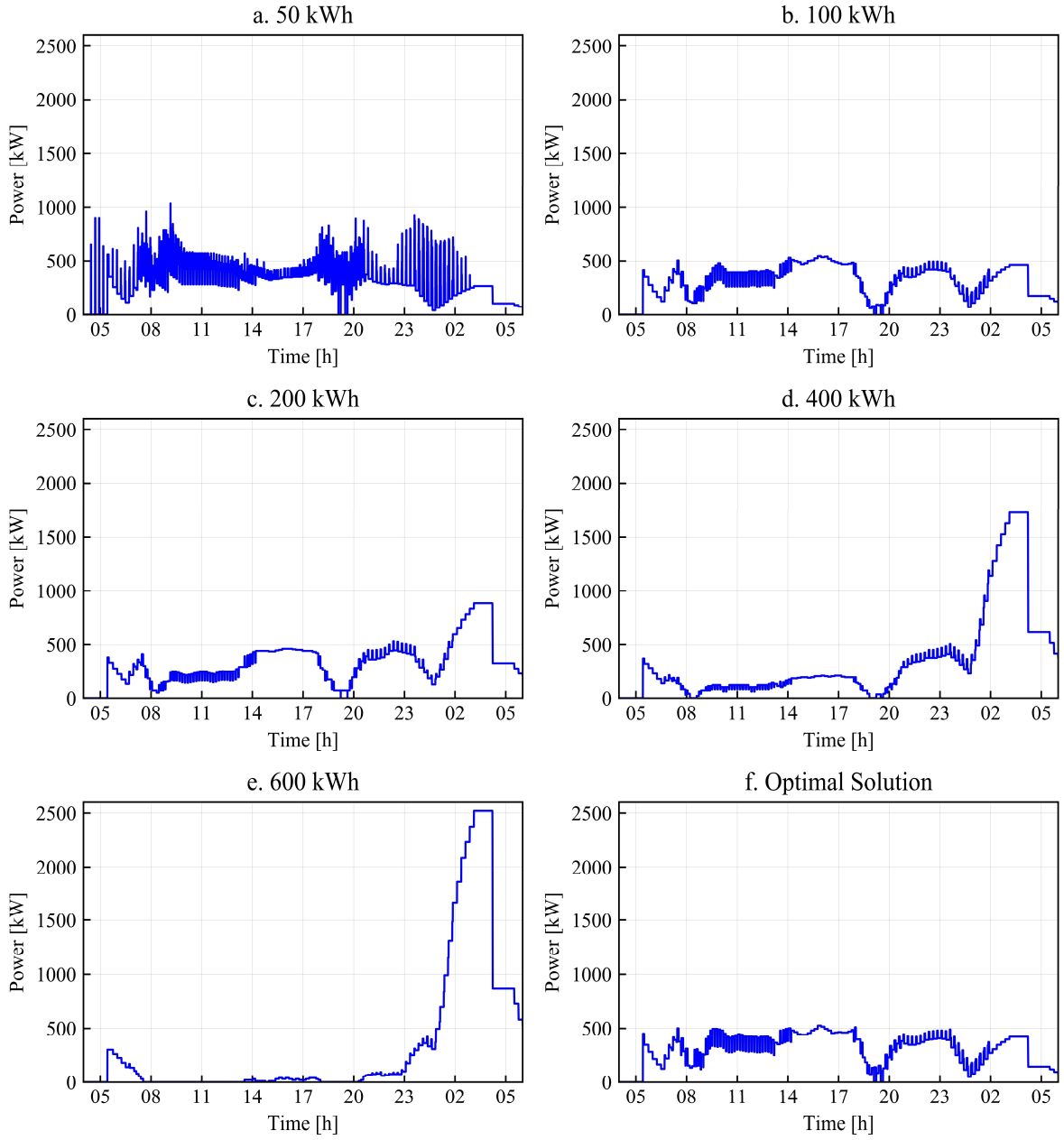


Figure 5.18: BEB cumulative power demand from the electric grid (Month of January)

The load factor is an indicative parameter that can present more insights on how leveled the charging load is. The load factor is defined as the ratio of the average power demand during the day, divided by the peak power. A high value of the load factor indicates that the power profile is well leveled, where the peak power does not deviate much from the average power demand.

Figure 5.19 shows the BEB power demand load factor at different battery sizes and under the proposed optimal solution (the bar located at the extreme right of Figure 5.19 – Load Factor = 0.447). At 50-*kWh* battery size, the load factor is around 0.2. This value increases and reaches 0.43 at 100-*kWh* battery size. Afterward, the load factor continuously decreases as battery size increases and it reaches 0.1 at 600-*kWh* battery size. For small batteries (below 100 *kWh*), high power peaks are observed during the day (between 9:00 hh: mm and 10:00 hh: mm) as previously presented in Figure 5.18 which results in a low load factor. For large batteries (above 100 *kWh*), BEBs equipped with larger batteries witness a very high power demand during the overnight charging event (after 02:00 hh: mm) as previously shown in Figure 5.18 and this also reduces the load factor.

Thus, BEBs equipped with battery sizes around 100 *kWh* result in the best load factor reaching 0.447 under the optimal proposed solution mainly due to the well-leveled power profile resulted from the proposed optimization methodology.

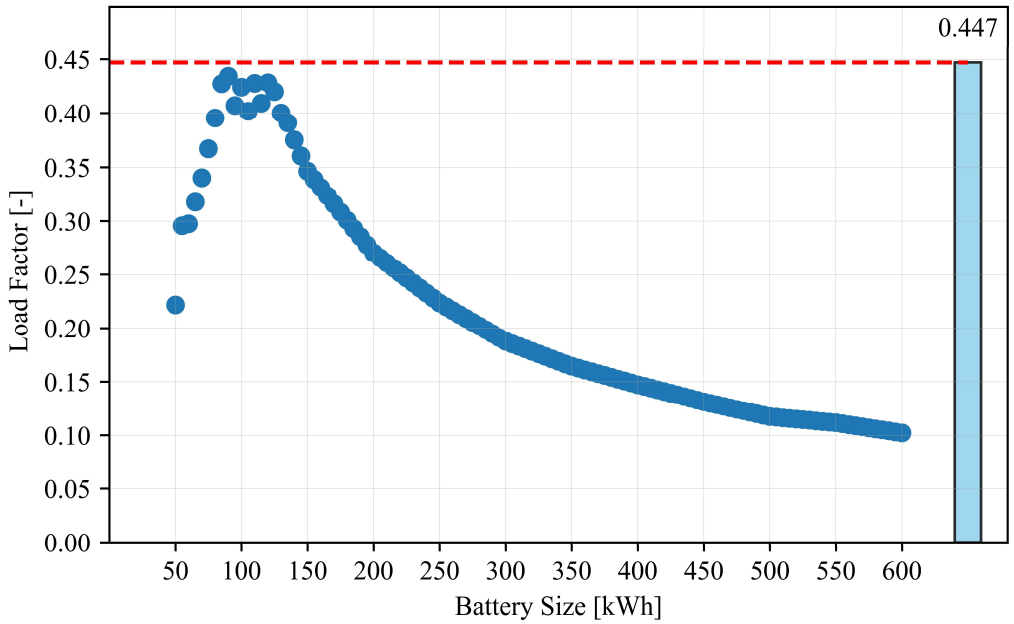


Figure 5.19: BEB power demand load factor at different battery sizes

In addition, BEB energy and charging needs highly vary as function of the different operating conditions, in particular the weather conditions. Figure 5.20 shows the optimal BEB power demand profiles from the electric grid under three different months. During January (coldest weather conditions), the peak power demand reaches 500 *kW* during the day. This value decreases to 320 *kW* for April (moderate cold), and 250 *kW* for August (moderately hot). The load factor is around 0.44 for all months under the optimal solution.

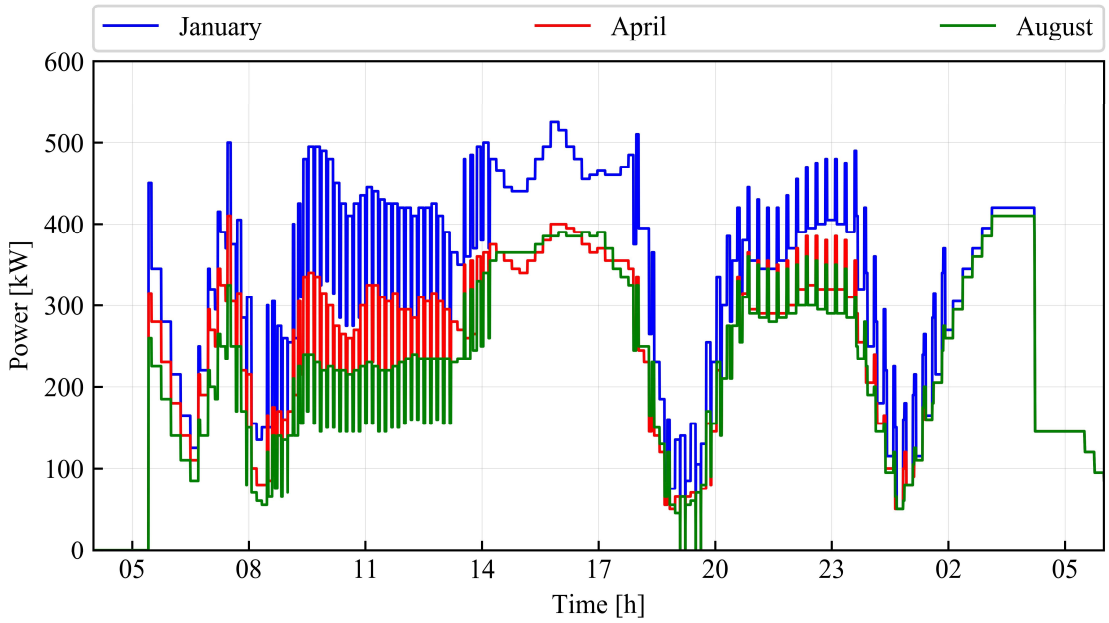


Figure 5.20: Optimal BEB power demand profiles from the electric grid under three different months

5.4.2.5 Sensitivity Analysis of the Different TCO parameters

The previously presented case study and the corresponding results are representative of a single bus line/ city. However, many parameters vary across different regions or countries, such as electricity tariffs and investment costs. In addition, several studies reveal that the cost of lithium-ion batteries and charging infrastructure is subject to continuous reduction with the recent advancements in battery and charging technologies. Furthermore, electric energy tariff highly varies from one region to another. Thus, it is interesting to conduct a parametric study by varying several cost-related parameters, in order to study their impact on the TCO of BEB deployment, optimal battery sizing, and optimal charging strategy. Based on the TCO segmentation analysis presented in Figure 5.16, the following cost parameters are considered in this parametric study: (1) Cost of Lithium-ion battery,(2) Demand charge tariff, and (3) Charger's cost.

5.4.2.5.1 Impact of Lithium-ion battery cost

The cost of Lithium-ion batteries is one of the main reasons behind BEB higher TCO when compared to diesel buses, or other alternative bus technologies. With the current advancements in battery technology, the cost of Lithium-ion batteries is expected to decrease down to 50 €/*kWh,* compared to the 580 €/*kWh* considered in this study at this point. Figure 5.21 shows the impact of Lithium-ion battery cost on BEB TCO at different battery sizes. Lithium-ion battery cost is varied from 50 €/*kWh* to 580 €/*kWh.*

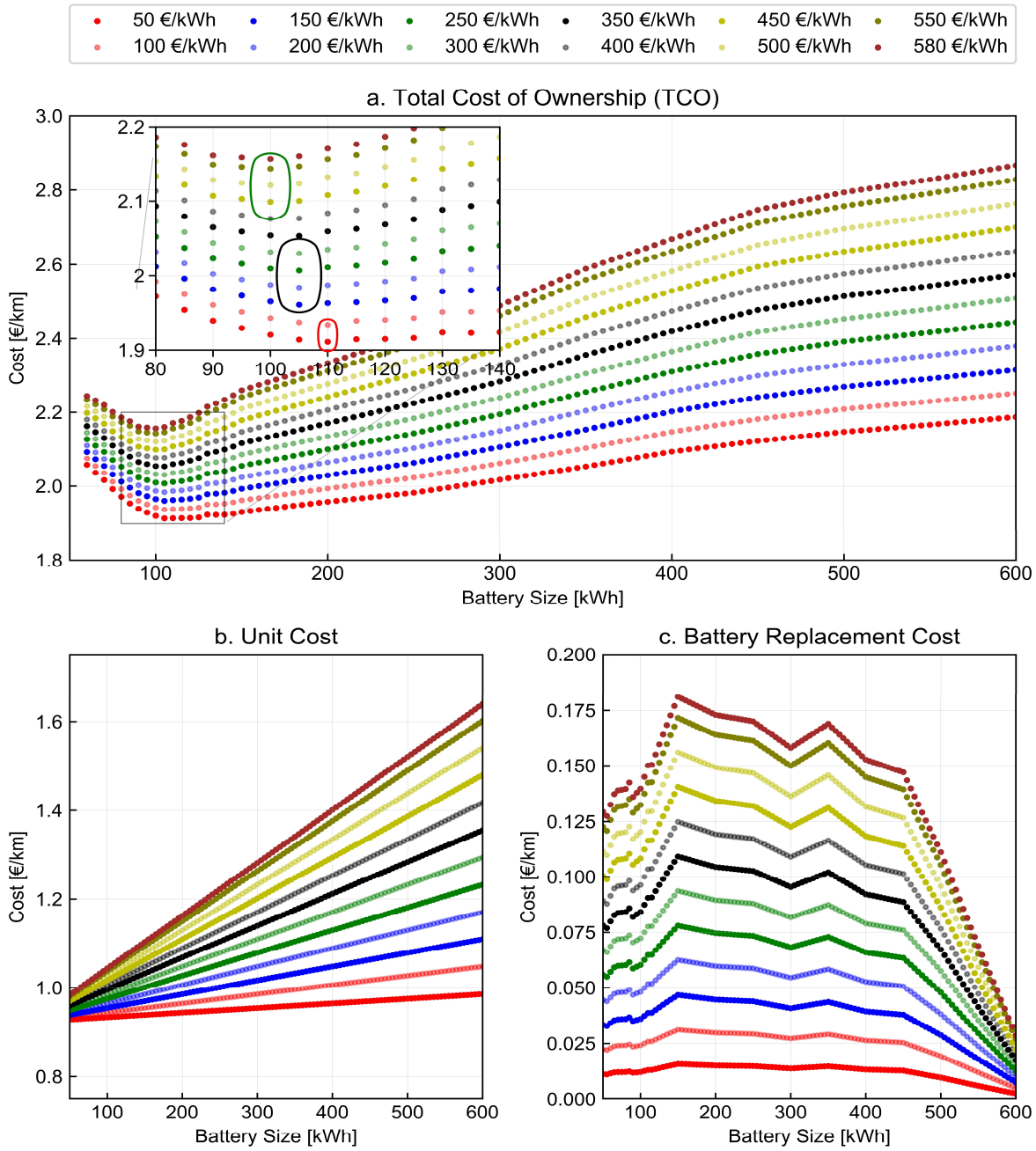


Figure 5.21: Impact of Lithium-ion battery cost on TCO

Similar behavior is observed regarding TCO variation as function of battery size at all lithium-ion battery costs. As shown in panel (a) of Figure 5.21, the TCO decreases from 50 *kWh* to around 100 *kWh* where it reaches its minimum, and then it starts increasing afterward continuously until 600 *kWh*. However, with lower lithium-ion battery cost, the TCO becomes less sensitive to the increase in battery size as the curves become less steep after its minimum (around 100 *kWh*). For example, for the case of 580 €/*kWh* (brown curve) Lithium-ion battery cost, the smallest battery size records a TCO of 2.21 €/*km*, which is the highest recorded TCO until the battery size reaches 160 *kWh*. On the contrary, for the case of 50 €/*kWh* (light-red curve) Lithium-ion battery cost, the smallest battery size records a TCO of 2.07 €/*km,* the highest recorded TCO until the battery size reaches 360 *kWh*. Mainly, a higher reduction in TCO is observed at the largest battery sizes. In other words, with lower Lithium-ion battery cost, larger batteries become more favorable.

Zooming at the curves' minima in panel (a) of Figure 5.21, a slight variation in the optimal battery size is observed where the optimal battery size (corresponds to the minimum TCO) is circled. With lower Lithium-ion battery cost, the optimal battery size slightly increases from 100 to 110 *kWh*.

In order to explain this behavior, Figure 5.21 panels (b) and (c) also show the cost components that are affected by the variation in Lithium-ion battery cost including the bus unit cost and battery replacement cost. The unit cost linearly increases with the increase in battery size regardless of the Lithium-ion battery cost, however, it becomes less sensitive to the increase in battery size at low Lithium-ion battery cost. At high Lithium-ion battery cost, the unit cost represents 45-55 % of the TCO, whereas, at lower Lithium-ion battery cost, the unit cost represents 42-44% of the TCO.

On the other hand, panel (c) of Figure 5.21 shows the battery replacement cost as function of battery size at different Lithium-ion battery costs. Similar behavior is observed regarding TCO variation as function of battery size at all lithium-ion battery costs. For a small battery size below 150 *kWh*, the battery replacement costs increase. Afterward, the battery replacement costs decrease for battery sizes larger than 150 *kWh*. The two main factors driving the battery replacement cost are the battery replacement frequency and the cost of Lithium-ion batteries. The two presented factors drive the battery replacement costs at different battery sizes. The battery replacement cost for small batteries is more sensitive to the variation in Lithium-ion battery cost mainly due to the higher frequency of battery replacement.

Although the variation in Lithium-ion battery cost has a considerable impact on the TCO, in specific unit cost and battery replacement cost, the optimal battery size resulting in the minimum TCO is always around 100 *kWh* for the presented case study despite the slight variation in unit cost and battery replacement cost across the different battery sizes at very low Lithium-ion battery cost. Medium batteries are still favored over small or large batteries and this is due to the following:

- Small batteries suffer a high infrastructure cost as shown in Figure 5.16 panel (c) when compared to medium-size batteries.
- Large batteries suffer a high demand charge and infrastructure cost as shown in Figure 5.16 panels (c) and (d) when compared to medium-size batteries.
- The variation in the energy cost as function of battery size is not significant as shown in Figure 5.16 panel (f).

5.4.2.5.2 Impact of demand charge tariff

The electricity demand charge is a significant part of the electric bill paid by the BEB operators and it can exceed 50% of the total electric bill. The demand charge tariff is set by local authorities/electricity suppliers, and it varies from one region to another. In addition, the demand charge tariff depends on the type of electricity supply, such as non-residential, industrial, etc. As there is no clear definition of the demand charge tariff worldwide, or in France, a parametric study is presented varying the demand charge tariff around the current tariffs deployed in Paris city (11.5 €/*kW*), where the value varies from 0 €/*kW* to 20 €/*kW*. All other cost parameters are held constant. Figure 5.22 shows the impact of demand charge tariff on BEB TCO at different battery sizes.

Similar behavior is observed regarding TCO variation as function of battery size at all demand charge tariffs. The TCO decreases from 50 *kWh* battery size to around 100 *kWh* where it reaches its minimum and then it starts increasing afterward continuously. Larger battery sizes are more sensitive to the variation in the demand charge tariff mainly due to the higher recorded demand charge at large battery sizes as explained in section 5.4.2.2. At a lower demand charge tariff, the TCO curve becomes less steep, i.e., less sensitive to the increase in battery size, after its minimum (around 100 *kWh*). For example, for the case of 20 €/*kW* (brown curve) demand charge tariff, the smallest battery size records a TCO of 2.3 €/*km*, which is the highest recorded TCO until the battery size reaches 140 *kWh*. On the contrary, for the case of 0 €/*kW* (red curve) demand charge tariff, the smallest battery size records a TCO of 2.19 €/*km,* the highest recorded

TCO until the battery size reaches 180 *kWh*. With the reduction in demand charge tariff, a higher reduction in TCO is observed at larger battery sizes.

Panel (a) of Figure 5.22 also zooms in on the optimal battery size corresponding to the minimum TCO. The optimal battery size slightly changes at different demand charge tariffs as it is always around 95-100 *kWh*.

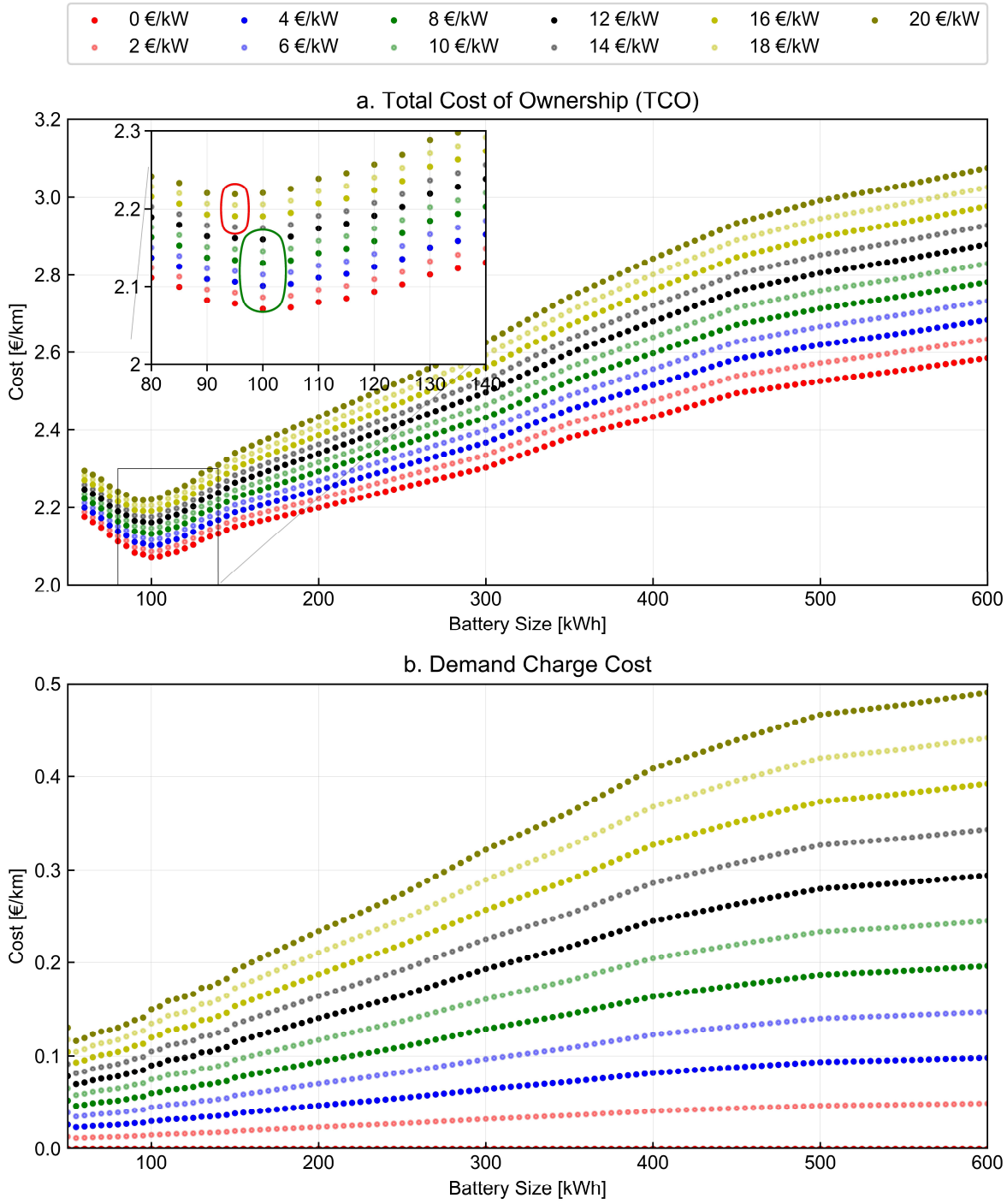


Figure 5.22: Impact of demand charge tariff on TCO

This behavior is better explained using panel (b) of Figure 5.22 where the demand charge cost is plot as function of the battery size at different demand charge tariffs. A higher variation in demand charge cost at different tariffs is observed for large batteries (above 150 *kWh*) when compared to small batteries (below 100 *kWh*), mainly due to the fact that the demand charge cost increases monotonically as function of battery size. That being said, small and medium-size batteries are less sensitive to the variation in demand charge tariff, and thus the optimal battery size, situated around 100 *kWh* battery size, is not highly affected by the variation in the demand charge tariff.

Despite the fact that the demand charge cost may represent 5 to 15% of the TCO, the TCO is still driven by other cost components, mainly the bus unit cost.

In order to better assess the impact of the demand charge tariff, the impact of Lithium-ion battery cost and demand charge tariff are both considered together as shown in Figure 5.23, where four different values of Lithium-ion battery cost are considered, and 2 demand charge tariffs are considered as well: a case of no demand charge tariff at 0 €/*kW* - panel (a) of Figure 5.23, and a case of very high demand charge tariff at 20 €/*kW* panel (b) Figure 5.23.

At 0 €/*kW* demand charge tariff- panel (a), as the Lithium-ion battery cost decreases, the optimal battery size corresponding to the minimum TCO increases. For example, at 580 €/*kWh* Lithium-ion battery cost, the optimal battery size is 100 kWh. This value increases to 125 *kWh* at 50 €/*kWh* lithium-ion battery cost. This behavior is explained by recalling that for large batteries, the unit cost, aging cost, and demand charge cost represent more than 75% of the TCO, whereas, for smaller batteries, these cost components represent around 55%. Thus, larger batteries witness a higher reduction in TCO at lower Lithium-ion battery costs and demand charge tariffs.

At 20 €/*kW* demand charge tariff- panel (b), as the Lithium-ion battery cost decreases, the optimal battery size corresponding to the minimum TCO is almost stable situated between 95 *kWh* to 105 *kWh*. Two opposing factors are taking place:

- A reduction in battery unit cost at lower Lithium-ion battery cost.
- An increase in the demand charge cost when compared to panel (a).

The first factor results in a higher reduction in the TCO of large batteries when compared to smaller batteries, where the latter results in a higher increase in the TCO of large batteries when compared to smaller batteries. Thus, the optimal battery size corresponding to the minimum TCO remains situated around 100 *kWh* in this case.

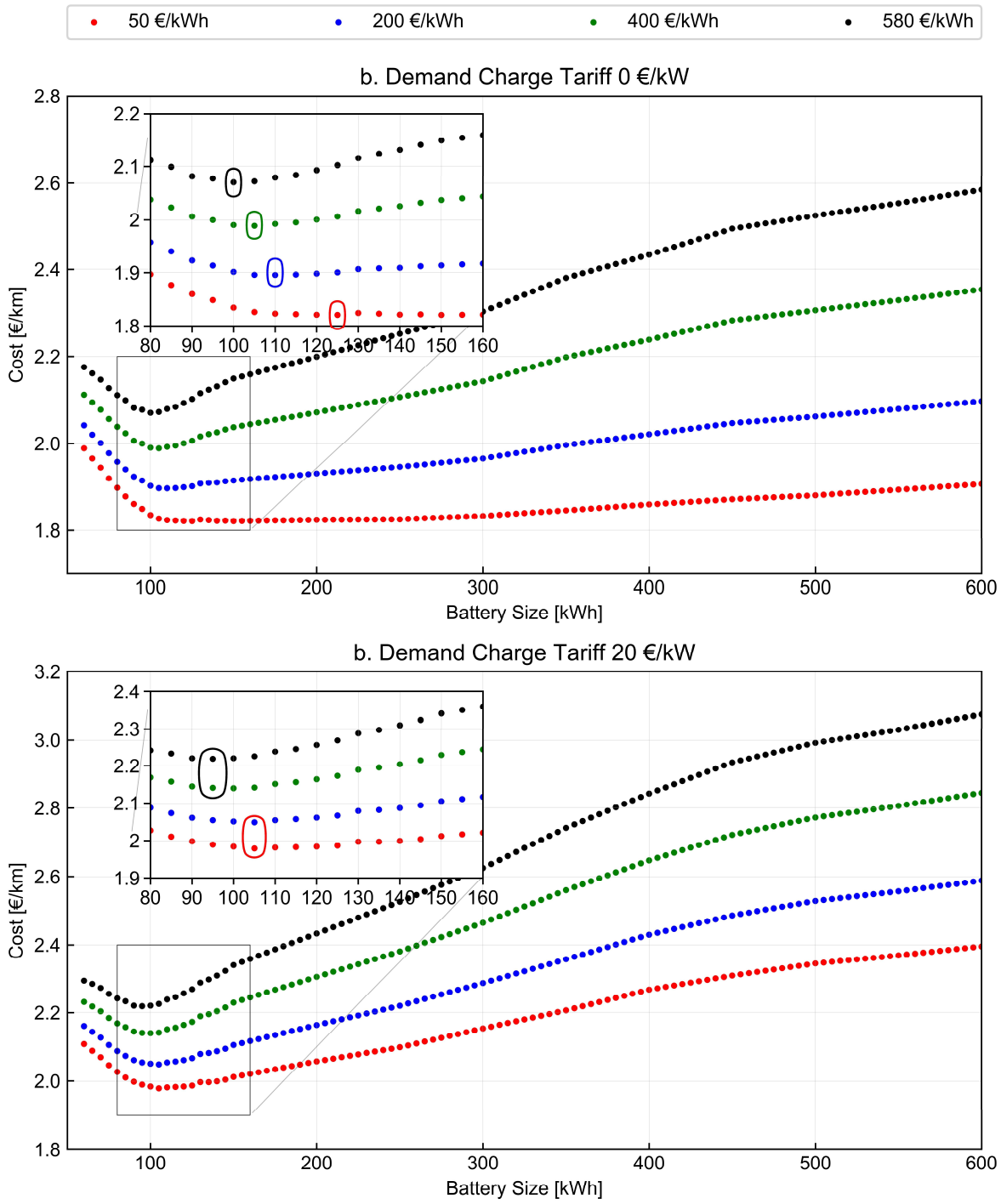


Figure 5.23: Impact of Lithium-ion battery cost and demand charge tariff on BEB TCO at different battery sizes

That being said, the variation in electricity demand charge tariff has a negligible impact on the choice of the optimal battery size if the cost of Lithium-ion batteries is very high, as the TCO is driven by the bus unit cost in this case. However, when the cost of Lithium-ion battery drops, the demand charge cost would become more significant and has a high impact on the TCO of BEB deployment, in particular at low demand charge tariffs. In addition, in the presented case

study, the maximum considered demand charge tariff is 20 €/*kW,* which is an assumption considered in this specific case study for Paris city. However, many studies reported a demand charge tariff exceeding 70 €/*kW* in other countries such as the USA, and thus the impact of the demand charge tariff might become even more significant.

5.4.2.5.3 Impact of the charger's cost

The cost of the charging technology is a main contributor to the TCO of BEB deployment, in specific the infrastructure cost. The infrastructure cost represents 5-15% of the TCO depending on the choice of the charging technology. Recall that in this thesis, the considered infrastructure costs are only those encountered by the bus operator such as chargers' acquisition and installation cost. Other infrastructure modifications especially those related to the electric grid are considered out of the scope of this study. A parametric study is conducted by varying the chargers' cost between its current rate of 460 €/*kW* to 250 €/*kW* to study its impact on the TCO, infrastructure cost, and optimal battery size and charging strategy as shown in Figure 5.24.

Panel (a) shows the TCO variation at different battery sizes and chargers' costs. Similar behavior is observed regarding TCO variation as function of battery size at all chargers' costs. The TCO decreases from 50 *kWh* battery size to around 100 *kWh* where it reaches its minimum and then it starts increasing afterward continuously. With higher chargers' cost, the TCO becomes more sensitive to the increase in battery size for small batteries as the curves become steeper between 50 - 100 *kWh* battery size.

Panel (a) of Figure 5.24 also zooms in on the optimal battery size corresponding to the minimum TCO. The optimal battery decreases from 100 *kWh* at high chargers' costs to 90 *kWh* at low chargers' costs (below 300 €/*kW*). Figure 5.24 panel (b) shows the infrastructure cost variation at different battery sizes for different chargers' costs. For very small battery sizes, the infrastructure cost is highest mainly due to the fast chargers needed at the stop stations for such small battery sizes. The infrastructure costs decrease as the battery size increases and it reaches around 250 *kWh* battery size for all chargers' costs. Afterward, infrastructure costs increase continuously.

That being said, the variation in chargers' cost has a negligible impact on the choice of the optimal battery size mainly because infrastructure costs represent 5% only of the TCO for the optimal battery size. It is important to recall the definition of infrastructure costs in the study as the cost of acquisition and installation of chargers, and that is the reason behind its low

contribution to the TCO. However, infrastructure costs may result in a larger portion of the TCO if other parameters are considered such as electric grid modifications.

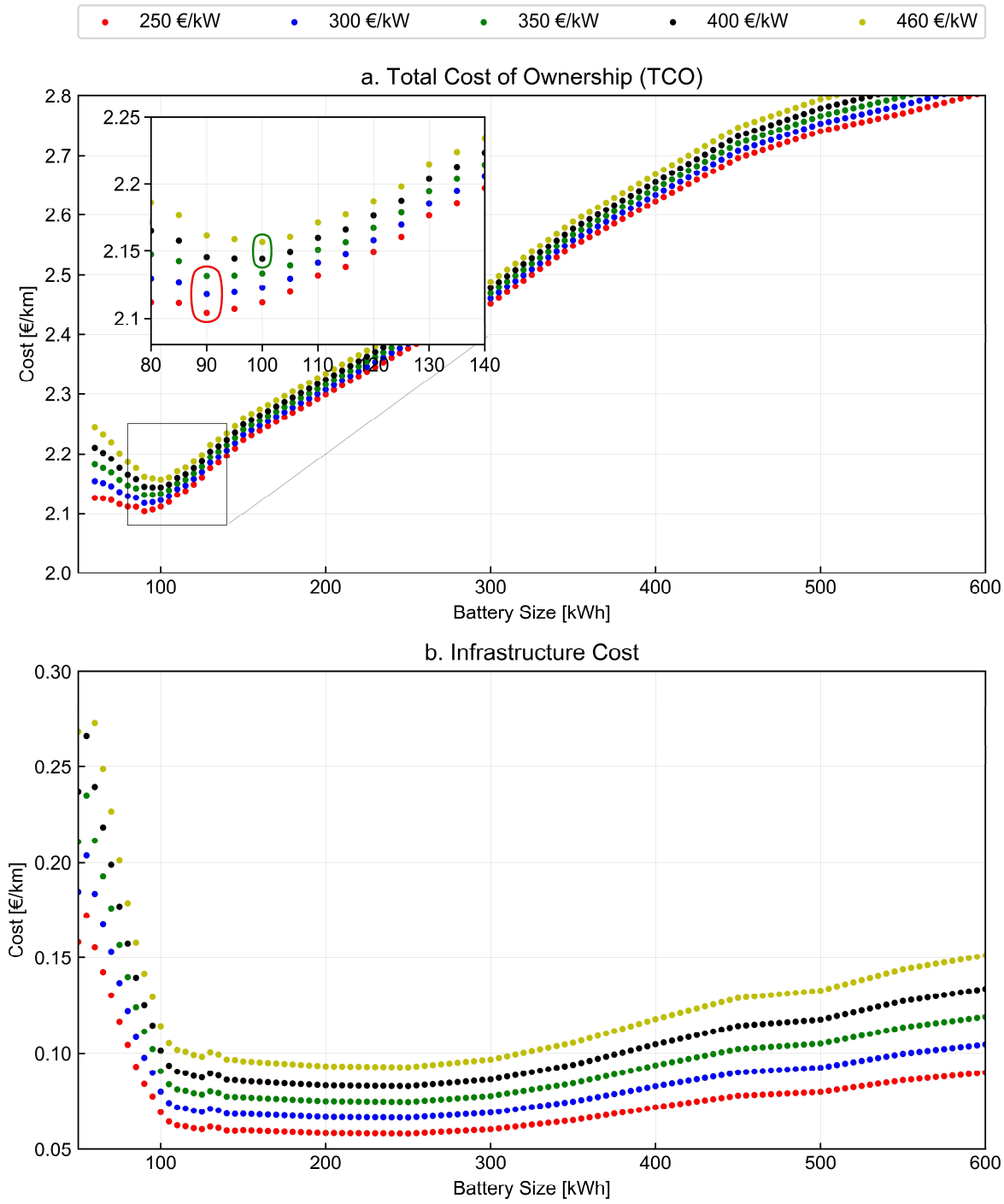


Figure 5.24: Impact of chargers' cost on TCO at different battery sizes

In this section, the main parameters impacting the TCO and optimal battery size and charging strategy are varied to study the behavior of the different cost components. This exercise helps

in understanding the different battery sizing needs and charging strategy for different regions or countries, as these cost parameters vary from one region to the other.

The cost of a Lithium-ion battery has the strongest influence on the TCO, and consequently on the choice of the optimal battery size and charging strategy. This is followed by the demand charge tariff as it has a considerable impact on the TCO, especially for low Lithium-ion battery cost, which is expected to decrease soon.

Nonetheless, this parametric study reveals that regardless of the variation of the cost parameters, medium battery sizes are still favorable (90-150 kWh), alongside an end-line charging strategy mainly due to their optimal trade-offs in terms of the different TCO cost components. More case studies for different bus lines are required in order to generalize this conclusion.

5.5 Conclusion

Charging of BEB is a process that incurs a very high number of variables that interact with each other and impact the TCO of BEB deployment and their operation as well. In addition to the battery size, the charging strategy directly drives the BEB TCO. This chapter presented an optimization-based methodology to minimize the TCO of BEB deployment while respecting their schedule constraints. The proposed methodology is composed of two consecutive optimization steps, a dynamic programming optimization routine is first applied to optimize the dynamic control variables such as charging energy and power during the day, and then followed by a genetic algorithm optimization routine to optimize the battery size for each BEB.

The proposed methodology is utilized in a case study representing a bus line operating in Paris city. For the presented case study, medium-sized batteries and end-line charging result in the optimal TCO. As they provide the optimal trade-off among the different TCO components ***Battery Unit Cost*** proportionally increases as function of the battery size, and thus medium size batteries do not suffer a very high battery cost. ***Infrastructure Cost*** is the highest for small batteries as they require frequent charging and at high while large batteries favor night charging at high power as well. Thus, medium batteries require the least expensive charging infrastructure. ***Demand Charge Cost*** continuously increases with battery size as more BEBs are charged simultaneously at night. ***Battery Replacement Cost*** is driven by the battery cost and the frequency of battery replacement. Small batteries suffer from a high replacement frequency but incur low battery costs, thus reducing the battery replacement cost. On the contrary, large batteries suffer high battery costs but very low replacement frequency. This also

results in reduced battery replacement costs. Medium batteries suffer the highest battery replacement cost. ***Energy Cost*** is not very sensitive relative to the different battery sizes and charging strategies. However, the different battery sizes encounter a tradeoff between the additional energy consumption for large batteries and the reduced charging costs at night.

The bus schedule has a huge impact on the choice of optimal battery size as it determines the available charging time slots during the day. BEBs that suffer from very short dwell times between consecutive trips are equipped with large batteries to avoid charging at very high power, which increases battery replacement, infrastructure, and demand charge costs. Although in this thesis the bus schedule is considered to be fixed through its operation during the year, it will be interesting to study the impact of a variable schedule per BEB as the bus schedule shows a considerable impact on the choice of optimal battery size.

The impact of BEB deployment on the electricity grid is thoroughly discussed for the presented case study. The results show the high discrepancy in maximum power demand and load factor for the different examined charging strategies and battery sizes. Small batteries that are charged frequently during the day and at high power result in a high-power load on the electric grid during the day. On the contrary, large batteries that favor nigh charging show minimal power demand from the electric grid during the day, however a very power demand at night as all BEBs are charged simultaneously. Medium batteries provide a good tradeoff and result in the maximum load factor in comparison to other battery sizes.

Finally, a sensitivity analysis is conducted by varying the main cost parameters that affect the TCO, mainly the cost of Lithium-ion battery, demand charge tariff, and charger's cost. The interest in this analysis is that these parameters vary across the different regions or countries, such as the electricity tariffs and investment cost, in addition to the fact that several studies reveal that the cost of lithium-ion batteries and charging infrastructure is subject to a continuous reduction over the next decade. The analysis shows that the cost of a Lithium-ion battery has the strongest influence on the TCO, optimal battery size, and charging strategy. It is followed by the demand charge tariff. The study reveals that for any combination of cost parameters, medium batteries (90-150 kWh) and end-line charging strategy provide the most economically effective solution to deploy BEB. More case studies for different bus lines are required in order to generalize this conclusion.

5.6 References

[1] Z. Chen, W. Liu, and Y. Yin, "Deployment of stationary and dynamic charging infrastructure for electric vehicles along traffic corridors," *Transp. Res. Part C Emerg. Technol.*, vol. 77, pp. 185–206, 2017, doi: 10.1016/j.trc.2017.01.021.

[2] A. Lajunen, "Lifecycle costs and charging requirements of electric buses with different charging methods," *J. Clean. Prod.*, vol. 172, pp. 56–67, 2018, doi: 10.1016/j.jclepro.2017.10.066.

[3] K. Elin, "Charging infrastructure for electric city buses," Royal Institute of Technology KTH, 2016.

[4] Z. Chen, Y. Yin, and Z. Song, "A cost-competitiveness analysis of charging infrastructure for electric bus operations," *Transp. Res. Part C Emerg. Technol.*, vol. 93, no. December 2017, pp. 351–366, 2018, doi: 10.1016/j.trc.2018.06.006.

[5] N. Qin, A. Gusrialdi, R. Paul Brooker, and A. T-Raissi, "Numerical analysis of electric bus fast charging strategies for demand charge reduction," *Transp. Res. Part A Policy Pract.*, vol. 94, pp. 386–396, 2016, doi: 10.1016/j.tra.2016.09.014.

[6] N. A. El-Taweel, M. Mohamed, and H. E. Farag, "Optimal design of charging stations for electrified transit networks," *2017 IEEE Transp. Electrif. Conf. Expo, ITEC 2017*, pp. 786–791, 2017, doi: 10.1109/ITEC.2017.7993369.

[7] A. Kunith, D. Goehlich, and R. Mendelevitch, "Planning and optimization of a fast-charging infrastructure for electric urban bus systems," in *International Conference on Traffic and Transport Engineering*, 2015, no. November.

[8] A. Houbbadi, R. Trigui, S. Pelissier, E. Redondo-Iglesias, and T. Bouton, "Optimal scheduling to manage an electric bus fleet overnight charging," in *Energies*, 2019, vol. 12, no. 14, pp. 1–17, doi: 10.3390/en12142727.

[9] A. Houbbadi, R. Trigui, S. Pelissier, T. Bouton, and E. Redondo-Iglesias, "Multi-Objective Optimisation of the Management of Electric Bus Fleet Charging," in *2017 IEEE Vehicle Power and Propulsion Conference, VPPC 2017 - Proceedings*, 2018, vol. 2018-Janua, pp. 1–6, doi: 10.1109/VPPC.2017.8331015.

[10] Y. Wang, Y. Huang, J. Xu, and N. Barclay, "Optimal recharging scheduling for urban

electric buses: A case study in Davis," *Transp. Res. Part E Logist. Transp. Rev.*, vol. 100, pp. 115–132, 2017, doi: 10.1016/j.tre.2017.01.001.

[11] Y. He, Z. Song, and Z. Liu, "Fast-charging station deployment for battery electric bus systems considering electricity demand charges," *Sustain. Cities Soc.*, vol. 48, no. April, 2019, doi: 10.1016/j.scs.2019.101530.

[12] B. R. Ke, C. Y. Chung, and Y. C. Chen, "Minimizing the costs of constructing an all plug-in electric bus transportation system: A case study in Penghu," *Appl. Energy*, vol. 177, pp. 649–660, 2016, doi: 10.1016/j.apenergy.2016.05.152.

[13] M. Rogge, E. Van Der Hurk, A. Larsen, and D. Uwe, "Electric bus fl eet size and mix problem with optimization of charging infrastructure," *Appl. Energy*, vol. 211, no. November 2017, pp. 282–295, 2018, doi: 10.1016/j.apenergy.2017.11.051.

[14] M. Xylia, M. Xylia, S. Leduc, P. Patrizio, S. Silveira, and F. Kraxner, "ScienceDirect ScienceDirect Developing a dynamic optimization model for electric bus charging Developing a dynamic optimization model for electric bus charging infrastructure infrastructure," *Transp. Res. Procedia*, vol. 27, pp. 776–783, 2017, doi: 10.1016/j.trpro.2017.12.075.

[15] R. Bellman, "Dynamic_Programming," 1954.

[16] C. Mansour and D. Clodic, "OPTIMIZED ENERGY MANAGEMENT CONTROL FOR THE TOYOTA HYBRID SYSTEM USING DYNAMIC PROGRAMMING ON A PREDICTED ROUTE WITH SHORT COMPUTATION TIME," *Int. J. Automot. Technol.*, vol. 13, no. 2, pp. 309–324, 2012, doi: 10.1007/s12239.

[17] M. L. Puterman, *Markov Decision Processes Discrete Stochastic Dynamic Programming*. John Wiley & Sons, 2014.

[18] Y. He, Z. Song, and Z. Liu, "Fast-charging station deployment for battery electric bus systems considering electricity demand charges," *Sustain. Cities Soc.*, vol. 48, no. October 2018, 2019, doi: 10.1016/j.scs.2019.101530.

[19] K. Sastry, D. Goldberg, and G. Kendall, "Chapter 4 Genetic Algorithms," in *Search Methodologies*, 2005, pp. 97–125.

[20] A. S. Fraser, "Simulation of genetic systems by automatic digital computers. II: Effects of linkage on rates under selection," *J. Biol. Sci.*, vol. 10, pp. 492–499, 1957.

[21] H. J. Bremermann, “The evolution of intelligence. The nervous system as a model of its environment,” Seattle, WA, 1958.

[22] J. H. Holland, “Adaptation in Natural and Artificial Systems,” Ann Arbor, MI, 1975.

**** End of Chapter 5 ****

Chapter 6

CONCLUSIONS AND PERSPECTIVES

Being the second most contributor to GHG emissions worldwide, the transport sector is subject to continuous development, in particular road transport as it accounts for more than three-quarters of these emissions. Several alternative vehicle technologies have been introduced and developed recently, however, oil-dependent mobility still holds the biggest market share due to the limited market penetration of these technologies, owing this to factors such as energy logistics, cost, and required infrastructure.

However, public transport, in particular transit buses, is less affected by these factors and this facilitates the deployment of alternative transport technologies. In this context, this thesis is involved in the development of sustainable public transit buses to reduce the reliance on oil-dependent mobility.

This thesis introduced a methodology capable of providing optimal battery sizing and charging strategy for BEB fleet to minimize the total cost of ownership of BEB deployment while ensuring no schedule disruption or service interruption during operation.

6.1 Synthesis and Conclusions

The analysis of new alternative public transit bus technologies was carried out in Chapter 1. The analysis considered diesel buses (DB), compressed natural gas buses (CNG), biofuel buses, hybrid electric buses (HEB) both series and parallel architectures, fuel cell electric buses (FCEB), and battery electric buses (BEB). The comparative analysis among these bus technologies was conducted based on their energy performance, emissions, economic performance, and operational features.

The presented analysis showed that BEB is the most promising solution to replace the current DB fleet thanks to their energy-efficient and environmental performance. However, BEB face many economic and operational challenges that prevent their massive deployment in the market.

In this thesis, solutions to ease the BEB deployment were studied from the bus operator's point of view by presenting cost-effective solutions. In addition to the high cost of BEB, the study discussed also the main challenges facing BEB operators which are range anxiety, the know-how of operation, and readiness of the electric grid.

First, it was essential to study the different energy systems encountered in BEB in order to evaluate their energy consumption and the total BEB energy consumption. In Chapter 2, the

BEB configuration was thoroughly presented and the bus architecture and components technology were introduced. Then, a comprehensive energy model for BEB was developed using a multi-physical approach, equation-based object-oriented programming. The model considers all the energy systems encountered in a BEB and they are: propulsion system, HVAC unit, and auxiliaries, in addition to the battery. The proposed models were validated against similar studies in the recent literature, or against data provided by bus operators.

Detailed energy analysis was conducted in Chapter 3 to study the energy performance of the BEB at the varying operating conditions it encounters during operation and to highlight the main factors showing a significant impact on its energy consumption. These operating conditions are driving conditions, weather conditions, and passengers' occupancy inside the BEB.

The driving conditions showed a significant impact on the propulsion system energy consumption as BEB operating along highly congested routes record a 35% increase in energy consumption in comparison to BEB operating at minimal levels of traffic. Besides, auxiliaries such as the steering pump and air compressor are highly affected by the BEB driving conditions as their energy consumption could double under high levels of traffic congestion. The HVAC unit average power demand is found to be increasing for trips with a high number of stops, mainly associated with frequent doors opening and closure increasing heat losses. Finally, the BEB total energy consumption drastically deteriorates for highly congested trips as it can increase by 50% for such driving conditions.

The weather conditions showed a considerable impact on the HVAC unit energy consumption and the total BEB energy consumption as well. The HVAC unit average power demand over a trip increases as external temperatures deviate from room temperature/thermal comfort temperature (19-26 °C). Extreme cold/hot conditions record the highest HVAC unit power demand reaching 25 kW in comparison to 2 kW for moderate weather conditions. In general, the BEB total energy consumption is highly affected by weather conditions, and the HVAC unit energy consumption could represent more than 50% of the total BEB energy consumption at extreme weather conditions, affecting the BEB driving range drastically.

On the other hand, the passenger's occupancy inside the BEB affects its energy consumption. The HVAC unit power demand is highly affected by passenger occupancy as it increases by 100% during cooling and by 15% during heating at maximum passenger occupancy. A high number of passengers rejects higher heat inside the bus and requires a higher amount of fresh

air. The propulsion system energy consumption linearly increases with a higher number of passengers on-board due to the additional weight. This increase could reach 15% when comparing an empty bus to a full one.

The BEB total energy consumption increases when high levels of traffic congestion are encountered or when external temperatures deviate from the thermal comfort temperature range of the bus cabin (estimated at 19 to 23 °C during winter and 23 to 26 °C during summer). The significant increase in BEB energy consumption at extreme operating conditions reduces the BEB driving range drastically.

This energy analysis gives valuable insights on required battery sizing for any BEB by simply identifying its operating conditions and assessing its energy consumption. A preliminary battery sizing framework was then introduced in this chapter. A case study was presented showing how the BEB required battery size is mainly driven by extreme operating conditions. In addition, a variety of recommendations and technical solutions that may reduce the battery size were introduced. Charging multiple times during the day was found to be the most effective solution to reduce the battery size, as the reduction could reach 80% for several charging events. However, this comes at a high cost and at a high risk of schedule disruption. Nonetheless, an adequate charging strategy could significantly reduce the BEB battery size, and thus reducing the total BEB costs without any disruption in operation.

The costs and operation of BEB are main challenges facing their deployment, and they are affected by the charging strategy and battery sizing. In Chapter 4, a techno-economic model for BEB line was developed. The model helps to assess the total cost of ownership (TCO) and operation of BEB for different battery sizes and charging strategies. The comprehensive TCO model considers the BEB unit costs, battery purchase and replacement costs, energy and power costs, infrastructure, and maintenance costs. Besides, BEB operation was realized by evaluating a punctuality index (PI) that reflects on the BEB departure delays to their schedule, resulting from daily charging events.

Simulation work was developed to assess the techno-economic performance of bus line number 21 in Paris. All stationary charging scenarios were considered: overnight charging (ONC), depot day charging (DDC), end-line charging (ELC), and opportunity charging (OC). For each charging scenario, the required battery size was estimated based on the method presented in Chapter 3. The TCO analysis for the four charging scenarios and their corresponding battery sizes revealed that the different charging strategies encounter tradeoffs among the TCO

components. The battery replacement cost is the highest during the OC scenario since the OC takes place at very high power which accelerates battery aging. The infrastructure cost is the highest for the OC scenario as well and lowest for ONC due to the high number of chargers used in the OC scenario and their high nominal power. The demand charge cost is the highest for the ONC scenario due to the fact that all BEBs charge at the same time during this scenario, thus their cumulative power demand is very high. The energy cost is very similar across the four different scenarios. The battery cost is the highest for the ONC scenario as it utilizes the largest battery size. Finally, the TCO is very high for the ONC scenario driven by the high battery cost and demand charge cost despite its low infrastructure and battery replacement costs. The other scenarios record similar TCO.

The TCO segmentation analysis revealed that there is room to reduce battery costs (acquisition and replacement), operating costs, and infrastructure costs as they are directly related to the choice of the battery size and the charging strategy (charging power, frequency, etc. …). However, this has a direct impact on the BEB operation, reflected in their punctuality index (PI). Decreasing the battery size directly reduces the TCO but deteriorates PI as such batteries are charged during the day resulting in some schedule delays. On the other hand, decreasing the maximum charging power reduces the TCO as demand charge costs, battery replacement costs, and infrastructure costs are reduced. On the contrary, the PI decreases due to the prolonged charging events resulting from reducing the charging power.

In Chapter 5, the potential to reduce the TCO of BEB deployment was realized by introducing an optimization methodology that aims at minimizing the TCO by optimizing the battery size and the charging strategy. The methodology is a 2-step optimization algorithm that utilizes both Dynamic programming and Genetic Algorithm optimization routines, where these techniques were coupled together to solve the problem. The optimization problem controls the size of the battery pack and the charging strategy (charging energy and power profiles for the BEB during the day).

The effectiveness of the proposed methodology was assessed by considering a case study for bus line 21 operating in Paris. For the presented case study, medium-sized batteries, around 100 *kWh*, coupled with end-line charging proved to be the most economically effective solution as they provided the optimal trade-off among the different TCO components. Battery unit cost is relatively low for a 100 *kWh* battery. The infrastructure cost is the lowest for such a charging strategy as it avoids frequent opportunity charging at high power from one hand, and it also avoids exclusive night charging at relatively higher power. The demand charge cost

continuously increases with battery size as more BEBs are charged simultaneously at night, and thus an end-line charging strategy encounters a low demand charge cost. Battery replacement cost is relatively high for the resulted optimal battery size and charging strategy, however, the reduction in other cost components compensates for this high battery replacement cost.

A further analysis was conducted to evaluate the impact of the BEB schedule on battery sizing as it defines the bus operating conditions and available charging time during the day. BEB that operate during peak hours or extreme weather conditions suffer a high energy consumption. Furthermore, buses that incur very short dwell times must be equipped with large batteries to avoid very high-power charging which increases battery replacement, infrastructure, and demand charge costs. Large batteries provide an energy reserve onboard that limits high-power charging during the day.

Besides, the BEB charging load was also analyzed as it may open a window on the impact of BEB charging on the electricity grid. The obtained results showed that the maximum charging load is reduced by a factor of 5 when comparing the optimal solution (medium-sized batteries coupled with end-line charging) to overnight charging BEBs equipped with large batteries, and by a factor of 3 in comparison to smaller battery sizes charged at the stop stations.

Finally, a sensitivity analysis was introduced where some cost parameters were modified as these parameters vary across the different regions and they are subject to continuous cost reduction. The analysis revealed that the Lithium-ion battery cost highly affects the choice of the optimal battery size and charging strategy. The study concluded that for any variation in these cost parameters, medium batteries (90-150 kWh) and end-line charging strategy provide the most economically effective solution for BEB deployment, respecting its operational constraints.

The proposed methodology provides a great potential to overcome BEB deployment technical and economic challenges, while the obtained results need further investigation in order to be generalized.

The work presented in this thesis resulted in two main contributions:

1. A systematic methodology capable of providing optimal battery sizing and charging strategy for the BEB fleet to minimize the total cost of ownership of BEB deployment, while ensuring no schedule disruption or service interruption during operation.

2. A tool composed of several layers that assists bus operators in the deployment of BEB. This tool allows the thorough evaluation of BEB energy performance and techno-economic performance. In addition, the proposed tool optimizes the required battery size and charging strategy to ease BEB deployment at minimal costs respecting the BEB schedule constraints.

6.2 Improvement and Future Work

The work presented in this thesis can benefit from some improvements, especially in regards of the considered modeling approach.

- The BEB energy model and its corresponding components must be experimentally validated in order to ensure a better prediction of the BEB energy behavior, rather than validating the model results to the reported values in the literature.

- Some components can be modeled using different approaches, in specific the battery thermal model and aging model, as they prove to affect the total BEB energy consumption and deployment cost significantly.

- The control strategy of the HVAC unit (including the BTMS) has a significant impact on its energy consumption, and thus it should be thoroughly studied to provide new control algorithms for further reduction of the HVAC energy consumption.

- There are several BTMS technologies and techniques that are being implemented in BEB meanwhile, and thus considering them in the model might enhance the model's representation of the current BEB operating on roads.

- The proposed optimization methodology to minimize TCO of BEB deployment is time-consuming. The computation time might be reduced by considering a reduced step size, however, its impact on the resulting solutions should be assessed.

- The results obtained in Chapter 4 and Chapter 5 are not generalizable as they are specific to the presented case study. A larger number of case studies, representing different real-life buses in operation, should be considered to generalize the results.

The work of this thesis opens several windows on other highly-related topics, that are essential to the deployment of BEB. Out of the numerous topics that could complete this thesis, or benefit from what has been presented in this thesis, the following topics, in particular, are of great interest:

1. The schedule of BEB shows a very high impact on the choice of optimal battery size and charging strategies of BEB. Rethinking bus scheduling is essential for BEB fleet. Current bus scheduling criteria are mainly developed to meet passengers' transportation needs utilizing diesel bus fleet. However, with bus fleet electrification, another dimension should be considered in bus scheduling and it is the charging of electric buses. Thus, rethinking the entire bus scheduling criteria by considering this aspect would provide room to ease the deployment of BEB.

2. Develop a BEB network model at a city/country level where all the operating bus lines are considered, along with their interaction. This would add another dimension to the analysis presented in this thesis as it comprehensively defines the required charging infrastructure of BEBs. In addition, this could help in thoroughly assessing the impact of bus fleet electrification on the electric grid.

3. The massive deployment of BEB, and passenger electric vehicles as well, would result in significant electric power demand that may require major infrastructure modification in electricity production or transmission. Thus, it will be interesting to thoroughly assess the impact of BEB deployment on the entire electricity market scheme including electricity generation, transmission, and distribution. In addition, this allows the real assessment of the environmental benefits of BEB as different electricity production means can be considered.

4. In an era when all energy systems during our daily life are interacting with each other, public transport buses are an integral part of the daily energy scheme. Coupling the BEB daily energy needs to other energy systems such as buildings, neighborhoods, or industrial sites presents an opportunity to further improve the energy efficiency of the mentioned systems. In addition, from the BEB perspective, the creation of such an energy network has numerous benefits including: (1) a fast responsive energy supply to the BEB, (2) numerous energy storage possibilities that can reduce the burden on the electrical grid, and (3) possibility to lower the BEB energy costs.

**** End of Conclusions and Perspectives ****

APPENDICES[3]

[3] The references used in each appendix are cited in their corresponding chapter's list of references

Appendix A :
Vapor Compression Cycle (VCC)

VCC is the most widely used refrigeration cycle in automobiles and buildings. In a typical ideal single-stage VCC, a refrigerant is circulated within the cycle, and it is subjected to 4 main processes as will be explained next. Figure 7.1 introduces a schematic of the VCC.

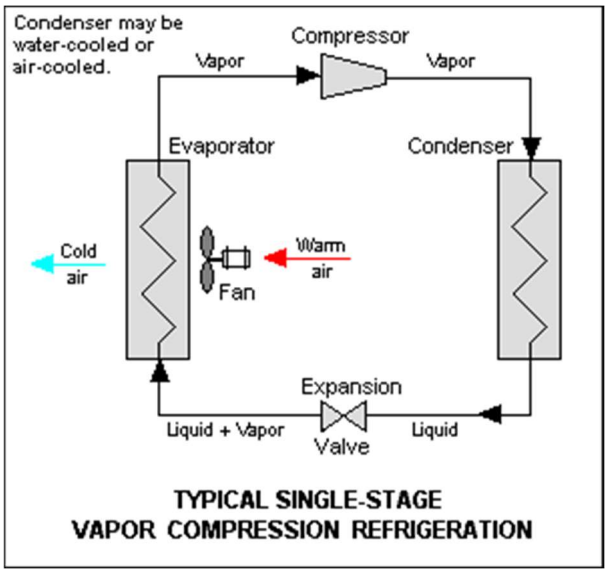


Figure 7.1: Ideal VCC schematic

1. Isentropic Compression

Refrigerant enters the compressor as a saturated vapor in the ideal cycle and gets compressed to a higher pressure. This compression process increases the temperature of the refrigerant where it becomes a superheated vapor. In the real VCC, the compression process is not isentropic as it incurs irreversibility.

2. Isobaric Condensation

The superheated refrigerant undergoes condensation using air flowing over the condenser's tubes. This heat exchange process is called heat rejection as the refrigerant heats the flowing air, whereas it cools the refrigerant until it becomes a condensed liquid. In the real VCC, the condensation process encounters some pressure losses, and thus it is not isobaric.

3. Isenthalpic Expansion

The saturated liquid refrigerant enters an expansion valve (throttle) where it undergoes a high reduction in pressure due to adiabatic flash evaporation (partial evaporation). This results in

temperature reduction, and the refrigerant becomes a mixture of liquid and vapor refrigerant. Real VCC do not achieve isenthalpic expansion.

4. Isobaric Evaporation

The refrigerant passes through the evaporator where the liquid part of the mixture gets evaporated by means of flowing air over the evaporator's tube. The refrigerant exits the evaporator as a saturated vapor. Similar to the condensation process, the real evaporation process incurs some pressure drop. In addition, the discharged refrigerant gets slightly heated in order to ensure no liquid particle entering the compressor for technological constraints.

Figure 7.2 and Figure 7.3 show the P-V and T-S diagrams of the ideal VCC, respectively.

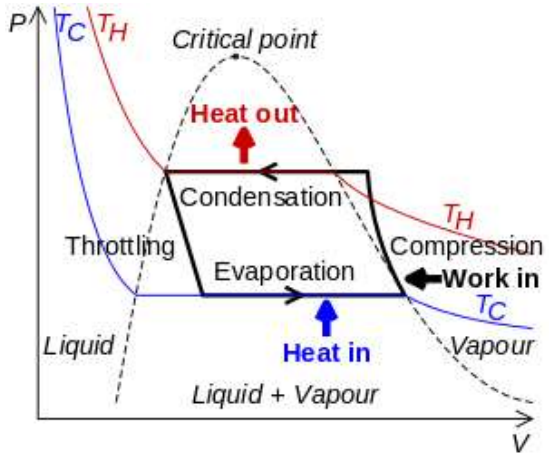


Figure 7.2: Ideal VCC P-V diagram

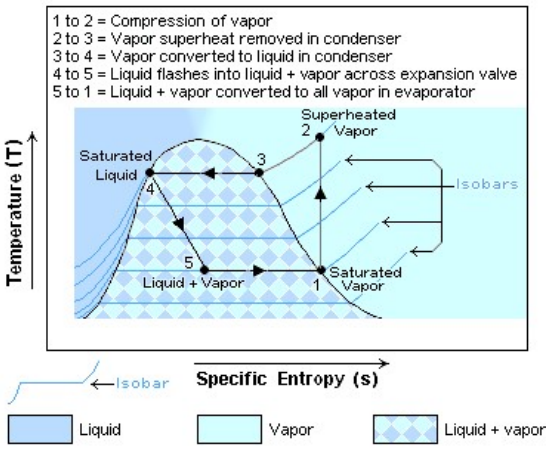


Figure 7.3: Ideal VCC T-S diagram

Refrigerant

Being a refrigerant of low GWP, refrigerant R1234yf is gaining increasing attention to replace refrigerant R134a in most automobile applications [97], [109]. Both refrigerants share similar thermodynamic properties as shown in Table 7.1.

Table 7.1: Thermodynamic properties of refrigerants R1234yf and R134a [109]

Property	R1234yf	R134a
Boiling Point at 1 atm (K)	243.7	247.08
Critical Temperature (K)	367.85	374.21
Critical Pressure (MPa)	3.38	4.06
Critical Density (kg/m^3)	478.01	511.9

Despite its environmental problems, many studies have shown that R134a achieves better performance when compared to R1234yf. VCC circulating R1234yf instead of R134a witness an up to 3% reduction in their Coefficient of Performance (COP) [96], [109]–[111].

Appendix B:
HP Components Modeling and Specifications

- **Compressor**

A scroll variable-speed compressor is used as it is the most used technology in HPs, especially for automotive applications, due to its high volumetric efficiency and lightweight [112]. The used compressor operates between 500 – 7000 *rpm*, and its volume of displacement is around 121 cm^3. The compressor data-sheet can be found in [113].

In the TSMedia AC library in Dymola, the compressor is modeled as a quasi-static device due to its fast response compared to the other HP components, namely the heat exchangers. The compressor model equations are presented in Table 7.2.

Table 7.2: Compressor model equations

Parameter: Description	Equation
$\dot{m}_{in}$: refrigerant mass flow rate at compressor inlet	$\dot{m}_{in} = \eta_v \,.\, \rho_{in} \,.\, V_d \,.\, \frac{\omega}{60}$ η_v: volumetric efficiency, V_d: displacement (Estimated from compressor datasheet) ω: rotational speed (control variable)
$\dot{m}_{out}$: refrigerant mass flow rate at compressor outlet.	$\dot{m}_{in} = \dot{m}_{out}$ No flow leakage
$\dot{W}_{shaft}$: compressor shaft power	$\dot{W}_{shaft} = P_{ise} + P_{fr}$
P_{ise}: isentropic power	$P_{ise} = \dot{m}_{in} \,.\, (\, h_{out,s} - h_{in})$
P_{Fr}: frictional power losses	$P_{Fr} = C_f \,.\, \omega^{E_f}$
C_f: friction coefficient	$C_f = 0.014 \,.\, \left(\frac{V_d}{33.10^{-6}}\right)^{1/3}$
E_f: friction exponent	$E_f = 2 \,.\, \left(\frac{V_d}{33.10^{-6}}\right)^{1/3}$
η_{ise}: isentropic efficiency	$\eta_{ise} = \frac{h_{out,s} - h_{in}}{h_{out} - h_{in}}$
h_{out}: refrigerant discharge actual enthalpy	$h_{out} = h_{in} + \frac{\dot{W}_{shaft}}{\dot{m}_{in}}$

Π: compression ratio	$\pi = \frac{P_2}{P_1}$
$P_{elec,em}$: electric machine driving the compressor: electric power	$P_{elec,em} = \frac{\dot{W}_{shaft}}{\eta_{em}}$ η_{em}: electric machine efficiency
I_{em}: electric machine load current	$I_{em} = \frac{P_{elec,em}}{V_{em}}$ V_{em}: electric machine voltage (equals the battery voltage)

- **Heat Exchangers**

Multi-port extruded tube (MPET) cross-flow heat exchangers are used in the HP. The modeling of the heat exchangers should consider the refrigerant phase change inside the heat exchangers. For this sake, a moving boundary model is considered in an approach similar to [114], [115]. The moving boundary dynamic approach considers energy and mass balance at a moving control volume, in addition to the energy balance at the tube wall as shown in Table 7.3.

Table 7.3: Moving boundary energy and mass balances for heat exchangers

Mass balance	$A\frac{d}{dt}\int_{z_{in}}^{z_{out}} \rho dz + \rho_{in} A \frac{dz_{in}}{dt} - \rho_{out} A \frac{dz_{out}}{dt} = \dot{m}_{in} - \dot{m}_{out}$
Energy balance	$A\frac{d}{dt}\int_{z_{in}}^{z_{out}} \rho h dz - AL\frac{dp}{dt} + A\rho_{in}h_{in}\frac{dz_{in}}{dt} - A\rho_{out}h_{out}\frac{dz_{out}}{dt} = \dot{m}_{in}h_{in} - \dot{m}_{out}h_{out} + qL$
Energy balance at the tube wall	$(C_p.\rho.A)_w \frac{\partial T_w}{\partial t} = p_i\alpha_i(T_r - T_w) + p_o\alpha_o(T_a - T_w)$

The equations presented in Table 7.3 are applied to every refrigerant phase within the heat exchangers. For example, the energy and mass balance equations in the evaporator are applied to the liquid-vapor mixture refrigerant and super-heated vapor refrigerant. So, in total, 4 equations represent the energy and mass balance of the refrigerant in the evaporator. On the contrary, 6 equations represent the energy and mass balance inside the condenser as the refrigerant changes phase twice inside the condenser from super-heated vapor to liquid-vapor mixture and finally to a sub-cooled liquid. This is achieved by applying Leibniz integration as discussed in [115].

- **Expansion Valve**

A thermostatic expansion valve is widely used in automotive applications. The expansion valve opening highly impacts the superheat level at the evaporator output. For this sake, the expansion valve opening is controlled by the HP control unit.

Table 7.4: Expansion valve model equations

Refrigerant flow rate across the expansion valve	$\dot{m} = C_d \,.\, A_{EXV}\sqrt{2 \,.\, \rho_3 \,.\, (P_h - P_l)}$ C_d: discharge coefficient P_h: high pressure P_l: low pressure
Isenthalpic Expansion	$h_{in} = h_{out}$

- **Fans**

The HVAC unit utilizes many fans for circulating air in and out of the bus. As shown in Figure 2.16, there are 1 air supply fans to the cabin, 2 evaporator fans (hidden inside the HP blocks), 1 exhaust air fan, and 1 BTMS fan. Centrifugal squirrel-cage Rosenberg fans are used in the HVAC system. The fans' characteristics curve is shown in Figure 7.4. The fan model equations are presented in Table 7.5.

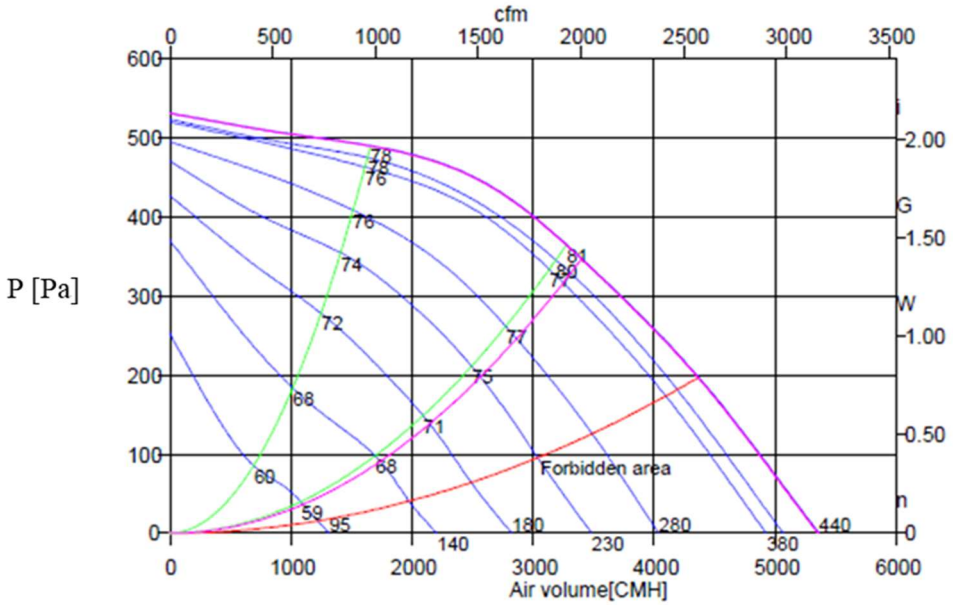


Figure 7.4: Fan pressure losses at different frequencies function of airflow rate

Table 7.5: Fan model equations

Parameter	Equation
Energy balance	$h_{out} = h_{in} + \frac{P_{shaft}}{\dot{m}_{in}}$
Mass balance	$\dot{m}_{in} + \dot{m}_{out} = 0$
$\dot{V}$: volumetric flow rate	$\dot{V} = \frac{\dot{m}_{in}}{\rho_{in}}$
P_{fl}: power transferred to the fluid	$P_{fl} = dp\,.\,\dot{V}$
P_{fan}: fan power	$P_{fan} = \frac{P_{hyd}}{\eta}$

Appendix C:

Propulsion System Validation Data

Table 7.6: Summary of scenarios and case studies used to validate the energy consumption of the propulsion system

		Bus Specifications					Battery		Driving Conditions	
Scenario #	Case Study #	Length [m]	Curb Weight [kg]	Drag Coef. [-]	EM - Power [kW]	Frontal Area [m^2]	Voltage [V]	Weight [kg]	Drive Cycle	Passengers #
1	1	12	13800	1.2	155	8.2	600 - 800	3564	MB	6
	2	12	13800	1.2	155	8.2	600 - 800	3564	NYC	6
	3	12	13800	1.2	155	8.2	600 - 800	3564	CSHV	6
	4	12	13800	1.2	155	8.2	600 - 800	3564	UDDS	6
	5	12	13800	1.2	155	8.2	600 - 800	3564	NYC	27
	6	12	13800	1.2	155	8.2	600 - 800	3564	NYC	50
	7	8	8800	1.2	75	6.2	600 - 800	1340	NYB	6
	8	8	8800	1.2	75	6.2	600 - 800	1340	MB	6
2	1	11.6	12500	0.66	275	8.28	600 - 800	1260	CSHV	3
	2	11.6	12500	0.66	275	8.28	600 - 800	1260	CSHV	7
	3	11.6	12500	0.66	275	8.28	600 - 800	1260	CSHV	15
	4	11.6	12500	0.66	275	8.28	600 - 800	1260	CSHV	26
	5	11.6	12500	0.66	275	8.28	600 - 800	1260	CSHV	38
3	1	12	12759	0.55	75	7.1	400	280	UDDS	1
4	1	12	9500	0.79	275	8.5	600 - 750	2500	OCTA	1
	2	12	9500	0.79	275	8.5	600 - 750	3250	OCTA	1
	3	12	9500	0.79	275	8.5	600 - 750	4100	OCTA	1
	4	12	9500	0.79	275	8.5	600 - 750	5400	OCTA	1
	5	12	9500	0.79	275	8.5	600 - 750	2500	MB	1
	6	12	9500	0.79	275	8.5	600 - 750	3250	MB	1
	7	12	9500	0.79	275	8.5	600 - 750	4100	MB	1

	8	12	9500	0.79	275	8.5	600 - 750	5400	MB	1
	9	12	9500	0.79	275	8.5	600 - 750	2500	NYB	1
	10	12	9500	0.79	275	8.5	600 - 750	3250	NYB	1
	11	12	9500	0.79	275	8.5	600 - 750	4100	NYB	1
	12	12	9500	0.79	275	8.5	600 - 750	5400	NYB	1
5	1	12	12500	0.66	155	8.28	600 - 800	2450	CSHV	10
	2	12	12500	0.66	155	8.28	600 - 800	2450	CSHV	38
	3	18	17500	0.66	155	8.28	600 - 800	3700	CSHV	30
	4	18	17500	0.66	155	8.28	600 - 800	3700	CSHV	75
	5	12	18500	0.66	155	10.35	600 - 800	4400	CSHV	30
	6	12	18500	0.66	155	10.35	600 - 800	4400	CSHV	75
6	1	12	10000	1.2	155	6.2	600 - 800	1515	NYB	22
	2	12	10000	1.2	155	6.2	600 - 800	1515	MB	22
	3	12	10000	1.2	155	6.2	600 - 800	1515	NYC	22
	4	12	10000	1.2	155	6.2	600 - 800	1515	CSHV	22
	5	12	10000	1.2	155	6.2	600 - 800	1515	UDDS	22

Table 7.7: Drive cycles specifications [116]

Cycle Name	Cycle ID	Duration [s]	Distance [km]	Average Speed [km/h]	Average Deceleration [m/s^2]	Idle Time [s]	Number of Stops
New York Bus	NYB	600	1.113	5.93	0.163	404	12
Manhattan Bus	MB	1089	3.32	10.98	0.188	395	21
New York Composite	NYC	1029	4.5	14.1	0.19	341	19
Orange County Transit Authority	OCTA	1909	11.845	19.84	0.237	407	31
Central Business District	CBD	569	3.64	20.43	0.2478	122	14
City Suburban Heavy Vehicle	CSHV	1780	12.1	21.86	0.167	385	19
Braunschweig	BRAU	1740	12.23	22.4	0.241	442	29
Urban Dynamometer	UDDS	1369	13.48	31.51	0.2248	259	17
Arterial	ART	291	3.6	39.71	0.276	48	4
Commuter	COM	329	7.248	70.28	0.82	40	1

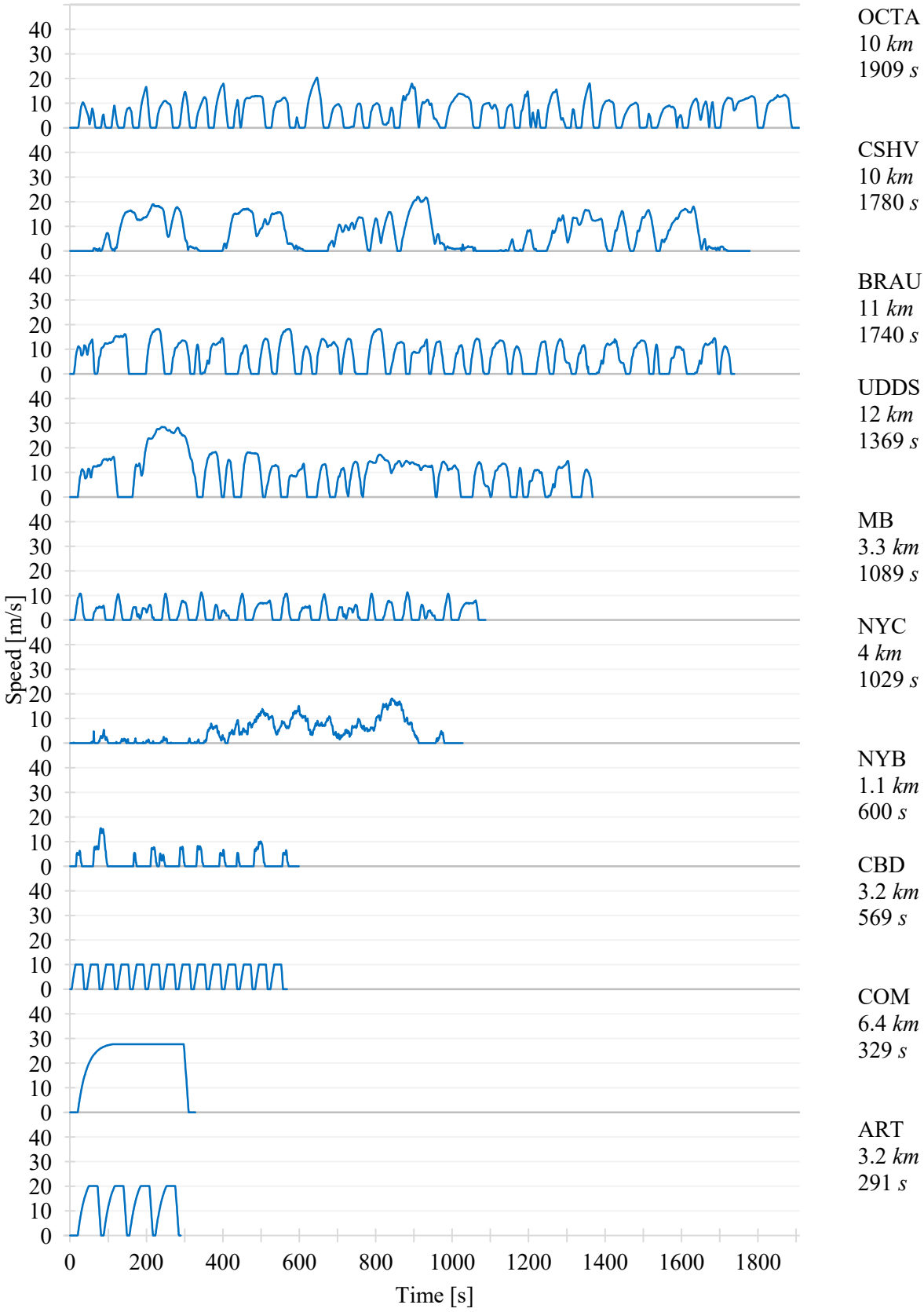


Figure 7.5: Velocity profiles of the test drive cycles used in model validation

Appendix D:
Comparative Energy Analysis of Battery Electric Bus and Diesel Bus

This appendix presents a comparative energy analysis of battery electric bus and diesel buses in order to highlight the BEB superior energy performance when compared to DB. First, the DB configuration is thoroughly described. Then, a sizing approach is presented to design the powertrain components for both BEB and DB according to APTA. A DB energy model is detailed similarly to the BEB energy model presented in Chapter 2. Finally, the energy performance of both buses is thoroughly evaluated.

- **Diesel Bus Configuration**

There are many technical differences between DB and BEB. Figure 7.6 shows the DB configuration highlighting the three main energy systems: (1) powertrain, (2) Cabin-HVAC, and (3) Auxiliaries. At the powertrain level, the DB consists of a diesel engine, a gearbox, a differential, wheels, and brakes in addition to its TCS. The cabin - HVAC system in DB is similar to the BEB system with the only difference lies in the compressor as it is directly driven by the diesel engine in this case, whereas the HVAC compressor in the BEB is driven by another electric motor apart from the traction motor allowing more flexibility in the compressor speed. Finally, the auxiliaries in DB are rather different from those in BEB. Most of these auxiliaries are pneumatic such as the doors, parking brakes, and suspension systems and they incur higher energy consumption compared to their electric counterparts in the BEB. Both buses share the same chassis parameters as shown in Table 2.3. Table 7.8 presents the auxiliaries technology in DB and BEB. Most of these auxiliaries are pneumatic in DB, whereas BEB take advantage of the already-established electric system and utilize electrically auxiliaries.

Table 7.8: Auxiliaries technology in DB and BEB

AUX	BEB	DB
Service Brakes	Pneumatic	Pneumatic
Parking Brakes	Electric	Pneumatic
Suspension System	Hydro-Electric	Pneumatic
Steering Pump	Hydro-Electric	Hydro-Electric
Lights	Electric	Electric
Wipers	Electric	Electric
Doors	Electric	Pneumatic

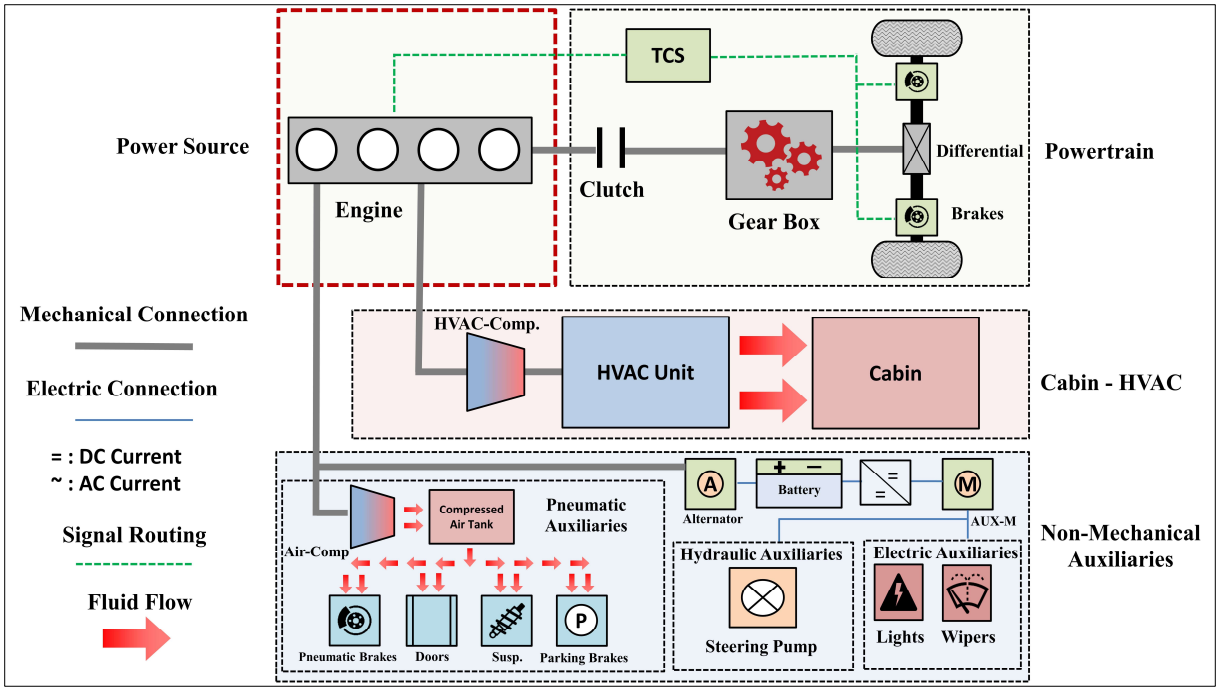


Figure 7.6: DB configuration

- **Sizing of Powertrain Components**

Prior to the development of the powertrain modeling, sizing its components is an essential step to make sure that they meet public transit performance specifications, and to ensure a fair comparison between both buses.

The APTA sets standards and performance specifications for public transit vehicles. Section 7 of the "Standard Bus Procurement Guidelines" TS. 7 "Power Requirements" defines the power requirement for a bus by introducing three main requirements the bus should overcome. These requirements are a top speed requirement, gradeability requirement, and acceleration requirement. Table 7.9 summarizes these requirements.

Table 7.9: Summary of bus performance requirement as set by APTA

Top Speed	Maintain a speed of 65 mph (105 km/h) on a straight level road	
Gradeability	Maintain a speed of 40 mph (65 km/h) on a 2.5% ascending grade	
	Speed mph (km/h)	Maximum time (Sec)
	10 (16)	5
	20 (32)	10
Acceleration	30 (48)	18
	40 (64)	30
	50 (80)	60
	Top speed	

In order to meet the first two requirements, the traction unit (Electric Motor or Diesel Engine) should be able to provide enough traction power to overcome the resistive forces and maintain the specified speeds at each grade level. Figure 7.7 shows the resistive forces' power as function of the bus speed for the BEB and DB, respectively. The resistive forces power is calculated according to the following equation:

$$P_{res} = \left(\frac{1}{2}.\rho.C_D.A_f.V^2 + M_{Veh}.g.\cos(\alpha).fr + M_{Veh}.g.\sin(\alpha)\right).V$$

The total weight of each bus is calculated as shown in Table 7.10.

Table 7.10: DB and BEB total mass segmentation

Components mass [kg]	Battery Electric Bus	Diesel Bus
Glider mass	11,600	11,600
Battery pack	4200	-
Engine + Fuel tank	-	1000
Transmission	80	250
EM	100	-
4 Auxiliary Electric Motors	100	-
Curb mass	**16080**	**12850**
Passenger mass	3400	3400
Total mass	**19480**	**15950**

The maximum traction power needed for the BEB is 142 *kW* and for the DB is 120 *kW*. This difference is due to the lower DB total weight. Concerning the diesel engine, an additional 55 *kW* is added to compensate for the thermal auxiliaries and other auxiliaries as they are driven by the engine. So finally, a 187 - kW electric motor is chosen for the BEB, and a 205 - kW diesel engine is chosen for the DB. These traction units are chosen based on existing engines and electric machines in ADVISOR libraries.

Concerning the acceleration requirement, the idea is to design the transmission ratios so that the chosen tractions units can supply enough torque to the wheels to follow the acceleration requirements. In the BEB, the whole transmission ratio (final drive and reduction gear) is designed to be equal to 27.5. As for the DB, the transmission system is quite different from the BEB. The gearbox is already chosen from ADVISOR libraries and the final drive ratio is designed to be equal to 4. Figure 7.8 shows the diesel engine maximum torque curve and the required engine torque at each gear ratio in order to follow the acceleration requirements. The required engine torque at all the gear ratios is below the engine maximum torque meaning that the powertrain complies with the acceleration requirements.

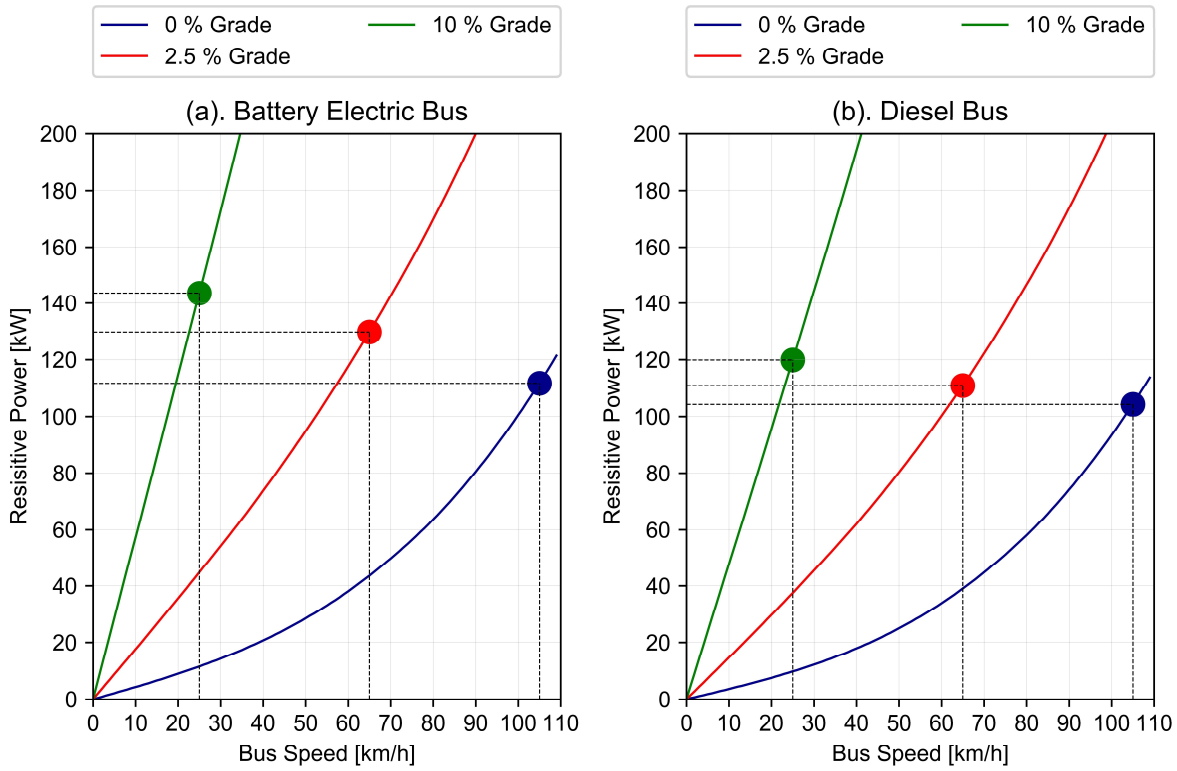


Figure 7.7: DB and BEB resistive power curve

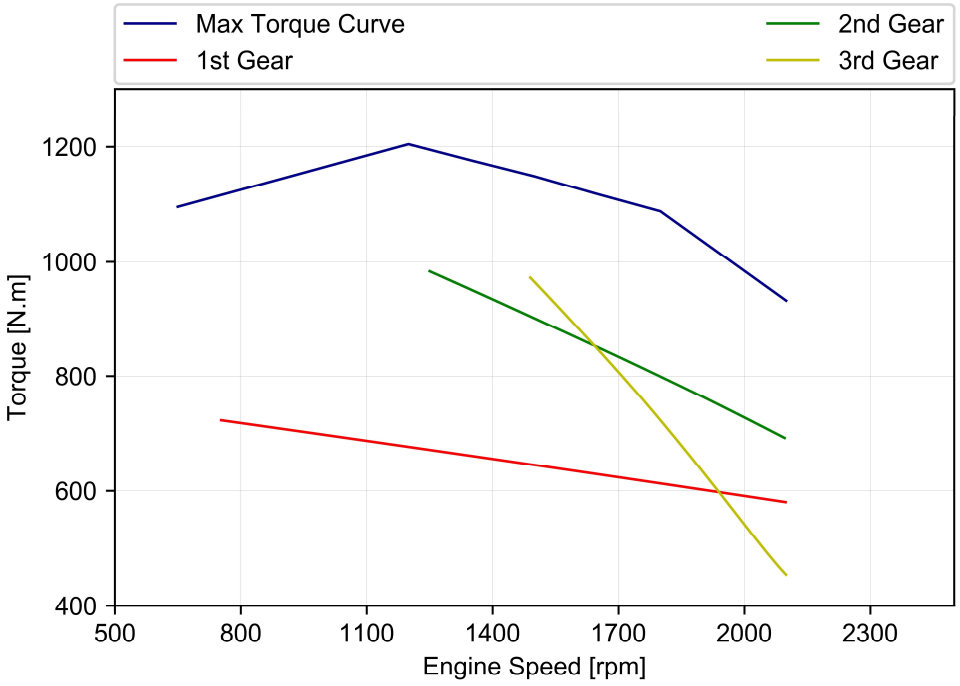


Figure 7.8: DB acceleration requirement curves

Finally, Table 7.11 summarizes the sizing results for both powertrains.

Table 7.11: Summary of DB and BEB component sizing

BEB	Electric Machine	Maximum Power	187 *kW*
		Maximum Torque	660 *N.m*
	Transmission	Reduction Gear Ratio	5.5
		Final Drive Ratio	5
DB	Diesel Engine	Maximum Power	205 *kW*
		Maximum Torque	1200 *N.m*
	Transmission	Gear Box Ratios	[3.43, 2.01, 1.43, 1]
		Final Drive Ratio	4

- **Diesel Bus Energy Model**

The main difference between the DB and the BEB powertrains lies in the traction unit and the transmission system. The engine is modeled by means of static maps and inertial components using the rotational mechanics library in Dymola. The engine dynamics can be ignored based on the quasi-static assumption and the engine fuel flow is only a function of its torque and rotational speed. Figure 7.9 shows the engine fuel flow map.

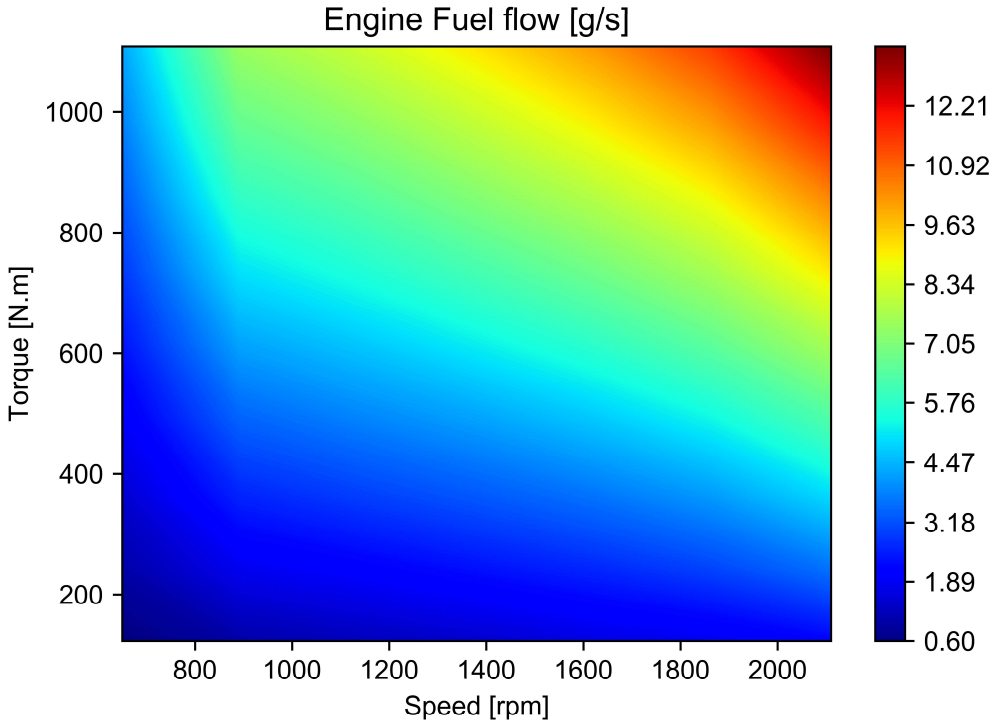


Figure 7.9: Engine fuel flow map

The engine fuel consumption is measured in Litres of diesel fuel per 100 km ($L/100\ km$). But in order to compare the energy consumption of both buses, the DB fuel consumption is

converted to its equivalent electric energy consumption (E_{DB}) measured in $kWh/\ km$ as shown in the following equation.

$$E_{DB} = \int_0^t \dot{m}(t).dt \,.\frac{Q_{LHV}}{D_{Total}}.\frac{1}{3.6e^6}$$

The diesel fuel flow rate $\dot{m}$ is calculated using linear interpolation based on the engine map.

As for the gearbox, it is a 4-speed gearbox with a maximum transmission efficiency of 95%. The largest gear ratio is 3.42 and the smallest ratio is 1. The gearbox is coupled to a differential with a final drive ratio equals to 4. The gearbox is modeled using Dymola rotational mechanics library by connecting a set of gears, synchronizers, and controllers all together as shown in Figure 7.10.

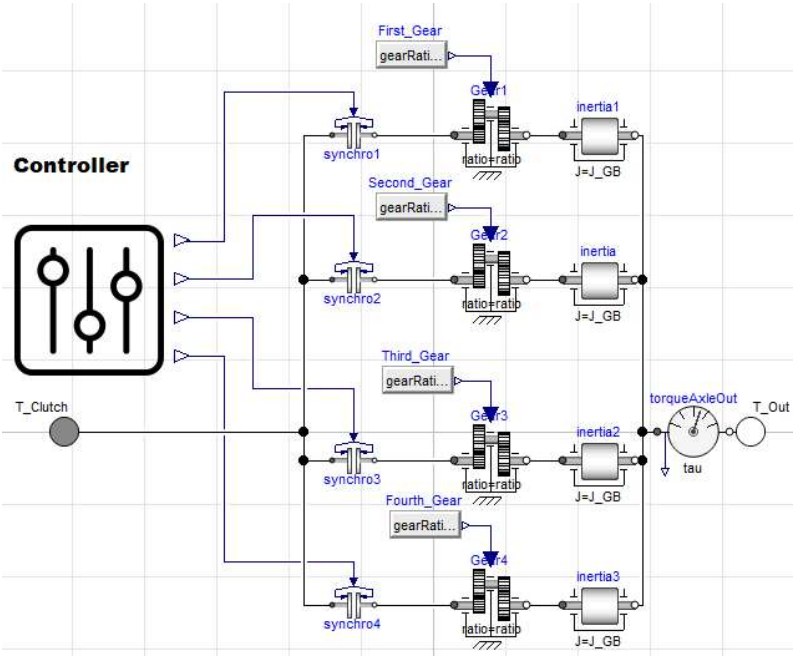


Figure 7.10: Gearbox Model of the DB in Dymola

- **Comparative Energy Analysis**

Using the introduced models, different simulations are conducted in order to evaluate the energy performance of both the BEB and the DB at different driving and weather conditions. Three levels of traffic are considered representing heavy traffic, normal traffic, and low traffic. Moreover, three different weather conditions are considered representing extreme cold weather conditions (-10 °C), cold weather conditions (10 °C), and hot weather conditions (40 °C). In this section, the performance of the different energy systems is analyzed.

- **Propulsion System**

Figure 7.11 shows the propulsion system energy consumption at different traffic conditions for both buses. Across all traffic conditions, the DB consumed more energy compared to the BEB. This is due to the powertrain efficiency in both buses. The engine efficiency in the DB ranges between 35%-40% whereas the electric motor efficiency in the BEB is around 80%.

As for the BEB, its traction energy consumption is not sensitive to the traffic conditions, and the consumption is always centered around 2 *kWh/km*. The main reason behind this stability is that the electric motor efficiency is less sensitive to the operating speed. However, the DB shows high sensitivity to the traffic conditions, and its consumption doubles at heavy traffic conditions compared to lower traffic. The first reason behind this increase in energy consumption is the diesel engine drop in efficiency at lower speeds representing heavy traffic conditions. The diesel engine efficiency can drop down to 10% at very low speeds causing this increase in traction energy consumption. In addition, engine consumption during idling is another reason that leads to this increase in consumption. Heavier traffic conditions cause more bus stops resulting in huge idling consumption

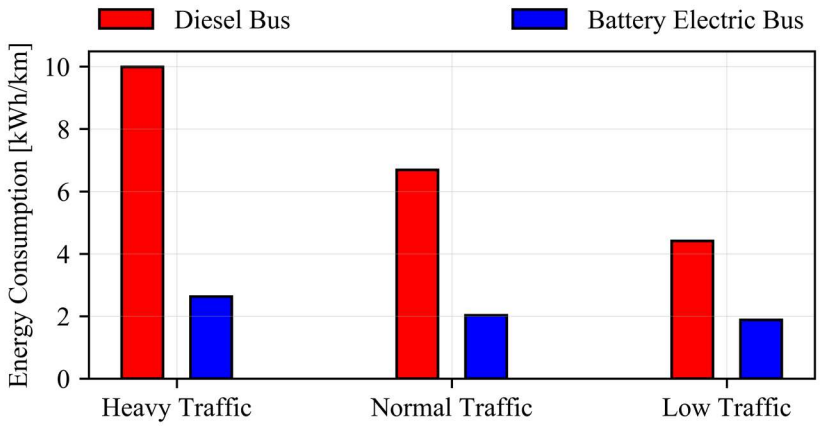


Figure 7.11: DB and BEB propulsion system energy consumption at different traffic conditions

It is interesting to segment the propulsion system energy consumption to better understand and evaluate the difference in energy consumption between BEB and DB. Figure 7.12 shows the propulsion system energy consumption segmentation for both buses at heavy, normal, and low traffic conditions respectively. The load is segmented as follows:

1. Energy consumed during the bus acceleration (Acceleration).
2. Energy consumed during the bus idling (Idling).
3. Energy recovered during the bus braking (BER).

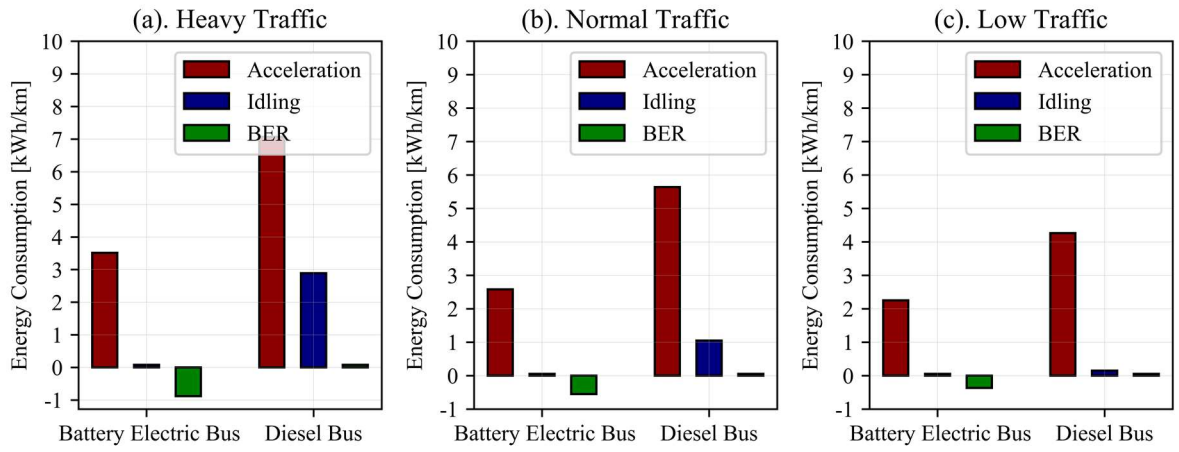


Figure 7.12: DB and BEB propulsion system energy segmentation

The acceleration energy consumption for both buses across all traffic conditions is directly related to the powertrain efficiency as discussed earlier. The BEB has higher propulsion efficiency and this is the first reason behind its lower energy consumption

As for the idling energy consumption, the DB encounters very high idling energy consumption during heavy traffic conditions due to frequent bus stops. This value decreases as traffic becomes less congested. On the other hand, the BEB encounters no idling energy consumption since its electric motor is turned off during bus layovers or stops due to traffic. The idling consumption represents almost 40% of the DB total propulsion energy consumption and this is the second reason behind its higher energy consumption.

Moreover, the BEB has the BER feature which is not possible in the case of the DB. The BER allows the BEB to recuperate part of its kinetic energy during braking resulting in a reduction in the total traction energy consumption that may reach 20% depending on the recuperation level. This highlights the last reason behind the BEB lower energy consumption.

- **Auxiliaries**

Traffic conditions do not only impact the traction load energy consumption, but it also affects the auxiliary's energy consumption. Figure 7.13 shows the auxiliaries' energy consumption at different traffic conditions for both buses. The DB is still recording higher energy consumption compared to the BEB mainly due to its reliance on a pneumatic auxiliary system with higher energy consumption and lower efficiency compared to the mostly all-electric auxiliary system in the BEB.

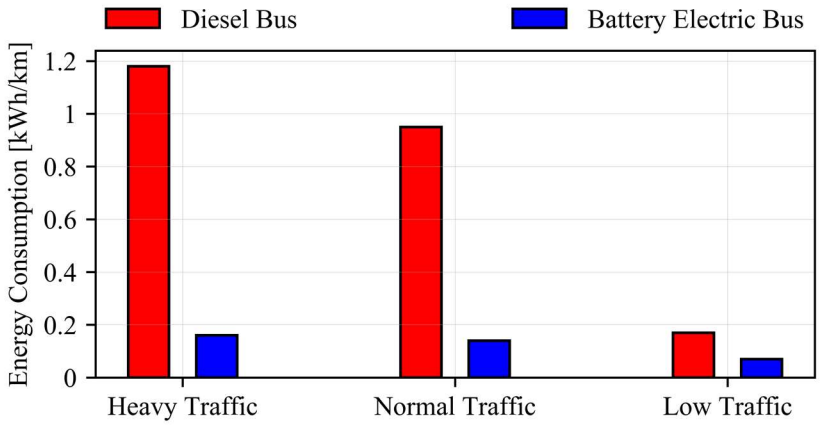


Figure 7.13: DB and BEB auxiliaries energy consumption at different traffic conditions

Moreover, heavier traffic conditions have a significant impact on the auxiliary's energy consumption. With heavier traffic conditions, the auxiliaries are used more frequently resulting in this increase in their energy consumption. For example, the service brakes are used more during heavier traffic conditions resulting in additional consumption. Furthermore, the steering pump hydraulic power demand is significantly higher at lower vehicle speeds which is the case at heavier traffic conditions resulting in higher energy consumption. In addition, heavier traffic conditions encounter more bus stops resulting in a more frequent actuation of the suspension system which is a significant energy load in heavy-duty vehicles.

- **HVAC Unit**

The weather conditions significantly affect the energy consumption of the bus especially if extreme weather conditions are considered. Figure 7.14 shows the HVAC unit energy consumption at different weather conditions for both buses. Both buses record very high energy consumption at extreme weather conditions. This consumption is almost equivalent to the propulsion energy consumption at extreme weather conditions. In other words, the energy needed to air-condition the bus is equal to the energy needed to propel the bus. For a BEB, this means a drastic reduction in its driving range creating schedule disruptions and disturbances in operation as it must be charged more frequently to compensate for this energy consumption due to air conditioning. The DB also witnesses a decrease in its driving range at extreme weather conditions, however, this is not a big concern as its refueling process is very fast compared to the BEB.

On another hand, the DB consumes almost as twice as the BEB to air-condition its cabin across all weather conditions. The main reason is that the HVAC system efficiency in the DB is way

lower than that in the BEB since the AC Comp. is driven by the engine in the DB which operates at lower efficiencies compared to the electric motor that operates the AC Comp. in the BEB. It is important to note that waste heat recovery from the diesel engine is not considered in this study. Waste heat recovery can help reduce the total energy demand for heating inside the DB.

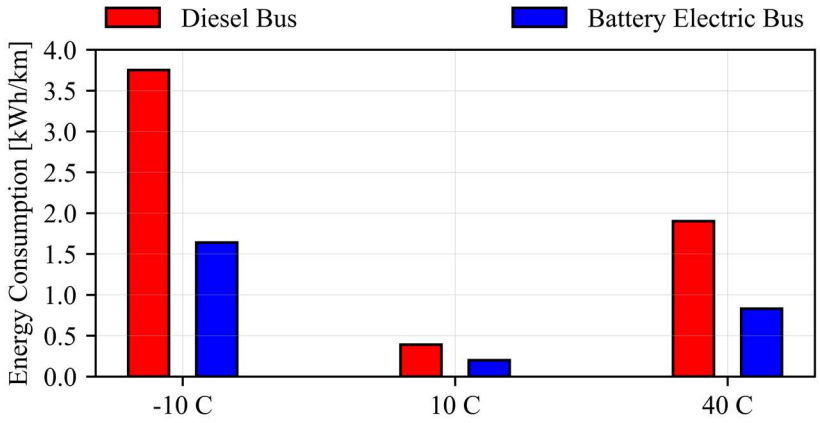


Figure 7.14: DB and BEB HVAC unit energy consumption at different weather conditions

This study comprehensively evaluates and compares the energy consumption of BEB and DB considering all the different energy loads encountered on the bus. Different simulations are conducted representing different driving and weather conditions. The results show that a BEB can consume up to 4 times less energy compared to the DB especially in heavy traffic conditions where most of this reduction comes from a reduction in the traction load energy consumption. The propulsion system energy consumption is further segmented and the analysis revealed that powertrain efficiency, diesel engine idling consumption, and BER feature all favor the BEB to have a way lower propulsion energy consumption compared to the DB.

Appendix E:
Development of the BEB Energy Consumption Maps

The BEB energy consumption maps are developed by simulating the dynamic BEB model presented in Chapter 2 at a variety of operating conditions.

- 10 drive cycles are considered (Table 7.7 in Appendix C) with the following specifications:
    - Trip average speed ranges between 5.93 and 70 *km/h*
    - Trip distance ranges between 1.113 and 13.48 *km*
    - Trip duration ranges between 10 and 31.81 minutes
    - Trip average acceleration ranges between 0.28 and 1.17 m/s^2
    - Trip average deceleration ranges between 0.16 and 0.82 m/s^2
    - Trip number of stop stations ranges between 1 and 31
    - Trip Idle time ranges between 0.67 and 7.36 minutes
- The external temperature varies from -10 to 40 $°C$, with a step of 1 $°C$ (51 cases).
- Solar flux varies between 0 and 700 W/m^2, with a step of 50 W/m^2 (15 cases)
- Passenger occupancy varies between 0 and 80 passengers, with a step of 5 passengers (17 cases).

Thus, a total of 10x51x15x17 = 130050 simulations is conducted to build the BEB energy consumption maps.

Linear interpolation is used to estimate the energy consumption of the BEB at specific operating conditions that are considered in these simulations. Finally, Table 7.12 summarizes the criteria used to develop BEB energy consumption maps for each energy system in the BEB.

Table 7.12: Summary of the criteria used to develop BEB energy consumption maps

Energy System		Concerned Parameters	Output	Number of Data Points
Propulsion		• Trip average speed (V_{avg}) • Passenger's Occupancy (n_P)	- A single 2-D map: $\overline{\mathrm{E}}_{\mathrm{Prop}} = f(V_{avg}, n_P)$	10 x 17 = 170 points
HVAC		• Temperature (T) • Solar Flux Intensity (SF) • Passenger's Occupancy (n_P) • Door Opening Frequency (R)	- Two 2-D maps • HVAC power without solar flux $P_{HVAC} = f(T, n_P)$ • Additional HVAC power due to solar flux $\mathrm{P}_{\mathrm{HVAC-SF}} = f(T, SF)$ • Correction factor to consider door opening losses $C_F = f(R)$	- Map1: 51 x 17 = 867 points - Map2: 51 x 15 = 765 points - Correction factor: 10 points
Auxiliaries	BTMS	• Temperature (T) • Passenger's Occupancy (n_P)	- A single 2-D map: $P_{BTMS} = f(T, n_P)$	51 x 17 = 867 points
	Pneumatic (Air Compressor)	• Trip Average deceleration D_{avg}	- A single 1-D graph: $P_{Pneu} = f(D_{avg})$	10 points

	Hydraulic (Steering Pump)	• Trip average speed (V_{avg})	- A single 1-D graph: $P_{Hyd} = f(V_{avg})$	10 points
	Electric and Suspension System	• Number of Stops *(NS)*	- A single 1-D graph: $P_{Ele-Sus} = f(NS)$	10 points

Appendix F:
Validation of the Map-Based BEB Energy Consumption Against Real-World Data

To verify the energy consumption of the map-based BEB energy consumption during typical real-world operating conditions against the dynamic model simulations, the model is simulated using the operating conditions of bus line number 21 in the city of Paris due to data availability. The bus drive cycle is shown in Figure 7.15, the distance covered per trip is 9.7 *km* during 1hour and 15 minutes resulting in an average speed of 8.3 *km/h*. Besides, three typical weather conditions for the city of Paris are considered representing the annual average temperature (12 °C), winter average temperature (5 °*C*), and summer average temperature (21 °*C*). As for the passenger's occupancy, three levels of occupancy are considered representing morning peak hours occupancy (51%), evening peak hours occupancy (72%), and off-peak hours occupancy (10.6%). The passenger's occupancy data during a typical working day for bus line number 21 in Paris are shown in Figure 7.16. The resulting energy consumption at these operating conditions is presented in Table 7.13. The map-based energy consumption is very close to the results yielded by the dynamic models' simulation, as the percentage error is always below 2%.

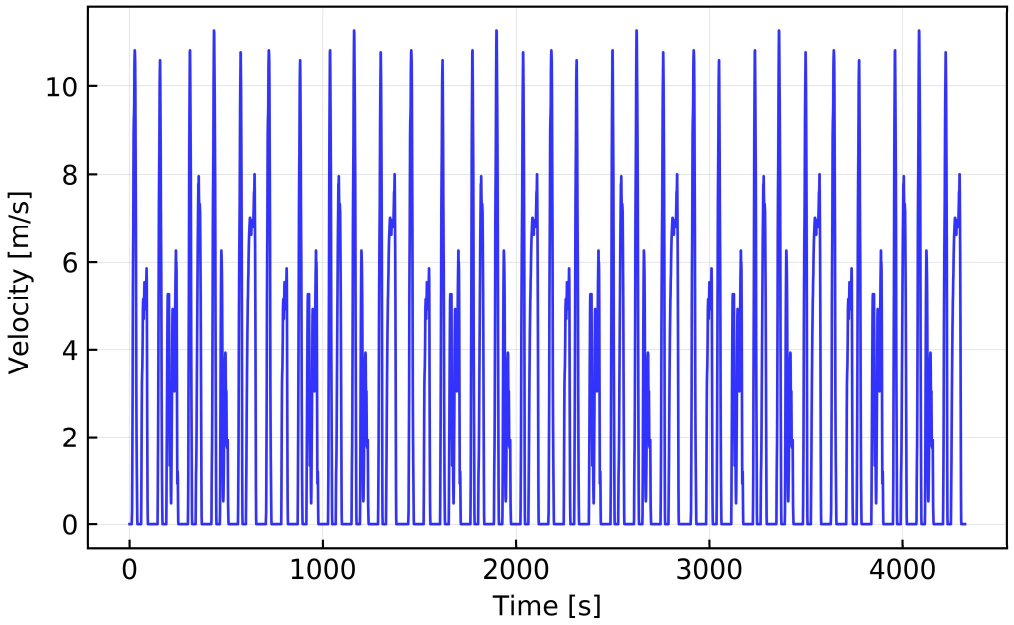


Figure 7.15: Velocity profile of bus line 21 in Paris

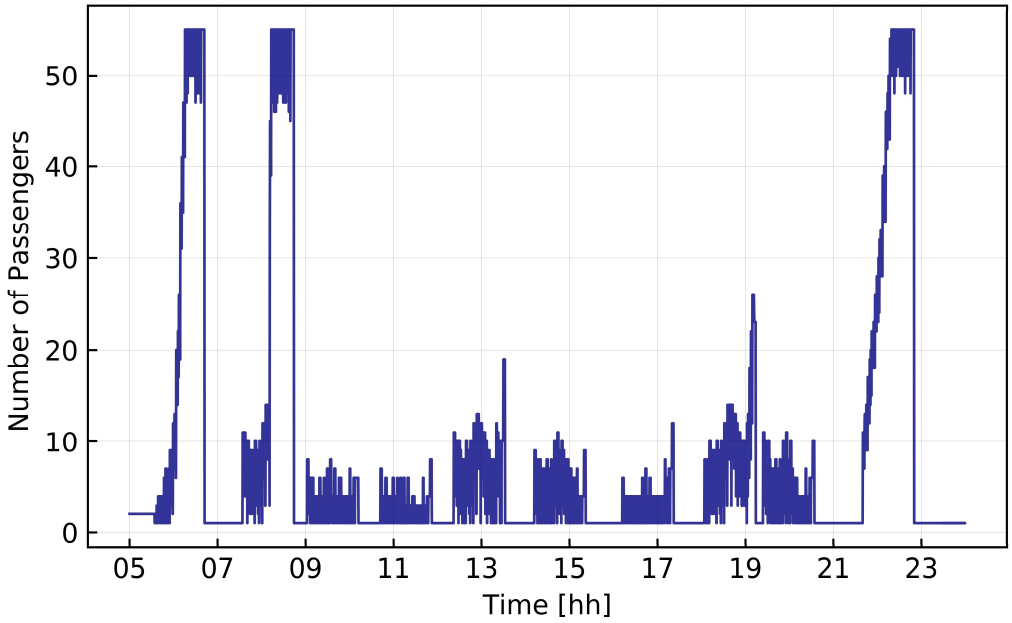


Figure 7.16: Passengers occupancy profile for bus line 21 in Paris (recorded on a Monday, July 2019)

Table 7.13: Validation of BEB map-based energy consumption (kWh/km)

		Occupancy Level		
		10.60%	51%	72%
Temperature: 12 °C	Simulation	2.35	2.37	2.4
	Maps	2.31	2.34	2.36
	% Error	**1.70%**	**1.27%**	**1.67%**
5 °C	Simulation	2.51	2.61	2.62
	Maps	2.47	2.56	2.57
	% Error	**1.59%**	**1.92%**	**1.91%**
21 °C	Simulation	1.97	2.07	2.1
	Maps	1.93	2.1	2.08
	% Error	**2.03%**	**-1.45%**	**0.95%**

Appendix G:

Supplement to Section 4.3.1

- **Passengers' Flow Interaction: Terminal Stations - BEBs**

Let $\mathcal{J}_T$ be a dynamic binary matrix of size 2 x n_B in order to detect which BEBs are parked at each terminal station.

$$\mathcal{J}_T\,(t) = \begin{bmatrix} I_{1,1} & \dots & I_{1,b} & \dots & I_{1,n_B} \\ I_{2,1} & \dots & I_{2,b} & \dots & I_{2,n_B} \end{bmatrix} \quad \forall\, B_b \in \mathcal{B} \tag{7.1}$$

$$I_{r,b}(t) = \begin{cases} 1, & \forall\ X_{B_b}(t) = X_{T^r} \wedge V_{B_b}(t) = 0 \\ 0, & \text{otherwise} \end{cases} \quad \forall\ I_{r,b} \in \mathcal{J}_T \tag{7.2}$$

$N_P^{T^r}$ is the number of passengers waiting at terminal station T^r as expressed in equation (7.3) where $\dot{n}_{In}^{T^r}$ is the passengers inward flow to the terminal station, and $\dot{n}_{out}^{T^r}$ is the passengers outward flow from the terminal station to the BEB. Similarly, $N_P^{B_b}$ is the number of passengers occupying BEB *b* at any instant *t* is expressed in equation (7.4).

$$N_P^{T^r}(t) = \int_0^t (\dot{n}_{In}^{T^r} - \dot{n}_{out}^{T^r}).\, dt \tag{7.3}$$

$$N_P^{B_b}(t) = \int_0^t (\dot{n}_{In}^{B_b} - \dot{n}_{out}^{B_b}).\, dt \tag{7.4}$$

The inward passengers' flow $\dot{n}_{In}^{T^r}$ to a terminal station is dependent on its location and time of the day, and it is an input to the BEB line model as expressed in equation (7.5).

$$\dot{n}_{In}^{T^r} = f(r, t) \tag{7.5}$$

Let t_d be the BEB departure time from the terminal station to start its return trip. The outward passengers' flow $\dot{n}_{Out}^{T^r}$ from a terminal station is expressed in equation (7.6).

$$\dot{n}_{out}^{T^r}(t) = \begin{cases} \sum_{b=1}^{n_B} I_{r,b}(t).\,\alpha\,, & \forall\, I_{r,b} \in \mathcal{J}_T \mid t < t_d \ \wedge N_P^{T^r}(t) > 0 \wedge N_P^{B_b}(t) < N_{P,Max}^{B} \forall\, B_b \in \mathcal{B} \\ 0, & \text{otherwise} \end{cases} \quad \forall\, T^r \in \mathcal{T} \tag{7.6}$$

α is a positive non-zero constant measured in (passengers/s) and $N_{P,Max}^{B}$ is the maximum allowable number of passengers on any bus.

The inward passengers' flow rate $\dot{n}_{In}^{B_b}$ to BEB B_b is dependent on the number of passengers waiting at the terminal station as described in equation (7.7).

$$\dot{n}_{In}^{B_b}(t) = \begin{cases} \sum_{r=1}^{2} I_{r,b}(t).\beta\,, & \forall\, I_{r,b} \in \mathcal{J}_{T,b} \subseteq \mathcal{J}_T \mid t < t_d \wedge N_P^{B_b}(t) < N_{P,Max}^{B} \wedge N_P^{T^r}(t) > 0\ \forall\, T^r \in \mathcal{T} \\ 0, & \text{otherwise} \end{cases} \quad \forall\, B_b \in \mathcal{B} \tag{7.7}$$

β is a positive non-zero constant measured in (passengers/s). $\mathcal{J}_{T,b}$ is a vertical sub-vector at column index *b* of matrix $\mathcal{J}_T$.

The outward passengers' flow $\dot{n}_{out}^{B_b}$ from BEB B_b at the terminal stations should ensure full discharge of passengers from the BEB as expressed in equation (7.8).

$$\dot{n}_{out}^{B_b}(t) = \begin{cases} \sum_{r=1}^{2} I_{r,b}(t).\kappa\,, & \forall\ I_{r,b} \in \mathcal{J}_{T,b} \subseteq \mathcal{J}_T \mid N_P^{B_b}(t) > 0\ \forall\, T^r \in \mathcal{T} \\ 0, & \text{otherwise} \end{cases} \quad \forall\, B_b \in \mathcal{B} \tag{7.8}$$

κ is a positive non-zero constant measured in (passengers/s).

Appendix H:
Battery Aging Model

Aging mechanisms are among the main challenges facing Lithium-ion batteries. Battery aging mechanism and degradation directly affect its performance as they result in capacity fade and resistance growth [81]. Throughout the battery lifetime, aging mechanisms reduce the battery charge capacity which explicitly yields to a reduction in the BEB driving range in the long run. Battery aging mechanisms are classified within two categories: (1) calendar aging and (2) cycle aging [82].

Calendar aging corresponds to the aging mechanisms resulting from battery storage [83], [84] mainly referred to as the self-discharge rate. The self-discharge rate is significantly affected by the storage conditions which may accelerate or slow down battery aging mechanisms [85]. Several studies across the literature report that the storage temperature and battery voltage have the highest effect on battery calendar aging [81], [86], [87]. High storage temperatures facilitate Lithium-ion corrosion reactions inducing capacity fade [88] whereas low storage temperatures limit these reactions. However, very low storage temperatures alter the battery chemistry and increase battery resistance [89].

On the contrary, cycle aging is mainly associated with the battery utilization patterns such as battery charging and discharge as well [81]. Two main factors impact Lithium-ion cycle aging: (1) SOC variation during charge/discharge and (2) charge/discharge rate. High SOC variation associated with deep charge/discharge accelerates cycle aging due to the degradation of the positive electrode [90]. In addition, high battery discharge/charge rates accelerate cycle aging mechanisms [91], [92].

Lithium-ion battery aging models are mainly divided into 3 parts: (1) electrochemical models, (2) equivalent circuit models, and (3) global performance models. Table 7.14 presents a summary of the different modeling approaches for Lithium-ion batteries aging.

For this thesis, global performance models are utilized to predict Lithium-ion batteries aging as they yield acceptable precision and computation complexity, and most importantly, the ability to couple such models to the developed BEB model.

Table 7.14: Summary of Lithium-ion batteries aging modeling approaches

Modeling Approach	Description	Model Performance
Electrochemical Models	Modeling the physical phenomena occurring inside the battery cells in detail providing a thorough understanding of these phenomena and their impact on battery aging [93]–[95].	Computation Complexity: --- Precision: +++ Data Requirement: - Coupling to BEB Model: ---
Equivalent Circuit Based Models	Simplified input-output models function of battery parameters mainly resistance, capacitance, and temperature. Models parameterization is obtained by running a large number of time-consuming tests [96]–[99].	Computation Complexity: - Precision: + Data Requirement: - Coupling to BEB Model: ++
Global Performance Models	Developing correlations between the different stress factors and the battery capacity fade through accelerated aging tests. Calendar and cycle aging are estimated separately[100]–[102].	Computation Complexity: - Precision: ++ Data Requirement: -- Coupling to BEB Model: ++

The proposed global performance model (GPM) for battery aging predicts battery cells capacity fade due to calendar aging and cycle aging. The normalized battery cell capacitance fade is expressed in equation (7.9) according to [103] where B is a pre-exponential factor, E_a is the activation energy of the reaction, R is the gas constant, T is the battery cell temperature and A_h is the charge throughput of the battery cell.

$$Q_{Loss} = B.\exp\left(\frac{E_a}{R.T}\right).(A_h)^z \tag{7.9}$$

The charge throughout A_h is the charged/discharged battery capacity over a certain period and it is expressed in equation (7.10) where N_{cyc} is the number of charge/discharge cycles. That being said, the charge throughput is directly related to time.

$$A_h = DOD.N_{cyc}.Q_{max} \tag{7.10}$$

$$DOD = 1 - SOC \tag{7.11}$$

The proposed equation considers both calendar and cycle aging. As mentioned earlier, calendar aging is the battery self-discharge overtime during storage, and it is highly affected by the storage temperature and time. As for the temperature effect, the Arrhenius equation is commonly used to describe the impact of temperature on calendar aging as presented in the exponential factor in equation (7.9). In addition, theories and experiments on battery calendar aging report a square-root time dependency as shown in [104]–[106] and this is also considered in the power-law factor z which is equal to 0.55.

On the other hand, cycle aging is directly affected by the battery depth of discharge (DOD) and charge/discharge rate. The battery cell DOD is explicitly considered in the charge throughput term whereas the charge/discharge rate, referred to as the C_{Rate}, affects the pre-exponential factor B and the activation energy E_a. The activation energy is expressed in equation (7.12) function of the C_{Rate}, where C_{Rate} is expressed in 7.13 as function the battery cell electric current I_{Cell} and cell charge capacity Q_{Cell}.

$$E_a = -31700 + 370.3.C_{Rate} \tag{7.12}$$

$$C_{Rate} = \frac{I_{Cell}}{C_{Cell}} \tag{7.13}$$

Finally, the pre-exponential factor B is function of the C_{Rate} as well and its value is extracted from data provided by [103]. Figure 7.17 presents the battery aging scheme highlighting the interactions among the battery electrical, thermal, and aging models.

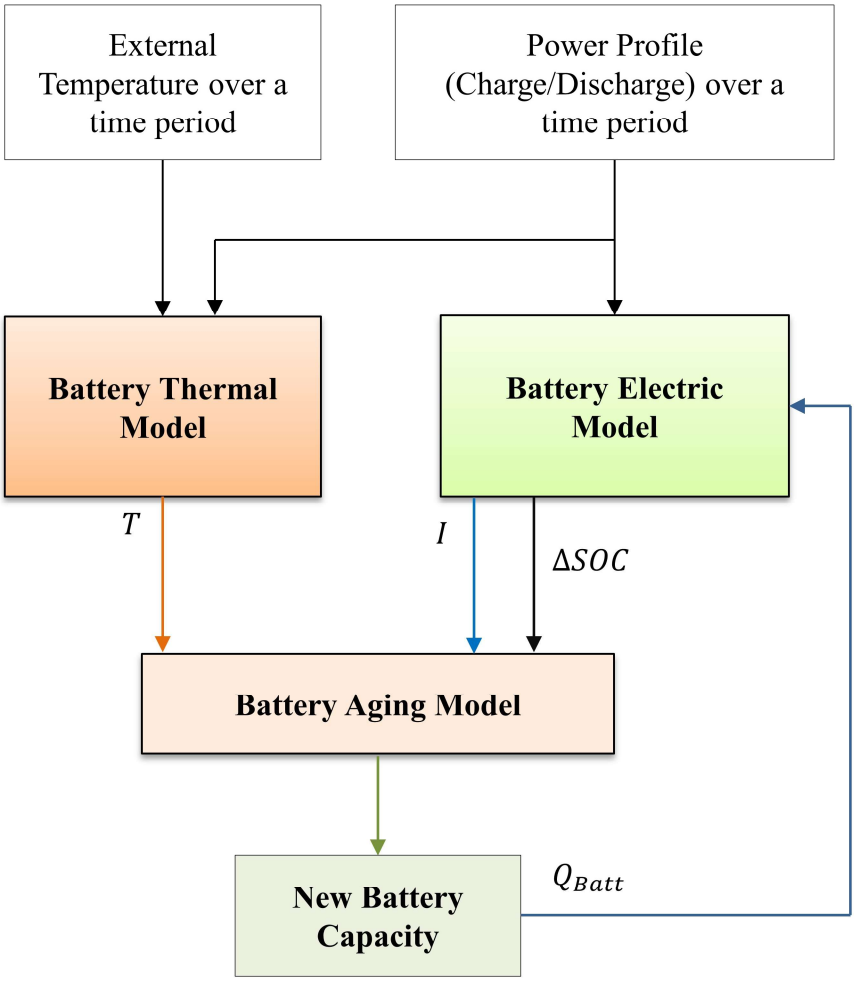


Figure 7.17: Scheme of battery aging model

Appendix I:
GA Global Optimum

In this study, a GA optimization methodology is utilized to minimize TCO. The search methodology implemented in GA-based optimization techniques may converge to a local minimum rather than the global minimum and thus sacrificing the solution optimality. For this sake, the GA optimization process is conducted at a variety of initial conditions in order to ensure that the resulting solution is the global optimal solution. Figure 7.18 shows GA objective function (TCO) variation as the number of generations increases using 5 different initial conditions. At all initial conditions, the algorithm converges to a single optimal solution verifying the global optimality of this solution.

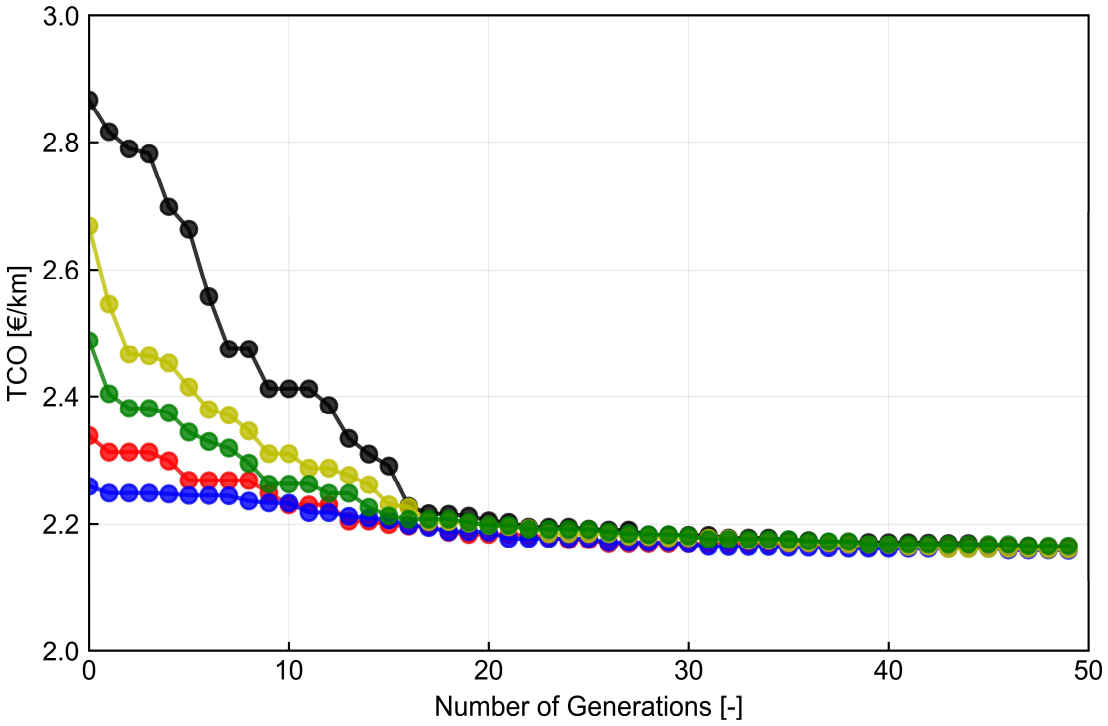


Figure 7.18: GA optimal solution at different initial conditions

This Page is Intentionally Left Blank

LIST OF PUBLICATIONS

Journal Publications

- **Comprehensive Energy Modeling Methodology for Battery Electric Buses**.

Hussein Basma, Charbel Mansour, Marc Haddad, Maroun Nemer, and Pascal Stabat. Published in: Energy, Sep- 2020. https://www.sciencedirect.com/science/article/abs/pii/S0360544220313487

- **Model and Optimal Control of Heat Pump System in Battery Electric Buses**

Rabih Al Haddad, Hussein Basma, and Charbel Mansour. Submitted to: Proceedings of the Institution of Mechanical Engineers, Part D – Journal of Automobile Engineering, 2020.

- **Energy Consumption and Battery Sizing for Different Types of Battery Electric Bus Service**

Hussein Basma, Charbel Mansour, Marc Haddad, Maroun Nemer, and Pascal Stabat. Submitted to: Transportation Research Part D: Transport and Environment, 2020.

International Conference Publications

- **Optimization of Battery Electric Bus Charging Under Varying Operating Conditions**

Hussein Basma, Charbel Mansour, Maroun Nemer, Marc Haddad, and Pascal Stabat. IEEE Vehicular Propulsion Power Conference (VPPC), Gijon, Spain, 2020.

- **Genetic Algorithm Control Strategy for Heat Pump System in Battery Electric Buses**

Rabih Al Haddad, Hussein Basma, and Charbel Mansour. IEEE Vehicular Propulsion Power Conference (VPPC), Gijon, Spain, 2020.

- **Analysis of Bus Fleet Electrification at Different Operating Conditions**

Hussein Basma, Charbel Mansour, Maroun Nemer, Pascal Stabat, and Marc Haddad. Published in: Proceedings of the 8th European Transport Research Arena, Helsinki, Finland, 2020. https://hal.archives-ouvertes.fr/hal-02611573/document

- **Comprehensive Energy Assessment of Battery Electric Buses and Diesel Buses**

Hussein Basma, Charbel Mansour, Marc Haddad, Maroun Nemer, and Pascal Stabat. Published in: Proceedings of the 32nd International Conference on Efficiency, Cost, Optimization, Simulation and Environmental Impact of Energy Systems, Wroclaw, Poland, 2019. https://hal.archives-ouvertes.fr/hal-02169856/document

- **Analysis of Heat Pump Performance in Battery Electric Buses**

Rabih Al Haddad, Hussein Basma, and Charbel Mansour. Published in: Proceedings of the 32nd International Conference on Efficiency, Cost, Optimization, Simulation and Environmental Impact of Energy Systems, Wroclaw, Poland, 2019. https://hal.archives-ouvertes.fr/hal-02169864/document

Work in Progress

- **A Techno-Economic Model of Battery Electric Bus Lines.**

Hussein Basma, Charbel Mansour, Marc Haddad, Maroun Nemer, and Pascal Stabat. To be submitted to Electric Power System Research.

- **Methodology for Optimal Battery Sizing and Charging Strategy for Battery Electric Buses.**

Hussein Basma, Charbel Mansour, Marc Haddad, Maroun Nemer, and Pascal Stabat. To be submitted to Transportation Research Part C: Emerging Technologies.

Résumé Français

9.1 Chapitre 1
INTRODUCTION

9.1.1 Contexte général

Plusieurs initiatives sont mises en œuvre à l'échelle mondiale pour réduire les émissions de gaz à effet de serre (GES) et les polluants locaux. Malgré les efforts déployés pour introduire des réglementations et des normes, les objectifs donnés en matière d'émissions ne sont pas atteints. Le secteur des transports compte 23 % des émissions de GES derrière la production d'électricité et de chaleur. Le transport routier incluant les véhicules particuliers et les poids lourds (camions et bus) est responsable de plus des trois quarts de ces émissions, tandis que les activités aériennes et ferroviaires représentent le reste.

Les émissions des bus et des camions enregistrent une augmentation au cours des 20 dernières années avec un taux moyen annuel de 2,2%. Malgré l'introduction et la mise en service de technologies alternatives ces dernières années, le pétrole détient toujours la plus grande partie du marché de la mobilité. Le déploiement de technologies alternatives pour le transport routier est lié étroitement à la logistique énergétique, au coût-bénéfice, à l'adaptation des infrastructures et à l'acceptation par le public. Cependant, les transports publics sont moins sensibles à ces facteurs, en particulier les bus de transport en commun. En effet, ces derniers circulent sur des itinéraires fixes en ayant des emplacements de départ et des terminaux centralisés, une infrastructure commune qui facilitent la mise en œuvre de technologies alternatives pour les bus de transport public.

9.1.2 Technologies alternatives de bus

Les technologies alternatives sont principalement classées en 3 catégories : (1) bus à combustibles fossiles, (2) bus à biocarburant et (3) bus électrifiés.

Les bus à combustibles fossiles alternatifs brûlent du gaz naturel comprimé (GNC) à l'aide d'un moteur à combustion interne (ICE) similairement aux bus diesel (BD). Le GNC est principalement composé de méthane (CH4), comprimé à 250-350 bars. Les biocarburants tels que le biodiesel ou l'éthanol sont aussi utilisés dans les ICE. Les deux technologies diffèrent par le système de stockage de carburant.

Les bus électrifiés sont alimentés en électricité, une machine électrique (ME) est utilisée pour propulser le bus. Ils sont classifiés selon la configuration de leur système de propulsion. Les bus électrifiés intègrent les bus électriques hybrides (BEH), les bus électriques à Pile A Combustible (PACO) et les bus électriques à batterie (BEB). Le BEH utilise à la fois un ICE et un ou plusieurs ME selon plusieurs architectures. En général, les architectures utilisées sont série ou parallèle pour décrire le type de connexion mécanique entre l'ICE et la ME. La PACO requiert de l'hydrogène pour produire de l'électricité. L'hydrogène est généralement produit à partir de combustibles fossiles via un reformeur. Enfin, le BEB est une technologie de bus électrique qui est alimentée par l'énergie électrique stockée dans la batterie.

9.1.3 Bus Electrique à Batterie

Le BEB est la solution la plus prometteuse pour remplacer les flottes de BD actuelles du fait de ses avantages environnementaux. Cependant, cette technologie est encore soumise à de nombreux défis. Cette section décrit les avantages du BEB par rapport au BD et aux autres technologies alternatives et les défis qui retardent leur déploiement à grande échelle.

- **Avantages**

Les BEB ont un grand potentiel pour réduire les émissions totales de GES du puits à la roue (*Well-to-Wheel* - WTW) par rapport au BD ou aux technologies alternatives. Les BEB sont capables de réduire les émissions WTW - GES de 41 à 98% par rapport au DB selon le mix énergétique de production d'électricité. Le graphique de gauche de la Figure 9.1 montre les émissions de GES WTW, WTT (*Well-to-Tank)* et TTW (*Tank-to-Wheel*) des différentes technologies de bus, et les étiquettes de données représentent des émissions de GES WTW par rapport à BD. Les émissions de GES minimales et maximales du BEB sont représentées par les barres d'erreur en considérant les meilleurs et les pires scénarios de mix énergétique de production d'électricité. D'une part, la performance environnementale du BEB est supérieure à celle des autres technologies alternatives, quel que soit le mix énergétique de production d'électricité excepté pour la performance de la PACO. La PACO compte une réduction de 74% des émissions de GES WTW par rapport au BD. Cependant, un mix énergétique de production d'électricité propre pourrait permettre de réduire de 98% les émissions de GES WTW du BEB.

D'autre part, le BEB représente un système efficace en énergie par rapport au BD et aux autres technologies alternatives. Le BEB permet une réduction de la consommation énergétique WTW par km du BEB. En effet, malgré une consommation énergétique relativement plus élevée pendant la phase de production d'électricité (WTT), les BEB présentent une consommation

d'énergie plus efficace à cause de leur faible besoin énergétique pendant la phase de fonctionnement (TTW) grâce à leurs systèmes de propulsion plus efficaces.

La réduction de la consommation énergétique WTW du BEB varie entre 9,68 et 50%, par rapport à BD, suivant les moyens de production d'électricité (graphique de droite de la Figure 9.1). Les chiffres affichés représentent le pourcentage de réduction de la consommation d'énergie par rapport au BD. Le BEB présente une efficacité énergétique supérieure par rapport aux technologies alternatives. Cependant, cette dernière se détériore considérablement suivant les moyens de production d'électricité.

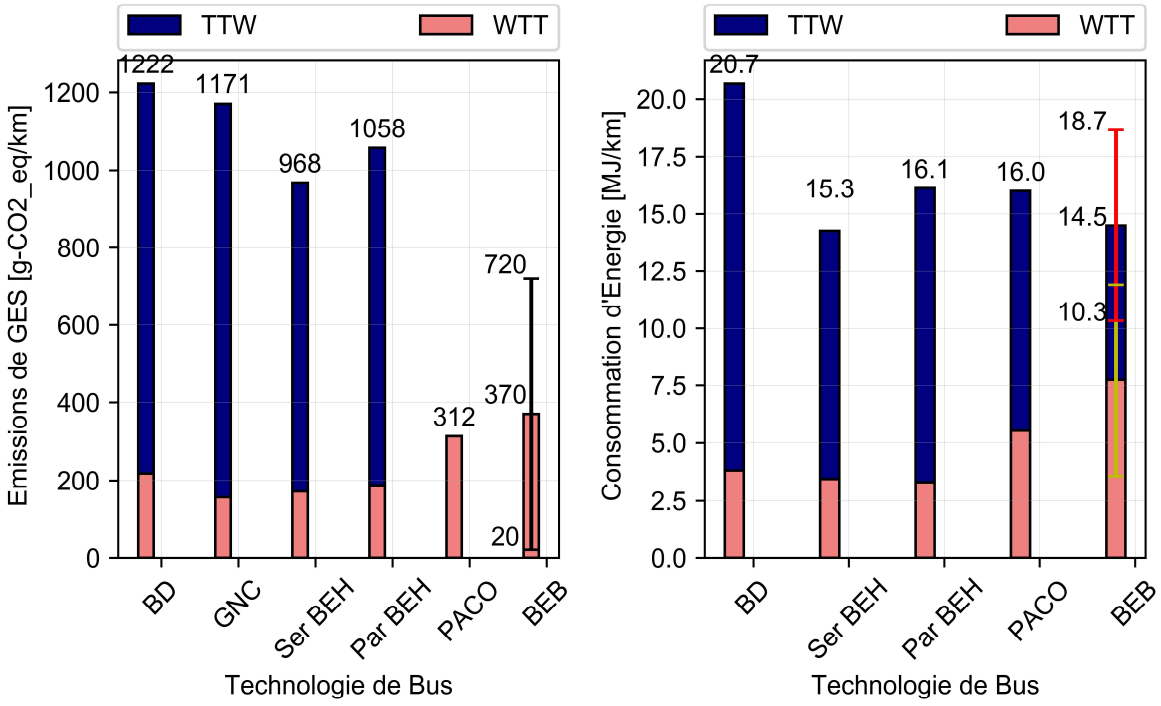


Figure 9.1: Émissions de GES et consommation d'énergie WTW, WTT et TTW des différentes technologies de bus

- **Défis**

Les BEB doivent faire face au défi lié à la performance économique. La performance économique des bus est décrite par leur coût total de possession (Total cost of ownership - TCO) qui comprend le coût unitaire, le coût de la maintenance, le coût du fonctionnement et le coût de l'infrastructure. La Figure 9.2 et la Figure 9.3 présentent le coût unitaire et le TCO pour les différentes technologies de bus. À l'exception de la PACO, le prix unitaire du BEB est le plus élevé, à cause du coût de la batterie. Le coût unitaire du BEB est proportionnel à la taille de sa batterie, en conséquence les BEB équipés de grosses batteries ont un coût unitaire plus élevé.

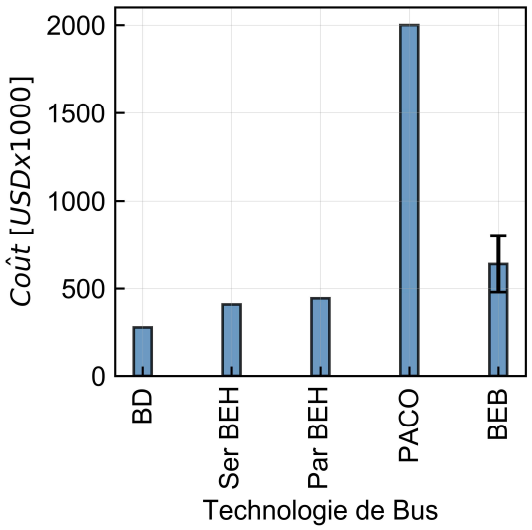


Figure 9.2: Coût unitaire du bus par technologie

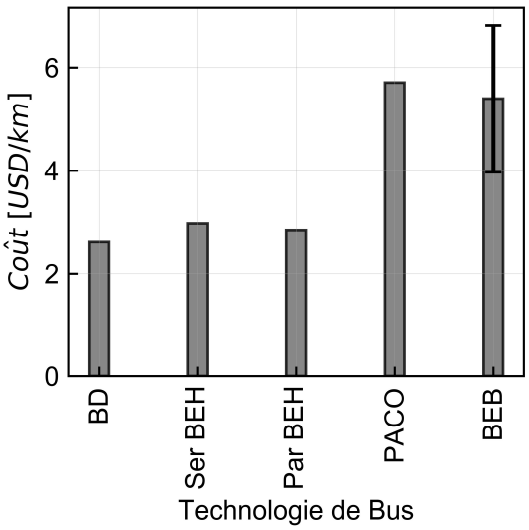


Figure 9.3: TCO du bus par technologie

De plus, les coûts de la maintenance et du fonctionnement des BEB sont inférieurs par rapport à ceux des autres technologies de bus ; en revanche les coûts de l'infrastructure sont les plus élevés, ce qui augmente considérablement leur TCO. Le TCO du BEB varie entre 3,97 et 6,83 $ / km selon la taille des batteries et les besoins en infrastructure.

Les caractéristiques opérationnelles des BEB (l'autonomie du bus, le temps de recharge et l'infrastructure) constituent un autre défi auquel cette technologie doit faire face.

L'autonomie est proportionnelle à la capacité de la batterie, cela contribue à l'ajout des coûts supplémentaires. L'autonomie des BEB ayant des batteries de grandes capacités peut atteindre jusqu'à 250 km, au détriment du prix unitaire qui est très élevé. Les technologies de bus sont deux fois plus autonomes par rapport aux BEB ; elle peut atteindre 450 km.

Le temps de recharge constitue une limite opérationnelle supplémentaire et un autre défi à relever. Cette fonctionnalité est fortement couplée avec l'autonomie des BEB car les batteries à haute capacité énergétique (équivalente à une autonomie élevée), ont un temps de recharge très long. En revanche, les batteries à faible capacité énergétique nécessitent un temps de recharge plus faible. Le temps de ravitaillement (temps de recharge) moyen est compris entre 5 et 10 minutes pour la plupart des technologies de bus ; en outre le temps de recharge des BEB peut atteindre 240 minutes. Le BEB peut être chargé en 10 minutes s'il est équipé d'une batterie de petite taille et de chargeurs rapides.

L'infrastructure de recharge, un aspect opérationnel du BEB, doit être pris en considération et étudié. Toutes les technologies alternatives nécessitent des modifications de l'infrastructure,

particulièrement pour le fonctionnement des BEB. D'abord, des stations de recharge sont à mettre en œuvre pour recharger les bus. Ensuite, le réseau électrique est impacté par l'installation des stations de recharge ; en conséquence des modifications du réseau sont nécessaires, en particulier dans les zones urbaines.

9.1.4 Déploiement de flottes de BEB

- **Les acteurs clés**

Plusieurs acteurs participent aux processus de déploiement du BEB. Chacun a des objectifs et des contraintes particuliers ; en conséquence il existe des différentes approches pour déployer le BEB à grande échelle. Principalement, ces acteurs sont classifiés en 3 catégories : (1) les opérateurs du BEB, (2) les acteurs de logistique énergétique et (3) les autorités de régulation.

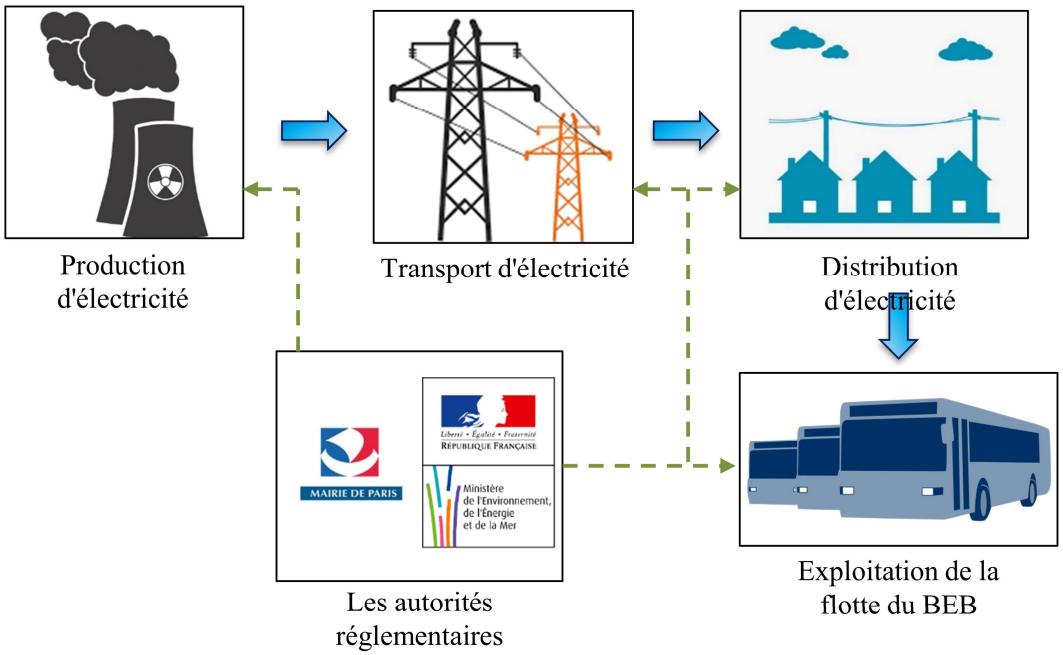


Figure 9.4: Schéma de déploiement du BEB

Les opérateurs du BEB sont responsables du fonctionnement de la flotte de BEB pour répondre aux besoins des voyageurs, en maintenant le fonctionnement sans interruption ou perturbation de l'horaire. Le déploiement des BEB entraîne des coûts supplémentaires pour l'opérateur appelés les coûts d'investissement : les coûts de l'achat des BEB et les coûts de l'infrastructure de recharge. En plus, l'opérateur prend en charge les coûts de l'énergie et de maintenance de la flotte, appelés les coûts du fonctionnement. Par conséquent, l'objectif principal de l'opérateur est de minimiser ces coûts en maintenant un fonctionnement ininterrompu de la flotte des bus.

Le déploiement des BEB amène à une augmentation de la demande en électricité, impactant ainsi le marché de l'électricité et les offres des fournisseurs d'électricité. De même, le déploiement du BEB augmente la demande en puissance car les bus nécessitent une recharge continue pendant la journée ou la nuit ; cela conduit à des modifications des infrastructures dans les réseaux de transport et de distribution d'électricité. Par conséquent, les objectifs du fournisseur d'énergie, de l'émetteur et du distributeur sont de minimiser les coûts supplémentaires de la production d'électricité et des modifications des infrastructures du réseau électrique.

Le rôle principal des autorités réglementaires (les gouvernements et les municipalités) est de réduire l'impact environnemental du secteur des transports. En parallèle, les autorités de régulation préfèrent les solutions rentables pour déployer les BEB puisqu'elles financent ces projets. Enfin, la satisfaction et le bien-être des citoyens (voyageurs) sont également des priorités pour les autorités de régulation.

L'objectif principal est d'étudier les leviers de facilitation du déploiement des BEB du point de vue des opérateurs de bus en présentant les solutions les plus rentables. La thèse suivante propose des solutions aux objectifs et aux priorités de tous les autres acteurs, en particulier ceux concernés par la logistique énergétique, en étudiant l'impact du déploiement des BEB sur le réseau électrique.

- **Défis des opérateurs du BEB**

Les trois principaux défis des opérateurs, sont (1) la gestion de l'autonomie limitée, (2) le savoir-faire d'exploitation et (3) la disponibilité opérationnelle du réseau électrique.

L'autonomie du BEB est le défi majeur auquel l'opérateur doit faire face à cause de la capacité énergétique limitée de la batterie et du temps de recharge long. Parmi les approches adoptées pour prolonger l'autonomie, les BEB sont équipés de batteries surdimensionnées à haute capacité énergétique ce qui conduit à l'augmentation du coût de la batterie. La recharge est réalisée principalement pendant la nuit lorsque le BEB est hors service et à faible puissance. Une autre approche consiste à réduire la capacité énergétique de la batterie et à recharger le BEB plus fréquemment pendant la journée. Cela réduit le coût de la batterie mais entraîne des coûts élevés de l'infrastructure à cause du besoin de mise en œuvre de plusieurs stations de recharge. Un compromis entre les coûts de déploiement du BEB et l'autonomie est à établir en fonction du choix de la capacité énergétique de la batterie.

La gestion d'une flotte de BEB présente plusieurs complications par rapport à la flotte de BD, principalement à cause de la recharge des BEB. La stratégie de recharge est essentielle pour garantir un bon fonctionnement de la flotte de BEB. Le fonctionnement d'une flotte de bus doit éviter : (1) les perturbations d'horaire et (2) l'interruption de service. Le choix de la stratégie de recharge détermine directement la technologie de recharge, les coûts correspondants et la gestion de la flotte de BEB. Par exemple, l'adoption d'une stratégie de recharge nocturne exige une recharge lente. Les coûts d'infrastructure de cette technologie sont faibles. Cependant, le risque d'interruption de service est élevé car il n'est pas possible de recharger le BEB pendant la journée. En revanche, l'adoption d'une stratégie basée sur une recharge quotidienne fréquente exige une recharge des BEB avec des chargeurs ultra-rapides entraînant des appels de puissance élevés. En plus de coûts de l'électricité accrus du fait des appels de puissance importants et sur des heures de pointe, les chargeurs sont coûteux et induisent des coûts élevés de l'infrastructure. Bien qu'une stratégie de recharge journalière fréquente réduise le risque d'interruption de service, une perturbation des horaires est très probable avec cette stratégie de recharge à cause des retards possibles qui résultent de la fréquence de recharge. Chaque stratégie de recharge est caractérisée par des coûts d'investissement différents et par une gestion spécifique de la flotte des BEB. En conséquence, le choix de la stratégie de recharge définit les coûts de déploiement des BEB et oriente le choix de la technologie de recharge.

Le déploiement massif de flottes de BEB soulève des questions sur la capacité du réseau électrique à accueillir une demande d'énergie supplémentaire et élevée. Les BEB représentent une faible part des véhicules électriques en comparaison des véhicules particuliers (VP) ; Cependant, la puissance de recharge des BEB appelée est élevée vu la taille des batteries des BEB. De plus, les bus, en général, parcourent plus de kilomètres par jour par rapport aux VP, ce qui augmente davantage la consommation énergétique quotidienne. Des contraintes supplémentaires sont alors imposées aux opérateurs des BEB par les distributeurs d'électricité. Ces contraintes affectent le choix des stratégies et des technologies de recharge ayant un impact sur le TCO du déploiement des BEB.

9.1.5 Formulation du problème

Les BEB représentent une solution prometteuse pour remplacer les flottes de bus actuelles consommant des énergies fossiles et pour éliminer leur fardeau environnemental grâce à leur efficacité énergétique élevée, à leurs émissions de GES plus faibles et à l'absence d'émission de polluants atmosphériques. Cependant, cette technologie doit faire face à plusieurs défis, en

particulier le TCO élevé et les caractéristiques opérationnelles comme l'autonomie, le temps de recharge et l'infrastructure. Différents acteurs clés interviennent dans le déploiement du BEB, notamment les opérateurs de bus, les fournisseurs d'énergie et les autorités publiques. Chaque acteur a ses propres objectifs et ses contraintes pour le déploiement des BEB qui doivent être pris en considération.

L'autonomie des BEB et la gestion de la flotte de BEB sont les principaux défis des opérateurs de bus afin d'assurer un bon fonctionnement continu sans interruption de service ou retard sur les horaires et répondre aux besoins des voyageurs à des coûts minimaux. Actuellement, deux approches principales sont envisagées dans le déploiement de BEB. La première consiste à équiper les BEB avec des batteries de très haute capacité énergétique accompagnées d'une recharge lente pendant la nuit. La deuxième consiste à équiper les BEB avec des petites batteries accompagnées de recharges fréquentes pendant la journée à des puissances très élevées. La première approche entraîne des coûts élevés de la batterie et une forte probabilité d'interruption de service, tandis que la seconde approche entraîne des coûts élevés de l'infrastructure et des perturbations des horaires.

Par conséquent, il est indispensable d'introduire une méthodologie capable de fournir un dimensionnement optimal des batteries et une stratégie de recharge pour la flotte de BEB afin de minimiser le coût total de possession TCO du déploiement du BEB, tout en garantissant l'absence de perturbation des horaires ou des interruptions de service.

9.1.6 Objectifs scientifiques

Cette thèse présente une méthodologie pour un dimensionnement des batteries et des stratégies de recharge optimales pour les BEB en utilisant une approche systématique. La modélisation des systèmes énergétiques multi-physiques, les simulations numériques et les algorithmes d'optimisation sont les principaux outils développés pour élaborer la méthodologie proposée.

Ainsi, cette thèse répond à la question de recherche principale suivante : Comment minimiser le coût total de déploiement des bus électriques à batterie pour faciliter leur intégration sur le marché et profiter au maximum de leurs bénéfices environnementaux ?

Afin de répondre à cette question, un lot de sous-questions est identifié :

1. Quels sont les différents systèmes énergétiques utilisés dans un BEB et comment évaluer leur consommation énergétique et la consommation énergétique totale du BEB ?

2. Comment la consommation énergétique d'un BEB change-t-elle dans différentes conditions de fonctionnement et quels sont les principaux facteurs ayant un impact significatif sur sa consommation énergétique ?
3. Quel est le dimensionnement approprié de la batterie pour un BEB compte tenu des besoins énergétiques en fonction des différentes conditions de fonctionnement ?
4. Comment évaluer le TCO et le fonctionnement des lignes de BEB et comment sont-ils impactés par le dimensionnement de la batterie et la stratégie de recharge ?
5. Quelle est la stratégie optimale de dimensionnement et de recharge de la batterie de la ligne de BEB en minimisant le TCO du déploiement des BEB en respectant les contraintes des horaires et de ponctualité ?

Chaque chapitre de cette thèse répond à une ou plusieurs questions comme indiqué ci-dessous. Pour cela, le plan suivant est élaboré afin de répondre aux questions de recherche listées :

11. Identifier l'architecture et la technologie des composants du BEB	Chapitre 2
12. Développer un modèle énergétique globale du BEB	
13. Valider le modèle de bus proposé	
14. Analyser et quantifier la consommation énergétique du BEB dans différentes conditions de fonctionnement	Chapitre 3
15. Évaluer la taille de la batterie de bus requise en fonction des conditions de fonctionnement	
16. Développer un modèle techno-économique pour les lignes de BEB	Chapitre 4
17. Analyser l'impact de la taille de la batterie et de la stratégie de recharge sur le TCO et sur le fonctionnement du BEB	
18. Développer une méthodologie pour minimiser le TCO du BEB	Chapitre 5
19. Appliquer la méthodologie proposée à travers une étude de cas réel à Paris	
20. Présenter les travaux supplémentaires en perspective qui améliorent ou complètent cette recherche	Chapitre 6

9.2 Chapitre 2
MODÈLE ÉNERGÉTIQUE du BUS ÉLECTRIQUE à BATTERIE

9.2.1 Introduction

Le déploiement massif du BEB doit répondre à différents enjeux tels que l'autonomie limitée des bus, le coût d'investissement élevé et la présence des infrastructures de recharge. L'autonomie limitée du BEB affecte le fonctionnement du bus pendant la journée ; cela entraîne des perturbations des horaires des bus. En outre, le coût de l'investissement du BEB, étroitement lié au coût de la batterie, est plus élevé que celui des bus diesel ou d'autres technologies de bus. De plus, le déploiement du BEB nécessite l'installation et la maintenance d'infrastructures de recharge engendrant des coûts supplémentaires élevés.

Un dimensionnement de la capacité énergétique de la batterie adapté, est essentiel pour surmonter les enjeux listés ci-dessus. En effet, les batteries à haute capacité énergétique augmentent l'autonomie du bus, mais en parallèle elles ont un coût d'investissement élevé et une consommation d'énergie supplémentaire à cause du poids de la batterie. En revanche, les petites batteries à faible capacité énergétique ayant une autonomie réduite ont un coût d'investissement moins élevé. D'autre part, le choix de la capacité énergétique de la batterie affecte les coûts de l'infrastructure de recharge. Les batteries à faible capacité énergétique sont chargées plus fréquemment et à des puissances élevées.

La batterie est la seule source d'énergie dans le bus ; elle doit être capable de fournir les besoins d'énergie pour tous les systèmes énergétiques de BEB. Ces derniers sont : le système de propulsion, le système HVAC et les auxiliaires. La consommation énergétique de l'unité HVAC regroupe les besoins énergétiques pour chauffer, ventiler et climatiser la cabine du bus afin de maintenir les conditions de confort thermique intérieur. D'autre part, le fonctionnement des auxiliaires requiert une quantité d'énergie non négligeable. Ces derniers regroupent les auxiliaires électriques, hydrauliques, pneumatiques et thermiques qui sont essentiels au fonctionnement du bus.

Par conséquent, une évaluation énergétique détaillée et complète pour le BEB est nécessaire en prenant en considération ces différents systèmes énergétiques.

L'objectif de ce chapitre est de présenter en détail l'architecture du bus, la technologie et l'approche de modélisation de chaque composant du bus. En plus, ce chapitre présente des critères utilisés pour valider les modèles proposés.

9.2.2 Etat de L'art

Plusieurs publications de la dernière décennie ont étudié et évalué la consommation énergétique du BEB. La plupart de ces études se concentrent sur la quantification de la consommation d'énergie du système de propulsion dans les bus ou sur l'évaluation de la consommation d'énergie du système HVAC. Ces études proposent différentes approches de modélisation pour les différents systèmes énergétiques de BEB. Ces études sont résumées dans Table 2.1.

La majorité des études évaluent la consommation d'énergie du système de propulsion. Ces études modélisent les composants du système de propulsion et évaluent leur performance énergétique dans certaines conditions de conduite tels que les cycles de conduite fixes, les topographies routières et la charge des passagers. Le modèle de la batterie est considéré comme un composant du système de propulsion.

Peu d'études examinent la consommation d'énergie du système HVAC dans les véhicules électriques. De plus, les quelques études modélisant le système HVAC utilisent des modèles thermiques statiques et simples pour la cabine et des modèles de système simplifiés sans stratégie de contrôle bien définie. En outre, la plupart des études de la consommation énergétique du système HVAC se limitent à des véhicules personnels. En plus, ces modèles proposés n'incluent pas l'intégralité des processus de transfert de chaleur qui ont lieu entre la cabine et son environnement, ce qui limite la précision du modèle et change les besoins thermiques.

En plus, la consommation énergétique des auxiliaires, a été étudié uniquement dans les bus hybrides et les bus diesel et souvent de manière simplifiée dans les différents modèles énergétiques présentés dans la littérature. Cependant, dans les véhicules lourds, les auxiliaires électriques, pneumatiques et hydrauliques ne sont pas négligeables et une approche de modélisation dynamique est indispensable pour estimer leur consommation d'énergie. En même temps, les auxiliaires thermiques de batterie sont des caractéristiques exclusives aux véhicules électrifiés et leur consommation d'énergie est importante dans les applications à haute énergie et densité de puissance.

En résumé, ce chapitre présente une méthodologie de modélisation complète pour évaluer la performance énergétique des différents systèmes énergétiques du BEB.

9.2.3 Configuration et spécification du bus

La configuration du bus est présentée dans Figure 9.5.

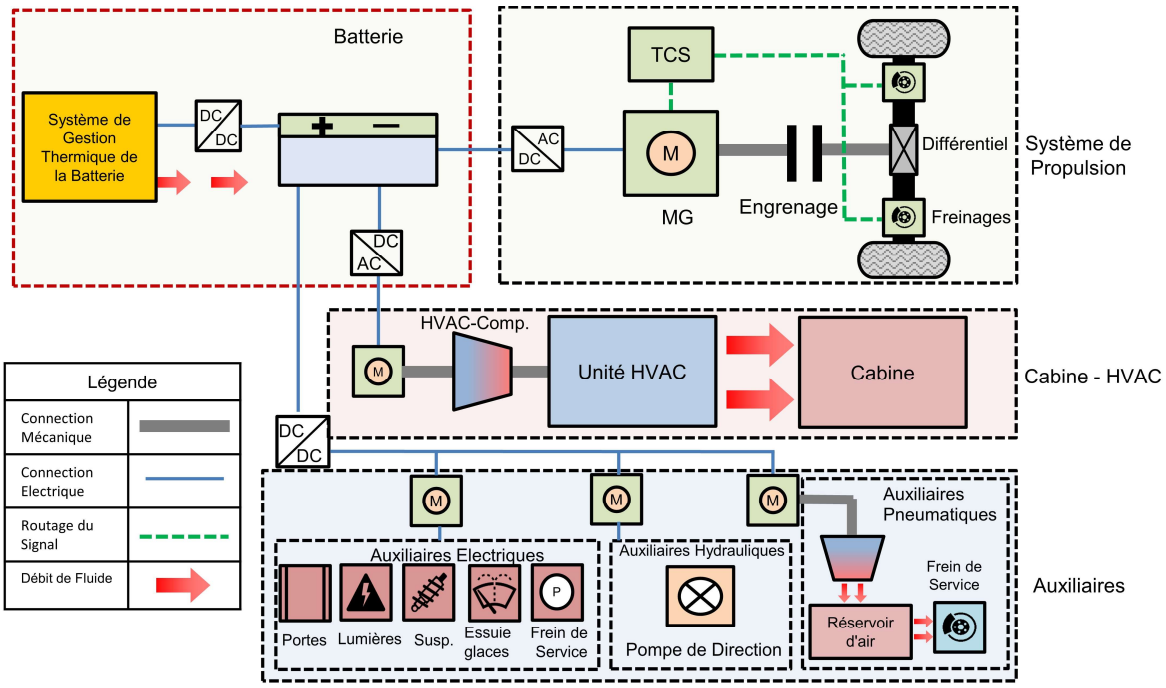


Figure 9.5: La configuration des composants du BEB

Les principaux composants du système de propulsion du bus (Motopropulseur), sont : l'unité de propulsion, l'unité de transmission et le système de freinage.

- L'unité de propulsion est une machine électrique (ME) alimentée par la batterie et contrôlée par une stratégie de contrôle du couple (*Torque Control Strategy* - TCS) pour assurer la propulsion et récupérer une partie de l'énergie de freinage. La ME fonctionne comme un moteur électrique pendant la propulsion. Cependant, pendant le freinage, elle fonctionne comme un générateur électrique : elle récupère une partie de l'énergie cinétique du véhicule et la convertit en énergie électrique pour recharger la batterie.
- L'unité de transmission consiste en un seul engrenage et un différentiel.
- Le système de freinage inclut les freins pneumatiques utilisés pour dissiper l'énergie de freinage non récupérée par la machine électrique. Il est contrôlé par le TCS.

L'unité HVAC permet le chauffage, le refroidissement, la ventilation et la déshumidification de la cabine de bus. L'unité HVAC est composée principalement de pompes à chaleur (PAC).

Les auxiliaires de bus sont des éléments essentiels pour le fonctionnement du bus et consomment une quantité d'énergie importante. Leur technologie diffère selon la technologie du bus. Dans les BEB, la plupart de ces caractéristiques sont électriques, cependant, les auxiliaires du bus diesel sont essentiellement hydrauliques et pneumatiques. La gestion thermique de la batterie (*Battery Thermal Management* - BTM) est un auxiliaire important et exclusif au BEB. Le BTM est essentiel dans des conditions météorologiques extrêmes pour assurer un fonctionnement efficace et sûr de la batterie. Ces auxiliaires sont résumés dans Tableau 9.1.

Tableau 9.1:Technologie des auxiliaires en BEB

Auxiliaires	Technologie
Frein de Service	Pneumatique
Freins de Stationnement	Electrique
Système de Suspension	Hydro- Electrique
Pompe de Direction	Hydro- Electrique
Lumières	Electrique
Essuie-glaces	Electrique
Portes	Electrique
BTM	Thermique

9.2.4 Modélisation

9.2.4.1 Batterie

Le BEB est équipé d'une batterie au lithium-ion qui est la technologie de batterie la plus utilisée dans les véhicules électriques. Le modèle électrothermique couplé de la batterie développé dans cette thèse, reproduit le comportement dynamique électrique et thermique des cellules de batterie. En vue d'estimer l'état de charge de la batterie (*state of charge* - SOC), la tension et le courant électrique, un modèle quasi-statique à circuit équivalent de Rint est considéré en utilisant des données empiriques de la batterie comme la tension et la résistance de la cellule de batterie en fonction du SOC de la batterie. La configuration des cellules de batterie (nombre de modules en série et en parallèle) détermine la capacité énergétique et la tension du pack de batteries, cette dernière est comprise entre 600 et 800 V. Le SOC de la batterie se situe entre 10 et 90%.

Le modèle thermique de la batterie à deux états (*two-state*) est développé, évalue les températures du noyau et de la surface de la cellule de batterie ainsi que la génération de chaleur interne résultant des réactions chimiques aux électrodes de la batterie. La technologie de

refroidissement à air actif (*active air cooling*) est adaptée pour refroidir la batterie en utilisant un ventilateur et un évaporateur connectés à l'unité HVAC. L'unité de refroidissement de batterie consomme de l'énergie électrique directement de la batterie. Un Schéma du modèle de batterie est présenté dans la Figure 9.6.

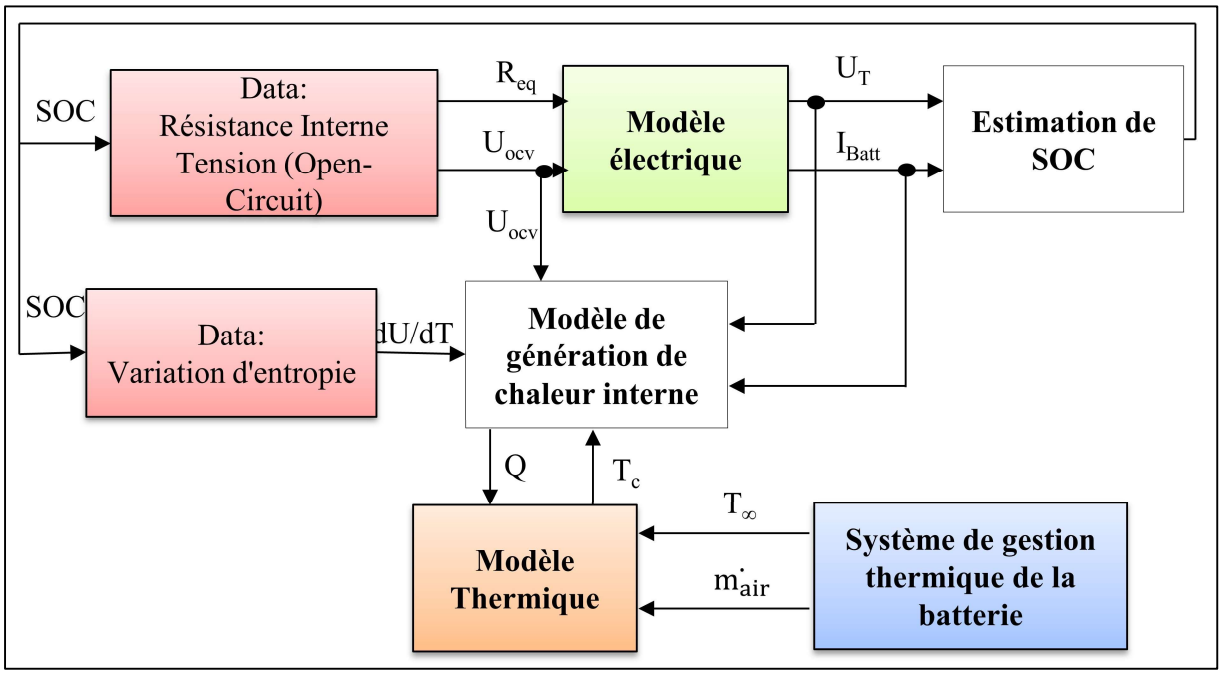


Figure 9.6: Schéma du modèle de batterie

9.2.4.2 Système de Propulsion

Les principaux composants du système de propulsion sont :

- la machine électrique (ME) : une machine électrique à induction AC triphasée est prise en considération. Elle est modélisée comme une cartographie d'efficacité statique qui inclut l'efficacité de la machine électrique et l'efficacité de l'onduleur en fonction du couple et de la vitesse de ME. De plus, des composants inertiels sont ajoutés au modèle de la ME pour détecter les performances dynamiques de la machine en imposant une résistance à la variation de vitesse de la ME.
- les systèmes de transmission et de freinage et les roues. Le bus à deux roues avant et deux roues arrière. Pendant la traction, le système de transmission (un engrenage et un différentiel) transmet le couple de traction de la ME aux roues arrière uniquement. Le différentiel répartit le couple entre les roues arrière en fonction du taux de patinage (*Slip Ratio)*. Le freinage est représenté en 2 modes : le freinage par friction (système pneumatique) et le freinage par récupération (*Brake Energy Recovery* – BER). Le

freinage régénératif est appliqué uniquement sur les roues arrière car elles sont couplées à la ME. Au contraire, le freinage par friction est appliqué aux roues arrière et avant.

- la stratégie de contrôle du couple (TCS) : Le TCS contrôle les couples de traction et de freinage dans le système de propulsion en analysant la demande du conducteur ; cette dernière est modélisée en PID. L'Organigramme de TCS est présenté sur la Figure 9.7.

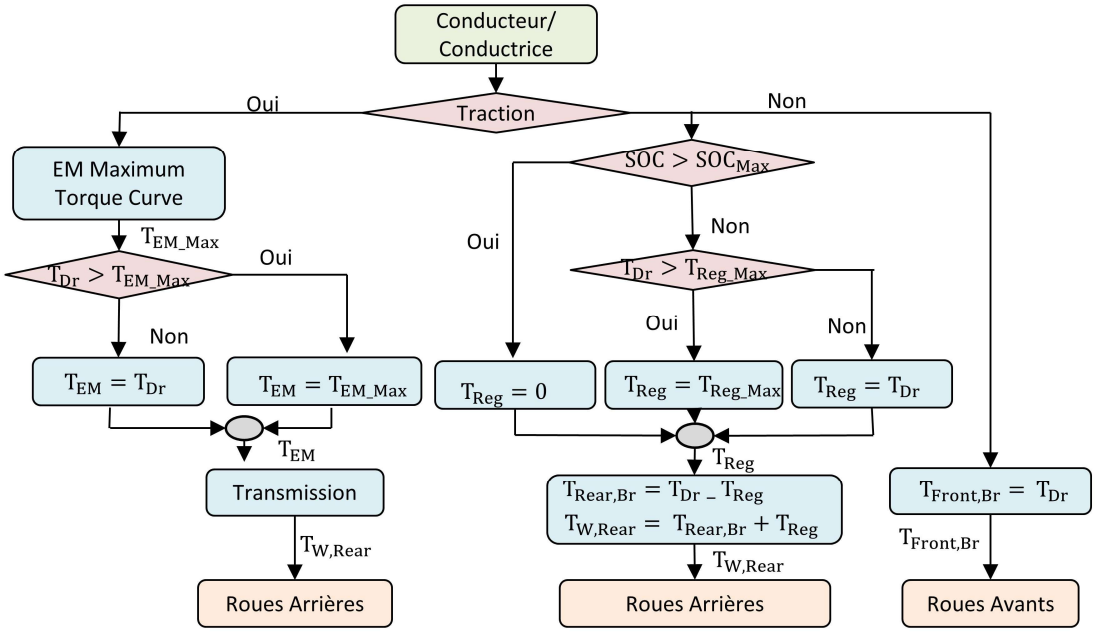


Figure 9.7: Organigramme de TCS

9.2.4.3 Cabine

Il est important d'évaluer la charge thermique de chauffage / refroidissement de la cabine pour étudier son impact sur l'autonomie du BEB. Un modèle thermique de la cabine est développé. Il consiste en quatre sous-modèles :(1) intérieur de la cabine, (2) parois, (3) passagers et (4) matériaux internes de la cabine. Ce modèle détermine la température de la cabine.

L'intérieur de la cabine est modélisé en un nœud thermique en utilisant une approche mono-zone qui considère les phases transitoires et stationnaires. Cette méthodologie d'évaluation énergétique est pratique pour la charge thermique dans le bus.

Les parois de la cabine représentent la carrosserie du bus (haut, bas, deux côtés, avant et arrière). Elles peuvent être opaques, ou vitrées. Les surfaces des parois sont déterminées par la géométrie du bus. Chaque paroi a deux interfaces : avec un l'environnement extérieur et l'intérieur de la cabine. Six modes d'échange thermique sont considérés dans ce modèle : (1) convection avec l'extérieur, (2) conduction à travers la paroi, (3) convection avec l'intérieur de la cabine, (4) rayonnement, (5) transmis et (6) rayonnement absorbé à travers le vitrage.

Chaque passager est modélisé comme une source de chaleur constante (70 *W* par personne). Le matériau interne de la cabine est un nœud thermique ayant une capacité thermique et une géométrie spécifique qui interagit avec l'intérieur de la cabine par convection et rayonnement.

A noter que l'ouverture fréquente des portes pendant le fonctionnement du bus a un impact sur la température intérieure de la cabine en raison de l'ouverture. Ces pertes d'énergie sont prises en compte dans le modèle de cabine en ajoutant un débit de chaleur variable entrant et/ou sortant de la cabine. Ce dernier dépend de la température ambiante, de la température de la cabine de bus et de la durée des portes ouvertes.

9.2.4.4 HVAC

L'unité HVAC consiste en 2 pompes à chaleur réversibles, un système de circulation d'air et un système de gestion thermique de la batterie.

La capacité de chauffage maximale requise est de 35 *kW* ; elle est obtenue à partir de calculs de charge thermique pour un bus de spécifications similaires. L'utilisation de plusieurs PAC dans les BEB est courante. 2 PAC réversibles sont considérées dans cette étude, chacune évaluée à 20 *kW* ; elles sont installées au milieu et à l'arrière du bus.

Le système de circulation d'air (*Air Circulation System* - ACS) est principalement composé de plusieurs ventilateurs (deux ventilateurs pour fournir l'air chaud/froid dans la cabine, un ventilateur d'extraction d'air pour évacuer l'air de la cabine et deux ventilateurs pour souffler de l'air extérieur), de registres (utilisés pour réguler le débit d'air) et de mélangeurs. Une partie de l'air extrait circule à travers un échangeur de chaleur air-air et le flux d'air frais récupère une partie de l'énergie de l'air extrait.

Le système de gestion thermique de la batterie (BTMS) est composé d'un ventilateur, d'un évaporateur et de registres d'air pour contrôler la source d'air (cabine, extérieur ou air extérieur / cabine climatisée). Un radiateur électrique à résistance est utilisé pour chauffer l'air en hiver.

Enfin, la consommation électrique totale de l'unité HVAC est la somme de la puissance nécessaire pour faire fonctionner les deux PAC, ACS et BTMS.

Des contrôleurs ON-OFF pour HVAC sont utilisés. La stratégie de contrôle vise à maintenir la température de la cabine à une valeur cible comprise entre des limites basses et hautes en contrôlant la vitesse du compresseur. Dans cette étude, le contrôleur ON-OFF est utilisé pour atteindre des conditions de confort thermique à l'intérieur de la cabine de bus avec une température comprise entre 19 et 23 °C. La température maximale de l'air soufflé et le débit

minimum d'air frais sont déterminés en tenant compte du confort des passagers à l'intérieur du bus. La quantité d'air frais requise dépend du nombre de passagers à l'intérieur du BEB. Dans le modèle, quatre niveaux d'occupation des passagers sont définis dans le contrôleur de l'unité HVAC : (1) Très faible : <10 passagers, (2) Faible : <25 passagers, (3) Moyen : <40 passagers, (4) Elevé:> 40 passagers

9.2.4.5 Auxiliaires

Les auxiliaires électriques dans les BEB sont modélisés par des demandes de puissance de la batterie. Les puissances appelées par les auxiliaires sont modélisées par un scénario de conduite.

La pompe de direction et le système de suspension constituent les principaux auxiliaires hydrauliques d'un bus. La pompe de direction doit toujours fournir la pression hydraulique requise pour le système de direction du bus. La consommation électrique de la pompe de direction peut être caractérisée en fonction de la vitesse du bus. Le système de suspension est un système hydrostatique utilisé pour soulever le bus (Δh = 65 mm). Le poids avant du bus correspond à la masse de l'essieu avant et à la masse du châssis supporté par l'essieu avant. De plus, on suppose que le poids de 1/3 des passagers est supporté par l'essieu avant en fonction de la géométrie du bus. L'efficacité du système de suspension est considérée comme constante à 70% et la durée du processus de levage est 3 secondes.

Le système pneumatique actionne principalement les freins de service des BEB. Les freins pneumatiques (*Air Brakes*) à friction utilisent l'air comprimé à 10 bars sur les pistons, de sorte qu'ils appliquent la pression nécessaire sur les plaquettes de frein pour décélérer le bus. Le système pneumatique du BEB consiste en un compresseur, un réservoir pour stocker l'air comprimé, une machine électrique du compresseur et un clapet pour réguler le débit d'air. Le système pneumatique doit toujours être capable de fournir un débit d'air comprimé suffisant pour actionner les freins de service au besoin. Pour cela, il est essentiel de surveiller le niveau d'air comprimé à l'intérieur du réservoir d'air. Un contrôleur ON-OFF est utilisé pour le compresseur afin de maintenir un niveau minimum d’air comprimé à 10 bars. Ce minimum est fixé à 50% du volume maximal du réservoir d'air. Lorsque le volume du réservoir d'air devient inférieur à 50% du volume maximal, le compresseur tourne à une vitesse maximale jusqu'à ce que le réservoir d'air se remplisse. Le débit du compresseur est de 240 l/min ; le compresseur consomme 2,7 *kW*. La vitesse du moteur électrique du compresseur est considérée fixe avec une efficacité constante de 80%. Enfin, Tableau 9.2 présente un résumé de la configuration du bus et des spécifications des composants.

Tableau 9.2: Résumé de la configuration du bus et des spécifications des composants

	Composant	Technologie	Paramètres	Valeur
Batterie	Pack de Batterie	Lithium-ion	Capacité énergétique/cellule	14.6 Wh
			Capacité de charge/cellule	4.3 Ah
			Masse de cellule	205 g
			Tension de cellule	2.4 - 4.1 V
			Résistance interne	3 - 20 $mohm$
	Unité de refroidissement	Refroidissement par air - Ventilateur	Débit d'air maximum du ventilateur	1000 CFM
			Pression statique du ventilateur	100 Pa
Propulsion	Machine Électrique	3-phase AC inductive	Puissance nominale	135 kW
			Couple nominale	650 $N.m$
			Peak torque	1000 $N.m$
	Transmission		Rapport de l'engrenage	5.5
			Rapport de la différentiel	5
			Efficacité	0.95
	Châssis		Masse de châssis	11600 kg
			Surface frontale	8.2 m^2
			Coefficient aérodynamique	0.55
			Coefficient roulement	0.008
			Rayon de roue	0.48 m
			Inertie de la roue	20.52 $kg.m^2$
HVAC	Cabine		Confort Thermique (hiver)	19-23 $°C$
			Confort Thermique (été)	23- 27 $°C$
	PAC	Cycle compression de vapeur	capacité de chauffage maximale	20 kW (x2)
			capacité de climatisation maximale	15 kW (x2)
Auxiliaires	Pneumatique	Compresseur	Débit nominal	4 L/s
			Puissance nominale	2700 W
	Hydraulique	Pompe de direction	Puissance	450-1000 W
	Electrique	Portes	Puissance	90 W
		Freinage de stationnement	Puissance	560 W
		Lumières	Puissance	500 W
		Essuie-glaces	Puissance	500 W

9.2.5 Validation des Modèles

Pour évaluer des modèles et hypothèses proposées, le modèle de BEB est validé en cinq parties :

- Validation de la consommation énergétique du système de propulsion
- Validation des besoins thermiques de la cabine de bus
- Validation de la consommation énergétique du système HVAC
- Validation de la consommation énergétique des auxiliaires
- Validation du modèle électrothermique couplé de la batterie

La Figure 9.8 montre les résultats de la validation du modèle. La modèle du système de propulsion est démontré en comparant sa consommation énergétique à la consommation obtenue dans la littérature. La comparaison de la consommation d'énergie est faite sur une variété de spécifications de bus, de conditions de conduite et de charges de passagers. Les scénarios et les études de cas sont présentés dans Table 2.20, Table 2.21, Table 2.22, Table 2.23, Table 7.6, et Table 7.7 Dans graphique (a), l'erreur moyenne de la consommation d'énergie du système de propulsion est toujours inférieure à 5% dans tous les scénarios.

La validation de la modélisation de la cabine est réalisée en comparant les charges thermiques estimées par le modèle à celles présentées dans la littérature pour différentes conditions météorologiques. Quatre scénarios de refroidissement sont envisagés (cas 2-5) où la température extérieure est comprise entre 32 et 36 °C, et un scénario de chauffage est considéré à -10 °C. Dans graphique (b), l'erreur est de moins de 5% pour tous les scénarios de refroidissement (cas 2-5), cependant le seul scénario de chauffage (cas 1) indique une erreur de 6,2%.

La performance de la PAC est démontrée en comparant la demande de puissance électrique du compresseur ou le COP de la PAC aux valeurs rapportées dans la littérature, principalement dans des études de validation expérimentale et de mesures de PAC dans les BEB ou dans des véhicules électriques en général. Dans graphique (c), tous les scénarios de refroidissement (cas 1 à 3) indiquent une erreur moyenne de moins de 4%, cependant les scénarios de chauffage (cas 4 à 5) montrent une erreur moyenne entre 2 et 3%. L'erreur la plus élevée est enregistrée dans le cas 5 à 6,8% (scénario de chauffage avec température extérieure à - 7 ° C).

Enfin, la validation des auxiliaires est effectuée en comparant la puissance moyenne des différents auxiliaires sur le cycle de conduite de Braunschweig. Dans Figure 9.8 – graphique (d), tous les auxiliaires enregistrent une erreur inférieure à 6%.

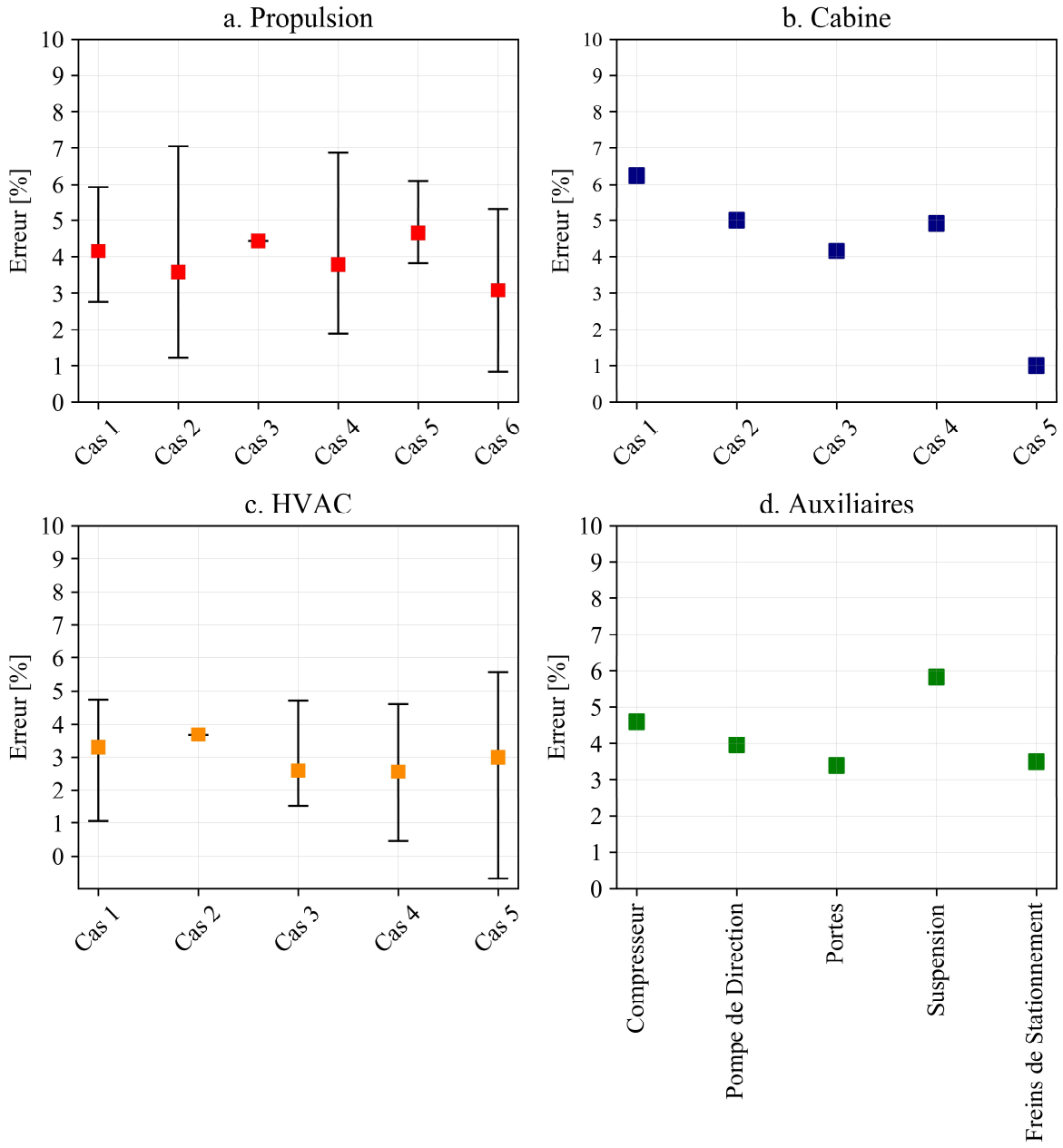


Figure 9.8: Validation du modèle de BEB

La validation du modèle électrothermique couplé de la batterie est présenté dans les Figure 9.9, Figure 9.10 et Tableau 9.3. Ils montrent le SOC de la batterie et les profils de température, Tc étant la température centrale de la cellule et Ts la température de surface de la cellule. Les profils de SOC sont très similaires et les légères fluctuations observées dans l'étude de référence sont dues au cycle d'épuisement de charge non constant. Les profils de température montrent une erreur élevée au début du cycle (23%). Cette valeur diminue à moins de 1% à la fin du cycle, principalement lorsque la moyenne temporelle mobile du cycle se rapproche de la moyenne totale (4C).

Tableau 9.3: Résumé de la validation du modèle électrothermique de la batterie

Temps	200 sec			400 sec			600 sec		
	Modèle	**Réf**	**Erreur**	**Modèle**	**Réf**	**Erreur**	**Modèle**	**Réf**	**Erreur**
SOC	0.73	0.7	4.2%	0.47	0.49	4.2%	0.19	0.18	5.5%
Tc [°C]	15.9	17.5	9.2%	19.51	20	2.4%	21.96	22	0.2%
Ts [°C]	11.2	13	13%	14.82	15	1.2%	18.74	18.9	0.8%

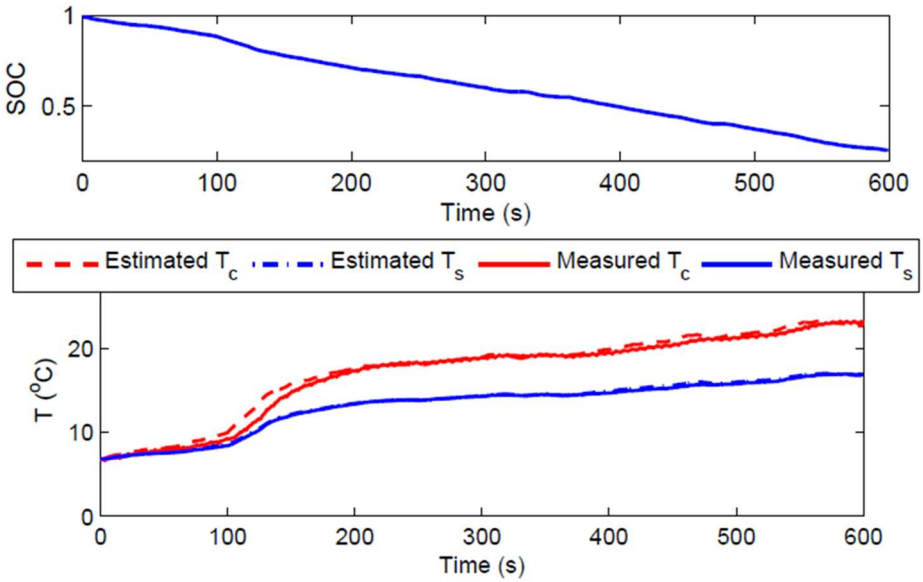


Figure 9.9: Résultats des tests de validation de la batterie (Référence)

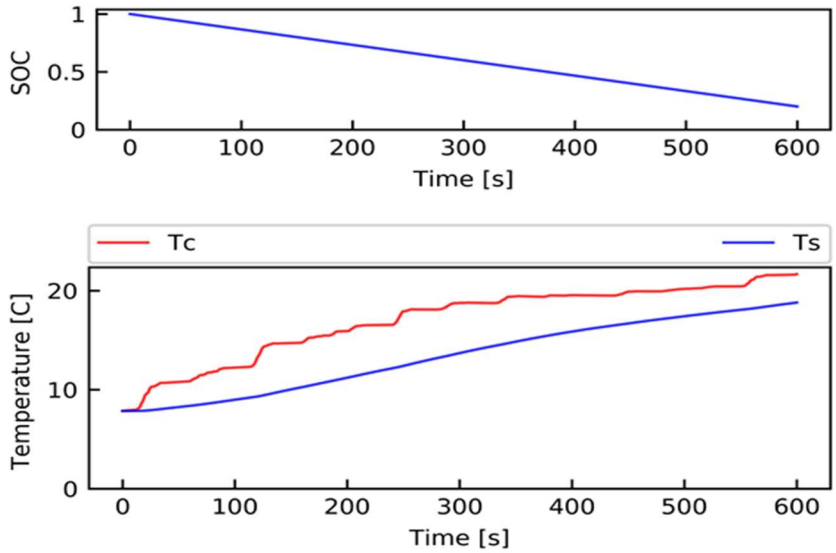


Figure 9.10: Résultats des tests de validation de la batterie (Simulation)

9.2.6 Conclusion

Ce chapitre présente une méthodologie de modélisation énergétique détaillée pour évaluer la consommation énergétique des BEB. Le modèle proposé prend en compte les différents systèmes énergétiques de BEB tels que le système de propulsion, le système HVAC et les auxiliaires. Le modèle intègre tous ces systèmes énergétiques dans une seule plateforme pour évaluer la consommation énergétique totale du bus. Un modèle de propulsion détaillé est présenté pour évaluer la consommation d'énergie du système de propulsion. Un modèle de cabine de véhicule électrique est modifié pour s'adapter à une application de bus et un modèle de HVAC est développé pour évaluer les besoins de chauffage et de refroidissement du bus et la consommation d'énergie qui en résulte. De plus, des modèles d'auxiliaires dynamiques sont développés tels que les auxiliaires pneumatiques, hydrauliques, électriques et thermiques.

Le modèle proposé est validé en termes de consommation d'énergie et de demande de puissance pour les différents systèmes énergétiques. Les résultats indiquent une marge d'erreur acceptable inférieure à 5% dans différentes conditions d'essai.

En conséquence, le modèle peut être utilisé pour estimer la consommation d'énergie des BEB dans différentes conditions de fonctionnement afin de calculer leur consommation d'énergie réelle. Cela est présenté dans le chapitre suivant.

9.3 Chapitre 3
La CONSOMMATION d'ÉNERGIE du BUS ÉLECTRIQUE à BATTERIE

9.3.1 Introduction

Une évaluation rigoureuse de la consommation d'énergie du BEB est nécessaire vu son autonomie limitée. Cette dernière est liée à la capacité énergétique limitée de la batterie ce qui n'est pas le cas des DB. A noter que, l'utilisation de l'unité HVAC et des autres auxiliaires pneumatiques, hydrauliques et électriques réduit davantage l'autonomie des BEB en consommant de l'énergie de la batterie. En conséquence, la consommation énergétique du groupe propulsif, de l'unité HVAC et des auxiliaires influence le dimensionnement de la capacité énergétique de la batterie.

La consommation énergétique des BEB varie énormément selon les conditions de fonctionnement. Ces dernières sont :

- les conditions de conduite qui incluent le profil de vitesse du bus, le comportement de conduite, la distance et la durée du trajet, la topographie de la route et le nombre d'arrêts.
- les conditions météorologiques comme la température et le flux solaire qui impactent les besoins thermiques du bus et affectant la consommation d'énergie de l'unité HVAC.
- la charge des passagers qui influence la consommation d'énergie du bus en raison du poids supplémentaire et des charges thermiques variables en fonction du nombre de passagers occupant le bus.

Peu d'études évaluent la consommation d'énergie du BEB selon plusieurs conditions de fonctionnement afin de quantifier sa consommation d'énergie réelle.

En effet, cette évaluation aide à dimensionner correctement la capacité énergétique de la batterie. Un dimensionnement approprié de la batterie permet d'affronter les défis de l'autonomie et des coûts liés au déploiement massif de BEB.

Par conséquent, il est essentiel de quantifier la consommation d'énergie du BEB dans diverses conditions de fonctionnement en adoptant une évaluation énergétique détaillée et complète pour le BEB en considérant ses différents systèmes énergétiques.

Ce chapitre répond aux questions suivantes :

- Comment la consommation énergétique d'un BEB change-t-elle dans différentes conditions de fonctionnement et quels sont les principaux facteurs ayant un impact significatif sur sa consommation énergétique ?
- Quel est le dimensionnement approprié de la batterie pour un BEB compte tenu des besoins énergétiques en fonction des différentes conditions de fonctionnement ?

La section 9.3.2 analyse l'impact des conditions de conduite sur la consommation d'énergie du BEB. Ensuite, les sections 9.3.3 et 9.3.4 analysent respectivement l'impact des conditions météorologiques et de la charge des passagers sur la consommation d'énergie du BEB. Enfin, la section 9.3.5 présente une méthodologie préliminaire pour le dimensionnement de la capacité énergétique de batterie.

9.3.2 L'impact des conditions de conduite

Le modèle de BEB est simulé sur tous les cycles de conduite présentés dans le Table 7.7, dont chacun représente des conditions de conduite spécifiques selon le niveau de trafic, le comportement du conducteur et le type d'itinéraire (itinéraire urbain ou interurbain déterminé en fonction du nombre d'arrêts par km). Les conditions météorologiques et la charge des passagers sont maintenues constantes dans les différentes simulations, et la température extérieure est fixée à 20 °C. La charge des passagers considérée est de 30 passagers ce qui équivaut à 60% du taux d'occupation.

La Figure 9.11 illustre la consommation d'énergie du système de propulsion aux différentes conditions de conduite. La figure montre l'énergie consommée pendant le mode d'accélération du bus, le mode Récupération d'énergie au freinage (BER) et la consommation totale d'énergie de propulsion, qui est la somme des 2 entités énergétiques citées. La consommation d'énergie du système de propulsion varie fortement selon les différentes conditions de conduite simulées. La consommation d'énergie la plus élevée est enregistrée pendant le cycle de conduite NYB à 2,62 *kWh/km*, tandis que la valeur la plus basse est enregistrée pendant le cycle de conduite CSHV à 1,7 *kWh/km*, ce qui représente une consommation d'énergie réduite de 35%. La principale raison de cette variation est liée à la vitesse moyenne du cycle de conduite. Sur la Figure 9.11, les cycles de conduite sont triés par ordre croissant de leurs vitesses moyennes. La consommation d'énergie diminue pour des vitesses moyennes plus élevées. Cela se traduit par une augmentation de la consommation d'énergie du système de propulsion avec plus de trafic. Avec des démarrages et des arrêts plus fréquents, l'EM ?? ne fonctionne pas dans des conditions

de régime stable, ce qui entraîne une consommation supplémentaire en raison d'accélérations fréquentes réduisant par conséquent son efficacité.

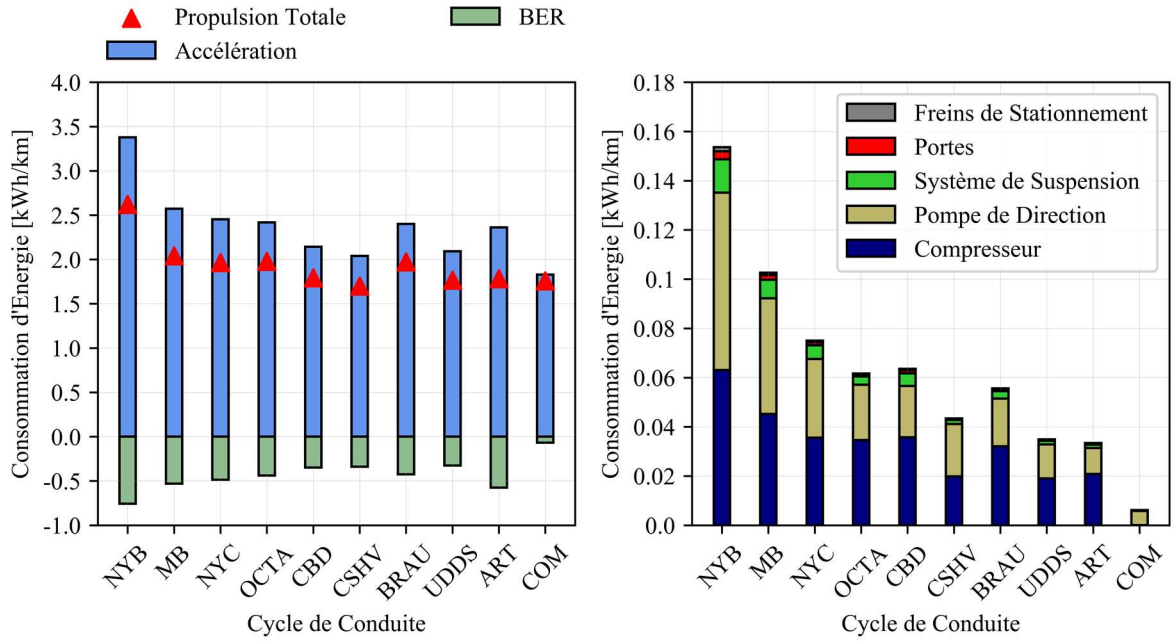


Figure 9.11: Consommation d'énergie du système de propulsion et des auxiliaires dans différentes conditions de conduite

En plus, la consommation d'énergie des différents auxiliaires varie selon les cycles de conduite. Elle est illustrée à la Figure 9.11. Le compresseur d'air et la pompe de direction sont les principaux consommateurs d'énergie, suivis du système de suspension. Les portes et les freins de stationnement représentent les auxiliaires électriques. La consommation énergétique totale des auxiliaires peut représenter jusqu'à 6% (NYB et MB) de la consommation totale d'énergie du BEB.

La demande de puissance de la pompe de direction est directement liée à la vitesse du bus. La consommation d'énergie de la pompe de direction augmente lorsque la vitesse moyenne du cycle augmente. Pareil, un trafic dense augmente la consommation d'énergie jusqu'à 3 fois par rapport à un trafic normal.

Les principaux auxiliaires pneumatiques d'un BEB sont les freins de service, alimentés par le compresseur d'air. Cette dernière est directement affectée par la fréquence et la puissance de freinage rencontrées lors du trajet. La consommation d'énergie du compresseur est plus élevée pour une décélération moyenne élevée du cycle de conduite. En d'autres termes, des conditions de trafic dense peuvent augmenter la consommation d'énergie du système pneumatique du BEB de 50% par rapport aux conditions de circulation standard (par exemple, les cycles de conduite

MB et NYC). Pour des décélérations supplémentaires, le besoin d'air comprimé augmente afin d'actionner les freins de service, ainsi le compresseur d'air est mis en marche plus fréquemment, ce qui augmente sa consommation d'énergie.

Les principaux auxiliaires électriques du BEB sont les portes et les freins de stationnement. En plus du système de suspension, ces auxiliaires ne sont actionnés que lorsque le bus s'arrête ; le nombre d'arrêts diffère selon les cycles de conduite. Le cycle ayant le nombre d'arrêts par km (NYB) le plus élevé enregistre la consommation d'énergie la plus grande avec une augmentation de 100% par rapport aux conditions de circulation standard des bus (cycles MB et NYC). A noter que, le nombre d'arrêts de bus par km est étroitement lié aux spécifications de l'itinéraire : ce dernier augmente dans les zones urbaines et à l'intérieur des centres-villes.

9.3.3 L'impact des conditions météorologiques

Le BEB est simulé pour plusieurs conditions météorologiques. La température extérieure varie entre -10 °C et 40 °C ; elles représentent les températures extrêmes enregistrées pour la ville de Paris. Les conditions de conduite et la charge des passagers sont maintenues constantes pour les différentes simulations. Le cycle de conduite MB est utilisé et la charge des passagers est fixée à 30 passagers ce qui équivaut à 60% du taux d'occupation.

La puissance moyenne de l'unité HVAC appelée est la plus élevée pour les conditions météorologiques extrêmes en raison de la charge thermique élevée dans ces conditions (Figure 9.12 graphique (a)). En plus, le COP du système HVAC dans des conditions extrêmes est très faible, ce qui dégrade la performance de l'unité HVAC. La puissance moyenne appelée diminue progressivement quand la température extérieure se rapproche de la température ambiante. Le chauffage ne fonctionne que pour des températures inférieures à 15°C et le refroidissement n'est actif que pour des températures supérieures à 20°C. Pour les conditions météorologiques extrêmes, la consommation d'énergie de l'unité HVAC est proche de celle du système de propulsion.

La variation de la température extérieure affecte la demande de puissance du BTMS de la même manière que la demande de puissance de l'unité HVAC. La Figure 9.12 graphique (b) montre l'appel de l'énergie électrique moyenne du BTMS pour différentes températures extérieures. La puissance moyenne BTMS appelée la plus élevée correspond aux conditions météorologiques extrêmes ; en effet l'air utilisé pour refroidir les cellules de la batterie nécessite un refroidissement dans des conditions extrêmement chaudes et un chauffage dans des conditions extrêmement froides. La puissance moyenne appelée du BTMS peut atteindre 6 kW

dans les conditions de chaleur extrêmes, ce qui correspond à un tiers de la demande totale de puissance de l'unité HVAC.

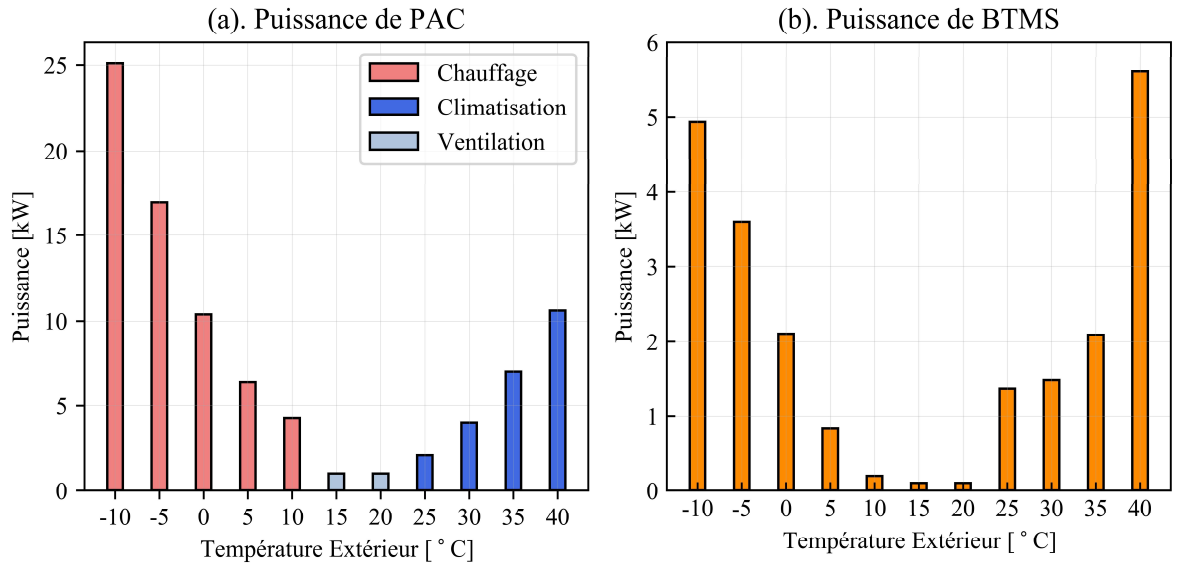


Figure 9.12: Demande de puissance moyenne pour HVAC et BTMS à différentes températures extérieures

9.3.4 L'impact de la charge des passagers

Dans cette section, l'effet de la charge de passagers du bus sur la consommation d'énergie est étudié. Le BEB est simulé pour quatre niveaux d'occupation : très faible : <10 passagers, faible : <25, moyen : <40 et élevé:> 40. Les simulations sont réalisées dans les mêmes conditions de conduite, représentées par le cycle de conduite MB et sous deux cas de conditions météorologiques illustrées par deux températures externes (0 °C pour émuler un scénario de chauffage de l'habitacle et 30 °C pour émuler un scénario de refroidissement de l'habitacle).

Figure 9.13 graphique (b) montre la demande moyenne de puissance électrique de l'unité HVAC pendant les états transitoires et stables à des niveaux d'occupation des passagers variables. Pour le scénario de chauffage à 0 °C, la demande de puissance moyenne augmente de 10,5 kW à 11,1 kW en variant les charges des passagers entre la valeur minimale et la maximale ; cela représente une augmentation de 5% de la demande de puissance. Au contraire, pour le scénario de refroidissement à 30°C, la demande de puissance moyenne augmente de 2,9 kW à 6 kW ; cela représente une augmentation de 100% de la demande de puissance. Les résultats montrent que l'évolution de la demande moyenne de puissance est moins sensible à l'augmentation du taux d'occupation du bus pour le scénario de chauffage par rapport au scénario de refroidissement. En effet, la charge élevée de passagers, résulte en un rejet

supplémentaire de chaleur dans le bus ce qui contribue à chauffer la cabine et à réduire les besoins en chauffage ; Au contraire, les passagers contribuent à augmenter les besoins de refroidissement.

De plus, l'augmentation de la charge des passagers a un impact sur la consommation d'énergie du système de propulsion. Cette consommation augmente de plus de 15% avec un taux d'occupation maximal par rapport à un bus vide (Figure 9.13 graphique(a)).

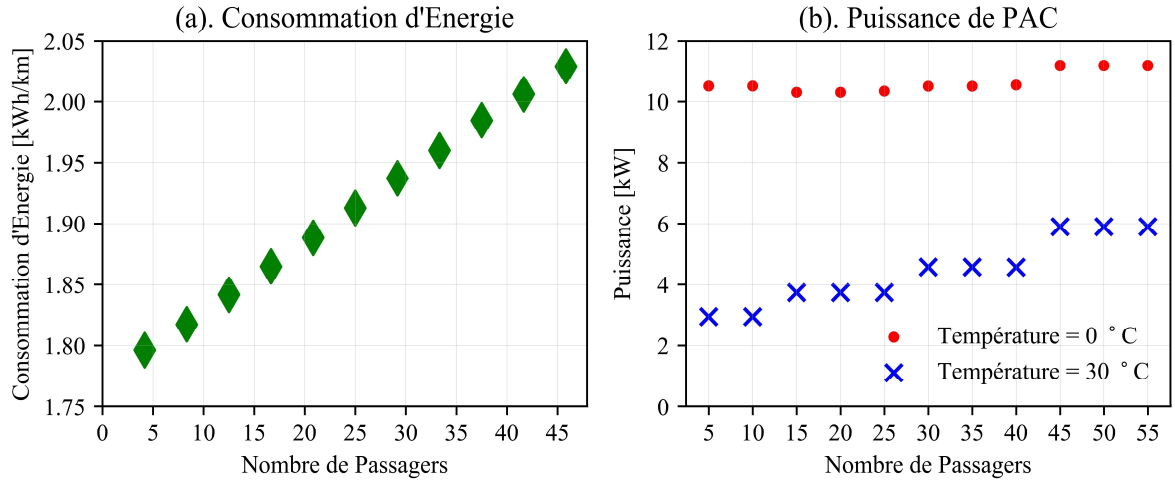


Figure 9.13: Consommation d'énergie / demande de puissance pour différentes charges de passagers

9.3.5 Méthodologie préliminaire pour le dimensionnement des batteries

Une étude sur l'impact des différentes conditions de fonctionnement sur la capacité énergétique des batteries est présentée. Elle détaille la méthodologie adaptée pour le dimensionnement approprié de la batterie en fonction des conditions de fonctionnement et présente les paramètres clés qui déterminent la taille de la batterie. En premier lieu, la méthodologie préliminaire de dimensionnement des batteries est présentée. Ensuite plusieurs études de cas sont considérées.

La méthodologie est basée sur quatre étapes représentées dans la Figure 9.14:

1. Détermination des conditions de fonctionnement du bus pour un voyage donné.
2. Détermination de la demande spécifique en énergie / puissance moyenne de chaque système énergétique dans le bus à l'aide des figures et des cartographies présentées.
3. Calcul de la consommation totale d'énergie du bus par voyage.
4. Estimation de la taille de la batterie en tenant compte de la fenêtre SOC disponible de la batterie et le nombre de voyages à effectuer avant une recharge complète de la batterie.

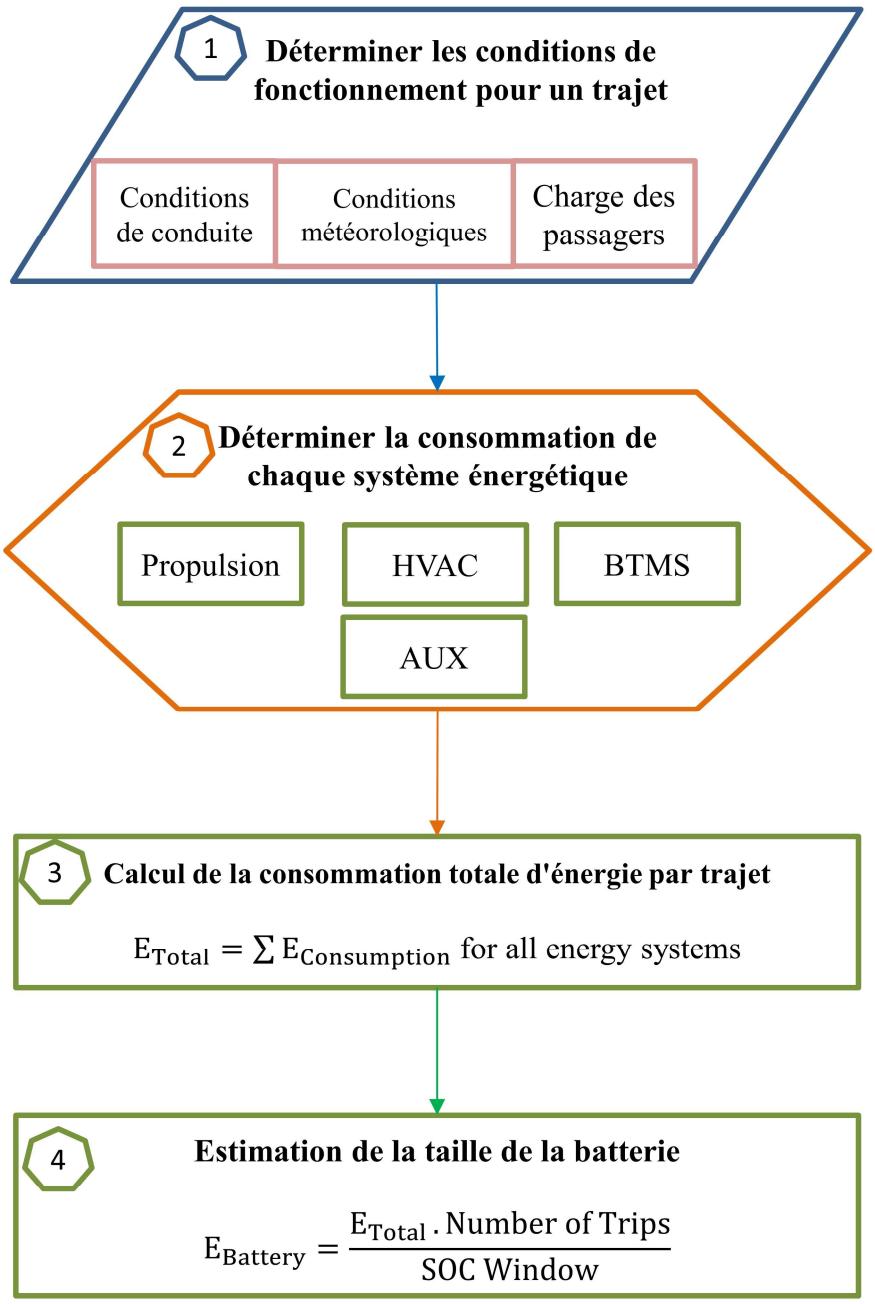


Figure 9.14: Organigramme de la méthodologie préliminaire de dimensionnement de batterie

Plusieurs études de cas sont investiguées afin d'évaluer l'impact des conditions de fonctionnement sur le dimensionnement des batteries. D'abord, un scénario de référence est présenté, le bus se recharge pendant la nuit. Les conditions de fonctionnement aller-retour de ce bus sont présentées dans Tableau 9.4. Trois types de conditions de fonctionnement sont considérés : (1) des conditions normales où toutes les conditions de fonctionnement sont calculées sur la base de données moyennes annuelles et (2 et 3) des conditions extrêmes.

Plusieurs solutions techniques sont étudiées pour réduire la taille de la batterie aux conditions extrêmes. Ces solutions, leur définition, leurs avantages et leurs inconvénients sont tous présentés dans le Tableau 9.5.

Tableau 9.4: Conditions de fonctionnement du scénario de référence

	Paramètre	Conditions Normales	Conditions Extrêmes 1	Conditions Extrêmes 2
Conditions de conduite	Vitesse moyenne	11 *km/h*	8 *km/h*	8 *km/h*
	Distance	20 *km*	20 *km*	20 *km*
	Durée	1.81 *h*	2.5 *h*	2.5 *h*
	Décélération moyenne	0.2 m/s^2	0.3 m/s^2	0.3 m/s^2
	Nombre d'arrêts	120	120	120
	Temps d'arrêt	0.51 *h*	0.51 *h*	0.51 *h*
Conditions météorologiques	Température	10 *°C*	-5 *°C*	35 *°C*
	Flux solaire	100 W/m^2	30 W/m^2	400 W/m^2
Charge de passagers		30	50	50
Informations Supplémentaires	SOC	0.7	0.7	0.7
	Nombre de voyages aller-retour	5	5	5
	Nombre de recharges par jour	1	1	1

Tableau 9.5: Résumé des solutions techniques pour la réduction de la taille de la batterie

Solutions Techniques	Capacité Energétique de la Batterie		Désavantages
	Conditions Extrême 1 (Froid)	Conditions Extrême 2 (Chaud)	
Scénario de référence	647 *kWh*	571 *kWh*	
Pré-conditionnement de la cabine	627 *kWh* **(-3%)**	557 *kWh* **(-2.4%)**	- Amélioration négligeable
Utilisation d'une source de chaleur alternative (pas de consommation électrique)	- remplacer 1 PAC 500 *kWh* **(-22%)** - remplacer 2 PAC 353 *kWh* **(-45%)**	Pas d'effet	- Non applicable pour les conditions de chaleur extrême
Réduction de la charge des passagers	- réduction de 30% 640 *kWh* **(-1%)** - réduction de 50% 655 *kWh* **(+1%)**	- réduction de 30% 528 *kWh* **(-5,2%)** - réduction de 50% 514 *kWh* **(-7,7%)**	- Pas amélioration dans les conditions de froid extrême - Réduction de la satisfaction des clients
Augmentation de la fenêtre de fonctionnement (SOC) de la batterie	- SOC = 80% 566 *kWh* **(-12,5%)** - SOC = 90% 503 *kWh* **(-22,5%)**	- SOC = 80% 500 *kWh* **(-10,2%)** - SOC = 90% 445 *kWh* **(-20,1%)**	- Accélération du vieillissement de la batterie et réduction de la durée de vie de la batterie
Réduction du nombre de voyages	- réduction de 20% 518 *kWh* **(-20%)** - réduction de 40% 388 *kWh* **(-40%)**	- réduction de 20% 457 *kWh* **(-20%)** - réduction de 40% 342 *kWh* **(-40%)**	- Utilisation de bus alternatifs interdits pour des raisons environnementales.
Augmentation du nombre de recharges par jour	- 3 fois par jour 258 *kWh* **(-60%)** - 5 fois par jour 130 *kWh* **(-80%)**	- 3 fois par jour 228 *kWh* **(-60%)** - 5 fois par jour 115 *kWh* **(-80%)**	- Coûts d'investissement supplémentaires (plus de chargeurs). - Risque de perturbation d'horaire

9.3.6 Conclusion

La taille de la batterie est étroitement liée à la consommation énergétique du BEB. Les batteries sont généralement surdimensionnées pour répondre aux besoins énergétiques du BEB dans des conditions météorologiques extrêmes. Bien que l'occurrence de ces conditions extrêmes soit rare, la taille de la batterie est surdimensionnée pour assurer un fonctionnement sans interruption du BEB dans ces conditions.

Le dimensionnement de la batterie du BEB est affecté par de nombreux facteurs, comme indiqué dans Tableau 9.5. Cependant, les modèles de recharge adoptés, tels que le nombre de recharges par jour, ont le plus d'impact. La recharge pendant la journée permet de réduire fortement la capacité de la batterie mais soulève des questions concernant les perturbations des horaires de bus. De plus, des coûts d'investissement supplémentaires sont à considérer. En outre, le choix de la technologie de recharge détermine la durée de recharge et les coûts d'investissement. Cependant, un dimensionnement approprié de la batterie associé à une stratégie de recharge adéquate peut garantir un fonctionnement fluide du bus sans interruption et à des coûts d'investissement faibles.

Cela nécessite un développement dédié car la stratégie de recharge du BEB est fortement affectée par l'horaire du bus, le nombre de bus en circulation sur le même trajet et la consommation d'énergie du bus en fonction des conditions de fonctionnement. Par conséquent, un modèle complet de ligne de bus est nécessaire pour évaluer ces solutions techniques.

9.4 Chapitre 4
MODÈLE TECHNO-ÉCONOMIQUE de LIGNE de BUS ÉLECTRIQUES à BATTERIE

9.4.1 Introduction

Le dimensionnement de la batterie est lié étroitement à la consommation énergétique du bus. La consommation énergétique du BEB dépend des conditions de fonctionnement du bus telles que les conditions de conduite, les conditions météorologiques et la charge des passagers. Par conséquent, la taille de la batterie est affectée par ces conditions. Généralement, les batteries sont dimensionnées en fonction de conditions de fonctionnement extrêmes telles que des températures extérieures très basses, des conditions de circulation denses et des charges de passagers élevés afin d'assurer un fonctionnement ininterrompu du bus. Cependant, le dimensionnement, basé sur des conditions d'utilisation rares, conduit à une augmentation des coûts de la batterie et un accroissement du poids du bus et réduit par suite sa capacité en passagers.

En parallèle, les stratégies de recharge du BEB affectent également la taille de la batterie. D'une part, la recharge du BEB pendant la nuit est associée à une batterie de grande taille, car la batterie doit répondre à tous les besoins énergétiques du BEB de la journée. La recharge nocturne utilise des chargeurs lents car il y a suffisamment de temps pour recharger les bus. D'autre part, la recharge répétitive diurne du BEB permet de réduire la taille de la batterie. Ces derniers scénarios de recharge sont associés à des chargeurs rapides en raison du temps limité disponible pour la recharge diurne des bus.

En plus, le dimensionnement des batteries et la stratégie de recharge de BEB sont déterminés par les conditions de fonctionnement des bus. Outre les conditions de conduite, les conditions météorologiques et la charge de passagers, l'horaire des BEB influence directement les stratégies de recharge. Les BEB qui opèrent sur des itinéraires très fréquentées ont principalement des horaires très chargés et effectuent un nombre élevé de trajets par jour, de sorte que le temps de recharge disponible pour ces bus pendant la journée est limité. Au contraire, les BEB interurbains opèrent sur des trajets plus longs entre les villes moins fréquemment, ce qui donne la possibilité de recharger pendant la journée.

En conséquence, afin d'évaluer les interactions entre le dimensionnement de la batterie, la stratégie de recharge et les conditions de fonctionnement du BEB, il est essentiel de développer un modèle technico-économique de la ligne BEB où ces composants sont considérés simultanément.

D'abord, les lignes de BEB fonctionnant actuellement à la pointe de la technologie et le schéma complet de recharge des BEB sont présentés. Ensuite, un modèle d'énergie de ligne de BEB détaillé est développé dans la section 9.4.3, suivi d'un modèle de fonctionnement de ligne de BEB dans la section 9.4.4 et d'un modèle TCO complet dans la section 9.4.5. La section 9.4.6 présente une étude de cas utilisant les modèles proposés, mettant en évidence l'impact des différentes stratégies de dimensionnement et de recharge des batteries sur le TCO et le fonctionnement des BEB. Enfin, dans la section 9.4.7 les principales conclusions de ce chapitre sont récapitulées.

9.4.2 État de l'art des lignes du BEB : dimensionnement des batteries, stratégie et technologie de recharge

Plusieurs villes dans le monde ont déjà mis en œuvre des projets d'électrification de leur flotte de bus. La Chine mène la course à l'électrification de la flotte de bus, où près de 99% des bus électriques mondiaux fonctionnent en Chine. Cela est dû aux promotions et aux incitations fixées par les autorités chinoises pour déployer rapidement les BEB. Par ailleurs, l'Europe est un grand marché des BEB où de nombreuses lignes de bus fonctionnent à 100% en BEB. Les Pays-Bas, la Suède et le Royaume-Uni sont les pays leaders dans l'électrification des flottes de bus, suivis par la France et l'Allemagne.

Table 4.1 présente une revue des lignes de BEB récentes en fonctionnement en Europe, en Chine et aux États-Unis. Il compare les différentes tailles de batterie et les stratégies de recharge adoptées dans chaque pays / ville.

En effet, une variété de tailles de batteries et de stratégies de recharge pour les lignes de BEB sont mises en œuvre dans le monde entier. Il est essentiel de bien définir la stratégie de recharge d'une ligne du BEB. Une stratégie de recharge intègre les quatre questions suivantes afin de garantir un service de BEB fluide et ininterrompu

• Où recharger ?

• Quand recharger ?

• Quelle quantité d'énergie à recharger ?

• A Quelle puissance de recharge ?

Premièrement, les bus peuvent se recharger au dépôt de bus, aux stations terminales de la ligne ou à une station d'arrêt quelconque de la ligne. Deuxièmement, les bus peuvent se recharger pendant la nuit quand ils sont hors service ou pendant la journée et ce à plusieurs reprises avec des fréquences variables. A noter qu'il est essentiel de déterminer la quantité d'énergie pour recharger les bus et la puissance requise. En effet, ces derniers permettent de déterminer la durée de recharge du bus et l'énergie disponible stockée dans la batterie. La stratégie de recharge définie en fonction des quatre questions posées et la taille de la batterie sont fortement liées. A titre d'exemple, la localisation des chargeurs au dépôt de bus implique une grande taille de batterie qui ne peut être rechargée que la nuit.

En général, la recharge des BEB est définie en identifiant les trois items suivants :

1. Infrastructure de recharge
2. Niveau de puissance de recharge
3. Type de système de recharge

- **Infrastructure de recharge**

L'infrastructure de recharge est définie par l'installation et l'emplacement des systèmes de recharge. Les types d'installations de recharge sont la recharge stationnaire et la recharge dynamique. Les installations de recharge stationnaires nécessitent le stationnement des bus à une station de recharge. Ce type d'infrastructure de recharge est le plus répandu dans le monde. En plus, la recharge stationnaire est classée en fonction de la méthode de recharge ou de l'emplacement. Il existe 3 méthodes de recharge stationnaire : (1) recharge de nuit (au dépôt), (2) recharge de fin de ligne (aux terminus) et (3) recharge d'opportunité (à des stations d'arrêt). Les installations de recharge dynamique, appelées « recharge en mouvement », peuvent charger les véhicules en mouvement. Les installations de recharge dynamique sont encore en cours de développement et nécessitent des tests supplémentaires.

- **Niveau de puissance de recharge**

Plusieurs normes définissent les niveaux de puissance de recharge des véhicules électriques. Les normes de la Society of Automobile Engineers (SAE) sont les normes les plus courantes utilisées pour les niveaux de puissance de recharge. La norme utilisée actuellement est la norme

SAE-J1772 ; elle catégorise les chargeurs en fonction de leur niveau de puissance. Les chargeurs sont classés en chargeurs CA (courant alternatif) ou CC (courant continu). Pour chaque type de chargeur, plusieurs niveaux de puissance de recharge sont considérés comme détaillé dans Table 4.2 et Table 4.3.

- **Type de système de recharge**

Le type de système de recharge est défini par le mode de transfert d'énergie de la source d'énergie à la batterie rechargeable. Trois modes de transfert d'énergie sont identifiés :

1. Système de recharge conductive
2. Système de recharge inductive
3. Echange de batterie (*battery swapping*)

Dans les systèmes de recharge conductive, le transfert de puissance de la source d'énergie à la batterie se fait par contact direct au moyen d'un conducteur. C'est le système de recharge le plus simple et le plus courant, caractérisé par une efficacité élevée.

Les systèmes de recharge inductive transfèrent l'énergie à la batterie à l'aide d'un champ électromagnétique sans aucun contact entre la source d'énergie et la batterie. Cette technologie est encore en cours de développement. Ces systèmes offrent des avantages supplémentaires tels que la sécurité électrique dans toutes les conditions météorologiques. Cependant, cette technologie est limitée par les coûts élevés et par une efficacité relativement faible et les pertes de puissance plus élevées par rapport aux systèmes de recharge conductive.

Le système d'échange de batterie (*Battery Swapping System* - BSS) permet à l'utilisateur d'échanger ses batteries à certaines stations BSS. Le BSS offre plus de flexibilité ce qui permet de prolonger la durée de vie de la batterie et de réduire la demande de puissance de pointe du réseau électrique. Cependant, les coûts et la sécurité du BSS sont toujours des questions.

La taille de la batterie et la stratégie de recharge adoptée pour une ligne BEB déterminent son fonctionnement et ses coûts. L'énergie disponible à bord et la durée de recharge affectent le fonctionnement du BEB. Les longues durées de recharge peuvent entraîner des perturbations dans le fonctionnement du BEB, en particulier si le bus circule sur des itinéraires très fréquentés et des horaires serrés. De plus, l'énergie disponible à bord détermine l'autonomie BEB disponible qui doit toujours être suffisante pour effectuer les trajets afin d'éviter toute interruption de service. D'autre part, les coûts du déploiement des BEB sont directement déterminés par le choix de la taille de la batterie et de la stratégie de recharge. Outre le coût de

la batterie, le coût des chargeurs est affecté par le choix de la technologie de recharge et de l'emplacement. Les chargeurs rapides haute puissance sont plus chers que les chargeurs lents, et le coût de l'installation d'une station de recharge au dépôt sont différents de ceux aux stations d'arrêt. En conséquence, chaque combinaison de taille de batterie et de stratégie de recharge entraîne des coûts différents et affecte différemment le fonctionnement de la ligne du BEB, l'objectif est de réduire les coûts et d'assurer un fonctionnement sans heurt.

Enfin, le fonctionnement et les coûts des lignes de BEB sont directement déterminés par la taille de la batterie et les stratégies de recharge adoptées. Par conséquent, ce chapitre répond à la question suivante :

- Comment évaluer le TCO et le fonctionnement des lignes de BEB et comment sont-ils impactés par le dimensionnement de la batterie et la stratégie de recharge ?

9.4.3 Modèle énergétique de la ligne du BEB

La Figure 9.15 montre un schéma d'une ligne du BEB. La ligne comprend des BEB, des chargeurs, des stations d'arrêt le long de la ligne, des stations terminales aux deux extrémités de la ligne et un dépôt. Les stations d'arrêt, les stations terminales et le dépôt peuvent être équipés de chargeurs pour recharger les BEB. Les conditions de fonctionnement de la ligne sont également définies, y compris les conditions météorologiques, les conditions de conduite et la charge des passagers. En outre, l'horaire de ligne est présenté dans la figure suivante ainsi que la stratégie de recharge.

Les stations d'arrêt le long de la ligne du BEB peuvent intégrer deux fonctions qui affectent le schéma énergétique global du système. Premièrement, les arrêts accueillent les passagers en attente de l'arrivée du bus ; le nombre de passagers à l'arrêt détermine directement la charge des passagers à l'intérieur du BEB, ce qui impacte la consommation d'énergie de tous les BEB opérant le long de la ligne. Deuxièmement, toute station d'arrêt est un emplacement potentiel pour installer un chargeur pour transférer de l'énergie aux BEB durant son arrêt à la station.

Les stations terminales sont des stations d'arrêt situées aux deux extrémités de la ligne du BEB. Les stations terminales peuvent être équipées de chargeurs pour transférer l'énergie vers les BEB. Cependant, la principale différence est que les BEB s'arrêtent normalement pour des durées plus longues dans les gares terminales.

Le dépôt est l'endroit où les bus sont garés lorsqu'ils ne fonctionnent pas pendant la journée ou lorsqu'ils sont hors service la nuit. Le dépôt de bus peut être situé à quelques kilomètres de l'une

des gares terminales de bus ou, dans certains cas, il peut servir de gare terminale. Au dépôt, les BEB peuvent être chargés car il s'agit également d'un emplacement potentiel pour installer des chargeurs. La recharge au dépôt a lieu principalement pendant la nuit lorsque les BEB sont hors service, ou pendant la journée si certains BEB ne fonctionnent pas pendant des longues durées.

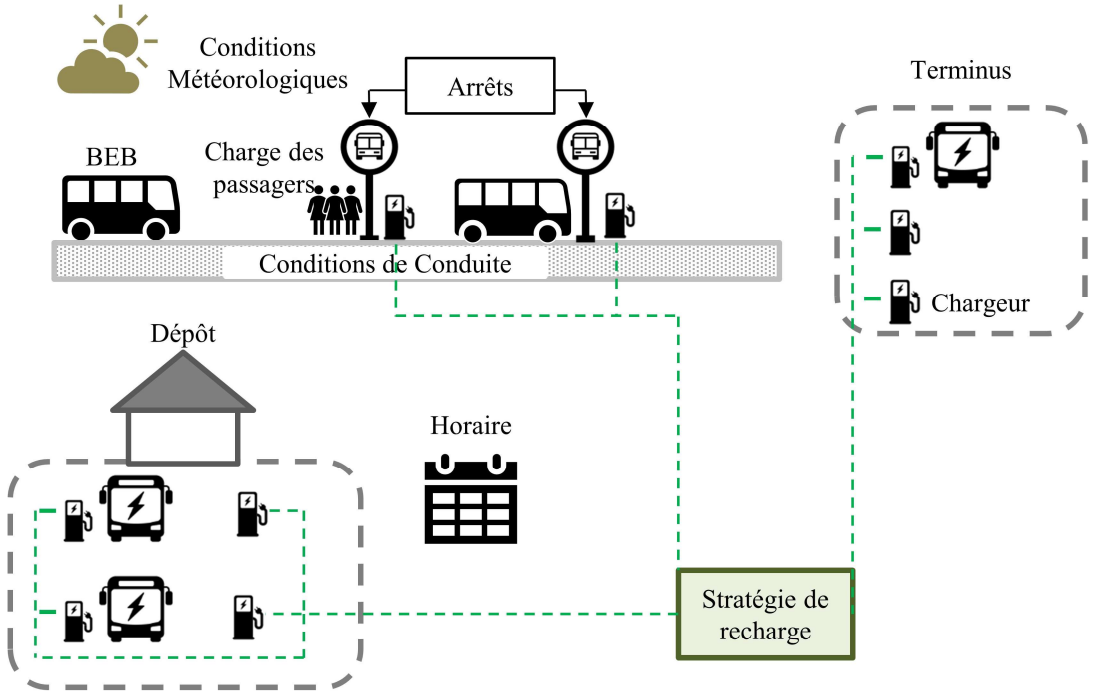


Figure 9.15: Schéma d'une ligne de BEB

De plus, les horaires des bus impactent le schéma énergétique de la ligne de BEB. Il est considéré comme une condition de fonctionnement supplémentaire. L'horaire détermine l'heure de départ des trajets pour chaque bus et le nombre quotidien de trajets par bus. Ainsi, les horaires impactent directement la consommation énergétique des BEB et la stratégie de recharge.

Enfin, la stratégie de recharge contrôle le flux de puissance des chargeurs vers les BEB.

9.4.4 Fonctionnement de la ligne du BEB

La tâche principale de toute ligne de bus est de faciliter la mobilité des passagers sur tout le trajet. Le fonctionnement de la ligne de bus doit garantir la satisfaction des passagers liée à la ponctualité des bus. Avec le déploiement des BEB, la capacité des BEB à suivre leur horaire prédéfini suscite des inquiétudes à cause de leurs besoins de recharge, ce qui peut entraîner des retards potentiels et perturber ainsi les horaires des BEB.

Le fonctionnement de la ligne du BEB est défini par deux caractéristiques principales : (1) % l'interruption d'horaire et (2) % l'interruption de service. Les bus doivent atteindre un certain niveau de ponctualité. En effet, le non-respect de ce niveau de ponctualité entraîne des pénalités qui devraient être payées par l'opérateur de bus.

- **Indice de ponctualité**

Le niveau de ponctualité est défini par un indice de ponctualité PI reflétant le nombre de trajets retardés et interrompus pour un échantillon de bus. Le contrat entre le Syndicat des Transports d'Ile-De-France et la Régie Autonome des Transports Parisiens, dans son l'annexe II – C, définit l'indice de ponctualité :« pour un trajet de bus programmé à un instant, l'indice de ponctualité est calculé en fonction du temps de retard, en référence à l'heure de départ programmée de la gare routière ».

Cette définition ne prend pas en compte l'interruption de service de bus, car actuellement avec les bus diesel actuels en service à Paris, les problèmes d'interruption de service due au manque d'énergie à bord sont absents. Dans cette thèse, il est considéré que si le service est interrompu lors d'un trajet de bus, un PI de 0% est attribué au trajet.

- **Structure des tarifs de pénalité**

Le tarif de pénalité est calculé en fonction de PI. Le montant annuel à payer en euros peut être positif ou négatif. Un montant positif indique le paiement d'une pénalité par l'opérateur et un montant négatif indique l'obtention d'un bonus. Un tarif maximal est imposé à la structure de pénalité. Il dépend de la taille du contrat entre l'opérateur et l'établissement public. Les opérateurs exploitant un grand nombre de lignes de bus sont soumis à des valeurs plus élevées.

9.4.5 TCO du déploiement des BEB

Le coût de déploiement des BEB peut être divisé en 5 composants principaux :

1. Coût unitaire du bus
2. Coût du fonctionnement
3. Coût de la maintenance
4. Coût de l'infrastructure
5. Coût du remplacement des batteries

- **Coût unitaire du bus**

Le coût unitaire est le coût d'achat d'un BEB. Il est plus cher par rapport au DB lié au coût supplémentaire des composants électriques (la batterie et la machine électrique). Il inclut un coût fixe et un coût variable dépendant de la taille de la batterie. Le coût de la batterie est considéré linéairement proportionnel à sa capacité énergétique.

- **Coût du fonctionnement du bus**

Le coût du fonctionnement des BEB sont les factures d'électricité payées par l'opérateur pour l'énergie électrique utilisée pour recharger les batteries des BEB. Une station de recharge est une station d'arrêt, une station terminale ou un dépôt équipé de chargeurs. Une station de recharge peut contenir un chargeur ou un ensemble de chargeurs, ce qui peut être le cas aux stations terminales et au dépôt. Chaque station de recharge est un nœud électrique qui est connecté au réseau électrique et engage une facture d'électricité. Ainsi, les coûts du fonctionnement d'une certaine ligne BEB, définis sur une période de facturation spécifique, sont la somme des factures d'électricité de toutes les stations de recharge pendant cette période de facturation.

Le coût du fonctionnement est directement lié à la consommation d'énergie des BEB et à la structure de la facture d'électricité fixée par les collectivités locales. La structure de la facture d'électricité diffère d'un pays à l'autre, voire d'une ville à l'autre d'un même pays. En général, la facture d'électricité inclut la consommation d'énergie et le coût des appels de puissance (*demand charge*).

Le coût de la consommation d'énergie électrique est proportionnel à la quantité d'énergie électrique consommée. Cependant, le tarif de l'énergie électrique peut varier au cours de la journée en fonction du mix de production d'électricité pendant la journée ou de la demande totale d'électricité sur le réseau.

L'autre composante de la facture d'électricité est un coût lié à la puissance installée. Le coût de la puissance est une redevance supplémentaire à payer par le consommateur et il est calculé en fonction de la demande de puissance de pointe pendant un intervalle de temps défini. Contrairement au coût de l'utilisation de l'énergie électrique, le coût de la puissance n'est pas cumulatif, il est considéré ponctuel proportionnel à la demande de puissance de pointe pendant une période de facturation définie. La demande de puissance de pointe est calculée comme étant la demande de puissance moyenne sur un intervalle de temps défini.

En plus, le coût du fonctionnement inclut les salaires des chauffeurs et des personnels rémunérés pour des services liés au fonctionnement de la ligne du BEB.

- **Coût de la Maintenance**

Les coûts de la maintenance intègrent des contrôles réguliers, la réparation ou le remplacement de composants dans le BEB. Les coûts de maintenance des BEB sont relativement inférieurs à ceux des DB à cause du nombre limité de pièces mécaniques en rotation. Les coûts d'entretien sont principalement mesurés par km. Ainsi, le coût de la maintenance d'une ligne BEB sur une période de temps est le coût unitaire de la maintenance multiplié par la distance parcourue par tous les BEB pendant cette période.

- **Coût de l'infrastructure**

Des modifications simples ou majeures de l'infrastructure sont nécessaires pour le déploiement des BEB. Le coût de la construction de stations de recharge sur la ligne de bus est relativement modéré. Cependant, un déploiement massif de BEB peut nécessiter des modifications au niveau du réseau électrique ou même des modifications dans la production d'électricité pour répondre à la demande supplémentaire d'électricité. Le scope de la thèse couvre le déploiement des BEB du point de vue de l'opérateur et, par conséquent, les coûts de l'infrastructure considérés se limitent à ceux associés à la construction et à l'installation de stations de recharge.

- **Coût du remplacement des batteries**

Le remplacement du système de stockage d'énergie est courant pour les BEB car la durée de vie de la batterie est plus courte que celle du BEB. Le coût du remplacement de la batterie est défini pour une année donnée. Pour une année, le coût du remplacement de la batterie est nul (pas de remplacement) ou égal au coût de la batterie (indiqué dans le coût unitaire).

- **Total Cost of Ownership**

Le « Total cost of ownership » (TCO) est une méthode très courante pour déterminer les coûts directs et indirects des lignes de bus urbains. Le TCO est utilisé pour calculer les coûts totaux obtenus pendant la durée de vie du système. Le modèle TCO proposé, quantifie ces coûts par kilomètre ; cela est utilisé pour l'évaluation du TCO des véhicules. Le TCO est calculé à partir de la somme de tous les éléments de coût mentionnés. De plus, la valeur de récupération de l'infrastructure et des batteries à la fin de la période d'étude est considérée.

9.4.6 Impact de la stratégie de recharge et de dimensionnement des batteries sur le fonctionnement et les coûts des lignes du BEB

Une étude de cas est présentée afin de démontrer l'impact du dimensionnement et de la stratégie de recharge des batteries sur le TCO et le fonctionnement d'une ligne de BEB en utilisant les modèles proposés. D'abord, les conditions de fonctionnement de la ligne et la fonction de coût sont paramétrés. Ensuite, les différentes stratégies de recharge et les tailles de batteries sont évaluées afin de quantifier leur impact sur les coûts et le fonctionnement de la ligne du BEB.

- **Etude de cas**

La ligne de bus 21 de la ville de Paris est représentée dans cette étude. Le point de départ est le stade Charlety dans le 13e arrondissement de Paris ; le terminus est la gare Saint-Lazare dans le 8e arrondissement de Paris. Le dépôt de la ligne de bus est situé à 1 km du Stade Charlety - Porte de Gentilly, il représente un dépôt et un terminal dans ce cas.

Quatre scénarios de recharge sont considérés. Ils représentent les tailles de batterie et les stratégies de recharge les plus courantes actuellement. La taille exacte de la batterie est calculée à partir du modèle du Chapitre 3. Tableau 9.6 présente ces scénarios.

Tableau 9.6: Scénarios de référence de l'étude de cas

Scénario		Taille de batterie	Stratégie de Recharge			
			Emplacement	**Période**	**Energie**	**Puissance**
1	**Overnight Charging (ONC)**	600 *kWh*	Dépôt	Nuit	SOC = SOC_{Max}	Minimum puissance requise pour SOC = : SOC_{Max} avant le départ de BEB
2	**Depot Day Charging (DDC)**	120 *kWh*	Dépôt	Jour/Nuit		
3	**End-Line Charging (ELC)**	80 *kWh*	Dépôt et Terminus	Jour/Nuit		
4	**Opportunity Charging (OC)**	60 *kWh*	Dépôt, Terminus et 8 arrêts	Jour, Nuit et pendant l'Opération (arrêts)		

- **Résultats et discussion**

La Figure 9.16 montre la segmentation du TCO suivant les scénarios. Le TCO est composé de 6 éléments : 1. Coût de la maintenance (MC), 2. Coût du fonctionnement (OC), 3. Coût de l'infrastructure (IC), 4. Coût de remplacement de la batterie (BRC), 5. Coût unitaire - Batterie (UCB) et 6. Coût unitaire - sans batteries (UCNB). Le scénario 1 (ONC) montre le TCO le plus élevé puisqu'il atteint 2,83 *€ / km*, tandis que le scénario 2 (DDC) rapporte le TCO le plus bas autour de 2,37 *€ / km*. Le TCO est relativement plus élevé dans le scénario 1 ayant un UCB élevé malgré son faible IC et OC. Le scénario de recharge de fin de ligne (ELC) et le scénario de recharge d'opportunité (OC) donnent un TCO identique de 2,39 *€ / km*.

Dans les 4 scénarios, MC et UCNB sont identiques car ils ne sont pas affectés par la taille de la batterie ni par la stratégie de recharge. Les autres composants TCO varient selon les scénarios.

Concernant l'UCB, les scénarios ayant les tailles de batterie les plus grandes engendrent des UCB les plus élevés.

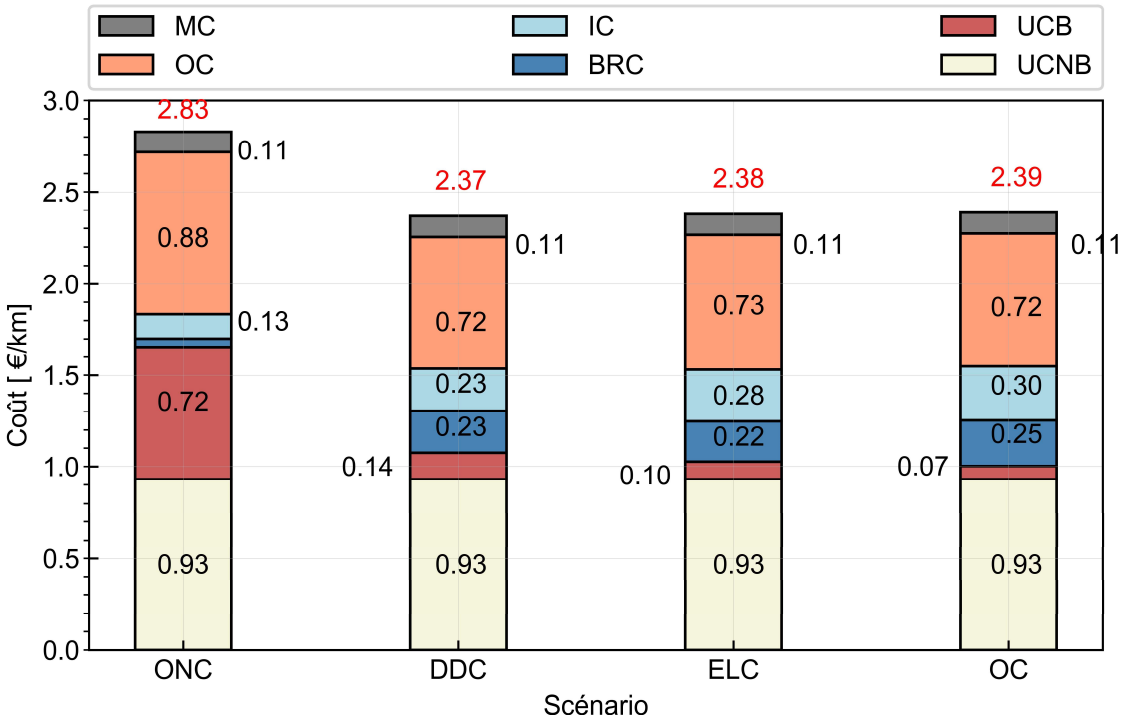


Figure 9.16: Segmentation du TCO dans les scénarios de référence

Pour le coût de remplacement des batteries (BRC), la batterie est remplacée lorsqu'elle atteint sa fin de vie, c'est à dire quand la capacité de charge est réduite de 20% par rapport à sa valeur maximale initiale. Les scénarios 2, 3 et 4 ont un BRC similaire, tandis que le scénario 1 à le

BRC le plus bas en raison de la recharge à faible puissance. Dans le scénario ONC, la durée de vie des batteries est d'environ 10,5 ans. Au contraire, les scénarios DDC, ELC et OC rapportent une durée de vie de la batterie de 2,8 ans, 2,7 ans, et 2,1 respectivement. Malgré le fait que la taille de la batterie dans le scénario ONC est beaucoup plus grande que les autres scénarios (et donc son coût de remplacement devrait être élevé), son BRC est faible en raison de la valeur de récupération de la batterie (la valeur de récupération de la batterie finale installée), car la batterie n'est utilisée que pendant 1,5 an supplémentaire.

Le coût des infrastructures (IC) représente les coûts d'acquisition et d'installation des chargeurs ; par la suite, ils sont directement liés au nombre de chargeurs à installer et à la puissance nominale correspondante. Le scénario OC au plus haut IC en raison des chargeurs rapides installés aux stations d'arrêt.

Pour les coûts d'opération (OC), ils sont les plus élevés pour le scénario ONC (0,88 *€ / km*) comparé aux autres scénarios (0,7 *€ / km)*. Cela est lié principalement à la consommation d'énergie plus élevée des batteries de grande taille et à la forte demande de puissance cumulative pour le scénario de recharge ONC.

La réduction du TCO du déploiement BEB est un point critique pour les opérateurs BEB ; ils sont soumis à de nombreuses contraintes concernant la qualité de service de la ligne BEB qui limitent leur capacité à réduire le TCO. La qualité de service est représentée par l'indice de ponctualité (PI) défini précédemment.

L'analyse de segmentation du TCO montre que l'opérateur dispose d'une marge de manœuvre pour réduire les coûts de la batterie (acquisition et remplacement), les coûts du fonctionnement et les coûts de l'infrastructure contrairement aux autres composantes de coût (coût unitaire et coût de maintenance).

Les coûts de la batterie, de fonctionnement et d'infrastructure sont directement liés au choix de la taille de la batterie et à la stratégie de recharge des BEB. La Figure 9.17 montre le compromis TCO - PI à différentes tailles de batterie et des puissances de recharge maximales pour le scénario DDC.

Tous les scénarios de base (cercles bleus avec des tons de couleur différents) ont un PI de 100% et n'ont aucune limitation sur la puissance de recharge maximum. Pour les autres scénarios sur la puissance de recharge, on définit un maximum autorisé de 100, 120 et 150 *kW*. La limitation de la puissance de recharge maximale peut conduire à des scénarios de recharge prolongés

entraînant des retards dans l'heure de départ des BEB réduisant ainsi le PI. Chaque trait plein représente une taille de batterie constante (K_b) et chaque trait en pointillé représente une puissance maximale constante (P_{max}).

À mesure que la puissance de recharge maximale autorisée diminue, le TCO diminue en raison d'une réduction du IC, du BRC et du coût de la puissance de l'OC. Cependant, cela entraîne une réduction du PI. Par exemple, pour une taille de batterie fixe de 120 *kWh* dans le scénario de base, la réduction de la puissance de recharge maximale autorisée à 100 *kW* réduit le TCO de 2,37 à 2,18 *€ / km* (8%), cependant, le PI est réduit de 100% à 85%. D'autre part, l'augmentation de la taille de la batterie augmente le TCO en raison des coûts de batterie supplémentaires et de la consommation d'énergie, mais des valeurs PI plus élevées sont obtenues. Cela est dû au fait que les batteries de plus grande taille nécessitent moins de recharge pendant la journée et sont donc moins sensibles à la puissance de recharge maximale autorisée.

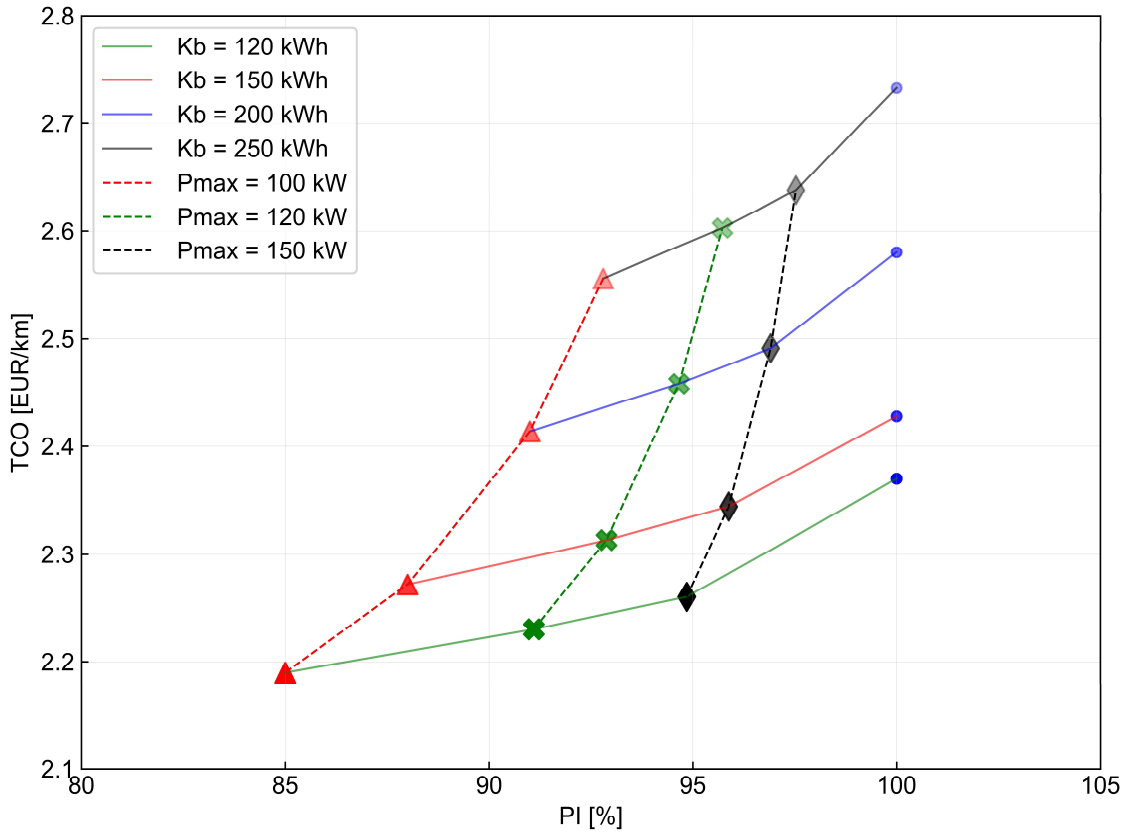


Figure 9.17: Compromis TCO - PI à différentes tailles de batterie et puissance de recharge maximum (DDC)

9.4.7 Conclusion

Le fonctionnement du BEB est sensible au dimensionnement de la batterie et à la stratégie de recharge adoptée. Un dimensionnement approprié de la batterie et une stratégie de recharge adéquate sont essentiels pour garantir un fonctionnement continu selon les horaires prédéfinis sans interruption du service. En outre, les coûts de déploiement des BEB dépendent également du choix du dimensionnement de la batterie et de la stratégie de recharge.

Le surdimensionnement des batteries peut aider à réduire les risques de perturbation d'horaire identifiés par l'indice de ponctualité (PI) ; mais cela se fait au détriment des coûts de batterie élevés et du TCO plus élevé en général. D'autre part, l'adoption d'une stratégie de recharge qui utilise des chargeurs de puissance élevée augmente le PI des BEB et réduit les risques de perturbation d'horaire. Ces stratégies de recharge entraînent un TCO élevé en raison du coût élevé des chargeurs en premier lieu, et des coûts de remplacement de batterie élevés en raison du vieillissement accéléré de la batterie.

Les différentes combinaisons de tailles de batteries et de stratégies de recharge entraînent différents couples TCO-PI. Pour cela, une stratégie optimale de dimensionnement et de recharge de la batterie est nécessaire pour minimiser le TCO du déploiement des BEB en maintenant des valeurs de PI acceptables (définies par les autorités locales).

9.5 Chapitre 5
Optimisation du dimensionnement de la batterie et stratégie de recharge des Bus Electriques à Batterie

9.5.1 Introduction

La recharge des BEB est un processus complexe avec des variables qui interagissent ensemble. Les variables du schéma de recharge peuvent être résumées en trois items principaux : (1) l'infrastructure de recharge, (2) le niveau de puissance de recharge et (3) le type du système de recharge. L'infrastructure de recharge caractérise les installations de recharge car elle définit l'emplacement de la recharge des BEB. La puissance de recharge détermine la puissance maximale des chargeurs à installer sur les différentes stations de recharge. Enfin, le type du système de recharge détermine le mode de transfert d'énergie de la source à la batterie (technologie). Ainsi, la stratégie de recharge combine tous ces éléments car elle définit l'infrastructure de recharge, le profil de puissance de recharge et la technologie de recharge.

Le dimensionnement des batteries et la stratégie de recharge des BEB déterminent directement le TCO du déploiement des BEB. Le TCO des BEB comprend les coûts d'acquisition des BEB, des batteries et des infrastructures et les coûts de fonctionnement, de maintenance et de remplacement des batteries. Le surdimensionnement des batteries conduit à une augmentation du coût d'acquisition des batteries et du TCO. D'autre part, la stratégie de recharge a également un impact sur le TCO des BEB. Des recharges fréquentes pendant la journée nécessitent l'installation d'un grand nombre de chargeurs ; cela conduit à l'augmentation des coûts de l'infrastructure. De plus, la recharge à des niveaux de puissance élevés nécessite l'installation de chargeurs spécifiques, à haute puissance, et à des coûts d'acquisition plus élevés.

En outre, le choix de la taille de la batterie et de la stratégie de recharge a un impact direct sur le fonctionnement des BEB et sur la ponctualité de leur horaire qui est caractérisée par l'indice de ponctualité (PI). L'adoption d'une stratégie de recharge utilisant des chargeurs à haute puissance pendant la journée permet de réduire le risque de perturbations d'horaire. Cependant, les BEB équipés de grosses batteries ne sont pas sujets à des perturbations d'horaire puisque les recharges se font pendant la nuit où ils sont mis hors service.

Une stratégie optimale de dimensionnement et de recharge des batteries minimisant le TCO du déploiement BEB tout en respectant les contraintes d'horaire des BEB est donc indispensable.

9.5.2 État de l'art

Plusieurs études ont été publiées sur la réduction des coûts du déploiement des BEB incluant un dimensionnement correct des batteries et adoptant des stratégies de recharge adéquates. Table 5.1 présente un résumé des études identifiées dans la littérature récente sur la réduction du coût de déploiement des BEB.

La plupart des études présentent des analyses comparatives ou des études de faisabilité des stratégies de recharge dans lesquelles la taille de la batterie et la puissance de recharge maximale sont considérées variables pour une infrastructure de recharge prédéfinie. D'autres études proposent des méthodes heuristiques pour réduire les coûts de déploiement des BEB.

D'autre part, des méthodes d'optimisation pour minimiser certaines composantes du coût du TCO des BEB ont été développées. Certaines études minimisent les coûts de l'acquisition des chargeurs en se basant sur un choix optimal de la localisation des stations de recharge et en identifiant la puissance maximale des chargeurs. D'autres études se concentrent sur la minimisation des coûts de remplacement des batteries.

Très peu d'études prennent en considération tous les éléments du coût du TCO des BEB. De plus, aucune étude présente une méthodologie d'optimisation qui minimise le TCO du déploiement des BEB incluant tous les éléments de coût (les coûts de l'acquisition de la batterie et des chargeurs, les coûts du remplacement de la batterie, les coûts de l'infrastructure, les coûts de l'énergie, le coût de la puissance et les coûts de dépenses) tout en respectant les contraintes d'horaire des BEB. De plus, à notre connaissance aucune étude présente une méthodologie globale qui permet d'optimiser pour une infrastructure de recharge spécifique, la taille de la batterie des BEB, la puissance, l'énergie et le temps de recharge.

En résumé, de cette étude bibliographique, nous avons identifié les besoins suivants : les limites des études dans la littérature ont été identifiées, lesquelles sont :

- Une méthodologie basée sur l'optimisation qui minimise le TCO du déploiement des BEB en considérant une fonction de coût complète tout en respectant les contraintes d'horaire.
- Une méthodologie généralisable pour tout type d'infrastructure de recharge et type de ligne de BEB, sans se limiter à une étude de cas spécifique.

- L'ajout de la taille de la batterie comme paramètre d'optimisation et non pas comme une donnée d'entrée.
- L'optimisation de toutes les variables de contrôle de la stratégie de recharge (la puissance, l'énergie, le temps et l'emplacement de recharge),

Dans cette partie, une méthodologie d'optimisation pour minimiser le TCO du déploiement des BEB en dimensionnant la batterie et en contrôlant la stratégie de recharge pour toute l'infrastructure de charge, tout en respectant les contraintes de ponctualité des BEB est développée. En résumé, ce chapitre répond à la question suivante :

Quelle est la stratégie optimale de dimensionnement et de recharge de la batterie qui minimise le TCO du déploiement des BEB tout en respectant les contraintes d'horaire et de ponctualité ?

9.5.3 Méthode

Pour minimiser le TCO du déploiement des BEB, il est essentiel d'optimiser les différentes variables de contrôle qui impactent le TCO. Comme mentionné en détail dans le Chapitre 4, la taille de la batterie et la stratégie de recharge des BEB déterminent le TCO du déploiement des BEB. La taille de la batterie est définie comme la capacité énergétique maximale de la batterie. En revanche, la stratégie de recharge inclut plusieurs variables : les profils d'énergie et de puissance de recharge des BEB pendant la journée, la puissance maximale et l'emplacement des chargeurs (l'infrastructure de recharge). Ces variables de contrôle sont classées en deux catégories : (1) Les variables de contrôle dynamiques, (2) Les variables de contrôle statiques.

Les profils d'énergie et de puissance de recharge des BEB pendant la journée sont des variables dynamiques car ils varient à chaque instant pendant le fonctionnement des BEB. Au contraire, la taille de la batterie et l'infrastructure de recharge sont des variables statiques fixes pendant le fonctionnement des BEB.

Chaque variable de contrôle a un impact sur une ou plusieurs composantes de coût du TCO. Les variables de contrôle dynamique (énergie de recharge quotidienne et profils de puissance) affectent principalement les coûts de fonctionnement et les coûts de remplacement de la batterie. D'un autre côté, les variables statiques affectent les coûts d'investissement (les coûts d'infrastructure et les coûts d'acquisition des batteries). Les coûts unitaires et de maintenance des BEB ne sont affectés par aucune variable de contrôle.

Ce problème ainsi formulé intègre un grand nombre de variables de contrôle de types différents (statiques et dynamiques). Pour cela, cette section présente une méthodologie d'optimisation

globale pour minimiser le TCO du déploiement BEB capable de prendre en considération toutes les variables de contrôle définies.

- **Cadre de Méthodologie**

La méthodologie est principalement composée de deux étapes d'optimisation où chaque étape utilise un algorithme d'optimisation spécifique et intègre un certain type de variables de contrôle. Dans la première étape, les variables de contrôle dynamique sont optimisées pour minimiser les coûts de fonctionnement et de remplacement de la batterie. Dans la deuxième étape, les variables de contrôle statiques sont optimisées pour minimiser le TCO tout en tenant en compte les variables de contrôle dynamique optimisées obtenues dans la première étape.

- **Méthode d'optimisation étape 1 : Programmation Dynamique (*Dynamic Programming* – DP)**

La programmation dynamique (DP) est une technique mathématique développée par Richard Bellman en 1954 pour fournir des solutions optimales aux problèmes de décision multi-étapes basées sur le principe de l'optimalité globale du problème. Cependant, cette technique présente certaines limitations liées au temps de calcul conséquent et à la nécessité d'une définition préalable de toutes les données définies tout au long de la période d'optimisation. Le choix de la DP pour cette étape d'optimisation est dû au fait qu'elle peut gérer un problème de décision dynamique en plusieurs étapes, ce qui est le cas dans l'étape d'optimisation 1. L'objectif de la DP est de minimiser les coûts totaux de l'énergie et du remplacement des batteries de chaque BEB sur une période d'optimisation en optimisant les variables de contrôle dynamiques (profils d'énergie et de puissance pour la recharge des BEB).

- **Méthode d'optimisation étape 2 : Algorithme Génétique (*Genetic Algorithm* – GA)**

« Les algorithmes génétiques (GA) sont des méthodes de recherche basées sur les principes de la sélection naturelle et de la génétique. » Pour faire évoluer un ensemble de solutions optimales, certaines mesures sont prises en compte pour distinguer les meilleures solutions. Dans les modèles mathématiques, ces mesures sont appelées fonctions objectives. Lors de la première étape d'optimisation, les variables de contrôle dynamique de chaque BEB sont optimisées pour chaque taille de batterie possible, minimisant ainsi les coûts de l'énergie et de remplacement de la batterie. Dans cette étape, le choix de la taille optimale de la batterie et ses variables de contrôle dynamique optimales correspondantes sont optimisées pour chaque BEB de la ligne, minimisant le TCO du déploiement du BEB.

La Figure 9.18 montre une schématisation de la méthodologie.

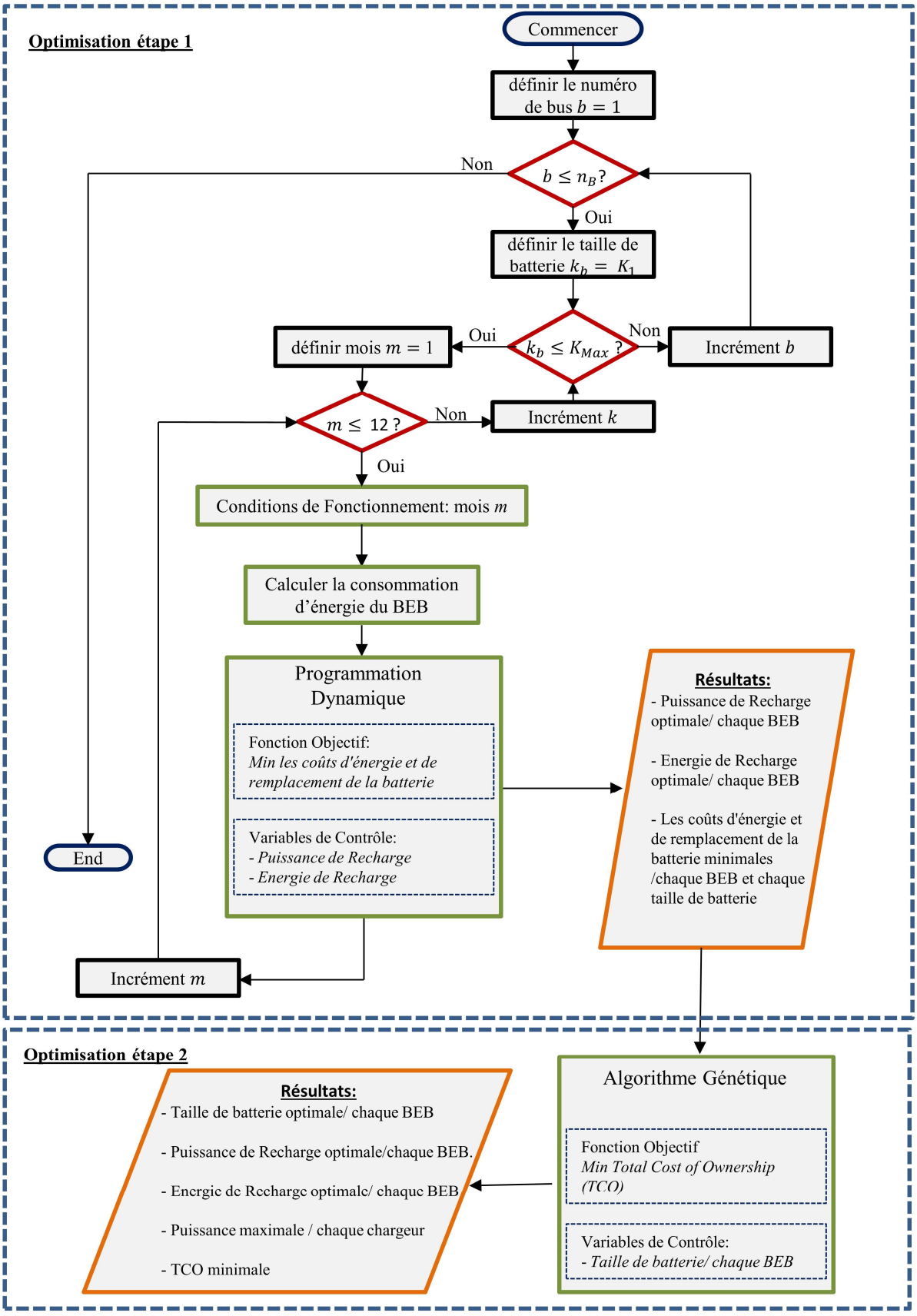


Figure 9.18: Schéma e de la méthodologie

9.5.4 Application et résultats

Dans cette section, une étude de cas est présentée en appliquant la méthodologie d'optimisation proposée. La ligne de bus 21 de la ville de Paris est étudiée.

D'abord, les résultats de l'étape de l'optimisation 1 (DP) sont présentés en analysant les stratégies de recharge optimales résultantes aux différentes tailles de batterie pour un seul BEB. Ensuite, les résultats de l'étape 2 de l'optimisation sont introduits ; ils mettent en évidence la taille optimale de la batterie et sa stratégie de recharge correspondante pour chaque BEB opérant le long de la ligne ainsi que l'infrastructure de recharge requise.

- **Stratégies de recharge optimales pour différentes tailles de batterie**

La Figure 9.19 montre la stratégie de recharge optimale pour différentes tailles de batterie pour le BEB numéro 1 au cours du mois de Janvier. Le graphique (a) de la Figure 9.19 présente la stratégie de recharge optimale pour une batterie de 50 *kWh*. Cette taille de batterie requiert une recharge au dépôt, au terminus et à 8 stations d'arrêt le long de l'itinéraire (4 dans chaque direction). Cela est dû à la capacité énergétique de la batterie sous-dimensionnée qui nécessite une recharge fréquente pendant la journée pour répondre aux besoins énergétiques du BEB. Les profils de puissance présentés dans le graphique (a) montrent que la puissance de recharge au dépôt et au terminal est comprise entre 50 et 100 *kW* pendant la journée ; cependant la recharge le long de l'itinéraire aux stations d'arrêt est de 200 *kW*. Cela est dû à la durée de recharge autorisée plus courte aux stations d'arrêt (30 secondes - 1 minute) par rapport à la recharge au dépôt ou au terminus.

De plus, la puissance de recharge fluctue fortement pendant la journée comme indiqué dans le graphique (a) à cause des conditions de fonctionnement quotidiennes variables, et donc des besoins énergétiques quotidiens variables du BEB. La puissance de recharge maximale au dépôt et au terminus est enregistrée entre 09 hh et 19 hh Elles représentent les heures de pointe ou les niveaux de congestion du trafic, la charge de passagers et en conséquence la demande d'énergie du BEB sont les plus élevés. De surcroît, les bus sont fréquents en heures de pointe ce qui réduit le temps de séjour des BEB au dépôt ou au terminus, et réduit donc le temps de recharge disponible des BEB.

Le bus 21 choisi est hors service après 02h30 du matin et garé au dépôt. A ce stade, la recharge pendant la nuit est à faible puissance (graphique a) car le BEB est rechargé à 15 *kW* pendant 3 heures.

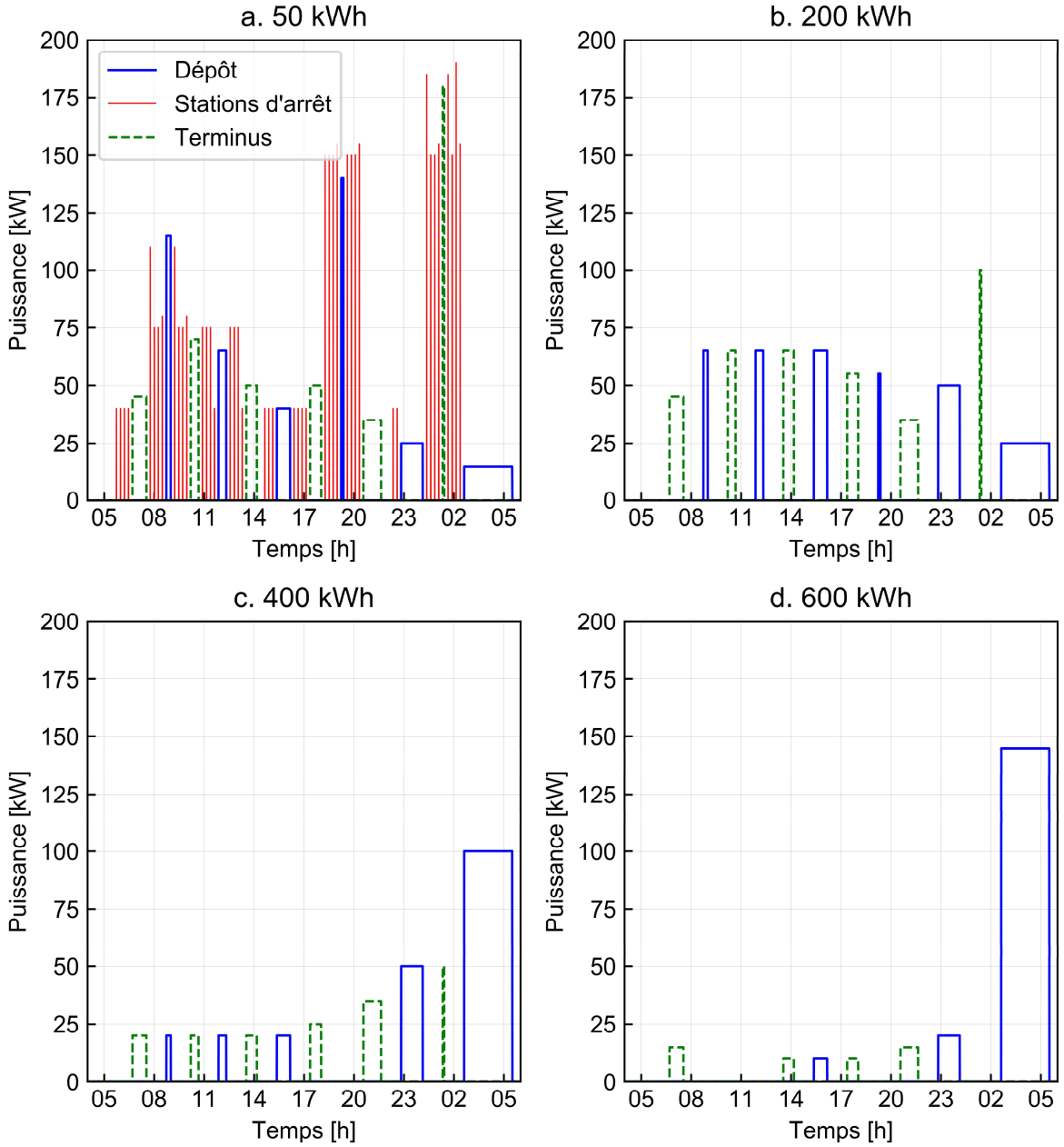


Figure 9.19: Stratégie de recharge optimale pour différentes tailles de batterie (BEB numéro 1 - mois de janvier)

D'autre part, les graphique (b), (c) et (d) montrent les stratégies de recharge optimales pour les tailles de batterie 200 *kWh*, 400 *kWh* et 600 *kWh* respectivement du BEB numéro 1 au cours du mois de Janvier. Pour ces tailles de batterie, les stratégies de recharge optimales sont uniquement au dépôt et au terminus. Cela est dû à la recharge à haute puissance aux stations d'arrêt qui accélère le vieillissement de la batterie et augmente ainsi les coûts de remplacement de la batterie. Il ressort clairement de la Figure 9.19 que la fréquence de recharge pendant la journée diminue à condition que la taille de la batterie soit plus grande. La fréquence de recharge pour les batteries de 200 kWh de 400 *kWh et de* 600 *kWh est* 11, 9, 6 recharges par jour. La

diminution de la fréquence de recharge pendant la journée des batteries de grande taille est associée au niveau d'énergie initial élevé de la batterie au début de journée.

Au contraire, la recharge pendant la nuit (après 02h30) est à une puissance plus élevée pour les batteries plus grosses. La batterie de 600 *kWh* est rechargée à 150 *kW* pendant la nuit. Cette valeur diminue à 100 *kW* pour la batterie de 400 *kWh* et à 25 *kW* pour la batterie de 200 kWh. Cela est dû à la plus faible énergie rechargée pendant la journée pour les BEB avec des grosses batteries. Les BEB équipés de grosses batteries favorisent la recharge de nuit à cause des tarifs d'électricité plus bas par rapport à ceux de la journée Les BEB équipés de grosses batteries peuvent répondre aux besoins énergétiques du BEB pendant la journée et avec une recharge minimale en raison de leur niveau d'énergie initial élevé. Cela permet de recharger la nuit à des tarifs d'électricité réduits, et donc de réduire les coûts de l'énergie.

Cependant, recharger uniquement la nuit peut entraîner une puissance de recharge très élevée qui accélère le vieillissement de la batterie et augmente ainsi les coûts du remplacement de la batterie. Pour cela, une certaine quantité d'énergie est rechargée pendant la journée afin de réduire la puissance de recharge la nuit. Cela entraîne une augmentation des coûts de l'énergie. Ainsi, la stratégie de recharge optimale pour chaque taille de batterie trouve le meilleur compromis entre les coûts d'énergie et les coûts du remplacement de la batterie.

- **Taille de batterie et infrastructure de recharge optimales**

Le graphique à gauche de la Figure 9.20 montre la taille de batterie optimale pour chaque BEB qui fonctionne sur la ligne proposée. Sur les 20 BEB opérant le long de la ligne, 13 BEB doivent être équipés de batteries de 90-100 *kWh*, 6 BEB équipés de batteries de 70-80 *kWh* et un seul BEB avec une batterie de 60 *kWh*. La taille optimale de la batterie pour chaque BEB dépend fortement de son horaire et de sa consommation d'énergie au cours de la journée ; cette dernière varie pour chaque BEB. En plus, le graphique à droite montre l'infrastructure de recharge optimale requise pour la ligne BEB proposée dans cette étude de cas. 20 chargeurs doivent être installés au dépôt avec des puissances maximales comprises entre 65 et 95 *kW*, la majorité de ces chargeurs est de 70 kW. 7 chargeurs supplémentaires à placer également au terminus et leurs puissances maximales varient entre de 100 à 115 kW. Aucun chargeur est à installer aux stations d'arrêt.

Afin d'analyser le choix des tailles de batterie optimales et de l'infrastructure de recharge requise, il est essentiel d'étudier le TCO pour différentes tailles de batterie. La Figure 9.21 présente les variations de tous les composants du coût du TCO en fonction de la taille de la

batterie. Pour simplifier l'analyse, tous les BEB sont équipés de la même taille de batterie ; la taille de batterie sur l'axe horizontal représente la taille de batterie de tous les BEB fonctionnant sur la ligne.

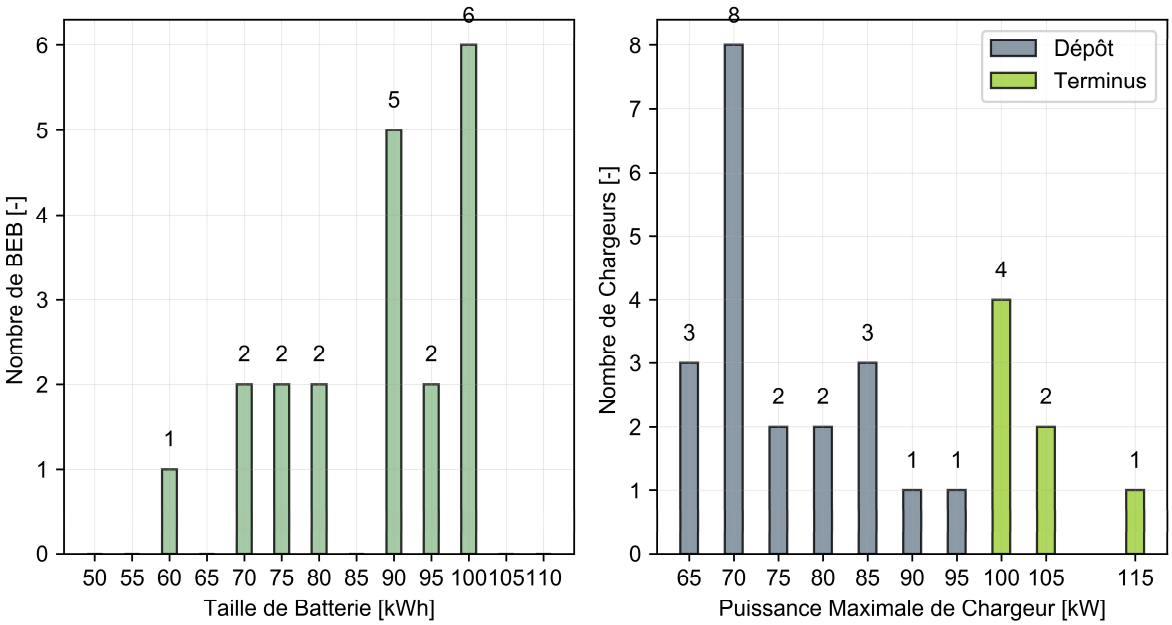


Figure 9.20: Taille de batterie optimale pour chaque BEB et infrastructure de recharge optimale requise

Dans le graphique (a), le TCO diminue de 2,27 à 2,157 *€/km* (réduction d'environ 6%) à condition que la taille de la batterie passe de 50 *kWh* à environ 100 *kWh*. À 100 *kWh* de capacité de batterie, le TCO atteint son minimum et commence à augmenter pour atteindre 2,87 *€/km* (augmentation d'environ 34%) pour une taille de batterie de 600 *kWh*.

Le coût unitaire est linéairement proportionnel avec la taille de la batterie. Il augmente de 1 *€/km* pour une batterie de 50 *kWh* à 1,6 *€/km* pour une batterie de 600 *kWh*. Le coût unitaire représente 45 à 55% du TCO ce qui représente le coût le plus important par rapport aux autres composantes du coût. La solution optimale présentée dans le diagramme à barres indique un coût unitaire égal à 1,029 *€/km*.

Le graphique (c) montre la variation des coûts de l'infrastructure en fonction de la taille de la batterie. Pour les batteries de très petite taille, le coût de l'infrastructure atteint 0,3 *€/km* pour une batterie de 50 *kWh*, principalement en raison des chargeurs rapides nécessaires aux stations d'arrêt pour les batteries de petite taille. Les coûts de l'infrastructure diminuent quand la taille de la batterie augmente et atteignent 0,1 *€/km* (réduction de 67%) pour une taille de batterie de 250 *kWh*. Pour les batteries de tailles moyennes (100 à 300 *kWh*), la recharge à la fin du trajet

est préférée par rapport à celle au dépôt, avec une puissance relativement inférieure par rapport aux batteries de taille plus petite. Cela se traduit par une réduction des coûts des chargeurs et donc par une réduction des coûts de l'infrastructure. Pour les batteries de taille supérieure à 300 *kWh*, les coûts de l'infrastructure augmentent pour atteindre 0,15 *€/km* pour une batterie de 600 *kWh* (augmentation de 50%). Les grosses batteries favorisent la recharge nocturne au dépôt plutôt que la recharge quotidienne fréquente, et donc l'ensemble des besoins énergétiques sont rechargés la nuit à une puissance relativement élevée dans cette étude de cas. Cela dépend fortement de la durée de charge la nuit, lorsque le bus est hors service.

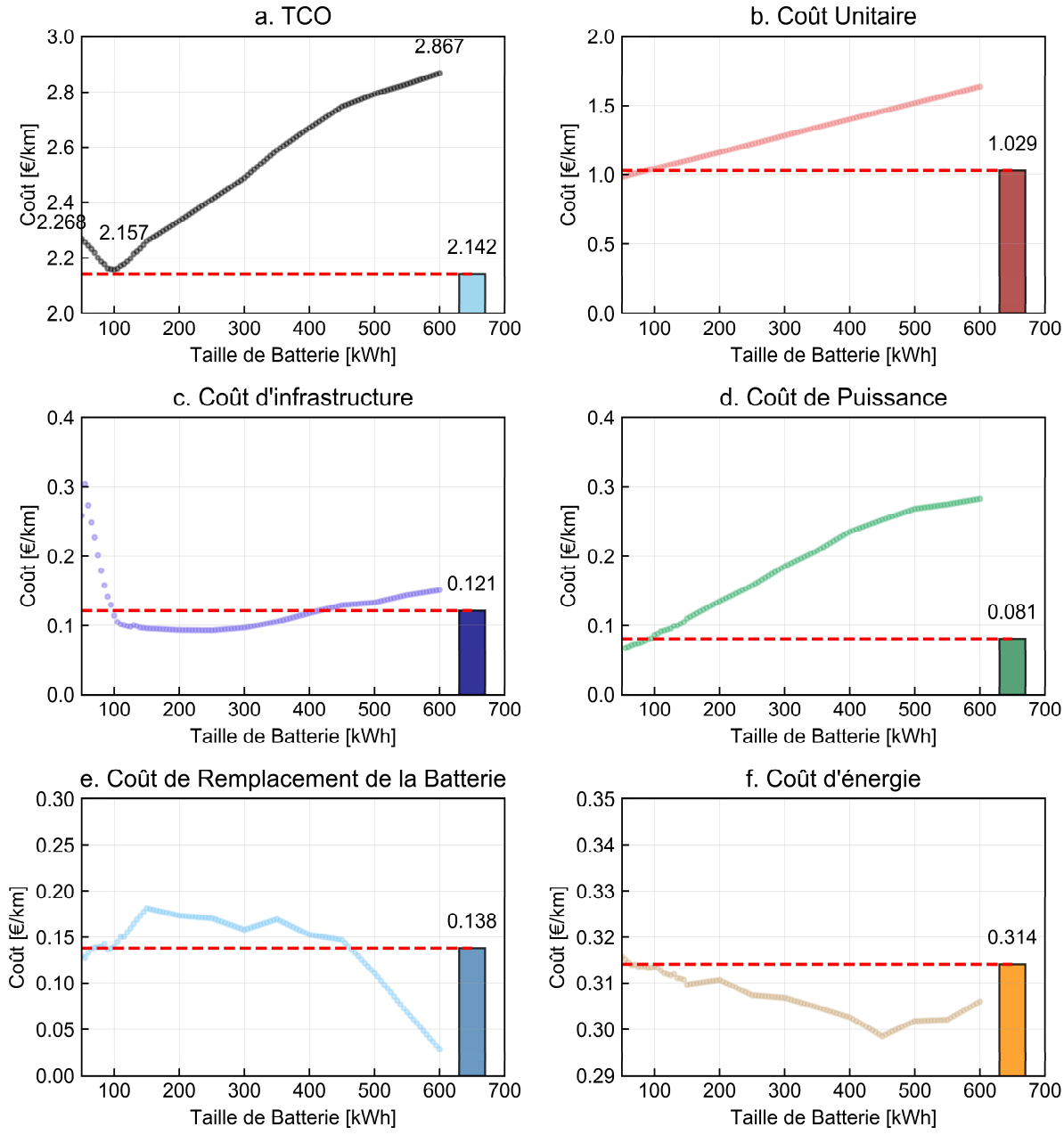


Figure 9.21: Segmentation du TCO

Le coût de la puissance n'est pas négligeable et pourrait dépasser les coûts de l'infrastructure, particulièrement pour les batteries de grande taille. Les coûts de la puissance augmentent strictement avec l'augmentation de la taille de la batterie. Même si les plus petites batteries sont rechargées à une puissance plus élevée pour chaque bus, elles enregistrent le coût de la puissance le plus bas du fait de la non-simultanéité des appels de puissance pour l'ensemble de la ligne de bus. Avec l'augmentation de la taille des batteries, la recharge est réalisée au terminus et au dépôt où les BEB sont rechargés simultanément ; cela entraîne une augmentation des coûts liés à la puissance souscrite.

Les coûts du remplacement des batteries diminuent lorsque la taille des batteries est élevée, car la fréquence de remplacement des batteries diminue en raison de leur recharge lente ralentissant leur phénomène de vieillissement. Cela dépasse les coûts élevés des batteries pour les grosses batteries. Cependant, pour des batteries de très petite taille, les coûts du remplacement des batteries sont en baisse. Malgré la fréquence élevée de remplacement de la batterie pour les petites batteries, les faibles coûts de la batterie à de telles tailles de batterie compensent la fréquence de remplacement élevée de la batterie due au vieillissement accéléré de la batterie.

La plus faible consommation énergétique des BEB correspond à des bus équipés de batteries de très petite taille. Cependant, la majorité de la recharge est réalisée en journée où un tarif d'électricité est élevé. En augmentant la taille de la batterie à 100-150 *kWh*, les consommations d'énergie augmentent ; A noter que, l'augmentation de la consommation énergétique des batteries de grande taille entraîne un accroissement de la facture énergétique inférieur à la baisse du coût de recharge la nuit à des tarifs réduits. Les coûts de l'énergie continuent de décroître pour des batteries de taille supérieure à 100-150 *kWh*. Enfin, pour les batteries de très grande taille (au-dessus de 450 *kWh*), l'augmentation des coûts liés à l'accroissement de la consommation énergétique l'emporte sur les avantages d'une recharge la nuit à tarifs réduits.

Enfin, la méthodologie proposée a le potentiel de réduire considérablement le TCO de BEB. Par rapport au BEB actuellement en service en France (Paris-Amiens- 350 kWh batterie et Bus 341 Paris- 240 kWh batterie), la réduction du TCO varie de 11 à 18%. De plus, par rapport aux autres bus circulant dans le monde, notamment avec de grandes batteries d'environ 600 kWh, la réduction du TCO peut atteindre 25%.

9.5.5 Conclusion

La recharge des BEB est un processus qui implique un très grand nombre de variables affectant le TCO du déploiement des BEB et leur fonctionnement. Outre la taille de la batterie, la stratégie

de recharge affecte directement le TCO des BEB. La méthodologie globale en deux étapes pour l'optimisation du TCO du déploiement des BEB en respectant les contraintes d'horaire est détaillée. D'abord, une optimisation de programmation dynamique est appliquée pour optimiser les variables de contrôle dynamique (l'énergie et la puissance de recharge pendant la journée) ; ensuite, une optimisation utilisant les algorithmes génétiques est appliquée pour optimiser la taille de la batterie pour chaque BEB.

Les résultats de l'application de la méthodologie sur une ligne de bus opérant dans la ville de Paris identifient un dimensionnement correct de la batterie et la stratégie de recharge des bus pour un TCO minimal. La réduction du TCO est de 25% par rapport aux tailles de batterie et à la stratégie de recharge actuellement adoptées.

9.6 Chapitre 6
CONCLUSIONS et PERSPECTIVES

En tant que deuxième contributeur mondial aux émissions de GES, le secteur des transports est soumis à un développement continu, en particulier le transport routier puisqu'il représente plus des trois quarts de ces émissions. Plusieurs technologies de véhicules alternatives ont été introduites et développées récemment, mais la mobilité dépendante du pétrole détient toujours la plus grande part de marché en raison de la pénétration limitée du marché de ces technologies, en raison de facteurs tels que la logistique énergétique, le coût et les infrastructures requises.

Cependant, les transports publics, en particulier les bus de transport en commun, sont moins affectés par ces facteurs, ce qui facilite le déploiement de technologies de transport alternatives. Dans ce contexte, cette thèse est impliquée dans le développement durable d'autobus de transport en commun afin de réduire la dépendance à pétrole.

Cette thèse présente une méthodologie systématique qui vise à développer des solutions pour surmonter ces défis en fournissant un dimensionnement des batteries et une stratégie de recharge optimales pour les BEB.

9.6.1 Synthèse et conclusions

L'analyse des nouvelles technologies alternatives de bus de transport en commun est réalisée au Chapitre 1. L'analyse prend en compte les bus diesel (BD), les bus au gaz naturel comprimé (GNC), les bus à biocarburant, les bus électriques hybrides (BEH) à la fois les architectures série et parallèle, les piles à combustible les bus électriques (PACO) et les bus électriques à batterie (BEB). L'analyse révèle que BEB est la solution la plus prometteuse pour remplacer la flotte DB actuelle grâce à ses performances énergétiques et environnementales. Cependant, BEB est confronté à de nombreux défis économiques et opérationnels qui empêchent son déploiement massif sur le marché.

Dans cette thèse, l'objectif est d'étudier le déploiement du BEB du point de vue de l'opérateur de bus en présentant des solutions rentables qui surmontent leurs défis. Outre le coût élevé du BEB, les principaux défis auxquels sont confrontés les opérateurs du BEB sont l'autonomie, le savoir-faire de fonctionnement et la disponibilité du réseau électrique.

Dans le Chapitre 2, la configuration du BEB est présentée en détail et l'architecture du bus et la technologie des composants sont présentées. Ensuite, un modèle énergétique complet pour du BEB est développé en utilisant une approche multi-physique. Le modèle prend en compte tous les systèmes énergétiques rencontrés dans un BEB et ce sont : le système de propulsion, l'unité HVAC et les auxiliaires, en plus de la batterie. Les modèles proposés sont validés par rapport à des études similaires dans la littérature récente, ou par rapport aux données fournies par les opérateurs de bus.

Une analyse énergétique détaillée est réalisée au Chapitre 3 pour étudier la performance énergétique du BEB aux différentes conditions de fonctionnement qu'il rencontre pendant son fonctionnement. Ces conditions d'exploitation sont les conditions de conduite, les conditions météorologiques et l'occupation de passagers.

L'impact des conditions de conduite est évalué en simulant le modèle du BEB. La consommation d'énergie du système de propulsion est très sensible aux conditions de conduite. Les routes très encombrées t augmenter la consommation d'énergie du système de propulsion de 35% par rapport aux BEB fonctionnant à des niveaux de trafic minimaux. De plus, les conditions de conduite ont un impact considérable sur la consommation d'énergie des auxiliaires, en particulier du compresseur d'air pneumatique.

Les conditions météorologiques ont un impact considérable sur la consommation d'énergie de l'unité HVAC et sur le BEB total. La demande de puissance moyenne de l'unité HVAC pendant un voyage augmente lorsque les températures externes s'écartent de la température ambiante / de la température de confort thermique (19-27 ° C). Les conditions extrêmement froides / chaudes enregistrent la demande de puissance de l'unité HVAC la plus élevée atteignant 25 kW en raison de la charge thermique élevée de la cabine et de la détérioration du COP de PAC. La demande de puissance de l'unité HVAC dans des conditions météorologiques modérées enregistre moins de 2 kW.

L'occupation des passagers influe sur la consommation d'énergie des bus. La demande de puissance de l'unité HVAC est fortement affectée par l'occupation des passagers car elle augmente de 100% pendant le refroidissement et de 15% pendant le chauffage. Un nombre élevé de passagers rejette une chaleur plus élevée à l'intérieur du bus et nécessite une plus grande quantité d'air frais. En outre, la consommation d'énergie du système de propulsion augmente linéairement avec un nombre plus élevé de passagers en raison du poids supplémentaire. Cette augmentation pourrait atteindre 15% en comparant un bus vide à un bus plein.

Cette analyse énergétique donne des informations précieuses sur le dimensionnement de la batterie requis pour tout BEB en identifiant simplement ses conditions de fonctionnement et en évaluant sa consommation d'énergie. Un cadre préliminaire de dimensionnement de la batterie est ensuite présenté dans ce chapitre. En outre, une variété de recommandations et de solutions techniques susceptibles de réduire la taille de la batterie sont présentées. Les stratégies de recharge adoptées, telles que le nombre d'événements de recharge quotidiens, ont un impact énorme sur la taille de la batterie.

Au Chapitre 4, un modèle techno-économique de la ligne du BEB est développé en temps réel afin d'évaluer les performances techno-économiques du BEB. Le modèle proposé dans ce chapitre permet d'évaluer le coût total de possession (TCO) du déploiement du BEB quelle que soit la taille de la batterie et la stratégie de recharge. Un modèle de coût est présenté où le TCO pour le déploiement du BEB est modélisé en tenant compte des coûts unitaires BEB, des coûts d'achat et de remplacement des batteries, des coûts d'énergie et de puissance, des coûts d'infrastructure et de maintenance. En outre, une approche pour évaluer le fonctionnement du BEB est présentée en évaluant un indice de ponctualité (IP) qui reflète les retards de départ des BEB dans leur horaire, résultant d'événements de recharge quotidiens.

Au Chapitre 5, le potentiel de réduction du TCO du déploiement de BEB est réalisé en introduisant une méthodologie d'optimisation qui vise à minimiser le TCO en optimisant la taille de la batterie et la stratégie de recharge. La méthodologie est un algorithme d'optimisation en 2 étapes qui utilise à la fois des routines d'optimisation de programmation dynamique et d'algorithme génétique, dans lesquelles ces techniques sont couplées pour résoudre le problème.

La méthodologie proposée est évaluée en considérant une étude de cas pour bus 21 opérant dans Paris. Pour l'étude de cas présentée, les batteries de taille moyenne couplées à une recharge de fin de ligne sont la solution la plus économique car ils offrent le compromis optimal entre les différents composants de TCO. Le coût unitaire de la batterie est très bas par rapport aux bus actuellement déployés (300 à 500 kWh). Le coût d'infrastructure est le plus bas car les batteries plus petites nécessitent une charge plus fréquente, qui est fournie par des événements de recharge d'opportunité à haute puissance. D'un autre côté, les batteries plus grandes favorisent une recharge la nuit où la majeure partie de la recharge de la batterie a lieu à une puissance relativement plus élevée. Le coût de puissance augmente continuellement avec la taille de la batterie car davantage de BEB sont chargés simultanément la nuit. Le coût de remplacement de la batterie pour les batteries de taille moyenne couplées à une recharge de fin de ligne est plus élevé par rapport aux batteries plus grandes, principalement en raison de la fréquence de

remplacement élevée de la batterie, cependant, la réduction des autres composants de coût compense ce coût de remplacement de batterie élevé. La méthodologie proposée offre un grand potentiel pour surmonter les défis techniques et économiques du déploiement du BEB, tandis que les résultats obtenus nécessitent une étude plus approfondie afin d'être généralisés.

Cette thèse a abouti à deux contributions principales :

1. Une méthodologie systématique capable de fournir un dimensionnement des batteries et une stratégie de recharge optimales pour la flotte de BEB afin de minimiser le coût total de possession du déploiement du BEB, tout en garantissant aucune interruption d'horaire ou interruption de service pendant le fonctionnement.
2. Un outil composé de plusieurs couches qui assiste les opérateurs de bus dans le déploiement de BEB. Cet outil permet une évaluation approfondie de la performance énergétique et des performances technico-économiques de BEB, fournissant des informations significatives sur la taille de batterie requise et la stratégie de recharge du bus et leur impact sur les coûts et le fonctionnement de la flotte de BEB. En outre, l'outil proposé optimise la taille de batterie requise et la stratégie de recharge pour faciliter le déploiement de BEB à faible coût et sans interruption de fonctionnement.

9.6.2 Perspectives

Les travaux de cette thèse ouvrent plusieurs fenêtres sur d'autres sujets très liés, essentiels au déploiement de BEB. Parmi les nombreux sujets qui pourraient compléter cette thèse, ou bénéficier de ce qui a été présenté dans cette thèse, les sujets suivants sont d'un grand intérêt :

1. Développer un modèle de réseau du BEB au niveau de la ville / du pays en tenant compte de toutes les lignes de bus avec leur interaction. Cela ajouterait une autre dimension à l'analyse présentée dans cette thèse, car elle définit de manière exhaustive l'infrastructure de recharge requise des BEB. En outre, cela pourrait aider à évaluer en profondeur l'impact de l'électrification de flotte de bus sur le réseau électrique.
2. L'horaires du BEB montre un impact très important sur le choix de la taille de batterie optimale et des stratégies de recharge. Les critères actuels de développement d'horaire des bus sont principalement élaborés pour répondre aux besoins de transport des passagers utilisant une flotte de bus diesel. Cependant, avec l'électrification de flotte de bus, une autre dimension doit être prise en compte dans le développement d'horaire des bus et c'est la recharge des bus électriques. Ainsi, repenser l'ensemble des critères de développement

d'horaire du bus en considérant cet aspect fournirait une marge de manœuvre pour faciliter le déploiement de BEB.

3. Le déploiement massif du BEB, ainsi que des véhicules électriques pour passagers, entraînerait une énorme demande d'énergie électrique qui pourrait nécessiter une modification majeure des infrastructures de production ou de transport d'électricité. Ainsi, il sera intéressant d'évaluer en profondeur l'impact du déploiement du BEB sur l'ensemble du schéma du marché de l'électricité, y compris la production, le transport et la distribution d'électricité. De plus, cela permet une réelle évaluation des bénéfices environnementaux du BEB car différents moyens de production d'électricité peuvent être envisagés.
4. À une époque où tous les systèmes énergétiques de notre vie quotidienne interagissent, les bus de transport public font partie intégrante du schéma énergétique quotidien. Le couplage des besoins énergétiques quotidiens du BEB à d'autres systèmes énergétiques tels que les bâtiments, les quartiers ou les sites industriels présente une opportunité d'améliorer encore l'efficacité énergétique des systèmes mentionnés. De plus, du point de vue du BEB, la création d'un tel réseau énergétique présente de nombreux avantages, notamment : (1) un approvisionnement énergétique réactif rapide au BEB, (2) de nombreuses possibilités de stockage d'énergie qui peuvent réduire la charge sur le réseau électrique, et (3) possibilité de réduire les coûts énergétiques du BEB.

The END

RÉSUMÉ

Les bus électriques à batterie (BEB) représentent une solution prometteuse pour remplacer les flottes de bus diesel actuelles consommant des énergies fossiles grâce à leur efficacité énergétique élevée et à leur potentiel de réduction des émissions de gaz à effet de serre et à l'absence d'émissions de polluants atmosphériques locaux. Cependant, cette technologie doit faire face à plusieurs défis, en particulier le coût total de possession (TCO) élevé et des contraintes opérationnelles comme l'autonomie des bus, le temps et le lieu de recharge. Cette thèse présente une méthodologie systématique qui vise à développer des solutions pour surmonter ces défis en fournissant un dimensionnement des batteries et une stratégie de recharge optimales pour les BEB. D'abord, un modèle énergétique multi-physique de bus est développé pour évaluer ses besoins énergétiques en prenant en considération ses différents systèmes énergétiques. Ensuite, la consommation d'énergie du bus est évaluée dans plusieurs conditions de fonctionnement afin de quantifier sa consommation d'énergie réelle. Un modèle techno-économique d'une ligne de bus est développé afin d'évaluer l'impact des différentes stratégies de dimensionnement et de recharge des batteries sur les coûts et le fonctionnement du BEB. Ensuite, un modèle TCO est introduit en tenant compte les coûts unitaires BEB, les coûts d'achat et de remplacement des batteries, les coûts d'électricité, les coûts d'infrastructure et de maintenance. L'analyse des résultats d'un cas d'étude à Paris souligne les compromis entre le TCO et les perturbations et les retards des horaires du BEB en fonction des différentes tailles de batterie et stratégies de recharge. Enfin, une méthodologie minimisant le TCO est proposée en déterminant un dimensionnement des batteries et une stratégie de recharge optimales pour la flotte de BEB tout en garantissant l'absence de perturbation des horaires ou des interruptions du service. Elle repose sur une optimisation en deux étapes qui utilise à la fois la programmation dynamique et un algorithme génétique. Les résultats montrent que la méthodologie proposée pourrait réduire le TCO du BEB entre 15-25% par rapport aux approches actuellement adoptées.

MOTS CLÉS

Bus électriques à batterie, Stratégie de recharge, Dimensionnement de batterie, Consommation d'énergie, Autonomie, flotte de bus, Optimisation, Programmation dynamique, Algorithme Génétique, Coût total.

ABSTRACT

Initiatives to decrease emissions from the transport sector are increasing worldwide by seeking alternative technologies to replace oil-based mobility. Battery Electric Buses (BEB) present a promising solution thanks to their high energy efficiency, low greenhouse gas emissions and the absence of local pollutant emissions. However, this technology still faces many challenges, especially its high total cost of ownership (TCO) and other operational factors such as the limited bus driving range, the high energy refueling time, and the required charging technologies and strategies. In this context, this thesis presents a systematic methodology that aims at developing solutions to help overcoming these challenges by providing optimal battery sizing and charging strategy for BEB. First, a comprehensive multi-physical bus energy model is developed to evaluate its energy needs considering all the energy systems encountered within. The energy consumption of the bus is then evaluated at a variety of operating conditions. Then, a techno-economic model of an entire bus line is developed in order to assess the impact of different battery sizing and charging strategies on the costs and operation of BEB. A TCO model is introduced considering the BEB unit costs, battery purchase and replacement costs, energy and power costs, infrastructure, and maintenance costs. A case study in Paris city is presented and the analysis reveals the resulting tradeoff between the TCO and BEB schedule disruptions and delays as function of different battery sizes and charging strategies. A methodology to minimize the TCO of BEB deployment is presented providing the optimal battery sizing and charging strategy for BEB, while respecting the BEB operation constraints. The methodology is a 2-step optimization algorithm that utilizes both Dynamic programming and Genetic Algorithm optimization routines. The results show that the proposed methodology could reduce the BEB TCO between 15-25% compared to the currently adopted approaches to deploy BEB.

KEYWORDS

Battery electric bus, charging strategy, battery sizing, energy consumption, Driving range, Bus fleet, optimization, Dynamic programming, Genetic algorithm, Total cost of Ownership.